Synthesis of Chiral Bimetallic Bipyridine-Bisoxazoline Complexes for Asymmetric Photocatalysis

Inaugural-Dissertation

zur Erlangung des Doktorgrades

der Mathematisch-Naturwissenschaftlichen Fakultät

der Heinrich-Heine-Universität Düsseldorf

vorgelegt von

David Doron Sokrates Thieltges

aus München

Düsseldorf, Mai 2023

aus dem Institut für Organische Chemie und Makromolekulare Chemie

der Heinrich-Heine-Universität Düsseldorf

Gedruckt mit der Genehmigung

der Mathematisch-Naturwissenschaftlichen Fakultät

der Heinrich-Heine-Universität Düsseldorf

Berichterstatter:

1. Prof. Dr. Constantin Czekelius
2. Prof. Dr. Thomas J. J. Müller

Datum der mündlichen Prüfung:

Ich versichere an Eides Statt, dass die Dissertation von mir selbstständig und ohne unzulässige fremde Hilfe unter Beachtung der „Grundsätze zur Sicherung guter wissenschaftlicher Praxis an der Heinrich-Heine-Universität Düsseldorf“ erstellt worden ist. Die Dissertation wurde in der vorgelegten oder in ähnlicher Form noch bei keiner anderen Institution eingereicht. Ich habe bisher keine erfolglosen Promotionsversuche unternommen.

Düsseldorf, den _____ _____

David Thieltges

Die vorliegende Arbeit wurde in der Zeit von Dezember 2017 bis Mai 2023 am Institut für Organische Chemie und Makromolekulare Chemie der Heinrich-Heine-Universität Düsseldorf unter Leitung von Prof. Dr. Constantin Czekelius angefertigt.

III

Danksagung

Mein besonderer Dank gilt Prof. Dr. Constantin Czekelius für die Aufnahme in die Arbeitsgruppe, für die interessante Aufgabenstellung, für sein Vertrauen und den Freiraum in der Bearbeitung des Projekts, sowie für seine fachliche und persönliche Unterstützung.

Ich danke weiterhin Prof. Dr. Thomas J. J. Müller für sein Zweitgutachten und die Möglichkeit essentielle photophysikalische Messungen in seinen Laboratorien durchzuführen. Des Weiteren möchte ich Priv.-Doz. Dr. Klaus Schaper, sowie Prof. Dr. Christian Ganter und Prof. Dr. Peter Gilch meinen Dank aussprechen, für ihre Hilfsbereitschaft und den fachlichen Austausch zu Fragestellungen aus ihrem jeweiligen Fachgebiet, der für dieses Forschungsprojekt von besonderer Bedeutung war.

Außerdem danke ich allen derzeitig aktiven und ehemaligen Mitarbeitern der Arbeitsgruppe C5, insbesondere meinen Mitstreitern aus Labor 27, für die angenehme Zusammenarbeit, für die positive und produktive Arbeitsatmosphäre, für den Austausch von Ratschlägen, Wissen und Erfahrungen, sowie für Freundschaften, die während der gemeinsamen Arbeit im Labor und darüber hinaus entstanden sind. Besonders danken möchte ich zudem bei Kai Baumgarten und Vivienne Wuttke für ihr Lektorat.

Ich danke meiner Familie für ihre Unterstützung und Motivation während des gesamten Studiums und der Promotion, insbesondere meinem Vater Philipp Zimmermann, dessen Unterstützung mir mein Studium und diese Arbeit ermöglicht hat. Auch meinem engsten Freundeskreis danke ich für offene Ohren und Ermutigung in schwierigen Arbeitsphasen.

Zuletzt möchte ich mich bei allen bedanken, die mich während meiner Promotion unterstützt haben, auch wenn sie nicht namentlich genannt wurden.

I. Table of Content

I. Abstract

This thesis aimed at the development of chiral bifunctional photocatalysts, that both serve to initiate photoredox reactivity and control stereoselectivity. The main focus was the comparison of heteroleptic ruthenium complexes of the form [Ru(R-bpy)$_2$(BOX-bpy)] with R = H, *t*Bu, OMe regarding the influence of substituents on the stereochemical outcome. The chiral bisoxazoline-bipyridine (BOX-bpy) ligands were synthesized by side-chain functionalization from 4,4'-dimethylbipyridine in a linear sequence of only four steps. Incorporation of the BOX-bpy ligand into the heteroleptic complexes paved the way for a comparative analysis of photophysical and electrochemical parameters, indicating that electron-donating substituents raise both the corresponding ligand orbitals and the metal-centred HOMO, while a BOX-bpy-centred orbital remains the energetically unaltered LUMO that preferably accepts an electron upon MLCT excitation. In order to determine the influence of the substituents on the preference for enantioselective transformations of Lewis acid-bound substrates with respect to racemic background reactions, five photoredox transformations were investigated. In an aerobic oxidation of a β-keto ester, the obtained enantiomeric excesses reflected the anticipated electronic influences. The results lay the foundation for further research on directed excitation in heteroleptic photocatalysts through rational modification of orbital energies for adjustment of reactivities on opposing catalyst sides towards spatially preferred photochemical activation of Lewis acid-bound substrates leading to enantioselective activation.

II. List of abbreviations

A	Acceptor
BOPA	Bis(oxazolinylphenyl)amide
BOX	Bis(oxazolin)
bpm	2,2'-Bipyrimidine
bpy	2,2'-Bipyridine
bpz	Bipyrazine ligand
CAMP	Cyclohexyl(2-methoxyphenyl)(methyl)phosphane
COD	Cyclooctadiene
COX-1	Cyclooxygenase-1
D	Donor
ΔG_{ES}	Gibbs free energy of lowest energy triplet MLCT
DET	Dexter energy transfer
dF(CF_3)ppy	2-(2,4-Difluorophenyl)-5-(trifluoromethyl)pyridine
DIOP	*O*-Isopropylidene-2,3-dihydroxy-1,4-bis(diphenylphosphino)butane
DIPAMP	(Ethane-1,2-diyl)bis[(2-methoxyphenyl)(phenyl)phosphane]
dmb	4,4‘-Dimethyl-2,2‘-bipyridine
DMF	*N*,*N*-Dimethylformamide
DNA	Deoxyribonucleic acid
DPZ	Dicyanopyrazine
dtbbpy	4,4'-Di-*tert*-butyl-2,2'-bipyridine
E_{00}	Energy difference between vibrationally relaxed ground and excited states
EA	Electron affinity
EDA	Electron donor acceptor
ee	Enantiomeric excess
E_{em}	Energy at emission maximum
EnT	Energy transfer
er	Enantiomeric ratio
EU	European Union
Fc	Ferrocen
Fc^+	Ferrocenium cation
FDA	U.S. Food and Drug Administration
FMN	Flavin mononucleotide
FRET	Förster resonance energy transfer
fs	Femtoseconds
GS	Ground state
HAT	Hydrogen atom transfer
HOMO	Highest occupied molecular orbital
IC	Internal conversion
IP	Ionization potential
ISC	Intersystem crossing
k_{fl}	Rate constant of fluorescence
k_{IC}	Rate constant of internal conversion
k_{nr}	Rate constant of non-radiative decay

k_{ph}	Rate constant of phosphorescence
LA	Lewis acid
λ_{GS}	Excess energy of ground state after phosphorescence
LC	Ligand-centred
LUMO	Lowest unoccupied molecular orbital
MC	Metal-centred
MLCT	Metal to ligand charge transfer
MO	Molecular orbital
NAD(P)H	Nicotinamide adenine dinucleotide phosphate
nm	Nanometer
nr	Non-radiative decay
ox	Oxidation
PCET	Proton-coupled electron transfer
PET	Photoinduced electron transfer
ph	Phosphorescnce
phen	1,10-Phenanthrolin
PHOX	Phosphinooxazoline
ppy	Phenylpyridine
ps	Picoseconds
PyBOX	Bis(oxazolinyl)pyridine
pz	Pyrazolo ligand
Q	Quencher
RB	Rose bengal
red	Reduction
RNA	Ribonucleic acid
SCE	Standard calomel electrode
SCS	Spin-center-shift
SET	Single electron transfer
SOMO	Singly occupied molecular orbital
TBHP	*tert*-Butyl hydroperoxide
UV	Ultra violett
vr	Vibrational relaxation

1 Introduction

Photoredox catalysis has become a major topic in chemical research in recent years and has added a variety of useful and previously unavailable transformations to the toolbox of organic synthesis.[1-6] Although there were sporadic publications on organic photoredox transformations since the 1970s, research associated with today's most popular photoredox catalyst $[Ru(bpy)_3]^{2+}$ (**7**) focused mainly on inorganic applications, e.g. water splitting or solar cells.[7-9] The versatility of this chemistry and its potential for synthetic methodology was not recognized by the chemical research community until the almost simultaneous appearance of three very diverse transformations: An efficient protocol developed by the MacMillan group in 2008 enabling an asymmetric α-alkylation of aldehydes **2** by merging photoredox- and organocatalysis is considered the initiator of the widespread and ever since growing interest in photoredox catalysis.[10] Almost at the same time, the Yoon group published a photoredox-catalyzed [2+2]-enone cycloaddition, followed by the Stephenson group introducing a visible light-induced reductive dehalogenation (**scheme 1**).[11, 12]

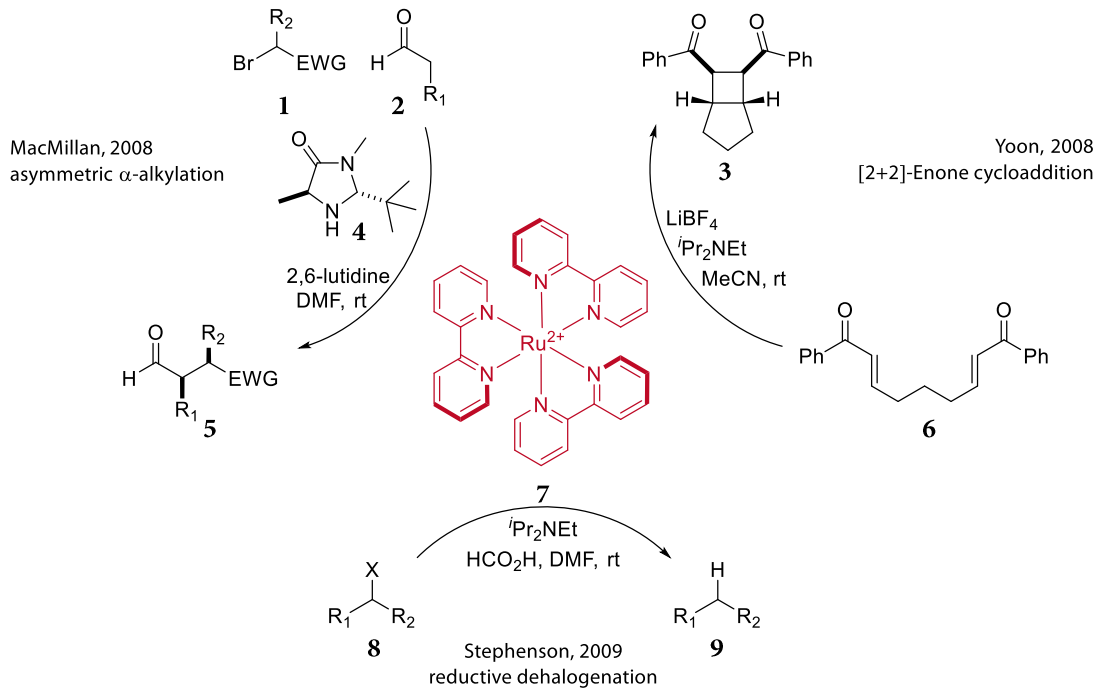

scheme 1. Selected examples of visible-light photoredox transformations that initiated the widespread interest in photoredox chemistry.[10-12]

Despite the diversity of these transformations, they share the photoredox catalyst $[Ru(bpy)_3]^{2+}$ (**7**), which possesses exceptional redox properties when excited by visible light (chapter 1.1) enabling single-electron-transfer (SET) or energy transfer to organic substrates and thus initiating a multitude of transformations involving radical intermediates (chapter 1.3). The MacMillan group exploited the photoredox catalyst for the reductive generation of α-carbonyl radicals to which chiral electron-rich enamines are readily added in a stereocontrolled fashion.[10] Oxidation of the resulting α-amino radicals - again by the photoredox catalyst - and regeneration of the organocatalyst **4** provides access to numerous enantioenriched α-alkylated aldehydes **5**.[10] In a similar way, the concept of organo-photoredox catalysis (chapter 1.3.1.1 and 1.3.2.1) was used to develop a variety of useful

transformations and served as inspiration for the establishment of further dual catalytic systems (chapter 1.3.1).[13-15] The Yoon group used photoredox catalysis for the reduction of an enone moiety **6**, which undergoes a stepwise cycloaddition to form cyclobutanes **3**.[11] As the redox potential of the photocatalyst **7** is insufficient for a direct reduction of the enone **6**, a Lewis acid co-catalyst was added which both facilitates the electron transfer and stabilizes the resulting radical anion, again suggesting the possibility of combining photoredox catalysis with an additional catalytic mode of activation.[11] Using photoredox catalysis, the Stephenson group succeeded in chemoselectively exchanging halogen substituents adjacent to electron-withdrawing groups, e.g. at α- or benzylic-positions, with hydrogen atoms by reductive dehalogenation in the presence of formic acid or Hantzsch ester serving as the hydrogen atom source.[12] This reaction is the foundation for later developments of the Stephenson group, e.g. a radical cyclization, wherein the intermediary radical adds intramolecularly to double or triple bonds before hydrogen atom abstraction.[16]

The fascination in photoredox catalysis that has persisted since these milestone publications reflects the variety of uncommon bond formations, enabled by the exploitation of radical reactivity, which greatly expands the repertoire of chemical transformations formerly dominated by ionic two-electron mechanisms.[3, 4] In contrast to established methods, the formation of these radicals does not require highly reactive radical initiators, that might lead to side reactions.[2, 3] Instead, the radical transformations can be initiated by simple irradiation with low-energy visible light from an ordinary household light bulb - a photochemical reaction setup that is very easy to implement without the need for specialized equipment.[3] Given their extraordinary photophysical and electrochemical properties (chapter 1.1), photoredox catalysts serve to convert the energy from visible light irradiation into usable electrochemical potential, thereby generating oxidants and reductants transiently at different points in the reaction mechanism, sometimes without the need for stoichiometric chemical oxidants or reductants.[3] Since visible light is of low energy and organic molecules typically do not absorb in the visible spectrum, the risk of side reactions resulting from photoexcitation is very low. [3, 17, 18]

Since 2008, research on photoredox catalysis has revealed a great number of novel transformations. By combining photoredox catalysis with other catalytic modes of activation such as organocatalysis (chapter 1.3.1.1 and 1.3.2.1), transition-metal catalysis (chapter 1.3.1.2 and 1.3.2.2) and even biocatalysis (chapter 1.3.1.3 and 1.3.2.3), the misconception that the reactivity of radical intermediates is incompatible with the increasing demand for selectivity was overcome and the spectrum of catalytic transformations was expanded by the branch of odd-electron-reactivity.[4] Thereby, a large number of catalyst derivatives including metal complexes analogous to $[Ru(bpy)_3]^{2+}$ (**7**), but also metal-free organic photoredox catalysts have been developed and their photophysical and electrochemical properties optimized for their respective transformation by precise fine tuning of the structure (chapter 1.1.3). Both the development of new photoredox catalysts and exploration of their reactivity, as well as the concept of dual catalysis are promising approaches for the further evolution of this fast growing field of chemistry. The combination of photoredox catalysis with asymmetric Lewis-acid activation within a single catalyst structure might thus be a promising strategy to further enrich the toolbox of synthetic organic chemists.

1.1 Photophysical principles and general mechanisms in photoredox catalysis

1.1.1 Structure and excited states of $[Ru(bpy)_3]^{2+}$ (**7**)

The ability of photoredox catalysts to initiate phototransformations by electron- or energy transfer on substrate molecules ultimately derives from the conversion of visible light energy into chemically available energy.[2, 3] The involved excited state species exhibits a different electronic structure and distinct physical properties and reactivities compared to the ground state, thus rendering the excitation a gate into another dimension of chemistry that is not accessible in the dark, with thermally activated ground state species.[17-23] The underlying photophysical processes are described in the following on the example of the most famous photoredox catalyst $[Ru(bpy)_3]^{2+}$ (**7**).

In the commonly used simplified representation of the frontier molecular orbitals in a single-configuration single-electron approximation of $[Ru(bpy)_3]^{2+}$ (**7**) in an octahedral field, three transitions are indicated, which are classified according to the nature of the involved starting and ending orbitals (ligand-centred or metal-centred) of the corresponding transition.[17-23] In the MO-diagram only the d-orbitals of the metal are considered while neglecting the orbital interaction involving the s-orbital and p-orbitals of the higher shell.[24] Furthermore, O_h-symmetry is assumed, although the ground state of $[Ru(bpy)_3]^{2+}$ (**7**) is better assigned to the point group D_3.[19-23] Two of the d-orbitals of the metal centre, d_{z2} and d_{x2-y2}, form ligand-centred σ-bonds with the lone pairs of the six nitrogen atoms (σ_{bpy}). The ligand-centred π-orbitals of the three aromatic bipyridine chelate ligands are non-bonding. Their antibonding, unoccupied counterparts (π_{bpy}^*) act as π-acceptor orbitals and expand the energetic gap between π_M (t_{2g} in O_h-symmetry, derived from d_{xy}, d_{xz} and d_{yz}) and σ_M^* (e_g^* in O_h-symmetry, derived from $d_{x^2-y^2}$ and d_{z^2}) by lowering the t_{2g} levels (that are nonbonding in pure σ-donor complexes) to such an extent, that σ_M^* lay higher than the π_{bpy}^*-acceptor orbitals of the bipyridine ligands.[24] This causes the lowest unoccupied molecular orbital (LUMO) to be ligand-centred and the lowest-energy excitation a metal-to-ligand-charge-transfer (MLCT).[17-23] In addition to this MLCT transition, which is responsible for the low-energy absorption in the visible region, the absorption spectrum exhibits higher-energy metal-centred (MC) and ligand-centred (LC) transitions (**figure 1**).[17-23]

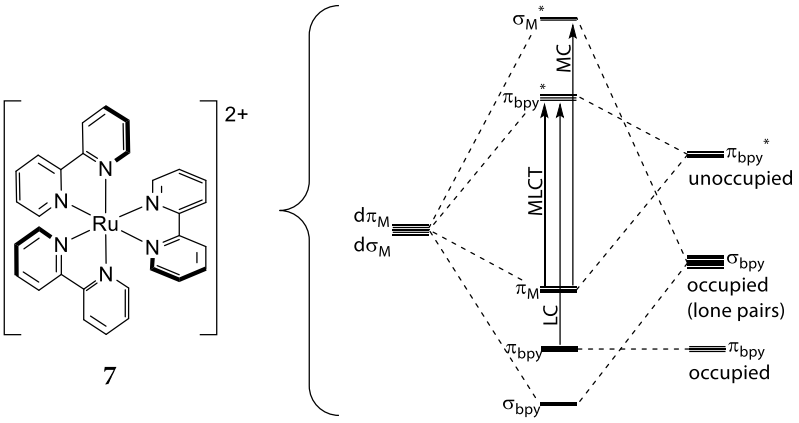

figure 1. Structure and simplified molecular orbital diagram of $[Ru(bpy)_3]^{2+}$ (**7**) in an octahedral field.[17-23]

The spin-allowed ^{1}MLCT transition (π_M -π_{bpy}*) causes the broad absorption band with a maximum at 452 nm in the visible range of the spectrum and is ultimately responsible for the unique redox properties of the excited photoredox catalyst (**spectrum 1**).[17-23] In a low temperature absorption spectrum (at 77 K in methanol-ethanol-glass) a direct spin-forbidden transition forming a triplet MLCT state (^{3}MLCT) in the low energy tail of the visible light MLCT band at about 550 nm is visible.[25] The occurrence of such spin-forbidden transitions is due to the heavy atom in the presence of which significant spin-orbit-coupling occurs.[26] Besides these low energy visible light MLCT excitations, there is another MLCT band near UV around 240 nm, resulting from the transition of an electron into higher antibonding ligand-centred orbitals.[17-23] Apart from these MLCT bands, the absorption spectrum shows two additional types of transitions: The narrow, intense band at 285 nm has been assigned to a spin-allowed ligand-centred (LC) transition (π_{bpy} - π_{bpy}*) by comparison with an absorption spectrum of the protonated ligand.[27] In addition, low intensity bands are indicated at 330 nm and 350 nm, which have been assigned to a metal-centred transition (MC) of an electron from the HOMO into metal-centred antibonding σ_M*-orbitals (π_M - σ_M*).[17-23] This symmetry forbidden d-d transition into antibonding orbitals regarding the ruthenium-bipyridine σ-bond is associated with a significant Ru-N bond elongation and promotes photodissociation of the ligand.[28-31]

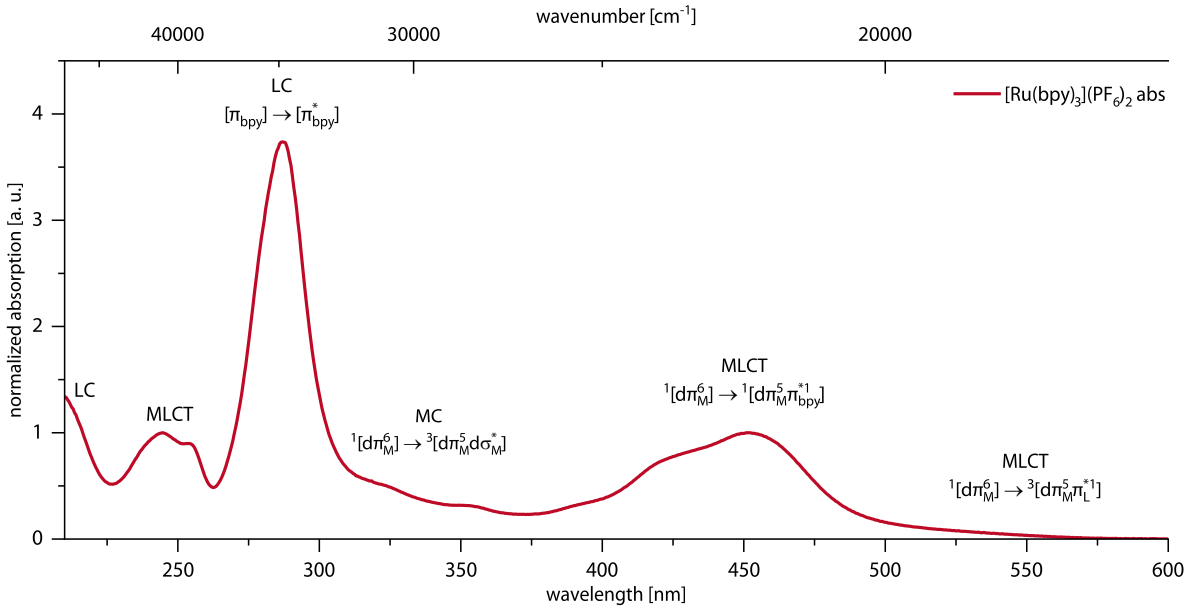

spectrum 1. UV/VIS absorption spectrum of $[Ru(bpy)_3]^{2+}$ (**7**) in MeCN at room temperature and assigned MLCT, LC and MC transitions.[17-23]

The visible light MLCT transition is primarily responsible for the unique photoredox properties. The deactivation pathways of the initially formed ^{1}MLCT state are shown in the Jablonski diagram (**scheme 2**). The absorption of light in the range of the visible light absorption maximum (452 nm) leads to the spin-allowed formation of a vibrationally excited ^{1}MLCT state, which after vibrational relaxation (vr) undergoes inter-system crossing (ISC) within about 100 fs with an efficiency close to unity due to spin-orbit coupling.[17-22] The vibrationally excited ^{3}MLCT state relaxes within about 20 ps to the lowest-energy ^{3}MLCT state.[22]

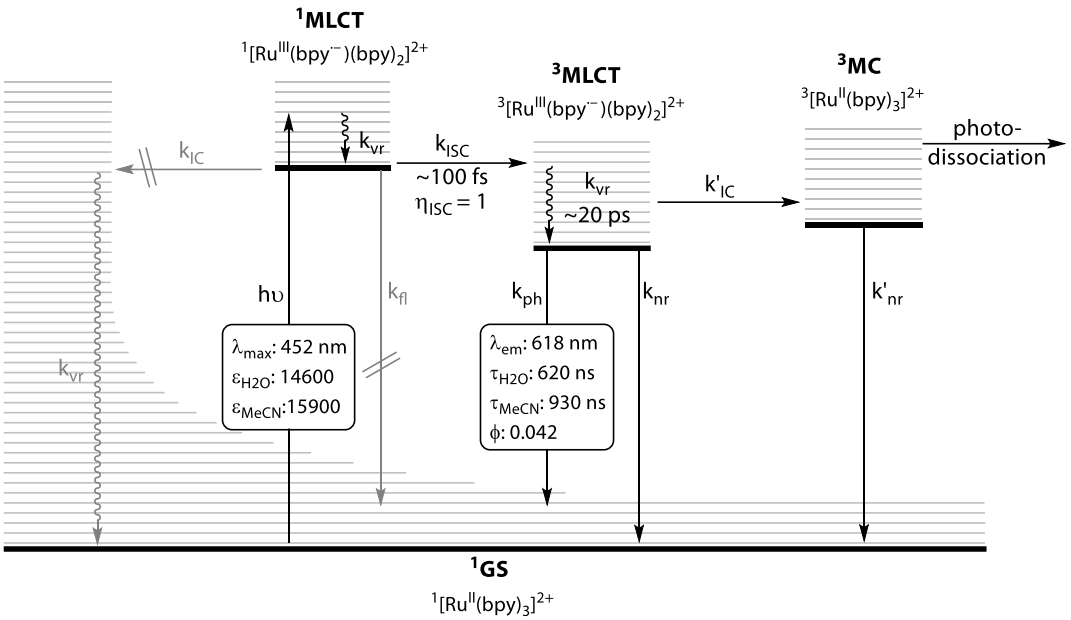

scheme 2. Jablonski-diagram showing the parameters and kinetics of ¹MLCT excitation and intramolecular decay pathways.[17-22]

Since the MLCT involves the transfer of an electron from the metal-centred HOMO to the ligand-centred LUMO, the excitation formally represents a simultaneous oxidation of the metal centre and reduction of a bipyridine ligand.[17-22, 32, 33] Considering the Franck-Condon principle of electronic excitation inside an unchanged molecular geometry, the ground state symmetry (D_3) should be maintained during initial excitation, resulting in delocalization of the negative charge across the three chelating ligands carrying 1/3 of the negative charge each ($[Ru^{III}(bpy^{1/3\cdot-})_3]^{2+}$).[34-36] A charge delocalization in a multichelate system does indeed occur within the first tens of femtoseconds, especially in non-relaxed MLCT states.[21] Also regarding the localization of the excited electron in the lowest energy ³MLCT, a long-term controversy persisted over the concepts of randomization of the excited electrons location across all ligands by fast interligand hopping versus its localization on one ligand, which was finally resolved in favour of the widely accepted concept of localized MLCT states ($[Ru^{III}(bpy^{-})(bpy)_2]^{2+}$) showing reduced C_2 symmetry with the help of a variety of photophysical measurements of ground and excited states, including low-temperature cyclic voltammetry and time-resolved spectroscopy methods (chapter 1.1.4).[37-46]

The MLCT state may return to the ground state *via* three deactivation pathways as shown in the Jablonski-diagram (**scheme 2**): Besides spin-forbidden phosphorescence (ph), non-radiative decay (nr) by heat dissipation or internal conversion (IC) of the excited electron to form a ³MC state can occur. Since the formation of the ³MC is associated with the occupation of an antibonding orbital regarding the metal-ligand bond (σ_M^*), the formation of this state is accompanied by a significant Ru-N bond elongation, i.e. geometry change which is better indicated by the relative position of Morse potential curves (**scheme 3**).[19-21, 28-31]

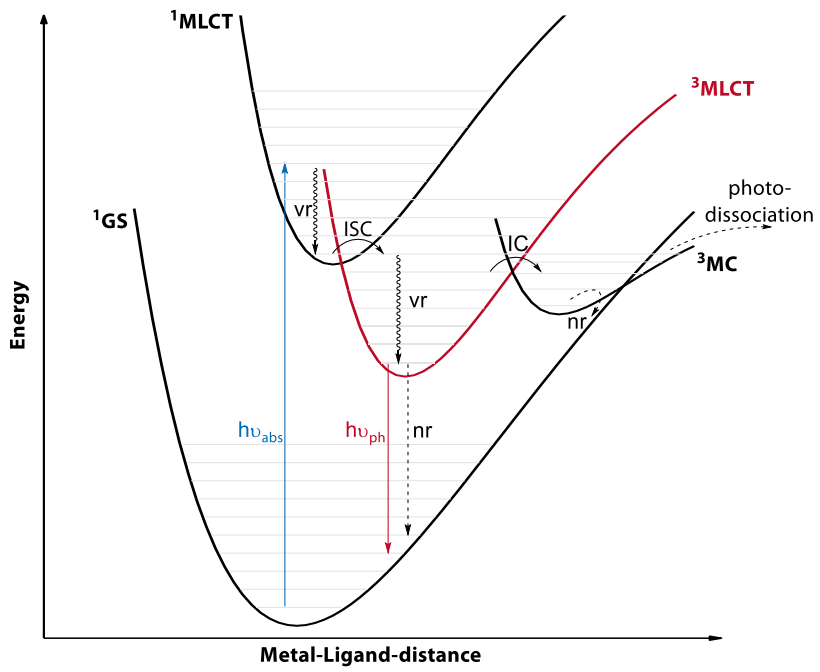

scheme 3. Morse-potentials showing the relative geometry changes of the different states and deactivation pathways thereof.[19-21, 28-31]

The ^{3}MC state undergoes either rapid non-radiative deactivation to the ground state or ligand loss, hence its lifetime is very short and no luminescence is observable. In contrast, the ^{3}MLCT state is not strongly displaced compared to the ground state and does not participate in efficient non-radiative decay.[19-21, 28-31] It exhibits luminescence and a remarkably long lifetime, dependant on several factors such as oxygen concentration, solvent and temperature, varying between 500 – 1000 ns (in H_2O, 620 ns; in MeCN, 930 ± 40 ns, both at 298 K).[17] This is sufficiently long to encounter a suitable reaction partner and release the energy contained in the ^{3}MLCT state through energy- or electron transfer reactions in order to return to the ground state.[17, 18]

The comparison of the deactivation pathways of ^{3}MLCT and ^{3}MC state exemplifies the dependency of the photophysical properties of a metal complex on the energetic order of the involved molecular orbitals and thus on the ligand field strength, i.e. the redox properties of the metal and the electronic properties of the ligand. In the case of $[Ru(bpy)_3]^{2+}$ (**7**) it is the interplay of the orbital- and redox properties of Ru(II) with the σ-donor and π-acceptor qualities of the bipyridine ligands that ultimately dictates the MLCT as the lowest energy transition and state, and leads to its longevity and resulting tendency towards alternative intermolecular deactivation pathways. The understanding of the underlying interplay between metal and ligand properties has provided several levers of rational catalyst design and a broad library of photocatalysts (chapter 1.1.3).

The energy of the ^{3}MLCT state remaining in excited $[Ru(bpy)_3]^{2+}$ (**7**) after absorption, ISC and relaxation is the available driving force for the initiation of photoredox transformations.[19]

1.1.2 Quenching of the ^{3}MLCT: Energy transfer and electron transfer

Excitation by visible light irradiation, intersystem crossing and relaxation results in a lowest energy ^{3}MLCT whose intramolecular deactivation pathways are slow and consequently its lifetime sufficiently long to enable it to encounter a suitable reaction partner and release the excess energy in intermolecular quenching pathways, i.e. energy transfer or electron transfer (oxidation or reduction), in order to return to the ground state (**scheme 4**).[17-22, 47, 48]

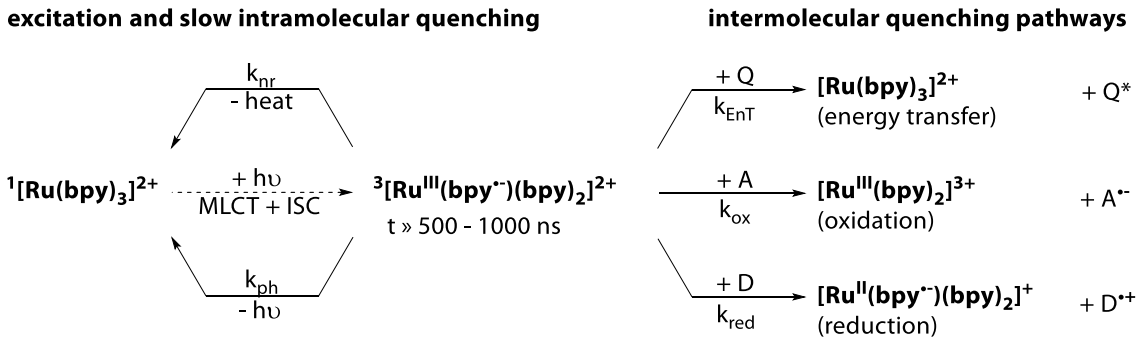

scheme 4. Comparison of slow intramolecular decay of the ^{3}MLCT-state and alternative intermolecular deactivation pathways.[17-22]

In the deactivation of the excited state by energy transfer, the excess energy is transferred to a suitable acceptor, which in turn enters an excited state.[18, 21, 49, 50] This could possibly proceed according to a trivial mechanism involving radiative energy release of the excited donor and subsequent absorption by the acceptor, however, the concept of energy transfer refers to non-radiative energy transfer processes.[18] Although the result of the energy transfer is always the deactivated donor and the excited acceptor, two energy transfer mechanisms are distinguished the physical origin of which is entirely different and the associated requirements, distance dependencies and occurrences are distinct (**scheme 5**).[18, 21, 49, 50]

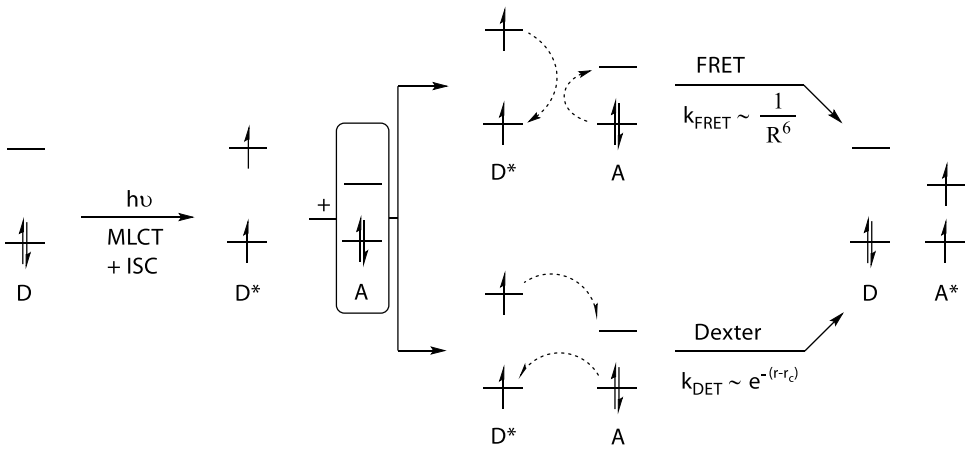

scheme 5. Comparison of intermolecular MLCT quenching by energy transfer following the FRET or the Dexter mechanism.[18, 21, 49, 50]

Förster resonance energy transfer (FRET) is a non-radiative process involving the coupling of the transition dipole moments of the donor and acceptor.[18, 21, 50] The dipolar nature of the mechanism allows energy transfer without orbital overlap, i.e. over long distances, making the process also known as a "through space" mechanism. For a

FRET process to proceed, spectral overlap of the emission band of the donor and the absorption band of the acceptor is required (**figure 2**).[18, 21, 50]

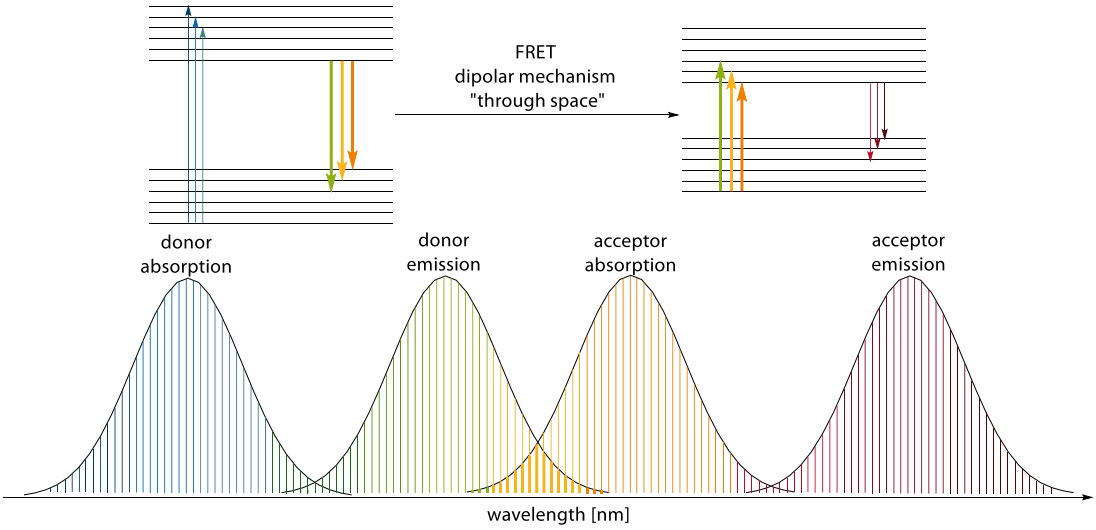

figure 2. FRET requirement of spectral overlap of donor emission and acceptor absorption shown in a simplified Jablonski-type diagram and in a representation of the absorption and emission bands of donor and acceptor.[18, 21, 50]

Since the organic substrates of photoredox processes usually do not absorb in the visible range, energy transfer processes following the dipolar FRET mechanism usually play a minor role.[18] Of greater importance is the Dexter energy transfer (DET), whose mechanism can be regarded as a combination of two simultaneous electron transfers. Such a process requires an orbital overlap, for which reason it is also referred to as a "through bond" process. This requirement leads to a much shorter distance within this process can take place efficiently.[18, 21, 49] While the rate constant of the dipolar FRET process is proportional to the inverse of the sixth power of the donor-acceptor distance and the mechanism is efficient in the range of longer distances of 10 – 100 Å, the rate constant of the DET process decreases exponentially and the process dominates at shorter distances < 10 Å.[21] Since molecular oxygen quenches the excited states of $[Ru(bpy)_3]^{2+}$ (**7**) and its analogues by Dexter energy transfer, physical measurements and chemical reactions are usually carried out under inert conditions using deoxygenated solvents unless oxygen is intended to be a reactant.[18, 51, 52]

Although there are some examples of photoredox transformations based on energy transfer, exploiting the unique redox properties of the charge separated excited states, which are both stronger oxidants and reductants compared to their corresponding ground states, dominates the field of photoredox catalysis.[18, 20, 21] In contrast to the Dexter process, the electron transfers take place one after the other, giving rise to two conceivable electron transfer quenching cycles that mainly differ in the order of steps. In both cases, the release of the excited electron from the reduced ligand ($\pi_{bpy}^{\star}$) as well as the receiving of an electron into the single-occupied metal-centred π_M orbital occurs. In the oxidative quenching cycle the excited state first acts as a reducing agent and transfers the excited electron to a suitable acceptor molecule. The resulting oxidized photocatalyst $[Ru^{III}(bpy)_3]^{3+}$ (**10**) still has one unpaired metal-centred electron and therefore readily accepts an electron from a donor molecule to turn over the photocatalytic cycle and regenerate the ground state.[18, 20, 21] In the reductive quenching cycle the order of redox

events is switched and the excited state first accepts an electron from a donor molecule into the metal-centred π_M-orbital before the unpaired excited electron is transferred from the π_{bpy}^*-orbital of the reduced ligand $[Ru^{II}(bpy^{\cdot-})(bpy)_2]^+$ (**11**) to an acceptor molecule in the second step (**scheme 6**). Which of these quenching cycles occurs depends on the available reaction partners and their respective redox potentials.[18-22]

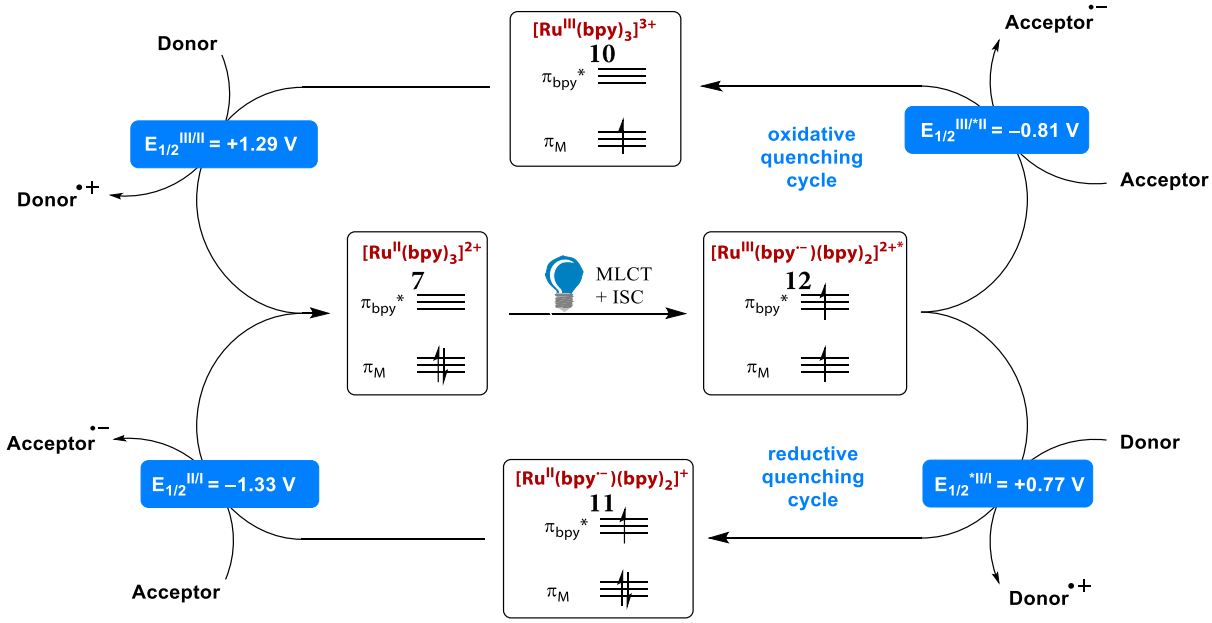

scheme 6. Comparison of oxidative and reductive photocatalytic quenching cycles.[18-22]

Since both quenching cycles contain two electron transfer events each, there arise three possible general types of transformations based on electron transfer (**scheme 7**).[3-6] In net oxidative reactions, a stoichiometric electron acceptor (oxidant) is added to the reaction mixture, which either serves to oxidatively quench the excited photocatalyst, forming $[Ru(bpy)_3]^{3+}$ (**10**) which is itself highly oxidizing, or to turnover the catalytic cycle, involving reductive quenching of the excited photocatalyst by the substrate.[3-6] Similarly, in net reductive reactions, a stoichiometric electron donor (reductant) is added, which either serves as a reductive quencher to generate the strongly reducing $[Ru^{II}(bpy^{\cdot-})(bpy)_2]^+$ (**11**) or to complete the oxidative quenching cycle by reducing $[Ru^{II}(bpy^{\cdot-})(bpy)_2]^+$ (**11**) resulting from the oxidation of the excited catalyst by the substrate.[3-6] Furthermore, a carefully designed interplay of the redox potentials of all involved intermediates enables redox neutral conversions which do not require a stoichiometric additive to complete the quenching cycles, but exploits the unique property of photoredox catalysis of forming oxidants and reductants at different stages of the reaction.[3-6] A prominent example of a net redox neutral photoredox transformation is Stephenson's atom transfer radical addition (ATRA) following the oxidative quenching cycle.[53] In this process, the excited photocatalyst **12** reduces an activated carbon-halogen bond, leading to the heterolytic cleavage of a halide to form an alkyl radical **20** and the oxidized photocatalyst **10**. After addition of the alkyl radical **20** to an alkene **21**, the resulting radical **22** is oxidized by $[Ru(bpy)_3]^{3+}$ (**10**) to a carbocation **18**, whereby the photocatalytic cycle is completed. The product **19** is then formed by nucleophilic trapping with the halide that was split off initially.[53]

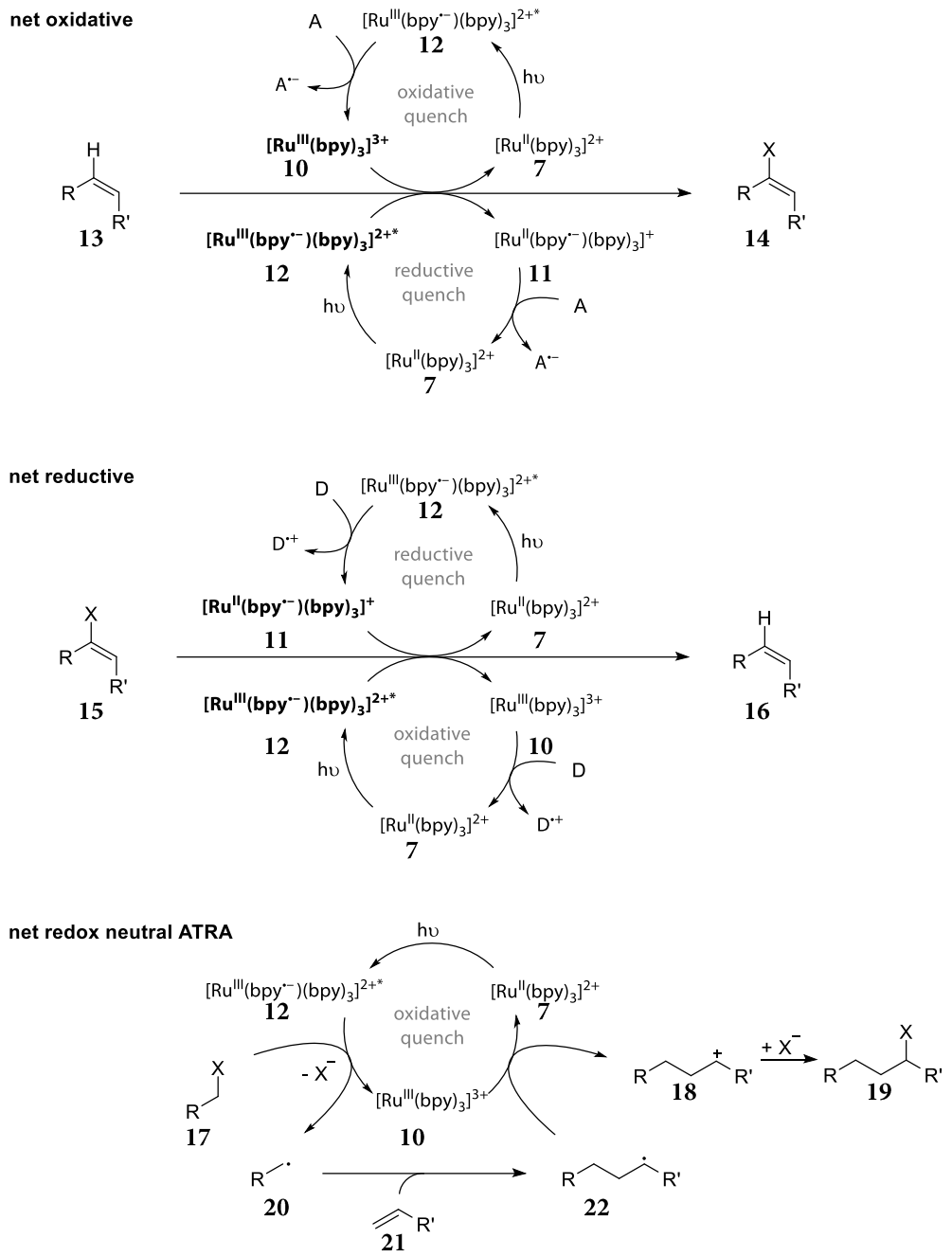

scheme 7. Comparison of net oxidizing, net reducing and net redox neutral photoredox transformations.[3-6, 53]

Net redox neutral photoredox reactions can also be achieved by combining the photoredox reactivity with catalytic amounts of another reversibly oxidizable or reducible additive. Since redox neutral photoredox systems do not require stoichiometric oxidants or reducing agents, they are particularly atom economic.[4]

The redox properties of a multitude of common organic chemicals have been analyzed by cyclic voltammetry.[54] In addition to these additives, several powerful tools for modifying the photophysical and electrochemical properties of photoredox catalysts and a broad library of photocatalysts have emerged allowing rational catalyst design for the development and optimization of new photoredox systems.[55, 56]

1.1.3 Redox properties of $[Ru(bpy)_3]^{2+}$ (**7**) and principles of rational modification of redox potentials

An electrochemical examination of $[Ru(bpy)_3]^{2+}$ (**7**) by cyclic voltammetry indicates multiple reversible redox events: One metal-centred oxidation and three peaks representing the stepwise reduction of the three bipyridine ligands (**figure 3**).[18, 20, 55] Furthermore, a peak of the internal standard ferrocene (Fc^+/Fc, bottom scale) is visible, which allows a conversion to other reference systems, like the standard calomel electrode (SCE, top scale).[57, 58] Starting at 0 V vs. SCE and following the IUPAC convention of a positively scanned potential, shows an oxidation peak at +0.38 V (vs. SCE) resulting from the oxidation of the internal standard ferrocene (Fc) to the ferrocenium cation (Fc^+).[57] A further increase of the potential to +1.27 V (vs. SCE) leads to the metal-centred oxidation of $[Ru^{II}(bpy)_3]^{2+}$ (**7**) to $[Ru^{III}(bpy)_3]^{3+}$ (**10**). After reversing the scan direction, the reductive sweep first reveals the corresponding (back-) reductions of the metal centre ($Ru^{III} \rightarrow Ru^{II}$), as well as of the internal standard ($Fc^+ \rightarrow Fc$). Further lowering of the potential results in three successive reductions at −1.35 V, −1.54 V and −1.78 V (vs. SCE), which can be assigned to the stepwise reduction of the three bipyridine ligands. After reversing the scan direction again and performing a positive potential scan, the corresponding (re-)oxidations of the reduced ligands to their neutral form are recognizable.[18, 20, 55]

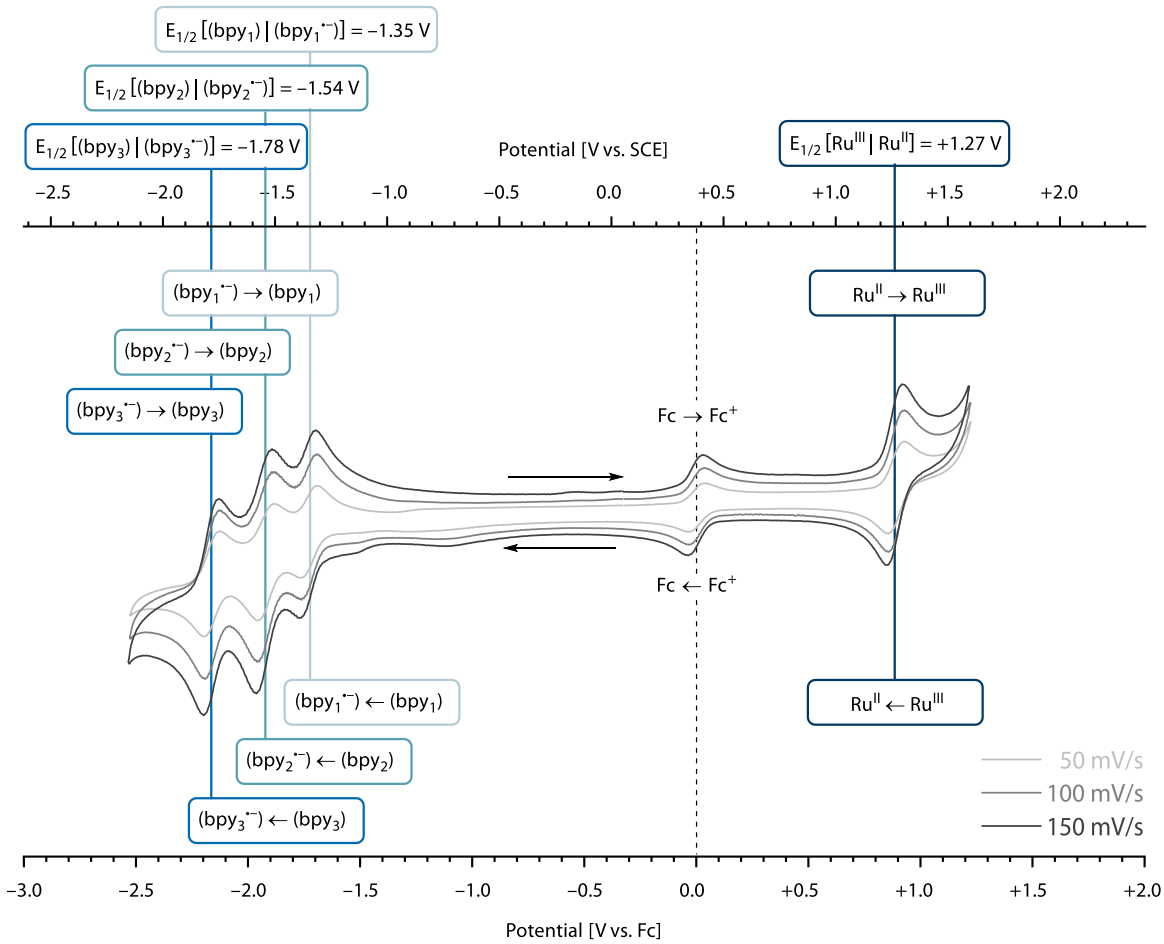

figure 3. Cyclic voltammogram of $[Ru(bpy)_3]^{2+}$ (**7**) measured at room temperature in MeCN with 0.25 M $TBAPF_6$ as supporting electrolyte at different scan rates (50 – 150 mV/s) using a glassy carbon working electrode, AgCl/Ag reference electrode and a Pt-disc counter electrode, referenced to the internal standard ferrocene (Fc^+/Fc, bottom scale) and to the standard-calomel-electrode (SCE, top scale).

The redox potentials of the metal-centred oxidation and the first ligand reduction are of particular importance for an understanding of the redox reactivity of $[Ru^{II}(bpy)_3]^{2+}$ (**7**) and analogues, given that the associated one-electron reduced or oxidized redox species dominate the reactivity. Furthermore, the orbitals involved in these redox processes are the same orbitals involved in the spectroscopic processes, hence an investigation of the electrochemical behaviour provides information about the MLCT excitation and vice versa.[32, 59-63] The MLCT-transition formally represents a simultaneous oxidation of the metal centre and a reduction of the ligands, leading to a separation of charges within the complex.[22, 32, 48] This process affects both the ionization potential (IP) and the electron affinity (EA) significantly. While the excited complex has a lower ionization potential and therefore releases its unpaired electron from the π_{bpy}^* orbital more readily, the electron hole remaining in the metal-centred π_M orbital is accompanied by an increase in electron affinity.[19, 64] As a result, the oxidized metal centre is a stronger oxidant and the reduced ligand is a stronger reductant than the ground state (**scheme 8**).[19, 64]

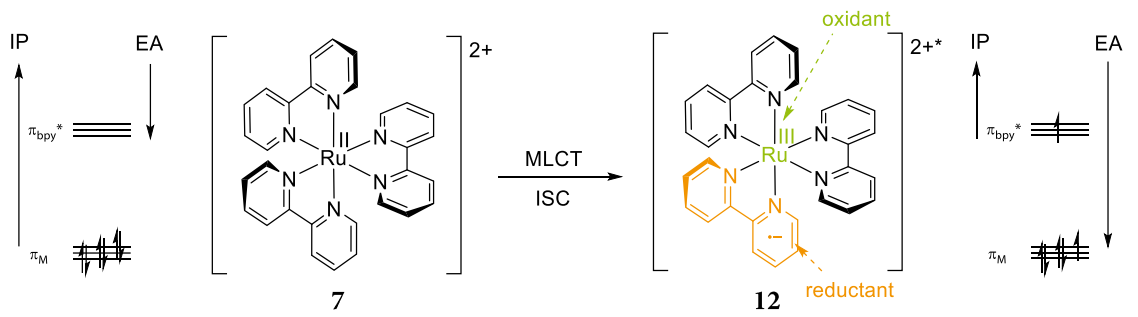

scheme 8. Excitation of $[Ru(bpy)_3]^{2+}$ (**7**) and metal to ligand charge transfer (MLCT).[19, 48, 64]

The corresponding redox potentials of the excited state reflect the excess energy resulting from the excitation with light and from the intramolecular charge separation.[17, 19, 22, 47, 48] The experimental determination is possible by electron transfer quenching experiments against quenchers of known potentials or by phase-modulated cyclic voltammetry.[65, 66] More commonly, however, these potentials are approximated from the ground state potentials. The underlying equations are based on Hess' Law following the thermodynamic cycles shown in **scheme 9**.[20, 32, 67] The redox potentials of the excited state are accordingly obtained by the addition or subtraction of the Gibbs free energy available in the ^{3}MLCT to or from the corresponding ground state potentials, which are readily accessible by cyclic voltammetry.[20, 32, 67]

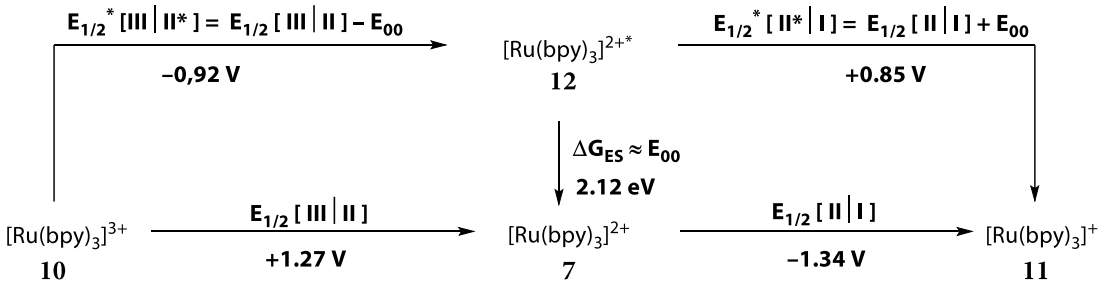

scheme 9. Thermodynamic cycle for the determination of the excited state redox potentials from ground state potentials and the excited state free energy.[20, 32, 67]

Since the determination of ΔG_{ES} is not trivial, it is instead approximated using the energy difference between the thermally equilibrated ^{3}MLCT and the zero vibrational level of the ground state, thereby neglecting the entropy change during excitation.[17, 19, 32, 33, 55, 56, 65, 68] This approximation can be justified by the small Stokes shift, indicating a similar shape, size and solvation, hence a similar entropy of the ground and excited state.[23, 47, 65, 69] The determination of E_{00} is possible by low-temperature spectroscopy and Franck-Condon-fit, as the direct $v = 0 \rightarrow v' = 0$ transition is resolved under these conditions.[17, 70] However, E_{00} is usually not determined but rather approximated from the energy of the emission maximum (E_{em}), thereby systematically neglecting the vertical nature of the transition. Instead, phosphorescence is assumed to represent an adiabatic transition to the relaxed ground state, although it leads to a vibrationally excited ground state the excess energy of which (λ_{GS}) is commonly neglected in this approach (**scheme 10**).[48, 56, 68, 70]

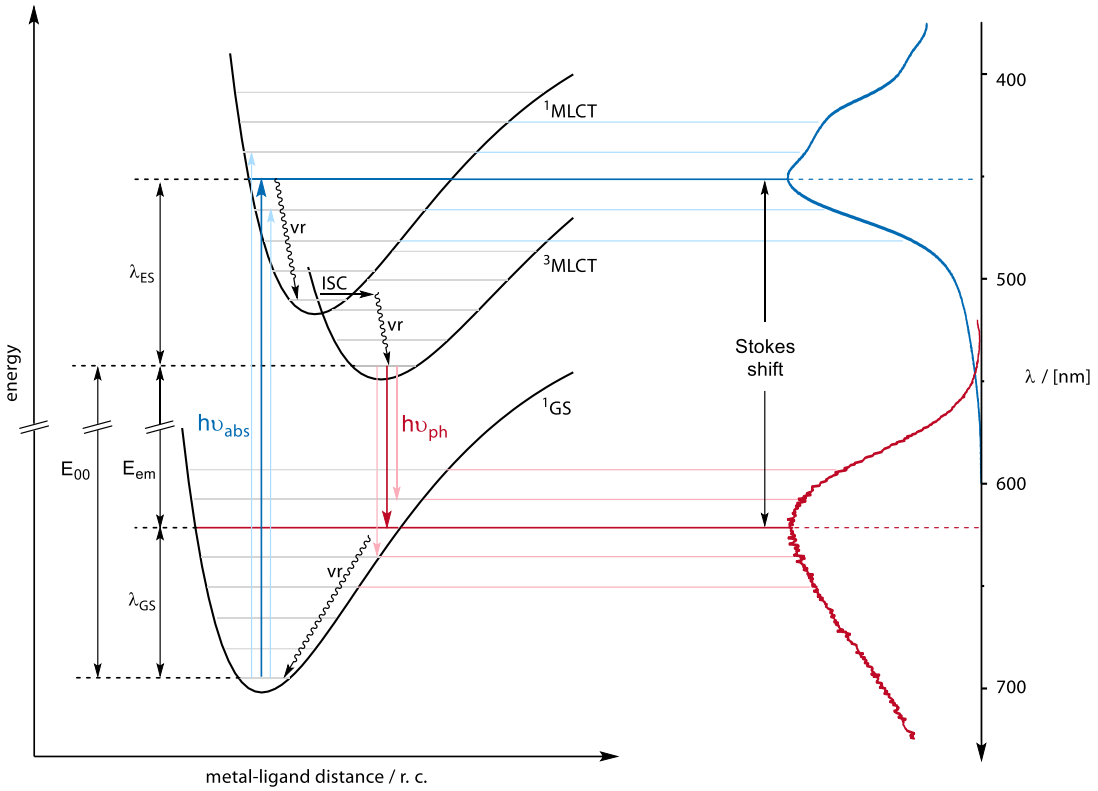

scheme 10. ^{1}MLCT excitation and radiative ^{3}MLCT deactivation in Morse potentials and relation to absorption and emission bands, as well as Stokes shift, including a comparison of the respective energy values for exact and approximate calculation of excited state redox potentials.[17]

The widely used approximations for the determination of the Gibbs free energy of the ^{3}MLCT state neglect both the entropy changes by approximating E_{00} as ΔG_{ES} as well as the vibrational energy (λ_{GS}) remaining in the ground state after phosphorescence by approximating E_{em} as E_{00} and therefore rather provide lower-limit values.[68] Given that the excitation is accompanied by simultaneous oxidation of the metal centre and reduction of a ligand, there are two parameters for rationally modifying the properties of photoredox catalysts based on an understanding of the underlying orbital interactions and photophysical processes following visible light excitation.[22, 32, 48] This becomes evident when examining the reduction potentials of structurally related oxidatively quenched catalyst complexes (**figure 4**): The exchange of a bipyridine ligand for two anionic pyrazolo ligands (pz) with strong

σ-donor properties leads to a stabilization of the Ru(III) centre and a significantly lowered reduction potential ($E_{1/2}$ $[[Ru^{III}(bpy)_2(pz)_2]^+|[Ru^{II}(bpy)_2(pz)_2]]$ = 0.30 V) compared to the reduction potential of prototypical $[Ru(bpy)_3]^{2+}$ (**7**) ($E_{1/2}$ $[[Ru^{III}(bpy)_3]^{3+}|[Ru^{II}(bpy)_3]^{2+}$ = 1.26 V). In contrast, the positive charge in the bipyrazine (bpz) derivative is less stabilized due to the electronegative heteroatoms and associated lowered π_{bpz}^* accepting orbitals, resulting in a greatly increased tendency to accept electrons ($E_{1/2}$ $[Ru^{III}(bpz)_3]^{3+}|[Ru^{II}(bpy)_3]^{2+}$ = 1.86 V).[48, 60-63, 68]

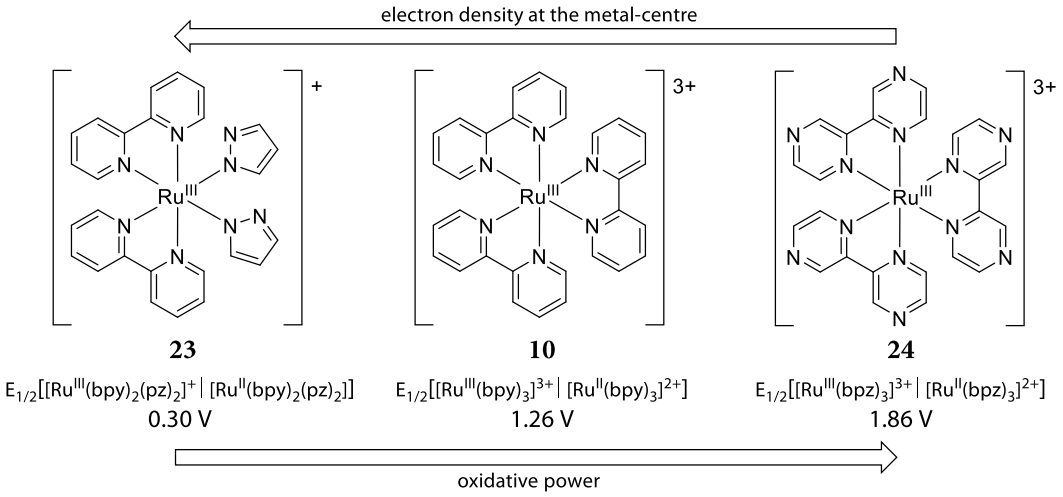

figure 4. Influence of substituents on reduction potentials of structurally related oxidatively quenched ruthenium complexes **23**, **10** and **24**.[48]

Similarly, the reduction potential of reductively quenched catalyst complexes is dependent on the electron density within the ligands (**figure 5**). The incorporation of inductively electron-donating methyl substituents increases the electron density in the ligands and raises the corresponding ligand-centred orbitals, which translates into a lowered reduction potential ($E_{1/2}$ $[Ru^{II}(dmb)_3]^{2+}|[Ru^{II}(dmb^{\cdot-})(dmb)_2]^+$ = −1.45 V) compared to $[Ru(bpy)_3]^{2+}$ (**7**) ($E_{1/2}$ $[Ru^{II}(bpy)_3]^{2+}|[Ru^{II}(bpy^{\cdot-})(bpy)_2]^+$ = −1.35 V).[48] In contrast, the incorporation of strongly electron-withdraw-

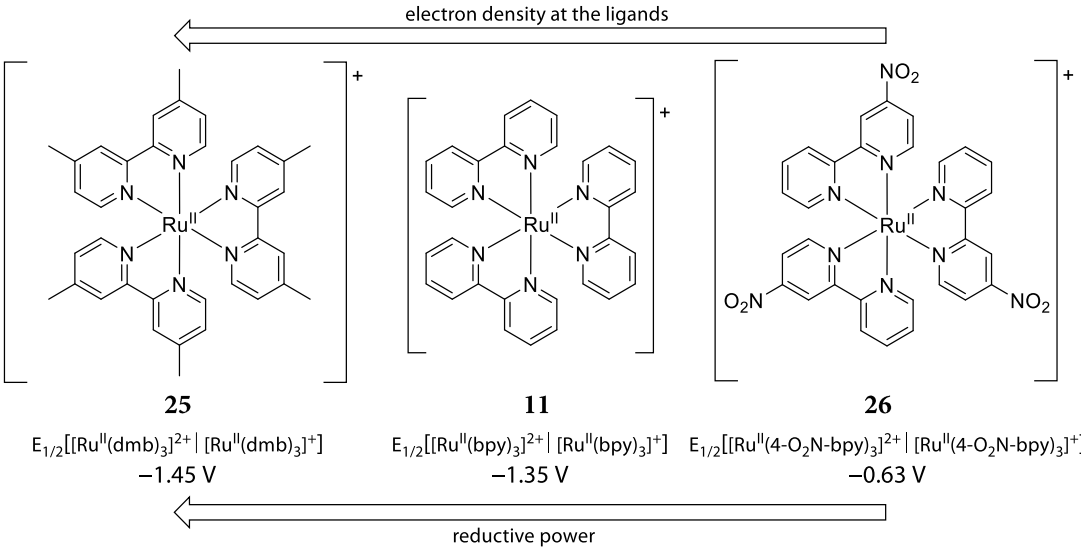

figure 5. Influence of substituents on reduction potential of structurally related reductively quenched ruthenium complexes **25**, **11** and **26**.[48]

ing nitro groups lowers the corresponding ligand orbital energies and leads to a reduced tendency to release electrons ($E_{1/2}$ $[Ru^{II}(4\text{-}O_2N\text{-}bpy)_3]^{2+}|[Ru^{II}(4\text{-}O_2N\text{-}bpy^{-})(bpy)_2]^{+}$ = −0.63 V).[48, 60-63, 68] The properties of the catalysts can also be adjusted by the choice of the central metal. The ligand field splitting depends on the metal, as it increases with the spatial extension of the d-orbitals and therefore with the period.[24, 30, 71] As a result, the energetic order of orbitals and therefore the nature of the lowest energy transitions can vary.[30, 72, 73] A comparison of the photophysical properties of complexes of Ru(II) ($4d^6$) with lighter Fe(II) ($3d^6$) and the heavier Os(II) ($5d^6$) and Ir(III) ($5d^6$) respectively illustrates this: In the case of Fe(II), the splitting in the octahedral ligand field is so small that the lowest excited state is metal-centred (MC) and not emissive. In contrast, the large splitting of the third-row transition metals exhibiting a $5d^6$ configuration is accompanied by an energetic elevation of the MC-states to such an extent that their non-radiative decay has no influence on the emission properties. In Ru(II) $4d^6$ complexes, the ligand field splitting falls between $3d^6$ (Fe(II)) and $5d^6$ (Os(II) & Ir(III)), rendering the ^{3}MC states thermally accessible from the ^{3}MLCT.[30, 72, 73] According to the energy gap law, the rate of non-radiative deactivation of excited triplet states decreases exponentially with their energy content.[22, 36, 70, 74] With a ^{3}MLCT energy content of Os(II) analogues of 1.6 eV, they consequently tend to undergo rapid non-radiative decay, therefore exhibiting low phosphorescence quantum yield ($\Phi < 0.1$) and lacking the long lifetimes required for intermolecular deactivation pathways.[72] In contrast, the ^{3}MLCT energy content of Ir(III) derivatives (2.1 - 3.0 eV) is even higher than that of $[Ru(bpy)_3]^{2+}$ (**7**) (2.1 eV), and therefore the energy is not affected by the energy gap law and is available for photoredox transformations.[72] Indeed, besides Ru(II)-based photoredox catalysts, mainly Ir(III) complexes are used extensively.

The charge of the metal ions also has an influence on the photophysical and electrochemical properties.[55, 72, 75] Direct comparison of potentials reveals that the triple charge in $[Ir^{III}(bpy)_3]^{3+}$ leads to facilitated ligand reduction ($E_{1/2}[[Ir^{III}(bpy)_3]^{3+}|[Ir^{III}(bpy^{-})(bpy)_2]^{2+}]$ = −1.1 V) compared to the double charged $[Ru(bpy)_3]^{2+}$ (**7**) ($E_{1/2}[[Ru^{II}(bpy)_3]^{2+}|[Ru^{II}(bpy^{-})(bpy)_2]^{+}]$ = −1.35 V), while the metal-centred oxidation is significantly hampered ($E_{1/2}[[Ir^{IV}(bpy)_3]^{4+}|[Ir^{III}(bpy)_3]^{3+}]$ = +2.1 V), compared to the oxidation of the ruthenium complex ($E_{1/2}[[Ru^{III}(bpy)_3]^{3+}|[Ru^{II}(bpy)_3]^{2+}]$ = +1.29 V). A more common ligand in Ir(III)-based photocatalysts is phenylpyridine (ppy), whose monoanionic phenyl fragment is available as a strong σ-donor and significantly facilitates metal-centred oxidation ($E_{1/2}[[Ir^{IV}(ppy)_3]^{+}|[Ir^{III}(ppy)_3]]$ = +0.77 V) (stronger reducing agent), while the ligand-centred reduction is hindered ($E_{1/2}[[Ir^{III}(ppy)_3]|[Ir^{III}(ppy^{-})(ppy)_2]^{-}]$ = −2.19 V).[55, 72, 75]

With the interest in photoredox transformations growing rapidly in recent years, the aforementioned principles of rational catalyst design have provided an extensive library of Ru(II)- and Ir(III)-based photoredox catalysts with varying electronic properties allowing the selection of the ideal catalyst for the intended transformation (**figure 6**).[55, 75] In addition, the field of metal-free organophotoredox catalysis has emerged, the underlying principles of which will however not be discussed here.[1, 15]

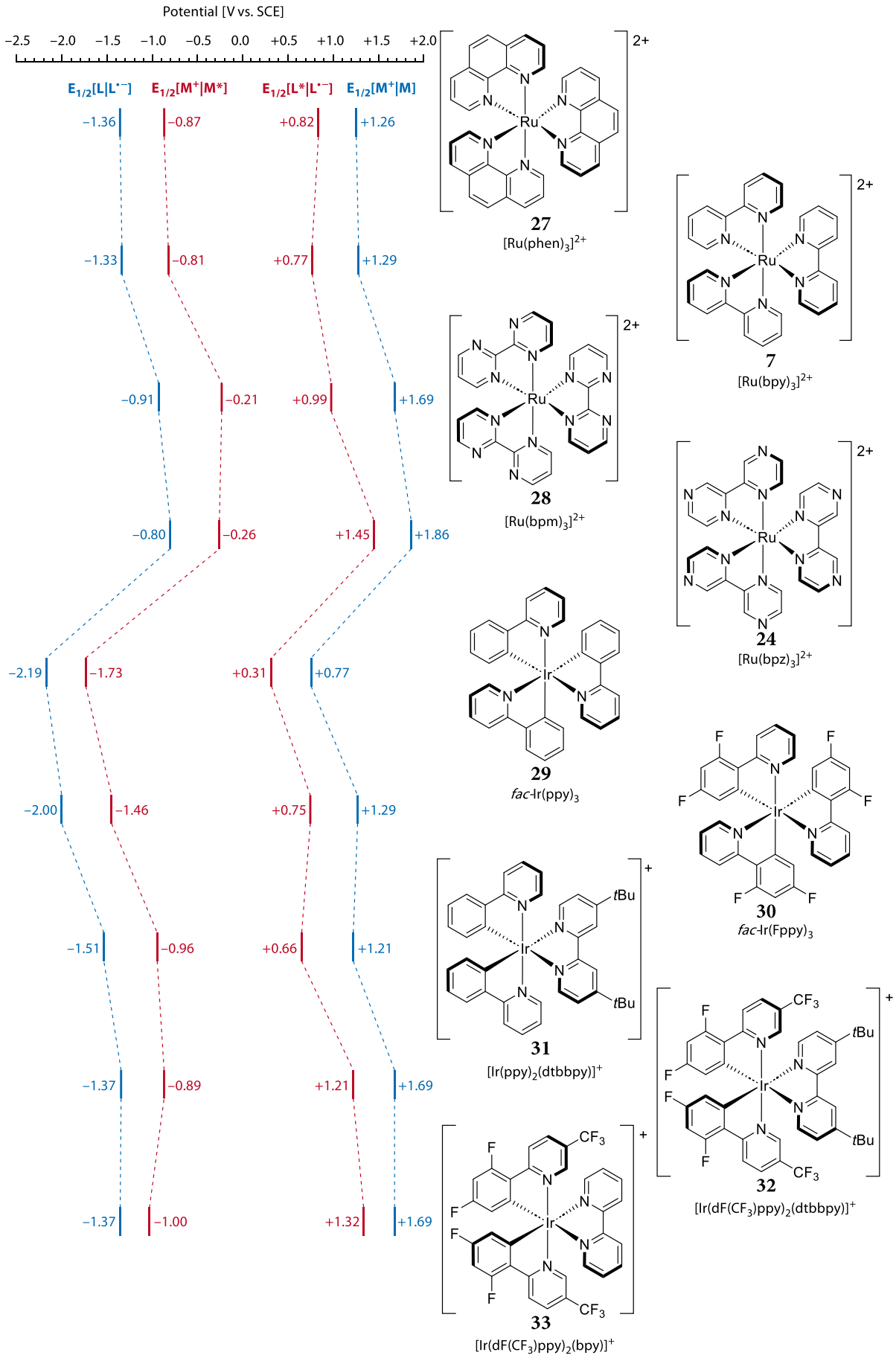

figure 6. Overview of common Ru(II)- and Ir(III)-photoredox catalysts and their ground state (blue) and excited state (red) redox potentials.[55, 75]

1.1.4 Localization of ^{3}MLCT states in $[Ru(bpy)_3]^{2+}$ (**7**) and in heteroleptic complexes

A closer look at the spatial orientation of involved orbitals in the lowest energy ^{3}MLCT state reveals a more complex picture of the electronic structure (**figure 7**). As an electron is transferred from the metal-centred HOMO to a ligand-centred π_{bpy}^*-orbital, an electron-hole remains on the metal that preferably enters an arrangement in which the electrostatic interaction with the excited electron is maximized.[22, 34, 35] As shown in **figure 7**, a lowest energy ^{3}MLCT state containing the excited electron localized on ligand a results in a preferred arrangement of the electron hole remaining on the metal in alignment with the reduced ligand and consequently in the d_{xy}-orbital.[22, 34, 35]

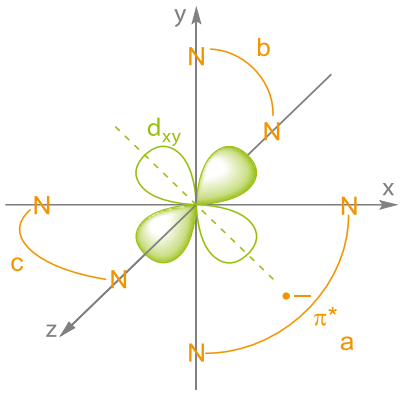

figure 7. Preferred spatial orientation of the excited electron in ligand a in arrangement with the electron hole remaining in the d_{xy}-orbital in the lowest-energy ^{3}MLCT.[22, 34]

With the excited electron at this bipyridine ligand, two additional higher-energy ^{3}MLCT states are conceivable wherein the electron hole is averted from the acceptor ligand, hence in d_{xz} and d_{yz} orbitals, respectively.[22, 34] Since each of the three bipyridine ligands can act as an acceptor, a total of three degenerate lowest energy triplet ^{3}MLCT excited states and two sets of two additional higher energy MLCT states per bipyridine ligand (nine MLCT states in total) are possible.[22, 34]

A completely different picture of the electronic structure emerges when examining excited states of heteroleptic complexes, whose lower symmetry can lead to the removal of the degeneracy of lowest energy ^{3}MLCT states.[76, 77] For the ligand reduction associated with the excitation, different ligands with individual π^* orbital energies and reduction potentials are available due to the incorporation of substituents. While electron-donating substituents on the ligand lead to an increase in the orbital energies and thus a decrease in the redox potential, electron-withdrawing residues cause the opposite effect (*vide supra*).[76, 77] Besides rational tuning of the general redox properties of photoredox catalysts, the systematic increase or decrease of the orbital energies of bipyridine ligands can serve to direct the excitation into selected ligand orbitals. In a variety of studies on the influence of substituents on the electrochemical and photophysical properties of heteroleptic complexes of the form $[Ru(X_2bpy)_2(bpy)]^{2+}$, containing substituents X that are more electron-donating than H (on the unsubstituted bpy ligand), correlations of redox potentials of the metal-centred and ligand-centred oxidation and reduction potentials, respectively, with the absorption and emission energies as well as substituent parameters that quantify their electronic properties have revealed some remarkable and consistent observations:[59, 60, 62, 63, 76, 78, 79]

(1) The potential of the first ligand reduction is approximately constant - i.e. regardless of strongly varying electronic properties of substituent X (summed Okamato-Brown parameters $\Sigma\sigma_p^+$: −1.04, *t*Bu; −3.12, OMe; −6.80, NMe_2).[63] This observation suggests the removal of degeneracy of the lowest-energy ^{3}MLCTs in heteroleptic complexes: While the electron rich ligand orbitals are energetically raised, the bipyridine ligand, which is common to all complexes, remains energetically unchanged, is reduced preferably.[20, 62, 63, 79] (2) The potential of the metal-centred oxidation event, on the other hand, varies strongly in response to the electron-donating nature of the substituents and correlates well with electronic substituent parameters.[63] This indicates that the π^* backbonding capabilities decrease with higher electron density in the ligand, which in turn translates into a destabilization of the metal-centred charge and a concomitant increase in the metal-centred orbital energies.[63] (3) The energy of the MLCT transition decreases with an increasing electron-donating nature of the substituents X, confirming the picture of approximately constant LUMO at the unsubstituted bipyridine and electronically elevated metal-centred orbital (HOMO).[59, 60, 62, 63, 76, 78, 7]

These observations can be summarized in the simplified MO diagram for heteroleptic complexes. The exchange of two bipyridine ligands in prototypical $[Ru(bpy)_3]^{2+}$ (**7**) for ligands with substituent of varying electron-donating properties leads to the removal of the degeneracy of lowest energy ^{3}MLCTs, since the π_M^* orbitals of electron-rich ligands are energetically elevated. Similarly, the π^* backbonding properties decrease, which is accompanied by a smaller stabilization of the metal-centred charge and associated elevation of the corresponding π_M orbitals.[59, 60, 62, 63, 76, 78, 7]

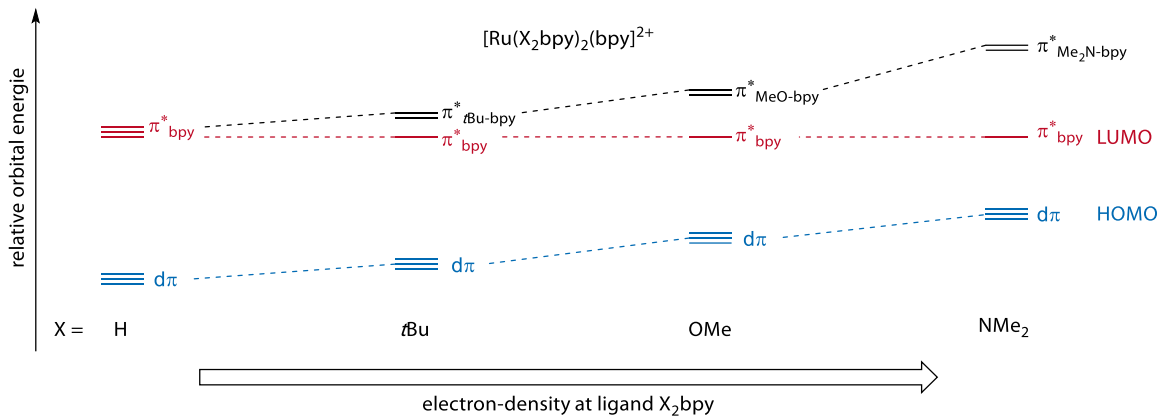

figure 8. Simplified MO diagram for comparing the relative orbital energies in heteroleptic complexes of varying electron density.

The idea of rationally removing the degeneracy in order to direct the MLCT excitation into the most reducible ligand orbital, will later become the basis for the development of heteroleptic photocatalysts (chapters 2 and 3.2.3).

1.2 Principles of asymmetric catalysis

1.2.1 Relevance and evolution of asymmetric catalysis

Most biological processes are asymmetric and their underlying biochemical building blocks are chiral.[80] For example, all proteinogenic amino acids are L-configured and most carbohydrates, e.g. ribose in DNA and RNA, show D-configuration.[81-83] The biological processes have developed over millions of years of evolution resulting in outstanding chemo-, regio- and stereoselectivity.[84] It is therefore not surprising that the interaction of exogenous substances with complex biochemical targets, such as receptors, is also strongly dependent on the three-dimensional molecular structure.[85-87] This was already expressed by Emil Fischer in 1894 in his lock-and-key analogy.[88] Nevertheless, another century was to pass before a rethinking in drug research occurred and it was realized once again that the mechanisms of action and pharmacological properties of enantiomers can differ greatly. While one structure shows the desired effect (eutomer), its enantiomer (distomer) may ideally show a weaker or no effect, but may at worst show entirely different effects.[89]

A prominent example of the devastating consequences of the different modes of action of enantiomers is thalidomide, which was promoted under the name contergan at the end of the 1950s as a non-prescription calmative and sleeping drug for pregnant women.[81, 83, 90, 91] While the (*R*)-enantiomer causes the desired sedative effect, the (*S*)-enantiomer exhibits teratogenic effects as it prevents the formation of blood vessels. As a result, the intake of the active substance, which was sold as a racemate, led to an accumulation of severe malformations in newborns.[81, 83, 90, 91] The thalidomide scandal triggered a change within regulatory requirements for active substances, however, another 20 years passed before the administration of racemic mixtures was generally questioned.[92] At the beginning of the 1980s, the non-active enantiomer was first identified as "isomeric ballast", an avoidable impurity of an exorbitant 50%, which had not been questioned until then.[89] The latter should be avoided when taking medicines to reduce side effects, but also for environmental reasons in the field of pesticides which are distributed in tons.[89] In 1992, the FDA published a policy statement for the development of new stereoisomeric drugs, which favoured the development of single-enantiomer drugs over racemates, but did not force it, followed by the EU in 1994 with a publication on the investigation of chiral active substances.[93, 94] This contributed to the steady increase in percentage of single-enantiomer drugs in synthetic chiral drugs from about 32% in 1985 - 1988 to about 90% in 2001 - 2004 (**figure 9**).[95] The 1990s were dominated by the chiral-switch concept, whereby previously racemic drugs were relaunched as single-enantiomers with the aim of achieving better effects and less complex pharmacodynamic and pharmacokinetic profiles at lower doses.[81, 85, 96] A prominent drug that has been subject to a chiral switch is (±)-ibuprofen, whose (*S*)-enantiomer is mainly responsible for the inhibition of the cyclooxygenase-1 (COX-1) enzyme and thus for the analgesic effect.[97, 98] In contrast to thalidomide, the (*R*)-enantiomer does not show any severe side effects, but undergoes a unidirectional metabolic inversion to the (*S*)-eutomer *in vivo*.[97, 98] The fact that a chiral switch from (±)-ibuprofen to (*S*)-(+)-ibuprofen was nevertheless carried out in 1994 exemplifies that not only the expectation of an accelerated onset of action, but also strategic considerations motivated pharmaceutical companies to perform the chiral switch.[85] Exploiting the extreme case of patentability of a selection invention, that disclosure of a class (racemate) does not constitute disclosure of its mem-

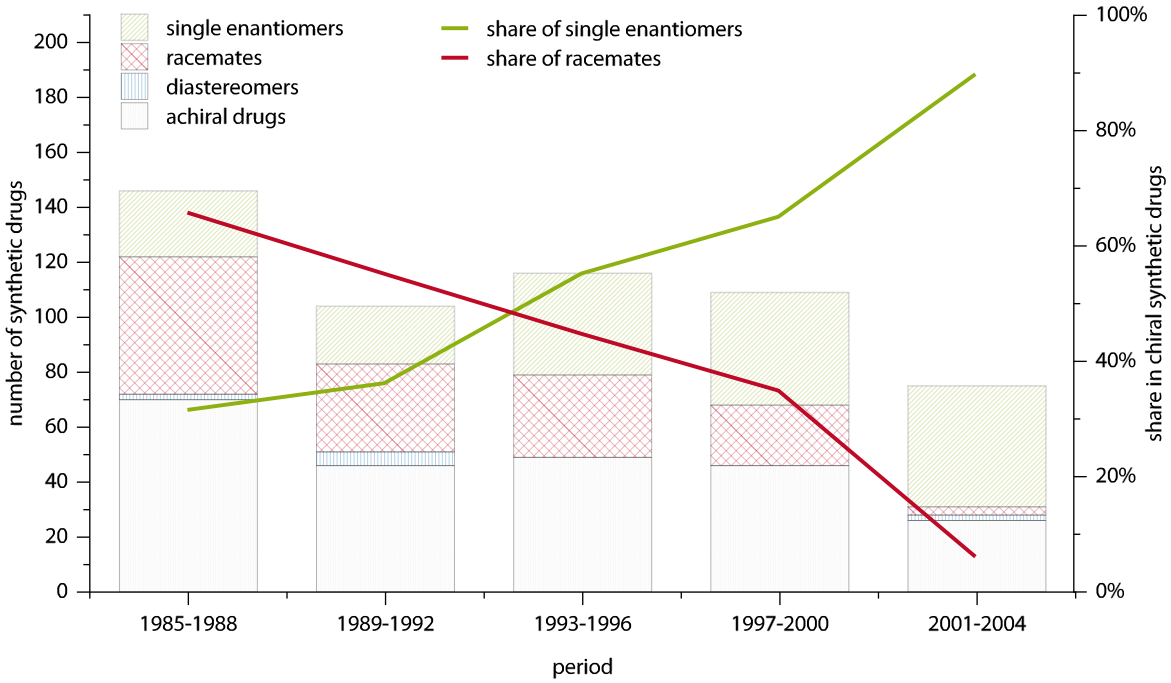

figure 9. Number of synthetic drugs and market shares of single enantiomers and racemates in chiral synthetic drugs in 1985 – 2004.[95]

bers (enantiomers), the chiral switch strategy can serve to extend intellectual property rights (such as patents), if the pharmacological properties of the enantiomers are sufficiently different from each other and from the racemate.[85] In this way, another three years of exclusive marketing of (*S*)-(+)-ibuprofen on the US market were effected.[85] Whatever the motivation behind the steadily growing demand for stereochemically defined substances is, it has been accompanied by the development of a variety of methods for the generation of single-enantiomers (chapters 1.2.2-1.2.4).

The most obvious approach to chiral compounds is the isolation of enantiopure substances from nature, namely from the chiral pool.[99] However, this very convenient and widespread approach has two limitations: Homochirality of biomolecules only allows the isolation of a certain configuration, moreover, the structural diversity is limited and potentially no natural structural motif may be suitable for the intended synthesis.[99] Therefore, a variety of physical and chemical methods for the isolation of enantiomers from racemic mixtures have been developed.[99] Besides the crystallization of a racemate and separation of the enantiomorphic crystals similar to the first separation of racemic ammonium tartrate according to Pasteur, the reversible diastereomeric interaction between a racemic solution and a chiral stationary phase in continuous flow can be used to separate enantiomers from racemates. (chiral chromatography).[100, 101] Different diastereomeric interactions can also be exploited when reacting a racemate with a chiral reaction partner that preferably forms the product with one enantiomer while the less reactive enantiomer accumulates.[102] Since this procedure relies on the difference in the activation barriers for the reactions of the individual enantiomers, which is directly related to rate constants of the diastereomeric transformations, this principle is also referred to as kinetic resolution.[102] A major limitation of this technique is the maximum yield of 50%, however, if the left-over enantiomer can be racemized simultaneously to the kinetic

resolution, which is thermodynamically favourable due to the increase in entropy, the reactive enantiomer is continuously regenerated and the yield limitation is overcome.[99, 103, 104] This principle is known as dynamic kinetic resolution.[99, 103, 104] Of even greater importance is the field of asymmetric synthesis, the underlying principles of which were first recognized by Emil Fischer in the diastereoselective addition of HCN to L-arabinose in 1890, thereby providing the foundation of the principle of intramolecular transfer of chiral information to a developing stereocentre and exploitation of diastereomeric transition states with different activation barriers.[105, 106] The concept of intramolecular chirality transfer has been used extensively by attaching stereogenic elements to achiral substrates prior to a stereoselective step and subsequent cleavage of the chiral fragment, known as chiral auxiliary.[107] Another milestone in the synthesis of chiral compounds and the birth of asymmetric organometallic catalysis was the observation that the transfer of chiral information also occurs intermolecularly using chiral man-made catalysts.[99] This was discovered in 1966 by Nozaki and Noyori in the asymmetric cyclopropanation of styrene (**35**) with diazoacetate in the presence of a chiral copper complex **34**.[99] After activation of the diazoacetate by the metal, the chiral ligand differentiates the sides of the approaching styrene, providing the *trans* and *cis* diastereomers in a 7:3 ratio and with moderate 6%*ee* and 10%*ee*, respectively (**equation 1**).[108]

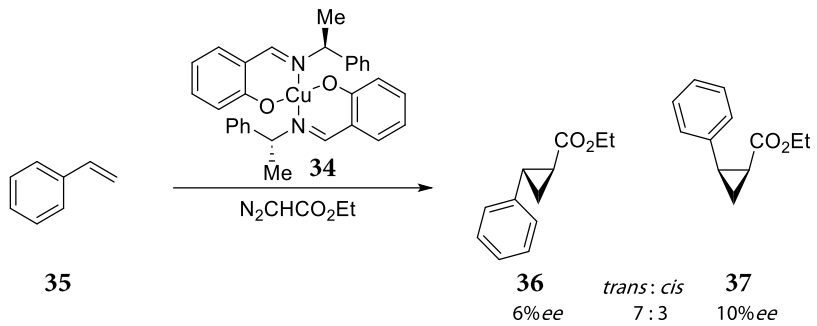

equation 1. First asymmetric metal catalysis by Nozaki and Noyori, employing chiral Cu-complex **34** for cyclopropanation of styrene (**35**).[108]

This was followed by pioneering work of Noyori and Knowles on the development of enantioselective hydrogenations, and of Sharpless on asymmetrically catalyzed oxidation reactions, for which they were awarded the Nobel Prize in 2001.[109-111] The intrinsic advantage of asymmetric catalysis over the chiral auxiliary strategy, which involves additional synthetic steps and the need for stoichiometric amounts of the auxiliary, was later summarized by Noyori as the "multiplication of chirality".[112] Towards the end of the 20th century, there was rapid growth in several areas of asymmetric catalysis. In the field of metal catalysis, a variety of asymmetric ligand structures was developed and different metal centres evaluated to explore diverse reactivity (chapter 1.2.2). The field of asymmetric biocatalysis also experienced rapid growth, influenced both by approaches on enzyme optimization through rational modifications, but particularly through the concept of directed evolution established by Frances Arnold (Nobel Prize 2018)(chapter 1.2.4).[113] In addition, the new concept of organocatalysis emerged, using small chiral organic molecules to catalyze a multitude of chemical reactions. The pioneering work of List and MacMillan in this field was honoured with the Nobel Prize in 2021 (chapter 1.2.3).[114] The underlying principles of asymmetric metal catalysis, organocatalysis and biocatalysis, as well as their use in asymmetric photo(redox) reactions, are explained in the following.

1.2.2 Development and principles of asymmetric metal catalysis

The development of asymmetric metal catalysis is largely driven by discoveries in the fields of asymmetric hydrogenations (reductions), asymmetric oxidations, as well as asymmetric C-C bond formations, the first example of which - a copper-catalyzed asymmetric cyclopropanation - by Nozaki and Noyori initiated research on asymmetric metal catalysis and exemplifies a fundamental requirement for the development of asymmetric metal-catalyzed reactions: In order for efficient asymmetric metal catalysis to be developed, the corresponding transformation must in principle be accelerated by coordination of metals to an involved substrate.[108-111] If a reaction is significantly catalyzed or ideally enabled by metal coordination, the stereochemical outcome in an asymmetric adaptation is not compromized by uncatalyzed, racemic background reactions. In this sense, the discovery of copper-catalyzed cyclopropanation with diazo components enabled the aforementioned asymmetric adaptation using a chiral Cu catalyst **34** by Nozaki and Noyori in 1966 (**equation 1**).[108]

While catalysis generally involves lowering of an activation barrier causing acceleration, in the case of asymmetric catalysis the reaction pathways leading to the two enantiomers experience a slightly different lowering and thus acceleration due to the stereogenic elements of the chiral ligands, thereby kinetically favouring the formation of one enantiomer. The fundamental principle of enantioselective metal catalysis is therefore the differentiation of prochiral fragments of the achiral substrate *via* diastereomeric transition states. Like diastereomeric compounds, possessing distinct physical properties and energy contents as a result of their individual three-dimensional structure, the reaction of an achiral substrate in the chiral environment of an asymmetric catalyst proceeds *via* diastereomeric transition states whose spatial structure and energy differ.[115] The difference in energy translates into a kinetic differentiation and thus directly into the ratio of enantiomers (*er*) that is formed. Therefore, the stereochemical outcome is ultimately dependent on the difference in Gibbs energies of the diastereomeric transition states $\Delta\Delta G^{\ddagger}$ (**figure 10**).[115] Considering the small energy difference of the ecliptic versus the staggered conformation in ethane of approximately 2.9 kcal/mol, emphasises the magnitude of the difference of $\Delta\Delta G^{\ddagger}$ that is required to achieve excellent enantiomeric excesses through kinetic stereocontrol and the inherent complexity of accurate predictions in rational catalyst development.

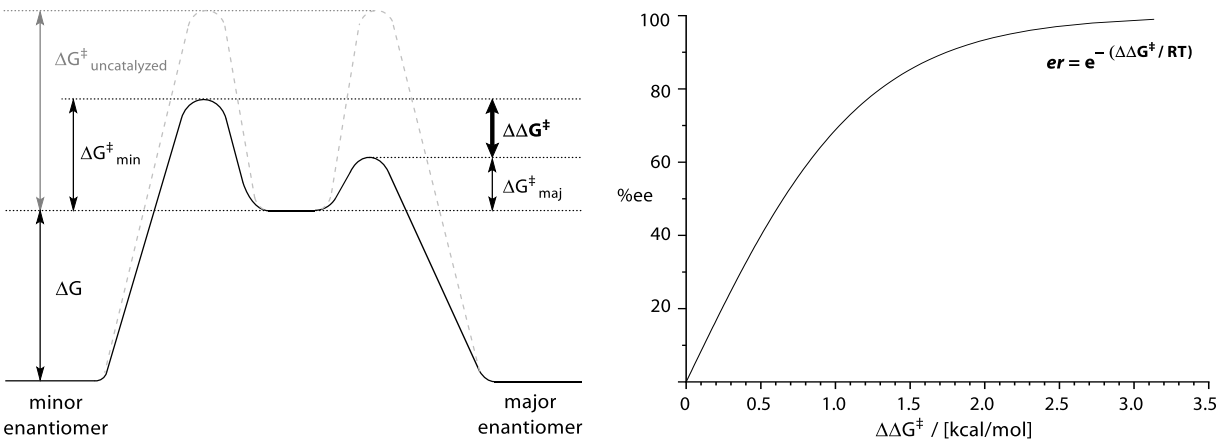

figure 10. Schematic representation of simplified energy profiles of uncatalyzed and asymmetrically catalyzed reaction pathways, leading to the formation of minor and major enantiomer *via* diastereomeric transition states of different energy content (left) and dependence of enantiomeric excess on the difference in transition state energies $\Delta\Delta G^{\ddagger}$.[115]

Similar to the asymmetric adaptation of Cu-catalyzed cyclopropanation, the discovery of metal-catalyzed Wilkinson hydrogenation using rhodium tris(triphenylphosphine)chloride in 1966 paved the way for the exploration of asymmetric hydrogenations.[116-118] In the early 1970s, Knowles was successful in utilizing a chiral rhodium complex with monodentate chiral-at-phosphorus ligand CAMP **38** which yielded a remarkable enantiomeric excess of 88%*ee* in the asymmetric reduction of an α-acetamidocinammic acid **39**, a key step in the synthesis of the anti-Parkinson drug L-DOPA (**41**) (**equation 2**).[116-118]

Around that time, Kagan and Dang published their bidentate C2-symmetric ligand DIOP and explained that the concept of incorporating identical phosphine fragments was intended to prevent potential isomerization of diastereomeric substrate-catalyst complexes.[119, 120] With this argument, Kagan and Dang drew attention to a more complex picture of energy profiles that emerges when the coordination of a prochiral substrate to the asymmetric metal catalyst precedes the enantioselectivity-determining step.[115] Since the coordination results in the formation of diastereomeric complexes, the stereochemical outcome is determined by the ratio between the energy barrier for interconversion of the diastereomeric complexes and the energy barriers leading to the product formation. In case of slow interconversion of the diastereomeric complexes (**figure 11**, left), the coordination of the substrate already determines the enantioselectivity of the reaction, whereas in the case of rapid interconversion of the diastereomeric complexes (**figure 11**, right), their ratio is less decisive, but the energy difference of the diastereomeric transition states leading to the products determines the stereochemical outcome (Curtin-Hammett conditions).[115] Even more equilibria between diastereomeric complexes and reaction pathways are obtained with ligands that show lower symmetry than C2.[115]

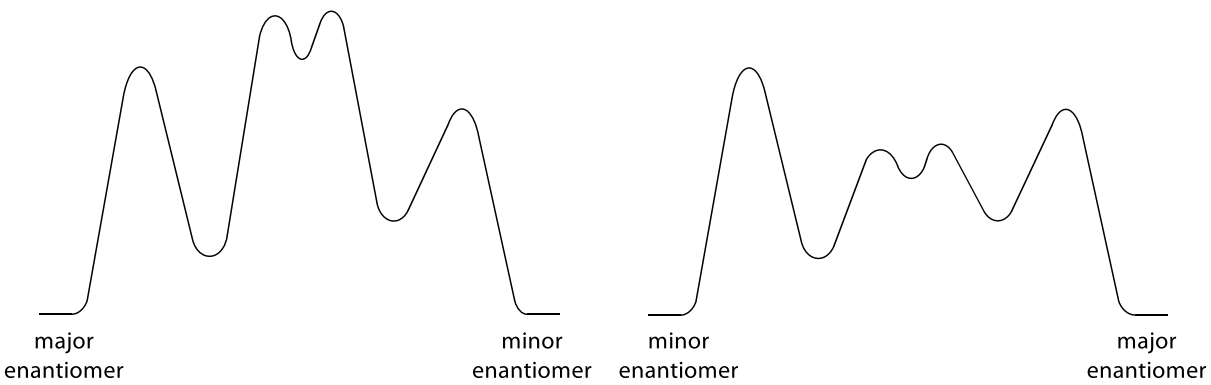

figure 11. Comparison of simplified energy profiles of asymmetric catalysis with prior substrate coordination to a C2-symmetric catalyst with slow (left) or fast (right) interconversion of diastereomeric catalyst-substrate complexes.[115]

In case of C2-symmetric catalyst complexes, only two diastereomeric substrate-catalyst complexes are obtained, as illustrated by the alignment of a prochiral double bond in the commonly used quadrant model, visualizing that protruding residues of C2-symmetric ligands occupy two opposing quadrants (grey), while the remaining two opposing quadrants (white) are less hindered (**figure 12**).[115]

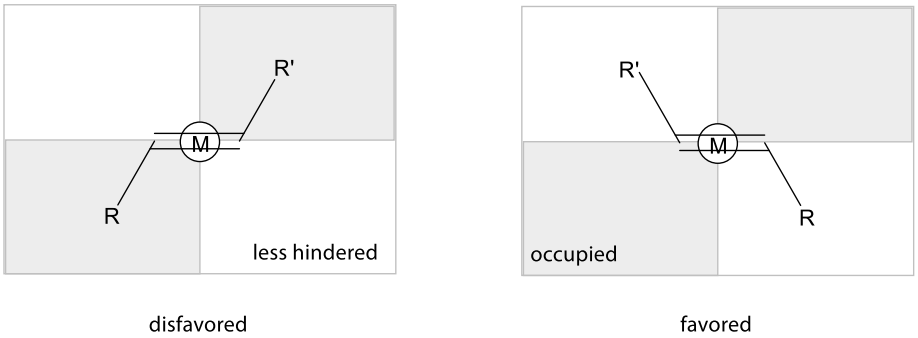

figure 12. Commonly used quadrant model illustrating the alignment of a prochiral double bond in front of a C2-symmetric catalyst; grey quadrants represent areas that are occupied by protruding ligand residues; white quadrants are less hindered.[115]

Certainly owing to the good enantioselectivities obtained with Kagan's and Dang's C2-symmetric DIOP ligand in the asymmetric reduction of α-acetamidocinammic acids (83%*ee*), their influential argumentation on C2 symmetry established a paradigm that was rarely questioned by the research community for several decades, but initiated the development of a large number of C2-symmetric ligands.[119, 120] Knowles also refined the L-DOPA synthesis by switching from the monodentate CAMP ligand (**38**) to the C2-symmetrical DIPAMP (**42**), thereby increasing the enantiomeric excess to 95%*ee* (**equation 2**).[121]

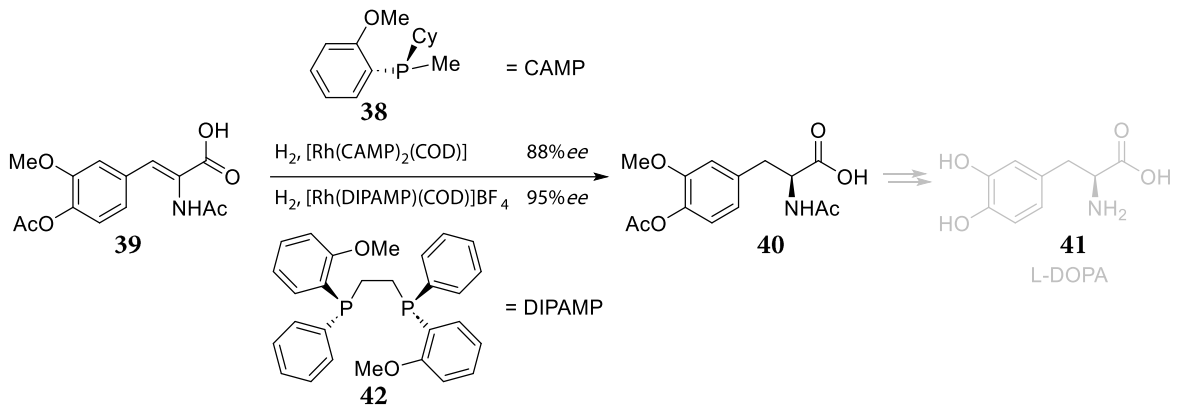

equation 2. Key step in the synthesis of L-DOPA: Reduction of α-acetamidocinnamic acids with originally used C1-symmetric CAMP ligand and with optimized C2-symmetric DIPAMP ligand.[118, 121]

Based on these initial achievements, the 1980s and 1990s were characterized by the discovery of further, mostly C2-symmetric ligands and reactivities. A milestone in asymmetric hydrogenation and, owing to its extraordinary versatility, for asymmetric metal catalysis in general, was the introduction of C2-symmetric axially chiral BINAP (**46**) by Noyori in 1980, the excellent selectivity of which can be used in a key step of the industrial synthesis of (−)-menthol (**47**) from myrcene (**43**) (**scheme 11**).[122-124] Another breakthrough was the use of Ru(II) instead of Rh(I), which on the one hand significantly extended the scope and on the other hand allowed the inversion of the preferred configuration in the reductive synthesis of amino acids.[110]

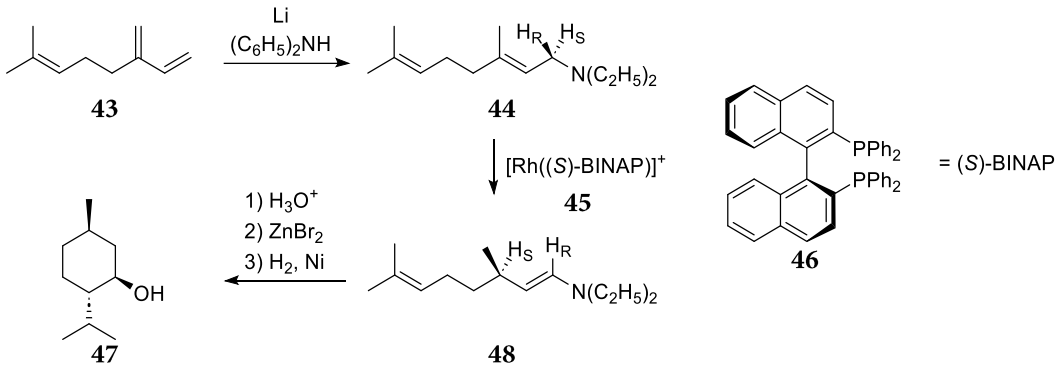

scheme 11. Takasago-menthol-synthesis employing asymmetric BINAP-ligand (**46**).[122-124]

In addition to these advancements in the field of asymmetric hydrogenation (reductions), Sharpless (Nobel laureate 2001) pioneered the field of asymmetric oxidations by publishing the first asymmetric epoxidation in 1980.[125] After attempts on the enantioselective adaptation of a molybdenum- and vanadium-catalyzed TBHP epoxidation, the breakthrough was achieved with the use of tartrates **51** and **54** that are easily accessible from the chiral pool as chiral ligands for an asymmetric titanium-catalyzed epoxidation of allylic alcohols **53**.[125] In 1988, Sharpless developed an asymmetric *cis*-dihydroxylation based on racemic osmium tetraoxide dihydroxylation, but in the presence of asymmetric cinchona alkaloid derivatives dihydroquinidine or dihydroquinine and employing only catalytic amounts of OsO_4 that are steadily regenerated by inexpensive stoichiometric oxidant additives.[126] Considering that the opening of an epoxide with an oxygen nucleophile produces a *trans*-1,2-diol derivative, Sharpless developed the corresponding synthetic counterpart with this dihydroxylation (**scheme 12**).[127]

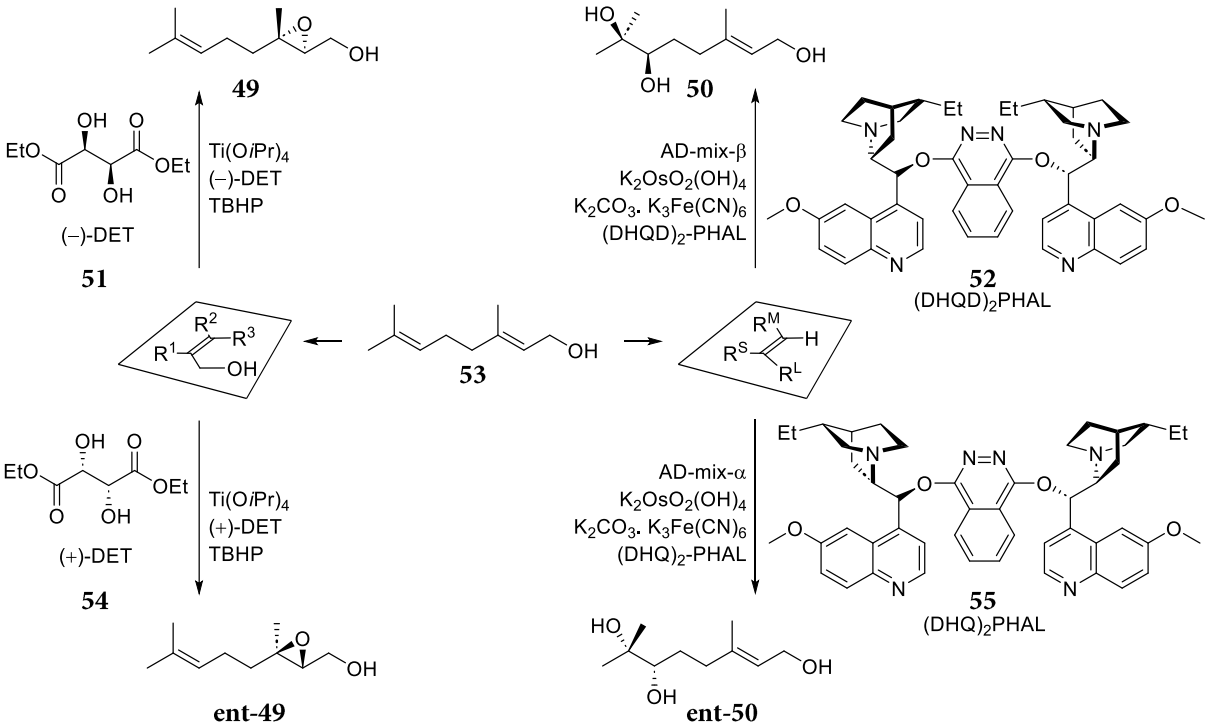

scheme 12. Asymmetric Sharpless epoxidation and asymmetric Sharpless dihydroxylation on the example of geraniol.[125, 126]

Inspired by the porphyrin ligands in the Heme group of oxidizing enzymes, Jacobsen and Katsuki developed a manganese-catalyzed epoxidation in 1990 employing the asymmetric salen ligand (**90**). In this way, the limitation of Sharpless epoxidation to allylic alcohols was overcome.[128, 129]

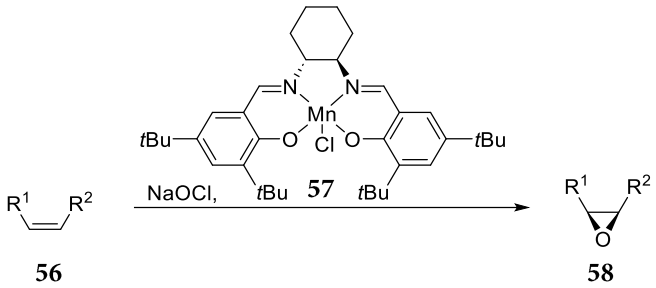

equation 3. Asymmetric Jacobsen epoxidation employing porphyrin inspired salen ligands (**90**).[128, 129]

In addition to these milestone publications on reductions and oxidations, asymmetric C-C bond formations have extensively been investigated. Compared to the asymmetric hydrogenations and oxidations discussed, this field is substantially more versatile, considering the variety of organic transformations involving C-C bond formations that can be activated by Lewis acids. As described above, initial research focused on asymmetric cyclopropanations.[108] Breakthroughs in this field were made in the late 1980s and early 1990s by the groups of Pfaltz, Masamune and Evans with the development of structurally related bisoxazolines **62**-**69** and semicorrines **59**-**61**, that also provided very good selectivities in numerous alternative transformations such as hydrosilylations, Mukaiyama aldol and Diels-Alder reactions (**figure 13**).[130-136]

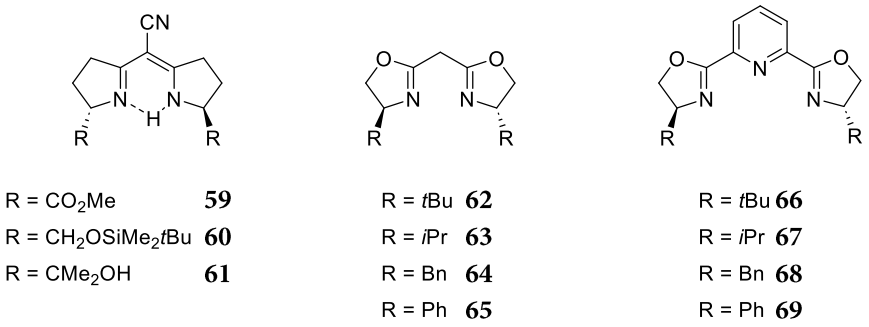

figure 13. Structures of semicorrines **59**-**61**, bisoxazolines **62**-**65** (BOX-ligands) and bis(oxazolinyl)pyridines **66**-**69** (PyBOX-ligands).[130-136]

In addition, a plethora of C-C bond forming reactions, including cycloadditions, aldol chemistry and analogous transformations, conjugate additions and alkene functionalizations, extending beyond the scope of this discussion of principles and milestones of asymmetric metal catalysis, was developed, frequently involving C2-symmetric ligands that were successful in the context of asymmetric hydrogenations and oxidations.[115, 127, 137]

Despite the success of C2-symmetric ligands, Achiwa *et al.* questioned the need for C2 symmetry in the early 1990s and developed a C1-symmetric modification of Kagan's DIOP (**72**) based on the consideration that the phosphine fragments fulfil different functions in the asymmetric intermediate complex: While the double bond standing *cis* to the PPh_2 residue serves enantioselection, more electron-rich *trans*-positioned PCy_2 fragments increases electron density at Rh, resulting in (1) an acceleration of the rate-determining oxidative addition of H_2 and (2) a more rigid

η^2-substrate positioning due to enhanced d-π* back-bonding. The C1-symmetric variant **73** indeed showed both higher catalytic activity and enantioselectivity (**equation 4**).[138-140]

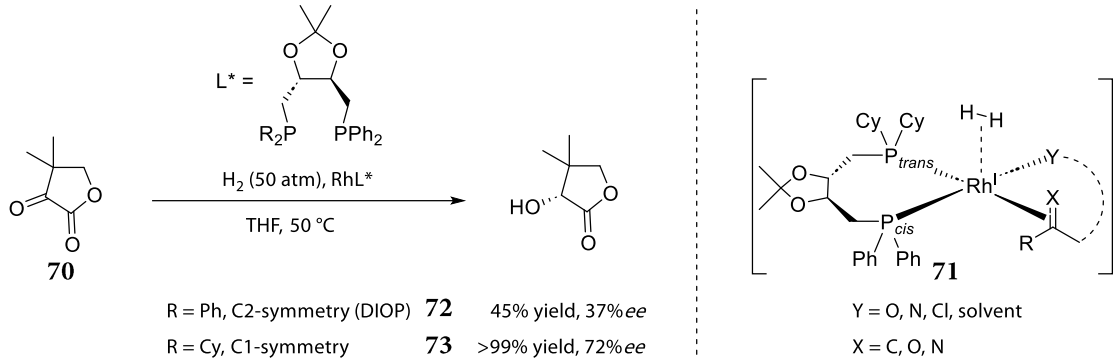

equation 4. Comparison of C2-symmetric DIOP (**72**) to C1-symmetric variant **73** in an asymmetric reduction according to Achiwa *et al.*[138-140]

The concept of desymmetrization led Pfaltz, Helmchen and Williams to the development of phosphinooxazoline (PHOX) ligands (**74-78**), that rely on a combination of one P- and one N- as coordinating atoms instead of bidentate substrate coordination with two identical P-atoms or N-atoms, resulting in an electronic desymmetrization due to different π-acceptor and σ-donor properties, respectively, and that have successfully been employed in a variety of allylic substitutions.[141-144]

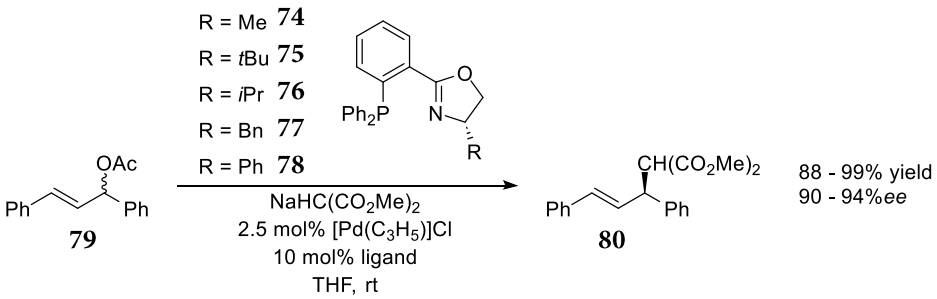

equation 5. Application of PHOX ligands (**74-78**) in a Pd-catalyzed asymmetric allylic substitution according to Williams *et al.*[142]

Some ligand structures and their corresponding metal complexes provided excellent selectivities in multiple, mechanistically unrelated reactions.[99, 145] These man-made catalysts exhibit a more universal scope than enzymes, while providing similar or matching selectivities. Adapting a term used in pharmaceutical chemistry to describe substances that are active on multiple biological targets, some ligand structures that have proven to provide excellent selectivities in a variety of different reactions are referred to as "privileged structures" (**figure 14**).[99, 145]

The origin of chirality differs significantly among the ligands.[115] In the structure of BOX (**62-65**), the chiral information originates from stereocentres in spatial proximity to the coordinated metal and thus reaction centre. In contrast, the stereocentres in Chiraphos (**81**) appear more remote and the chiral information is translated to the reaction centre *via* a favourable skewed conformation of the metallacycle in which the backbone methyl substituents occupy pseudo-equatorial positions causing the P-bound phenyl groups to protrude, in analogy to the quadrant diagram discussed above (**figure 12**). In contrast, the widely used BINAP (**46**) or BINOL (**86**) exhibit

axial chirality, as although the two napthyl fragments are connected by a single bond, the rotation barrier is so large due to the hydrogen atoms at the C8 and C8' positions, as well as potentially large residues X, that the configuration is stable even at high temperatures. The single bond nevertheless allows the coordination of metals of different radii, since the distance between the coordinating residues X can vary by rotation around the central aryl-aryl bond.[115]

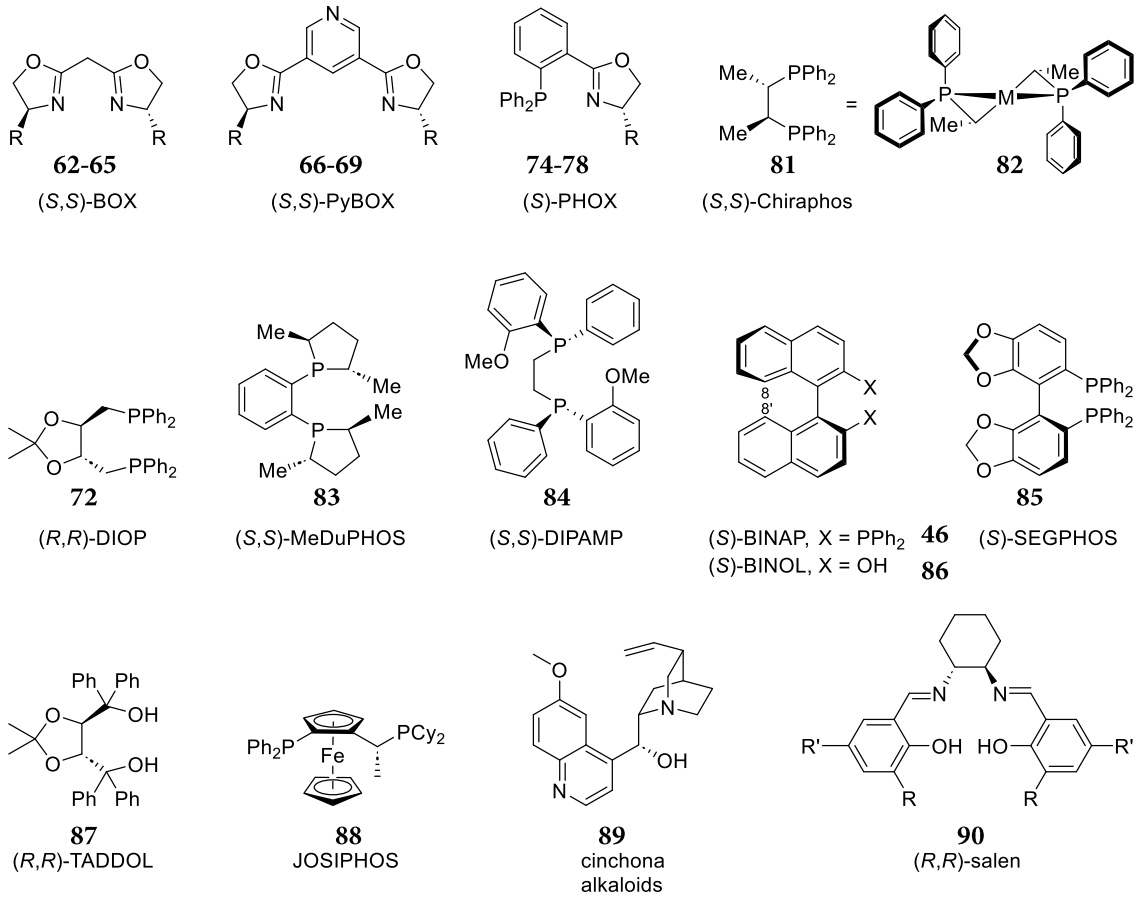

figure 14. Overview of common asymmetric ligand structures ("privileged ligands").[115, 145]

The versatile applications of these privileged structures in highly diverse reactivities render them an obvious starting point for the exploration of new asymmetric transformations. Some of them have also been successfully incorporated in asymmetric phototransformations, both in dual metal photoredox catalysts (chapter 1.3.1) as well as in bifunctional single catalyst approaches (chapter 1.3.2).

1.2.3 Development and principles of asymmetric organocatalysis

Organocatalysis is the latest emerging approach to asymmetric catalysis, which received prominence following two milestone publications in year 2000 by List and MacMillan, who were awarded the Nobel Prize 2021 for their achievements in the area.[114, 146, 147] Although the history of related catalysis dates back to the 1970s when Hajos and Parrish (Hofmann-La Roche) and Eder, Sauer and Wiechert (Schering AG) discovered a L-proline (**95**) catalyzed intramolecular aldol reaction known as the Hajos-Parrish-Eder-Sauer-Wiechert reaction, its underlying principles and potential for organic synthesis were not recognized.[148-151]

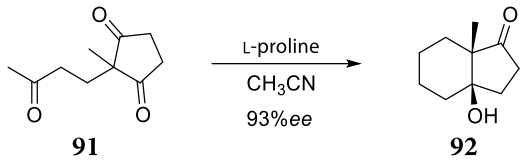

equation 6. Hajos-Parrish-Eder-Sauer-Wiechert reaction: L-Proline-catalyzed asymmetric Robinson-annulation.[150, 151]

Inspired by metal-free aldolase enzymes exploiting an enamine-based mechanism, in the year 2000 List *et al.* achieved an asymmetric L-proline (**95**) catalyzed aldol reaction of acetone (**93**) with various aldehydes **94**.[114, 147] A screening of primary amino acids and cyclic amino acids of varying ring size and substitution patterns revealed that both the pyrrolidine ring and the carboxylic acid are required for efficient catalysis and good enantioselectivities.[147] This observation suggested a metal-free Zimmermann-Traxler-type transition state, illustrating two modes of action of the organocatalyst **95**: The enamine formation increases the nucleophilicity compared to acetone (**93**) and creates a chiral environment, furthermore the carboxylic acid acts as an acid/base co-catalyst, thereby both activating the aldehyde **94** towards a nucleophilic attack as well as directing the aldehyde **94** towards the favoured Re-facial attack (**equation 7**).[147]

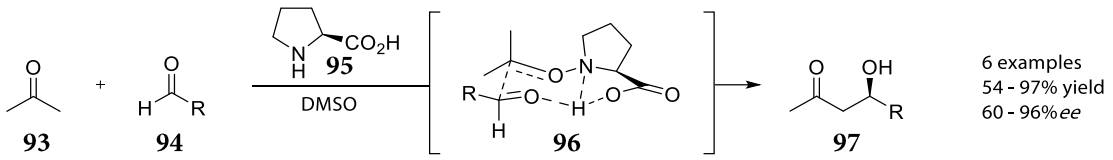

equation 7. L-proline catalyzed asymmetric aldol reaction by List *et al.*[147]

In the same year, MacMillan *et al.* realized the close similarity between the organocatalytic idea and the established Lewis acid (LA) catalysis, given that analogous to the LA coordination to a carbonyl group, also the condensation with an amine activates by LUMO lowering while the iminium ion formation remains reversible thereby ensuring the catalytic turnover (**scheme 13**).[146]

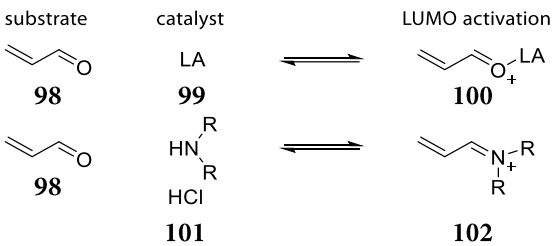

scheme 13. Comparison of LUMO-activating Lewis-acid catalysis and iminium-catalysis.[146]

Realizing this similarity, MacMillan *et al.* foresaw the potential use of chiral amines as asymmetric organocatalysts in many transformations that had previously been metal-catalyzed and proved his concept in organocatalyzed Diels-Alder reactions of α,β-unsaturated carbonyl compounds **104** with different dienes.[114, 146] Besides L-proline (**95**), several chiral secondary amines, both cyclic and acylic, were evaluated, with the phenylalanine-derived imidazoline **103** providing the best selectivity. The latter controls stereoselectivity both by favouring the formation of the (*E*)-iminium ion and by shielding the *Re* side of the iminium ion (**equation 8**).[146]

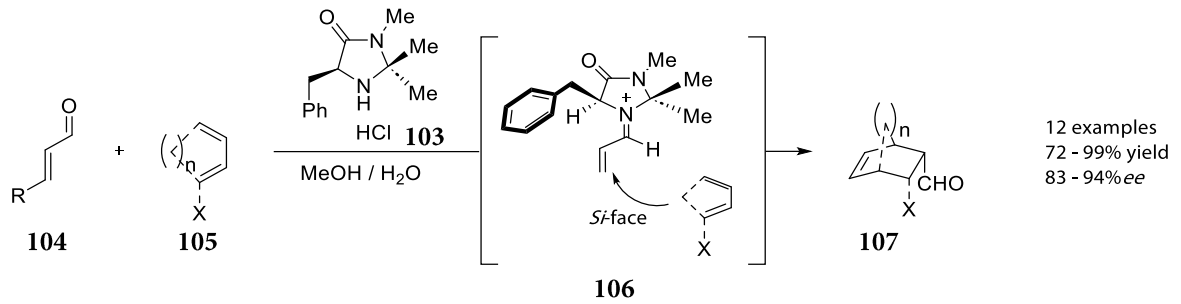

equation 8. Organocatalyzed asymmetric Diels-Alder-reaction by MacMillan *et al.*[146]

The aforementioned milestone publications illustrate two fundamental activation principles of organocatalysis: Simple carbonyl compounds **108** undergo condensation with chiral secondary amines **112** to form chiral enamines **111**, which contain an energetically raised HOMO and are in turn activated towards reaction with the LUMO or SOMO (single-occupied molecular orbital) of electrophiles or electrophilic radicals. In contrast, α,β-unsaturated carbonyl compounds **109** form chiral iminium ions **113** with energetically lowered LUMO, showing an increased electrophilicity for the reaction with nucleophiles in conjugate additions.[152]

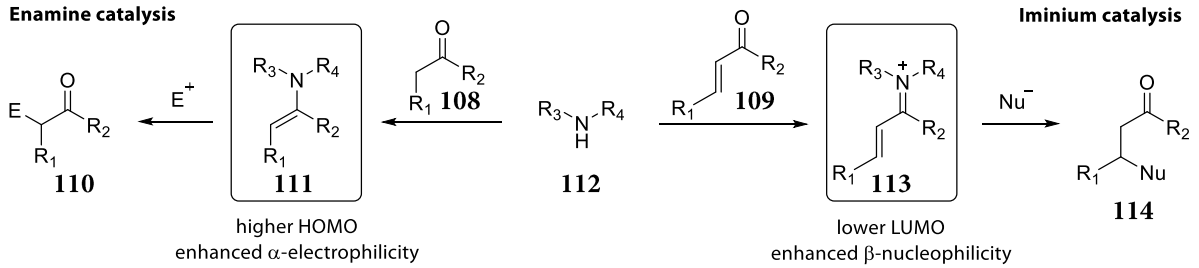

scheme 14. Comparison of the activation principles of enamine and iminium ion catalysis.[152]

In addition to these very common mechanisms of activation, organocatalysis also comprises activation by hydrogen bonding or Brønsted bases and acids, usually in the form of chiral organic ions.[153, 154]

In recent decades, research in organocatalysis has provided various chiral secondary amines, and similar to privileged ligand structures, some have repeatedly provided satisfactory results (**figure 15**).[152] Remarkably, cinchona alkaloid structures **116** have also been used as metal-free organocatalysts. Moreover, the bifunctional nature of L-proline (**95**) and its electrophile-directing carboxyl group can be modified analogously to the Jorgensen-Hayashi catalyst **115** to reverse the direction by shielding one side of the enamine **118**.[152]

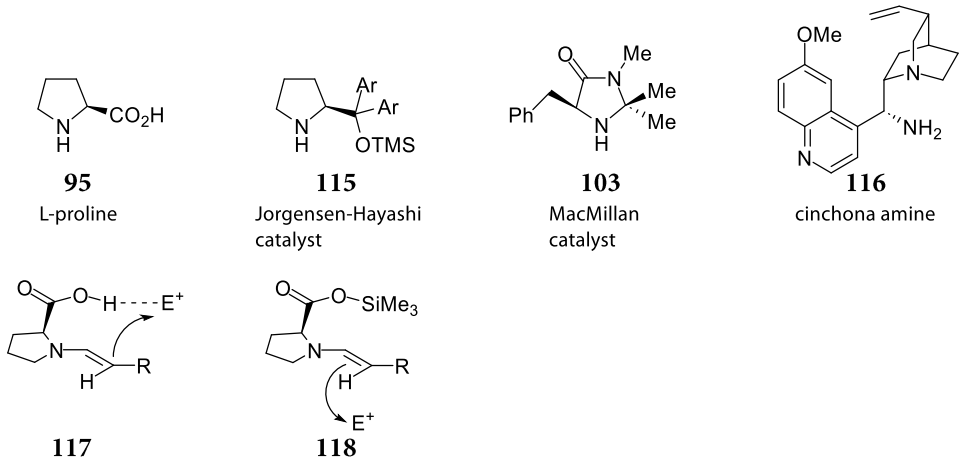

figure 15. Commonly employed organocatalysts and comparison of electrophile directing carboxylic acid **117** and sterically shielding silylester **118** in L-proline (**95**) and Jorgensen-Hayashi-catalyst **115**, respectively.[152]

The versatility of organocatalysis predicted by MacMillan became a reality, in part because of several advantages over metal and biocatalysis. For example, organocatalysts are either available from the chiral pool or can be easily and inexpensively synthesized therefrom, without the need for expensive metals some of which may leave toxic impurities. Moreover, many reactions proceed without exclusion of air and water and are very well scalable.[155] Also in the context of photoredox reactivity, a large number of asymmetric transformations involving odd-electron species has been carried out by organocatalysis (chapters 1.3.1.1 and 1.3.2.1).[1, 15]

1.2.4 Development and principles of asymmetric biocatalysis

The use of biocatalysts dates back to ancient times, exploiting the fermentation of sugar **121** to alcohol **119** in the production of beer or wine, and of lactose to lactic acid in cheese production.[156, 157] But even beyond food production, some large-scale industrial processes predate detailed structural elucidation or mechanistic understanding and range from the synthesis of glycerol (**123**) by yeast fermentation for the production of explosives in World War I, to the benzoin-type condensation of benzaldehyde (**124**) with acetaldehyde (**125**) produced *in situ* from glucose (**121**) by yeast to yield a precursor **126** of L-ephedrine (**127**).[84, 156, 158-160] A patent for this process was filed as early as 1934 without any knowledge of a mechanism and it is still used today.[156, 161]

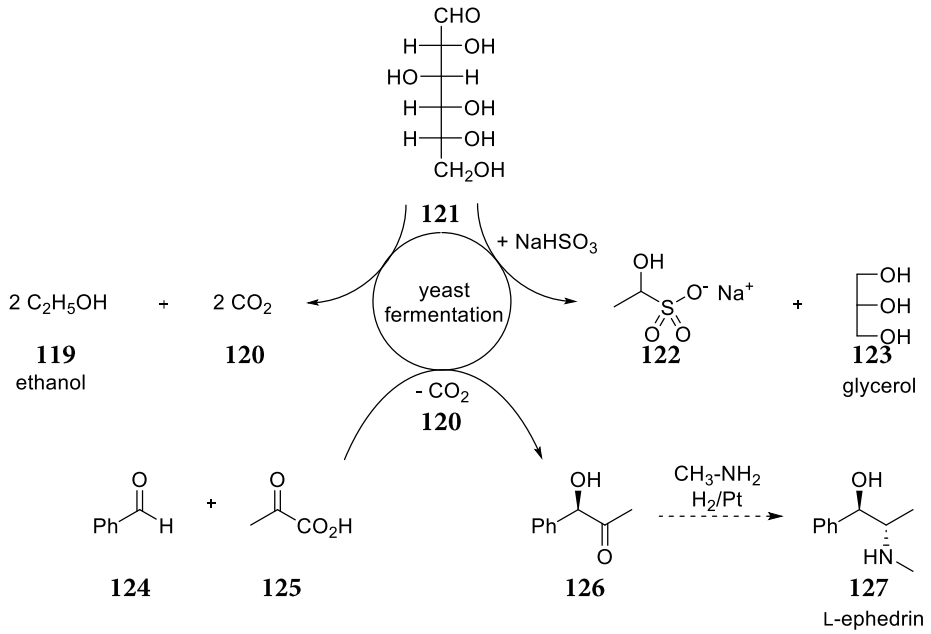

scheme 15. Selected examples of historical applications of biocatalysis: Production of alcohol **119** (top left) and glycerol (**123**) (top right) from glucose (**121**) and stereoselective benzoin-type condensation for the synthesis of a precursor **126** of L-ephedrin (**127**) (bottom).[84, 156, 158-161]

Biocatalysts can be whole cell organisms, single enzymes, crude enzyme preparations or immobilized enzymes. The actual catalyst is usually an enzyme, i.e. a complex structure, often comprising several hundred amino acids, that evolution has created over millions of years in order to perform a biochemical transformation precisely, with superior chemo-, regio- and stereoselectivity.[84, 162] An example of the extraordinary regioselectivity is a key step of the Reichstein synthesis of ascorbic acid (**130**) from D-glucose (**121**). After reduction to D-sorbitol (**128**), regioselective oxidation of a secondary hydroxyl group besides three more secondary and two primary hydroxyl groups to L-sorbose (**129**) takes place by Acetobacter suboxydans (**scheme 16**).[163, 164]

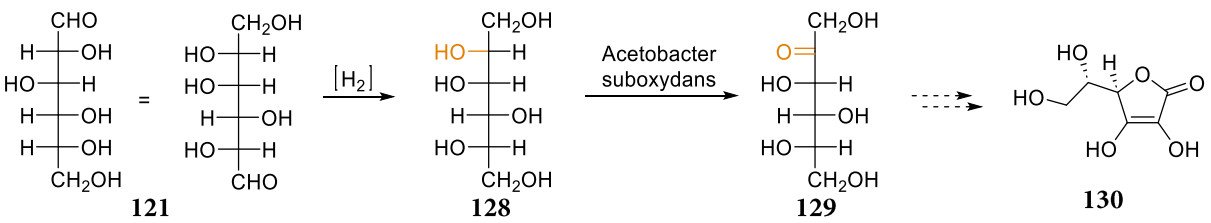

scheme 16. Key step in the Reichstein synthesis of L-ascorbic acid (**130**) from D-glucose (**121**): Regioselective oxidation of D-sorbitol (**128**) to L-sorbose (**129**).[163, 164]

A key step in the industrial synthesis of hydrocortisone (**133**) also illustrates the remarkable regio- and stereoselectivity of biocatalysis. The selective C-H oxidation at C11 of progesterone (**131**) is achieved using Rhizopus nigricans (**scheme 17**).[84]

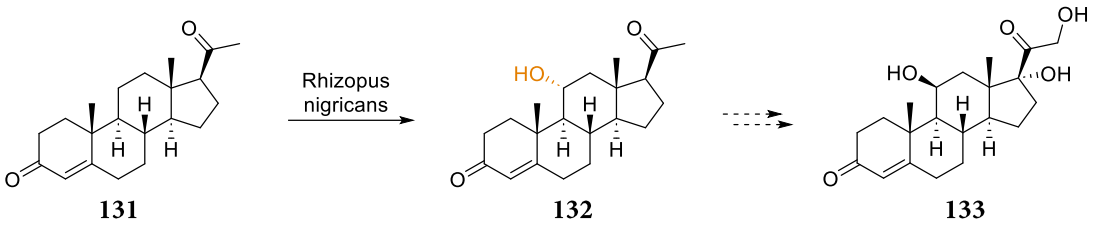

scheme 17. Biocatalytic C-H oxidation at C11 of progesterone (**131**) by Rhizopus nigricans in the industrial synthesis of hydrocortisone (**133**).[84]

Although biocatalysts were already used extensively in industrial processes without mechanistic understanding and were rather used as a black box for the corresponding transformation, it was not until the 1950s that methods for structural elucidation were advanced sufficiently to shed some light into the dark.[84] In 1951, Sanger (Nobel laureate 1958) succeeded in determining the first enzyme primary structure on the example on the amino acid sequence of insulin.[156, 165] Progress in the field of X-ray crystallography led to the first structural elucidations at the end of the 1950s.[166, 167] The mechanistic understanding of involved coenzymes such as NAD(P)H (**309**) or thiamine also developed increasingly, but several decades passed and pioneering work in the field of genetic engineering, such as the decoding of the genetic code and the development of methods for DNA modification and recombinant DNA, had to be achieved before enzymes became available in sufficient quantities for industrial applications and mechanistic insights could be gained through enzyme modifications.[156]

Despite the very large enzyme structures relative to metal catalysts and organocatalysts, the same fundamental chemical principles and principles of catalysis apply in the active centre. Therefore, depending on whether the active site contains a metal, enzymes can be regarded either as complex, oversized organocatalysts or as giant organometallic catalysts.[84] However, the outstanding selectivity results not only from an energetic differentiation favouring one of several competing transition states, but also from a synergy of multiple interactions between the reaction partners and the relatively large specialized tertiary structure that serves to precisely align substrates in the active centre.[84]

The obvious desire to extend such selectivity to unnatural substrates and reactivities and to increase the applicability of biocatalysts under non-natural conditions motivated researchers to pursue rational enzyme optimizations in the 1980s.[84, 156, 168-173] Frances Arnold achieved a breakthrough in the early 1990s by establishing the concept of directed evolution, for which she was awarded the 2018 Nobel Prize in Chemistry.[113] Aware of the superiority of nature, this concept is based on an interplay of alternating random mutation and subsequent selection.[174] In this approach, a randomly mutated gene is expressed in a bacterium, producing enzymes the properties of which are subsequently evaluated in the desired transformation before ineffective enzymes are sorted out and the promising gene sequences undergo another cycle of random mutation.[113, 174] Using this concept, Arnold investigated the solvent limitation of enzymes on the example of subtilisin, that breaks down casein, and found that its third generation of directed evolution showed a 256-fold improvement in performance in 65% DMF

compared to the original enzyme. This was the result of 10 random mutations, the advantages of which were not predictable by rational enzyme design.[113, 174]

The outstanding selectivities, the steadily growing capabilities of enzyme engineering and the fact that catalysis in general, but biocatalysis in particular, meets many of the principles of green chemistry, led to a steep increase from 60 industrial biocatalyzed processes in 1990 to several hundred in 2019.[156, 175] The ongoing search for new reactivities also led to the recent discovery, that irradiation with visible light can induce new reactivities. Biocatalysts containing a photoactive fragment, e.g. flavin-dependent ene-reductases, were irradiated with visible light, enabling new, unnatural transformations involving single-electron species (chapter 1.3.2.3).[176-180] Furthermore, combinations of enzyme catalysts with a separate photocatalyst were also investigated (chapter 1.3.1.3).[181-185]

1.3 Asymmetric photoredox catalysis

Since pioneering reports by MacMillan, Yoon and Stephenson in 2008, research in the field of photoredox catalysis has dominated the chemical literature and added a variety of useful transformations to the repertoire of organic synthesis.[2, 4, 10-12, 186] Exploiting photosensitizers to harvest abundant, inexpensive and environmentally benign visible light energy and to convert it into chemically available energy under mild conditions and with simple experimental setup opened a new dimension of chemical transformations involving odd-electron species that were regarded as difficult to control before.[187]

Considering the increasing demand for enantiopure material, this type of chemical reactivity has been extensively combined with the concepts of asymmetric metal-, organo- and biocatalysis, resulting in a variety of asymmetric photoredox transformations. The catalyst concepts may be further divided into dual catalytic systems, in which a photoredox catalyst is present besides an asymmetric catalyst (chapter 1.3.1), and single bifunctional catalysts, which both initiate the photoredox reactivity and cause the asymmetric induction (chapter 1.3.2).[187, 188]

1.3.1 Asymmetric dual catalyst approaches

1.3.1.1 Asymmetric dual organophotoredox catalysis

1.3.1.1.1 Asymmetric dual organophotoredox catalysis *via* chiral enamines

The great research interest in photoredox catalysis was inspired, in part by a milestone publication by MacMillan *et al.* who established an asymmetric α-alkylation by combining a photoredox catalytic cycle with an organocatalytic cycle (**equation 9**).[10] The asymmetric organocatalyst condensates with an aldehyde to form a chiral enamine **135** with energetically raised HOMO, that is involved in two steps: First, it serves for the reductive quenching of the excited photocatalyst **12**, yielding the reduced photocatalyst $[Ru(bpy)_3]^+$ (**11**), which is itself a sufficiently strong reductant to reduce an α-halocarbonyl compound **1** to the corresponding α-carbonyl radical **138** upon release of a halide anion. Second, the elevated HOMO in the chiral enamine **135** results in an activation towards a reaction with the electrophilic radical **138** the stereochemical outcome of which is influenced by the chiral imidazolidinone substructure. The resulting radical **139** is subsequently oxidized in a chain propagation mechanism by the α-halocarbonyl substrate **1**, generating an iminium ion **136** which liberates the enantioenriched α-alkylated product **5** and regenerates the organocatalyst **4** upon hydrolysis (**scheme 18**).[10]

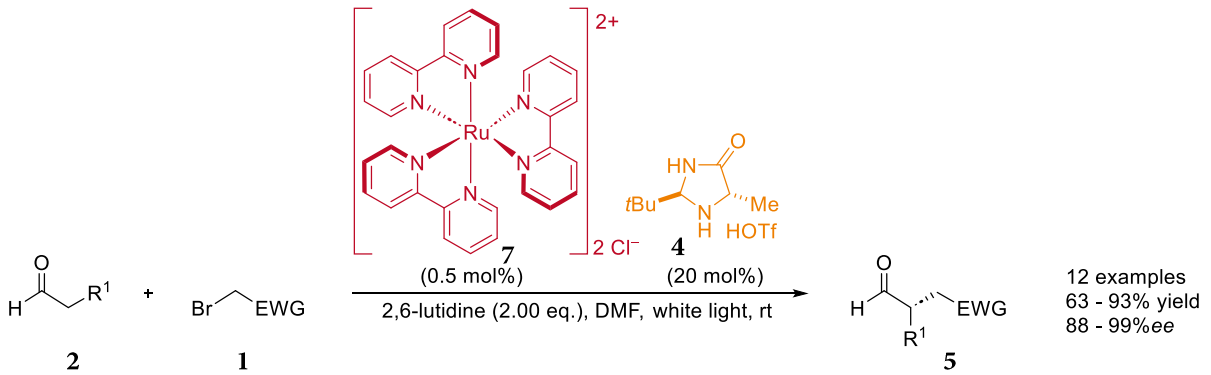

equation 9. Asymmetric α-alkylation of aldehydes according to MacMillan *et al.*[10]

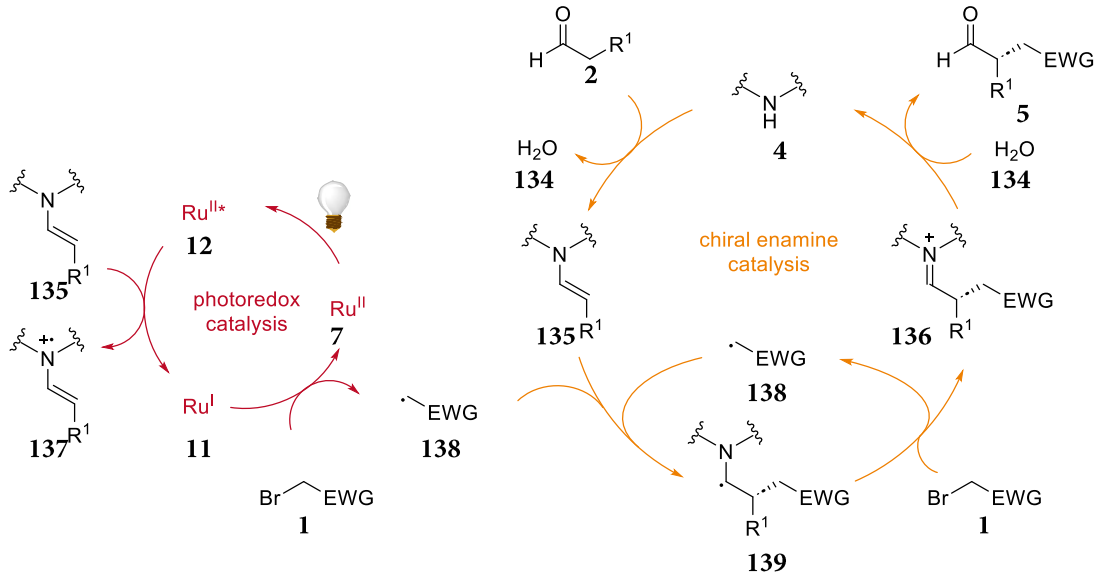

scheme 18. Mechanism of the asymmetric α-alkylation of aldehydes proposed by MacMillan *et al.*[10]

This principle was extended to other α-functionalizations such as α-trifluoromethylations and α-perfluoroalkylations and the underlying reactivity was also optimized for alternative photocatalysts.[187, 189] Using the first-row analogue $[Fe(bpy)_3]Br_2$ and the non-transition-metal complex Al(salen)Cl, Cozzi *et al.* achieved a closely related α-alkylation, however, the excited photocatalysts directly served to reduce the alkyl radical precursor in contrast to MacMillan's original $[Ru(bpy)_3]^{2+}$ (**7**) catalyzed reaction.[190, 191] Related α-alkylations have also been optimized for metal-free photosensitizers such as Eosin-Y by König and Zeitler *et al.* or rose bengal by Ferroud *et al.*[192, 193] Luo *et al.* applied MacMillan's mechanistic principle to the α-alkylation of β-ketocarbonyl compounds **140** and **144**, obtaining all-carbon quaternary stereocentres (**scheme 19**).[194] For this purpose, an acyclic organocatalyst **142** was used, that contributed to high stereoinduction by H-bonding interaction of the protonated amine with the carbonyl group of the electrophilic radical.[194]

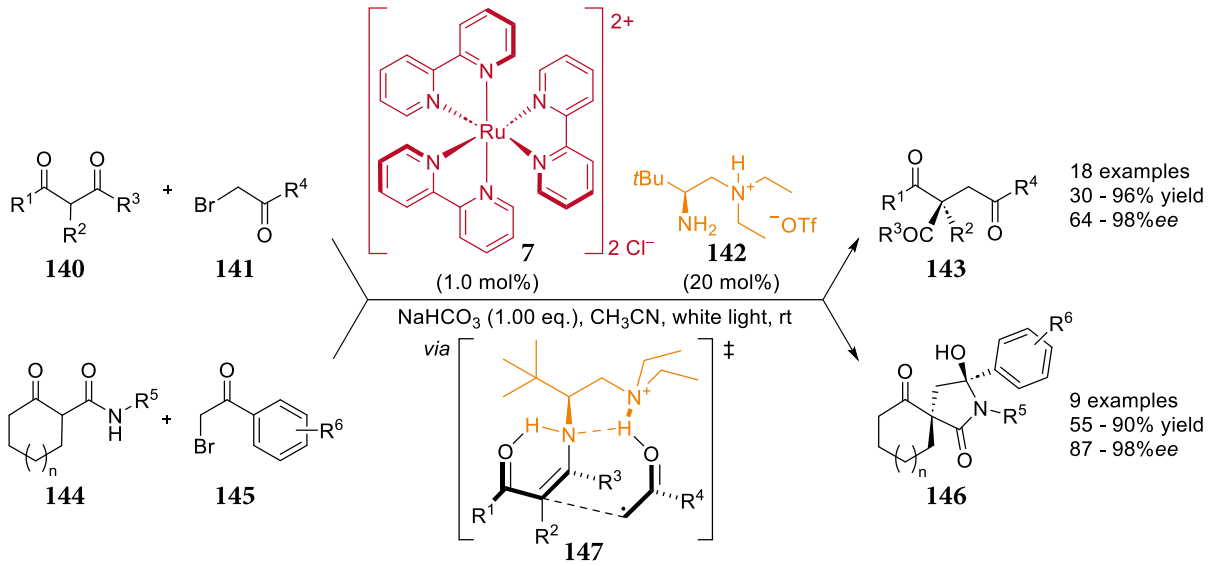

scheme 19. Asymmetric α-alkylation of β-ketocarbonyls **140** and **144** providing access to all-carbon quarternary stereocentres and associated model of stereoinduction according to Luo *et al.*[194]

Employing electron-deficient benzyl bromides and the stronger reducing photocatalyst *fac*-Ir(ppy)$_3$ (**29**), MacMillan expanded the scope of the general reactivity to an asymmetric α-benzylation of aldehydes **149**.[195]

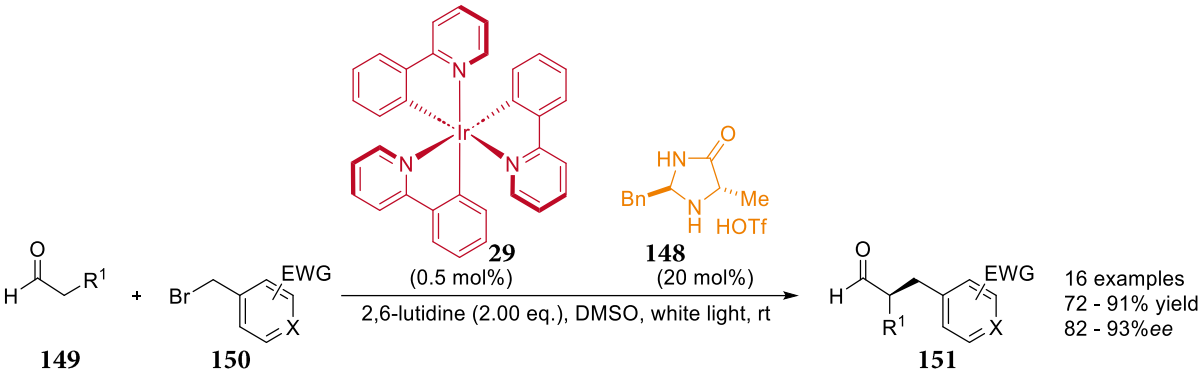

equation 10. Enantioselective α-benzylation of aldehydes according to MacMillan *et al.*[195]

A few years later and inspired by DNA biosynthesis involving a spin-centre-shift to cleave a C-O bond, MacMillan *et al.* developed an asymmetric α-benzylation employing benzylic alcohols **154** as radical precursors, thereby avoiding the additional step of converting them into halides or other suitable leaving groups.[196] The mechanism proceeds *via* the reduction of the heteroaromatic **154** and spin-centre shift (SCS) to cleave off water (**134**) and generate the benzyl radical **157**. After addition to the chiral enamine **161**, oxidation by the Ir(IV) species **158** follows, closing the photocatalytic cycle and generating an iminium ion **162** that releases the product **155** upon hydrolysis (**scheme 20**).[196]

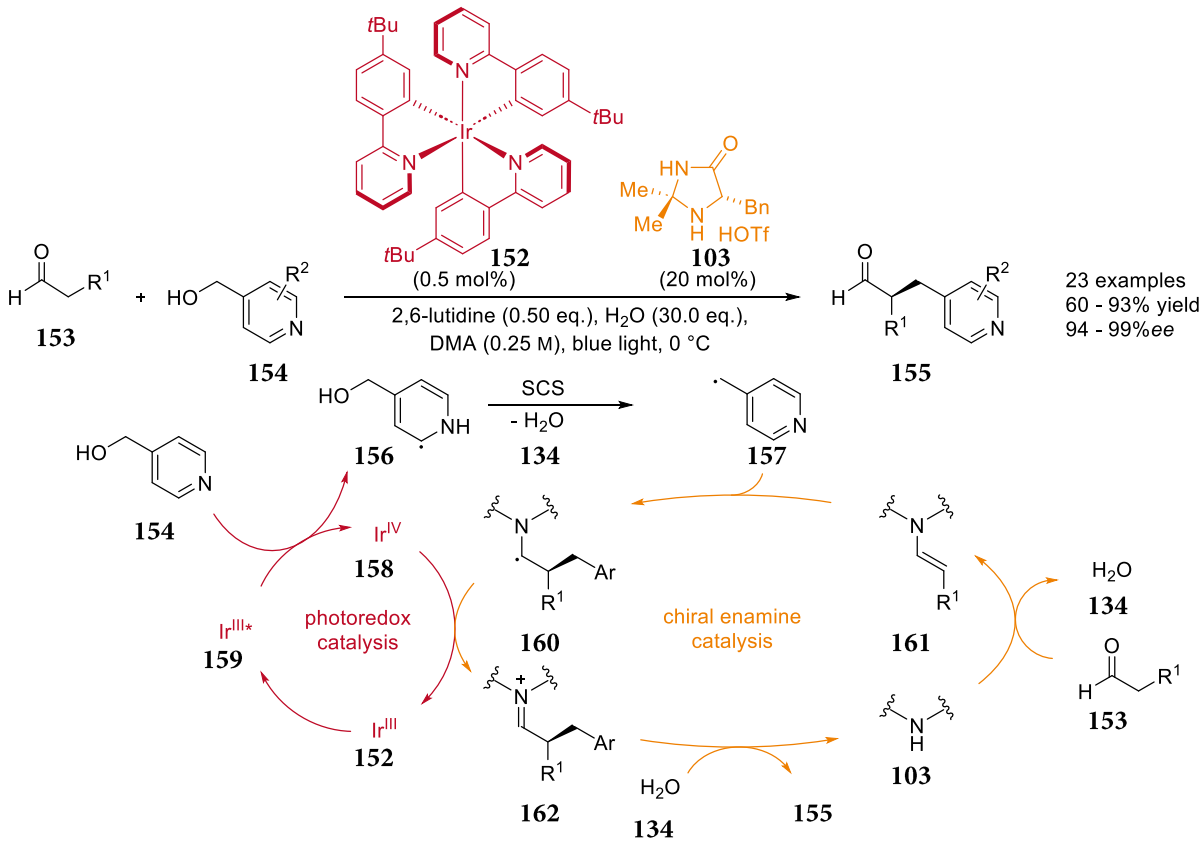

scheme 20. Spin-centre-shift enabled direct enantioselective α-benzylation of aldehydes **153** with alcohols **154** and proposed mechanism according to MacMillan *et al.*[196]

Another elegant approach of asymmetric α-functionalizations based on the combination of photoredox reactivity with asymmetric enamine organocatalysis is MacMillan's direct α-alkylation using simple olefins.[187, 188, 197] Besides the synthetic utility of employing simple olefins, the underlying mechanistic concept, involving the interplay of three individual catalytic cycles to ensure redox neutrality, is particularly noteworthy. The photoexcited iridium complex **173** oxidizes the chiral enamine **174** to form an electrophilic enaminyl radical **179** that readily adds to suitable olefins **165** and **169**. MacMillan *et al.* succeeded in identifying thiophenol **163** as a suitable hydrogen atom source, which transfers the hydrogen atom only after alkene addition (rather than to the enaminyl radical cation **179**). The resulting iminium ion **175** releases the product **164** or **170** upon hydrolysis. The thiyl radical **178** is reduced by the Ir(II) species **177**, thereby turning over both the photocatalytic and the HAT catalytic cycle. In this way, a variety of intra- and intermolecular cyclizations were performed in high enantioselectivities (**scheme 21**).[197]

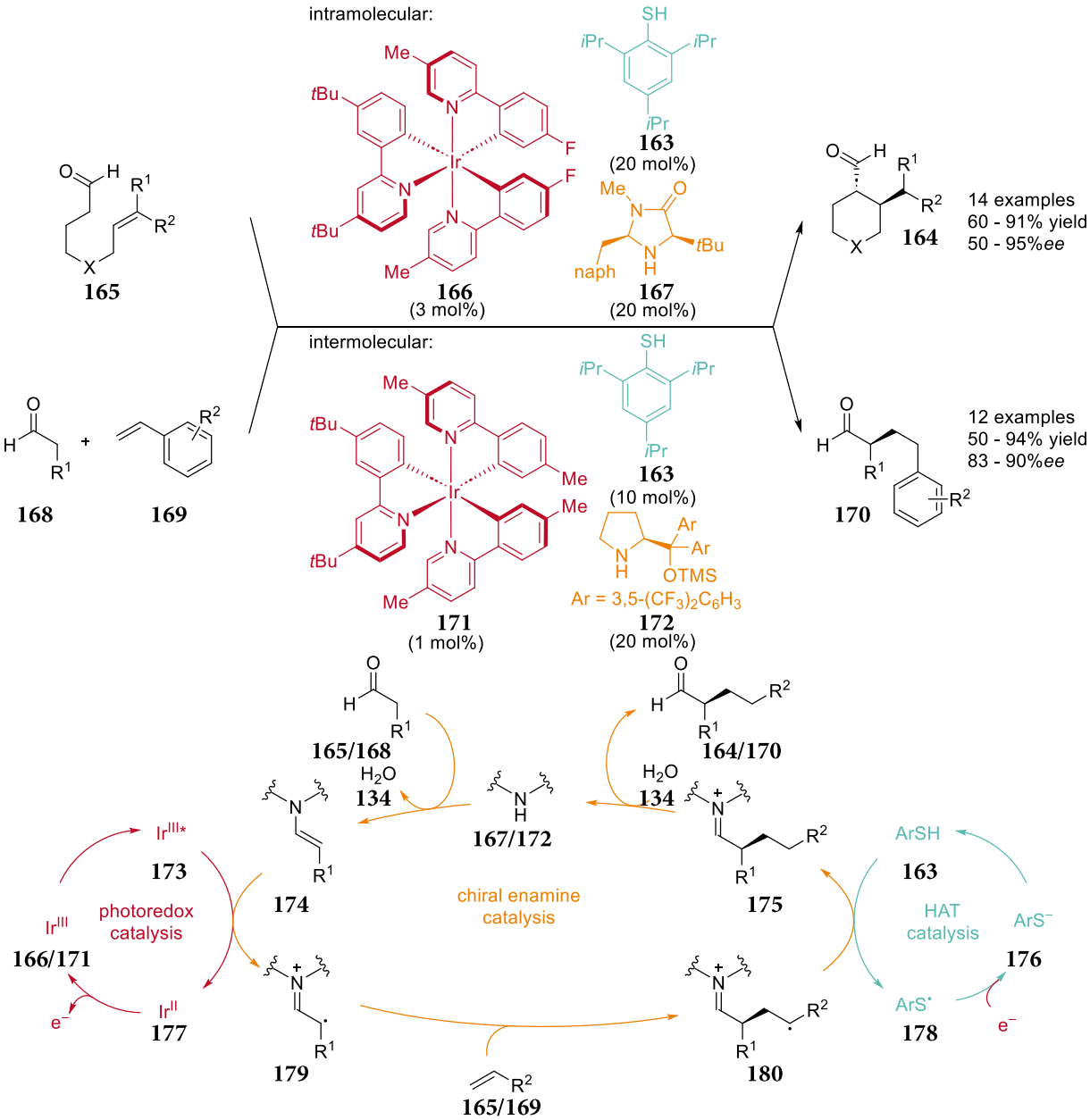

scheme 21. Mechanism and conditions of MacMillan's intra- and intermolecular α-alkylation of aldehydes using simple olefins.[197]

1.3.1.1.2 Asymmetric dual organophotoredox catalysis *via* chiral iminium-ions

Besides combining photoredox reactivity with organocatalysis based on chiral enamines, in most cases aiming at asymmetric α-functionalizations of carbonyl compounds, some transformations have been developed that involve chiral iminium ions, and mostly focus on asymmetric β-functionalizations of Michael systems.[187, 188] Condensation with the chiral organocatalyst lowers the LUMO of the α,β-unsaturated carbonyl compounds, resulting in the activation of the chiral iminium ion towards the addition of nucleophiles or nucleophilic radicals. Melchiorre *et al.* exploited this concept and developed an approach to quaternary stereocentres the broad applicability of which was demonstrated by the use of two non-related light-induced pathways involving different photoredox catalysts (**scheme 22**).[198]

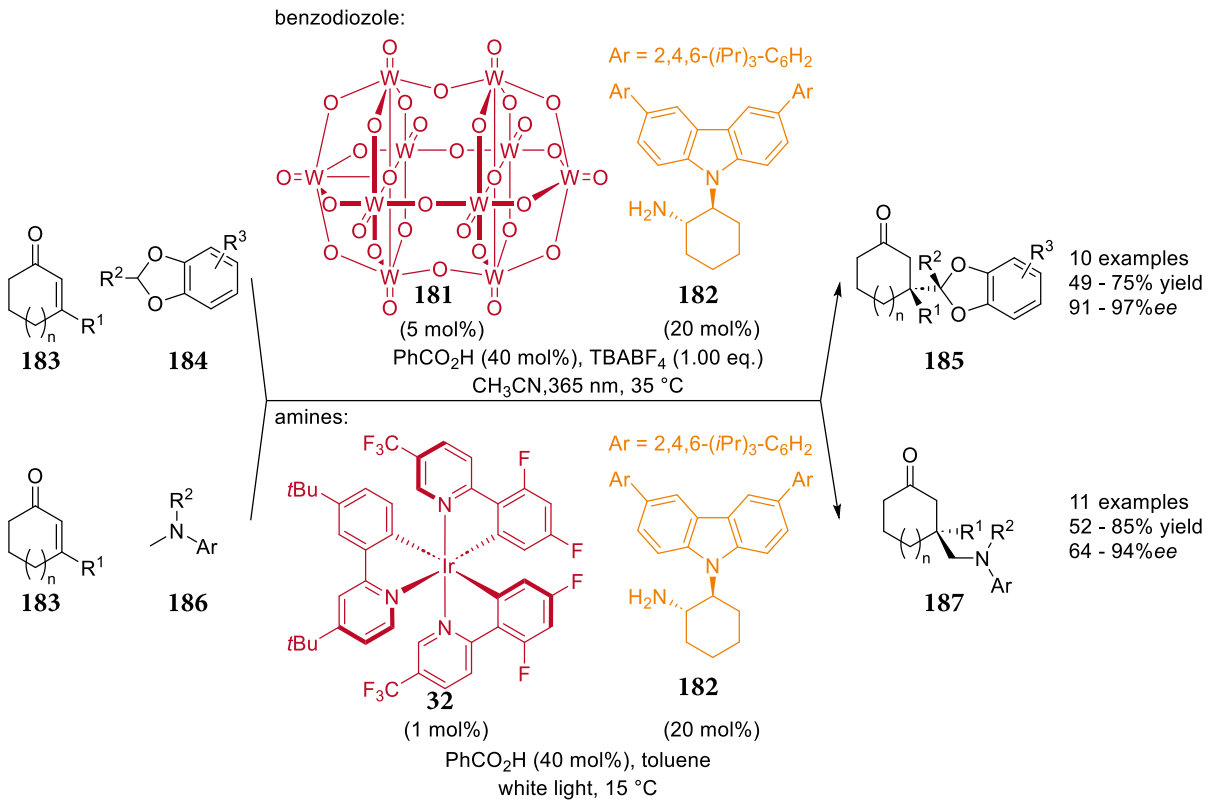

scheme 22. Asymmetric catalytic formation of quaternary carbons by iminium ion trapping of radicals according to Melchiorre *et al.*[198]

For the benzodiazole substrate **184**, tetrabutylammonium decatungstate (TBADT) (**181**) was used, which upon excitation acts as a hydrogen-atom transfer catalyst and homolytically cleaves the C-H bond on the benzodiozole **184**, generating a nucleophilic carbon-centred radical **188**.[198] For the tertiary amine substrate **186**, $Ir(dF(CF_3)ppy)_2(dtbbpy)PF_6$ (**32**) was used as the photocatalyst, which oxidizes the amine **186** to form α-amino radicals **188**. In both cases, nucleophilic carbon-centred radicals are formed which add in a stereocontrolled fashion to the chiral iminium ion **193** formed from the organocatalyst **182** and a cyclohexenone substrate **183**. A chiral cyclohexyl diamine **182** containing a redox active carbozole unit was used as the organocatalyst. The latter initiates intramolecular SET to form an enamine, which rapidly tautomerises to an imine **190**. The carbazole

radical cation **194** is then reduced, closing the photocatalytic cycle and releasing the product **185/187** upon hydrolysis.[187, 188, 198]

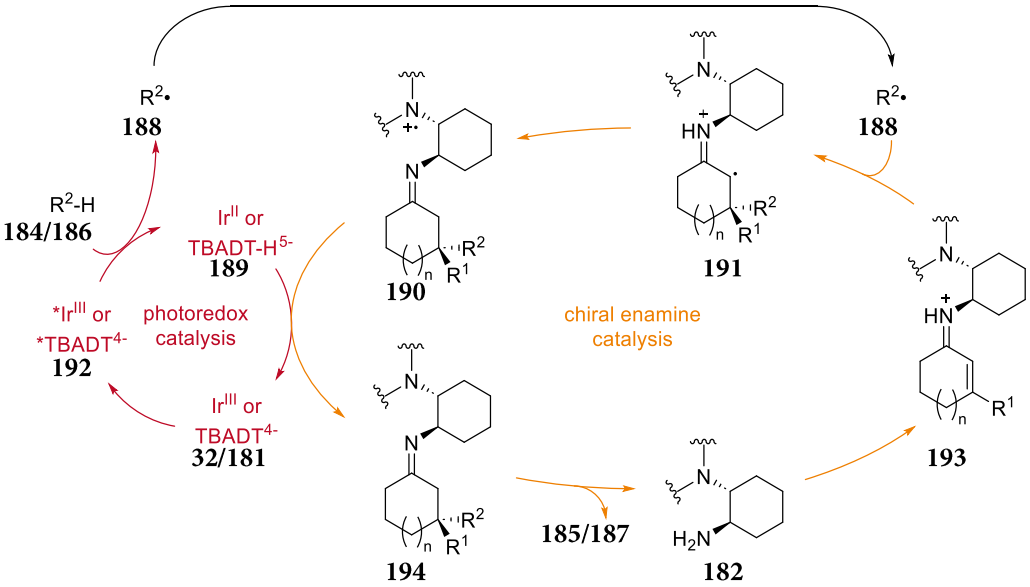

scheme 23. Mechanism of the asymmetric catalytic formation of quaternary carbons *via* iminium ions proposed by Melchiorre *et al.*[198]

The underlying mechanistic principle was subsequently extended by Yu *et al.* to asymmetric hydroacylation of aromatic enals **196** using α-ketoacids **197**.[187, 188, 199] In this process, excited $[Ru(bpz)_3](PF_6)_2$ (**24**) serves to induce oxidative decarboxylation of the α-keto acid **197** and generation of an acyl radical, which adds to the chiral iminium ion in a similar way to the β-functionalization discussed earlier. The resulting enaminyl radical is oxidized by a Ru(I) species, giving rise to the 1,4-dicarbonyl product **198** by hydrolysis.[199]

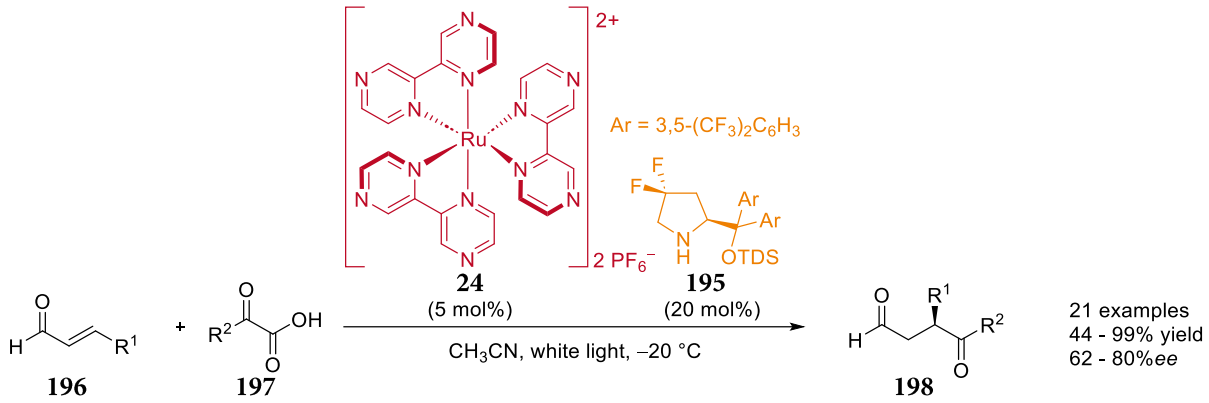

equation 11. Asymmetric hydroacylation of enals **196** with α-ketoacids **197** according to Yu *et al.*[199]

1.3.1.1.3 Asymmetric dual organophotoredox catalysis *via* H-Bonding, Brønsted acid or base catalysis

Besides the discussed combinations of photoredox catalysis with organocatalysis based on chiral enamines or chiral imines, the field of asymmetric organophotoredox catalysis also includes the combination with chiral hydrogen-bonding catalysts or chiral Brønsted acids or bases.[187, 188] All these concepts share the principle of transferring chirality from chiral counterions to intermediately formed (radical) ions. In addition, the hydrogen-bonding interaction often leads to the modification of redox potentials of involved substrates.

An example is the enantioselective reduction of 1,2-diketones **201** by Jiang *et al.* using a guanidinium salt **200** as H-bonding organocatalyst.[200] The excited dicyanopyrazine photocatalyst (DPZ) (**206**) is reductively quenched by a tertiary amine **202** (*N*-napththyl-tetrahydroisoquinoline). The reduced photocatalyst **205** reduces the substrate **201** to generate a ketyl radical anion **204** that forms a hydrogen bond with the chiral guanidinium salt **200**. In this chiral environment, reduction to the anion **209** is caused by another equivalent of the tertiary amine **202**. After enantioselective protonation, the enantioenriched α-hydroxyketone **203** is released from the organocatalyst **200** (**scheme 24**).[200]

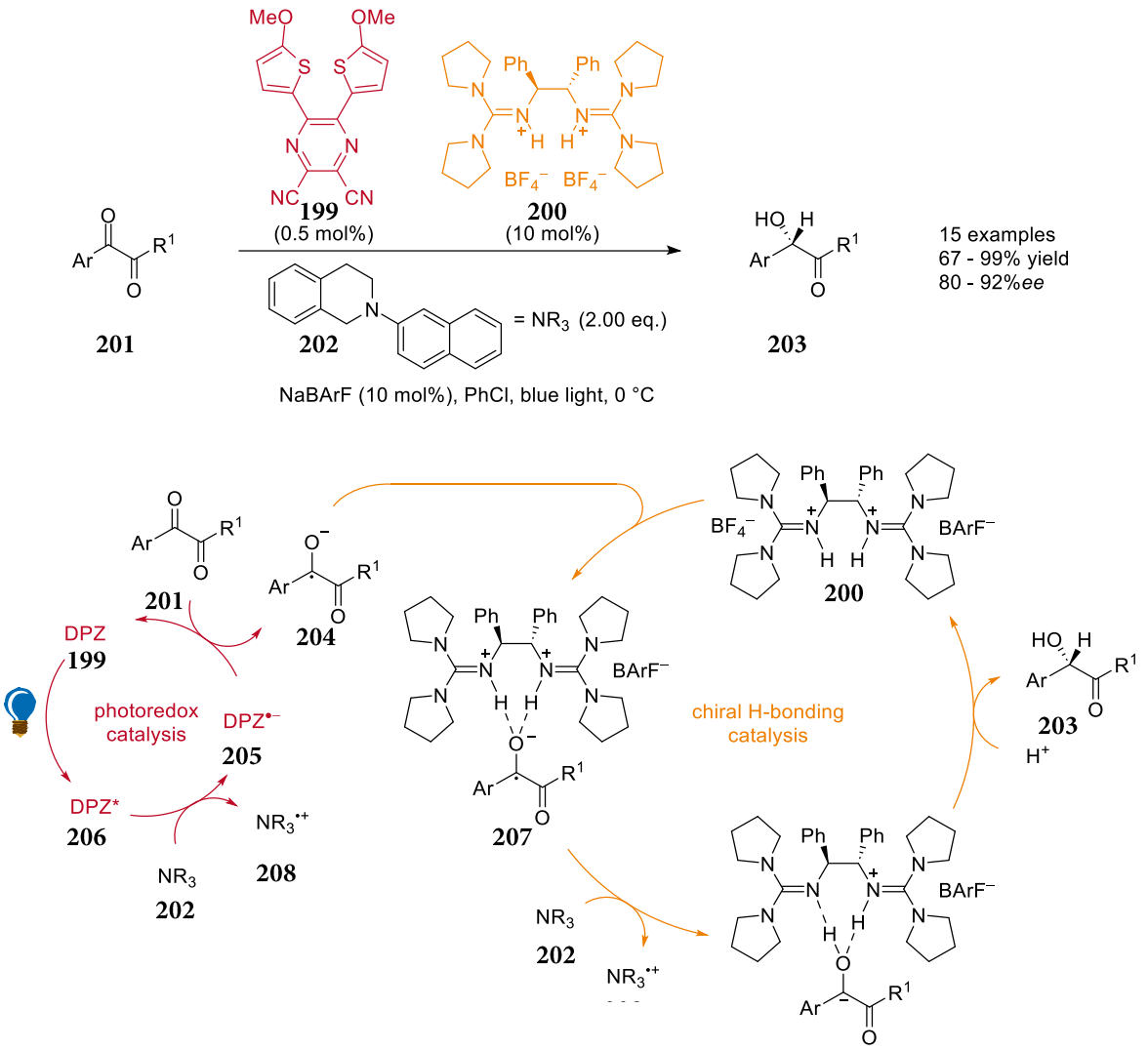

scheme 24. Catalytic enantioselective reduction of 1,2-diketones **201** by the combination of photoredox catalysis and chiral H-bonding organocatalysis and proposed mechanism thereof according to Jiang *et al.*[200]

Chiral Brønsted base catalysis was also successfully combined with photoredox catalysis.[187, 188] Recently, Knowles *et al.* succeeded in developing an intramolecular hydroamination by exploiting a triple catalytic system, consisting of a photoredox catalytic cycle, a Brønsted base catalytic cycle and a HAT catalytic cycle.[201]

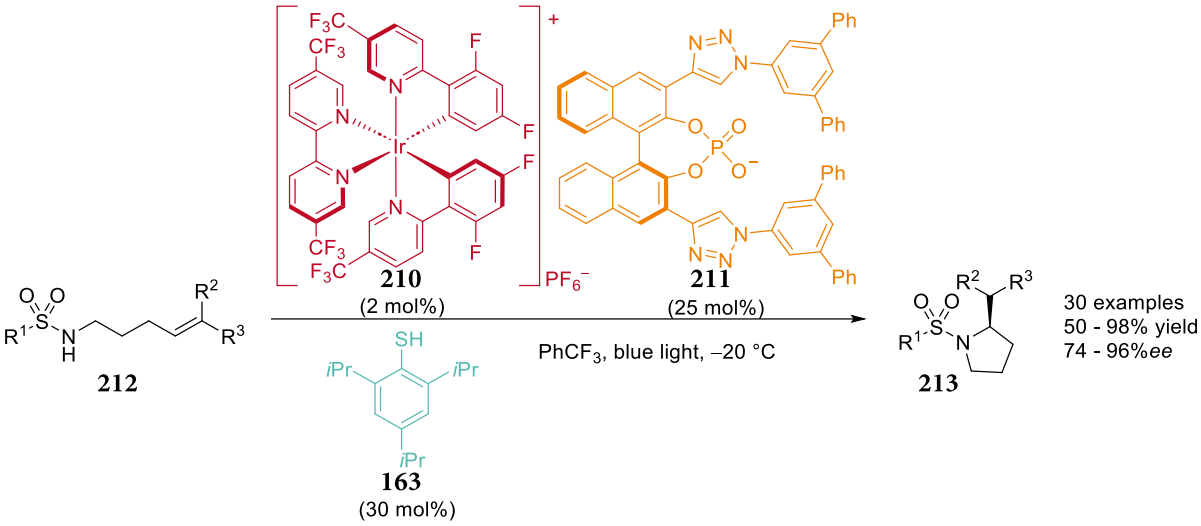

equation 12. Enantioselective hydroamination of alkenes with sulfonamides enabled by proton-coupled electron transfer.[201]

The hydrogen bonding interaction of the sulfonamide **212** with the chiral BINOL-phosphate anion **211** activates the substrate **212** towards oxidation by the excited photocatalyst **217**, rendering this step a proton-coupled-electron-transfer (PCET).[201] After stereocontrolled 5-exo-dig cyclization, the product **213** is formed by hydrogen atom abstraction from the thiol cocatalyst **163**. The resulting thiyl radical **178** is reduced to thiol **163** by the photocatalyst **210** in the presence of phosphoric acid **216**, thereby turning over all three catalytic cycles simultaneously.[201]

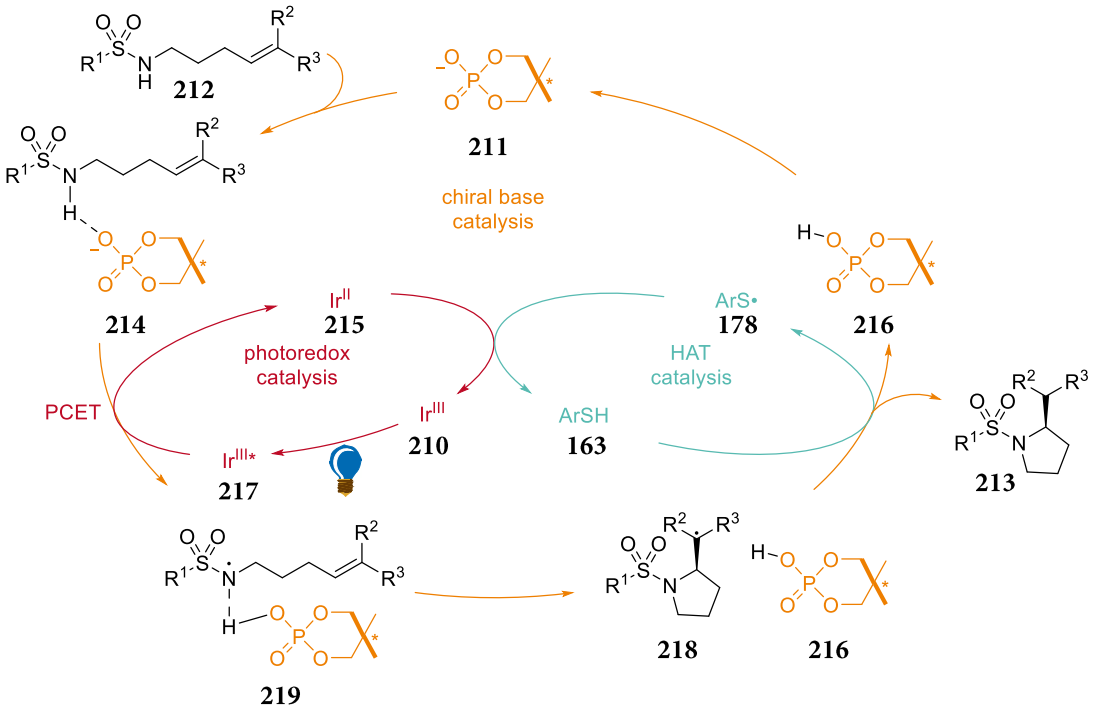

scheme 25. Mechanism of the triple catalytic enantioselective hydroamination of alkenes with sulfonamides.[201]

The combination of chiral Brønsted acids with photoredox reactivity has led to a wide variety of transformations, ranging from conjugate additions involving enantioselective protonation to cycloadditions or reductions for the synthesis of furoindolines and pyrolloindolines. Common principles often include proton-coupled electron transfer and directing effects of phosphate groups, as well as LUMO lowering to facilitate nucleophilic attacks.[187, 188] An example is the enantioselective coupling of α-bromoketones **222** with *N*-aryl-α-aminoacids **221** by Jiang *et al.*[202] Thereby, the deprotonated amino acid **224** is oxidized by the excited photocatalyst, inducing a decarboxylation with formation of an α-amino radical **226**. Reductive debromination completes the photocatalytic cycle and generates an α-carbonyl radical **227**. In the chiral environment of the chiral phosphoric acid **220**, which functions as a bifunctional H-bonding catalyst by both stabilizing the electrophilic α-carbonyl radical species **227** and activating the nucleophilic α-amino radical species **226**, enantioselective radical cross-coupling occurs.[202]

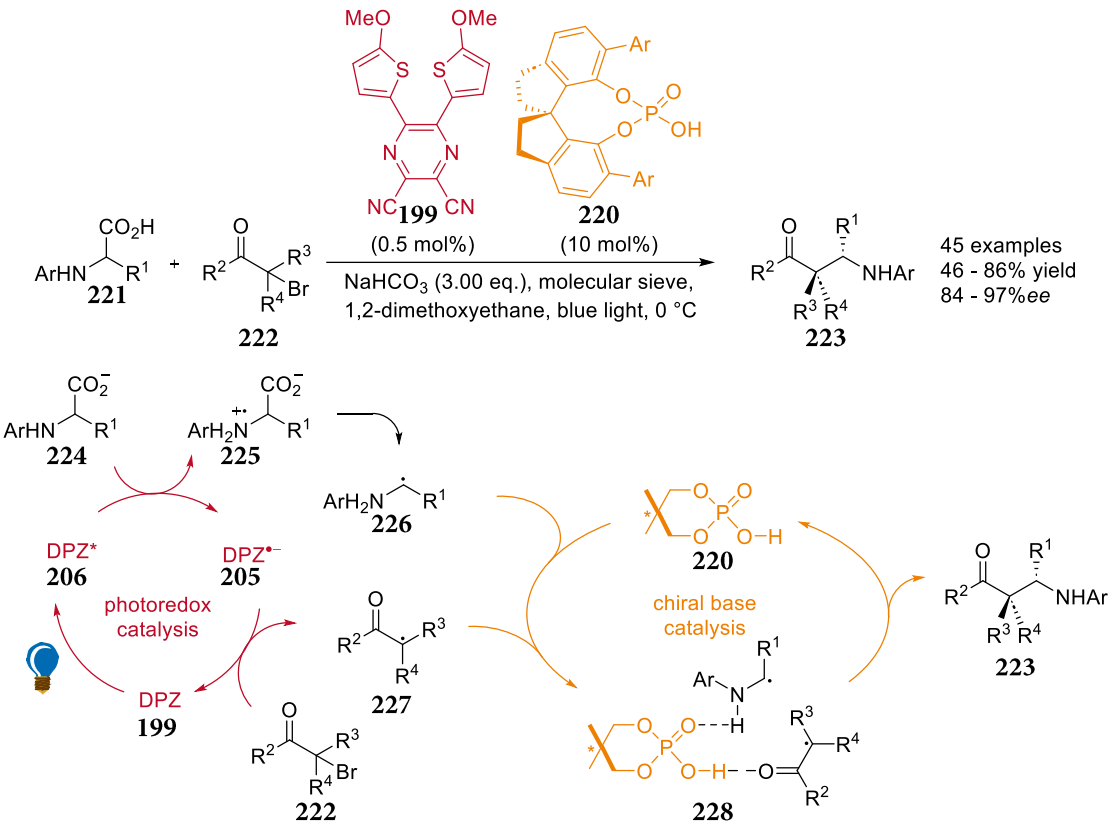

scheme 26. Enantioselective radical-radical coupling of α-bromoketones **222** with *N*-aryl-α-aminoacids **221** and mechanism thereof according to Jiang *et al.*[202]

1.3.1.2 Asymmetric dual metallaphotoredox catalysis

The combination of chiral metal catalysis with photoredox reactivity has produced a multitude of useful transformations. On the one hand, coordination to a chiral Lewis acid ensures a chiral environment in the enantiodetermining step; moreover, it leads to increased electrophilicity, lowered reduction potentials and stabilized (radical)anion intermediates due to electron withdrawal.

1.3.1.2.1 Dual metallaphotoredox catalysis exploiting enhanced electrophilicity for asymmetric radical addition

An important mechanistic principle of asymmetric metallaphotoredox catalysis is the exploitation of the electrophilicity of electron-deficient alkenes **233**, enhanced by Lewis acid coordination, for the enantioselective addition of radicals **229**, known as a photo-Giese-type reactions.[187] The common mechanistic principle of such transformations is based on reductive quenching of the excited photocatalyst **234** (PC) by a radical precursor containing a suitable leaving group **230**. The resulting radical **229** readily undergoes stereoselective conjugate addition to the asymmetrically activated Michael acceptor **233**. The resulting radical **232** completes the photocatalytic cycle and generates a Lewis acid enolate **236** that releases the enantiomerically enriched product **238** by protonation and keto-enol tautomerism. The Lewis acid serves for chirality transfer and accelerates the rate-determining step of conjugate addition (**scheme 27**).[187]

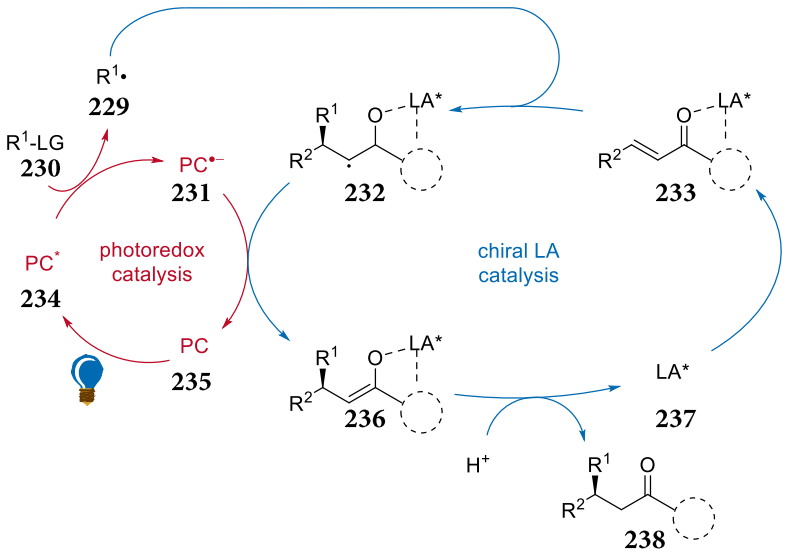

scheme 27. General mechanistic principle of asymmetric Lewis acid-catalyzed photo-Giese-type reactions.[187]

Based on this mechanism, a variety of transformations has been developed that differ in the source of the nucleophilic radicals. While Yoon *et al.* and Shibasaki *et al.* generated α-amino radicals from the corresponding trimethyl silanes **239**, Meggers *et al.* and Xiao *et al.* generated alkyl radicals from trifluoroborates **240** and Hantzsch esters **241**, respectively.[203-206] Furthermore, the Michael acceptors incorporate different heteroatom-containing groups in addition to the carbonyl group to ensure rigid two-point coordination to the chiral Lewis acid.[187, 188] Many different photocatalysts and chiral ligands were successfully employed. While Yoon *et al.* used the prototypical $[Ru(bpy)_3]Cl_2$ (**7**) and a C2-symmetric PyBOX ligand **245**, Shibasaki *et al.* used $Ir(ppy)_2(dtbbpy)PF_6$ (**31**) and a Cu complex with an axially chiral Segphos derivative (**85**).[203, 204] Both Meggers *et al.*

and Xiao *et al.* used the metal-free organic acridinium photocatalyst, but different chiral Lewis acids: Meggers *et al.* employed a chiral-at-metal rhodium complex **246**, the photophysical properties enabled its use as a bifunctional asymmetric photocatalyst in later research (chapter 1.3.2.2).[205] Indeed, a similar asymmetric photo-Giese-type reaction with dihydropyridines as alkyl radical precursors was developed by Meggers *et al.* in 2018 using the chiral-at-metal-complex without an additional photoredox catalyst.[207] Inspired by these results and the structure of Megger's chiral-at-metal complex, Xiao *et al.* designed a chiral Co-complex **247** whose tetradentate ligand also provided very good enantioselectivities due to its high configurational stability (**scheme 28**).[206]

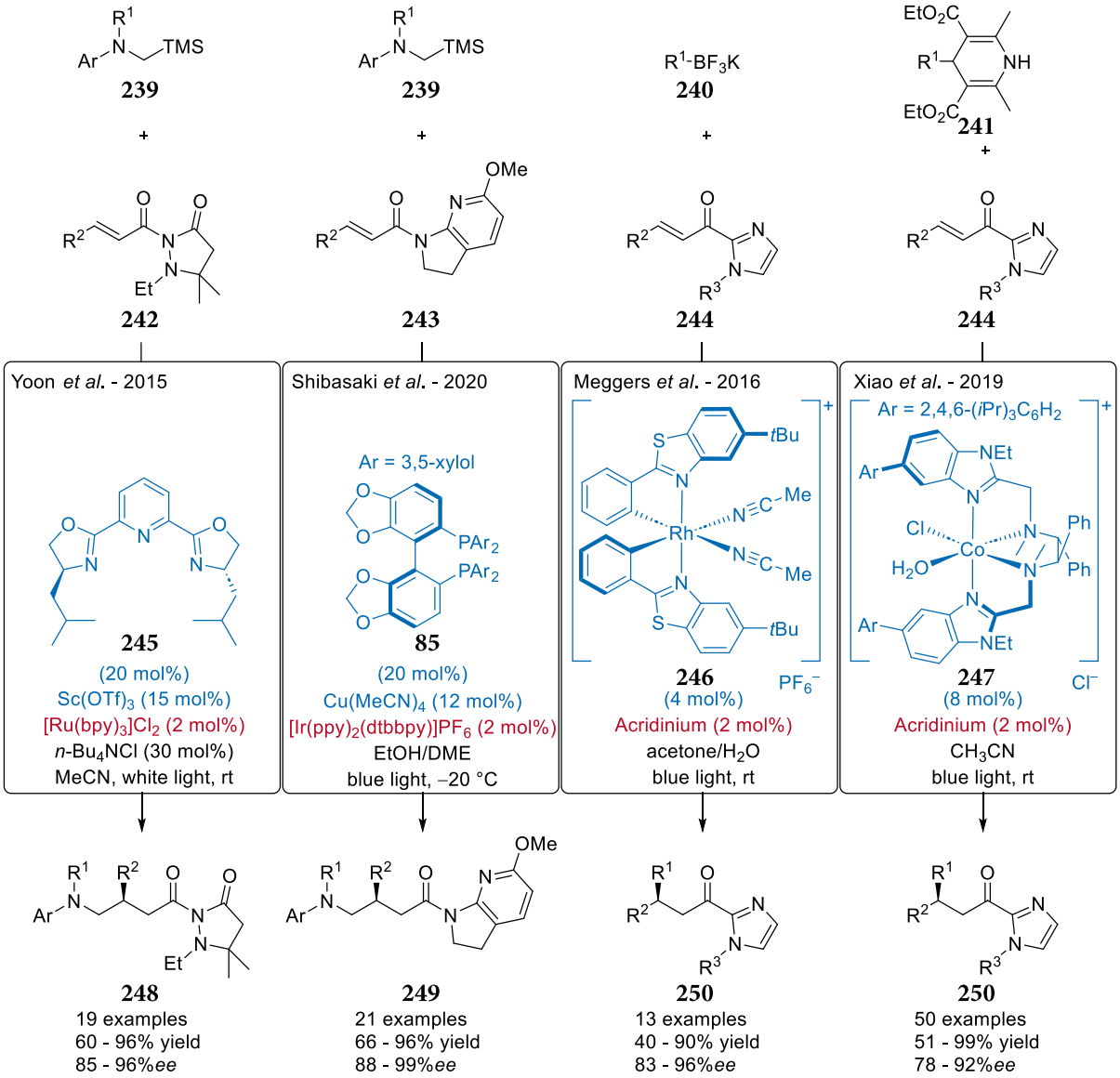

scheme 28. Selected examples of asymmetric metallaphotoredox-catalyzed photo-Giese-type reactions.[187, 188, 203-206]

Meggers applied this principle to a γ-selective C(sp^3)-H functionalization of amides, demonstrating that triple catalytic systems are also accessible involving Lewis acid catalysis. [187, 188, 208] Interaction of the amide **252** with the phosphate base catalyst adjusts the redox properties to induce a PCET that generates a *N*-centred amide radical **255** and a reduced photocatalyst **257**. The amide radical undergoes a 1,5-hydrogen atom transfer (HAT) to generate a

more stable terminal C-centred radical **256**. According to the previously discussed mechanism of the conjugate radical addition, this C-centred radical adds to the chiral Rh-coordinated substrate (**scheme 27**). However, Meggers *et al.* proposed the following alternative mechanism, which differs mainly in the order of the steps, especially that of the conjugate addition and reduction by the reduced photocatalyst **257**. According to this mechanism, reduction of the Rh substrate complex **261** occurs prior to radical-radical coupling in the chiral environment. The base catalytic cycle is then closed by protonation of the rhodium enolate **259**, enabling the product **254** to be exchanged for a new α,β-unsaturated 2-acylimidazole substrate **253** (**scheme 29**).[208]

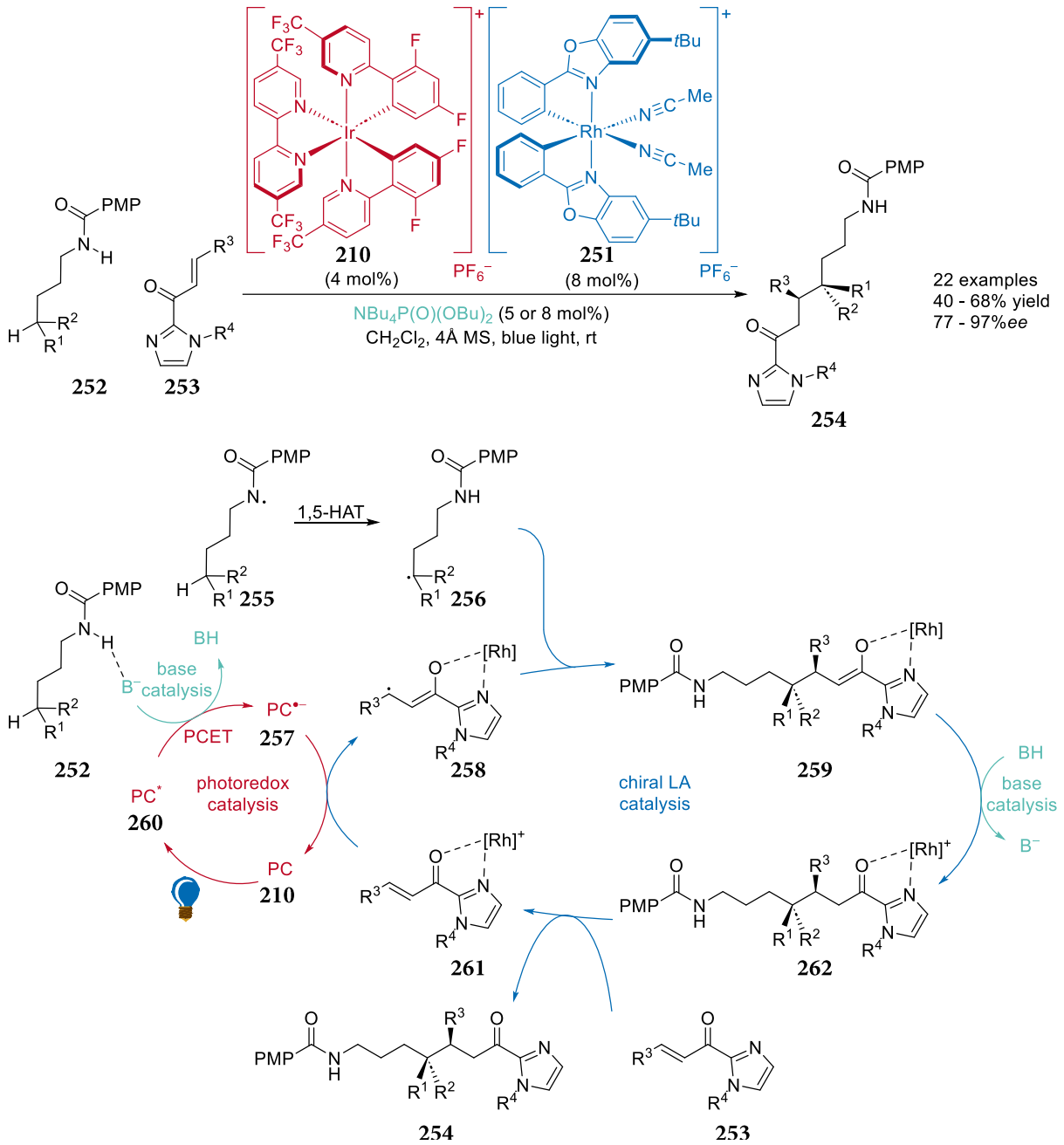

scheme 29. Triple catalytic asymmetric γ-selective C(sp³)-H functionalization of amides **252** and mechanism thereof by Meggers *et al.*[208]

1.3.1.2.2 Dual metallaphotoredox catalysis exploiting lowered redox potentials for photocatalytic reduction

Mechanisms of this type exploit the lowering of redox potentials of carbonyl groups, michael systems or imines caused by Lewis acid coordination for the generation of asymmetrically coordinated radicals, which either undergo radical radical coupling with a radical generated elsewhere in the mechanism, or add to a double bond.[187, 188]

One example is Megger's synthesis of 1,2-amino alcohols **265**.[209] As in previous examples, an α-silylamine **263** serves as radical precursor and reductively quenches the excited photocatalyst **12** to form an α-amino radical **267** and release a TMS cation **272**. The latter plays a crucial role as it serves as an *in situ* generated additional Lewis acid. A chiral-at-metal rhodium complex **246**, as well as the TMS-cation **272**, activate the 2-acylimidazole substrate **264** and allow its reduction to a ketyl radical **268**. Cross-coupling with the α-amino radical **267** in the chiral environment of the rhodium complex **246** and desilylation yields the enantiomerically enriched 1,2-amino alcohol **265**.[209]

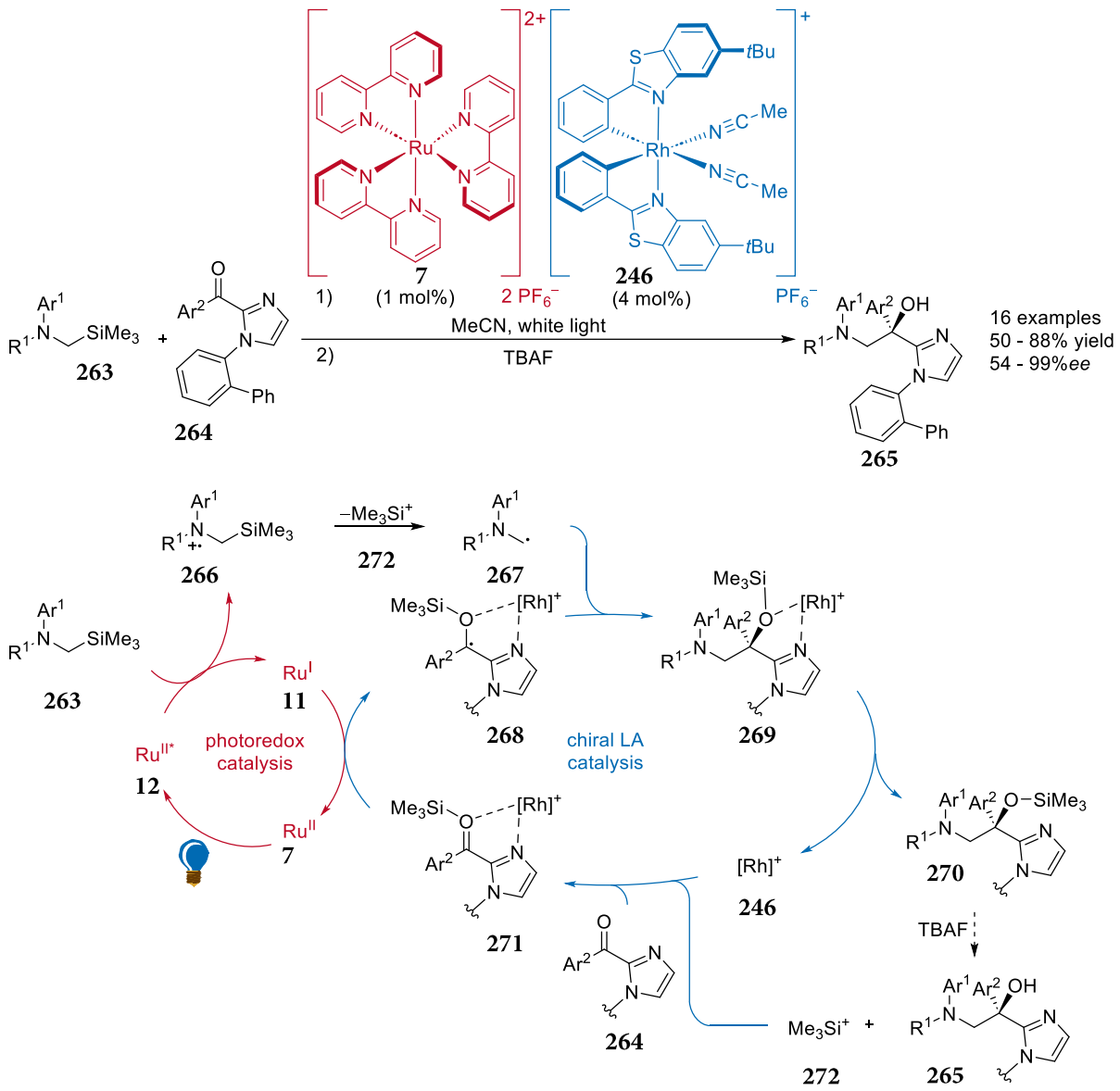

scheme 30. Enantioselective photocatalytic synthesis of 1,2-aminoalcohols **265** and mechanism thereof according to Meggers *et al.*[209]

This general principle of exploiting lowered redox potential of Lewis-acid coordinated substrates is also the foundation of many transformations by Yoon *et al.* who used Lewis acid activation to lower the potential of enones and cyclopropyl ketones for the reduction to allylic ketyl radicals and distonic radicals, respectively. In this way, they developed several initially racemic and then enantioselective (2+2) and (3+2) cycloadditions, first intra- then intermolecularly.[11, 210, 211] Their initial success was an intramolecular (2+2) cycloaddition of bis(enones) **6**, which revealed that Lewis acid activation was required for the key step of the first enone reduction.[11] The allylic ketyl radical **274** underwent intramolecular 5-exo-dig conjugate addition to form an α-carbonyl radical, that reacts with the lithium enolate to form the cyclobutane fragment.[11] Soon after, this reactivity was extended to an intermolecular crossed (2+2) cycloaddition.[210] The requirement of a Lewis acid for the reduction to an allylic ketyl radical, suggested an asymmetric adaptation with asymmetrically coordinated Lewis acids. Due to the kinetic lability of lanthanide complexes, i.e. to ensure the turnover from chelating product to monodentate substrate, chiral gadolinium and europium complexes were evaluated.[211] Since no or very little evidence of enantioselectivity was detected with the privileged ligand structures BINOL (**86**), TADDOL (**87**) and PyBOX (**66-69**), Yoon *et al.* developed a C1-symmetric Schiff-base ligand **281** (**scheme 31**).[211]

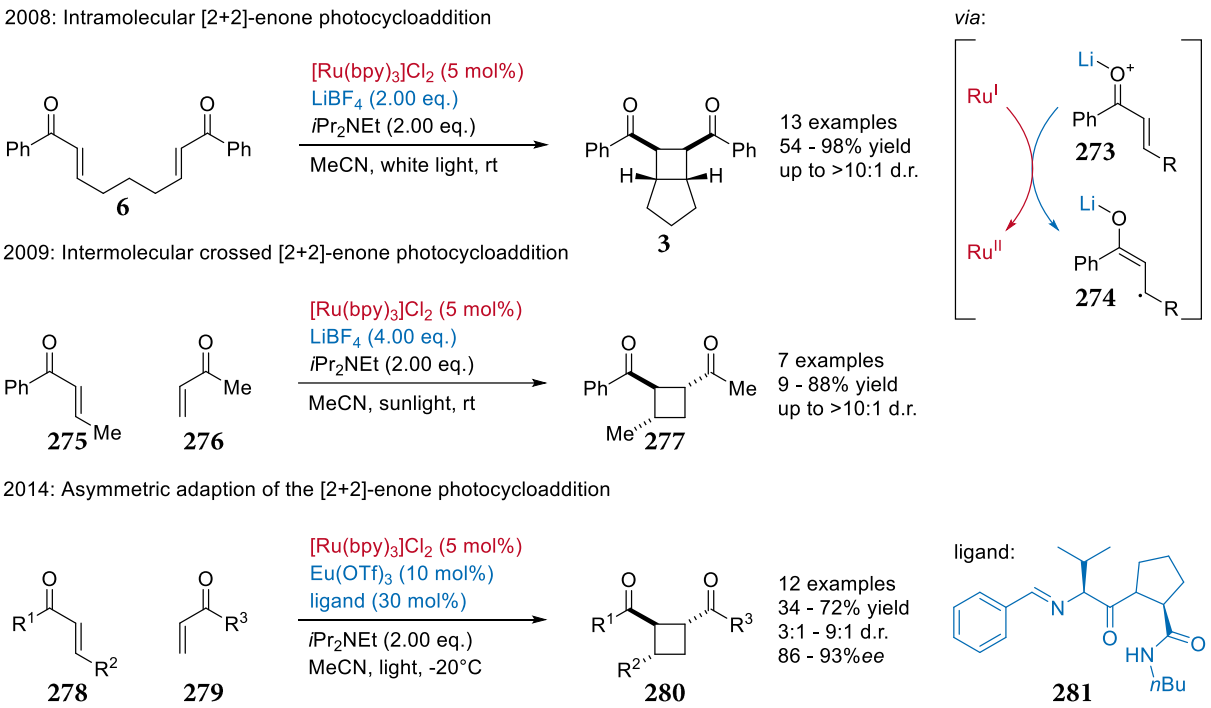

scheme 31. Development of an asymmetric (2+2)-enone photocycloaddition from racemic intra- and intermolecular (2+2)-enone photocyclizations by replacement of the required formerly achiral Lewis acid $LiBF_4$ with a chiral Schiff base **281** coordinated lanthanide complex according to Yoon *et al.*[11, 210, 211]

With cyclopropyl ketones **282** and **285** instead of enones **6**, **275**, **276**, **278** and **279**, the reduction proceeds to a ketyl radical that opens the cyclopropyl ring and forms the distonic radical **284**, paving the way for a formal (3+2)-photocycloaddition with formation of cyclopentanes **283** and **287** instead of cyclobutanes **3**, **277** and **280** (**scheme 33**).[212, 213] Following the initial intramolecular proof of concept, an extension to an intermolecular variant followed in 2016, as well as the asymmetric adaptation thereof (**scheme 32**). In this study, lanthanides were again

used as Lewis acids and a screening of asymmetric PyBOX ligands with different stereodiscriminating residues resulted in the best selectivities using *s*-Bu-PyBOX **288.**[212, 213]

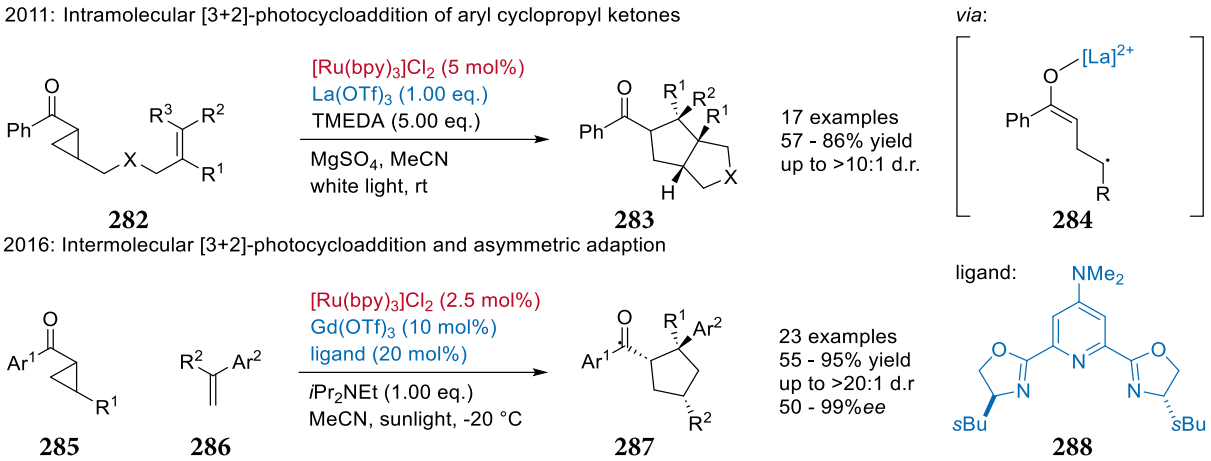

scheme 32. Intra- and intermolecular (3+2)-photocycloaddition and asymmetric adaption thereof by Yoon *et al.*[212, 213]

Mechanistically, after ring closure, either a reduction of the LA-activated cyclopropyl ketone substrate **285** takes place in the sense of a chain propagation or an oxidation to the product by the amine radical cation **291** occurs by means of a chain termination (**scheme 33**).[213]

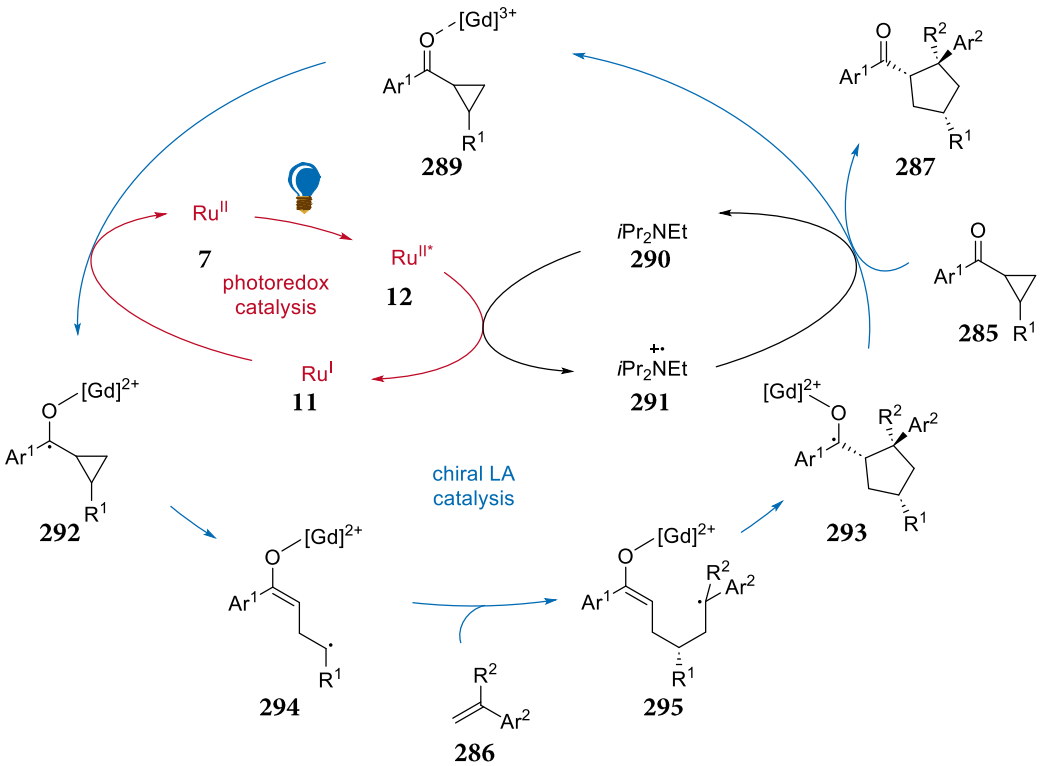

scheme 33. Mechanism of the (3+2)-photocycloaddition on the example of the asymmetric intermolecular variant proposed by Yoon *et al.*[213]

1.3.1.2.3 Dual metallaphotoredox catalysis exploiting chirale enolates as reductive quencher

In contrast to the previously discussed transformations, the LA-coordination-modified redox potentials allow direct reductive quenching of the excited photocatalyst by the substrate complex **303** rather than by a radical precursor containing a suitable leaving group or a quenching additive.[187, 188] Using chiral-at-rhodium complex **246** for substrate activation and chirality transfer, Meggers *et al.* achieved enantioselective α-aminations and α-alkylations of 2-acylimidazoles **298** employing aryl azides **296** and α-diazo esters **299** as radical precursors, respectively.[214] The excited photocatalyst **12** is reductively quenched by the rhodium-coordinated substrate **303**. The electron-deficient radical precursor **296** or **299** is reduced by the Ru(I) species **11**, thereby turning over the initiating photocatalytic cycle. Depending on whether an aryl azide **296** or diazo ester **299** was used, a nitrogen or a carbon-centred radical (**304** or **305**) is formed after the elimination of the only by-product, nitrogen. The radical **304** or **305** adds selectively to the chiral rhodium enolate **303** to form the ketyl radical **302**. The latter can then either reduce another equivalent of the electron-deficient radical precursor **296** or **299** in the sense of radical propagation, or convert to the Rh-coordinated product **301** by reductive quenching of the excited photocatalyst **12**. The enantiomerically enriched product **297** or **300** is released by exchange for a new 2-acylimidazole substrate **298** (**scheme 34**).[214]

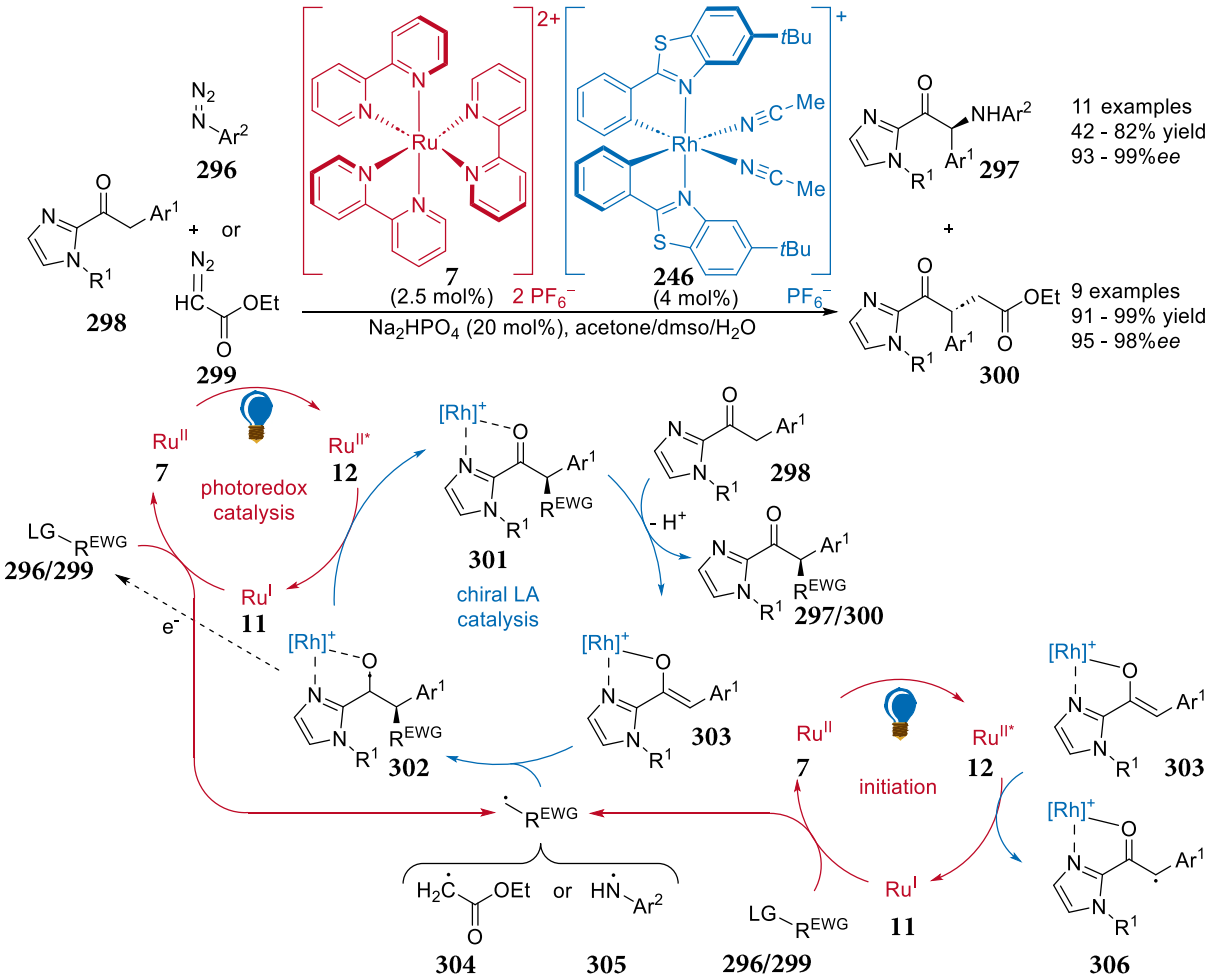

scheme 34. Mechanism of enantioselective α-alkylation and α-amination of 2-acylimidazoles **298** according to Meggers *et al.*[214]

1.3.1.3 Asymmetric dual biophotoredox catalysis

The combination of biocatalysis with photoredox reactivity has produced several interesting transformations in recent years, aiming at the exploitation of the outstanding selectivity of biocatalysts. The approaches focus both on the combination of an established photocatalyst with enzyme catalysts but more commonly on the utilization of redox-active cofactors such as NAD(P)H (**310**) (nicotinamide dinucleotide (phosphate)) or flavin mononucleotide (FMN) the redox potentials of which are modulated by photoexcitation, paving the way for an expansion of the natural ground state reactivity of enzymes.[177] The substrate activation relies on principles of H-bonding organocatalysis, on the one hand modifying the corresponding redox potentials and on the other hand spatially arranging the involved reaction partners for enantioselective HAT (hydrogen atom transfer) key steps.[188, 215, 216] Hyster *et al.* developed a concept of biophotoredox catalysis using rose bengal (RB) (**315**) as an external photosensitizer for deacetoxylation of α-acetoxyketone **308** with NADPH-dependent ene-reductases.[177] To prevent racemic background reactions outside the enzyme, a substrate was chosen whose redox potential is adjusted through hydrogen bonding with a tyrosine residue within the chiral environment of the active site. After reductive quenching of the excited photocatalyst **314** by NADPH (**310**), the activated substrate **313** is reduced to the ketyl radical **317**. A spin-centre shift leads to deacetoxylation and the formation of an α-carbonyl radical **318**. The selectivity-determining step is the hydrogen atom transfer of NADPH (**310**) from the back of the substrate radical **318**. A SET of NADP radical onto the ground state photocatalyst closes the catalytic cycle (**scheme 35**).[177]

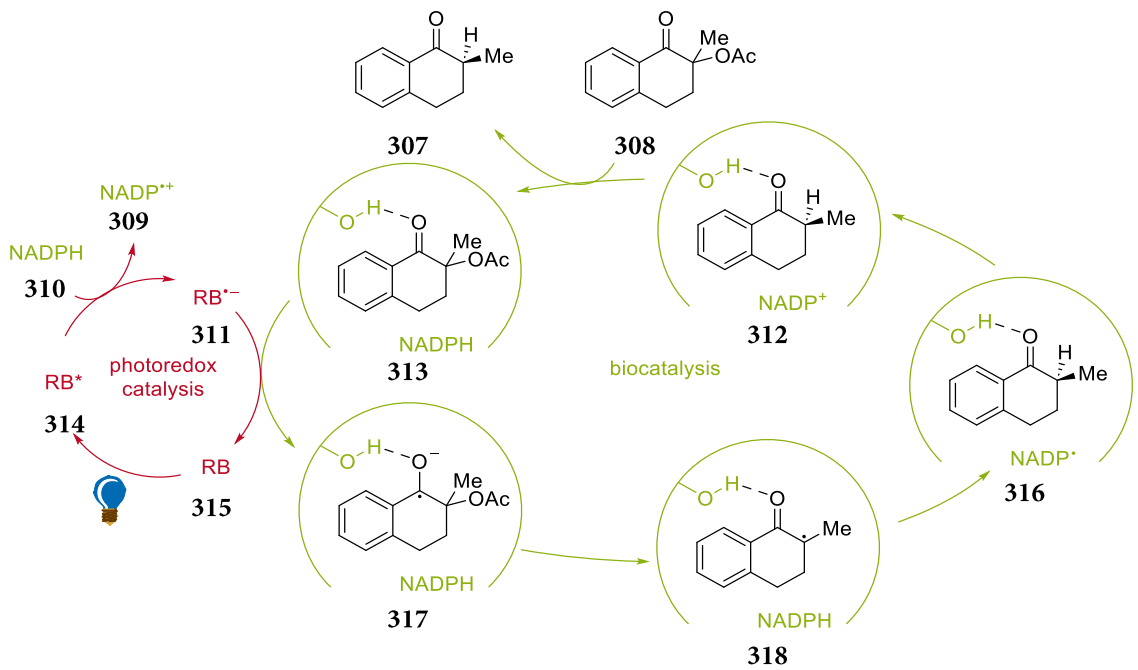

scheme 35. Mechanism of the asymmetric biophotoredox deacetoxylation of α-acetoxyketones **308** with NADPH-dependent ene-reductases according to Hyster *et al.*[177]

Given that some enzymes or their cofactors themselves show modified redox potentials and thus reactivities when irradiated, such an extension of natural enzyme reactivity by irradiation in the sense of single bifunctional catalysts (chapter 1.3.2.3) is even more common than the combination with an external photosensitizer.

1.3.2 Asymmetric single bifunctional catalyst approaches

In addition to combining established concepts of asymmetric organo-, metal- and biocatalysis with photoredox catalysts in the sense of separate, dual catalytic systems, some bifunctional catalysts have been developed that combine different concepts of asymmetric induction with photoredox reactivity within one catalyst.[187]

1.3.2.1 Asymmetric bifunctional organo-photoredox catalysis

Many of the different activation concepts of asymmetric organocatalysis have been incorporated into bifunctional photocatalyst concepts. Pioneering work in the field of bifunctional organo photocatalysis dates back to 2005 and work by Bach *et al.* who achieved the first enantioselective photoreaction by linking a benzophenone fragment with a chiral bicyclolactame *via* a rigid oxazole unit.[217] After photoinduced electron transfer (PET), cyclization occurred by intramolecular conjugate addition of an intermediate α-amino radical to C-4 of a quinolone fragment (transition state **319**). In this process, the substrate **320** is positioned in the chiral environment by two H-bonding interactions (**equation 13**).[217]

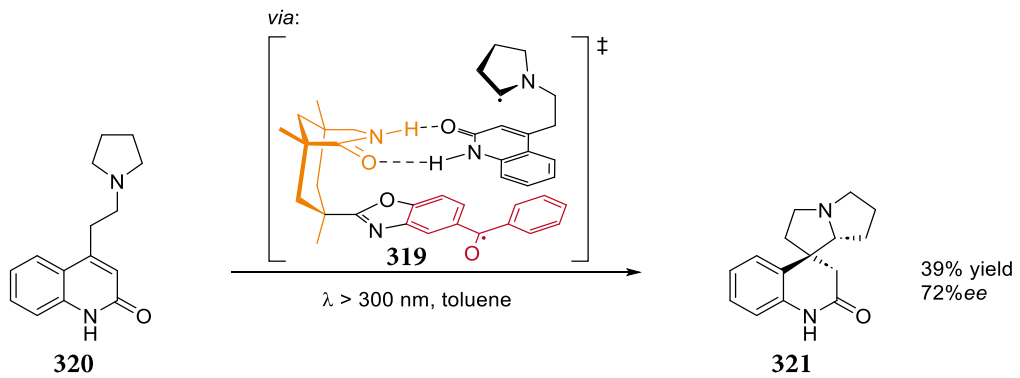

equation 13. Asymmetric intramolecular cyclization employing bifunctional organo-photocatalyst according to Bach *et al.*[217]

This general concept of covalently connecting a photosensitizer with an asymmetric H-bonding organocatalyst was modified and adapted several times using a thioxanthone structure as the photoactive element due to its significant absorption in the visible spectrum.[218] Similar to the initial work, the thioxanthone fragment was linked to different chiral H-bonding fragments, such as bicyclolactame or thiourea fragments, and used in intra- and intermolecular photocyclizations (**scheme 36**).[218-220] However, the latter construct yielded only modest enantiomeric excesses (12%*ee*).[220] In 2020, the thioxanthone fragment was linked to the commonly used (privileged) chiral BINOL-phosphate acid fragment, enabling intermolecular (2+2)-photocycloadditions of cyclic β-carboxyl enones **332** and olefins **333**.[221] The interaction of the substrate with the chiral Brønsted acid not only serves to attach the substrate **332** in the chiral environment, but also to modify its triplet energy. Since it was not possible to determine the enantiomeric excess by chiral HPLC, a derivatization was carried out by benzylation, revealing up to 86%*ee* (**scheme 36**).[221]

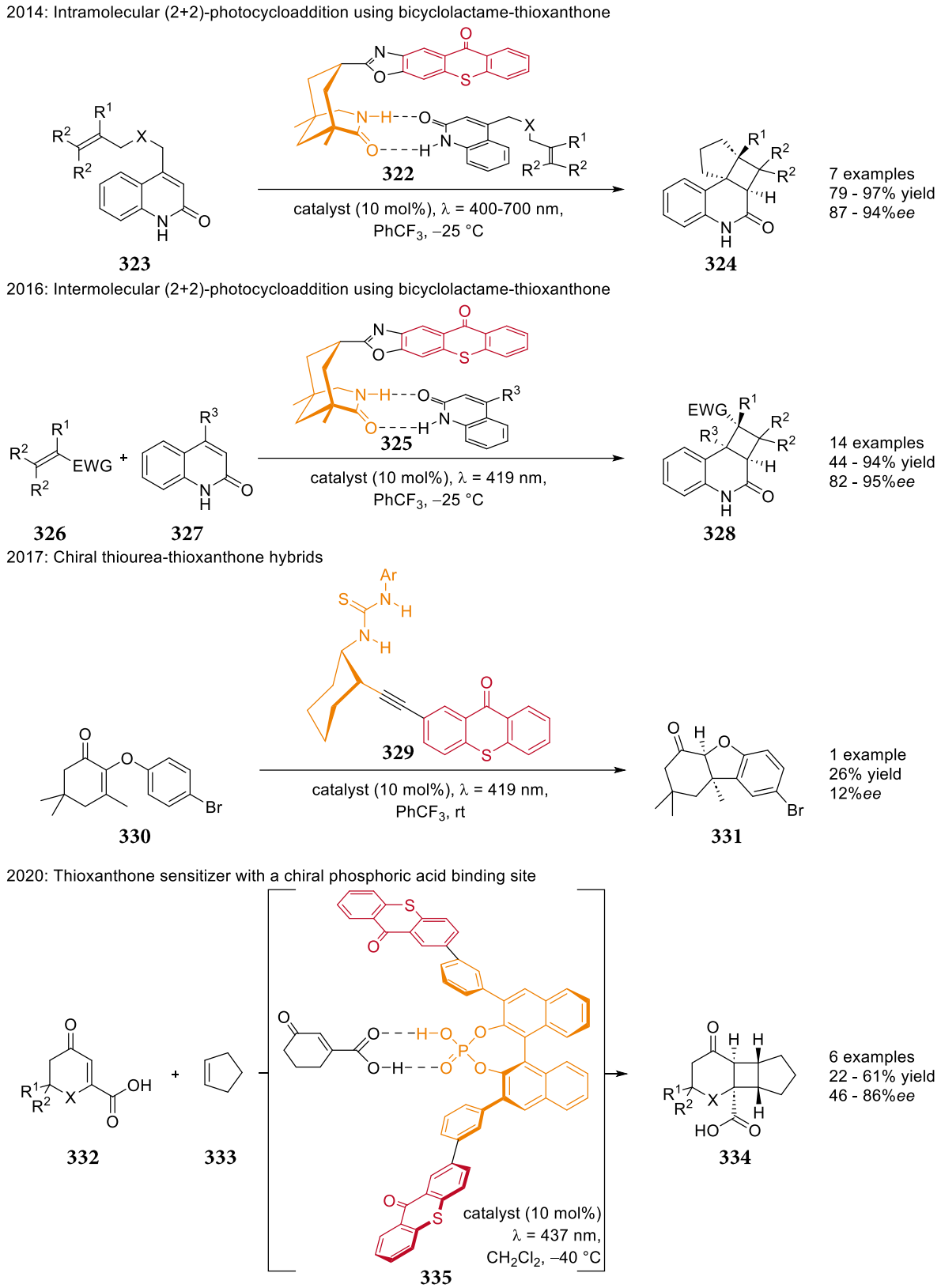

scheme 36. Selected examples of bifuncitonal asymmetric H-bonding thioxanthone photosensitizers and their application in asymmetric phototransformations by Bach *et al.*[218-221]

Structurally closely related is a concept by Aleman that links the thioxanthone structure with MacMillan's imidazolidinone organocatalyst **336**.[10, 222] It was used for an adaptation of MacMillan's pioneering α-alkylation of aldehydes **337** (**equation 14**), following the intially reported mechanism (**scheme 18**).[10, 222]

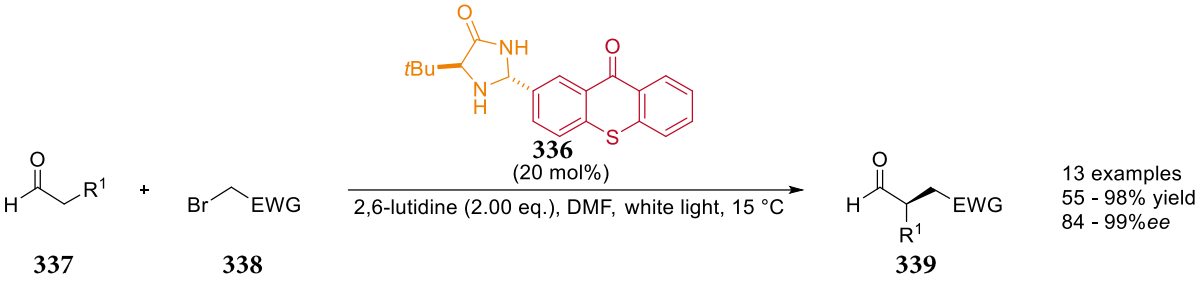

equation 14. Bifunctional photoaminocatalyst for the α-alkylation of aldehydes **337** according to Aleman *et al.*[222]

Besides these covalently linked catalyst concepts, some non-covalently connected combinations of chiral anions with cationic photocatalysts are also considered bifunctional organo-photocatalysts.[187] The chiral induction is usually based on the interaction of a substrate or intermediately formed radical cations with anionic axially chiral BINOL derivatives. Such chiral anions have been combined with organic photocatalysts, such as Fukuzumi's mesityl acridinium catalyst (Mes-Acr$^+$ (**340**)) or Nicewicz oxopyrylium catalyst (**348**), as well as with metal-based photoredox catalysts.

Luo *et al.* achieved an anti-Markovnikov hydroetherification based on the interaction of the chiral BINOL phosphate anion **341** with radical cations **342** formed by reductive quenching of the photoexcited Mes-Acr$^+$ catalyst.[223] The chiral anion **341** not only transfers chirality, but also mediates a proton transfer to the reduced phenylmalonodinitrile additive, which forms the product by H-atom transfer to the cyclized radical (**equation 15**).[223]

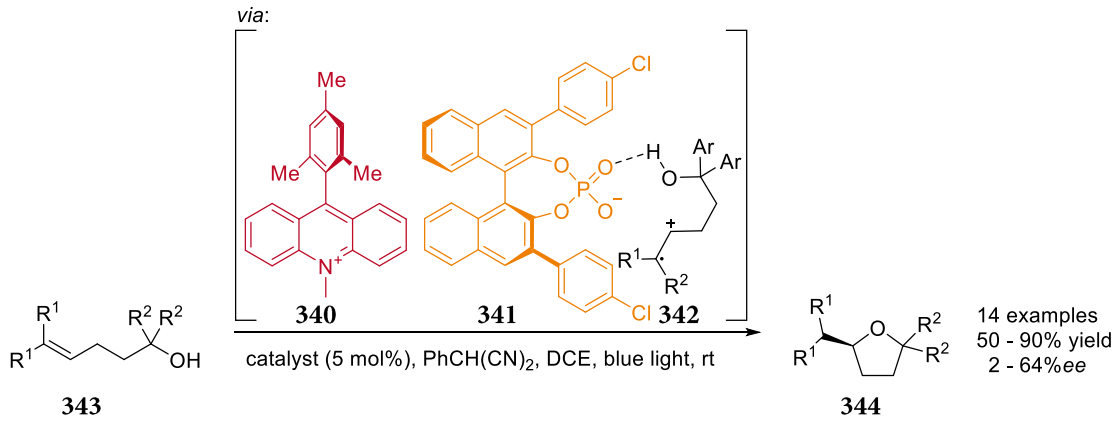

equation 15. Anti-Markovnikov hydroetherification with non covalently connected anionic chiral BINOL-phosphate **341** and cationic mesityl acridinium photocatalyst **340** as well as transition state of proposed H-bonding interaction between chiral phosphate **341** and key radical cation intermediate **342** according to Luo *et al.*[223]

Soon after and also based on ion-paired cationic photocatalyst **348** with an anionic chiral anion **349**, an intra- and intermolecular Diels-Alder reaction was published by Nicewicz *et al.*, proceeding *via* a cation radical intermediate **350**.[187, 224] It was assumed that these common intermediates resulting from dienophile oxidation

should pair with the chiral anion even without any additional coordinating functional group, such as a carbonyl group or hydroxyl group. Indeed, an inverse correlation of enantioselectivity and solvent dielectric constant confirmed that close ion pairing is required for chirality transfer. Furthermore, a catalyst screening revealed that only *N*-triflylphosphoramides **349** with sterically demanding substituents at positions 3 and 3'- of the BINOL backbone gave satisfactory results, which was attributed to lower nucleophilicity of the anions and thus increased reactivity. Using the combination of cationic oxopyrylium photocatalyst **348** and anionic *N*-triflylphosphoramide **349**, three intra- and three intermolecular cation-radical Diels-Alder transformations with moderate selectivities of up to 50%*ee* were achieved (**scheme 37**).[224]

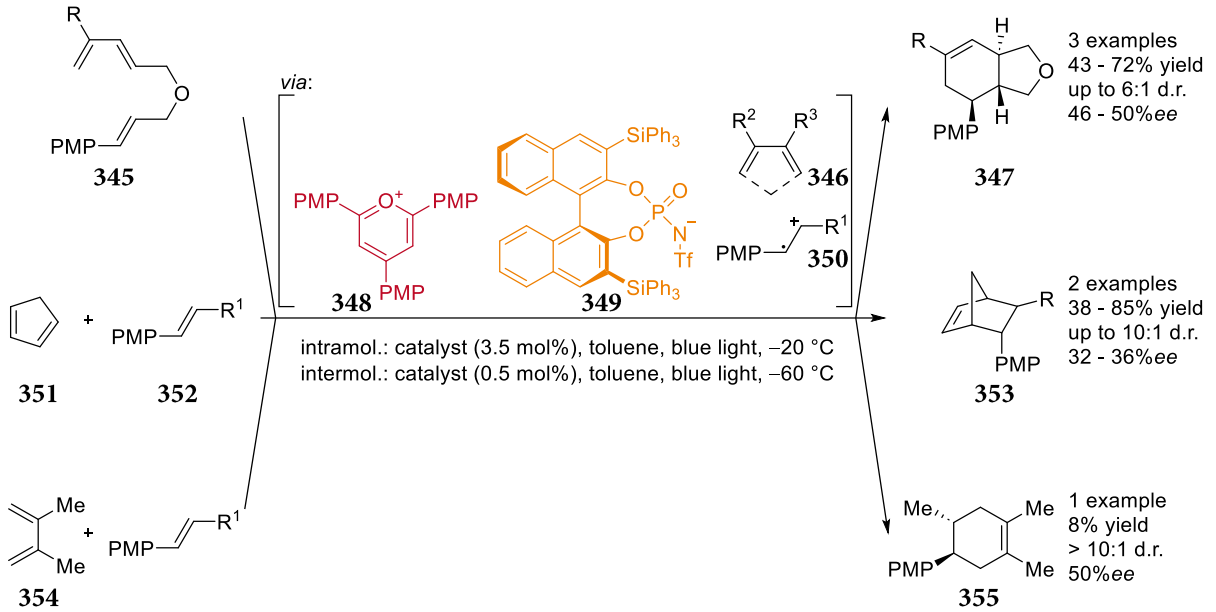

scheme 37. Asymmetric cation radical Diels-Alder reaction using a bifunctional ion-pair catalyst consisting of a cationic oxopyrylium photocatalyst **348** and an asymmetric BINOL-derived *N*-triflylphosphoramide anion **349** according to Nicewicz *et al.*[224]

Ooi *et al.* developed a related concept using an ion pair of a BINOL-derived chiral borate **356** as a non-nucleophilic anion for a cationic iridium photocatalyst **32**.[187, 225] The chiral anion **356** serves as an H-bond acceptor for urea derivatives of cyclopropylamine substrates **357**. The urea group in the substrate **357** not only functions as a directing group, but is also redox active as it is oxidized by the excited photocatalyst (*$[Ir^{III}]^+$ **360**) to form a *N*-centred radical cation **362**. The reduced $[Ir^{II}]$-complex **361** is uncharged, leaving the chiral borate ($^-$[B] **356**) for interaction with the substrate radical cation **362**. As in previously discussed (3+2)-cycloaddition of cyclopropyl derivatives (*vide infra*), further transformation proceeds *via* a distonic radical **363** that is derived from an equilibrium with the *N*-centred radical cation **362** by ring opening and that readily adds to α-alkylstyrenes **358**. This is followed by an enantiodetermining 5-exo-trig cyclization in the chiral environment of the anion. Final reduction yields the uncharged urea-cyclopentane **359** and regenerates the cationic $[Ir^{III}]^+$ complex **32** along with the chiral anion $[B]^-$ **356**. Alternatively, the cyclization can be followed by direct oxidation of a substrate **357** in the sense of radical propagation. By reaction with diethylenetriamine at 130 °C, the synthesis of chiral aminocyclopentanes with vicinal tertiary and quaternary stereocentres was achieved in this way (**scheme 38**).[225]

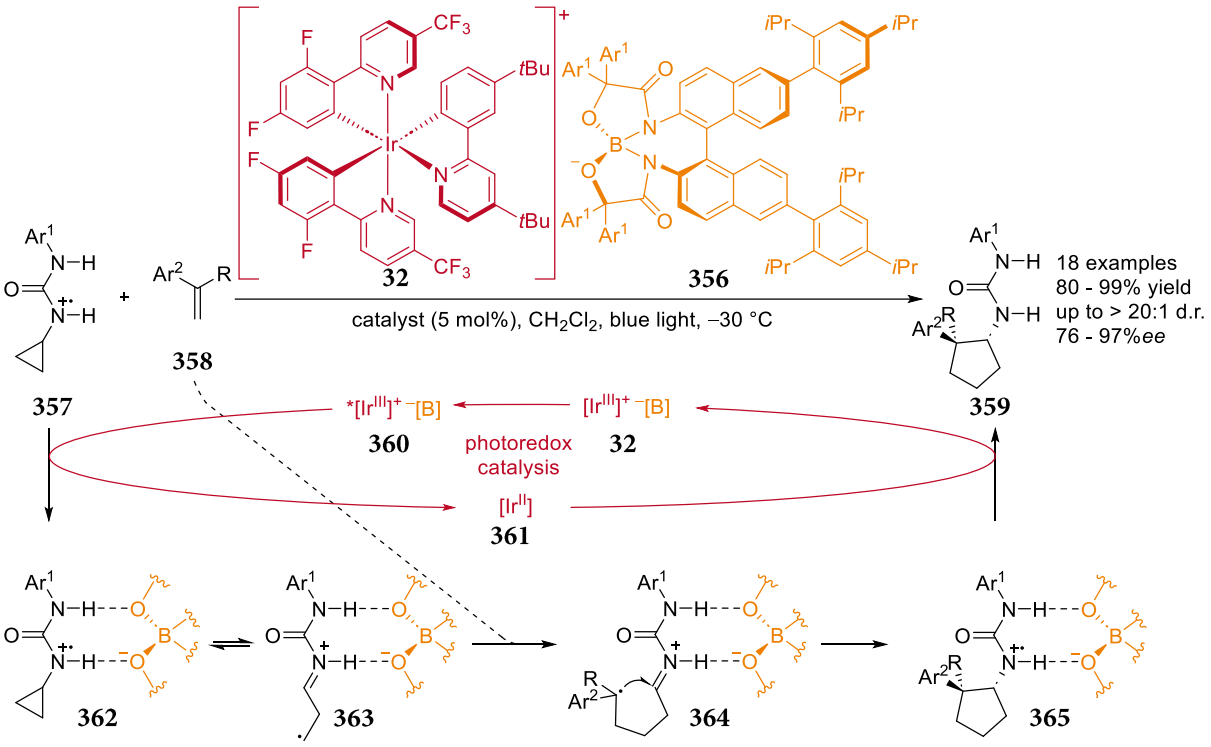

scheme 38. Asymmetric (3+2)-photocycloaddition of *N*-cyclopropylurea derivatives **357** with alkylstyrenes **358** using a bifunctional ion-pair consisting of a cationic Ir-photocatalyst **32** and an asymmetric BINOL-derived borate anion **356** according to Ooi *et al.*[225]

1.3.2.2 Asymmetric bifunctional metallaphotoredox catalysis

Bifunctional metal catalysts, which are responsible for both the asymmetric induction in the enantiodetermining step and for initiating photoredox reactivity, can be classified according to the origin of chirality.[187] Most approaches focus on the exploitation of chiral-at-ligand complexes and the ability of some to function both as photoredox and asymmetric catalyst structures, but also chiral-at-metal complexes were employed as bifunctional chiral photoredox catalysts by Meggers *et al.* The most commonly used chiral-at-metal complexes are characterized by a helical chiral arrangement of either 2-phenyl-benzoxazole or 2-phenyl-benzothiazole ligands in left-handed (Λ-enantiomer) and right-handed (Δ-enantiomer) screw-sense configuration (**figure 16**).[226]

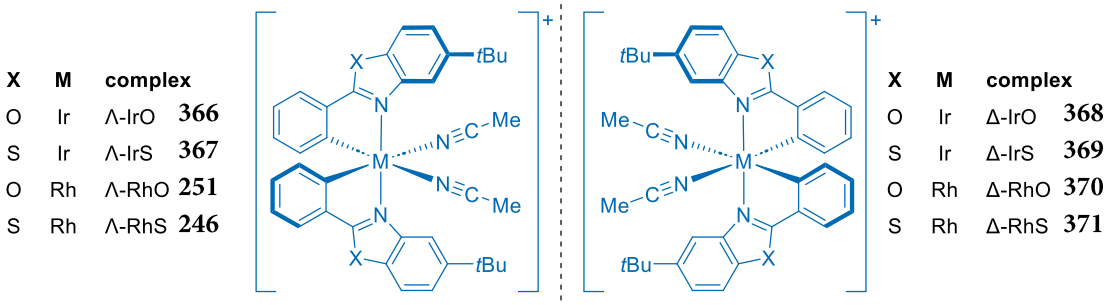

figure 16. Enantiomers of chiral-at-iridium **366**-**369** and chiral-at-rhodium **251**, **246**, **370** and **371** complexes with helical chiral arrangement of benzoxazole or benzothiazole ligands.[226]

In their initial application in 2014, Λ-IrO (**366**) and Δ-IrO (**368**) served as chiral Lewis acids in a non-photoredox related Friedel-Crafts alkylation.[227] As discussed earlier, they were subsequently employed successfully as chiral Lewis acids in combination with a photosensitizer (chapter 1.3.1.2).[205, 208, 209, 214, 228] Shortly after their initial application, Meggers *et al.* showed in a seminal report from 2014 that the chiral-at-Ir complex **367** or the corresponding substrate complex itself can serve not only for asymmetric induction but also as a photosensitizer for the asymmetric α-alkylation of 2-acylimidazoles **372**.[229]

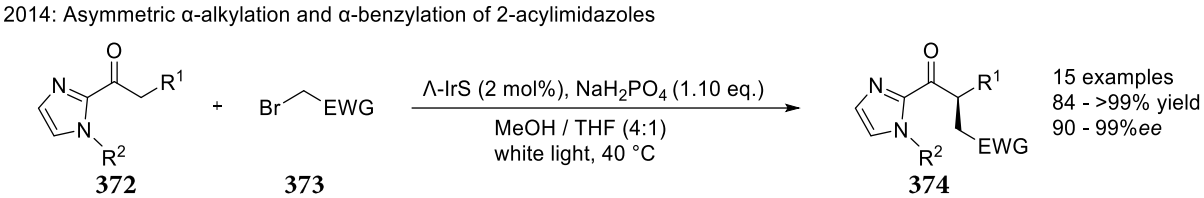

equation 16. Initial application of bifunctional chiral-at-Ir complex **367** for asymmetric induction and as a photosensitizer in the asymmetric α-alkylation and α-benzylation of 2-acylimidazoles **372** according to Meggers *et al.*[229]

The mechanism proceeds *via* the exchange of labile acetonitrile ligands against 2-acylimidazole enolates, resulting in the photoactive complex **375**, which upon visible light irradiation is capable of reducing electron-deficient radical precursors **373**.[229] The electrophilic radical **379** adds to the chiral enolate **382** in a stereocontrolled fashion, forming a ketyl radical **381** that either closes the photocatalytic cycle or initiates the formation of another electrophilic radical **379** according to a radical propagation mechanism (**scheme 39**).[229]

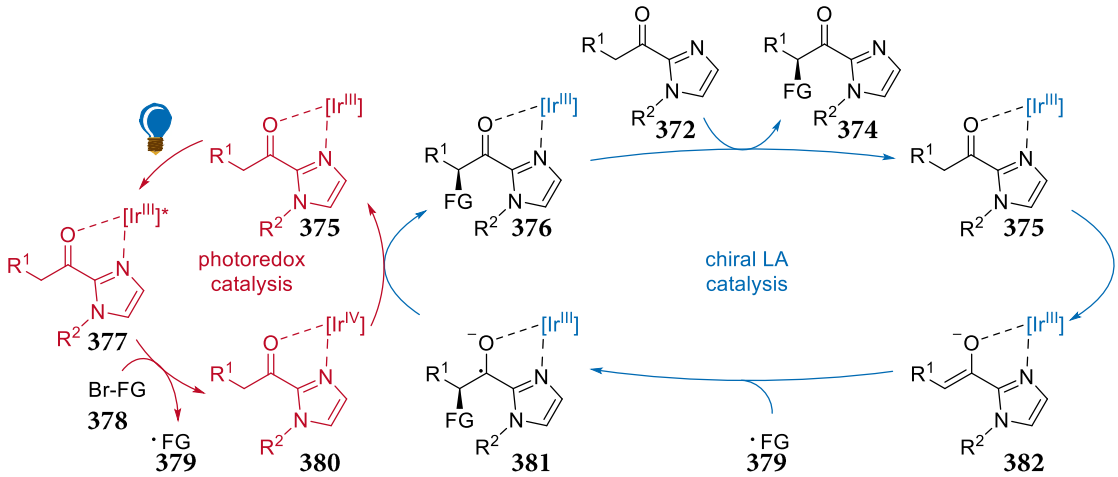

scheme 39. Mechanism of the initial application of bifunctional chiral-at-metal photocatalysts in the asymmetric α-alkylation and general mechanism of subsequent α-functionalizations.[229]

The high enantioselectivities of this transformation and all subsequent transformations involving chiral-at-metal complexes arise from steric shielding of one side of the substrate by the protruding *tert*-butyl residue of the helical-chiral 2-phenylbenzoxazole or 2-phenylbenzothiazole ligands.[207, 209, 226, 229-231] The optimization of the α-alkylation revealed an increase of yield, selectivity and decrease of reaction time from 97% yield, 95%*ee* and 3 h to quantitative yield, 99%*ee* with half the reaction time due to the switch from the benzoxazole to the benzothiazole fragment.[229] This was attributed to the longer C-S bond resulting in a decrease in the distance between the coordinated substrate and the stereodiscriminating *t*Bu group (**figure 17**).[229] In some later photoredox applications, the chiral-at-Rh analogue showed superior performance to the Ir catalyst, which was attributed to faster ligand exchange and turnover.[226]

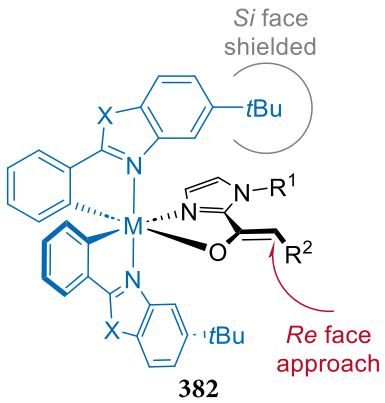

figure 17. Model of stereoinduction for transformations involving chiral-at-metal complexes on the example of Meggers α-functionalization of 2-acyl-imidazoles.[229]

In the following years, a variety of versatile transformations were developed using chiral-at-metal complexes as chiral photosensitizers. Based on the mechanism of the α-alkylation, the reactivity was extended to asymmetric α-trichloromethylation of 2-acylimidazoles and 2-acylpyridines (**383**), as well as to α-perfluoroalkylations of 2-acylimidazoles **386** providing excellent enantioselectivities of up to >99.9%*ee*.[232, 233]

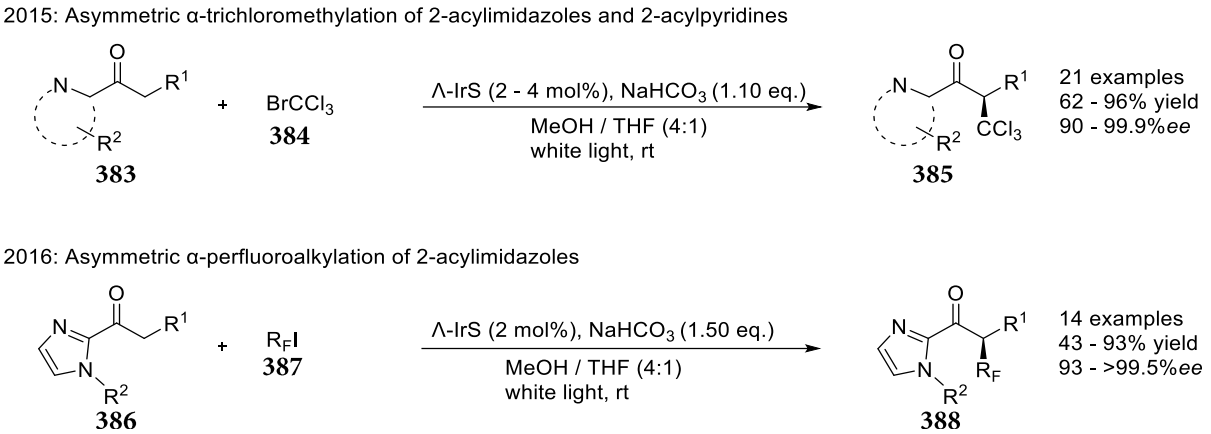

scheme 40. Application of the bifunctional chiral-at-metal complex **367** in the asymmetric α-trichloromethylation and α-perfluoroalkylation by Meggers *et al.*[232, 233]

In addition to the α-functionalization of metal enolates, chiral-at-rhodium complex **391** has been successfully employed in an asymmetric β-C-H-functionalization.[234] Exploiting the strongly reducing excited rhodium enolate **394** for a SET and β-proton transfer onto a 1,2-dicarbonyl compound **390**, radical coupling in the chiral environment and protonation yields the product of β-functionalization **392** involving two adjacent stereocentres (**scheme 41**).[234]

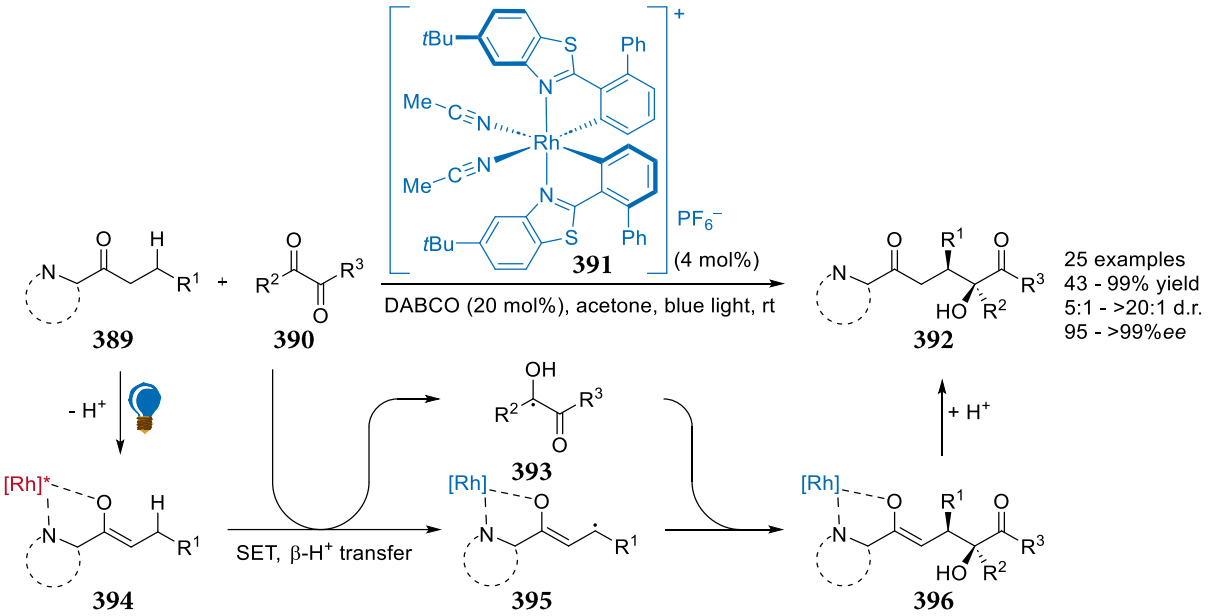

scheme 41. Asymmetric β-C-H-functionalization of 2-acylimidazoles and 2-acylpyridines (**389**) with 1,2-dicarbonyl compounds **390** using bifunctional chiral-at-rhodium catalyst **391** according to Meggers *et al.*[234]

Besides these transformations in which the excited chiral-at-metal complex served as a reducing agent, it can also function as an oxidant, as shown in the asymmetric conjugate addition of alkyl radicals to chiral Rh-acylenones.[207] The excited state Rhodium enolate complex **403** oxidizes an alkyl-Hantzsch ester **398** to liberate an alkyl radical **401** that recombines with the asymmetrically coordinated β-carbonyl radical **404** in the enantiodetermining step (**scheme 42**).[207]

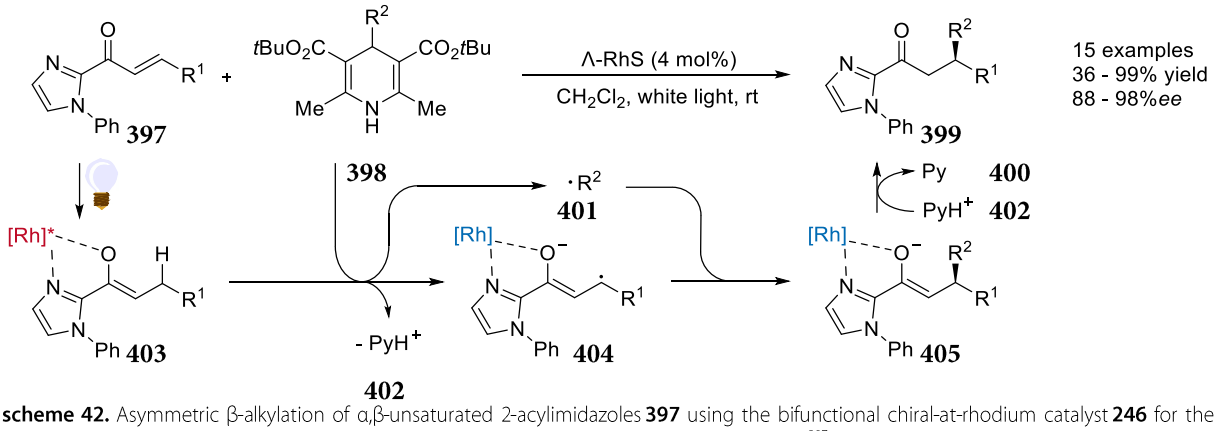

scheme 42. Asymmetric β-alkylation of α,β-unsaturated 2-acylimidazoles **397** using the bifunctional chiral-at-rhodium catalyst **246** for the oxidative generation of alkyl radicals **401** from Hantzsch esters **398** according to Meggers *et al.*[207]

In addition, the chiral-at-metal complexes have been used in asymmetric (2+2) photocycloadditions of metal enones and in (3+2) photocycloadditions of cyclopropyl ketones.[231, 235] In the (2+2)-cyclization, ISC of the excited metal enones **409** is followed by selective addition to the alkene **407**. Another ISC paves the way for ring closure yielding asymmetric cyclobutanes **408** with vicinal all-carbon quaternary stereocentres with excellent selectivities (**scheme 43**).[231]

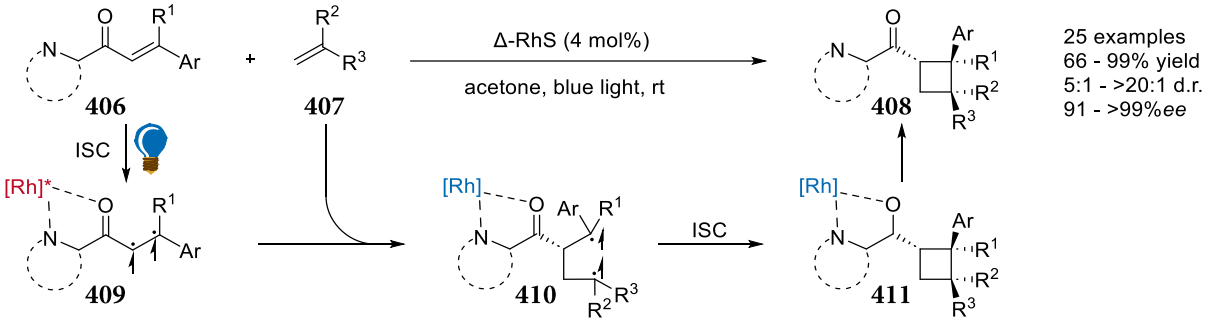

scheme 43. Asymmetric (2+2)-photocycloaddition of enones **406** using the bifunctional chiral-at-rhodium catalyst **371** for the synthesis of cyclobutanes **408** with vicinal all-carbon quaternary stereocentres according to Meggers *et al.*[231]

The (3+2)-cycloaddition follows a mechanisms which is related to the photocyclizations described by Yoon *et al.*[212, 213] Thus, a reduction of a coordinated cyclopropyl ketone initiates ring opening to the key distonic radical intermediate **416**, which undergoes a (3+2) cycloaddition with a variety of alkenes and alkynes (**413**) in the chiral environment. Final oxidation releases the product **414** and turns over the catalytic cycle (**scheme 44**).[235]

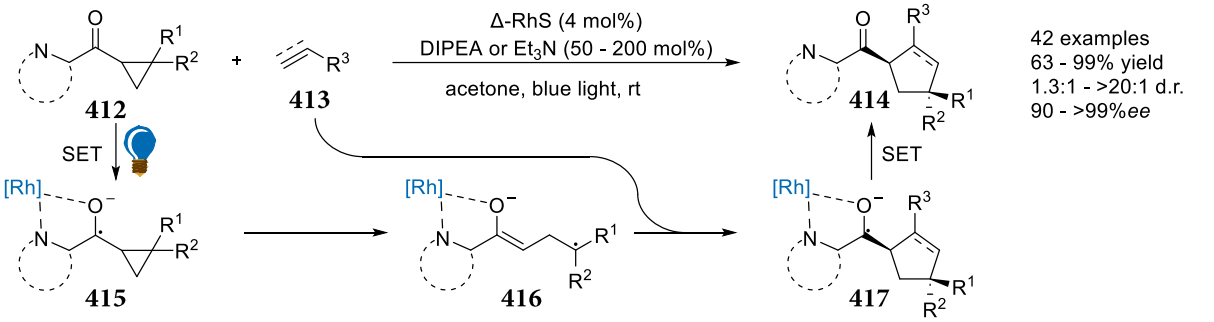

scheme 44. Asymmetric (3+2)-photocycloaddition of cyclopropyl ketones **412** with alkenes and alkynes (**413**) using the bifunctional chiral-at-rhodium catalyst **371** according to Meggers *et al.*[235]

In bifunctional asymmetric photocatalysts that both initiate photoredox reactivity and serve for chirality transfer, the chiral information can also originate from chiral ligands.[187] In a seminal report by Fu and Peters *et al.* from 2016, chiral Cu-spirophosphine complexes were used for asymmetric cross-coupling of racemic tertiary α-haloamides **419** with carbazoles **420**.[187, 236] After deprotonation of the carbazole **420** and coordination to the chiral copper complex **427**, the excited Cu(I)-carbazolide **423** reduces the α-chloro carbonyl compound **419** to the corresponding α-carbonyl radical **422**. The C-N bond formation occurs after addition of the alkyl radical **422** and enantiodetermining reductive elimination (**scheme 45**).[236]

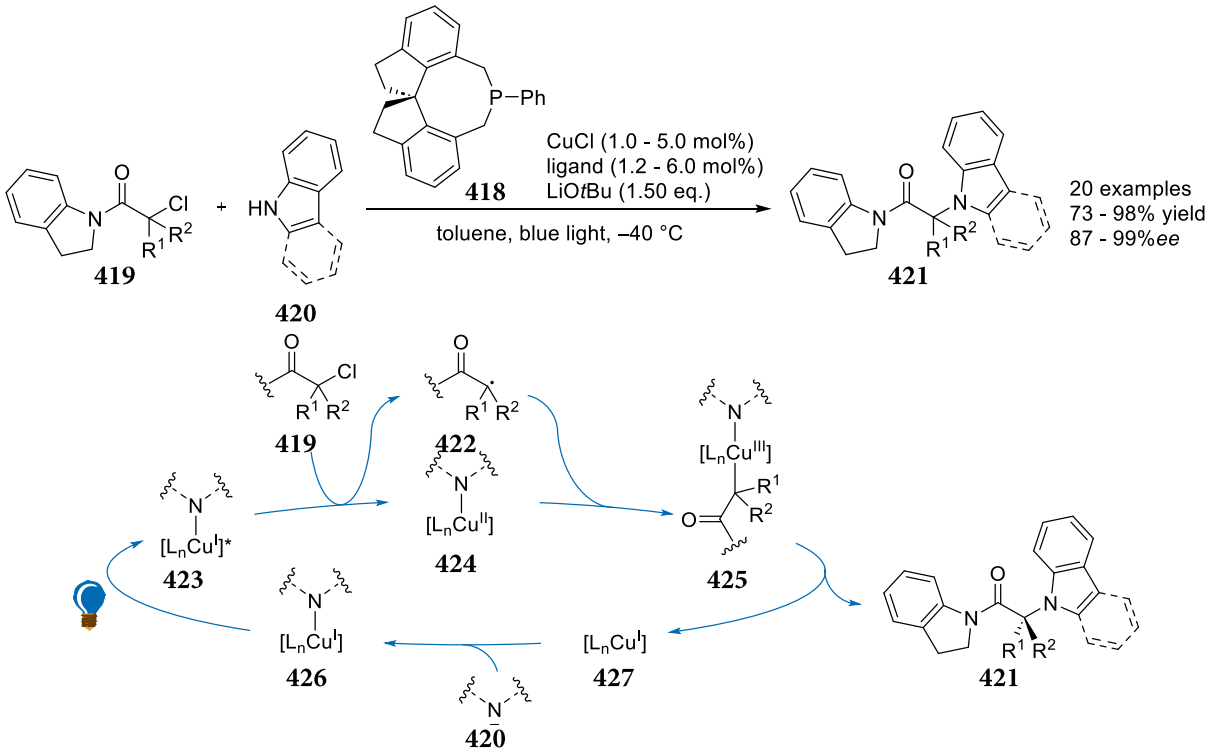

scheme 45. Asymmetric copper-catalyzed C-N cross coupling and mechanism thereof according to Peters and Fu *et al.* [236]

This seminal report was followed by further transformations based on asymmetric Cu complexes, often involving bisoxazoline-like ligands.[187] Mechanistically similar, Wang and Xu *et al.* succeeded in developing a multicomponent asymmetric cyanofluoroalkylation of alkenes **431**.[237] A perfluoroalkyl radical **437** from the oxidative quenching of excited Cu(I) complex **440** adds to an alkene **431**. The resulting radical forms a Cu(III) species **441**, allowing enantioselective reductive elimination to give the product **436** and close the cycle. Screening of several privileged structures (BINAP **46**, BINOL-phosphate, salen **90**) revealed the class of bisoxazolines to be particularly promising, of which the cyclopropylindanoyl-BOX-ligand **428** gave the best results (**scheme 46**).[237]

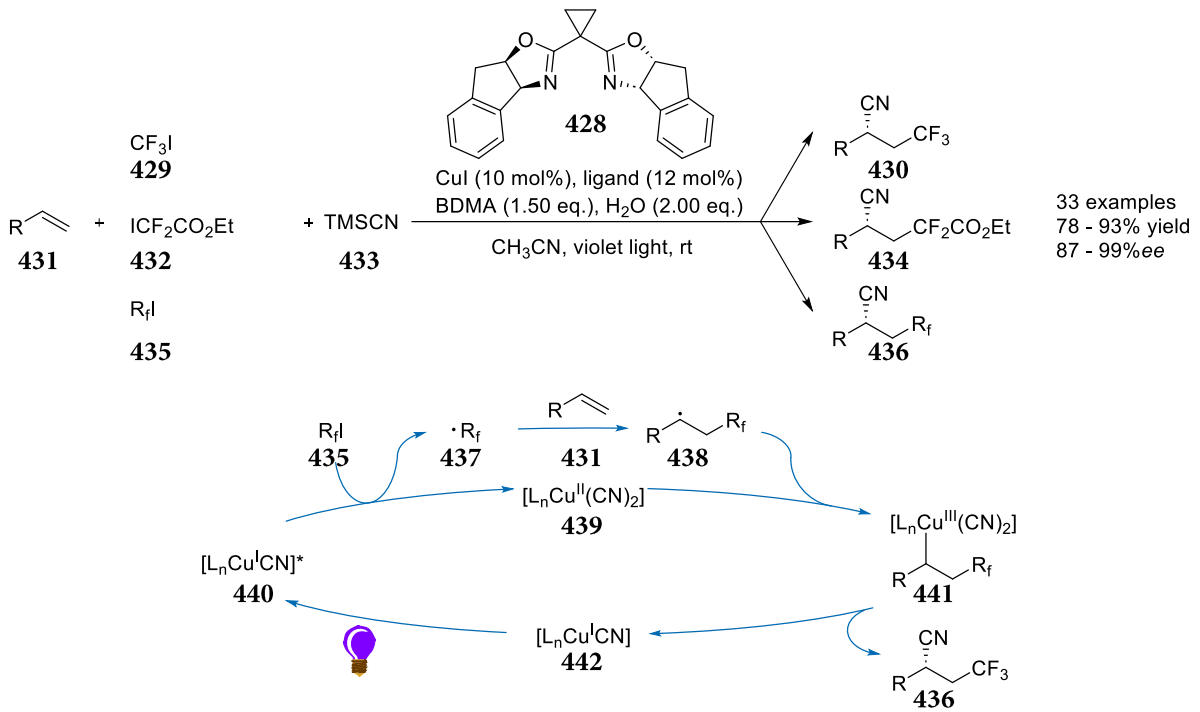

scheme 46. Asymmetric cyanofluoroalkylation of alkenes **431** using copper bisoxazoline as bifunctional catalyst and mechanism thereof according to Wang and Xu *et al.*[237]

Zhang and Zhang *et al.* also succeeded in a dual alkene functionalization, however involving the attachment of two alkyl residues (dual carbofunctionalization).[187, 238] This transformation also follows a similar mechanism, although with the additional formation of the photoactive Cu-acetylide species **453**, which reduces the alkyl iodide radical precursor **446** after excitation with visible light. Analogous to previous mechanisms, the addition to the alkene **444**, subsequent coordination to the complex **451** and enantiodetermining reductive elimination takes place. The chirality transfer occurred from the BOX-related BOPA (bis(oxazolinylphenyl)amide) ligand (**443**) (**scheme 47**).[238]

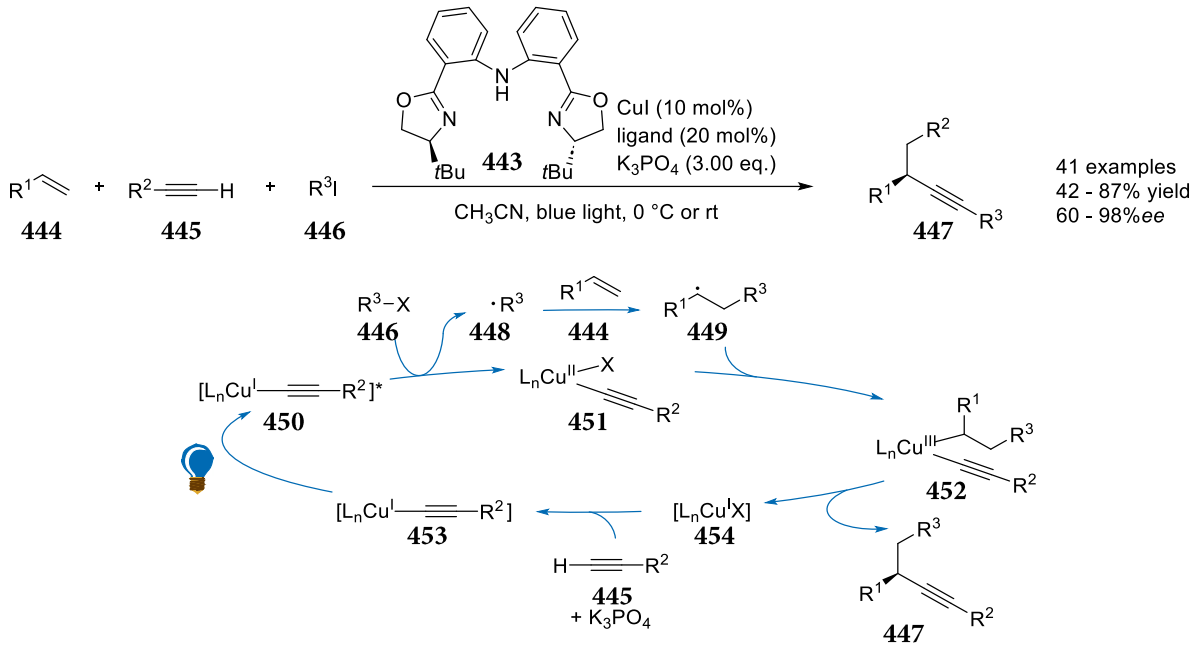

scheme 47. Asymmetric copper-catalyzed photoinduced dual carbofunctionalization of alkenes and mechanism thereof according to Zhang and Zhang *et al.*[238]

Also employing Cu-BOX complexes, Gong *et al.* achieved various useful transformations, such as an α-alkylation and α-aminoalkylation of imines, as well as an aerobic cross-dehydrogenative coupling, although exploiting different mechanisms.[187, 239] In the initial alkylation of imines **455** and **459**, the oxidation of alkyl trifluoroborate radical precursors **456** or **460** by the excited Cu(II)-BOX complex **466** occurs upon irradiation with visible light. The corresponding alkyl radical **463** adds to the Cu-coordinated imine substrate **468** in the chiral environment, generating a coordinated enantioenriched amino radical cation **465** that is reduced to the coordinated product **469** by the reduced Cu(I) species **464** (**scheme 48**).[239]

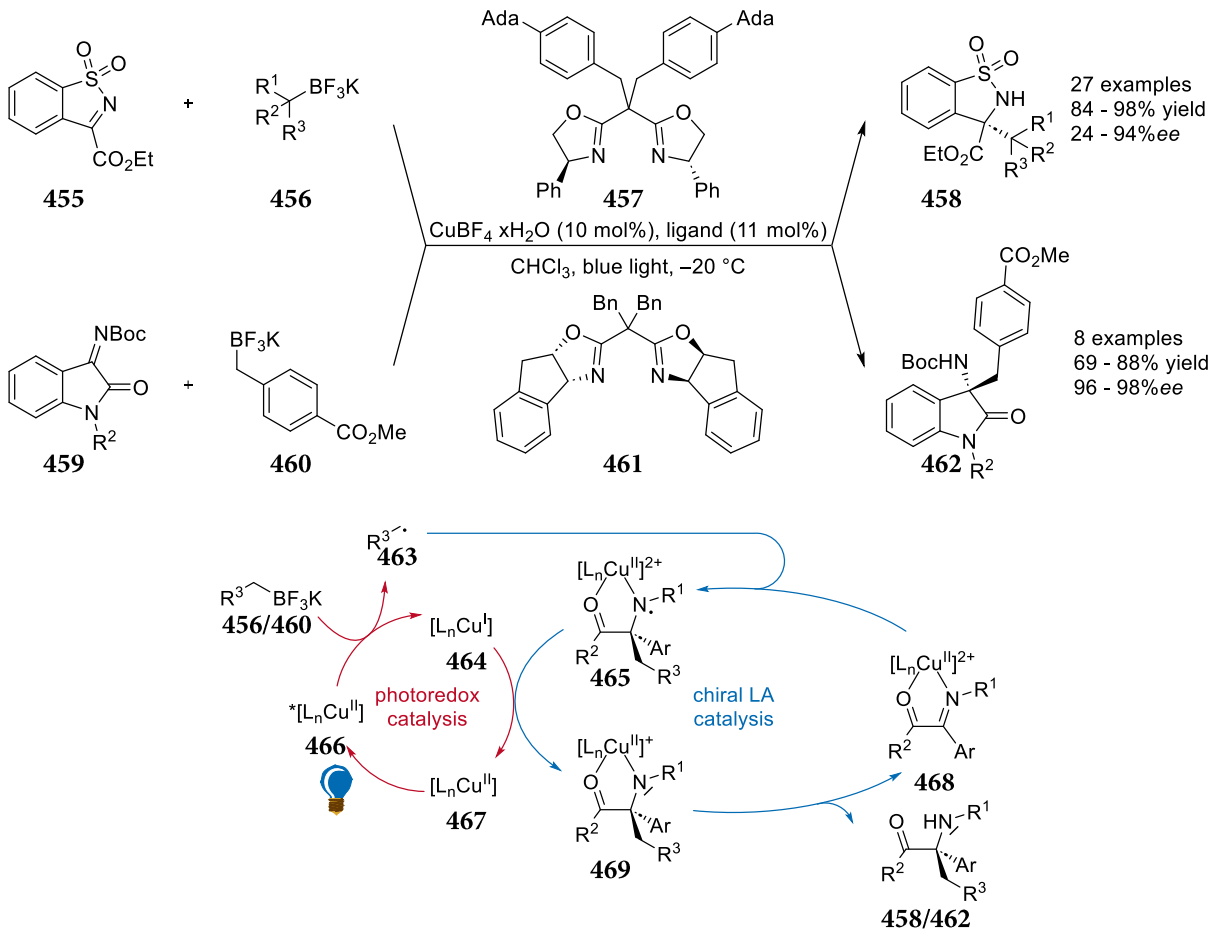

scheme 48. Asymmetric copper-catalyzed photoinduced alkylation of imines **455** and **459** and mechanism thereof according to Gong *et al.*[239]

Also based on Cu-BOX complexes, shortly afterwards Gong *et al.* succeeded in an enantioselective α-aminoalkylation of acylic imines **470**, wherein the photoactive species **476** is formed *in situ*.[187, 240] Initially, the silylamine radical precursor **471** is oxidized by the ground state Cu(II) complex **479**. The released α-amino radical **478** reacts selectively with a coordinated imine substrate **477** in the chiral environment of the BOX ligand **472**. The reduced Cu(I) complex **476** formed at the beginning is photoactive and, after excitation, capable of reducing the *N*-centred radical **475** to give the enantioenriched diamine **473**.[240]

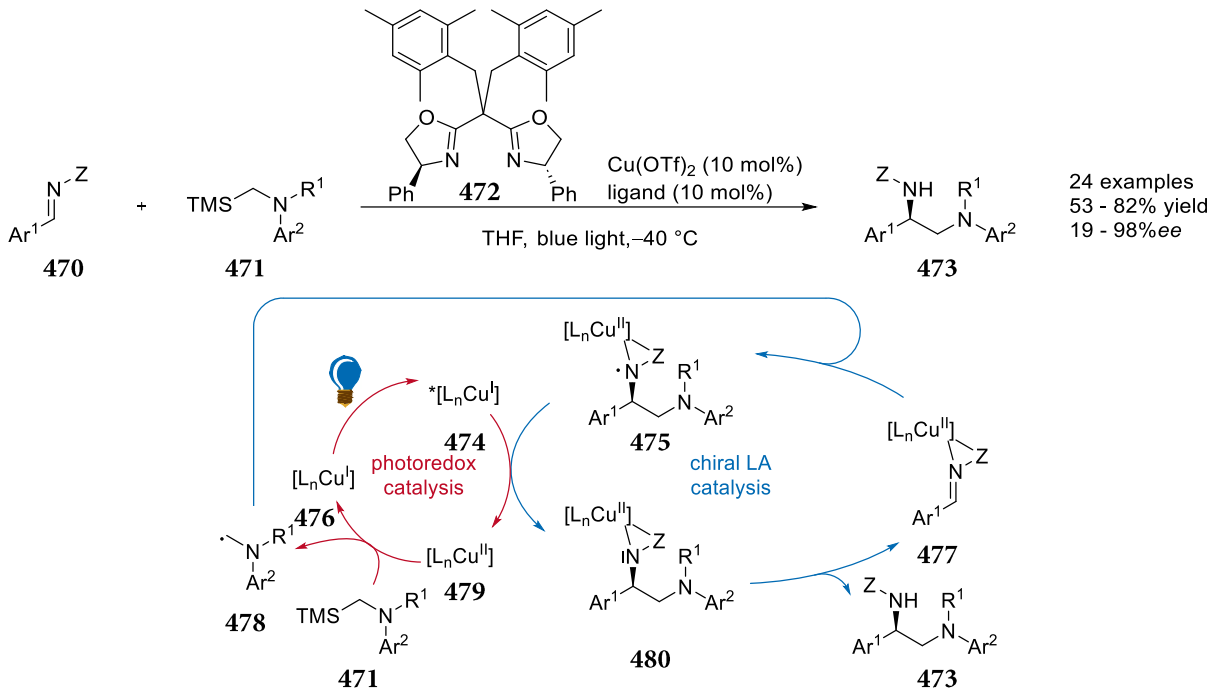

scheme 49. Asymmetric copper-catalyzed α-aminoalkylation of acyclic imines **470** and mechanism thereof according to Gong *et al.*[240]

In a mechanistically different approach, the Cu photocatalytic cycle serves on the one hand for the visible light-induced oxidation of a xanthene derivative **483**, and on the other hand for the reduction of atmospheric oxygen **491** to the hyperoxide anion (**488**), paving the way for the formation of a xanthene peroxide **490**, which upon protonation forms the xanthenyl cation **494** - the actual electrophile of this transformation.[187, 241] In the chiral environment, the enantiodetermining C-C bond linkage with the Cu-enolate **495** takes place (**scheme 50**).[241]

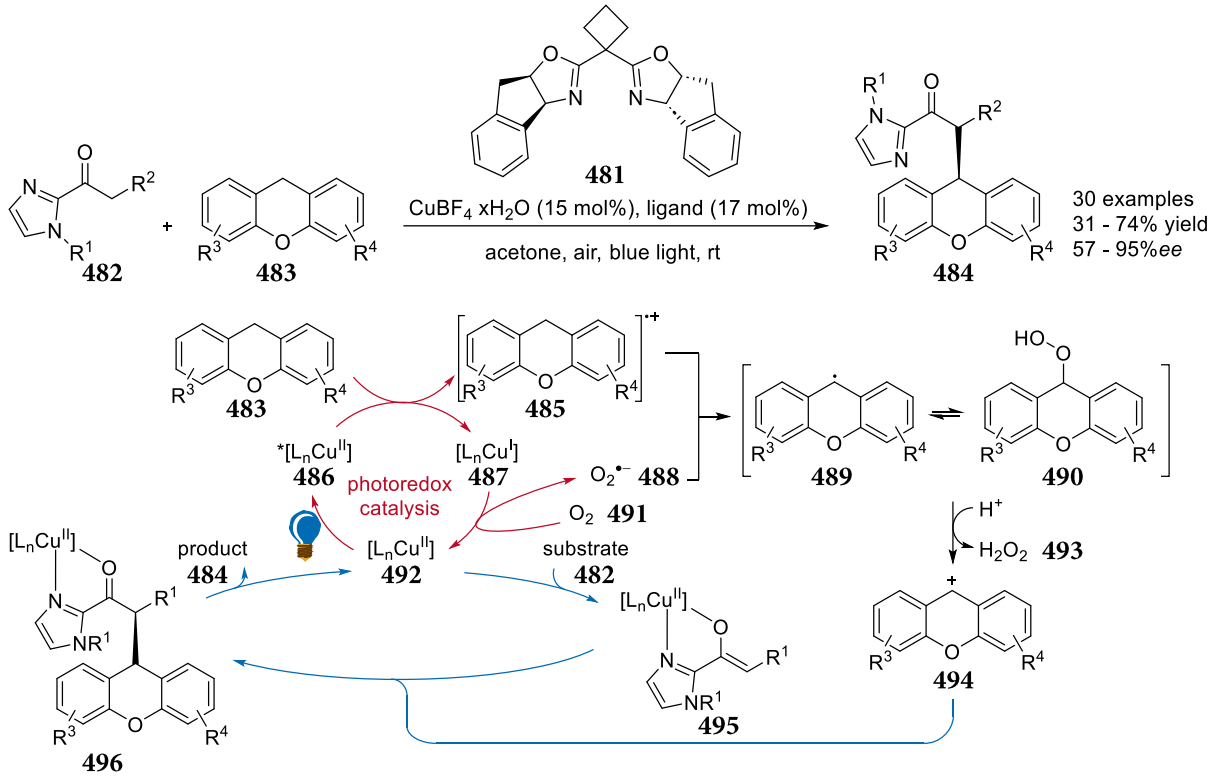

scheme 50. Asymmetric copper-catalyzed aerobic cross-dehydrogenative coupling of C(sp^3)-H bonds and mechanism thereof according to Gong *et al.*[241]

In addition to these versatile Cu-based approaches, the chirality of which was mostly based on bisoxazoline derivatives, bifunctional nickel complexes have also successfully combined with chiral bisoxazoline derivatives and employed as bifunctional catalysts.[187] The first example is a conjugate addition of α-amino radicals **501** that are released from silylamine radical precursors **499** upon oxidation by the excited Ni(II)-DBFOX complex **505**.[242] The radical undergoes stereocontrolled conjugate addition with the substrate **504** that is activated by coordination. The resulting α-carbonyl radical **503** is reduced by the reduced nickel complex **502**, allowing the enantioenriched product **500** to be released upon protonation (**scheme 51**).[242]

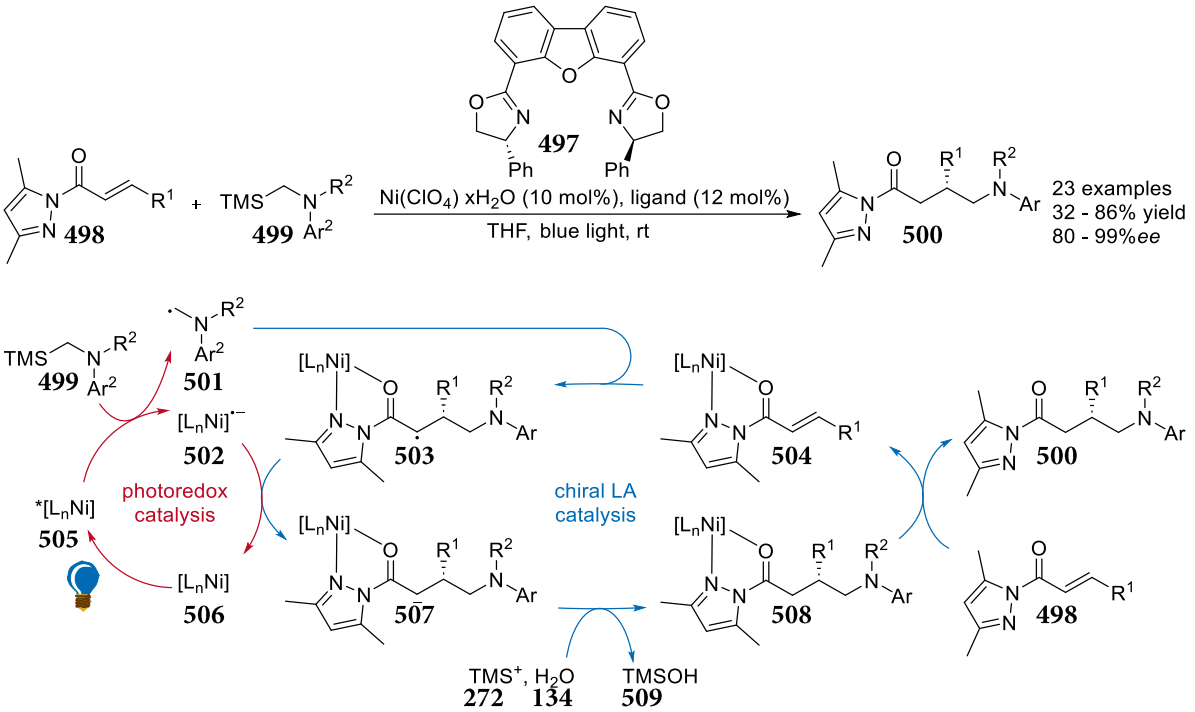

scheme 51. Asymmetric nickel-catalyzed aminoalkylation of enones **498** and mechanism thereof according to Gong *et al.*[242]

Furthermore, Xiao *et al.* developed a bifunctional BOX-Ni-based catalyst concept that, unlike all previous chiral-at-ligand approaches, does not rely on the photocatalytic activity of involved Cu or Ni complexes, but instead, similar to some of the single-catalyst approaches in the field of organophotoredox catalysis, covalently links the chiral BOX-Ni fragment to a thioxanthone structure that serves as a photosensitizer.[243] The bifunctional catalyst was successfully used in an asymmetric aerobic oxidation of β-ketoesters **511**. While the thioxanthone fragment serves to generate singlet oxygen (**514**) by energy transfer to atmospheric oxygen (**491**), the chiral BOX-Ni complex **510** provides substrate activation and a chiral environment for the transformation with singlet oxygen (**514**) (**scheme 52**).[243]

In contrast to the previously discussed single catalyst approaches, this catalyst concept of linking an established asymmetric ligand for substrate activation and an established photosensitizer for initiating the desired photochemistry offers the advantage that established photosensitizers allow access to more diverse phototransformations. For good reason, certain chemical structures have emerged as commonly used photocatalysts, while others have emerged as privileged ligands. Although many useful transformations have been

developed using for example chiral-at-metal complexes as photocatalysts, the complexes involved typically exhibit weaker absorption and shorter lifetimes than commonly used photocatalysts.[243] The concept of combining an established asymmetric ligand structure (BOX) with an established photocatalyst ($[Ru(bpy)_3]^{2+}$ (**7**)) will later become the basis for the development of bifunctional asymmetric BOX-substituted ruthenium photocatalysts (chapter 2).

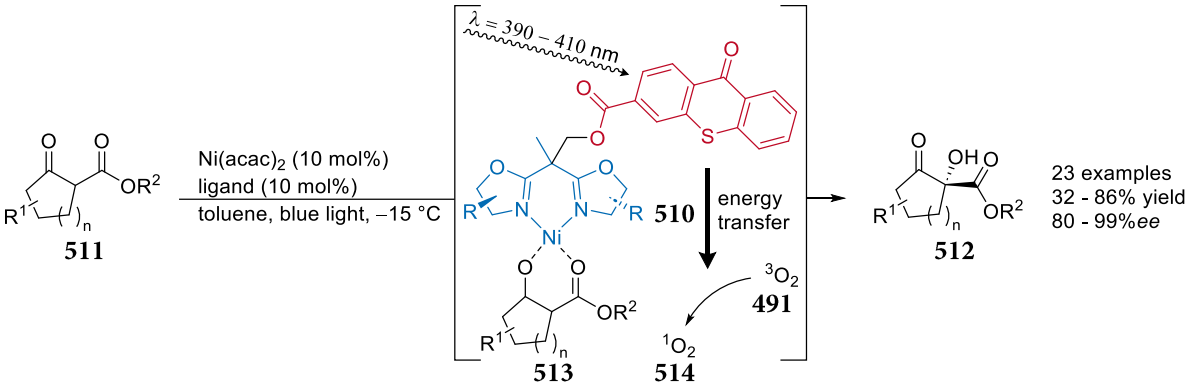

scheme 52. Asymmetric nickel-catalyzed photoinduced aerobic oxidation of β-ketoesters **511** according to Xiao *et al.*[243]

1.3.2.3 Enzymes as asymmetric bifunctional photoredox catalysts

Exploiting the observation that redox potentials of some cofactors can be significantly modified by visible light irradiation, initial attempts to combine photoredox reactivity with asymmetric biocatalysis were based on the principle that the cofactors involved serve as radical initiators.[176] The first example by Hyster *et al.* used various NAD(P)H-dependent ketoreductases (such as RasADH and LKADH) as radical initiators for a dehalogenation of α-bromolactones **516** followed by an enantioselective HAT. Taking advantage of the change in the redox potentials of such cofactors **310** from about 0.57 V vs. SCE in the ground state to about 2.60 V vs SCE in the excited state, a charge transfer excitation of the substrate **516** and cofactor **310** in close proximity occurs. After cleavage of a bromide anion, an enantioselective hydrogen atom transfer occurs. Exchange of the product **515** or **517** for the reactant **516** and of the cofactor **309** for a new equivalent **310** completes the catalytic cycle. Light excitation turned the carbonyl reductase into an initiator of radical transformation and chiral H-atom donor (**scheme 53**).[176]

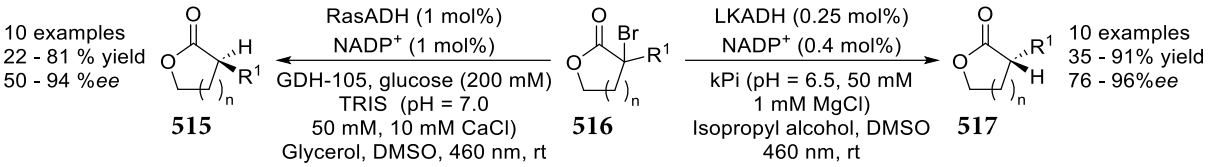

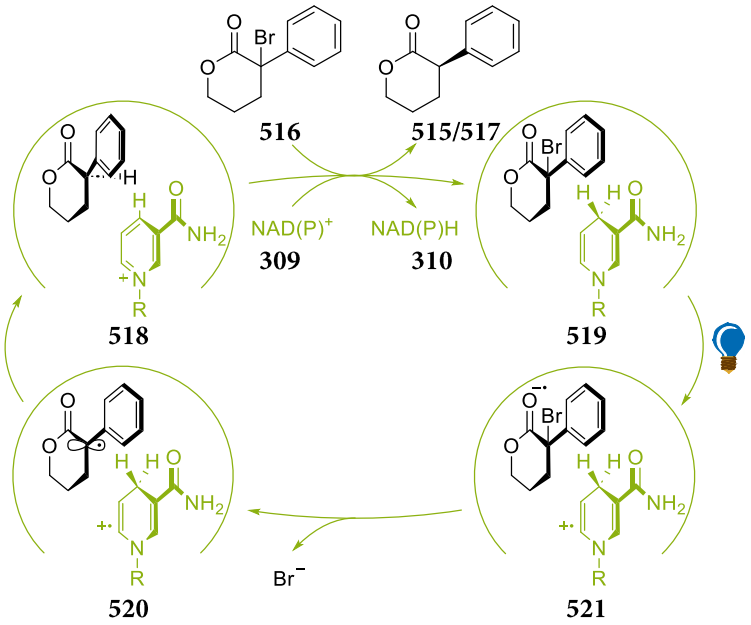

scheme 53. Asymmetric reductive dehalogenation with ketoreductases according to Hyster *et al.*[176]

Following the initial biophotoredox concept, flavin-dependent ene-reductases were also used for asymmetric radical cyclizations of α-chloroamides **522** to β-stereogenic lactams **523**.[178] Taking advantage of the lowering of the potential of flavin hydroquinones from –0.45 V vs. SCE in the ground state to –2.26 V vs SCE in the excited state, numerous asymmetric cyclizations ranging from 5-exo-trig to 8-endo-trig with different substitution patterns and employing different ene-reductases were achieved. The excitation of an electron-donor-acceptor (EDA) complex **525** by irradiation leads to the reduction of the C-Cl bond accompanied by chloride cleavage. The α-carbonyl radical **527** undergoes enantioselective cyclization followed by HAT. Exchange of the product **523** for

a new substrate **522** and regeneration of the flavin by NADPH (**310**) completes the catalytic cycle. In this example, substrate activation as well as spatial arrangement is also achieved by interaction of the carbonyl group with some side chains (His and Asn) of the active site (**scheme 54**).[178]

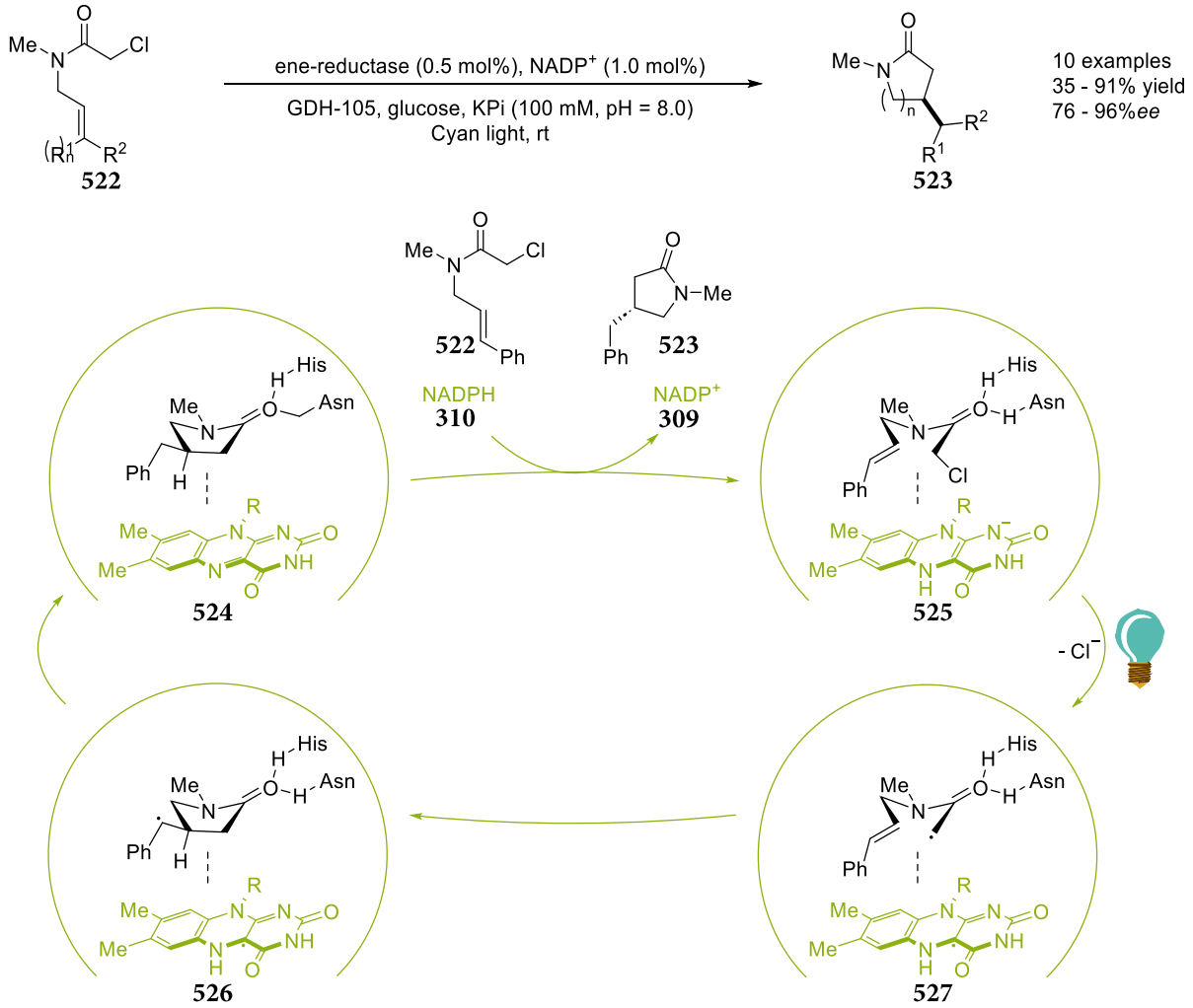

scheme 54. Asymmetric radical cyclization by photoexcited flavin dependent ene-reductases according to Biegasiewicz *et al.*[178]

2 Objective of the project

The present thesis aims to combine an established photocatalyst structure with asymmetric Lewis acid catalysis in one chiral bimetallic photocatalyst structure. Therefore, a chiral ligand structure, bisoxazoline (R-BOX), will be covalently connected to at least one 4 position of 2,2'-bipyridine (bpy) resulting in double (**528**, **530**) or triple (**529, 531**) bidentate BOX-bipyridine ligands (R-BOX-bpy), the bipyridine fragments of which can form a $[Ru(bpy)_3]^{2+}$-type photocatalyst substructure and whose chiral BOX fragments might coordinate to a substrate-activating Lewis acid (L.A.) (**figure 18**).

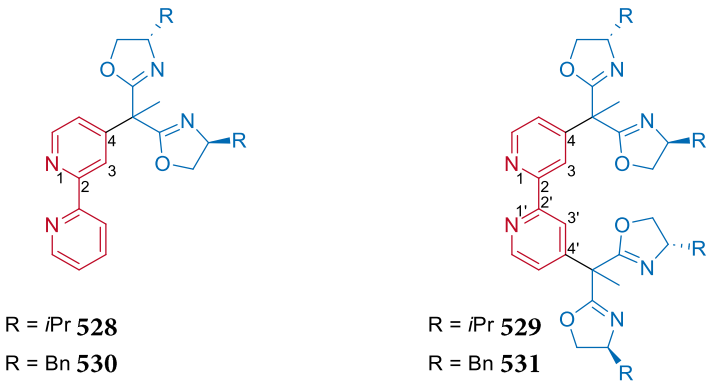

figure 18. Targeted ligand structures for combining a bipyridine fragment with a chiral bisoxazoline.

Based on the most common photocatalyst structure $[Ru(bpy)_3]^{2+}$ (**7**), the desired bimetallic complex might be obtained by the synthesis of a Ru(II) complex wherein the metal centre is octahedrally surrounded by three bidentate bipyridine ligands, of which at least one is R-BOX-bpy **528-531**. This incorporation of a R-BOX-bpy **528-531** might extend the versatile reactivity of visible light photoredox catalysis by enantioselective transition metal catalysis thus giving access to asymmetric phototransformations. The simplest imaginable catalyst structure $[Ru(bpy)_2(R\text{-}BOX\text{-}bpy)]^{2+}$ **532** or **533** containing two unmodified bipyridines and one R-BOX-bpy **528-531** is shown in **figure 19**.

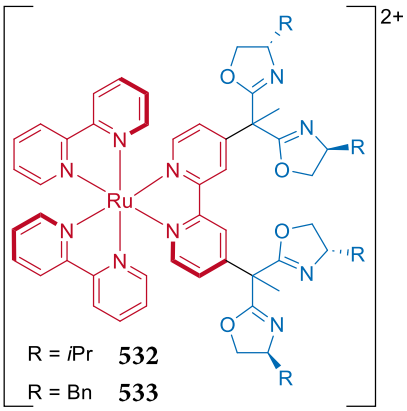

figure 19. Simplest heteroleptic bimetallic catalyst $[Ru(bpy)_2(R\text{-}BOX\text{-}bpy)]^{2+}$ **532** or **533**.

Efficient asymmetric induction by the BOX fragment requires the corresponding transformation to occur preferentially in the chiral environment of the BOX fragment. Given that both electron transfer and energy transfer are strongly distance dependent,[17, 21] the structure shown above might despite substrate activation by the chiral Lewis acid suffer from a competition with the racemic background reaction in proximity to the unsubstituted bipyridine ligands thus leading to a poorly controlled stereochemical outcome. Accordingly, during irradiation and MLCT, the electron should be excited into orbitals of the unsubstituted catalyst side, so that electron transfer to the substrate occurs preferentially from this side. This is illustrated by the imaginable SETs onto a generalized substrate structure **534** which is suitable for Lewis acid coordination (**scheme 55**).

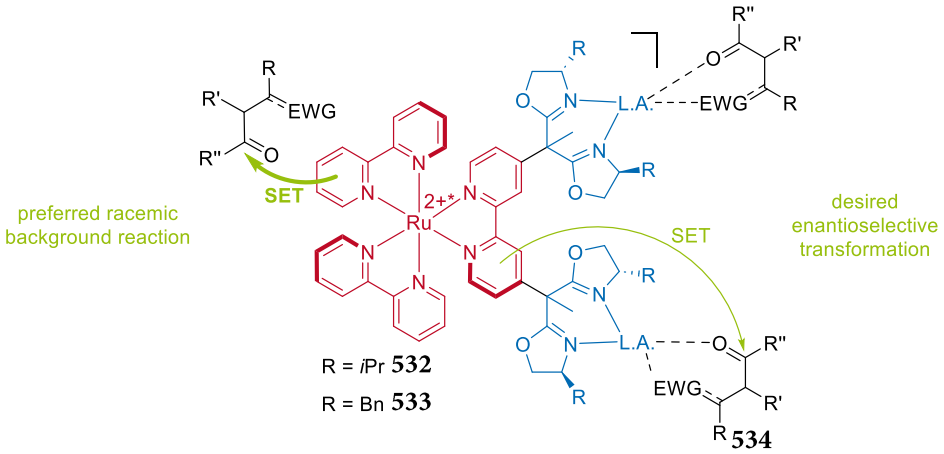

scheme 55. Competition between SETs onto a generalized substrate **534** structure inside or outside the chiral BOX environment.

The mentioned challenges could be overcome by focusing on substrates whose redox potentials lie outside the redox capabilities of the photocatalyst, allowing transformations only to occur upon prior Lewis acid activation of the substrates and the associated modification of the orbital energies and redox potentials. Although this concept of dual photoredox catalysis has been successfully applied in a number of reactions it is inherently constrained to only those substrates or functional groups that have a precisely adjusted range of redox potentials.[11, 211, 244, 245] More desirable is a catalyst concept **535**, whose intrinsic design of structure as well as resulting orbital energies reduce the racemic background reactions to a minimum. For this purpose, the averted catalyst side of the BOX fragment needs to be shielded (**figure 20**).

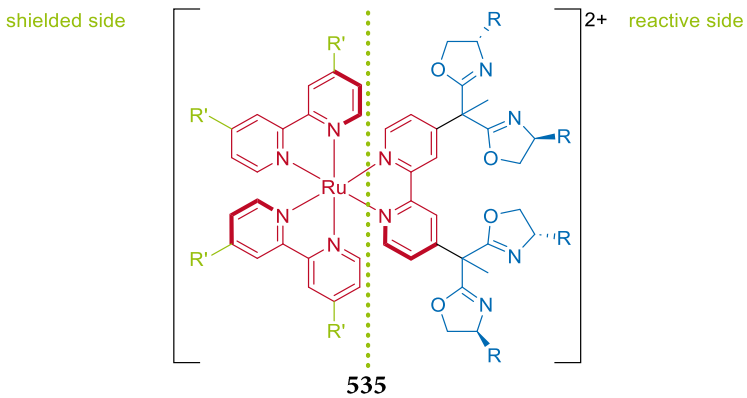

figure 20. Schematic representation of the required separation of heteroleptic bimetallic complexes into shielded and reactive sides.

The most obvious type of shielding could be provided by sterically demanding substituents that enlarge the distance between substrate and photocatalyst core to such an extent that efficient electron transfer is as or less likely than on the BOX-substituted side. Although *tert*-butyl substituents cannot nearly meet the steric demand of the BOX fragments, comparison of the photocatalysts without shielding $[Ru(bpy)_2(R\text{-}BOX\text{-}bpy)]^{2+}$ **532** or **533** and with *tert*-butyl-substituted backbone in $[Ru(t\text{Bu-}bpy)_2(R\text{-}BOX\text{-}bpy)]^{2+}$ **536** or **538** could provide insight into general prospects for the success of steric backbone shielding, especially since the slightly electron-donating *tert*-butyl substituents might increase the orbital energies thereby rendering the π^* orbitals of the less electron-rich R-BOX-bpy side in the complexes **536** and **538** the LUMO. An alternative concept of shielding could explicitly exploit this change in orbital energies, specifically making excitation into a π^*-orbital at the BOX-bpy side more likely, thereby favoring electron transfer to substrates in close proximity to the BOX-bpy fragment. The incorporation of electron-donating methoxy substituents should electronically disfavor the backside, since the π^*-orbitals of the methoxybipyridine fragments should be significantly higher in energy and thus rendering the π^*-orbital of the BOX-bpy ligand the LUMO (**figure 21**).

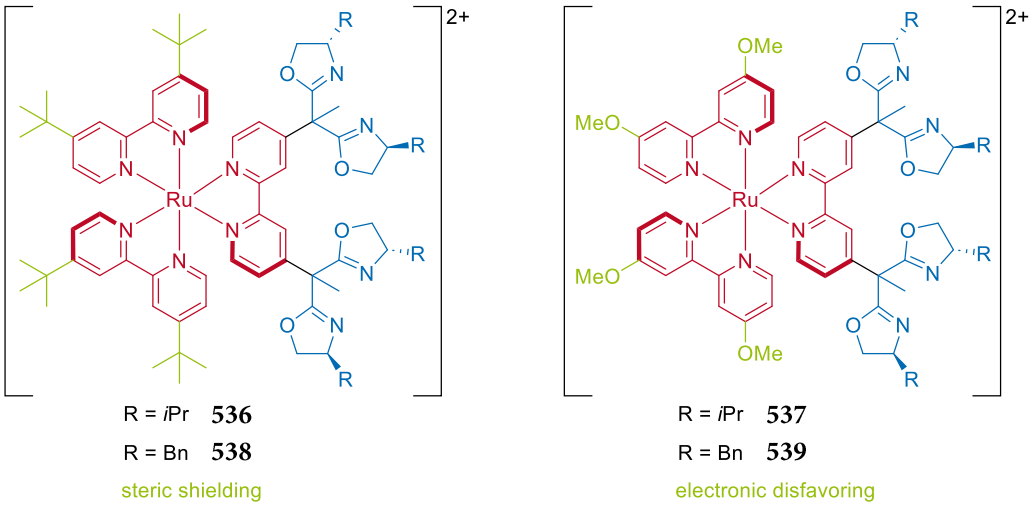

figure 21. Heteroleptic bimetallic photocatalysts **536-539** with sterically or electronically disfavored symmetric sides.

Instead of a heteroleptic complex **536-539** with only one reactive BOX-bpy fragment and two sterically (*t*Bu-bpy) or electronically (MeO-bpy) disfavoring bipyridine fragments, the synthesis of homoleptic $[Ru(R\text{-}BOX\text{-}bpy)_3]^{2+}$ catalysts **540-543** could eliminate the need for shielding of an achiral side required in the heteroleptic complexes **536-539**. In the homoleptic complexes **540-543** the asymmetric outer BOX ligand sphere completely surrounds the photocatalyst core and could coordinate up to six substrate-activating Lewis acids in a chiral environment. With both electron and energy transfers being strongly distance-dependent,[17, 21] substrates in close proximity to the asymmetric Lewis acid surrounding will preferentially engage in photoinduced transformations. Although racemic background reactions could potentially occur outside the BOX ligand sphere, the probability should exponentially decrease with the distance. Despite the advantages of these catalyst structures, its synthesis could be particularly difficult due to the double or triple bidentate structure of the BOX-bpy ligands **528-531** (**figure 22**).

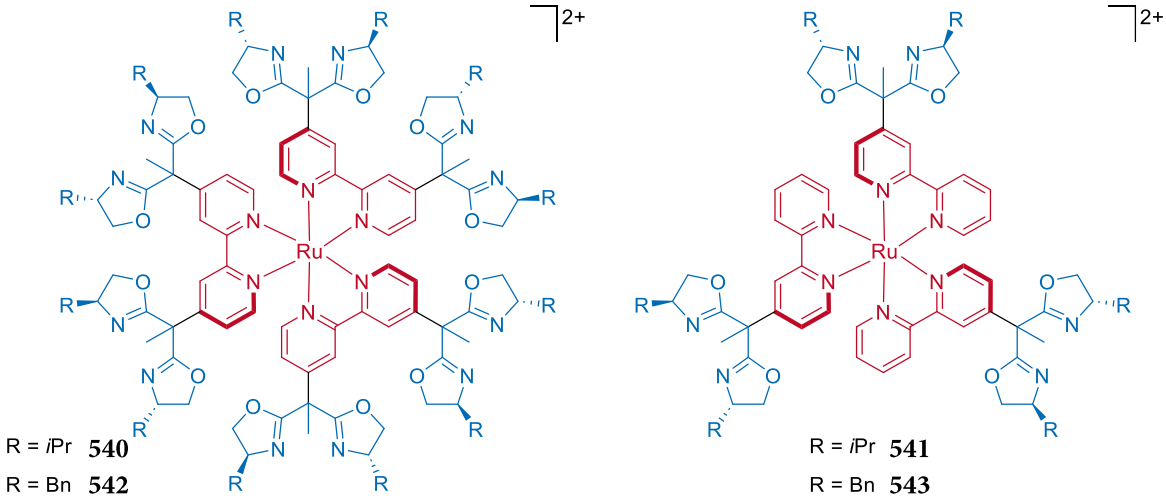

figure 22. Homoleptic complexes of the form $[Ru(R\text{-}BOX\text{-}bpy)_3]^{2+}$ **540-543**.

After successful ligand synthesis, R-BOX-bpy **528-531** can be used in the synthesis of Ru-tris diimine complexes of the homoleptic form $[Ru(R\text{-}BOX\text{-}bpy)_3]^{2+}$ **540-543** or the heteroleptic form $[Ru(R'bpy)_2(R\text{-}BOX\text{-}bpy)]^{2+}$ **536-539**. Given a greater risk of racemic background reactions for the heteroleptic case, different residues R' should be incorporated on the achiral backside ligands, in particular *tert*-butyl for steric shielding as well as methoxy for electronic disfavoring. For better comparability of the shielding concepts and to determine the change in catalyst performance as well as photophysical properties caused by the incorporation of R-BOX compared to $[Ru(bpy)_3]^{2+}$ (**7**), the heteroleptic complex without substituents in the achiral backbone $[Ru(bpy)_2(R\text{-}BOX\text{-}bpy)]^{2+}$ **532** and **533** should also be prepared. In order to obtain information about the change in reactivity of these catalysts, and for complete characterization of the novel photoredox catalysts, they should be investigated by photophysical and electrochemical measurements, and the obtained values compared with the prototypical $[Ru(bpy)_3]^{2+}$ (**7**). In case of the heteroleptic catalysts **536-539**, the changes of orbital energies with respect to the substituents in the catalyst backside should be analyzed in order to gain insight into the potential success of the concept of electronically disfavoring MLCT excitation into orbitals of the achiral catalyst side.

Ultimately, the asymmetric bifunctional photoredox catalysts **532**, **533**, **536-543** should be evaluated in suitable transformations both for their fundamental catalytic activity as well as efficiency of stereoinduction by the asymmetric BOX fragments. In the case of the heteroleptic complexes **536-539**, the different shielding concepts could be compared, hence the substituent influence on the resulting enantiomeric excess of the achiral side of the catalyst could be investigated. Since the catalysts aim to link asymmetric Lewis acid catalysis with photoredox reactivity, suitable transformations for evaluation of the catalysts employ substrates that might be coordinated by a Lewis acid in the chiral environment of the BOX fragments, e.g., 1,3-dicarbonyl compounds.

The synthesis of the novel asymmetric bifunctional catalyst structures and the exploration of the conceptually novel approach of electronic disfavoring of an achiral catalyst side by rational modification of excited-state orbital energies, by both photophysical and electrochemical investigation, as well as by comparison of the catalysts in photoredox transformations, may establish the foundation for a new type of dual asymmetric photoredox catalysis.

3 Results and discussion

3.1 Synthesis of BOX substituted bipyridine ligands **528-531**

3.1.1 BOX-bipyridine **528-531** synthesis *via* substitution on 4-halopyridines and bipyridine coupling

The synthesis of BOX-substituted bipyridine ligands could be carried out by the synthesis of a BOX-pyridine fragment **544** and **545** and subsequent coupling to the bipyridine, either in the sense of homocoupling with another BOX-pyridine fragment **544** or **545**, or with an elsewise- or unsubstituted pyridine.[246-248] This retrosynthetic approach traces the synthesis back to the linkage of a halopyridine **551** or **553** with a malonic acid derivative e.g. malonic acid ester **554** or malonodinitrile **552**. To separate the conjugated π-system of bipyridine from the bisoxazoline fragment, the malonylpyridine **549** or **550** could be methylated at the benzylic α-position. Nitrile substituents could then be converted into oxazoline rings with a chiral amino alcohol in the presence of a Lewis acid.[249-252] For ester substituents the BOX-fragment could be obtained by amide formation with a chiral amino alcohol and conversion of the terminal hydroxy groups into suitable leaving groups and subsequent intramolecular nucleophilic substitution.[252-258] Alternatively, ring closure could be achieved under dehydrating conditions or by Lewis-acid activation.[132, 259-265] The BOX-pyridine fragment **544** or **545** could then be coupled with itself or with a different pyridine derivative to form the bipyridine ligands **528-531** (**scheme 56**).

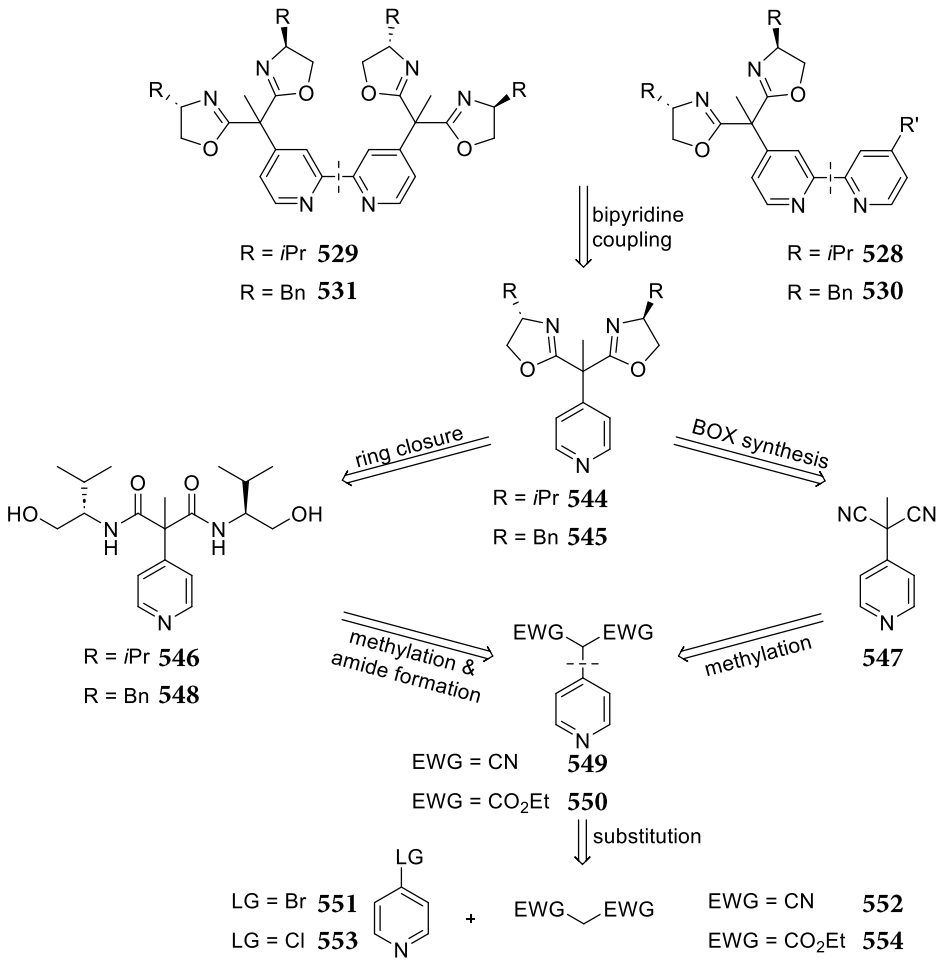

scheme 56. Retrosynthetic approach *via* substitution on 4-halopyridines **551** and **553** and bipyridine coupling.

3.1.1.1 Ullmann-type coupling for the synthesis of malonylpyridin **550**

In order to obtain malonylpyridine **550**, a copper(I) iodide-catalyzed heteroarylation according to Zeng *et al.* was investigated. They successfully performed the heteroarylation with a variety of pyridine derivatives at the 2-, 3- and 4-position of the heterocycle in good to excellent yields. Zeng *et al.* obtained the desired 4-malonylpyridine **550** in very good yield (81%) (**equation 17**).[266]

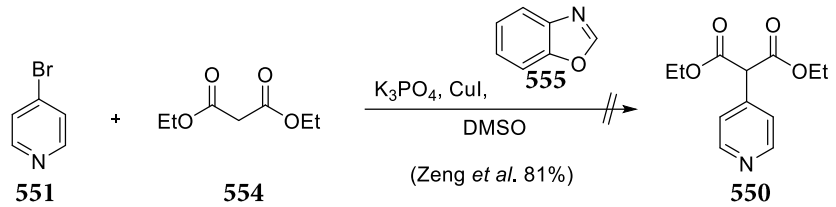

equation 17. Ullman-type coupling for the heteroarylation of diethylmalonate (**554**) according to Zeng *et al.*[266]

In optimizing the reaction conditions, Zeng *et al.* screened different ligands, Cu(I) sources, bases, solvents, temperatures, and stoichiometry. Best results were obtained using 8 mol% Cu(I), 12 mol% benzoxazole (**555**) as ligand, 1.5 eq. diethylmalonate (**554**) and 3.0 eq. K_3PO_4 in degassed DMSO under an argon atmosphere after six hours at 50 °C. Without any ligand, only product traces were obtained and using other ligands provided significantly lower yields (<43%). Alternative bases (Cs_2CO_3, K_2CO_3, NaOAc, Et_3N, DIPEA, Py) or solvents (DMF, 1,4-dioxane, toluene, THF) resulted in less or no product formation.[266]

The mechanism of the Ullmann coupling or the Ullmann reaction involves the formation of a Cu-π-complex **564** followed by an oxidative addition of the aryl halide (bromopyridine **551**). After reductive elimination and dissociation of the π-bound product the Cu(I) halide can react with another potassium malonate **557** to form the copper malonate **562**. The mechanism proposed by the authors is similar to the Ullmann reaction. Alternatively, a radical mechanism *via* a pyridyl radical is conceivable. Thereby, the Cu(I) malonate **562** cleaves the halogen-carbon bond reductively. The pyridyl radical **559** could then oxidatively add to the Cu(II) malonate **560** to form a Cu(III) species **566** which, in analogy to the mechanism of the Ullmann reaction, reductively eliminates the product **550** to complete the cycle. A direct, one-step conversion to the product **550** is also possible.[267]

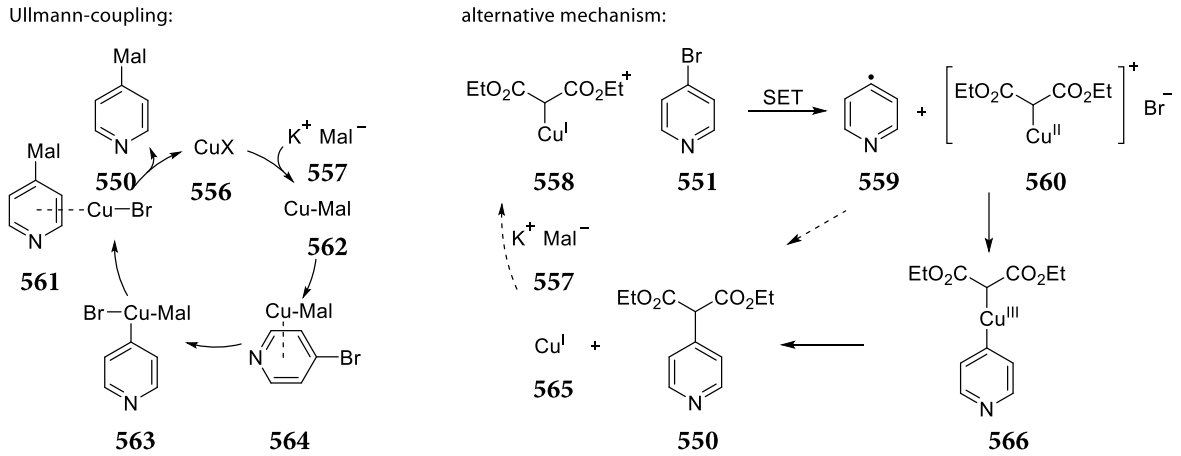

scheme 57. Potential mechanisms for the Ullmann-type heteroarylation of diethylmalonate **554**.[267]

The results reported by Zeng *et al.* failed to be reproduced in several approaches. First, 4-bromopyridine (**551**) was prepared from its hydrochloride and under the published conditions allowed to react with distilled diethylmalonate (**554**), K_3PO_4 and freshly purchased benzoxazole (**555**) in degassed DMSO (p.a.) under nitrogen atmosphere. However, no conversion was observed on TLC. In another approach, a mixture of 4-bromopyridine hydrochloride, benzoxazole (**555**) and distilled diethylmalonate (**554**) in freshly distilled DMSO was first degassed and then mixed with CuI (**556**) and finally with a slightly increased amount of K_3PO_4 in a strong nitrogen counterflow. As again no conversion was detectable, the ligand benzoxazole (**555**) was first purified by column chromatography and finally by sublimation. However, even the use of highly purified benzoxazole (**555**) did not lead to product formation. Finally, 4-bromopyridine hydrochloride was degassed with sublimed benzoxazole (**555**) and distilled diethylmalonate (**554**) in distilled DMSO under an argon atmosphere. CuI was added to the mixture in a strong argon counterflow, followed by K_3PO_4, but again no product formation was observed.

The absence of product formation could be explained by two deviations from the literature conditions: Instead of setting up the reactions in an argon glovebox, the experiments were carried out using high-purity chemicals in thoroughly freeze-pump-thaw degassed solvents using general Schlenk technique. Furthermore, 4-bromopyridine hydrochloride was used in three experiments instead of 4-bromopyridine (**551**). However, the latter should have formed *in situ* due to the use of a larger amount of base.

In order to covalently connect a malonic acid derivative to a Pyridine-ring further experiments investigated the nucleophilic aromatic substitution.

3.1.1.2 Nucleophilic aromatic substitution for the synthesis of malonylpyridine **549** and **550**

Another synthetic route for linking a pyridine ring to a malonic acid derivative is the nucleophilic aromatic substitution of a 4-halopyridine **551** or **553** with a malonate ester **554** or malonodinitrile (**552**) (**equation 18**). Different base-solvent combinations and reaction temperatures were evaluated. The parameters and results of selected experiments are summarized in **table 1**.

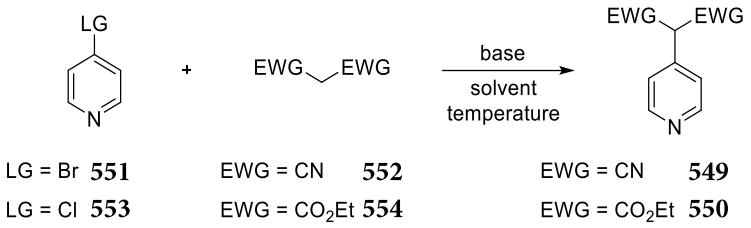

equation 18. Nucleophilic aromatic substitution for the synthesis of malonylpyridines **549** and **550**.

table 1. Reaction parameters and results of selective modifications of the nucleophilic aromatic substitution.

entry	LG	EWG	base	solvent	temperature	yield
1	Br	CO_2Et	NaH	THF	rt → reflux	---
2	Br	CN	K_2CO_3	Et_2O	rt → reflux	---
3	Br	CN	K_2CO_3	DMF	rt	---
4	Cl	CN	Piperidine	DMF	rt → reflux	---
5	Cl	CN	Piperidine	EtOH	rt → reflux	traces
6	Cl	CN	*n*-BuLi	THF	–78 °C	---
7	Cl	CN	LiHMDS	THF	–70 °C → reflux	---
8	Cl	CN	KHMDS	THF	–50 °C → rt	---
9	Cl	CN	NaHMDS	THF	rt	---

Given the relatively low electron density compared to benzene, nucleophilic aromatic substitutions on pyridines typically proceed very well. The mesomeric structures suggest that nucleophilic substitutions occur particularly at positions 2 and 4. This distribution of electron density is also reflected in studies on the relative reactivity of chloropyridines with NaOEt in EtOH at 20 °C (**scheme 58**).[248]

The investigation of the nucleophilic aromatic substitution showed that neither irreversible bases (NaH), nor inorganic bases (K_2CO_3), nor organic bases (piperidine) have selectively initiated the desired substitution in different solvents and at different temperatures (entries 1 – 4). In a similar, literature-known substitution with phenylpyridine chloride, good yields were obtained using piperidine in both DMF and EtOH.[268] However, only product traces were detected in NMR after refluxing with piperidine in EtOH.

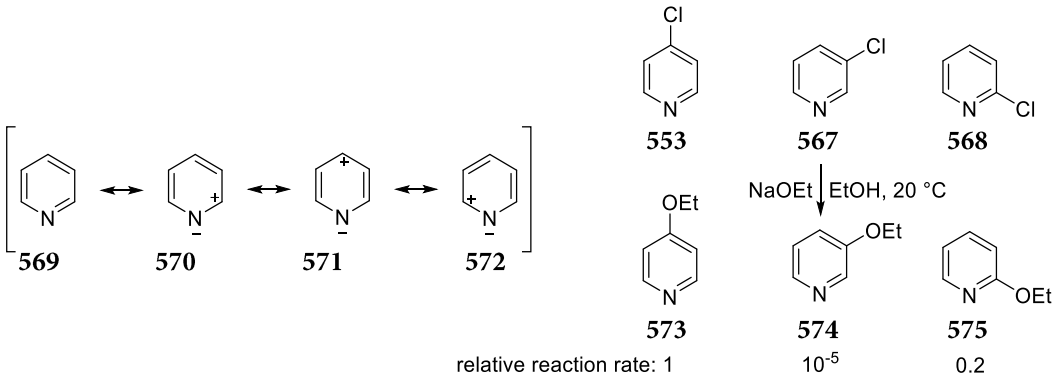

scheme 58. Mesomeric structures of pyridine and relative reactivity of chloropyridines with NaOEt in EtOH at 20 °C.[248]

The dominantly formed side product appeared to be a piperidylnitrile-like species **577** resulting from the addition of the base to malonodinitrile. In further approaches, stronger bases were evaluated. Using *n*-butyllithium, the quantitative formation of a substance which appeared to have either the mass of 4-chloro-2-butylpyridine (**576**) or 4-butylpyridine hydrochloride (**578**) was detected in TLC-MS within 15 minutes at −78 °C (entry 6). This is plausible, since analogous to the Ziegler reaction of pyridines with alkyl or aryllithium compounds, a hydride substitution can take place in the 2-position due to the directing effect of nitrogen (**scheme 59**).[248] Alternatively, the *n*-butyl anion could also have exchanged the chloride substituent and the product might have been detected as the corresponding hydrochloride in TLC-MS. When more sterically demanding HMDS bases were used, neither TLC-MS nor crude NMR detected product formation (entries 7 – 9).

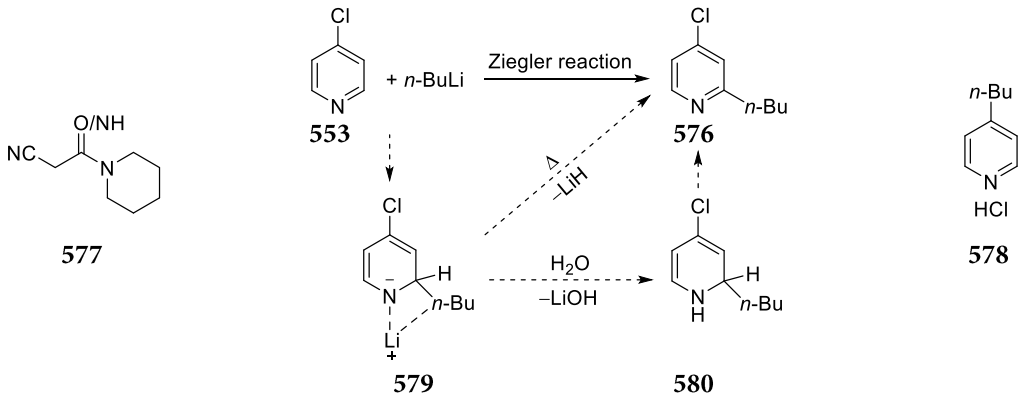

scheme 59. Detected side products **576**-**578** and potential side reaction of the nucleophilic aromatic substitution.

Since nucleophilic aromatic substitutions at the 4-positions of pyridines are generally favoured and all investigated bases should be able to deprotonate the malonic acid derivatives (malonodinitrile **552**, pKa = 11.1, diethylmalonate **554**, pKa = 15.9) the problem could arise from the leaving group.[269, 270] Therefore, the synthetic route involving final coupling of a BOX-pyridine **544** or **545** with another pyridine-derivative to a bipyridine ligand was not pursued further and instead the synthesis of bipyridine derivatives with better leaving groups was begun. Theses derivatives might not only be used to link the bipyridine with malonic acid derivatives, but possibly also to link directly with a bisoxazoline fragment, thereby giving access to the bisoxazoline bipyridine ligands **528** and **530** in a very convergent synthetic route.

3.1.2 BOX-bipyridine **528** and **530** synthesis *via* S_NAr on bipyridine derivatives

A straightforward synthetic approach for a BOX-substituted bipyridine derivative might be the nucleophilic substitution on a bipyridine bearing a suitable leaving group (**scheme 60**). Conversion of bipyridine **587** into the *N*-oxide **588** allows a selective nitration at the 4-position. Subsequent reduction of both the nitro group and the *N*-oxide would provide the aminobipyridine **590** thus paving the way for a Balz-Schiemann sequence to give 4-fluorobipyridine **585** *via* the corresponding diazonium salt **582**, both of which might serve as bipyridines with suitable leaving groups. Simultaneously, the synthesis of the BOX fragments **581** and **584** could be performed either from a malonate ester **554** or from malonodinitrile **552**.[132, 249-265, 271-273] This approach does not require the final coupling of two pyridine fragments to form a bipyridine and may not only be used to link the bipyridine with malonic acid derivatives **552** or **554**, but possibly also to link directly with the bisoxazoline fragments **581** or **584**. In this way, the bisoxazoline bipyridine ligands **528** and **530** could be accessible in a very convergent synthetic route. The convergence of the resulting route makes this approach particularly worth considering, not because the total number of synthetic steps is small, but because the separate syntheses of the bipyridine **582** or **584** and the BOX fragments **581** or **584** may possibly proceed more smoothly. However, this retrosynthetic analysis only provides access to 4-BOX-bipyridines **528** and **530**, not to 4,4'-DiBOX-bipyridines **529** and **531**.

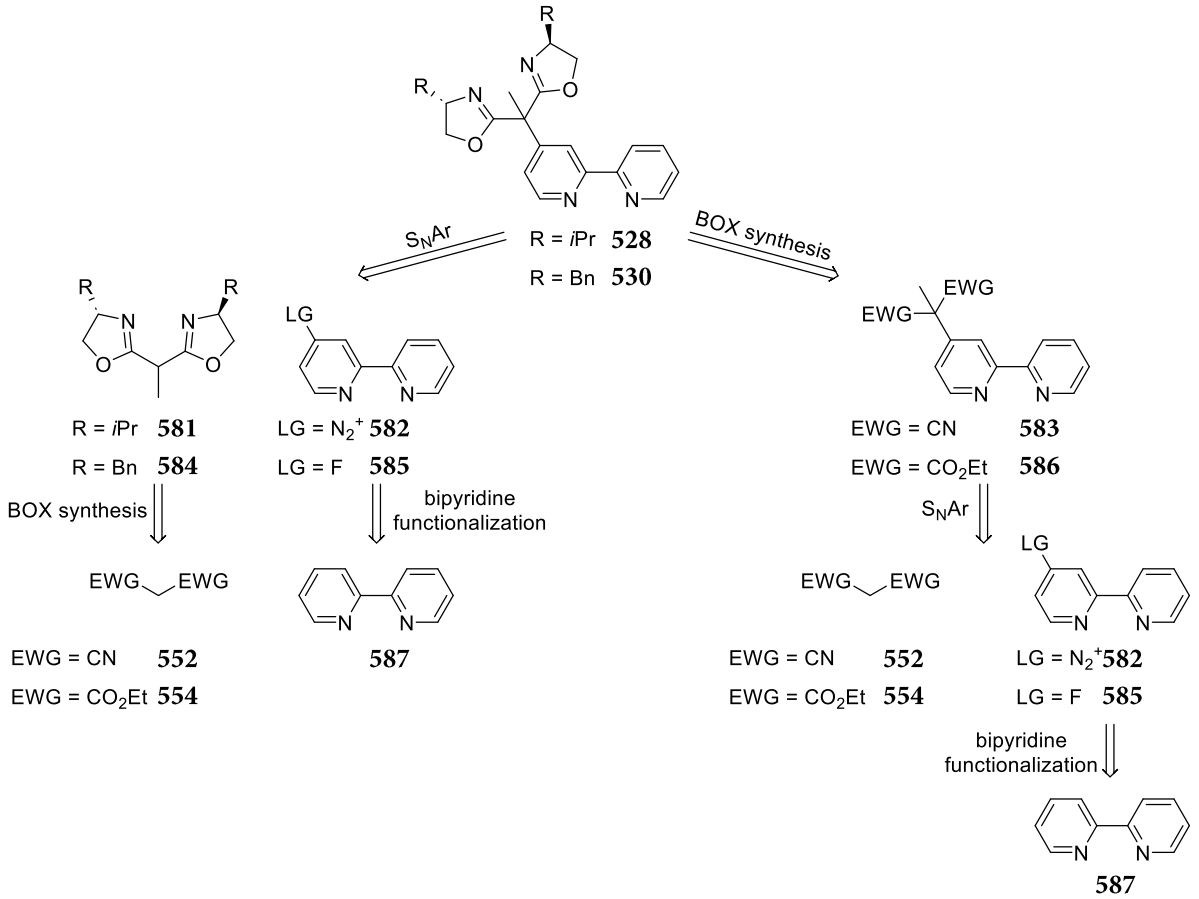

scheme 60. Retrosynthetic approach *via* nucleophilic aromatic substitution on bipyridine derivatives.

3.1.2.1 Synthesis of 4-diazobipyridine **582** and 4-fluorobipyridine **585**

The synthesis of 4-fluorobipyridine **585** was performed starting from bipyridine **587** by conversion to the *N*-oxide **588**, selective nitration at the 4-position, reduction to 4-aminobipyridine **590** and a Balz-Schiemann sequence (**scheme 61**).

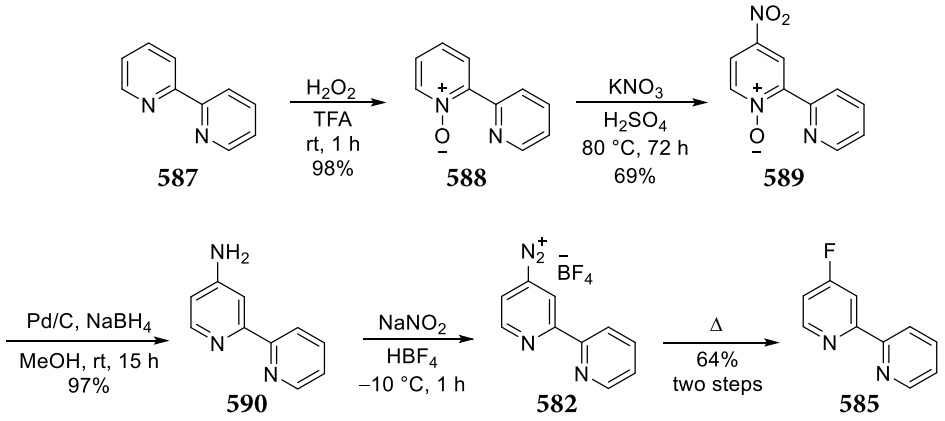

scheme 61. Synthetic route for the synthesis of 4-fluorobipyridine **585** from bipyridine **587**.

Pyridine *N*-oxides allow ring functionalizations that are not possible in pyridine or only under harsh conditions. Thus, the reaction of pyridine in nitrating acid at 300 °C leads to nitration at the 3-position in a very poor yield of 15%.[248] Since the connection between the BOX fragment and bipyridine is ultimately desired at position 4 of the heterocycle, which according to the mesomeric structures does not preferentially participate in electrophilic aromatic substitutions, bipyridine was converted into the corresponding *N*-oxide **588**. The mesomeric structures of the bipyridine *N*-oxide **588** show that it has an increased reactivity in nucleophilic substitutions as well as in electrophilic substitutions, paving the way for electrophilic ring functionalizations at 4-position (**scheme 62**).[248]

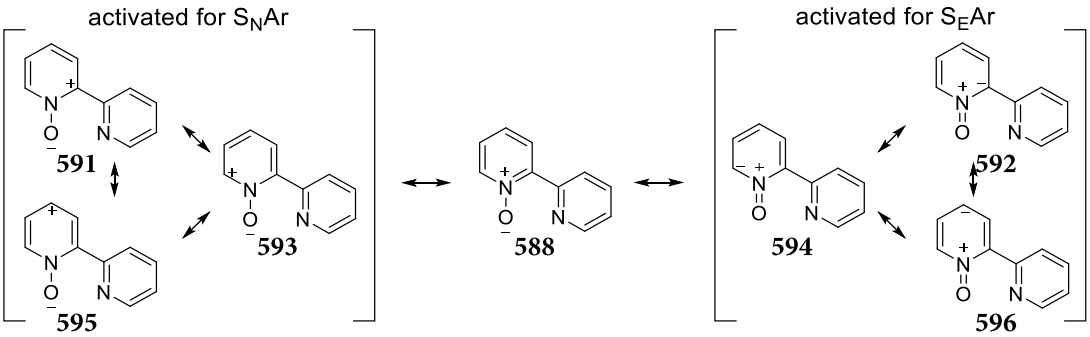

scheme 62. Mesomeric structures of bipyridine *N*-oxide **588**.

The *N*-oxide **588** was quantitatively formed within one hour by stirring bipyridine (**587**) in trifluoroacetic acid with hydrogen peroxide solution. Extraction with chloroform and washing with NaOH to neutralize and remove acid residues gave the *N*-oxide **588** in an excellent yield of 98%. The subsequent nitration was carried out by heating the *N*-oxide **588** with KNO_3 in concentrated sulphuric acid, whereby the nitrosyl cation readily added to the *para*-position regarding the *N*-oxide as favored by the mesomeric structure **596**. During the workup, the nitrating acid had to be neutralized to cause precipitation of the 4-nitro-bipyridine *N*-oxide **589**. Thereby, the pH value had to

be precisely adjusted to pH = 9.5 in order to prevent nucleophilic substitution by hydroxide anions, indicated by the sudden colour change of the yellow solution to dark green (**scheme 63**).

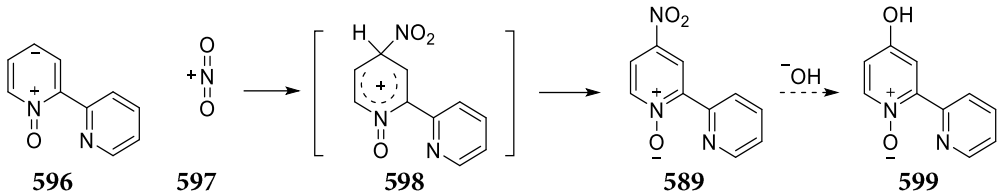

scheme 63. Nitration of bipyridine-*N*-oxide by electrophilic aromatic substitution and side-reaction occurring during workup at pH > 9.5.

Experiments attempting to control the rapid pH change using less concentrated NaOH resulted in a significantly reduced yield due to dilution. Thus, for maximizing the yield, a 25% NaOH solution was used to neutralize and in order to fine adjust the pH value and prevent degradation of the product, a pH meter was used. In this way, the yield of 4-nitrobipyridine-*N*-oxide **589** was maximized to 69%. The subsequent reduction of both the nitro group and the *N*-oxide proceeded smoothly with Pd/C and $NaBH_4$ and yielded the corresponding amine **590** in excellent yield (97%) setting the stage for a Balz-Schiemann-sequence.[269]

As part of the Balz-Schiemann sequence, initially sodium nitrite in tetrafluoroboric acid was used to obtain the diazonium salt **582**, which was filtered off as a beige solid and dried over phosphorus pentoxide to avoid hydrolytic side reactions. The dry diazonium salt **582** was then heated without solvent under inert conditions until a controlled decomposition to 4-fluorobipyridine **585** occurred, indicated by an alteration of the beige solid to a brownish substance. Several experiments revealed that a temperature of about 60 °C leads to the formation of 4-fluorobipyridine **585**. The Balz-Schiemann sequence provided 4-fluorobipyridine **585** in a maximum yield of 64% over two steps.

The described synthetic sequence provides access to 4-fluorobipyridine **585** from bipyridine **587** in a total yield of 42% over 6 linear steps. Since the diazonium salt **582** showed remarkable stability and the leaving group (nitrogen) should also be suitable for nucleophilic aromatic substitutions, the diazonium salt **582** was not entirely converted into 4-fluoropyridine **585** but kept for substitution experiments.

3.1.2.2 Synthesis of chiral bisoxazolines

In order to evaluate a very convergent synthetic approach of directly linking a bisoxazoline with a bipyridine derivative and to establish an enantioselective dual-catalyzed photoredox transformation with separate photoredox- and Lewis acid BOX catalyst, different synthetic strategies for the synthesis of non-, mono- and dimethylated BOX derivatives (BOX **612**, MeBOX **581**, Me_2BOX **613** - **614**) were investigated. In all BOX syntheses, the chiral information originates from the chiral pool: Reduction of naturally occurring amino acids (L-valine (**600**), L-phenylalanine (**601**)) with $LiAlH_4$ provides access to chiral amino alcohols **603** and **604**, which react with different malonic acid derivatives (**554, 605** - **607**) to form bisoxazolines (**581**, **612** - **614**) (**scheme 64**).

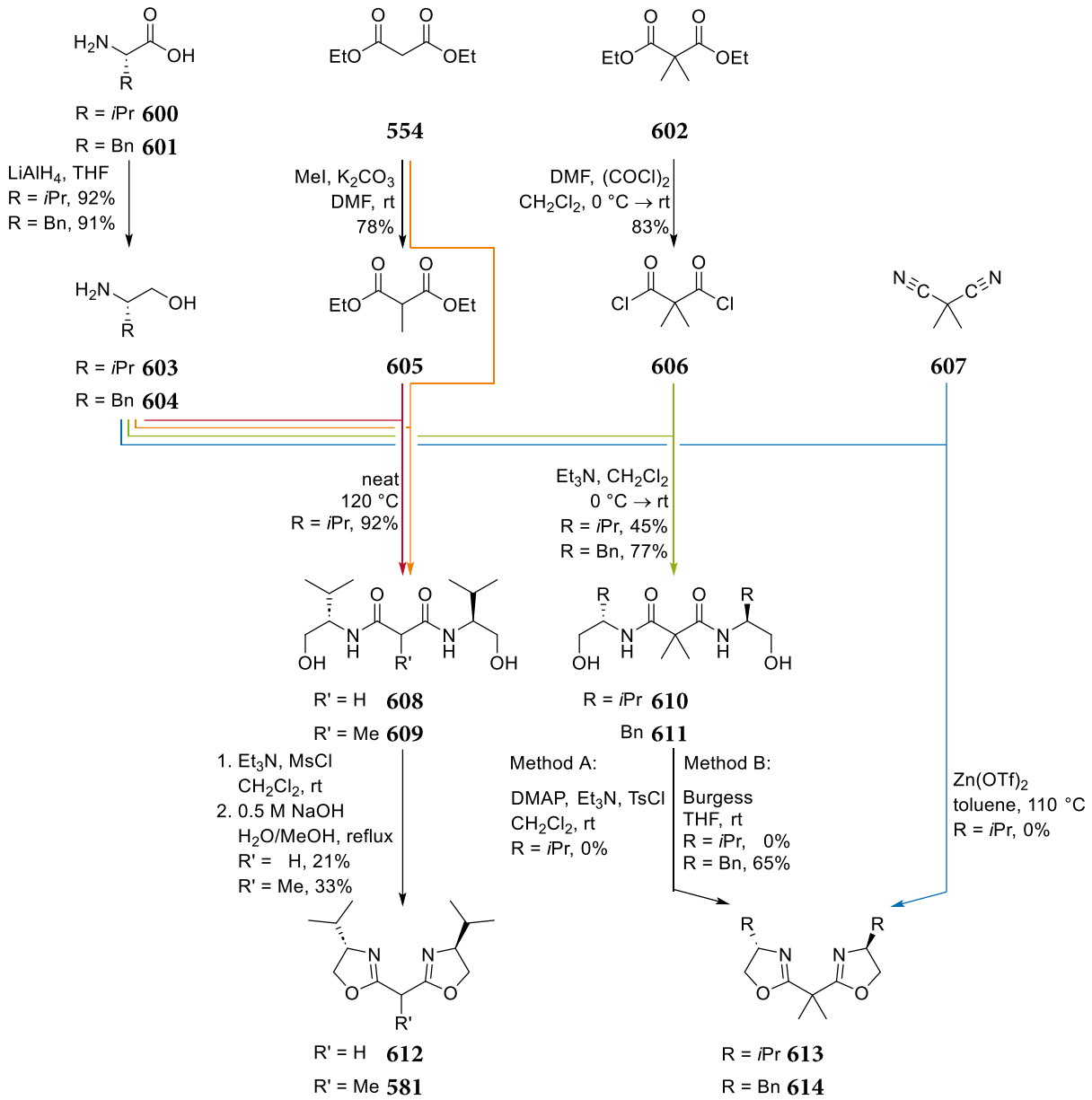

scheme 64. Evaluated synthetic approaches for the synthesis of bisoxazoline derivatives **581**, **612** - **614**.

After reduction of the amino acids **600** and **601**, the isolation of the amino alcohols **603** and **604** from the reaction mixture, i.e. the separation from the Li/Al salts, was particularly challenging, making the work-up strategy the

critical factor for obtaining very good yields. Three work-up strategies were examined: Repeated refluxing of the Li/Al salts in a THF/water mixture yielded L-valinol (**603**) in a maximum yield of 37%. Through addition of a sodium-potassium-tartrate solution, which coordinates the Li/Al salts the crude product became extractable with diethyl ether, increasing the maximum yield to 55%. In case of L-phenylalaninol (**604**) product isolation by refluxing the crude mixture in diethyl ether was achieved in a yield of 61%. As the amino alcohols **603** and **604** are very polar and highly soluble in water, it was assumed that a further improvement of the yield is only possible by a complete removal of the water. Therefore, after extraction from the Li/Al salts by repeated refluxing in a THF/water mixture, the THF was removed under reduced pressure and the remaining aqueous residues were dried with chloroform on an inverse Dean-Stark-apparatus. In this way the yields for L-valinol (**603**) and L-phenylalaninol (**604**) were increased to 92% and 91%, respectively.

With the chiral aminoalcohols **603** and **604** at hand, the BOX-derivate **612** without substituent at the bridging atom (R' = H) was first prepared by formation of a diamide **608**. For this purpose, diethyl malonate (**554**) was heated to 120 °C in excess L-valinol (**603**) (neat). After removal of malonate residues by column chromatography, the diamide **608** was selectively obtained in excellent yield (92%) by increasing the polarity of the eluent. Excess L-valinol (**603**) remained stuck to the column by this method; later approaches showed that the excess L-valinol (**603**) can be recovered by distillation during the workup process.

The diamide **608** was subjected to the most common two-step ring closing sequence for the conversion into bisoxazolines.[256] For this purpose, the diamide **608** was deprotonated at the hydroxy groups with triethylamine and converted into the dimesylate with methanesulfonyl chloride. The crude product was then refluxed in NaOH solution in H_2O/MeOH. The base serves to deprotonate the amide nitrogen-bound protons to induce the intramolecular mesylate substitution. In competition with this ring-closing mechanism, however, hydroxide anions may also participate in intermolecular nucleophilic mesylate substitution (**scheme 65**). This side reaction is equivalent to a reverse reaction to the diamide **608** and could be a possible reason for the low yield of 21% over two steps.

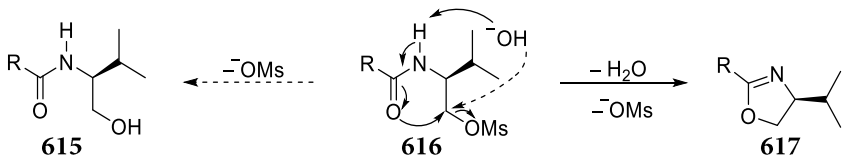

scheme 65. Base induced intramolecular cyclization for oxazoline ring formation and competing back reaction to the hydroxyamide.

In this way, the unmethylated BOX derivative **612** was obtained in a yield of 19% over three linear steps from diethylmalonate (**554**). Next, a monomethylated BOX derivative **581** for subsequent linkage to a bipyridine derivative was prepared. The methyl group serves to separate the conjugated π-system of the bipyridine from the BOX fragment, since a hydrogen atom on the bridging carbon atom would allow imine-enamine tautomerism to extent the conjugated π-system of the ligand and significantly alter the photophysical properties in comparison to $[Ru(bpy)_3]^{2+}$ (**7**). The α-methylation of diethylmalonate (**554**) proceeded smoothly in good yields (78%) and set

the stage for the formation of a diamide **609** as well as the subsequent ring closing sequence, which was performed in the same way as for the unmethylated derivative however in a higher yield of 28% over four linear steps from diethylmalonate (**554**), albeit the additional step of the α-methylation.

To establish an enantioselective photoredox transformation with separate photocatalyst and BOX-Lewis acid complex, the synthesis of dimethylated BOX derivatives **613** and **614** was investigated. Due to the modest yield in the ring closing sequence in the synthesis of the non- or monomethylated BOX derivatives **612** and **581**, alternative synthetic strategies, either again *via* diamides **610** and **611** and alternative ring closing methods, or by direct synthesis from dimethylmalonodinitrile **607** with a Lewis acid were examined. Although the preparation of the diamide by heating a mixture of malonate and aminoalcohol gave satisfactory yields for the synthesis of the diamides **608** and **609**, the synthesis of dimethylated diamides **610** and **611** was carried out *via* the corresponding malonic acid dichloride **606**, as besides L-valinol (**603**) (containing an isopropyl residue) also L-phenylalaninol (**604**) (containing a benzyl residue) was to be incorporated and since the latter is a solid at room temperature and a reaction in molten aminoalcohol **604** was not considered, the acid chloride **606** enabled diamide synthesis under mild conditions. The malonic acid dichloride **606** was generated using DMF and oxalyl chloride and obtained in very good yield (83%) by fractional distillation with minor impurities by acid (< 2%). Reaction of the dichloride **606** with L-valinol (**603**) or L-phenylalaninol (**604**) in the presence of triethylamine gave the corresponding dimethylated diamides **610** and **611** in moderate (45%) or good (77%) yields, respectively. Two distinct ring closing strategies for the conversion of the diamides **610** and **611** into bisoxazolines were investigated. The first method evaluated was another very common approach reported by Evans *et al.* (**scheme 64**, method A), which strongly resembles the two-step ring closing sequence, but which converts the bis(malonamide) **610** in the presence of DMAP, triethylamine, and toluenesulfonylchloride into a bistosylate that cyclizes to the bisoxazoline **613** under the reaction conditions without the need for isolation of the intermediate and initiation of the cyclization by another base, e.g. by refluxing the intermediate in aqueous sodium hydroxide solution.[258] After extraction and removal of the solvent the bisoxazoline **613** can be isolated from the crude product by extraction with hot *n*-pentane. In this way, however, ^{1}H-NMR analysis revealed toluene signals that were traced back to residual *para*-toluenesulfonic acid. Thus, as recommended for further purification to obtain analytically pure samples, the mixture was subjected to a Kugelrohr distillation carried out on a modified rotary evaporator. High vacuum was applied to the apparatus and the rotating flask containing the product mixture was heated to a maximum of 120 °C in an oil bath. The product was condensed by cooling the rotating adjacent Kugelrohr distilling bulbs with liquid nitrogen. However, ^{1}H-NMR analysis showed that the impurity assumed to be *para*-toluenesulfonic acid increased. This indicated that more distillation flasks connected in series are required to separate *para*-toluenesulfonic acid and the bisoxazoline **613**. Due to the encountered problems during purification, a ring closing procedure was investigated involving the Burgess dehydration reagent **619**.[260, 261, 274] The Burgess reagent **619** is an inner salt that binds a γ-hydroxyamide **615** at its terminal hydroxy group while splitting off a triethylammonium cation to form a methoxycarbonyl sulfamate **620**. Assuming a six-membered transition

state, the oxazoline ring **617** might be formed by proton transfer resulting in the fragmentation of the sulfamate into sulfur trioxide and a (methoxycarbonyl)amide anion (**scheme 66**).

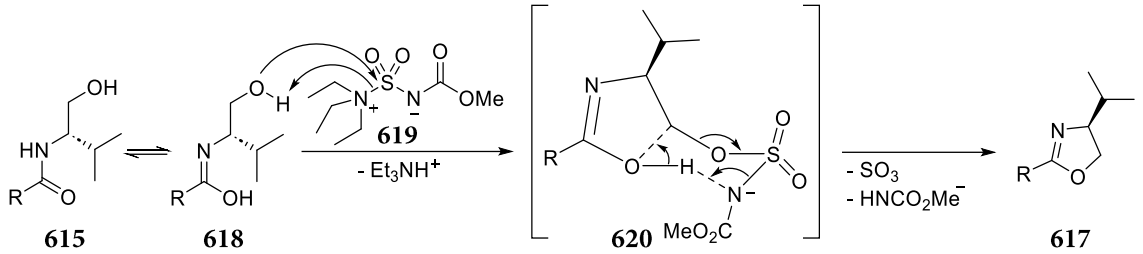

scheme 66. Assumed mechanism of the conversion of γ-hydroxyamides **615** into oxazolines **617** by cyclodehydration using Burgess reagent **619**.

In this way, no product has been obtained using the *i*Pr-hydroxyamide **610**, probably as a result of the use of an older batch of Burgess reagent **619** which, despite storage at −20 °C in a nitrogen glovebox, showed signs of a change in appearance from an off-white solid to a yellow solid with sporadic sticky clumps and significantly reduced solubility in THF. With a benzyl-hydroxyamide **611** and using a new batch of the Burgess reagent **619**, a yield of 65% was obtained. A completely different synthetic strategy employs malonodinitrile **607**, which reacts with amino alcohols in the presence of a suitable Lewis acid to give bisoxazolines.[249-252] To achieve a high yield of bisoxazoline **613**, stoichiometric amounts of $Zn(OTf)_2$ must be used in this direct synthesis. By refluxing the mixture in toluene for 24 hours, excellent yields (90%) were described. However, when sub-stoichiometric amounts were used, only partial ring formation was observed giving the bisoxazoline in a mixture with a monocyclized oxazoline.[275] When the literature-known procedure was performed, the mixture of L-valinol (**603**) and malonodinitrile (**607**) was refluxed in the presence of stoichiometric amounts of $Zn(OTf)_2$ (stored in a nitrogen glovebox) in toluene for twice the reaction time (48 h) to ensure complete conversion to the bisoxazoline **613**. Nevertheless, only the monooxazoline **621** was obtained in a yield of 81%, clearly indicated by the ratio of integrals of methyl- and ring protons or isopropyl signals.

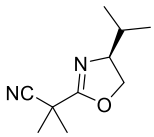

621

figure 23. Obtained monooxazoline side product **621** from the BOX-synthesis from malonodinitriles.

The demand for stoichiometric amounts of zinc triflate may be due to its catalytic inactivation by the water that is released during the reaction. Given the very selective formation of the monooxazoline by-product **621**, it was assumed that stoichiometric amounts of zinc triflate should not be related to the amount of malonodinitrile but to the number of rings to be formed (twice the amount). At this point, since enough material was produced following the other routes, the synthesis of bisoxazolines was not further optimized and the bisoxazolines prepared so far were used either for the enantioselective adaptation of photoreactions (chapter 3.4) or for the linkage with bipyridine derivatives (chapter 3.1.2.3).

3.1.2.3 Nucleophilic aromatic substitution on 4-diazobipyridine **582** and 4-fluorobipyridine **585**

As discussed previously, pyridine derivatives react more readily in nucleophilic aromatic substitutions due to the lower electron density compared to benzene, besides the mesomeric structures suggest that such transformations occur preferentially at positions 2 and 4. Nevertheless, several attempts to obtain malonylpyridine derivatives by nucleophilic substitution failed with 4-bromopyridine (**551**) and 4-chloropyridine (**553**) (chapter 3.1.1.2). Assuming that the reaction was hampered by the absence of a suitable leaving group, 4-fluorobipyridine **585** and its precursor 4-diazobipyridine **582** were synthesized and evaluated in substitution reactions with both the malonate ester **605** and BOX-derivative **581** (**scheme 67**). Different base/solvent combinations and temperatures were investigated. The parameters and results of selected experiments are summarized in **table 2**.

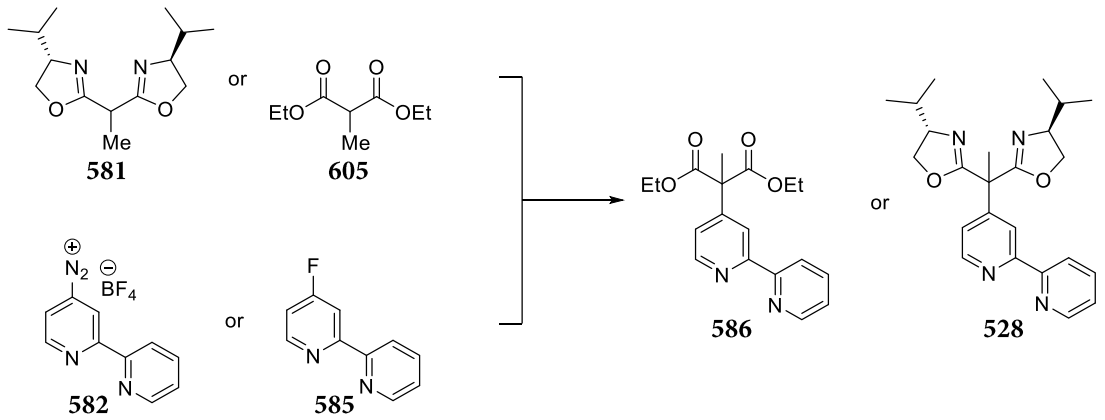

scheme 67. Nucleophilic aromatic substitution on 4-diazobipyridine **582** and 4-fluorobiyridine **585** with 2-methyldiethylmalonate (**605**) and monomethylated BOX **581**.

table 2. Reaction parameters and results of selected experiments on the nucleophilic aromatic substitution.

entry	nucleophile	bipyridine	base	solvent	temperature	yield [%]
1	**605**	**582**	NaH	DMF	rt	---
2	**605**	**582**	NaH	THF	reflux	---
3	**605**	**582**	KHMDS	DMF	rt	---
4	**581**	**582**	KO*t*Bu	DMF	rt	---
5	**581**	**582**	*t*BuLi	THF	–78 °C → rt	---
6	**581**	**585**	KO*t*Bu	DMF	150 °C	---
7	**581**	**585**	*t*BuLi	THF	–78 °C → rt	traces
8	**581**	**585**	*t*BuLi	THF	–78 °C → rt	traces
9	**581**	**585**	*t*BuLi	THF	–78 °C → rt	*t*Bu-bipyridin
10	**581**	**585**	LDA	THF	–78 °C → rt	traces

For the optimization of a nucleophilic aromatic substitution reaction, the quality of a leaving group in terms of the stability of the cleaved fragment is not the only critical factor. Nucleophilic aromatic substitutions proceed *via* an

addition-elimination mechanism. The first step, i.e. the addition, is comparatively slow, as the aromaticity is lost, whereas the subsequent elimination is fast, since the aromaticity is restored. Although the stability of the leaving group may increase the rate of the second step, the total reaction rate remains unaffected since the addition step is the bottleneck of the reaction. Although the fluoride anion is a less stable leaving group than chloride or bromide, the negative hyperconjugation may contribute to both an activation of the heteroaromatic for nucleophilic aromatic substitutions and a stabilization of the intermediate obtained after loss of aromaticity. Unfortunately, several approaches with the use of both malonate ester **605** and monomethylated BOX **581** employing 4-fluorobipyridine **585** using various bases (NaH, KHMDS, KO*t*Bu, *t*BuLi) failed (entries 1 - 5). Neither TLC-MS nor NMR allowed detection of product formation. Therefore, the diazonium salt **582** was used in further approaches. Hoping for a highly convergent synthetic route, monomethylated BOX **581** was continued to be used as the nucleophilic component. To force reactivity, the previously unsuccessful combination of KO*t*Bu in DMF was tested again at elevated temperature. Upon addition of the diazonium salt **582** an immediate nitrogen release was observed. This could either be the result of a Balz-Schiemann-type conversion to fluorobipyridine **585** or a side reaction of the diazonium salt **582** with DMF (although, the corresponding *ortho*-hydroxyaldehyde was not detected).[276] The reaction indicated that the cleavage of nitrogen occurs rapidly, so further bases were investigated at low temperature. Using *t*BuLi, the mass of the protonated BOX-bipyridine **528** was detected by TLC-MS for the first time. Since it was a very small scale experiment, only traces of a substance with a similar ^{1}H-NMR spectrum to BOX-bipyridine **528** was obtained after column chromatography (entry 7). Since the integrals did not fit and the purification by column chromatography was complicated, it was assumed that the obtained product was still contaminated with monomethylated BOX **581**. Therefore, the reaction with *t*BuLi was repeated. This time the product mass BOX-bipyridine **528** + NH_4^+ was detected by TLC-MS. Again, the removal of BOX residues by column chromatography was not successful and only trace amounts of the product were obtained (entry 8). As the experiment was performed a third time, a substance with the mass of 4-*tert*-butyl-bipyridine was found dominantly in TLC-MS and a ^{1}H-NMR spectrum was obtained, which, in addition to bipyridine signals, included a singulet at 1.54 ppm with approximately 7 H; due to the low concentration, the integrals might be incorrect and the singulet interpreted as a *tert*-butyl residue (entry 9). The formation of *tert*-butyl bipyridine suggests that even the sterically demanding *t*Bu anion is too nucleophilic for the very good leaving group N_2. In a further approach, the even bulkier and less nucleophilic LDA was used (entry 10). After purification, however, the reaction again gave only traces of a substance similar to BOX-bipyridine **528**, purification of which was not successful. This synthetic approach would formally represent a very convergent synthetic route, although it requires the separate synthesis of both BOX **581** and a bipyridine derivative **582** or **585**, resulting in 10 total steps on top of the relatively unsuccessful nucleophilic aromatic substitution. Therefore, the route for the synthesis of BOX bipyridine by nucleophilic aromatic substitution was not pursued any further. Instead, the development of a synthetic route for DiBOX-bipyridine derivatives **529** and **531** by side chain functionalization of dimethylbipyridine **626** was the focus of the following experiments, providing access to the desired ligand structure in only four linear steps.

3.1.3 BOX-bipyridine **529** and **531** synthesis *via* side-chain functionalization of dimethylbipyridine **626**

Another retrosynthetic approach exploits the extraordinary kinetic acidity of the heterobenzylic protons for the stepwise conversion of 4,4'-dimethylbipyridine **626** into their corresponding methylene bases,[248] which should readily undergo nucleophilic addition to ethyl chloroformate (**627**), thus giving access to 4,4'-dimalonylbipyridine. Subsequent methylation at the benzylic α-positions would separate the conjugated π-system of the bipyridine from the bisoxazoline fragment and provide access to the central compound **625** of this synthetic approach. From there, the BOX-bipyridines **529** and **531** could be accessible either *via* formation of hydroxyamides **622** and **623**, that can be transformed into the corresponding bisoxazolines **529** and **531** by a multitude of pathways including Lewis-acid activation,[132, 264, 265] dehydratization[132, 259-263] and (most commonly) conversion of the terminal hydroxy groups into leaving groups followed by intramolecular nucleophilic substitution.[252-258] Alternatively, the methylated dimalonylbipyridine **625** could be converted into the tetranitrile **624** by dehydratization of a bis(malonamide) or a bis(dioxime) and provide access to the desired bisoxazoline-substituted bipyridines **529** and **531** by the direct reaction with chiral aminoalcohols in the presence of a Lewis acid or *via* the addition of aminoalcohols to iminohydrochlorides.[249-252, 254, 271-273] This synthetic approach requires only four linear steps and allows varying the steric demands of the bisoxazoline residues at a late stage of synthesis by using differently substituted aminoalcohols. However, this strategy involves the intrinsic challenge that the corresponding transformations must take place at four reaction centres on almost every stage. Obtaining high conversions is of particular importance due to potentially difficult to separate (since similar) product mixtures (**scheme 68**).

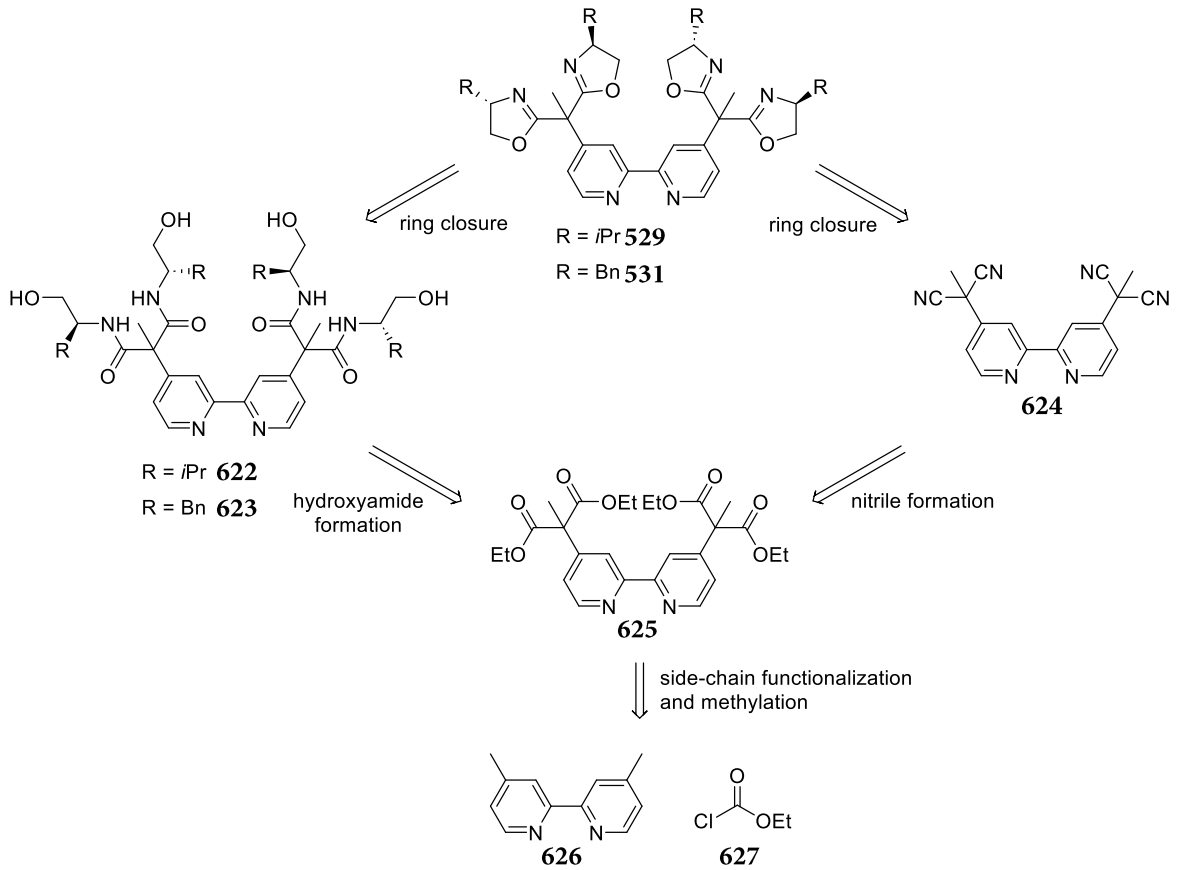

scheme 68. Retrosynthetic approach *via* side-chain functionalization of 4,4'-dimethylbipyridine **626**.

3.1.3.1 Synthesis of 4,4'-dimalonyl-bipyridine **636** by heterobenzylic functionalization

Heterobenzylic protons show a kinetic acidity that is 10^5 times higher than that of benzene derivatives. This becomes evident by H/D exchange experiments of 2-, 3- or 4-picoline (**628**, **631**, **633**)(relative rates: 130:1:1810 in MeOD, MeONa at 20 °C, toluene = 10^{-5}). This is due to the resonance stabilization of the carbanions with participation of the heteroatom when deprotonating at positions 2 and 4 (**scheme 69**).[248]

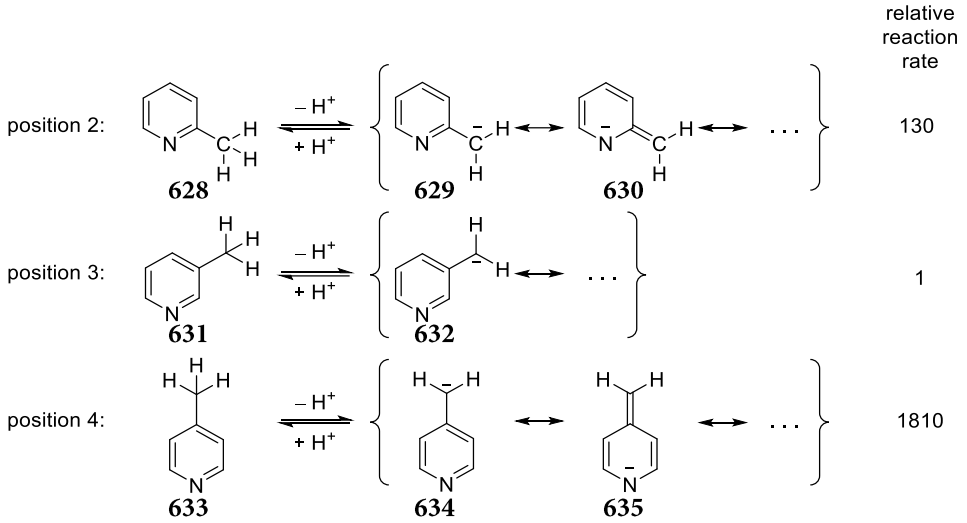

scheme 69. Mesomeric structures of deprotonated picolines and relative reaction rates.[248]

Given the equilibrium between 2- and 4-alkylpyridines with their methylene bases that readily react as nucleophilic enamines, attempts were made to synthesize bis(diethylmalonyl)bipyridine **636** by side-chain functionalization of 4,4'-dimethylbipyridine **626** (dmb) through deprotonation with LDA and reaction with ethyl chloroformate (**627**).

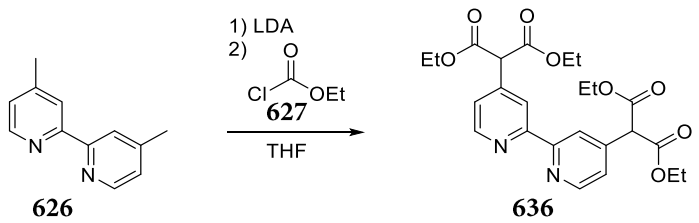

equation 19. Side-chain functionalization of 4,4'-dimethylbipyridine **626**.

The deprotonation of dimethylbipyridine **626** with 2.2 eq. LDA caused an immediate change of colour of the solution to deep red. After addition of 2.5 eq. ethyl chloroformate (**627**), the quick colour change from red to yellow indicated that all methylene bases were added to the electrophile. Only ten minutes after the addition of LDA and ethyl chloroformate (**627**) the formation of mono-, di-, tri- and tetrasubstituted bipyridine-derivatives was confirmed by TLC-MS (**figure 24**).

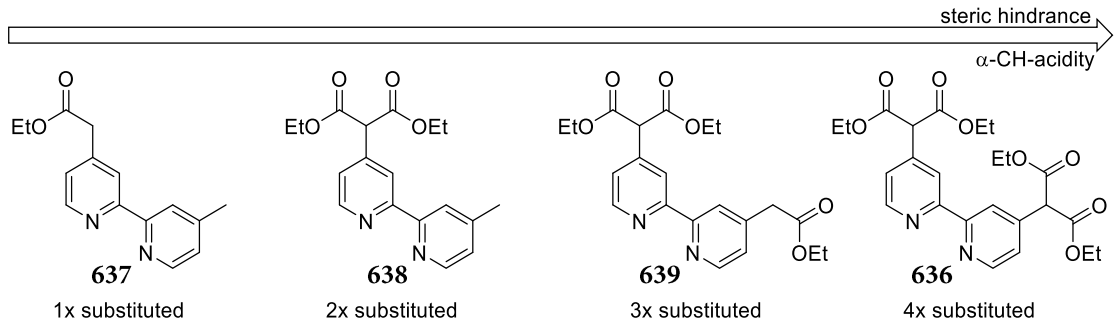

figure 24. Assumed substitution patterns related to the product masses detected 10 minutes after addition of LDA and ethyl chloroformate (**627**).

The substances shown in **figure 24** are most likely formed, since the acidity increases with the number of electron-withdrawing substituents and the formation of the pentasubstituted product was not detected, presumably due to steric hindrance. Accordingly, despite increasing acidity, the formation of the isomers shown in **figure 25** is possible but unfavorable due to steric hindrance or pK_a considerations.

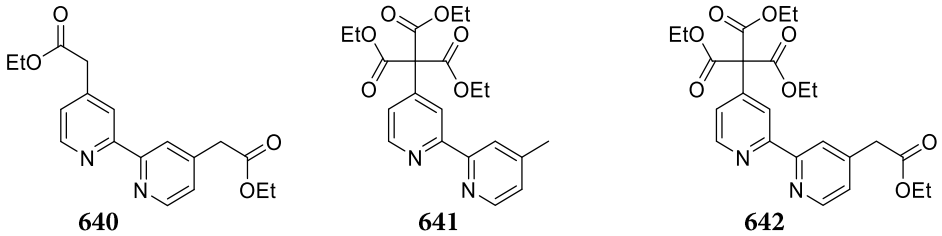

figure 25. Possible but due to pK_a or steric hindrance unfavored isomers.

As the BOX-synthesis requires a malonate moiety only the (tetrasubstituted) dimalonate bipyridine **636** as well as the (disubstituted) malonate bipyridine **638** are of interest for the following synthetic route. Since the selective termination of the reaction at the disubstituted derivative **638** seemed impossible, a total of 6.1 equivalents of both LDA and ethyl chloroformate (**627**) were added alternatingly to achieve high conversion to the tetrasubstituted dimalonate bipyridine **636**. Applying these conditions resulted in the product distribution shown in **equation 20**.

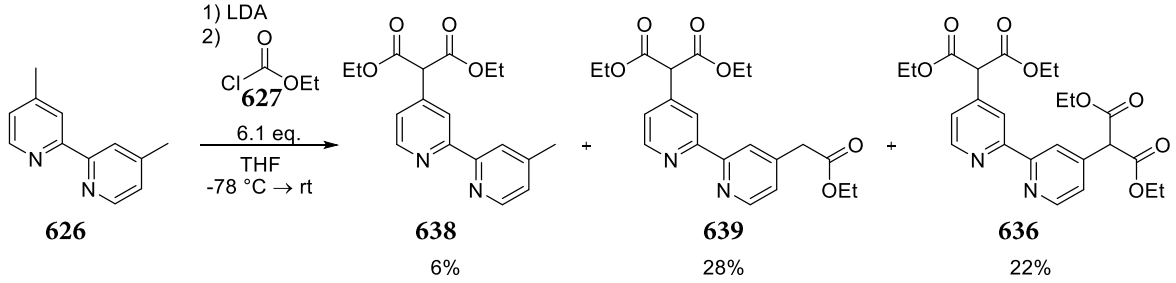

equation 20. Product distribution from the side chain functionalization of dimethylbipyridine (**626**) with LDA and ethyl chloroformate (**627**).

In an attempt to convert a mixture of disubstituted and trisubstituted bipyridines **638** and **639** in an analogous reaction with LDA and ethyl chloroformate (**627**) to the tetrasubstituted bipyridine **636**, one excess equivalent of each led for the first time to the formation of the pentasubstituted product. This is probably a consequence of the along with the degree of substitution increasing acidity. In previous reactions, the formation was not observed, as

excess equivalents of base reacted with residues of other excess equivalents of ethyl chloroformate (**627**). In order to increase the yield of the tetrasubstituted derivative, a direct addition of both 4.4 eq. LDA and ethyl chloroformate (**627**) was performed. As multiple simultaneous deprotonations are unlikely, the excess equivalents reacted quickly to form a substance with the mass of ethyl diisopropyl carbamate (**643**) (**figure 26**).

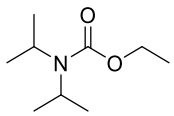

643

figure 26. Presumably formed side product ethyl diisopropyl carbamate (**643**) derived from excess equivalents of LDA and ethyl chloroformate (**627**).

Therefore, in all further approaches LDA and ethyl chloroformate (**627**) were repeatedly added alternatingly until the conversion to the tetrasubstituted product **636** did no longer appear to increase. Thereby, a maximum yield of 25% was obtained. In the corresponding experiment the formation of the sticky black mass was also observed, presumably resulting from the side reaction of excess equivalents. Accordingly, the precise addition of equivalent amounts of LDA and ethyl chloroformate (**627**) must be ensured. Since the pK_a decreases with a growing degree of substitution, the higher substituted derivatives are preferably deprotonated in a mixture of different degrees of substitution. The formation of the pentasubstituted product is generally possible; therefore the conversion of di- or trisubstituted bipyridine **638** and **639** in a mixture with the tetrasubstituted bipyridine **636** is not possible. Accordingly, the overall yield could only be increased by ensuring an evenly increasing degree of substitution. Since a mixture of mono-, di-, tri- and tetrasubstituted bipyridine was detected by TLC-MS after only 10 minutes and after the addition of 2.2 eq. of LDA and 2.5 eq. ethyl chloroformate (**627**), controlling the degree of substitution is a major challenge. Especially since it cannot be avoided that after addition of one equivalent of ethyl chloroformate (**627**) to a quantitatively deprotonated solution of dimethylbipyridine **626**, the initially formed monosubstituted derivatives might participate in a deprotonation by unsubstituted dimethylbipyridine anions, thereby leading to a neutralization of the unsubstituted derivatives and at the same time paving the way for the second substitution of the already substituted derivatives. To solve this problem, after quantitative deprotonation a very fast addition of the electrophile should take place, allowing the dimethylbipyridine anions to react uniformly with one equivalent each without time for reprotonation. Since a sticky black substance was observed in all reactions, possibly as a result of the side reaction of excess equivalents to ethyl diisopropyl carbamate **643**, the reaction should be performed using a mechanical stirrer. Applying these conditions increased the maximum yield of the tetrasubstituted product **636** to 30%. In the corresponding experiment the formation of the sticky black mass was again observed, although great attention was given to the precise addition of one equivalent of reactant for every cycle of functionalization. Although a maximum yield of only 30% of dimalonylbipyridine **636** was obtained, the described strategy provides access to malonylsubstituted (bi-)pyridine derivatives for the first time. Furthermore, the present synthetic approach provides access to the ligand structure DiBOX-bpy **613** by side chain functionalization of 4,4'-dimethylbipyridine **626** in only four linear steps, thus a yield of 30% is limiting but

significantly more efficient compared to the convergent synthetic approach (see chapter 3.1.2) consisting of 10 linear steps.

3.1.3.2 Methylation at heterobenzylic α-position

The dimalonyl bipyridine derivative **636** was methylated at the benzylic α-positions. The methylation was performed by deprotonation with potassium carbonate in DMF and subsequent addition of methyl iodide. After 24 hours a complete conversion to the product **625** was detected by TLC-MS. Precipitation of the product from chloroform/*n*-hexane gave the dimethylmalonyl bipyridine **625** in very good yield (85%) as colorless crystals (**equation 21**).

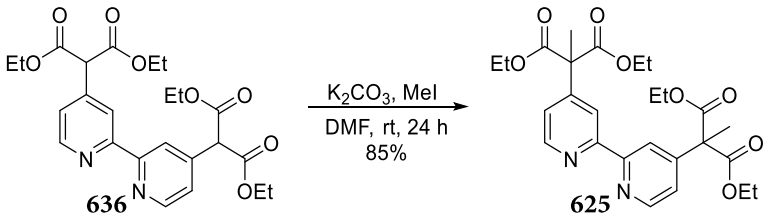

equation 21. Methylation of dimalonylbipyridine **636** at the benzylic α-positions.

Installing a methyl group at this position and thereby removing the remaining α-carbonyl-proton prevents imine-enamine-tautomerism in the final BOX-bipyridine product **529** and therefore separates the aromatic bipyridine fragment from the BOX-ligand. Besides slightly electron-withdrawing inductive effect of the BOX-fragments, the BOX-bipyridine ligand should as a result not exhibit significantly altered photophysical- or electrochemical properties, when implemented into a $[Ru(R\text{-}bpy)_3]^{2+}$ type catalyst structure (**scheme 70**).

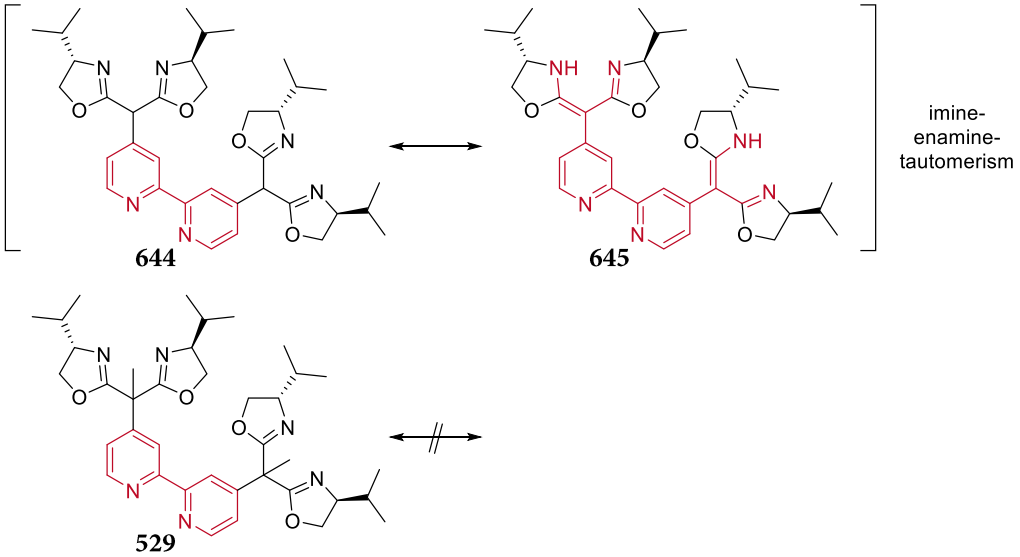

scheme 70. Imine-enamine-tautomerism DiBOX-bipyridine-derivatives with and without methyl group.

Given this central key molecule of the present synthetic route, bis(2-methyldiethylmalonyl)bipyridine (DiMeMal-bpy) **625**, the stage was set for the synthesis of BOX-substituted bipyridine ligands **529**. As mentioned earlier, the synthesis of bisoxazolines from malonic acid esters can be carried out in two ways, essentially consisting of the

same main steps, however, due to the different sequential order of the steps, proceeding *via* significantly differing intermediates as summarized in **scheme 71**.

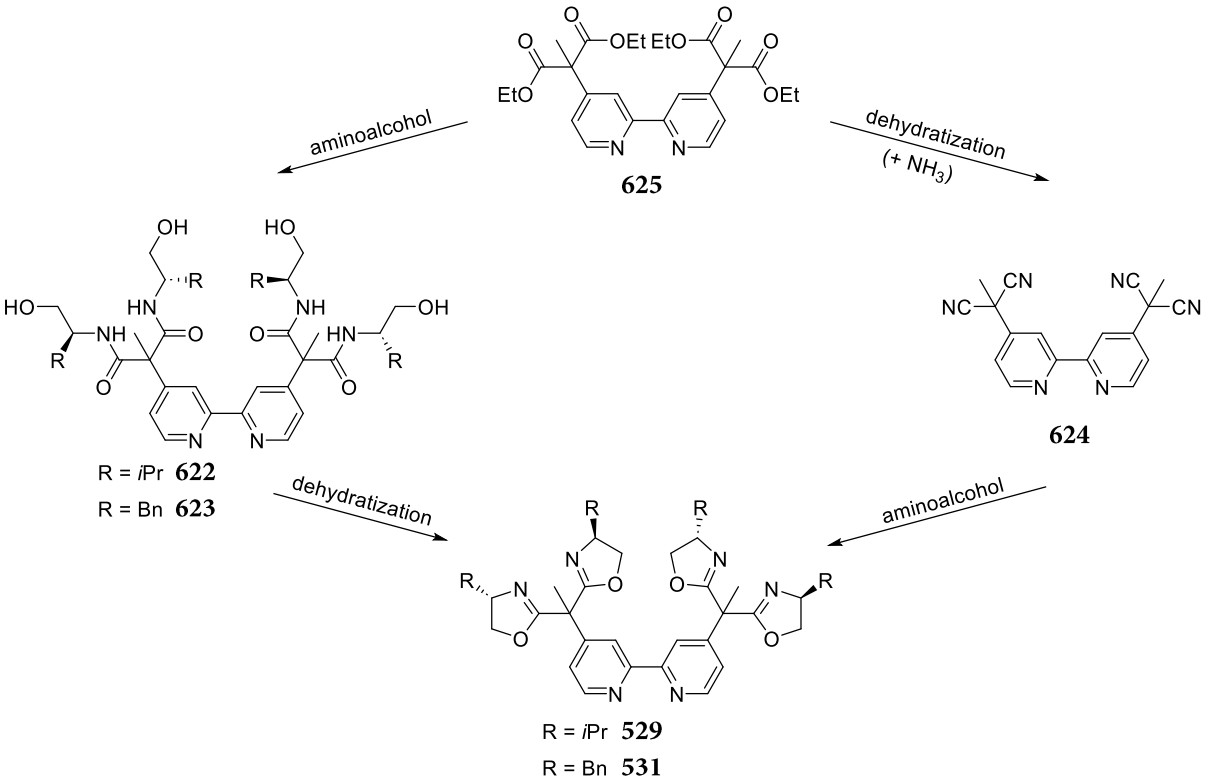

scheme 71. General pathways for the synthesis of bisoxazolines from malonate esters.

Starting from DiMeMal-bpy **625**, a tetra-γ-hydroxyamide **622** and **623** can be synthesized through attachment of chiral aminoalcohols (chapter 3.1.3.3). The subsequent ring closure of the γ-hydroxymalonamide fragments to the bisoxazoline substructures formally represents a dehydration, achievable by a variety of synthetic strategies, including Lewis-acid catalysis,[132, 264, 265] dehydrating reagents[132, 259-263] or most commonly *via* conversion of the terminal hydroxygroups into suitable leaving groups followed by intramolecular nucleophilic substitution[252-258] (chapter 3.1.3.3.4). Alternatively, after conversion of the bis(malonyl)bipyridine **625** with ammonia into a malonamide, it can first be dehydrated to obtain a bis(malonodinitrile) **624** (chapter 3.1.3.4.1), which in a second step can be converted into bisoxazolines **529** with chiral amino alcohols in the presence of suitable Lewis acids (chapter 3.1.3.4).[249-252, 277-279]

3.1.3.3 Synthesis of BOX-bipyridine **529** and **531** *via* γ-hydroxyamides **622** and **623**

3.1.3.3.1 Synthesis of *i*Pr-tetra-γ-hydroxyamide **622**

In analogy to the procedure described for the synthesis of bisoxazolines from malonate esters (chapter 3.1.2.2), the bis(2-methyldiethylmalonyl)bipyridine (**625**) was heated in excess L-valinol (**603**), aiming at the formation of the tetra-γ-hydroxymalonamide-bipyridine **622** (**equation 22**).

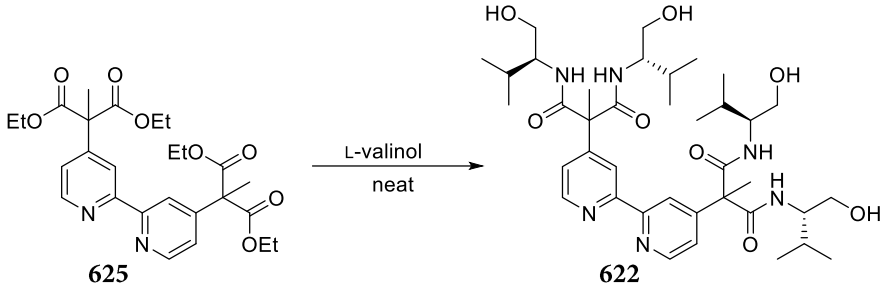

equation 22. Synthesis of the *i*Pr-tetra-γ-hydroxyamide **622** from malonylbipyridine **625**.

Due to the steric demands of the product **622** and intermediates the formation of the tetra-γ-hydroxyamide **622** is very slow. Attempts to increase the reaction rate by raising the temperature (above 75 °C) failed, given that water residues, possibly originating from the highly hygroscopic L-valinol (**603**), might trigger a partial saponification of the ethyl ester groups. The resulting β-amido carboxylic acids **647** can undergo decarboxylation reactions at elevated temperatures, thereby yielding the bisamide **649** containing only two amide strains and two heterobenzylic protons generated by saponification and decarboxylation in a yield of 86% (**scheme 72**).

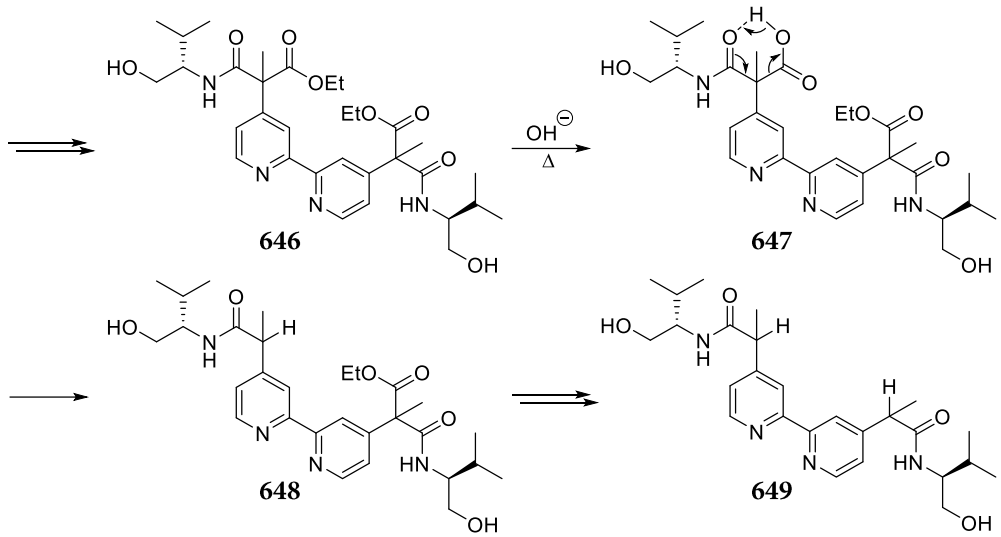

scheme 72. Observed saponification decarboxylation sequence yielding the bisamide **649** as side product.

The obtained bisamide **649** could potentially be used for the synthesis of unsymmetrically substituted bisoxazolines, but this pathway was not further investigated. In order to avoid such saponification-decarboxylation sequences, further approaches were performed in L-valinol (**603**) that was previously dried on an inverse Dean-Stark trap and thereafter distilled under high vacuum into the reaction flask. The malonylbipyridine **625** was then added in a nitrogen counterflow and the reaction mixture was first heated slightly above the melting point of

L-valinol (**603**). However, at this temperature the reaction was so slow that after 48 hours the lower intermediates (mono- and diamide) were only slightly indicated. Therefore, the reaction mixture was gradually heated to 80 °C within three days, and catalytic amounts of sodium hydride were added to the reaction mixture,[280] while regularly monitoring the conversion and the intermediates. In this way, after a total of seven days, only the product **622** mixed with the diamide **646** was detectable on TLC-MS. The formation of the diamide **646** proceeded comparatively unhindered, while the binding of two further valinol-amide strands is probably hindered sterically. This assumption is supported by the observation that the reaction mixture had to be stirred at 75 °C for another 10 days before complete conversion to the product **622**. In a smaller scale, product formation under the optimized conditions was first observed after 48 hours. After 5 days the tetra-γ-hydroxyamide **622** was dominant on TLC-MS. During workup, the main impurity excess L-valinol (**603**) was easily regained by vacuum distillation of the crude mixture. The residue was then subjected to a short silica column and finally purified by precipitation from dichloromethane/*n*-hexane to give the tetraamide **622** as a colourless crystalline solid in excellent yields (95%). This process was also successful on a gram scale (**equation 23**).

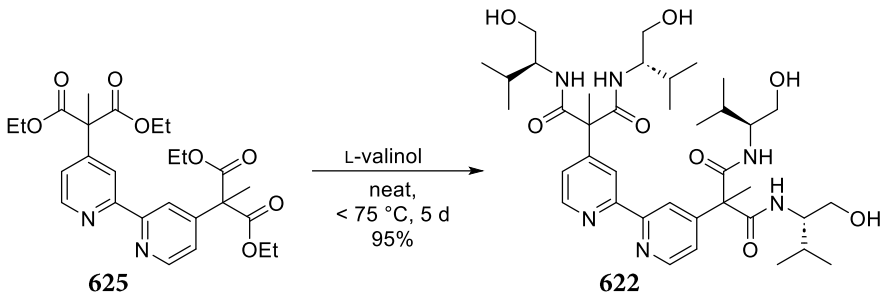

equation 23. Optimized conditions for the synthesis of the *i*Pr-tetra-γ-hydroxyamide-bipyridine derivative **622**.

3.1.3.3.2 Synthesis of Bn-tetra-γ-hydroxyamide **623**

An advantage of the synthetic strategy for BOX-bipyridine derivatives *via* side-chain functionalization is that during amide formation a broad scope for diversification arises at a late synthetic stage. By using different amino alcohols, the steric demands of the BOX residues should be precisely adjustable. Thus, instead of using L-valinol (**603**), ultimately leading to isopropyl residues in the BOX fragments, some attempts have been made employing L-phenylalaninol (**604**), aiming for benzyl residues. Given that L-phenylalaninol (**604**) is a solid at room temperature the amide formation by heating malonylbipyridine **625** in the molten aminoalcohol (**604**) (neat) was not considered an option at first. Therefore, different solvents for the formation of the tetraamide **623** with L-phenylalaninol (**604**) were investigated, the results of which are summarized in **equation 24**.

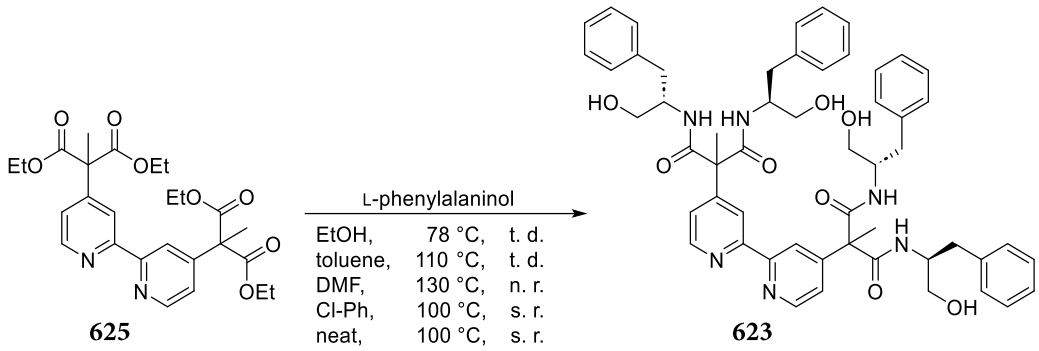

equation 24. Conditions and results of selected experiments for the formation of the Bn-tetra-γ-hydroxyamide-bipyridine derivative **623**. t. d. = traces detected in TLC-MS, n. r. = no reaction, s. r. = side reaction.

For this purpose, malonylbipyridine **625**, L-phenylalaninol (**604**) and catalytic amounts of sodium hydride were dissolved in ethanol, toluene or DMF and stirred for five days at 78 °C, 110 °C or 130 °C, respectively. Although TLC-MS investigations of the experiments in ethanol (78 °C) and toluene (110 °C) indicated the formation of the product **623** after 24 hours, it could not be excluded that the assumed product signal was only the result of a contamination in the background noise when repeatedly measuring blank spectra. During further TLC-MS analyses no further increase in product formation was detected. However, the formation of a species with the mass of bis-γ-hydroxyamide (m/z 711.1) was repeatedly detected in ethanol and toluene (**figure 27**).

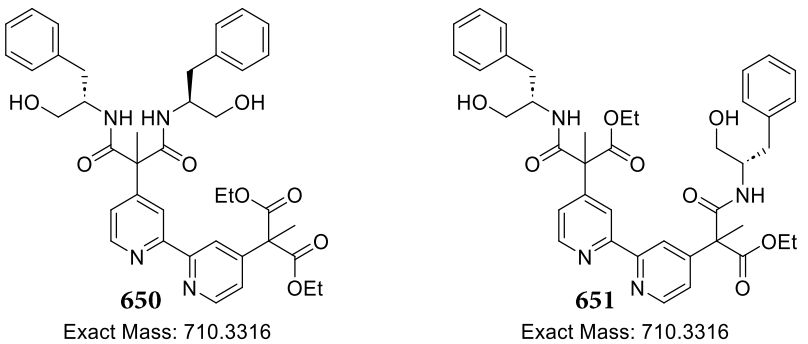

figure 27. Assumed structures of bis-γ-hydroxyamides **650** and **651** related to the detected mass.

Due to the greater steric demand of the benzyl residues in L-phenylalaninol (**604**), the formation of the desired tetraamide **623** could be even more hindered (and thus slower) than the amide formation with L-valinol (**603**). To accelerate the reaction, it was performed again in chlorobenzene, the increased polarity of which should be accompanied by improved solubility of both the reactants as well as the ethanolate or ethanol molecules released during the reaction. After 40 hours, a TLC showed the complete turnover of the reactant, as well as two new spots of significantly higher polarity. The analysis of these spots by TLC-MS indicated both the excess L-phenylalaninol (**604**) (m/z 152.1) and the formation of the tetra-γ-hydroxyamide product **623**: Although the product mass (m/z 921.4) in the mass spectrum of the TLC spot was merely indicated with low intensity besides a dominant peak at m/z 567.4, a closer examination revealed a set of peaks with a mass difference of 44 and a linear increase of intensity from m/z 830.9 (tetra-γ-hydroxymalonamide after fragmentation of one benzyl residue **653**) to m/z 567.4. The fragments with a mass of 44 could be traced back to the separation of 2-hydroxyethyl radicals **654** or isocyanic acid (**656**). The observation suggests a stepwise fragmentation of the product **623** to a species **658** with m/z 567.4 under the conditions of mass spectrometry (**scheme 73**)

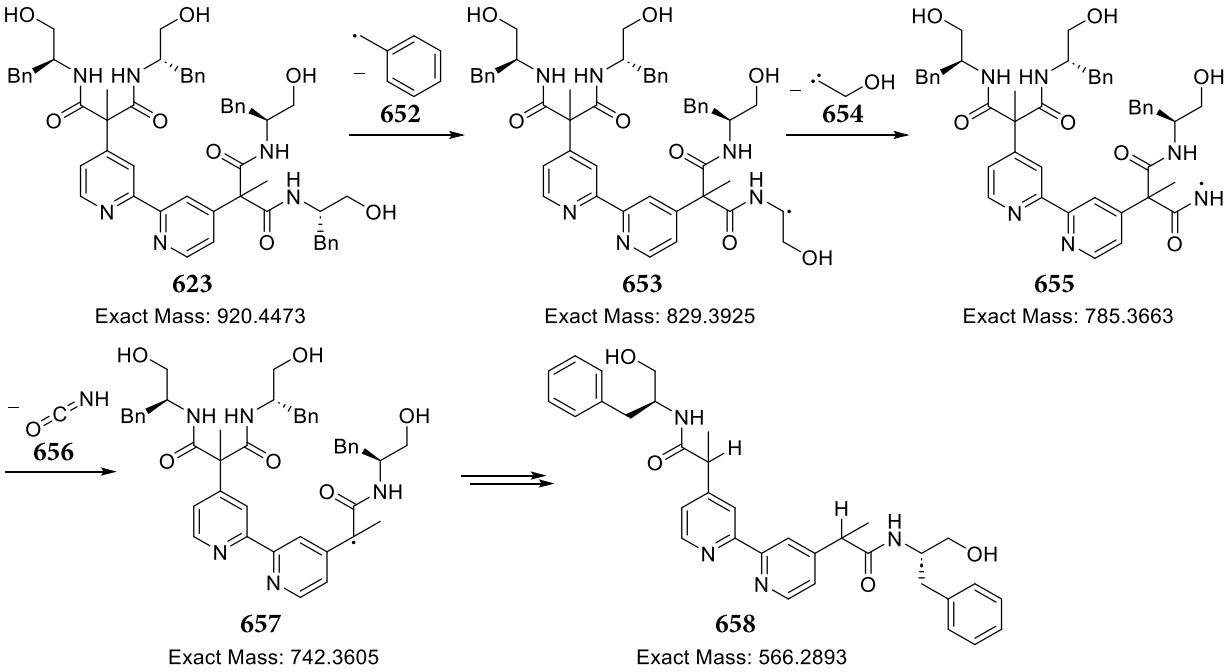

scheme 73. Conceivable mechanism for the detected fragmentation pattern in TLC-MS.

Alternatively, the dominant peak at m/z 567.4 might, in analogy to the observed side product formation in the synthesis of *i*Pr-tetra-γ-hydroxyamide **622** (chapter 3.1.3.3.1), be traced back to a saponification-decarboxylation sequence, ultimately leading to the same bisamide **658** (**scheme 74**).

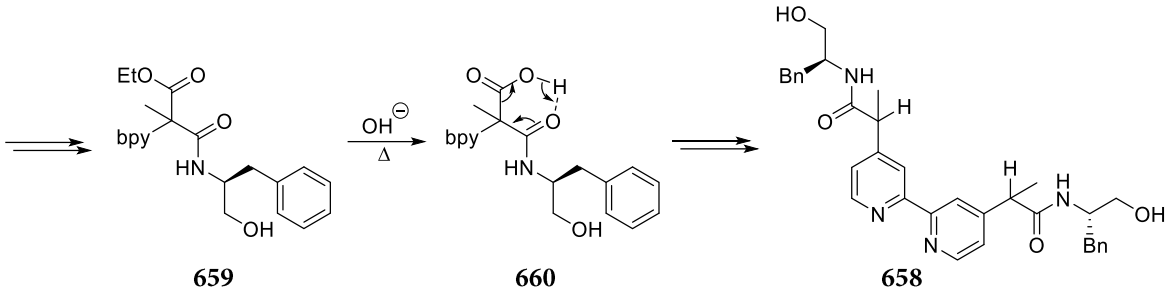

scheme 74. Saponification decarboxylation sequence yielding the bisamide **658** as side product.

After work-up by removal of the solvent and column chromatography, no substance was isolated with an ^{1}H-NMR spectrum containing the characteristic bipyridine signals. Similar to the *i*Pr-bisamide **649**, the Bn-bisamide **658** could itself be a compound that is nearly insoluble even in an eluent mixture of dichloromethane/methanol/ammonia and could thus not be washed off the silica gel.

To enforce the formation of the benzyl-substituted tetra-γ-hydroxyamide **623**, the reactants malonylbipyridine **625** and L-phenylalaninol (**604**), which are solids at room temperature, were gradually heated with catalytic amounts of NaH up to the melting temperature of the amino alcohol (**604**) (first observed at bath temperature 95 °C) and ultimately stirred at 100 °C for 65 hours. TLC-MS analysis indicated the complete conversion of malonylbipyridine **625** to a very polar species that showed the same fragmentation pattern as in the amide formation in chlorobenzene. For product isolation, most of the excess L-phenylalaninol (**604**) was recovered by sublimation. The residue was purified by column chromatography, but again no bipyridine derivative was obtained. Perhaps the investigated reaction temperatures were too high for the amide formation, since especially 2-arylmalonate derivatives are prone to undergo thermal decarboxylation.[281] Therefore, the synthesis of BOX-substituted bipyridines containing benzyl residues **531** *via* hydroxyamide **623** was not pursued further and instead the synthesis of bis(malonodinitrile)-bipyridines **624** as precursors for the synthesis of Bn-BOX-bpy **531** was approached.

3.1.3.3.3 Alternative approaches for the synthesis of γ-hydroxyamides

3.1.3.3.3.1 Side-chain functionalization of dimethylbipyridine **626** with isocyanate **662**

In addition to the synthesis by amide formation from malonylbipyridine **625** an alternative approach for the synthesis of the tetraamide was evaluated, starting from dimethylbipyridine **626**. It was assumed that the high reactivity of *in situ* generated *O*-TBDMS-valinol-isocyanates **662** could be used for the direct formation of a tetraamide **663** from dimethylbipyridine **626** (**scheme 75**).

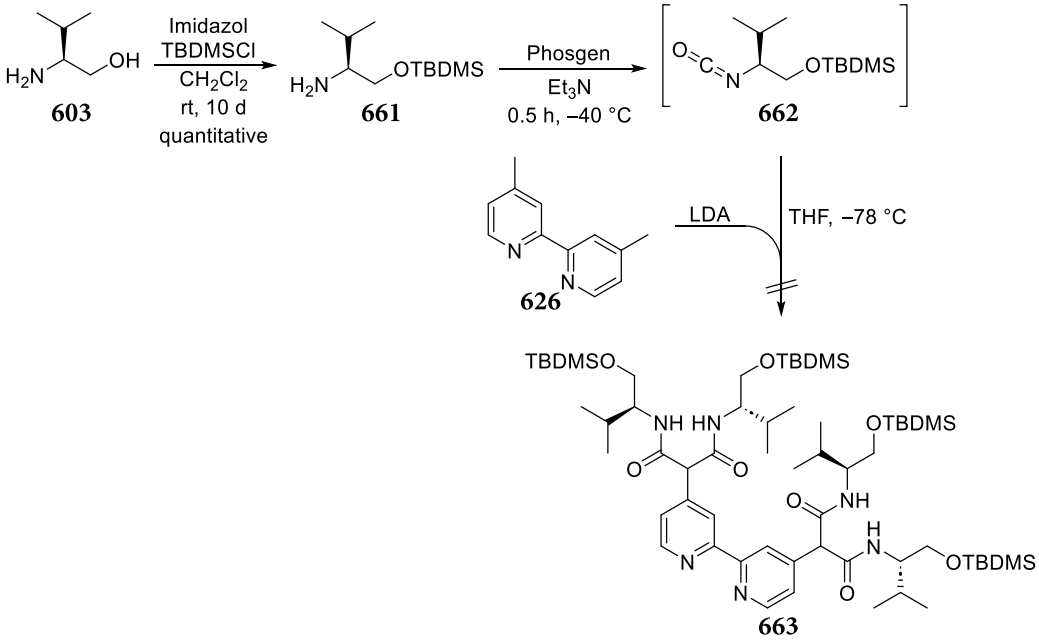

scheme 75. Alternative synthetic approach for the direct synthesis of a tetraamide-bipyridine species **663** from dimethylbipyridine **626**.

For this purpose, L-Valinol (**603**) was protected at the hydroxy group in quantitative yield using imidazole and TBDMSCl in dichloromethane. The TBDMS protected L-Valinol **661** was then converted with phosgene in triethylamine to the corresponding isocyanate **662**. After 30 minutes, a white suspension was formed whose NMR spectroscopic analysis indicated the absence of amino group signals. The white suspension was then added to a deep red solution of dimethylbipyridine **626** and LDA. No decoloration of the solution was observed (in analogy to the side chain functionalization in chapter 3.1.3.1) and also no signs of product formation were detected by TLC-MS. In a second experiment, the mixture of dimethylbipyridine **626** and LDA was added to a suspension of the isocyanate **662**, but again the desired reaction was not observed. Preliminary stages of tetraamide (i.e. mono-, di-, triamide) were also not detected. Although this synthetic approach would have allowed the direct formation of a tetraamide species **663** from dimethylbipyridine **626**, a subsequent methylation would have been necessary in order to separate the π-system of bipyridine from the BOX fragment. Furthermore, this synthetic approach requires two additional steps (TBDMS protection and deprotection) and was therefore not pursued any further.

3.1.3.3.3.2 Synthesis of Bn-tetra-γ-hydroxyamides **623** *via* malonic acid derivatives

Furthermore, an alternative strategy for the synthesis of the benzyl-tetra-γ-hydroxymalonamide **623** was evaluated, involving the bis(2-methylmalonic acid) **664** which was obtained by saponification of malonylbipyridine **625** with potassium hydroxide in very good yield (83%). The bis(malonic acid) **664** was then treated with L-phenylalaninol (**604**) in the presence of the carbodiimide coupling reagent EDC HCl and DMAP. However, neither the formation of the product **623** nor the formation of lower intermediates could be detected under these conditions.

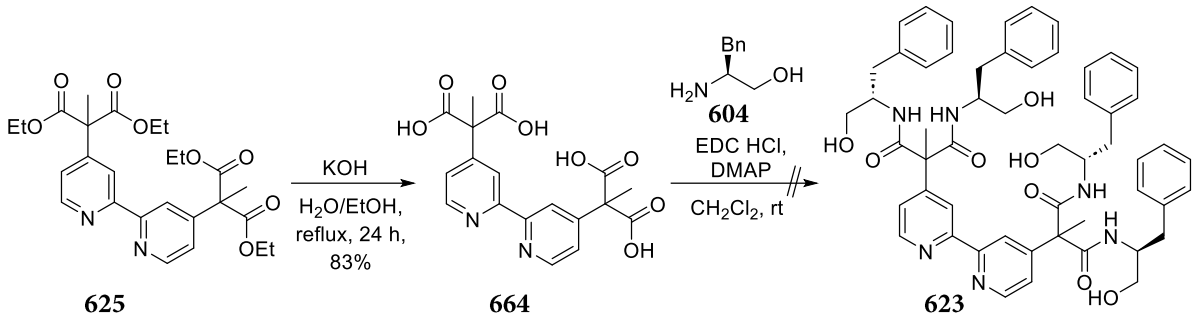

scheme 76. Attempted synthesis of Bn-γ-hydroxyamide **623** *via* bis(2-methylmalonic acid) **664**.

Possibly the linkage of the tetraacid **664** with the amino alcohol **604** requires prior activation *via* the acid chloride. Since acid chlorides are highly reactive and often unstable, and since four carboxyl groups would have to be activated simultaneously in the molecule, which also corresponds to an additional synthetic step, this procedure was not pursued further. Instead, further approaches focused on the conversion of isopropyl-tetra-γ-hydroxyamide bipyridine **622** to the corresponding *i*Pr-BOX-bpy ligands **529** (chapter 3.1.3.3.4).

3.1.3.3.4 Ring-closing-strategies for the conversion of γ-hydroxyamide **622** into BOX-bipyridine **529**

The synthesis of oxazoline structures can essentially be performed by two established synthetic strategies: By reaction of nitriles with aminoalcohols in the presence of suitable Lewis acids (chapter 3.1.3.4),[249-252] or by ring closure of γ-hydroxyamides, like *i*Pr-tetra-γ-hydroxyamide **622**. A multitude of conditions for initiating the ring closure has been successfully applied: Ring closure was achieved by activation of γ-hydroxyamides with Lewis acids,[132, 264] e.g. dimethyltin dichloride or trifluoroborane diethyl etherate. Due to the toxicity and high reactivity accompanied by potential loss of selectivity, several different ring-closing methods have evolved, which are characterized by milder conditions and are essentially based on two principles: (a) The dehydration by use of hydrophilic substances, e.g. calcium hydride, Burgess reagent or diethylaminosulfur trifluoride (DAST), or reaction setups with continuous removal of water using Dean-Stark-trap (chapter 3.1.3.3.4.2) or (b) the conversion of the terminal hydroxy groups into suitable leaving groups, e.g. mesylates, tosylates or chlorides, followed by intramolecular nucleophilic substitutions.[132, 259-263] Mitsunobu-type conditions were also successfully used for cyclization (chapter 3.1.3.3.4.1).[255, 260, 261] An overview of the desired transformation and different literature-known conditions is given in **scheme 77**.

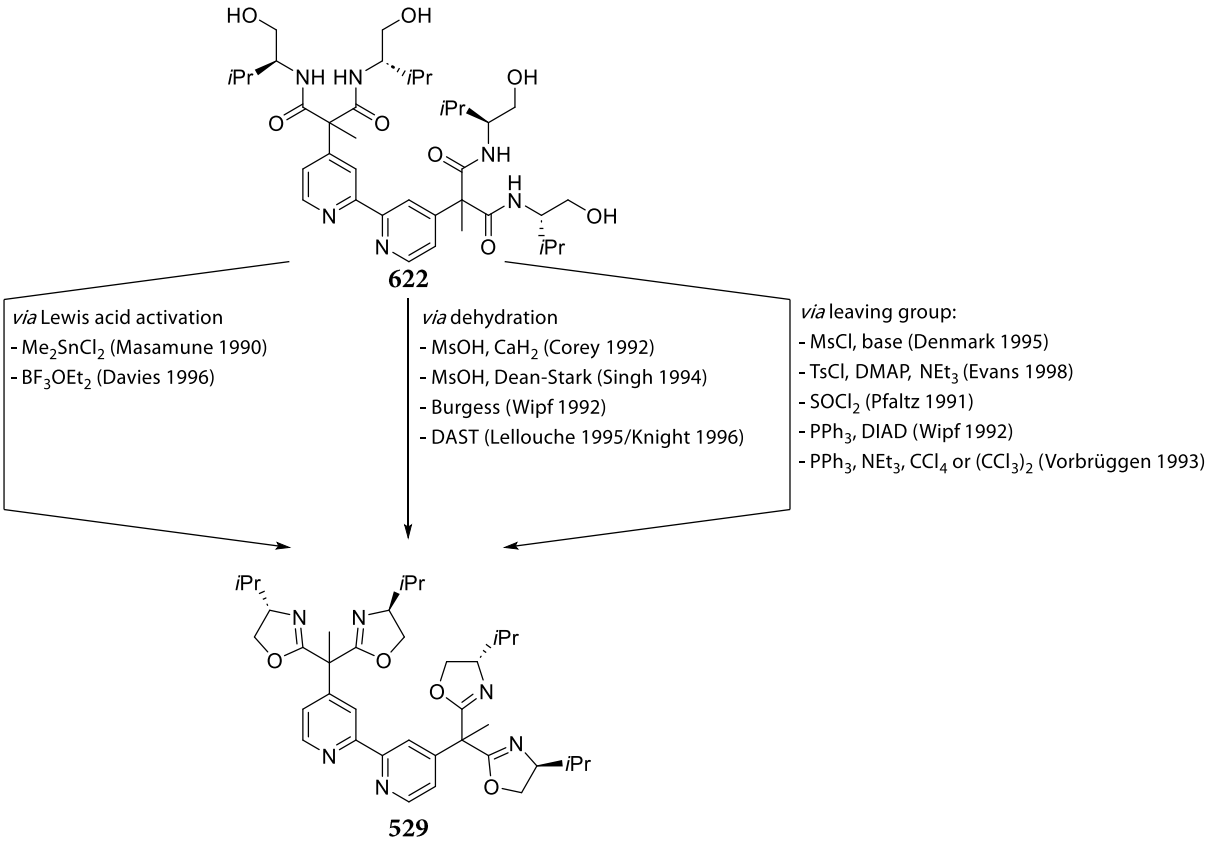

scheme 77. Common synthetic strategies for the synthesis of bisoxazolines from γ-hydroxyamides.[132, 252-265]

3.1.3.3.4.1 Cyclodehydration *via* leaving group and intramolecular substitution

Of all the ring closing strategies described, the route *via* suitable leaving groups has found particularly widespread application in the literature. Therefore, the first approaches focussed on the conversion of the terminal hydroxy groups in the tetra-γ-hydroxyamide **622** into mesylate leaving groups, followed by an intramolecular nucleophilic substitution induced by deprotonation at the amide nitrogen atom (**equation 25**).[256]

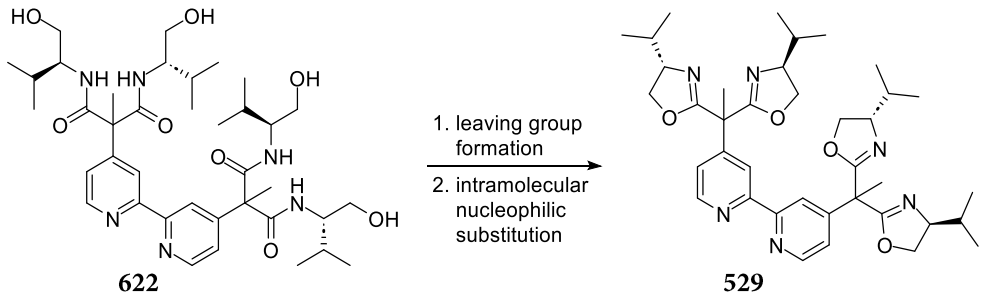

equation 25. Two-step ring closing sequence *via* leaving group and intramolecular substitution.

As in the preparation of the tetraamide **622**, both steps must take place at four reaction centres. It was therefore initially assumed that the mesylation step would require a longer time. To ensure complete conversion, the mesylation was stirred for at least 24 h in the first approaches. In later experiments, the required reaction time was examined by repeated TLC-MS analysis every five minutes revealing that the conversion to the tetramesylate was almost completed after only 25 minutes. However, this investigation is only possible indirectly because the reaction product and its precursors tend to eliminate methanesulfonic acid and therefore only partly or completely eliminated reaction products were available for conclusions on the progress of the reaction. Some repeatedly detected masses and potential corresponding molecular structures are shown in **figure 28**.

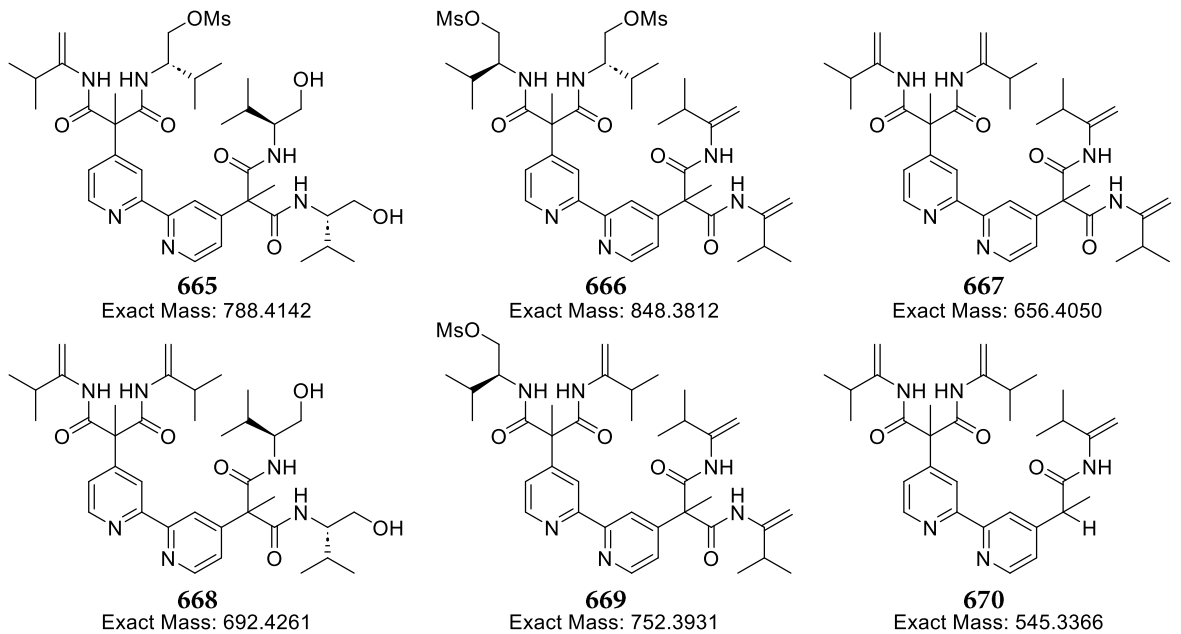

figure 28. Detected masses and potential corresponding molecular structures.

The mass of the tetraene **667** is of particular importance, as this is probably related to the tetramesylate. This assumption is confirmed by closer examination of the time-resolved spectrum shortly after injection which showed exclusively the mass of the tetramesylate (m/z 1040). However, within a few seconds the remaining signals emerged, resulting from gradual elimination under the conditions of mass spectrometry.

Although after 25 minutes there were still traces of di- and trimesylate detectable, a subsequent experiment showed that not even the addition of 10 eq. Et_3N and a total of 15 eq. MsCl (3.75-fold excess) was sufficient to reach complete conversion to the tetramesylate. Neither do longer reaction times lead to quantitative conversion; instead, formation of additional unknown side products was detected after 4.5 h. The tetramesylate although contaminated with small amounts of di- or trimesylate was then heated in a solution of sodium hydroxide in a mixture of water and methanol in order to initiate the ring closure.[256] As discussed in chapter 3.1.2.2, the base serves to deprotonate the amide nitrogen atom, allowing the ring closure to occur by intramolecular substitution of a mesylate group. In a competitive reaction an intermolecular nucleophilic substitution of the mesylate, by hydroxide anions or water, might result in a conversion back to the γ-hydroxyamide (**scheme 78**).

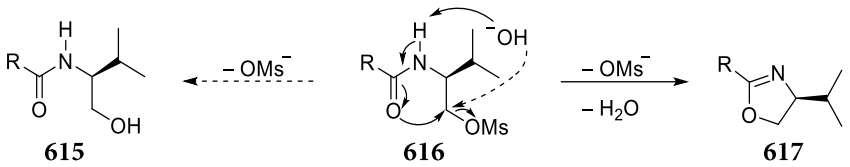

scheme 78. Mechanism of the base induced ring closure and potential side reaction.

This could explain why in several experiments a mixture of the desired Di-*i*Pr-MeBOX bipyridine **529** and a species with a mass of 675.1 g/mol, possibly corresponding to a compound containing three oxazoline rings and one amide fragment **671**, was obtained (**figure 29**).

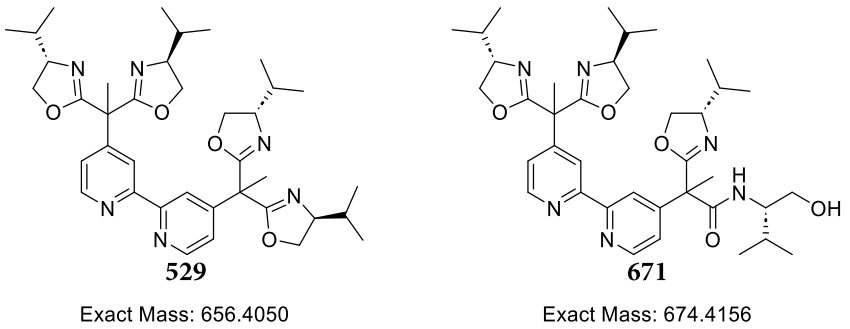

figure 29. Di-*i*Pr-MeBOX-bpy **529** and the inseparable side product of the ring-closing-reaction.

Since the separation of this mixture was neither possible by column chromatography nor by precipitation or recrystallization, the mixture was subjected to another mesylation-ring-closing sequence. After only 10 minutes the dominant formation of a spot indicating the mesylation of the free hydroxy group was detected by TLC-MS. Since the TLC did not change over one hour, an aqueous extraction was performed to prepare the ring closure. However, TLC-MS confirmed that the mesylate group is already substituted during the workup. Therefore, mesylation was repeated and the solvent dichloromethane was removed in a high vacuum *via* the schlenkline

before the ring closure, hoping that any residual triethylammonium chloride and methanesulfonyl chloride or methanesulfonic acid would not interfere the subsequent step. DMF and potassium *tert*-butoxide were then added as a non-nucleophilic solvent-base combination and the mixture was stirred for three days. After this time, however, the formation of a substance with a mass of 728.4 g/mol was observed, suggesting a ring opening reaction of all rings providing the tetraamide **622**. Possibly the solvent used was contaminated with residual water and the potassium *tert*-butoxide reacted to *tert*-butanol and potassium hydroxide. The latter could have caused the side reaction described above. In conclusion, the additional mesylation and ring closure using DMF and potassium *tert*-butoxide did not facilitate the separation of the desired BOX-bpy ligand **529** and the partly uncyclized precursor **671** shown in **figure 29**. In subsequent experiments, other leaving groups as well as other solvents and non-nucleophilic bases for initiating the intramolecular substitution were evaluated. In analogy to a procedure according to Evans *et al.*, triethylamine and tosyl chloride were added to the *i*Pr-tetra-γ-hydroxyamide **622**.[258] This combination was intended both to convert the hydroxy groups into tosylate leaving groups and to initiate the intramolecular nucleophilic substitution. However, tosylation was only detected after the addition of catalytic quantities of DMAP, and only besides a large number of side products. Product formation appeared more clearly after the addition of a large excess of triethylamine, tosyl chloride and DMAP as well as heating the reaction mixture to 40 °C, although continuing to occur alongside intermediates with only three closed amide chains or species whose TLC-MS analyses indicated the loss of one or two rings or amide chains. Since also a second attempt with DIPEA instead of triethylamine did not lead to an increase in selectivity, the tosylation strategy was not pursued further. In the following approaches, the hydroxyamide **622** was first mesylated with methanesulfonyl chloride and triethylamine in dichloromethane at −18 °C for 45 minutes before the solvent was removed inertly over the schlenkline in high vacuum and the residue was mixed with different non-nucleophilic bases and suitable solvents to initiate ring closure by intramolecular substitution. Both the combination of potassium *tert*-butoxide in THF and of diisopropylethylamine in THF showed significant product formation in TLC-MS analysis, but some masses again indicated the loss of ring fragments or amide strands. Only when using LiHMDS, Di-*i*Pr-MeBOX-bpy **529** could be isolated in a yield of 52% with only minor impurities resulting from the ring-loss side-product. In an experiment in which no more mesylated species could be detected after some time, it was observed that addition of further LiHMDS resulted in a significant increase in the amount of BOX-bpy **529**, possibly because lithium acts as a Lewis acid activator while HMDS acts as a dehydration reagent. This observation became the basis for further experiments on cyclodehydration with dehydrating reagents or continuous removal of water (chapter 3.1.3.3.4.2). Finally the ring closure was evaluated applying Mitsunobu-type conditions.[255, 260, 261] After two days at room temperature, the formation of triphenylphosphine oxide was observed, but product formation was only indicated besides five other side-products.

As no ring closure variant through conversion of the terminal hydroxy groups into suitable leaving groups and intramolecular nucleophilic substitution selectively delivered the desired *i*Pr-BOX-bpy **529** ligand in satisfactory yield, further approaches focused on dehydration strategies (chapter 3.1.3.3.4.2).

3.1.3.3.4.2 Cyclodehydration *via* dehydrating reagents or continuous water removal

Since the formation of oxazoline rings from hydroxyamide fragments formally represents a dehydration, several established dehydration strategies were evaluated (**equation 26**).

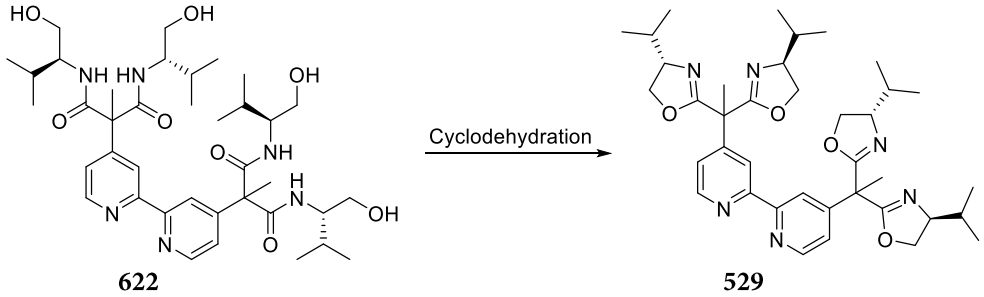

equation 26. Synthesis of Di-*i*Pr-MeBOX-bpy **529** by cyclodehydration.

Following a procedure by Corey *et al.* and Singh *et al.*, the reaction mixture consisting of hydroxyamide **622** and methanesulfonic acid was refluxed in dichloromethane in an apparatus including a schlenk frit loaded with calcium hydride for continuous removal of water from the refluxing solvent.[259, 262] Under these conditions only mono dehydration was detected on TLC-MS after five days. Although calcium hydride is frequently used as a drying reagent due to its hydrophilic properties, e.g. in the purification of solvents, and is thus capable of binding water that has been split off during the dehydration thereby removing it from the equilibrium by the release of hydrogen and calcium hydroxide (which is neutralized by the methanesulfonic acid) it is however not involved mechanistically in the initiation of the dehydration.

Subsequent approaches focused on the use of the Burgess dehydrating reagent **619**.[274] As discussed for the cyclodehydration of hydroxyamides **615** in the synthesis of BOX **613** (chapter 3.1.2.2), it is an inner salt that assumably forms a methoxycarbonyl sulfamate **620** with the terminal hydroxy group and subsequently through a six-membered transition state and fragmentation of sulfur trioxide and a ((methoxycarbonyl)amide anion generates the oxazoline ring **617** (**scheme 79**).

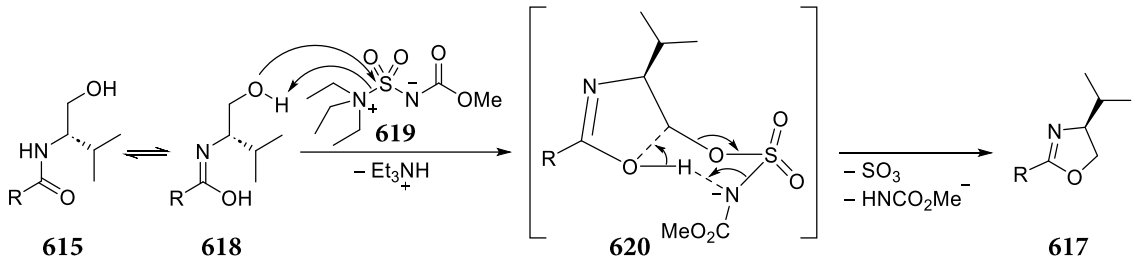

scheme 79. Mechanism of the oxazolin formation from γ-hydroxyamides by Burgess dehydration.

Despite the use of an older batch of Burgess reagent **619** (recognizable by orange/reddish discoloration), a test approach of the Burgess cyclodehydration showed the most selective ring-closure with dominant product formation so far, for which reason all other strategies, both *via* intramolecular substitution of suitable leaving groups (chapter 3.1.3.3.4.1) as well as alternative dehydrations, were not further investigated. Instead, cyclodehydration was optimized with a new batch of the Burgess reagent **619**. It was always handled inside the

glovebox and then added as a solution in dry THF to a solution of the γ-hydroxyamide **622**. Since 4.4 eq. did not provide full conversion after three days, further 2.2 eq. were added. In this way, complete consumption of the starting material was observed mainly providing the desired target molecule Di-*i*Pr-BOX-bpy **529**, besides minor impurities of not completely cyclized intermediates. Identical observations were obtained in subsequent approaches using 6.0 eq. Burgess reagent **619** and a reaction time of 24 h. Extended reaction times did not appear to increase conversion to the BOX-bpy **529**. Maybe the addition of more than 0.5 excess equivalents per ring are required for a quantitative conversion to the product, to account for the fragility of the burgess reagent **619**. Purification attempts failed on silica gel with eluents consisting of highly polar mixtures of dichloromethane/methanol/ammonia, that even elute very polar compounds with a strong tendency to tailing as clear spots. Using reverse phase HPLC (C18) with a gradient composed of water:methanol, the isolation of pure BOX-bpy **529** after removal of methanol under reduced pressure and of water at the lyophilizator was successful in a yield of 70%.

For simplifying the purification, different solvent mixtures were investigated for purification by precipitation. Before that, the salts derived from the Burgess reagent **619** were removed by washing a solution of the crude product with water. Since the separation of a few solid particles was observed in an NMR tube containing a solution of the crude product in acetonitrile and only one spot was visible on the TLC, an attempt was made to purify the crude product by the addition of a small amount of acetonitrile. However, this approach resulted in only a slight cloudiness and no significant purification after filtration. After addition of an excess amount of *n*-hexane to a concentrated solution of the crude product in dichloromethane, a significant white precipitate was formed, which was initially misinterpreted as product precipitation. In fact, this process led to the precipitation of all side-products, i.e. not fully cyclized intermediates, and after filtration and removal of the solvent the desired ligand **529** was obtained in a yield of 75%. Therefore, this purification method not only provides higher yield than obtained by RP-HPLC, the desired ligand structure can also be obtained requiring considerably less experimental effort and time (**equation 27**).

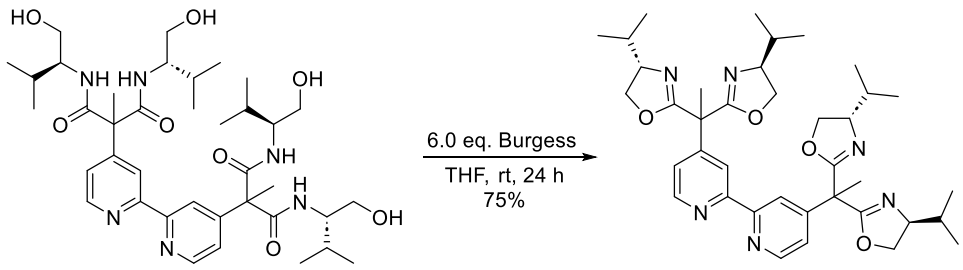

622 **529**

equation 27. Optimized conditions for the Burgess cyclodehydration of the γ-hydroxytetraamide **622** to BOX-bpy **529**.

In summary, the desired ligand structure **529** was obtained in only four steps by side-chain functionalization of dimethylbipyridine **626** in an overall yield of 18% (**scheme 80**). The yield limiting factor turned out to be the benzylic acylation by consecutive benzylic deprotonation and reaction with ethyl chloroformate **627**, given that increasing degrees of substitution are accompanied by decreasing pk_a and thus selective functionalization of lower-

substituted intermediates in mixtures with higher-substituted species, i.e. control of the degree of substitution, is very challenging. Another key step of the synthetic sequence is the ring closing reaction, which only proceeded in low selectivity and yield using the more conventional routes of conversion of the terminal hydroxyl groups into leaving groups and intramolecular substitution. A major difficulty arises from the requirement of four reaction centres to undergo the transformation, just as in the benzylic acylation and amide formation. Upon examination of numerous ring closing procedures, the Burgess dehydration reagent **619** provided the most selective formation of the desired BOX-bpy ligand **529**. In addition to the low total number of synthetic steps, another remarkable advantage of the developed synthetic route is the ability to obtain each reaction product in its pure form by simple precipitation. Without the need for time-consuming and uneconomical column chromatography, the presented synthetic route is therefore straightforward and easily scalable.

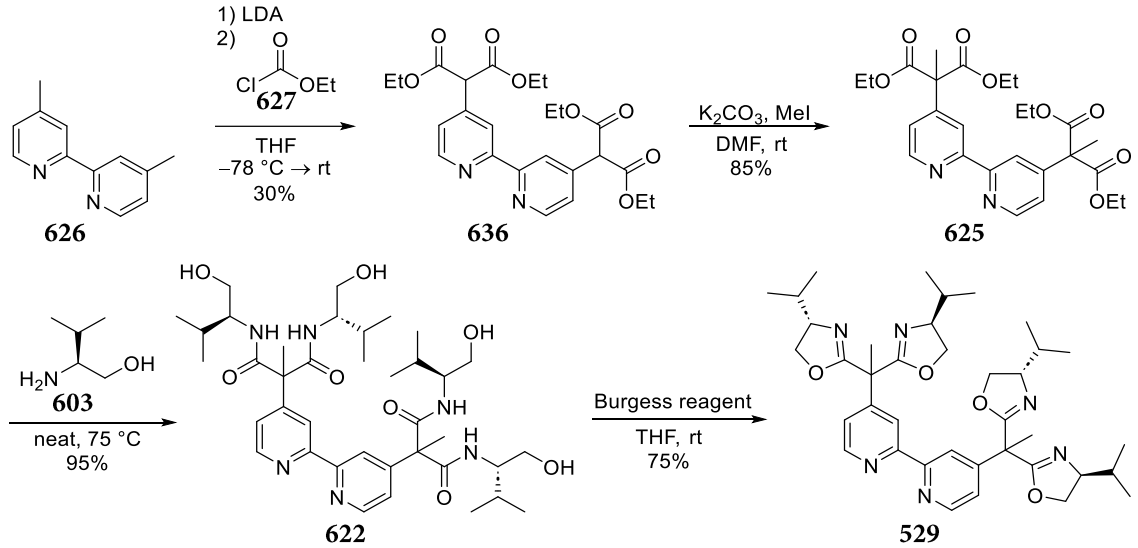

scheme 80. Synthetic route for the synthesis of BOX-bpy **529** from dimethylbipyridine **626** by side-chain functionalization.

3.1.3.4 Synthesis of BOX-bipyridine **531** *via* tetranitrile **624**

After some attempts for the synthesis of BOX-substituted bipyridines with benzyl instead of isopropyl residues failed *via* the conventional way based on γ-hydroxyamides due to decarboxylation reactions during amide formation, it was assumed that an alternative route could be used to link the malonylbipyridine derivative **625** with chiral amino alcohols. This strategy exploits that nitriles react with amino alcohols in the presence of suitable Lewis acids to form oxazolines. Similarly, malonodinitrile derivatives can be used as precursors for the bisoxazoline synthesis. For the synthesis of benzyl-BOX-substituted bipyridine derivatives it was therefore attempted to convert the malonylbipyridine **625** into the tetranitrile **624** which could then be further converted with L-phenylalaninol (**604**) to the desired ligand Di-Bn-MeBOX-bpy **531** (**scheme 81**).

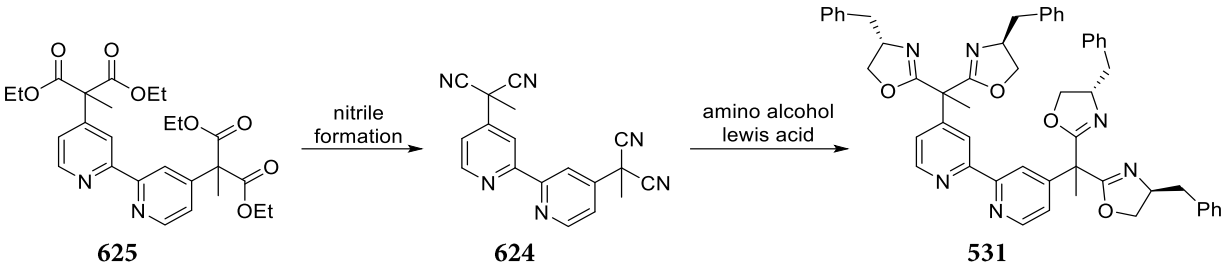

scheme 81. Synthetic approach for DiMeBOX-bpy ligands *via* tetranitrile.

3.1.3.4.1 Synthesis of the tetranitril-bipyridine **624**

The synthesis of the bis(malonodinitrile)-bipyridine **624** starting from malonylbipyridine **625** could be performed in two ways: By reduction to the alcohol and Swern oxidation, malonate esters could be converted into aldehydes, which subsequently might be condensed with hydroxylamine to form the oxime derivative **672**.[282] Dehydration of the oxime with the Burgess reagent would result in the formation of the tetranitrile **624**.[279] In a similar, but significantly shorter route, the malonate esters could be treated with ammonia to form a bis(malonamide) **673**, which in turn could be dehydrated using the Burgess reagent to form the tetranitrile **624**.[277, 283, 284] Due to the smaller number of steps, all attempts focused on the nitrile synthesis *via* the bis(malonamide) **673** (**scheme 82**).

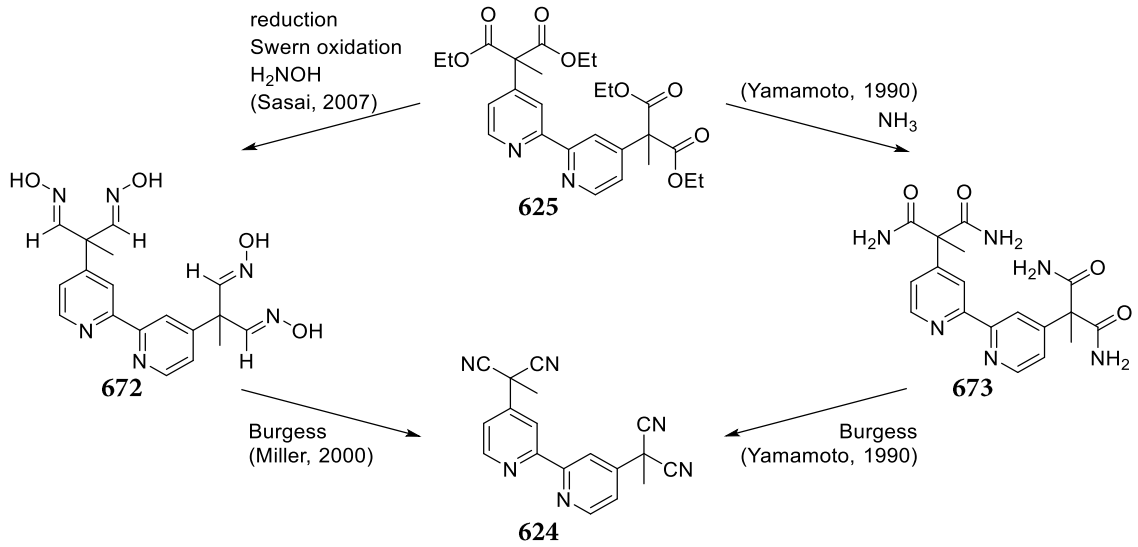

scheme 82. Conceivable synthetic strategies for the conversion of malonate ester **625** into the tetranitrile **624**.[277, 279, 282-284]

In an attempt to convert the malonate ester **625** into the bis(malonamide) **673** a solution of malonylbipyridine **625** in ethanol was stirred with an aqueous ammonia solution at room temperature. After three weeks under these conditions the formation of small amounts of monoamide was detected by TLC-MS, revealing that the reaction time using these conditions is impractical for the synthesis of larger amounts of tetranitrile **624.**

To enforce the amide formation in another approach an ethanolic solution of malonylbipyridine **625** was saturated with ammonia by bubbling ammonia gas into the solution. After the air was pushed out of the tubes a significant decrease of bubble quantity and size was visible at the gas bubbler, indicating the dissolution of ammonia in ethanol. A slight increase of the reaction volume was also visible. After replacing the gas bubbler with an empty balloon, the reaction mixture was stirred at room temperature for 4 days. After this time, besides the dominant educt spot (m/z 501), the formation of small amounts of the monoamide (m/z 472) could be detected by TLC-MS. To increase the reaction rate, a few milliliters of liquid ammonia were added to the reaction solution using an ammonia condenser and the solution was stirred at −78 °C for another 24 hours. After this time the formation of a new spot with the mass m/z 429.2 was clearly visible, which was misinterpreted as product mass minus one proton plus two sodium cations ($[M + 2\ Na - H]^+$). Therefore the solvent was removed and the residue was mixed with about 3 mL of condensed ammonia in a pressure tube at room temperature for another week. At this point, in addition to weakly indicated product formation, a large number of other spots appeared, which indicated di- and triamide formation. Moreover, some masses were detected to which no further significance was attributed at this point. Assuming that the large number of spots might be caused by the repeatedly changed reaction conditions and since the formation of tetraamide **673** seemed to take much longer, a new approach was initiated in liquid ammonia in the pressure tube and analyzed after three weeks. At this point, even more spots were visible than in the previous test approach, but only two of them were formed dominantly. After isolation by column chromatography, ^{1}H-NMR spectroscopy showed that neither of the two dominant spots was the tetraamide **673**, but instead the decarboxylation products **674** and **675** shown in **figure 30**.

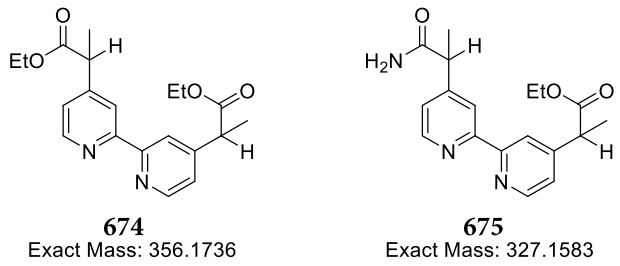

figure 30. Isolated side products resulting from decarboxylation during an attempt to form the tetraamide **673**.

When comparing these results with the masses detected in the previous approach, it was found that some species were already formed during the reaction with condensed ammonia, and that although the masses of all amide intermediates were detected, all partially or completely decarboxylated intermediates were also detected to the same or greater extent. Since decarboxylation requires hydrolysis to the acid and the problems only occurred after the use of condensed ammonia, larger quantities of water could have entered the reaction mixture during the

condensation process. During the condensation process, no special attention was paid to inert handling, instead the ammonia condenser was simply attached to the reaction flask or the ammonia gas was fed through a hose into an open pressure tube cooled to –78 °C. Condensed traces of water pave the way for a saponification to the acid which then readily decarboxylates. The synthesis of α,α-disubstituted malonamides from malonate esters has previously been described as hindered and 2-arylmalonates are known to be involved in decarboxylation reactions.[281] As the synthesis of the *i*Pr-substituted BOX-bpy ligand **529** through cyclodehydration of hydroxyamide **622** showed promising results at this stage, the synthesis of the benzyl-substituted BOX-bpy ligand **531** through the tetranitrile **624** was not pursued further and focus was placed on the incorporation of the *i*Pr-BOX-bpy-ligand **529** into Ruthenium-complexes (chapter 3.2).

3.2 Synthesis of BOX-substituted photocatalysts

3.2.1 Synthesis of Ru(II)-precursors **677** and **683**

The desired photocatalysts of the general formular $[Ru(BOX\text{-}bpy)_3]X_2$ (chapter 3.2.2) and $[Ru(R\text{-}bpy)_2(BOX\text{-}bpy)]X_2$ (chapter 3.2.3), respectively, are Ru(II) complexes. Although the synthesis of Ru(II) complexes can be achieved from $RuCl_3$ x H_2O (**676**) by simultaneous ligand attachment and reduction, the use of Ru(II) precursors can contribute to a simplification of the complex formation since only the ligand coordination and no longer the reduction of the metal centre has to take place.[285-289] Two very common Ru(II) precursors, *cis*-$RuCl_2(dmso)_4$ **677** and $Ru(COD)Cl_2$ **683**, were prepared and used in the synthesis of the photocatalysts.[290-293]

3.2.1.1 *cis,fac*-$RuCl_2$(dmso-*S*)$_3$(dmso-*O*) (**677**)

The first synthesis for *cis*-$Ru(dmso)_4Cl_2$ **677** was performed in 1971 by James *et al.* by bubbling hydrogen gas through a solution of $RuCl_3$ x H_2O (**676**) (often assumed to be the trihydrate) in DMSO at 80 °C and subsequent recrystallization from acetone/DMSO.[290] Two years later, Evans *et al.* reported that this tedious procedure was not necessary and instead a short (15 min) refluxing of $RuCl_3$ x H_2O (**676**) in DMSO followed by precipitation with acetone and recrystallization from DMSO/acetone was sufficient.[291]

In the first approach, to ensure complete conversion and successful reduction, a mixture of $RuCl_3$ x H_2O (**676**) was stirred under a hydrogen atmosphere for 48 h at 80 °C in DMSO through which hydrogen had previously been bubbled. A distinct color change from opaque black to clear orange was visible. After cooling and addition of acetone, *cis*-$RuCl_2(dmso)_4$ **677** crystallized in the form of cubic yellow crystals in a yield of 53%.

Several approaches were carried out to increase the yield and simplify the reaction setup following the procedure by Evans *et al.*[291] However, refluxing $RuCl_3$ x H_2O (**676**) for 15 min in DMSO followed by concentrating the red solution on the rotary evaporator and adding acetone resulted in only a very small amount of bright precipitate, which was filtered off and washed with Et_2O. Given the low yield, the filtrate was concentrated again and the residue dissolved in acetone. Addition of Et_2O led to the precipitation of a large amount of a black solid that visually resembled the starting material $RuCl_3$ x H_2O (**676**), suggesting that under the reaction conditions or after the short reaction time, most of the $RuCl_3$ x H_2O (**676**) was not reduced and converted into the desired DMSO complex.

According to Alessio *et al.* the success of the reaction can be significantly increased by refluxing the $RuCl_3$ x H_2O (**676**) in EtOH for several hours and filtration of undissolved residues prior to the heating period in DMSO.[292] This procedure also increases the reproducibility of the synthesis, which is problematic due to varying quality and composition of the starting material $RuCl_3$ x H_2O (**676**): Although $RuCl_3$ x H_2O (**676**) is usually formulated as $RuCl_3$ x 3 H_2O (**676**), it is actually a mixture of Ru(III) and Ru(IV) species with varying numbers of water equivalents.[286, 294] Furthermore, an extended reaction time of more than 2 h was recommended. In this way, the Ru(II) precursor *cis*-$RuCl_2(dmso)_4$ **677** was obtained in a yield of 64%.

The analysis of the obtained complexes was initially performed by elemental analysis which confirmed the desired elemental composition, however, due to both the heteroleptic nature of the desired complex and the fact that DMSO ligands (**680**) preferentially bind to Ru(II) at the sulfur atom, yet coordination *via* the oxygen atom is also possible and thus the formation of multiple isomeric structures is conceivable, elemental analysis is insufficient for the confirmation of the actual structure.

The most common description of the complex, *cis*-$RuCl_2(dmso)_4$ **677** also ignores the fact that the thermodynamically most favorable structure, confirmed by x-ray crystallography, should be correctly referred to as *cis,fac*-$RuCl_2$(dmso-*S*)$_3$(dmso-*O*) (**677**), considering that other isomers can also be formed: Hence, further studies on the synthesis, as well as structure and stability of isomers, revealed that heating $RuCl_3$ x H_2O (**676**) in DMSO to merely 70 °C specifically produces the isomer *trans*-$RuCl_2$(dmso-*S*)$_4$ (**678**), suggesting that this is the kinetic product.[294, 295] Furthermore, irradiation of *cis,fac*-$RuCl_2$(dmso-*S*)$_3$(dmso-*O*) (**677**) at room temperature can initiate isomerization to the *trans*-$RuCl_2$(dmso-*S*)$_4$ derivative (**678**), which can likewise isomerize back to the thermodynamically more stable *cis,fac*-$RuCl_2$(dmso-*S*)$_3$(dmso-*O*) (**677**) when heated (**scheme 83**).[292, 294]

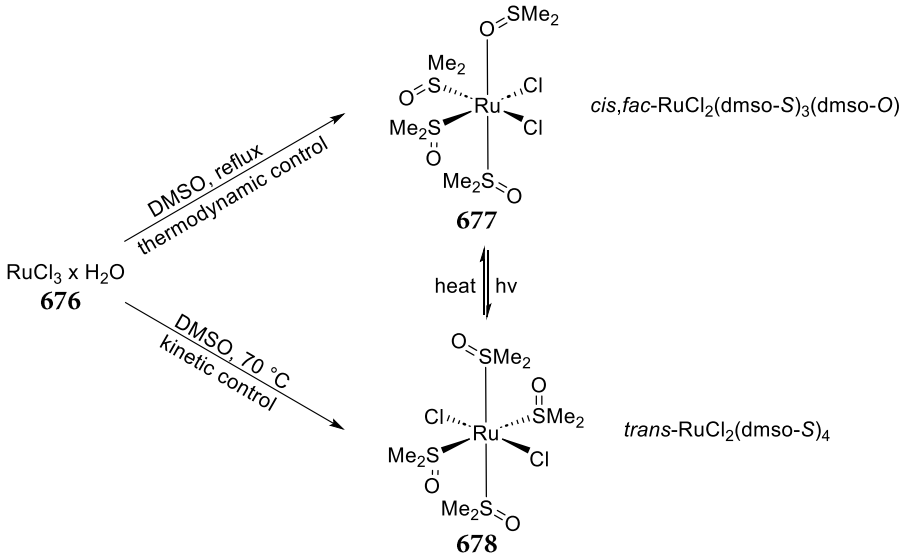

scheme 83. Synthesis and equilibrium of isomers of $RuCl_2(dmso)_4$.[292, 294, 295]

Due to the isomerization described above, the reaction products obtained were further analyzed by ^{1}H-NMR spectroscopy, which proved to be challenging since the *O*-bound DMSO ligand (**680**) is particularly labile and exchanges quickly for stronger σ- and π-donors. Residual water in commercial $CDCl_3$ initiates a partial hydrolysis, resulting in additional sets of signals that were initially misinterpreted as impurities or ascribed to signs of partial isomerization to *trans*-$RuCl_2(dmso)_4$ (**678**). Upon comparison with the literature, the obtained signals were assigned to the desired *cis,fac*-$RuCl_2$(dmso-*S*)$_3$(dmso-*O*) (**677**) in addition to further signals resulting from *cis,fac*-$RuCl_2$(dmso-*S*)$_3$(H_2O) (**spectrum 2**).[294]

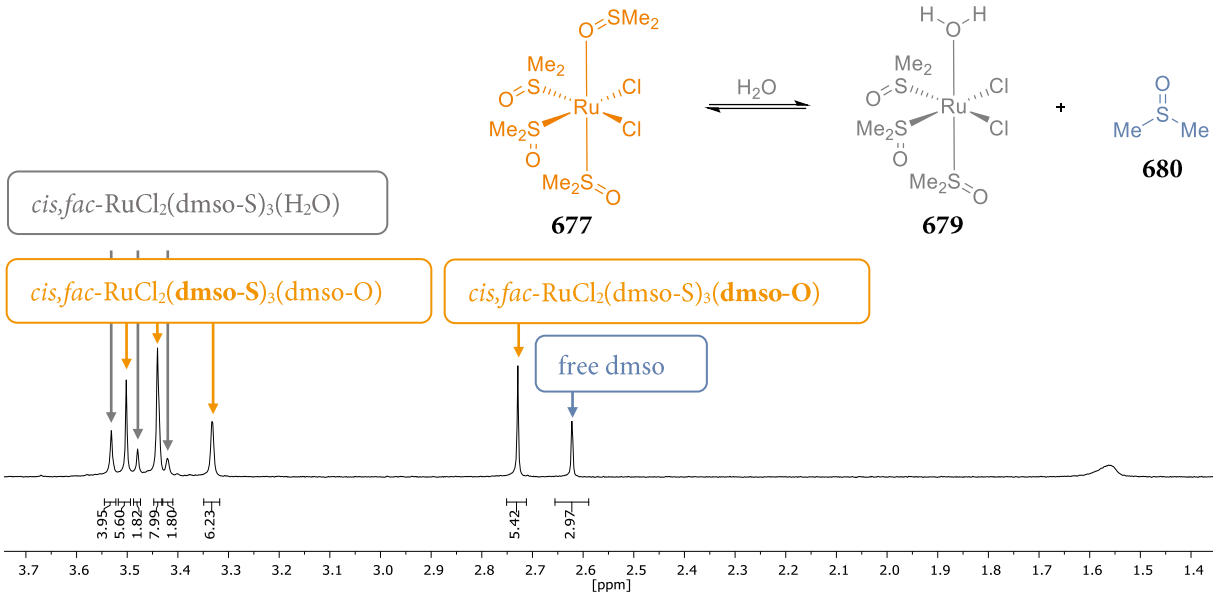

spectrum 2. Detailed ^{1}H-NMR analysis of *cis,fac*-$RuCl_2$(dmso-S)$_3$(dmso-O) (**677**) and its partial hydrolysis in commercial $CDCl_3$.

3.2.1.2 μ-Chloro-(η^4-cycloocta-1,5-diene)ruthenium(II)-polymer (**683**)

Less common but yet very successfully employed in the synthesis of Ru(II) complexes of the type Ru(R-bpy)$_2$Cl$_2$ is the stable ruthenium(II) precursor [$RuCl_2$(η^4-COD)]$_x$ (**683**), which was prepared by refluxing $RuCl_3$ x H_2O (**676**) and cyclooctadiene (COD) for 48 h in degassed ethanol acting as a reducing agent (**equation 28**).

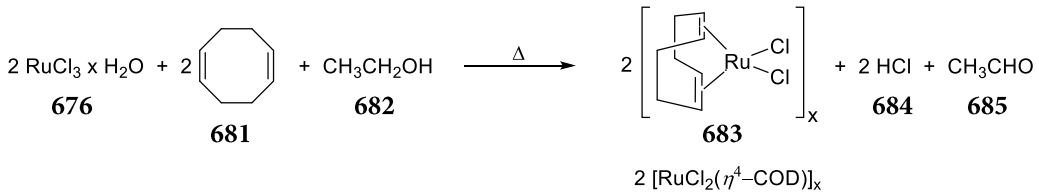

equation 28. Synthesis of [$RuCl_2$(η^4-COD)]$_x$ (**683**).

Filtering off the brown precipitate and washing with EtOH and Et_2O gave the complex in excellent yield. Due to the polymeric structure of the generalized form [$RuCl_2$(η^4-COD)]$_x$ with x > 2, no further analysis of the structure is typically performed and the poorly soluble brown product is used in further reactions without further purification.

3.2.2 Synthesis of homoleptic photocatalyst $[Ru(BOX\text{-}bpy)_3]^{2+}$ **540**

3.2.2.1 Direct synthetic approaches

The initial complexation experiments focused on the synthesis of a homoleptic Ru(II) complex **540** containing an inner sphere wherein the metal centre is surrounded by three bipyridine substructures, resulting in a $[Ru(bpy)_3]^{2+}$-derived photocatalyst with a photoredox active core completely surrounded by a chiral BOX sphere. Due to the distance dependency of electron transfers, substrates that are in close proximity to the chiral BOX fragments should preferably react. Another advantage compared to a heteroleptic complex version (featuring only one BOX-bpy ligand **529**) is that besides the low risk of racemic background reactions at a larger distance to the chiral BOX fragments, there is no risk of racemic background reactions on opposite sides to the BOX fragment.

For the synthesis of the octahedral complex $[Ru(BOX\text{-}bpy)_3]^{2+}$ **540**, three equivalents of the BOX-bpy ligand **529** were mixed with different Ru(II) sources and refluxed in various solvents. The parameters and results of selected experiments are summarized in **table 3**.

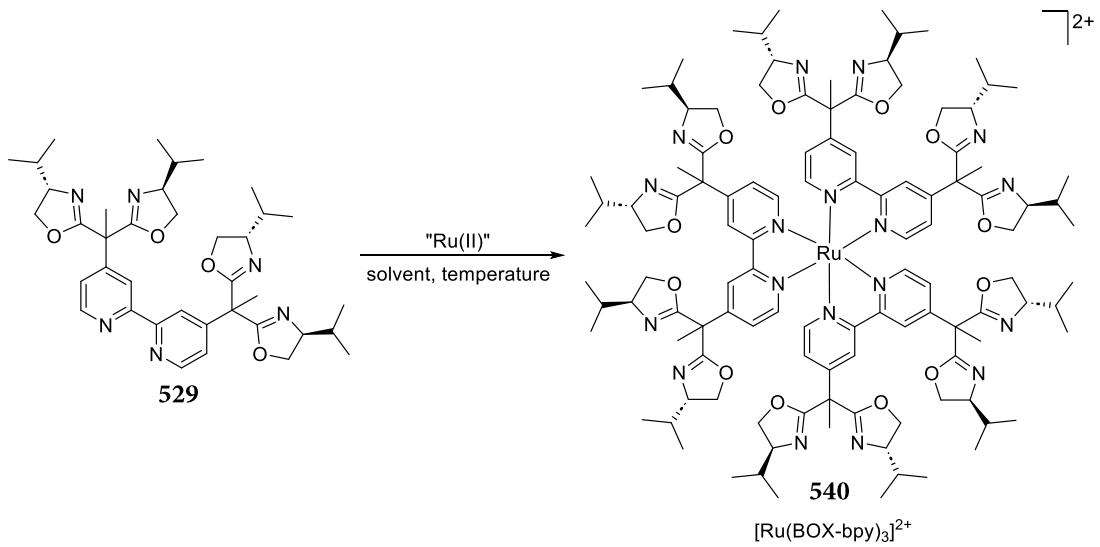

equation 29. Investigated synthesis of the homoleptic BOX-substituted photocatalyst **540**.

table 3. Parameters and results of selected experiments for the direct synthesis of $[Ru(BOX\text{-}bpy)_3]^{2+}$ **540**.

entry	Ru(II)	solvent	T [°C]	t [h]	yield
1	$RuCl_3$ / NaH_2PO_2	H_2O / EtOH	100	24	---
2	$RuCl_2(dmso)_4$	MeOH	reflux (65)	3	42%*
3	$RuCl_2(dmso)_4$	EtOH	reflux (78)	24	---
4	$RuCl_2(dmso)_4$	MeCN	reflux (82)	120	---

*including inseparable impurities of partly hydrated complexes

In analogy to a literature known $[Ru(bpy)_3]^{2+}$ (**7**) synthesis, the initial complexation experiment was performed by reaction of $RuCl_3$ x H_2O (**676**) with three equivalents of the ligand **529** in a reducing aqueous solution of sodium hypophosphite (entry 1).[296] Due to the low solubility of the ligand in water (even at 100 °C), a small amount of

ethanol was added and the solution was refluxed for 24 h. The reaction mixture showed streaks in the orange coloration characteristic for ruthenium tris(bipyridine) complexes, besides some undissolved deep red or black particles, possibly traceable to residues of the ruthenium source. An attempt to precipitate the complex by the addition of solid potassium chloride and attempts of recrystallization from water failed.

Extraction with ethyl acetate and concentrating *in vacuo* gave a red film of the crude product which was analyzed by MALDI-TOF. The formation of the desired photocatalyst **540** could not be observed. Instead, the mass spectrum indicated the formation of a ruthenium complex containing only two BOX-bpy ligands and two water molecules occupying the remaining coordination sides **686** (**figure 31**, left). It was suspected that the complexation of the bulky BOX-bpy ligand **529** was sterically too hindered under the investigated complexation conditions and that a stepwise complexation or prolonged reaction times might be required in analogy to literature known syntheses of sterically demanding substituted ruthenium tris(bipyridine) derivatives. The crude product, containing the intermediate **686** was redissolved in ethanol und mixed with one more equivalent of ligand, however the desired complex formation could not be detected.

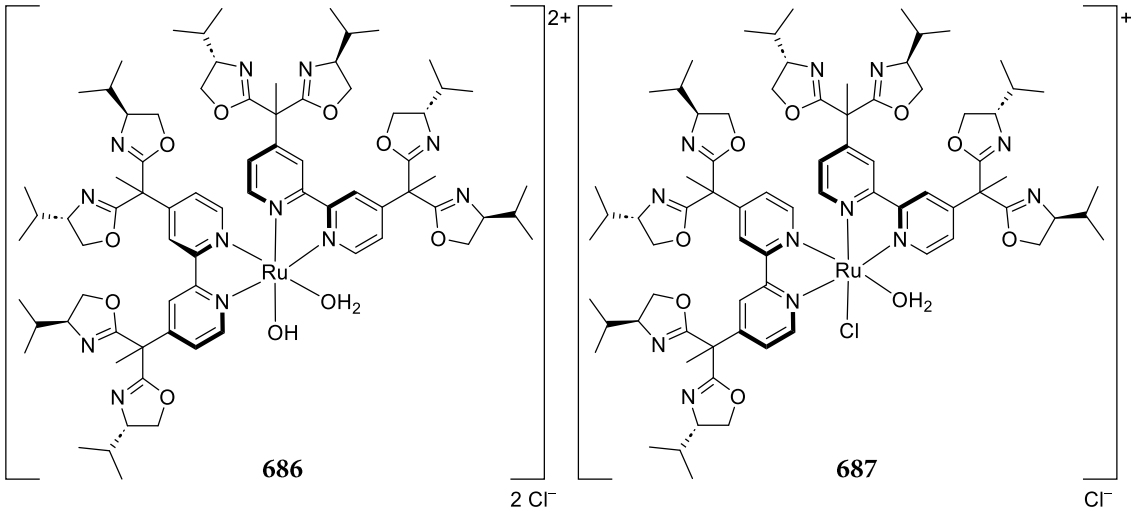

figure 31. Isolated intermediates of the formation of the homoleptic complex **540**.

To simplify the complexation reaction, the Ru(II) precursor *cis,fac*-$RuCl_2$(dmso-*S*)$_3$(dmso-*O*) (**677**) was used in subsequent approaches (entries 2 - 4). In this way, only the coordination of the BOX-bpy ligands **529** and not also its reduction to Ru(II) has to take place. After the Ru(II) precursor was refluxed with three equivalents of the BOX-bpy ligand **529** for three hours in methanol a small sample was taken from the reaction mixture and analyzed by mass spectrometry, confirming for the first time the desired complex formation based on a set of peaks at half the complex mass (m/z 1035.7) with the splitting pattern of a doubly charged substance. Another dominant peakset indicated a single-charged compound containing only two BOX-bpy ligands **529**, one chloride and one water ligand $[Ru(BOX\text{-}bpy)_2(H_2O)Cl]^+$ (**687**) (**figure 31**, right). Furthermore, a large number of peak sets with masses far above the desired complex mass were detected, frequently at a distance of a mass difference of m/z 18, which was attributed to the formation of higher multinuclear complex clusters **688** (**figure 32**) with different degrees of

water incorporation. Attempts to isolate the complex **540** in its pure form by column chromatography or crystallization failed. Only a partial separation of by-products succeeded, yielding a red film containing the product besides clearly detectable species from both mono- (m/z 1044.6) and double hydration (m/z 1053.1) (entry 2) (**spectrum 3**).

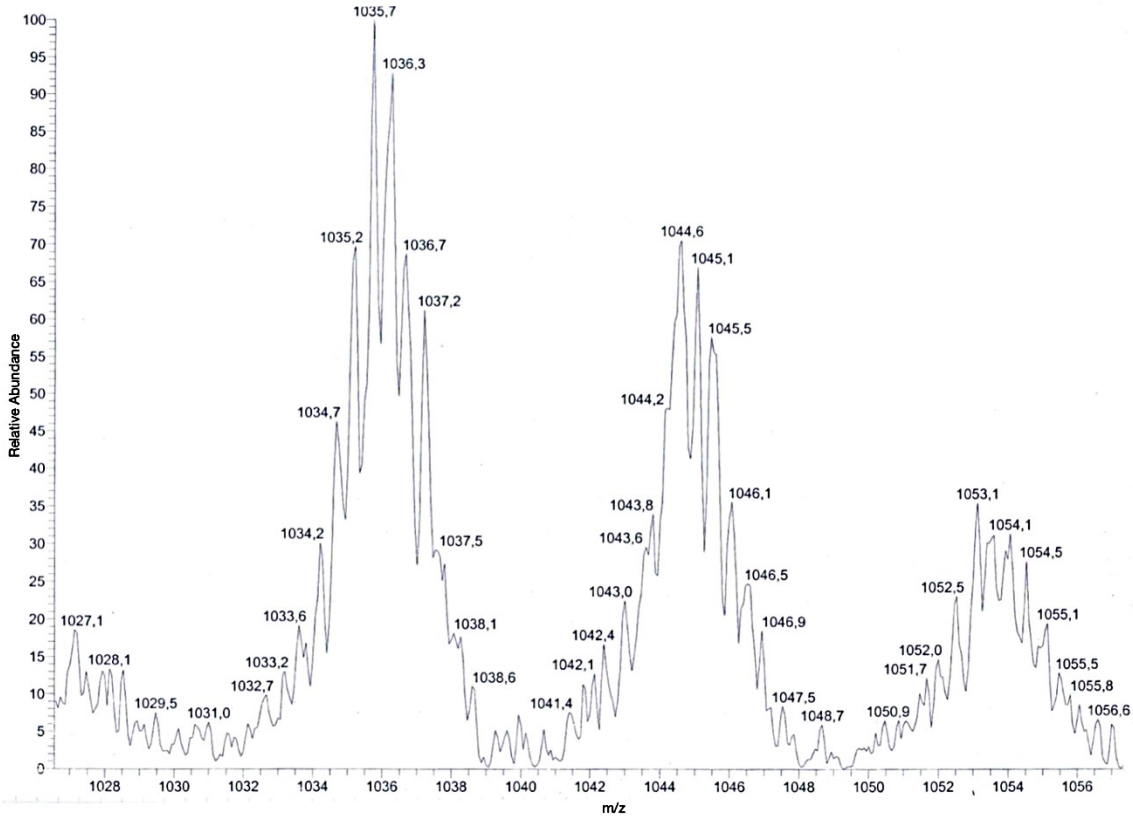

spectrum 3. Mass spectrum of the isolated substance indicating the formation of the desired [Ru(BOX-bpy)$_3$]$^{2+}$ **540** (M: 2071 g/mol, m/z 1035) besides peaksets for mono- and double hydrated side-products.

Hoping for the formation of [Ru(BOX-bpy)$_3$]$^{2+}$ **540**, hypothesized as the thermodynamically most favorable complex structure, the Ru(II) precursor **677** was refluxed in EtOH and MeCN for prolonged reaction times of 24 h and 120 h, respectively. The desired complex formation could not be detected by mass spectrometry. Instead, the mass of an intermediate was again detected, this time containing two BOX-bpy ligands **529**, one chloride and one dmso ([Ru(BOX-bpy)$_2$Cl(dmso)]$^+$, m/z 1527.6960). Moreover, evidence of partial and complete oxazoline ring opening by hydration was again observed (BOX-bpy + H_2O: m/z 675, BOX-bpy + 4 H_2O m/z 729) (**scheme 84**).

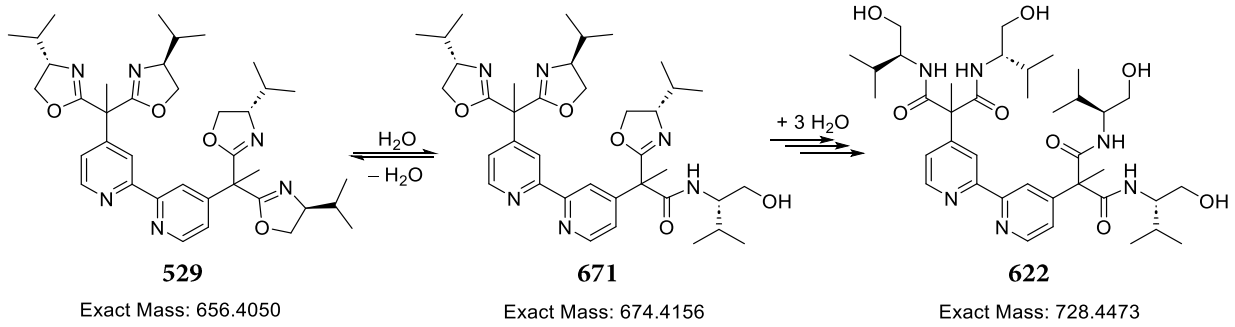

scheme 84. Side products resulting from hydrating ring opening.

In addition, these approaches also showed a large number of unassignable peaks, often lying above the mass of $[Ru(BOX\text{-}bpy)_3]^{2+}$ **540** (m/z 1035.7) and therefore possibly resulting from the formation of multinuclear clusters **688** (**figure 32**).

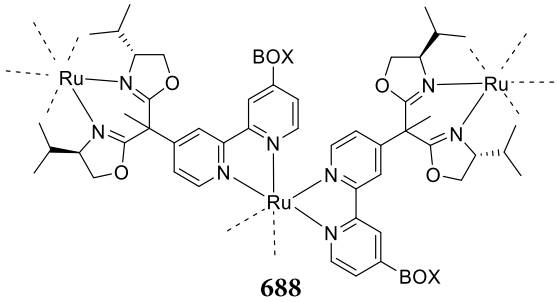

figure 32. Conceivable formation of higher multinuclear clusters.

The formation of ruthenium bridged complexes is a direct consequence of the triple bidentate ligand structure. Although the relatively large ruthenium cation should preferably be coordinated by the bipyridine fragments, some ruthenium-bisoxazoline complexes have already been prepared, and the conducted experiments confirmed that even prolonged refluxing does not selectively lead to the complex assumed to be the thermodynamically most favorable structure.[297, 298] Furthermore, all approaches show the partial addition of water, presumably due to a hydrating ring opening of the oxazoline fragments, which were previously formed by cyclodehydration (chapter 3.1.3.3.4.2).

A conceivable way for preventing both clustering and ring opening hydration might be to block the BOX fragments with a suitable Lewis acid, thus using an L.A.-BOX-bpy precomplex. The Lewis acid could protect the ring structure from ring opening by keeping the oxazoline rings in their coordinating position. Moreover, precomplexation converts the BOX-bpy ligand **529** from a triple-bidentate to a mono-bidentate structure, leaving only the bipyridine fragment available for attachment to Ru(II). Therefore, direct synthesis of the homoleptic complex $[Ru(BOX\text{-}bpy)_3]^{2+}$ **540** was not pursued further and subsequent studies focused on the formation of precomplexes of the form L.A.-BOX-bpy, as well as complexation experiments thereof (chapter 3.2.2.2).

3.2.2.2 Complexation through blocking of BOX-fragments by Lewis acids

To increase selectivity and prevent the formation of multinuclear clusters in the synthesis of the homoleptic photocatalyst **540**, several experiments focused on blocking the BOX substructures. Therefore, experiments were performed regarding the use of Lewis acids for the saturation of the coordination sides of the BOX fragments (chapter 3.2.2.2.1), along with complexation tests involving the presence of Lewis acids (chapter 3.2.2.2.2).

3.2.2.2.1 ^{1}H-NMR-investigations on interactions of Lewis acids with BOX-bpy **529**

During preliminary complexation experiments for the synthesis of a homoleptic Ru(II) complex **540** with BOX-bpy ligands **529**, it was expected that under thermodynamic control, the bipyridine fragments should preferentially coordinate to the central metal ion due to the relationship between the ion size and the bite angle of the bipyridine and BOX fragments. However, the experiments indicated in all approaches that the formation of multinuclear clusters cannot be prevented due to the triple bidentate structure. Therefore, it was assumed that prior formation of a precomplex of the form L.A.-BOX-bpy, i.e. blocking of the coordination sides of the BOX fragments by a suitable Lewis acid, might result in a monodentate ligand structure that should coordinate to ruthenium *via* the bipyridine fragments in a more controlled manner.

A suitable Lewis acid is characterized by its ability to contribute to selective blocking of the BOX fragments in solution. It should be distinguished between Lewis acids that only serve to block the BOX fragments for efficient complex synthesis and Lewis acids whose properties are suitable for later application in the bimetallic photocatalyst. For this purpose, the Lewis acid must, for instance, allow efficient exchange of reaction products for new substrates. In addition, the redox properties of the Lewis acid should be suitable for incorporation in the photocatalyst: Either redox-inert Lewis acids that do not affect the photoredox reactivity or Lewis acids whose redox properties lead to a mediating effect or enrich the redox reactivity should be used. In case of Lewis acids, which are not suitable for later application in the photoreaction, they should not coordinate to the BOX fragment too strongly, allowing their removal after formation of the precomplex and subsequent Ru-complex generation.

Considering the described criteria, as well as published results on common Lewis acids in asymmetric BOX catalysis in general and asymmetric dual transition metal photoredox catalysis in particular, Zn(II), Mg(II), Cu(II), Ni(II), Eu(III), Gd(III) were considered as potential Lewis acids.[244, 299, 300] Thereof, Zn(II) and Mg(II) as common Lewis acids in asymmetric BOX catalysis were considered to be weakly coordinated, photoredox inert representatives, while Cu(II) and Ni(II) appear to be more strongly coordinated and redox active ions - the complexes of which have been reported to be photoredox catalysts themselves or the redox behaviour of which is systematically utilized in dual lewis acid photoredox catalysis.[301-306] These properties render copper and nickel less interesting for a proof of concept of bimetallic photoredox catalysis due to potential complication of catalytic steps. In addition to complicating the overall catalytic system, redox-active Lewis acids, could furthermore counteract the concept of exploiting the distance dependancy of electron transfers, i.e. gaining stereocontrol by shielding the photoredox active core by a chiral BOX sphere, through acting as redox mediators. The aforementioned lanthanides have been successfully used in asymmetric photoredox transformations presumably due to their high kinetic lability facilitating catalyst turnover.[244]

In order to investigate the suitability of the Lewis acids for the preparation of a precomplex in detail, their tendency to coordinate in solution primarily to BOX fragments or to bipyridine fragments was investigated by ^{1}H-NMR spectroscopy by gradually increasing the $ZnCl_2$ concentration in an NMR sample containing BOX-bipyridine **529** (**spectrum 4**).

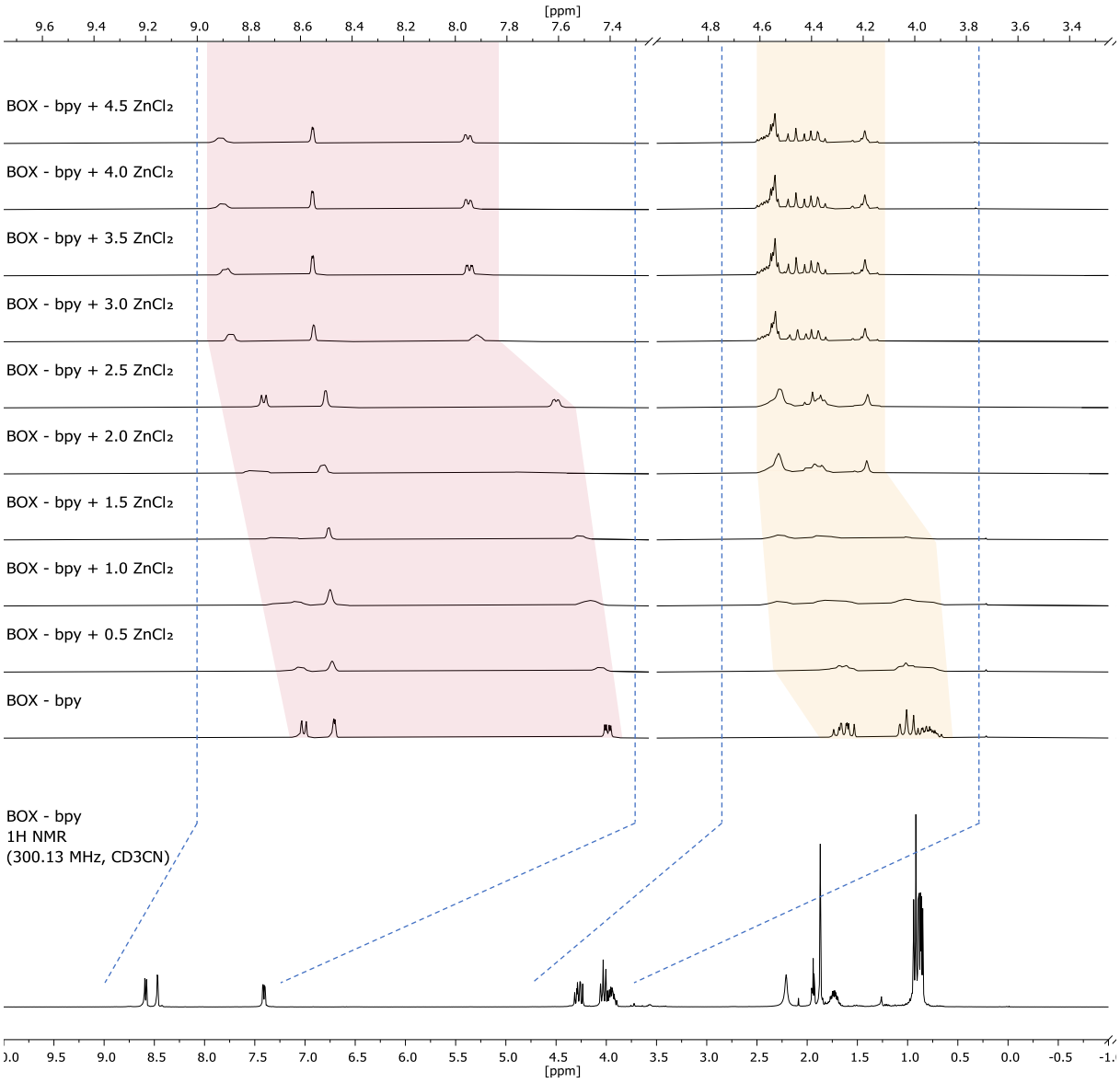

spectrum 4. ^{1}H-NMR analysis of BOX-bpy **529** in the presence of different amounts of $ZnCl_2$.

A full spectrum of the BOX-bpy ligand **529** is shown at the bottom. Above this, the stacked spectra of the NMR samples with corresponding equivalents of $ZnCl_2$ are shown. For better visibility, the superimposed spectra have been trimmed to enlarge only the bpy-ring signals (red) and the oxazoline-ring signals (yellow) (**spectrum 4**).

Examination of the spectra clearly shows that the addition of < 2.0 eq. $ZnCl_2$ causes a gradual low-field shift of all signals, which appear diffuse due to the presence of multiple species with varying $ZnCl_2$ interaction and the associated signal broadening. Upon addition of > 2.0 eq. $ZnCl_2$ an obvious clearing of the oxazoline ring signals is evident due to complete saturation of all bisoxazolines with $ZnCl_2$. this is also indicated by the unchanging chemical

shift of the oxazoline signals. In contrast, the bipyridine signals show a constant form and chemical shift only upon addition of > 3.0 eq. $ZnCl_2$.

When a similar experiment was performed with dimethylbipyridine **626** instead of BOX-bpy **529**, chemical shift and signal shape were constant for > 1.0 $ZnCl_2$, suggesting that Zn(II) certainly coordinates to bipyridine fragments when no BOX-fragments are available. In summary, this NMR experiment clearly demonstrates that $ZnCl_2$ preferentially coordinates to the BOX fragment prior to coordination of the bipyridine fragments (**figure 33**). Zn(II) could therefore be a suitable Lewis acid for blocking the BOX fragments in the synthesis of $[Ru(X_2Zn\text{-}BOX\text{-}bpy)_3]^{2+}$, and a complexation experiment was therefore carried out in the presence of $Zn(OTf)_2$ (chapter 3.2.2.2.2).

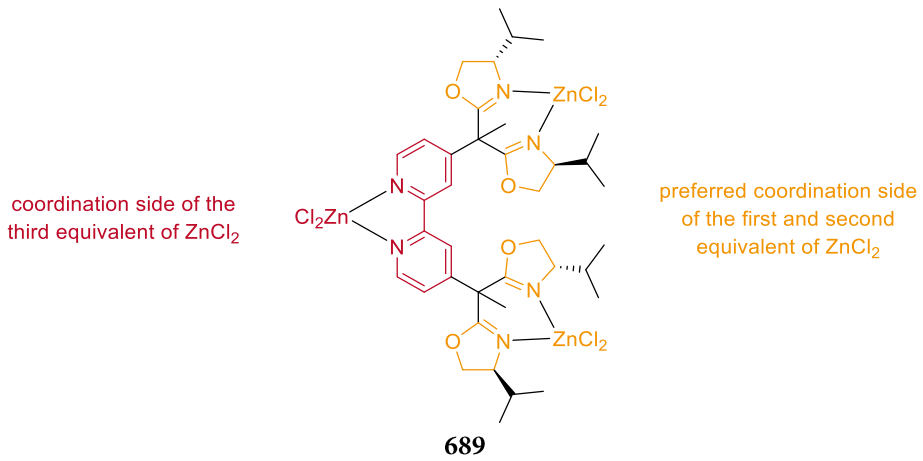

figure 33. Comparison of the coordination of $ZnCl_2$ at the BOX fragments and at bipyridine.

The NMR sample was transferred into a separating funnel, dissolved in dichloromethane and washed with water before it was measured again by NMR spectroscopy. The obtained spectrum showed no deviation from the original spectrum of the ligand **529** before addition of $ZnCl_2$, i.e. no residues of L.A., indicating that although Zn(II) shows a preference for the BOX fragments it is not bound to BOX sufficiently strong to block it permanently.

3.2.2.2.2 Complexation in the presence of a Lewis acid

Several problems were encountered in the direct synthesis of the homoleptic photocatalyst $[Ru(BOX\text{-}bpy)_3]^{2+}$ **540** (chapter 3.2.2.1). For instance, several attempts yielded only intermediates resulting from double ligand coordination. When *cis*-$RuCl_2(dmso)_4$ **677** is reacted with chelating ligands, all four dmso ligands are usually exchanged first; to force the third ligand coordination, the complexes of the form $RuCl_2(R\text{-}bpy)_2$ may be converted into the corresponding solvate complex **690** by abstraction of the chloride ligands with a silver salt. The solvate complex **690** should then react more readily with another equivalent of the ligand. Furthermore, the formation of multinuclear clusters was observed in all previous approaches as a consequence of the triple bidentate ligand structure. ^{1}H-NMR experiments on the tendency of Lewis acids to coordinate rather to the BOX or to the bpy fragment have shown that Zn(II) coordinates preferentially to the BOX fragments in solution (chapter 3.2.2.2.1). It was therefore hypothesized that stepwise complexation in the presence of zinc triflate (blocking the BOX fragments) should first lead to the formation of an intermediate of the form $[RuCl_2((OTf)_2Zn\text{-}BOX\text{-}bpy)_2]$. Addition of silver triflate should then abstract the chloride ligands and thereby generate a solvate complex **690**, which should react readily with another equivalent of the ligand **529** to form the desired L.A.-saturated photocatalyst of the form $[Ru((OTf)_2Zn\text{-}BOX\text{-}bpy)_3]^{2+}$ **691** (**scheme 85**).

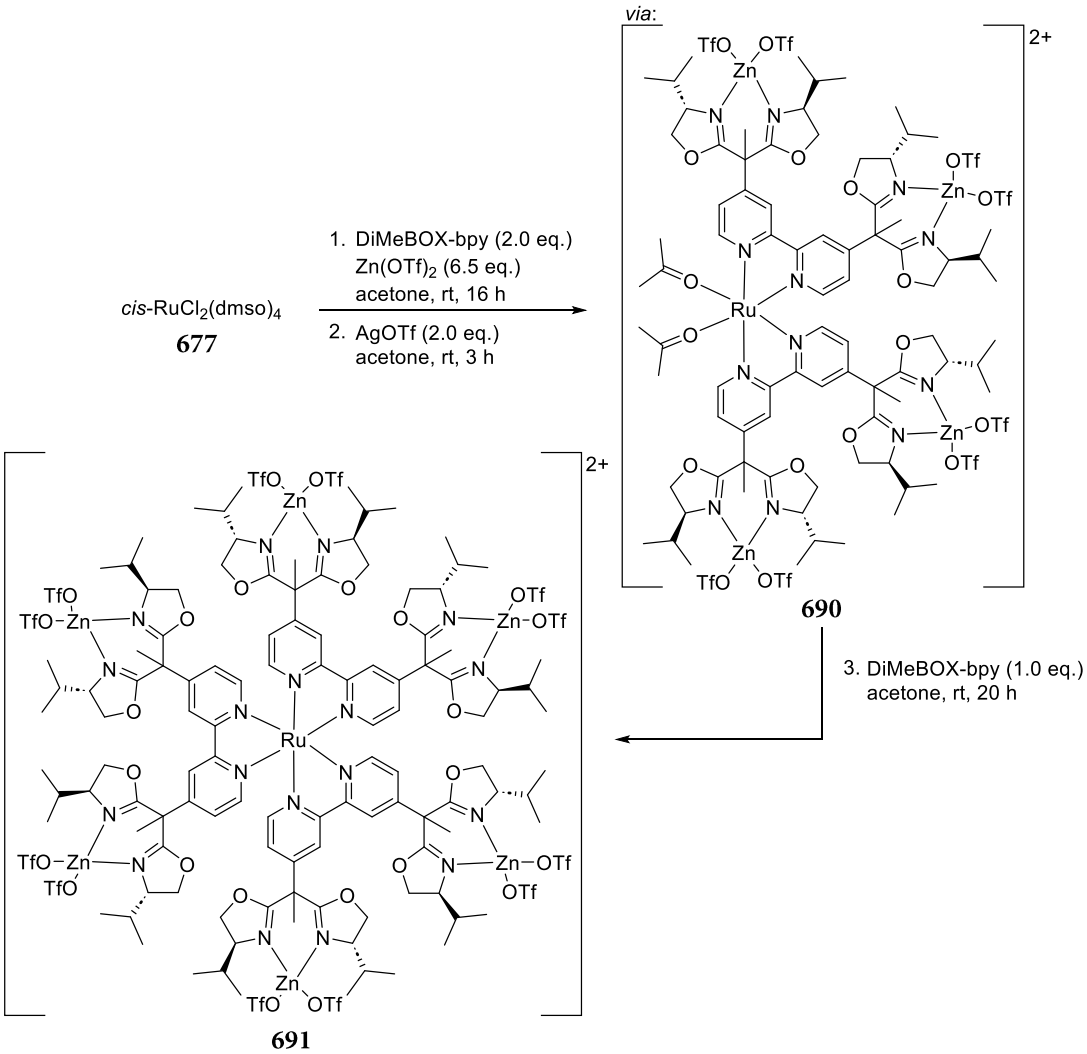

scheme 85. Attempted stepwise synthesis of the homoleptic complex **691** by blocking the BOX fragments with $Zn(OTf)_2$.

Immediately after the addition of the first two ligand equivalents to a solution of *cis*-$RuCl_2(dmso)_4$ **677**, TLC analysis showed seven yellow spots on top of the unreacted ligand spot. Addition of zinc triflate reduced the number of spots within 30 minutes to one dominant yellow spot, plus three additional spots of lower intensity. Since this development indicated the successful increase in selectivity through blocking of the BOX fragments, the reaction mixture was stirred for an additional 16 h at room temperature. After this time, however, the dominant yellow spot had disappeared and instead the formation of 10 spots of equal intensity was evident. This observation might indicate that although the blocking of BOX fragments by Zn(II) is kinetically preferable, the formation of BOX-Ru substructures is thermodynamically more stable and thus, after prolonged reaction time, the Zn(II)-ions were partly displaced by Ru(II) complexes. The intended reaction sequence was nevertheless continued by abstracting any remaining chloride ligands with silver triflate, resulting in a decrease in the number of spots to 6. After inert filtration of the formed silver chloride through a syringe filter, another equivalent of the ligand was added. By TLC, it was observed that 12 spots were present after two hours, which reduced to 9 spots within 20 hours with two slightly more dominant spots. After cooling and precipitation with KPF_6 solution, a black solid was obtained the ^{1}H-NMR analysis of which showed highly broadened unevaluable signals. Such signal broadening may either be the result of overlaying of a large number of very similar but not identical species or may be explained by paramagnetism of Ru(III). In summary, the described procedure neither yielded the fully Zn-coordinated complex $[Ru((OTf)_2Zn\text{-}BOX\text{-}bpy)_3]^{2+}$ **691** nor $[Ru(BOX\text{-}bpy)_3]^{2+}$ **540**. The replacement of the dmso ligands by two chelating ligands can initiate the isomerization of the remaining chlorido ligands depending on the complexation conditions and ligand type, with contradictory observations in the literature and predictions not possible when using slightly varying ligands.[307] For efficient incorporation of the third BOX-bpy **529** equivalent, two adjacent coordination sides are required, however, the thermodynamically preferred derivatives of the type *cis*-$RuCl_2(L\text{-}L)_2$ are usually formed at high temperatures, conditions under which the kinetically preferred BOX-Zn substructures are presumably labile, thereby preventing efficient blocking of the BOX fragments by the Lewis acid. Since the concept of synthesizing the homoleptic complex $[Ru(BOX\text{-}bpy)_3]^{2+}$ **540** by blocking the BOX fragments with a Lewis acid failed, alternative strategies, such as constructing the BOX fragments on the side chain of ruthenium complexes with ligands that are precursors of BOX-bpy **529** (chapter 3.2.2.3) or synthesizing heteroleptic BOX-substituted complexes of the form $[Ru(R\text{-}bpy)_2(BOX\text{-}bpy)]^{2+}$ (chapter 3.2.3), were evaluated.

3.2.2.3 Synthesis of $[Ru(BOX\text{-}bpy)_3]^{2+}$ **540** by side-chain functionalization of $[Ru(R\text{-}bpy)_3]^{2+}$-complexes

The selectivity problem arising from the triple-bidentate ligand structure in the reaction of BOX-bpy **529** with a Ru(II)-source (chapter 3.2.2.1) could instead of blocking the BOX fragments by a Lewis acid (chapter 3.2.2.2) also be solved by building up the BOX substituents by side-chain functionalization using a simplified photocatalyst precursor. In this way, the chelating bisoxazoline substructures that led to bridging and formation of multinuclear clusters in the direct complex synthesis would be formed after coordination of the bipyridine substructures around a central Ru(II) ion. For this purpose, the starting material of the ligand synthesis, 4,4'-dimethylbipyridine (dmb) **626**, was reacted with *cis*-$RuCl_2(dmso)_4$ **677** by heating in ethylene glycol/water to give the corresponding homoleptic precursor complex of the form $[Ru(dmb)_3](PF_6)_2$ (**692**) in excellent yield (99%) (**equation 30**).

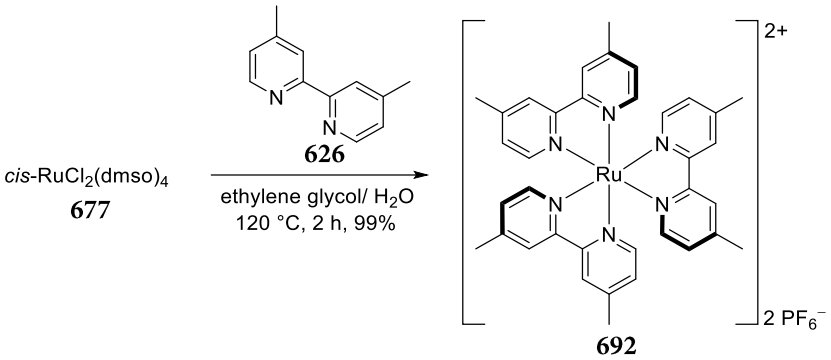

equation 30. Synthesis of $[Ru(dmb)_3](PF_6)_2$ **692**.

Following the ligand synthesis by side-chain functionalization (chapter 3.1.3.1), the obtained precomplex was subjected to a modified deprotonation addition sequence. Due to the electron-withdrawing effect of the Ru(II) ion, it was assumed that deprotonation at the heterobenzylic position should proceed under milder conditions than in the functionalization of the free ligand. Therefore, instead of LDA, which despite its steric demand readily adds to ethyl chloroformate **627**, the non-nucleophilic base Cs_2CO_3 was used. This way an alternating addition of base and ethyl chloroformate **627** was assumed to be no longer necessary. However, after workup by precipitation with saturated NH_4PF_6 solution, only the starting material was isolated (**equation 31**).

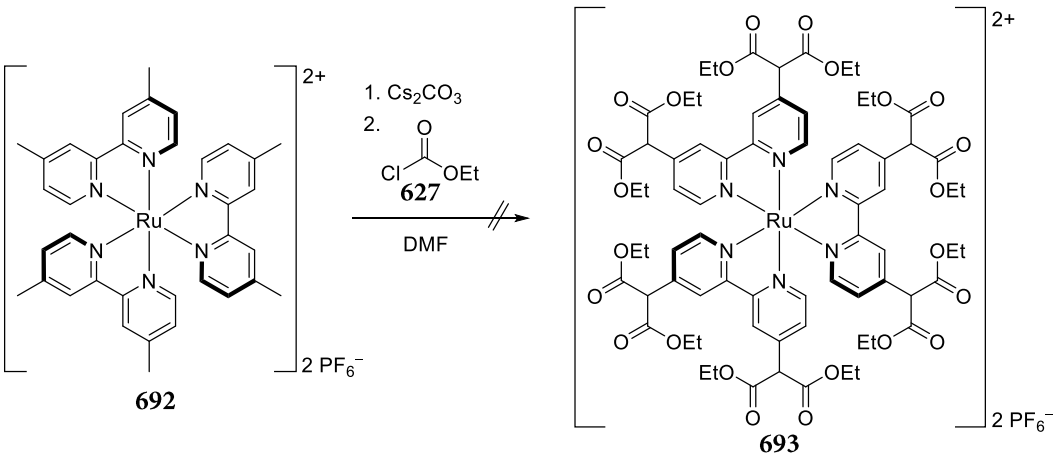

equation 31. Attempted side-chain functionalization of $[Ru(dmb)_3](PF_6)_2$ (**692**).

Perhaps the employed base was too weak for deprotonation despite the reduction in pk_a value due to metal coordination. The lack of conversion was previously not detected by TLC, as precise differentiation of such polar compounds by TLC is very difficult. Since the desired heterobenzylic functionalization was the bottleneck of the ligand synthesis anyway, a later entry into complex functionalization was approached. Therefore, either the already functionalized malonyl-bipyridine (mal-bpy) derivative **625** (chapter 3.1.3.2) or the tetra-γ-hydroxyamide-bipyridine derivative **622** (chapter 3.1.3.3.1) could be employed to prepare precursor complexes, starting from which the BOX fragments could be synthesized. Assuming that the γ-hydroxyamide strands might be sterically hindered and prone to bridging due to the large number of heteroatoms, focus was placed on the complexation of malonyl-bpy **625** to obtain a complex of the form $[Ru(mal\text{-}bpy)_3](PF_6)_2$ **694**. In analogy to the above mentioned synthesis of $[Ru(dmb)_3](PF_6)_2$ **693**, malonyl-bipyridine **625** was mixed with *cis*-$RuCl_2(dmso)_4$ **677** in ethyleneglycol/water and heated to 120 °C, providing the desired complex **693** in a moderate yield (65%) (**equation 32**) .

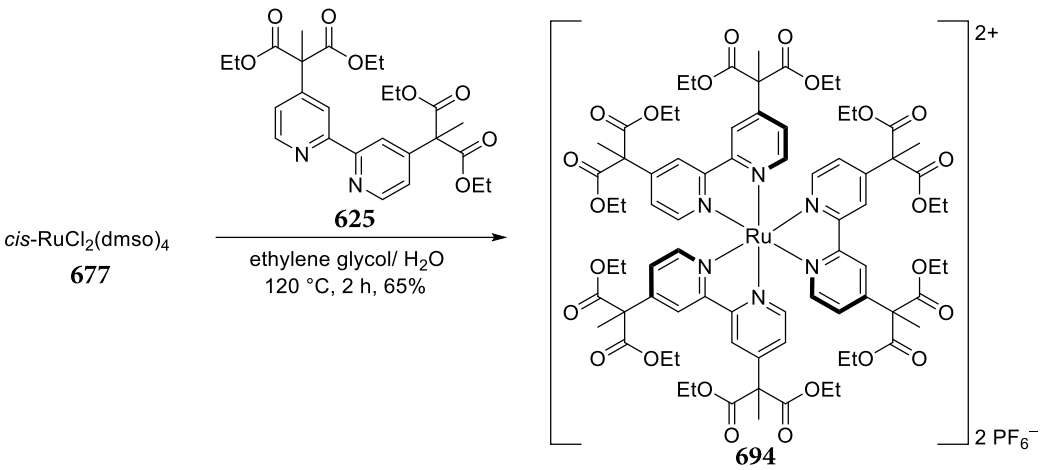

equation 32. Synthesis of $[Ru(mal\text{-}bpy)_3](PF_6)_2$ **694**.

Following the most successful established ligand synthesis (chapter 3.1.3.3.1), the resulting complex was reacted neat with freshly dried and distilled L-valinol (**603**) (**equation 32**). Already during the synthesis of the free ligand **529**, the amide formation must take place at four reaction centres, which is why this step required a particularly long reaction time. However, in the case of side-chain functionalization of the complex, amide formation must take place at 12 ester groups to form the product complex **695**, which is why the mixture was stirred for three weeks, before excess L-valinol (**603**) was distilled off and the residue was purified by column chromatography.

A complex species was obtained whose ^{1}H-NMR spectroscopic analysis clearly showed the disappearance of the ester signals from the reactant complex **694**. However, the ratio of the integrals of the valinol-amide strands relative to the unchanged bipyridine signals and methyl group signals, was found to be only half of that expected for the product **695**, suggesting in analogy to the side reaction observed during amide formation in the synthesis of the

free ligand, decarboxylation may have occurred (chapter 3.1.3.3.1) (**scheme 86**). It is possible that the involved complex species are even more prone to undergo decarboxylation due to metal coordination.

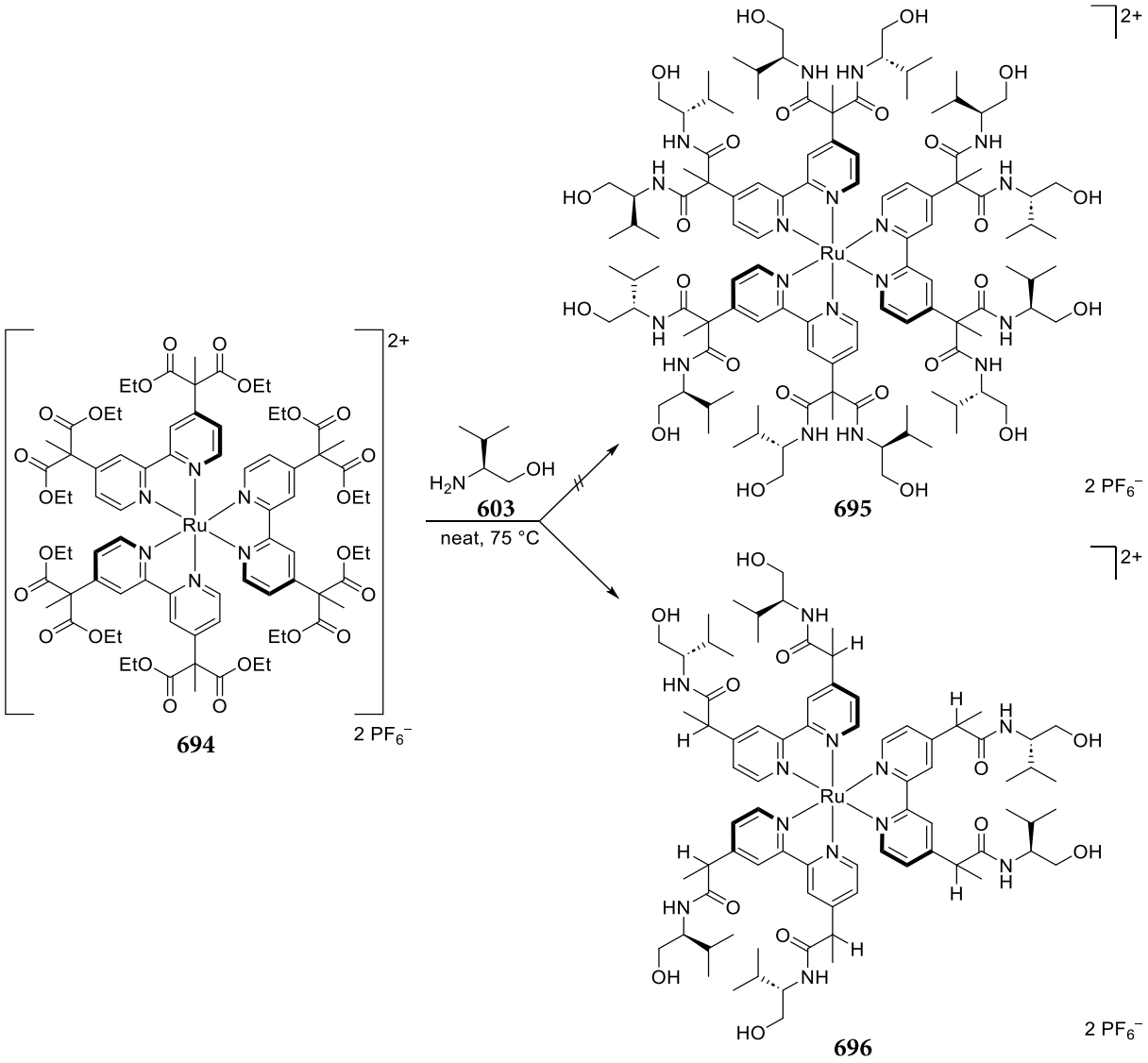

scheme 86. Attempted side-chain-functionalization of $[Ru(mal\text{-}bpy)_3](PF_6)_2$ **694** and assumed decarboxylated side product **696**.

With these results, the concept of synthesizing the catalyst by side-chain functionalization of precomplexes prepared from preliminary stages of the ligand was not successful, and the last chance of using tetra-γ-hydroxyamide-bpy **622** was not considered to simplify the complex synthesis for the reasons mentioned above, thus further experiments focused on the synthesis of heteroleptic photocatalysts (chapter 3.2.3).

3.2.3 Synthesis of heteroleptic photocatalysts $[Ru(R\text{-}bpy)_2(BOX\text{-}bpy)]^{2+}$ **532**, **536** and **537**

An alternative photocatalyst concept envisions heteroleptic complexes of the general form $[Ru(R\text{-}bpy)_2(BOX\text{-}bpy)]X_2$, containing only one asymmetric BOX-bpy ligand **529**. The heteroleptic nature allows for a conceptual separation of the complexes into an asymmetric and a symmetric side. To achieve satisfactory asymmetric induction, it is important to ensure that phototransformations occur preferentially in close proximity to the BOX-bpy ligand **529**. Although photoinduced electron transfer onto suitable substrate, e.g. α-bromocarbonyl compounds, is facilitated by the electron-withdrawing effect of Lewis acids that are asymmetrically coordinated at the BOX fragments, there is an increased risk of undesired racemic background reactions on the opposite side of the BOX fragment in the heteroleptic complex, unless the phototransformation has been tuned in such a way that the involved substrates only react after their redox potential has been lowered by Lewis acid coordination.[11, 211, 244, 245] Aiming at the enantioselective adaption of previously established racemic phototransformations that were developed using racemic $[Ru(bpy)_3]^{2+}$ (**7**) complexes and thus readily react without Lewis acid activation, the risk of racemic background reactions on the BOX-bpy side must be lowered in a different way.

For this purpose, the racemic side has to be shielded, which can be achieved mainly in two ways: The most obvious way of shielding could be of steric nature and involve the incorporation of, for example, *tert*-butyl groups to equalize the distance between the photoredox active catalyst core and the substrate on all sides of the catalyst or to increase it on the symmetric side. In the resulting complex of the form $[Ru(t\text{Bu-}bpy)_2(BOX\text{-}bpy)]^{2+}$ **536**, the preference for enantioselective transformation should therefore be based 1. on the activating effect of the Lewis acid, and 2. on the exploitation of the distance dependancy of electron transfers (**figure 34**, left). An alternative shielding approach could be of electronic type and increase the electron density on the BOX averted side by incorporation of alkoxy substituents in such a way that removal of degeneracy of excited triplet MLCTs results and, during photoexcitation, the electron is preferentially excited into orbitals on the BOX-substituted catalyst side (**figure 34**, right).

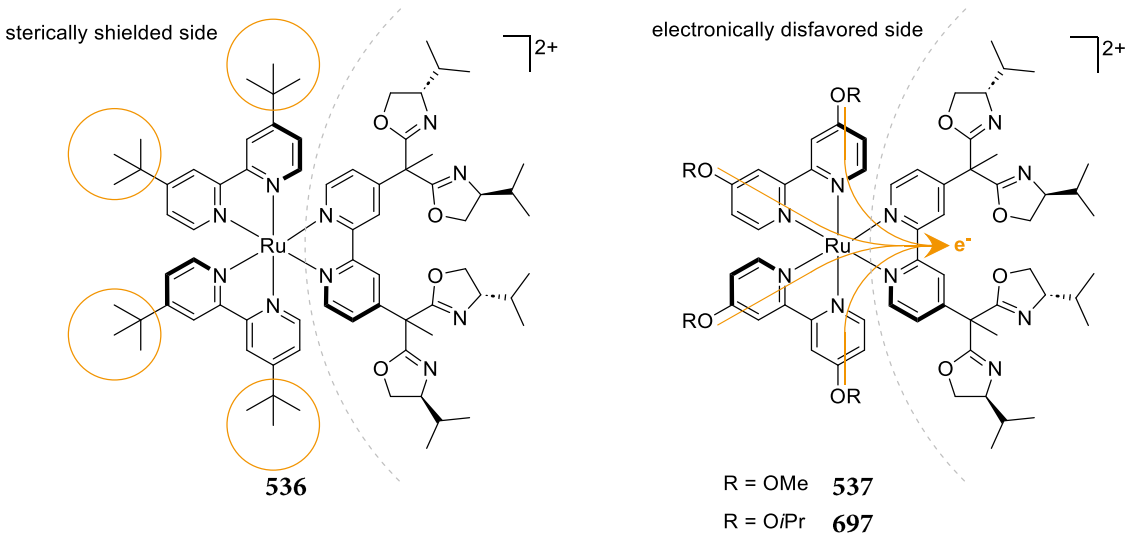

figure 34. Envisioned steric shielding and electronic disfavoring of achiral sides in heteroleptic photocatalysts **536, 537** and **697**

3.2.3.1 Synthesis of precursor complexes $Ru(R\text{-}bpy)_2Cl_2$ **701-703**

For the synthesis of heteroleptic complexes of the form $[Ru(R\text{-}bpy)_2(BOX\text{-}bpy)]^{2+}$ (**536, 537** and **697**), several approaches focused initially on the synthesis of precursor complexes of the form *cis*-$Ru(R\text{-}bpy)_2Cl_2$ **701-703**, allowing BOX-bpy **529** to be incorporated at a later stage (**scheme 87**). These structures can be obtained by simple refluxing of a mixture of $RuCl_3$ x H_2O **676** with two equivalents of the corresponding ligand **698-700** in reducing solvents, e.g. alcohols or DMF. Under these conditions, however, relatively long reaction times are usually required, thus synthetic methods have been developed using sugars as reducing additives, allowing greatly shortened reaction times.[308] Moreover, the synthesis can be carried out using Ru(II) sources such as *cis*-$RuCl_2(dmso)_4$ **677** or $RuCl_2(\eta^4\text{-}COD)$ **683**. As both the concept of steric shielding and electronic disfavoring should be evaluated, a variety of approaches to the synthesis of precursor complexes with different bipyridine derivatives **698-700** were carried out. In addition to commercially available *tert*-butyl-bipyridine **698** and methoxy-bipyridine **699**, isopropyloxy-bipyridine **700** was also used, as it was hypothesized that the heteroleptic complex obtainable with it could embody a symbiosis of steric shielding and electronic disfavoring. The parameters and results of selected experiments of the synthesis of precursor complexes are summarized in **table 4**.

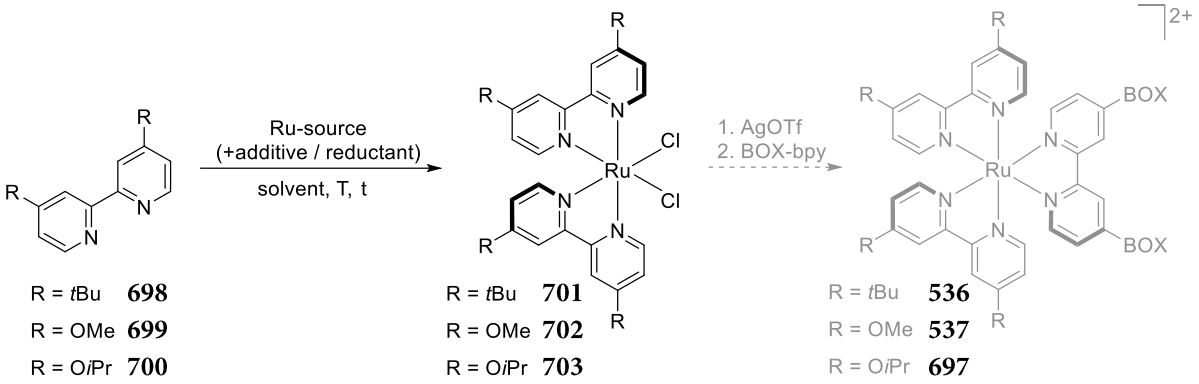

scheme 87. Synthesis of precursor complexes **701**, **702** and **703** for the synthesis of heteroleptic BOX-substituted complexes **536**, **537** and **697**.

Starting from dimethoxybipyridine **699**, refluxing in a mixture of hydrogen bromide and acetic acid gave dihydroxybipyridine **704** in a moderate yield of 67%.[309] The dihydroxy derivative **704** was reacted with an excess of isopropyl bromide in the presence of potassium carbonate to neutralize the hydrogen bromide released during the reaction, and catalytic amounts of potassium iodide to accelerate the substitution by intermediate formation of the more reactive alkyl iodide. In a small scale, diisopropyloxybipyridine **700** was obtained in quantitative yield, on a larger scale, the product was obtained in very good yield of 84% (**scheme 88**).

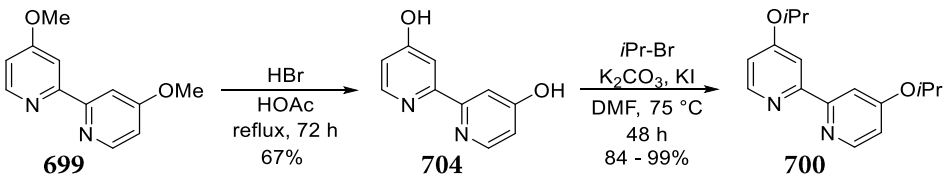

scheme 88. Synthesis of diisopropyloxybipyridine **700** from dimethoxybipyridine **699**.

table 4. Parameters and results of selected experiments on the synthesis of different precursor complexes of the form Ru(R-bpy)Cl_2.

entry	bpy-R	Ru source	c(Ru)	additive [eq.]	reductant	solvent	T [°C]	t [min]	yield
1	*t*Bu	$RuCl_3$ xH_2O	0.038 M	LiCl [40]	glucose / ascorbic acid	H_2O / $HOCH_2CH_2OH$	110	60	---
2	*t*Bu	$RuCl_3$ xH_2O	0.041 M	LiCl [40]	glucose / ascorbic acid	H_2O / $HOCH_2CH_2OH$	110	100	---
3	*t*Bu	$RuCl_3$ xH_2O	0.273 M	LiCl [5.7]	glucose / ascorbic acid	H_2O / $HOCH_2CH_2OH$	110	75	---
4	OMe	$RuCl_3$ xH_2O	0.038 M	LiCl [40]	glucose / ascorbic acid	H_2O / $HOCH_2CH_2OH$	110	30	---
5	OMe	$RuCl_3$ xH_2O	0.038 M	LiCl [40]	glucose / ascorbic acid	H_2O / $HOCH_2CH_2OH$	110	60	---
6	OiPr	$RuCl_3$ xH_2O	0.038 M	LiCl [13]	glucose / ascorbic acid	H_2O / $HOCH_2CH_2OH$	110	60	---
7	*t*Bu	$RuCl_3$ xH_2O	0.191 M	LiCl [6.8]	---	DMF	156	480	---
8	*t*Bu	$RuCl_2(dmso)_4$	0.012 M	LiCl [10]	---	DMF	130	150	---
9	OMe	$RuCl_2(dmso)_4$	0.012 M	LiCl [10]	---	DMF	130	150	---
10	O*i*Pr	$RuCl_2(dmso)_4$	0.012 M	LiCl [10]	---	DMF	130	150	---
11	OMe	$RuCl_2(dmso)_4$	0.011 M	---	---	$CHCl_3$	61.2	180	---
12	O*i*Pr	$RuCl_2(dmso)_4$	0.011 M	---	---	$CHCl_3$	61.2	180	---
13	*t*Bu	$Ru(COD)Cl_2$	0.200 M	---	---	*o*-$C_6H_4Cl_2$	140	180	32%
14	*t*Bu	$Ru(COD)Cl_2$	0.200 M	---	---	*o*-$C_6H_4Cl_2$	140	180	82%
15	OMe	$Ru(COD)Cl_2$	0.198 M	---	---	*o*-$C_6H_4Cl_2$	140	180	---
16	O*i*Pr	$Ru(COD)Cl_2$	0.195 M	---	---	*o*-$C_6H_4Cl_2$	140 → 180	360	---
17	OMe	$Ru(COD)Cl_2$	0.198 M	---	---	*o*-$C_6H_4Cl_2$	180	180	83%

The initial experiments were carried out according to a modified protocol by Cheruzel *et al.*, who optimized the synthesis of bis(bipyridine)-ruthenium(II) complexes from $RuCl_3$ x H_2O (**676**) in the presence of reducing additives, e.g. glucose and ascorbic acid and successfully synthesized both *cis*-Ru(*t*Bu-bpy)$_2$Cl$_2$ (**701**) and *cis*-Ru(MeO-bpy)$_2$Cl$_2$ (**702**) in a short time and in good yields.[308] They performed the reaction in the presence of a large excess of lithium chloride which serves to prevent the addition of a third ligand and formation of a homoleptic complex of the form [Ru(R-bpy)$_3$]$^{2+}$ (**714-716**). Although accurate analyses of such complexes by structure-resolving techniques such as ^{1}H-NMR are rather uncommon and often the crude product is used in the next complexation step without further analysis or purification, all complexation approaches were subjected to thorough ^{1}H-NMR analysis. This serves on the one hand to minimize potential losses of the ligand **529** in the development of a complex synthesis, but also to establish a more reproducible synthetic route. Following the published results with R = *t*Bu provided a dark violet microcrystalline solid in quantitative yield, assuming the observed substance was indeed *cis*-Ru(*t*Bu-bpy)Cl$_2$ (**701**), however the unambiguous confirmation of the successful synthesis by ^{1}H-NMR spectroscopy proved to be challenging (entries 1 – 2). Hence, two separate *tert*-butyl signals comprising 18H each were clearly detectable, indicating a desymmetrization compared to the free ligand **529**, which is only to be expected for the desired product *cis*-Ru(*t*Bu-bpy)Cl$_2$ (**701**) or a precursor of the form *cis,cis*-Ru(*t*Bu-bpy)Cl$_2$X$_2$ (**705**), however the aromatic region showed only four equally intense signals. The appearance of four signals cannot be rationalized easily by any of the conceivable species **701-716** (**figure 35**) since complexes of higher symmetry should carry only three aromatic hydrogen atoms due to the *tert*-butyl substituent at the 4- or 4'-position of the bipyridine fragment and thus show only three signals. Low symmetry complexes, on the other hand, should exhibit three signals each for rings that are *trans* to chloride or *trans* to other ligands (bpy or X), i.e. a total of six signals.

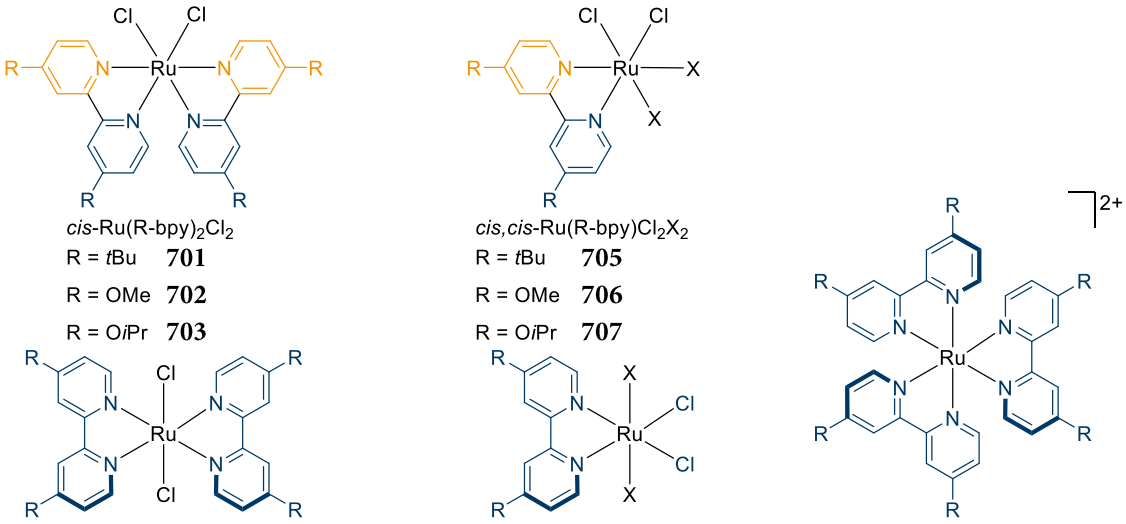

figure 35. Classification of conceivable complexes according to their symmetry: Top – low symmetry species, bottom – high symmetry species.

Based on the appearance of the obtained complex, which was in agreement with several publications, it was assumed that it might be the *trans*-derivative **708** with three bipyridine-signals in addition to an unknown impurity, the integral of which coincidentally showed similar intensity. The complex was therefore used in a test run of the subsequent complexation and indeed successfully afforded the first heteroleptic complex (chapter 3.2.3.2). Subsequent approaches focused on the goal of obtaining a more comprehensible ^{1}H-NMR analysis in order to employ a better defined substance in the final complexation step than in this test approach.

The reaction was repeated with extended reaction time (entry 2) to ensure that the thermodynamically more favorable *cis*-derivative **701** was obtained. A similar spectrum was obtained, but with significantly broadened signals indicating paramagnetic Ru(III) and thus a failed reduction. By mass spectrometry, the product mass was confirmed, but the detected compound did not show ionization by protonation or similar. The results obtained indicated a failed reduction of the paramagnetic Ru(III) and formation of a species of the type [Ru(*t*Bu-bpy)$_2$Cl$_2$]Cl, which was reported previously.[308] The reason might be that the reaction mixture was not degassed by freeze-pump-thaw but only by bubbling nitrogen into the reaction mixture, although no information was provided in the literature about prior degassing or required inert handling: Instead, these types of structures are typically filtered off under air by Büchner filtration and sometimes dried and stored under air. Also, the commercially available Ru(bpy)$_2$Cl$_2$ (**717**) does not require any specifically mentioned inert handling. Nevertheless, all further approaches were performed in thoroughly degassed solvent.

In the subsequent reaction (entry 3), the concentration was substantially increased. Purification *via* a short aluminium oxide column allowed the separation of a small amount of a side-product, the mass spectrum of which showed dominantly the product mass in addition to a large amount of free ligand **698**. The ^{1}H-NMR spectrum displayed only three signals in the aromatic region, indicating that it was the *trans*-derivative **708**. Furthermore, a larger amount of a substance was obtained, whose mass spectrum likewise dominantly contained the product mass, in addition to a small amount of the free ligand **698**, and whose ^{1}H-NMR spectrum showed for the first time the (for symmetry reasons) expected number of signals in the aromatic region, in addition to minor *trans*-product **708** signals.

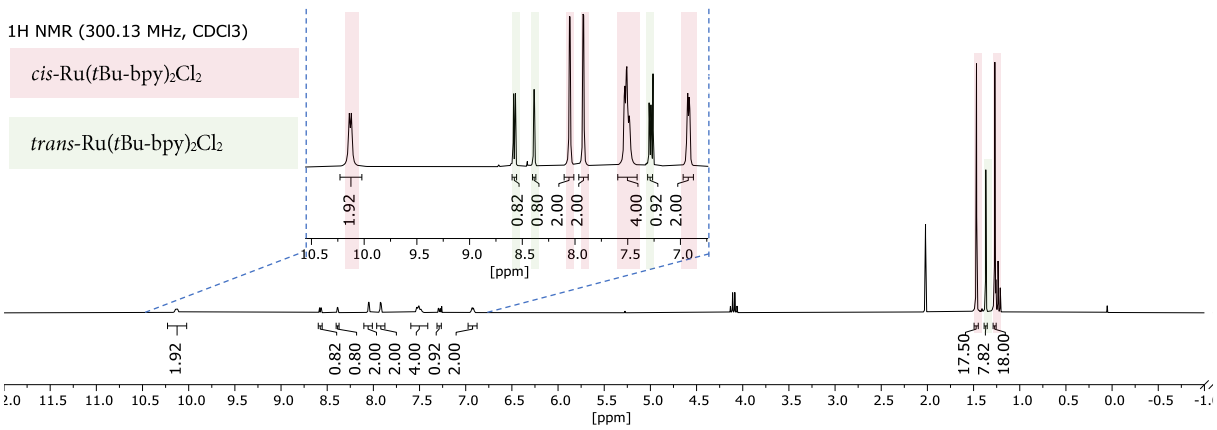

spectrum 5. ^{1}H-NMR of the obtained mixture of *cis*-Ru(*t*Bu-bpy)$_2$Cl$_2$ (**701**) and *trans*-Ru(*t*Bu-bpy)$_2$Cl$_2$ (**708**).

When similar conditions were applied using 4,4'-methoxybipyridine **699** (entry 4) the appearance of the obtained reaction product did not match the reference in the literature describing a smooth shiny violet microcrystalline solid. Instead, a brown powder was obtained exhibiting very poor solubility in many common solvents, thus hampering ^{1}H-NMR analysis. Nonetheless, very small ^{1}H-NMR signals were obtained in both d_4-MeOH and d_3-MeCN, although these included only three aromatic bipyridine signals and one methoxy signal. For symmetry reasons, six aromatic signals are expected for all desired *cis*-$RuCl_2$(R-bpy)$_2$ derivatives (**701**-**703**), as well as two peak sets for the corresponding residue (*t*Bu, OMe, O*i*Pr). Therefore, the observed signals can only be attributed to free dimethoxybipyridine **699** or an isomer of higher symmetry (**709**, **712**, **715**). The reaction was repeated with extended reaction time and using twice the amount of ascorbic acid to ensure successful reduction (entry 5). After cooling and precipitation, a shiny, deep violet microcrystalline solid was indeed obtained, the appearance of which changed, however, to a dark brown powder as it was dried by a stream of air over the Büchner funnel. It is possible that the change in appearance was associated with a transformation of the substance that was drying. The ^{1}H-NMR spectrum showed the same signals as in the previous experiment; after a week, additional signals became visible in the aromatic region and around the methoxysignals, either as a result of ligand dissociation or particularly slow dissolution of the desired *cis*-$RuCl_2$(MeO-bpy)$_2$ (**702**). The encountered problem, as well as a thorough analysis of the compound, have not been reported previously.

It was hypothesized that the observed difficulties could be overcome by employing a different alkyl residue. Therefore, diisopropyloxybipyridine **700** was subjected to the conditions of previous approaches (entry 6). Precipitation and filtration provided a black solid, that partly dissolved in acetone. In the ^{1}H-NMR, the solubilized substance showed the ligand signals clearly shifted (possibly due to Ru coordination), but similar to previous attempts (with R = OMe), only 3 signals in the aromatic region and only one signal set for the *i*Pr residues. The mass spectrum indicated the mass of the product probably because the *trans*-product **709** was formed. Furthermore, the mass of the homoleptic complex $[Ru(iPrO\text{-}bpy)_3]^{2+}$ (**716**) was visible. In contrast, the acetone-insoluble substance showed a doubled set of signals for the *i*Pr residues but only three clearly resolved aromatic signals with 2H each, in addition to two strongly broadened, not clearly identifiable signals with 4H and 2H, respectively, thus a total of 12 aromatic protons as expected for the desired *cis*-product **703** and also in the mass spectrum a peak set with an isotopic pattern typical for ruthenium was recognizable in the region of the product mass. However, the desired mass could not be found by HRMS-ESI.

In summary, all approaches starting from $RuCl_3$ x H_2O (**676**) aiming to shorten the reaction time by using external reducing agents (sugars and ascorbic acid) were characterized by low selectivity, problematic purification and difficulties in confirming *cis*-$RuCl_2$(R-bpy)$_2$ (**701**-**703**) unambiguously (entries 1 - 6). Therefore, further approaches focused on alternative synthetic methods. The *t*Bu-ligand was refluxed with $RuCl_3$ x H_2O (**676**) in the presence of LiCl in thoroughly degassed DMF (entry 7). This approach aimed at the tendency of DMF to decompose at high temperatures, resulting in the release of dimethylamine, which can act as a reducing agent.[308] However, as there is no sudden decomposition of all DMF molecules above a certain temperature, it was suspected

that a significantly prolonged reaction time of 8 h is required for a complete reduction of the Ru(III) source. After repeated purification experiments by column chromatography in mixtures of dichloromethane/methanol/ammonia-solution or benzene/acetone, a dark purple compound was obtained the ^{1}H-NMR spectrum of which contained the expected signals for a *cis*-RuX_2(*t*Bu-bpy)$_2$ species as well as DMF signals whose integrals indicated that two DMF molecules were coordinated to Ruthenium (X = DMF). It is possible that the mixture was refluxed for too long, allowing the chlorido ligands to be exchanged for solvent molecules. Since it was assumed that the reduction of Ru(III) by DMF requires a prolonged reaction time, the most obvious solution was to use Ru(II) precursors in subsequent approaches.

Using *cis*-$RuCl_2$(dmso)$_4$ **677** for the complexation of *t*Bu-bipyridine in DMF, several species were obtained after column chromatography, the ^{1}H-NMR spectra of which exhibited several signals similar to those for Ru-bound DMSO in the spectrum of the Ru(II) precursor (entry 8). With R = OMe, obtaining a pure substance was not possible by both column chromatography and precipitation, resulting in ^{1}H-NMR spectra that did not allow reliable analysis due to the large number of signals, some of which were poorly resolved (entry 9). With R = O*i*Pr, the expected number of signals in the aromatic region was again obtained in this way, but the integral of the isopropyl signals relative to aromatic signals showed only half of the expected protons, suggesting the formation of another asymmetric intermediate for example of the general form *cis,cis*-RuX_2Cl_2(*i*PrO-bpy) **707** (entry 10). Indeed, the formation of such a species for X = dmso was confirmed by mass spectrometry, besides two dominant peak sets at much higher masses (m/z 852 and m/z 1011), which could not be explained by any obvious potential side reaction (m/z [Ru(*i*PrO-bpy)$_3$]$^{2+}$: 918; m/z $RuCl_2$(dmf)$_2$(*i*PrO-bpy) 792; m/z $RuCl_2$(dmso)$_2$(*i*PrO-bpy) 600).

On one hand, the results indicate that an exchange of chlorido ligands against DMF molecules takes place at prolonged reaction times, on the other hand, too short reaction times apparently lead to an incomplete exchange of dmso ligands against two bpy ligands. Therefore, two complexation approaches were carried out with R = OMe and R = O*i*Pr at extended reaction time but in non-coordinating chloroform (entries 11 – 12). In both approaches, the formation of a large number of spots was evident on TLC. The precipitation from acetone with Et_2O, as described for these types of complexes, only slightly reduced the number of spots in the case of R = OMe. It is possible that the absence of LiCl was responsible for the formation of many byproducts.

Ultimately, further approaches were made using the Ru(II) precursor $RuCl_2$(COD) **683**, the use of which was reported to provide access to the desired *cis*-complexes: Heating the precursor **683** with 2 equivalents of the ligand **702** in 1,2-dichlorobenzene to 180 °C for 2 h according to Meyer *et al.* or to 140 °C for 3 h according to Du Bois *et al.* has been reported to provide access to *cis*-Ru(MeO-bpy)Cl_2 **702** in excellent yields.[62, 310] However, the authors did not perform any further analysis and instead assumed the amount of their crude product to be pure product and used it in subsequent steps.

In the reaction of Ru(COD)Cl_2 **683** with *t*Bu-bpy **698** according to Du Bois *et al.* the product was precipitated with *n*-hexane in a very microcrystalline form, so that filtration through a Büchner funnel fitted with filter paper repeatedly failed to collect all solid particles.[310] The first filtration gave a sample indeed containing dominantly

cis-$RuCl_2$(*t*Bu-bpy)$_2$ (**701**) next to little impurity of free ligand **698** or any symmetric derivative, e.g., *trans*-$RuCl_2$(*t*Bu-bpy)$_2$ (**708**), in a poor yield of 14%. The second filtration gave the desired complex without traces of other Ru complexes, but mixed with residues of the solvent 1,2-dichlorobenzene (bp 180 °C); ^{1}H-NMR allowed the determination of a yield of 32% from this sample (entry 13).

When the reaction was repeated, the work-up strategy was optimized by removing the supernatant solution from the precipitated product after sedimentation using a syringe and repeatedly purifying the residual solid within the flask by slurrying with *n*-hexane, sedimentation and removal of the supernatant solution. In this way, most of the dichlorobenzene was washed out. After drying in high vacuum, the substance was obtained in a yield of 98%, however, after ^{1}H-NMR analysis and consideration of the remaining contamination with dichlorobenzene, the substance was obtained in a yield of 82% (entry 14). The *cis*-$RuCl_2$(*t*Bu-bpy)$_2$ (**701**) obtained was not further purified, since residues of the non-coordinating solvent should not have a negative effect on the subsequent reaction.

Following the same procedure according to Du Bois *et al.* using dimethoxybipyridine **699** led to the isolation of a brown solid, the ^{1}H-NMR analysis of which showed only one dominant set of signals with 3 aromatic signals (2[310] **709** Employing *i*PrO-bpy **700** under the same conditions gave similar results (entry 16), however besides dominant signs of the *trans*-product **710** another set of signal was visible indicating that it might have been a mixture of *cis*-product **703** and *trans*-isomer **710**. Given that most approaches so far, especially when employing alkoxy-bipyridines **699** and **700**, led primarily to the formation of the *trans*-isomers **709** and **710** it was assumed that these might be kinetically favored while the formation of the desired *cis*-products **702** and **703** requires even higher temperatures. Therefore, according to Meyer *et al.* the crude *cis*/*trans*-mixture obtained was dissolved in dichlorobenzene again and heated to 180 °C for another three hours hoping for an isomerization to the *cis*-isomer **703** (entry 16).[62] However, the spectrum obtained in this way did not show a change in the *cis*/*trans*-ratio. The conditions of the Meyer group were examined again using methoxy-bipyridine **699** (entry 17).[62] After 3 h at 180 °C *n*-hexane was added and the precipitate repeatedly washed inside the flask by carefully removing the supernatant liquid followed by addition of clean *n*-hexane to the solid residue. Although the reaction was performed in a small 100 mg scale, the washing procedure was repeated with a total of 120 mL *n*-hexane. ^{1}H-NMR-analysis of the solid in $CDCl_3$, did not show any signals similar to MeO-bpy **699**, probably as a result of a significantly increased dipole of the *cis*-derivative **702** and associated altered solubility. When the substance was analyzed as a solution in DMSO-d_6 the formation of the desired *cis*-complex Ru(MeO-bpy)$_2$$Cl_2$ **702** was indeed unambiguously confirmed on the basis of 6 aromatic signals and two MeO-signals (**spectrum 6**).

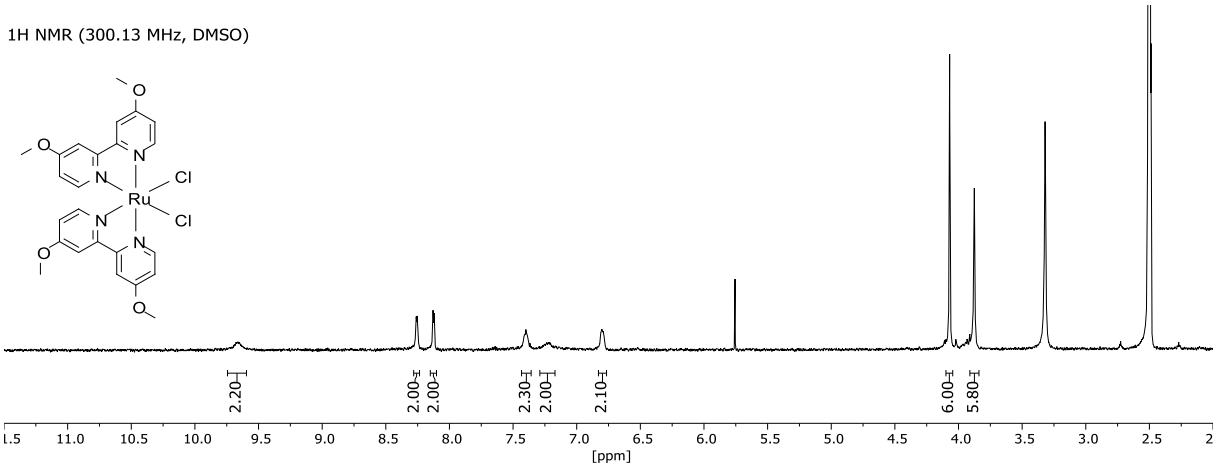

spectrum 6. ^{1}H-NMR spectrum confirming the formation of *cis*-Ru(MeO-bpy)Cl_2 (**702**).

In summary, the synthesis utilizing the $RuCl_2$(COD) precursor **683** provided the best results, presumably because the exchange of the η^4-bound COD ligand **681** automatically leads to the exposure of 4 coordination sides and thus there is less risk of only partial exchange of dmso ligands. For the synthesis of the *t*Bu precursor complex **701**, a maximum yield of 82% was obtained at 140 °C, whereas an even higher temperature of 180 °C is required when MeO-bipyridine **699** is employed. Since the methoxy derivative **702** is sufficient to qualitatively investigate the concept of electronically directed excitation, the synthesis of the isopropyloxy derivative **703** was not further investigated. Instead, subsequent approaches focused on the incorporation of BOX-bpy **529** into the *cis*-Ru(R-bpy)Cl_2 precursor complexes **701** and **702**.

3.2.3.2 Incorporation of BOX-bpy **529** into heteroleptic photocatalysts **532**, **536** and **537**

The synthesis of heteroleptic photocatalysts of the general formula $[Ru(R\text{-}bpy)_2(BOX\text{-}bpy)]^{2+}$ was approached starting from the corresponding precursor complexes (**717**, **701**, **702**) (chapter 3.2.3.1) by reaction with BOX-bpy **529** following two different pathways (**scheme 89**). The reaction parameters and results of selected transformations are summarized in **table 5**.

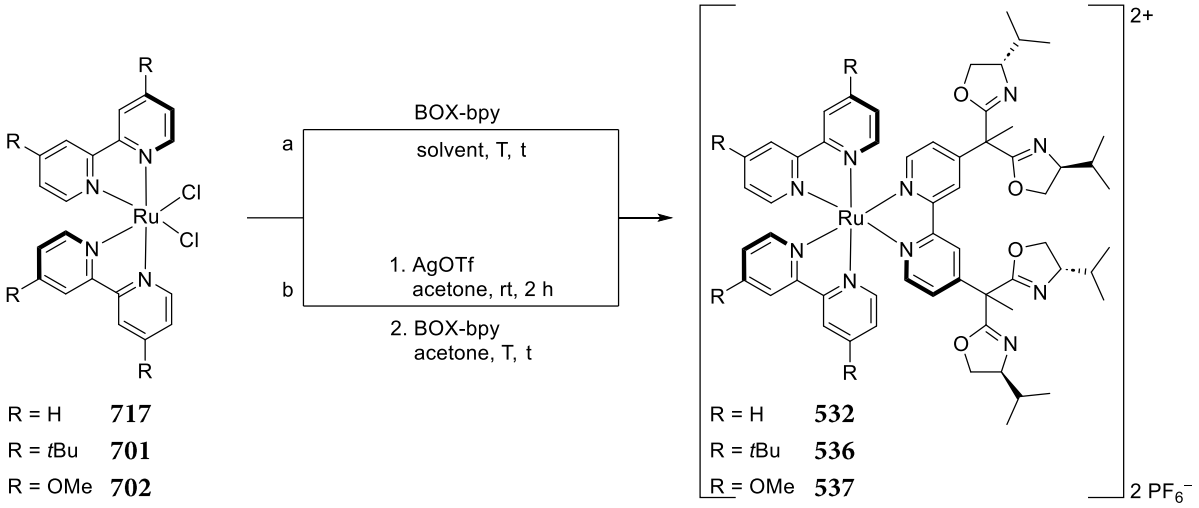

scheme 89. Evaluated procedures for the synthesis of heteroleptic photocatalysts **532**, **536** and **537**.

table 5. Parameters and results of selected experiments for the synthesis of heteroleptic photocatalysts **532**, **536** and **537**.

entry	R	n(Ru) [µmol]	procedure	solvent	additive	T [°C]	t [h]	yield [%]
1	H	48.0	a	H_2O / MeOH	---	100	1.5	---
2	H	48.0	a	MeCN	---	82	18	---
3	H	72.6	b	acetone	AgOTf	56	2 + 18	33
4	H	72.6	b	acetone	AgOTf	56	2 + 3.5	46
5	H	76.6	b	acetone	AgOTf	50	2 + 3	42
6	H	165	b	acetone	AgOTf	50	2 + 3	46
7	H	155	B	acetone	AgOTf	50	2 + 3	60
8	*t*Bu	91.4	b	acetone	AgOTf	50	2 + 3	44
9	*t*Bu	64.0	b	acetone	AgOTf	50	2 + 4	52
10	*t*Bu	165	b	acetone	AgOTf	50	2 + 3	52
11	OMe	88.7	b	acetone	AgOTf	50	2 + 3	37
12	OMe	165	B	acetone	AgOTf	50	2 + 3	46

The initial experiments investigated whether simple heating of a solution of a commercially available precursor complex **717** with BOX-bpy **529** leads to exchange of the chlorido ligands and incorporation of BOX-bpy **529** to form the desired heteroleptic complexes **532**, **536** and **537**. After 1.5 h at 100 °C in a mixture of H_2O/MeOH

(entry 1), a ^{1}H-NMR spectrum was obtained that showed product-like signals at the expected chemical shifts, yet signal analysis was severely hampered by signal broadening caused either by the oxidation of the metal centre to paramagnetic Ru(III) or the overlapping of a large number of structurally related species. The latter was confirmed by mass spectrometry which included the signal sets of a multitude of Ru complexes although not of the product mass. In addition, the mass resulting from the hydrating oxazoline ring opening was clearly detectable. Based on the assumption that a longer reaction time might be required for the replacement of the chlorido ligands and also for the formation of the thermodynamically most favorable complex, as well as to prevent hydrating ring openings, an analogous mixture was refluxed in acetonitrile (without H_2O) for 20 h (entry 2). However, instead of the desired complex $[Ru(bpy)_2(BOX\text{-}bpy)]^{2+}$ (**532**) (M 1070.4469, m/z 535.2229) or the precursor $Ru(bpy)_2Cl_2$ **717** (M 483.9796, m/z 483.9796) or by-products from single or double exchange of the chlorido ligands against MeCN. ($[Ru(bpy)_2(MeCN)Cl]^+$, M 490.0372, m/z 490.0367; $[Ru(bpy)_2(MeCN)_2]^{2+}$ M 496.0938, m/z 248.0469) a dominant signal set with Ru-type splitting and single charge around the mass of 639.141 was obtained, the assignment of which was not successful.

Further approaches therefore pursued an alternative complexation strategy (procedure b) based on exploiting the extraordinary affinity of silver salts for the formation of silver chloride: The corresponding precomplex was dissolved in acetone, mixed with silver triflate and stirred for 2 h at room temperature, aiming at the formation of the acetone complex $[Ru(R\text{-}bpy)_2(acetone)]^{2+}$. In the second step the acetone ligands should be readily exchanged for the chelating BOX-bpy ligand **529** under mild conditions (50 °C). When *cis*-$Ru(bpy)_2Cl_2$ (**717**) was subjected to these conditions, the silver chloride formed in the first step was separated by Schlenk filtration of the supernatant solution into another flask, to which a solution of BOX-bpy **529** was added. After refluxing overnight, concentration *in vacuo* and purification by precipitation as hexafluorophosphate salt as well as column chromatography followed by washing with KPF_6-solution, the desired heteroleptic complex $[Ru(bpy)_2(BOX\text{-}bpy)](PF_6)_2$ (**532**) was obtained for the first time in a yield of 33% (entry 3). During an attempt to develop a simplified purification strategy of the very polar complex compound by reverse-phase HPLC (H_2O/MeCN 80:20), the product was lost. Under the same conditions, $[Ru(bpy)_2(BOX\text{-}bpy)]^{2+}$ (**532**) was prepared multiple times (entry 4 - 7), but with considerably less experimental effort due to the use of syringe filtration for the separation of the complex solution from precipitated silver salts. During these experiments an optimized reaction time of only about 3 h was determined by TLC. the desired complex **532** was obtained reproducably in a moderate yield of 42 - 60%.

With these conditions at hand, the reaction was carried out again using the previously prepared precursor complexes *cis*-$RuCl_2(tBu\text{-}bpy)_2$ (**701**) and *cis*-$RuCl_2(MeO\text{-}bpy)_2$ (**702**). After removal of the solvent, the residues were purified by column chromatography and the obtained substances washed with KPF_6 to ensure saturation of the cationic complexes with well-defined hexafluorophosphate anions. In this way, the sterically shielded heteroleptic complex $[Ru(tBu\text{-}bpy)_2(BOX\text{-}bpy)](PF_6)_2$ (**536**) and the electronically modified complex

[Ru(MeO-bpy)$_2$(BOX-bpy)](PF$_6$)$_2$ (**537**) were obtained in yields of 44 – 52% and 37 – 46%, respectively. The scale of the reaction had no discernible influence on the resulting yields.

Despite the similarities of the three catalyst structures, they differ in ^{1}H-NMR spectroscopic analyses not only in the signal sets of the residues located in the 4-positions of the achiral catalyst sides (R = H, *t*Bu, MeO) but also in the splitting pattern of aromatic signals, resulting both from electronic differences of the substituents and the relative position of the rings to each other. In the ^{1}H-NMR spectrum of the heteroleptic complex with R = H four aromatic signals can be identified, three of which have an integral of 6H and probably represent the bipyridine protons at ring positions 3, 5 and 6. The fourth of the signals comprises only 4H, possibly originating from the hydrogen atoms at the 4-positions of the unsubstituted bipyridine ligands (**spectrum 7**).

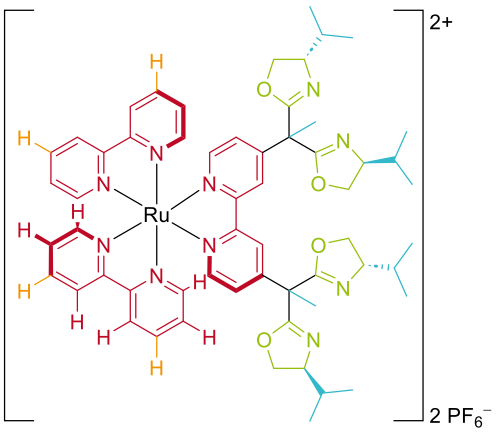

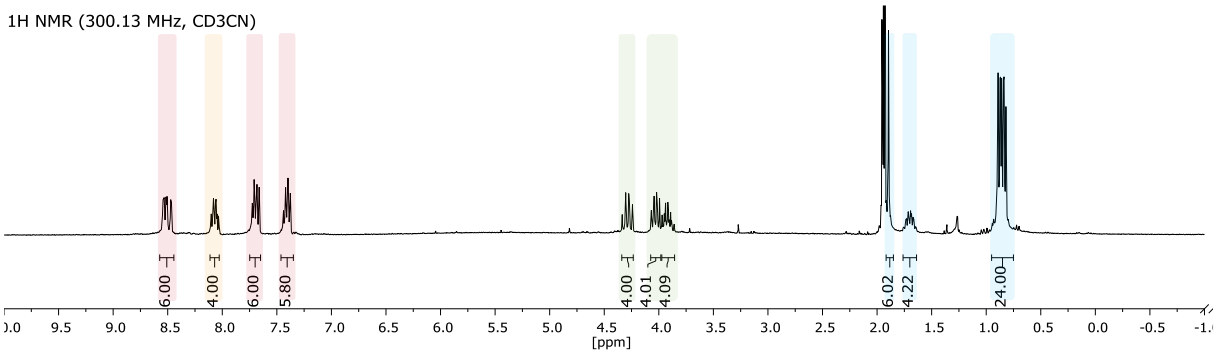

spectrum 7. ^{1}H-NMR analysis of [Ru(bpy)$_2$(BOX-bpy)](PF$_6$)$_2$ (**532**).

In the ^{1}H-NMR spectrum of the heteroleptic complex with R = *t*Bu **536**, the successful synthesis is evident from the correct ratio of the *tert*-butyl signal and the signals of isopropyl residues of the BOX-fragments (36H/24H). In the aromatic region, despite the substituents at the four positions of all pyridine rings and the resulting remaining of only 3H per pyridine ring, a splitting into four signals with the relative intensities 6H, 2H, 4H, 6H is recognizable. Given that there are 6 rings with 3 aromatic protons each, this splitting probably results from electronic differences of the individual pyridine rings, which differ on the one hand in their own substituent and on the other hand in the type of the pyridine ring in *trans* position. Due to the stronger electron-donating nature of the *tert*-butyl substituents compared to the BOX-fragments, one group of hydrogen atoms could be more strongly shielded and thus high-field shifted in the *t*Bu-substituted rings than the hydrogen atoms at the BOX-substituted pyridine rings.

Another interpretation could attribute the splitting not to the electronic effects of the ring substituents, but to the relative positions of the six-rings to each other, i.e. ligand effects. The distinction could therefore also result from the fact that four pyridine rings are located *trans* to a *tert*-butyl-substituted pyridine ring, while only two pyridine rings are located *trans* to a BOX-substituted pyridine ring. Which of these analyses is correct remains unclear, but the fact that there is a splitting of one type of signal and thus an electronic distinction between the asymmetric BOX-bpy side and the symmetric *t*Bu-bpy side suggests that in the course of the photoreaction there might occur an electronic disfavoring in addition to the steric shielding of the *tert*-butyl residues, which was originally intended to be achieved and investigated using alkoxy-substituted derivative **537** (**spectrum 8**).

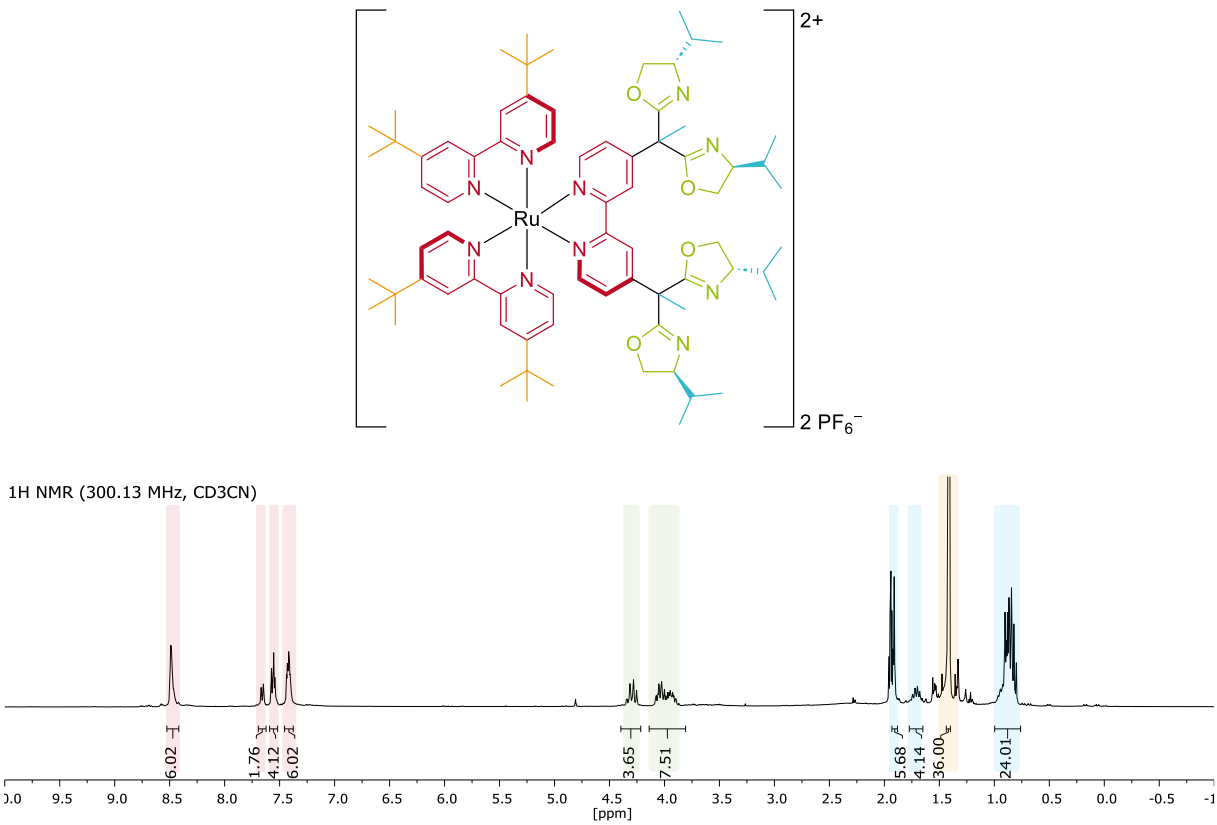

spectrum 8. ^{1}H-NMR analysis of **[**Ru(*t*Bu-bpy)$_2$(BOX-bpy)**]**(PF$_6$)$_2$ (**536**).

In the methoxy-substituted derivative **537**, a splitting of the aromatic signals into a total of six signals is observed, of which three signals exhibit an integral of 2H and the remaining three signals show an integral of 4H. Despite the identical substitution pattern compared to the *t*Bu-substituted catalyst, the splitting of the aromatic signals differs significantly. This might be due to the much stronger electron-donating nature of the methoxy substituents, making all the effects used previously to explain the splitting patterns of the ring protons even more pronounced than in the *t*Bu complex **536**. While the *t*Bu residues exhibit a slight electron-donating inductive effect, the stronger electron-donating mesomeric effects of the MeO residues cause a more significant distinguishability of the six rings. All six rings carry three hydrogen atoms at positions 3, 5 and 6. Since four of the six rings carry strongly electron-donating MeO substituents, this presumably results in one signal per ring position with one proton originating from each MeO-substituted ring, thus 3 signals with 4H each. The two comparatively electron-poor

BOX-substituted pyridine rings also carry three hydrogen atoms each at the ring positions mentioned, likewise resulting in three signals. However, since there are only two BOX-substituted rings, the integral of these signals is only 2H. Alternatively, it might be argued by the relative position of the rings to each other, in particular with the *trans* effect. Since four of six rings are *trans* to a methoxy-substituted ring, but only two rings are *trans* to a BOX-substituted ring, a similar splitting into two signal sets with 3 signals each, one of them with integral four and the other with integral two, is reasonable. Despite the strong electron-donating nature of the MeO-substituents, splitting and signal position are not exclusively dominated by the direct influences of the ring substituents, but are also influenced by the relative position of the rings to each other, which can also be seen on close inspection of the MeO-signal (at 3.98 – 4.01 ppm): It is not just a singlet with 12H for all four MeO-groups, but two singlets with 6H each, accounting for the relative position of the rings to each other (**spectrum 9**).

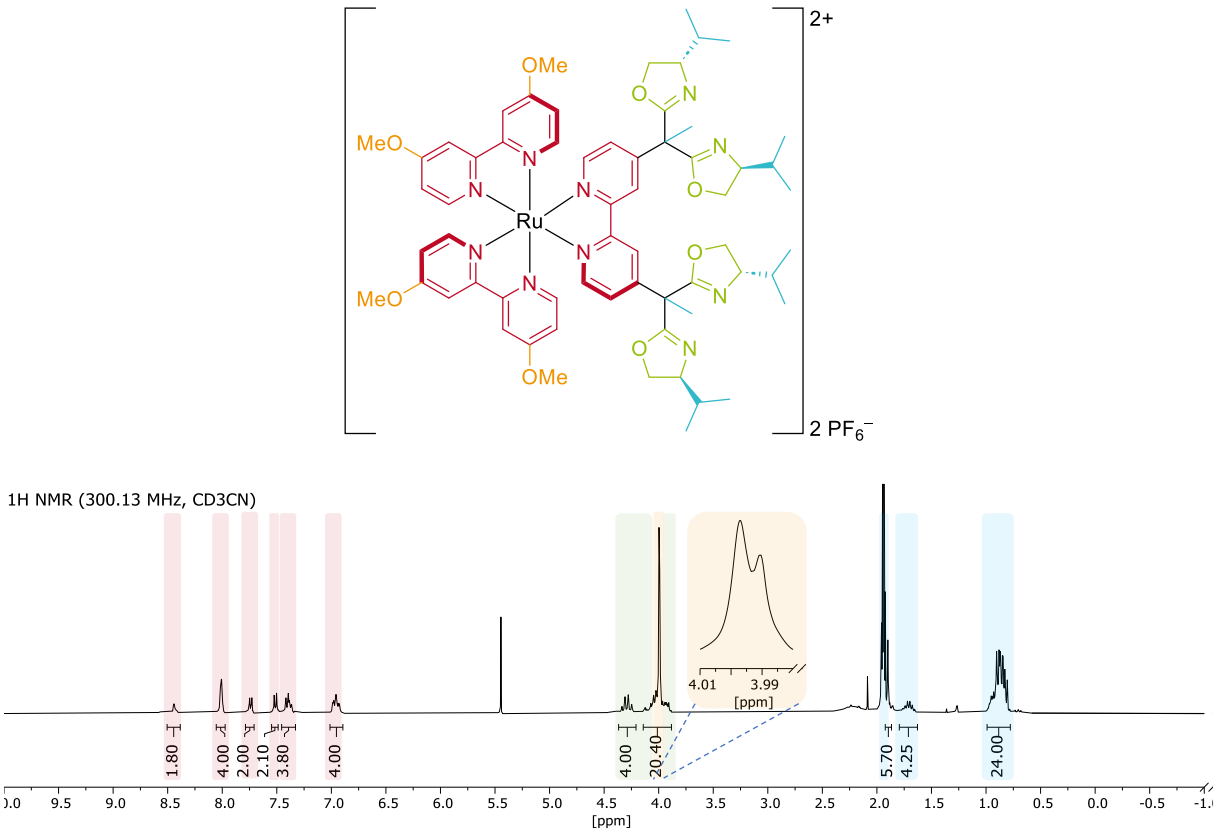

spectrum 9. ^{1}H-NMR analysis of [Ru(MeO-bpy)$_2$(BOX-bpy)]**(PF$_6$)$_2$ (537)**.

Although the synthesis of the originally targeted homoleptic catalyst complex [Ru(BOX-bpy)$_3$](PF$_6$)$_2$ (**540**) failed, the synthesis of three significantly different heteroleptic complexes **532**, **536** and **537** succeeded. During the investigation of substituent influences on the enantiomeric excess, [Ru(bpy)$_2$(BOX-bpy)](PF$_6$)$_2$ (**532**) serves as a reference system without shielding, allowing the evaluation of both the concept of steric shielding using [Ru(*t*Bu-bpy)$_2$(BOX-bpy)](PF$_6$)$_2$ (**536**) and the conceptually new concept of electronically directed excitation using [Ru(MeO-bpy)$_2$(BOX-bpy)](PF$_6$)$_2$ (**537**).

3.3 Photophysical and electrochemical properties of the photocatalysts **532**, **536** and **537**

Before evaluating the heteroleptic complexes **532**, **536** and **537** in asymmetric photoredox transformations, some photophysical and electrochemical characterizations were performed. Irrespective whether the targeted reactivity is based on energy transfer or electron transfer, knowledge of the underlying parameters allows predictions about thermodynamically possible reactions, since the orbital energies or redox potentials of the substrates must fit the catalyst system.

As discussed in the introductory chapter on photophysical properties of $[Ru(bpy)_3]^{2+}$ (**7**) (chapter 1.1), visible light irradiation causes excitation of an electron from a metal-centred d-orbital (HOMO) into ligand-centred π* orbitals forming a short-lived ^{1}MLCT-state. After thermal relaxation and intersystem crossing, a long-lived ^{3}MLCT state is formed, which is responsible for the photoredox reactivity of such structures. In homoleptic $[Ru(bpy)_3]^{2+}$ (**7**), three equivalent π_1^* orbitals are available for excitation, ultimately resulting in three degenerate low-energy ^{3}MLCT states consisting of a formally oxidized metal centre surrounded by a reduced bipyridyl radical anion and two neutral bipyridines (**equation 33**).[20, 22]

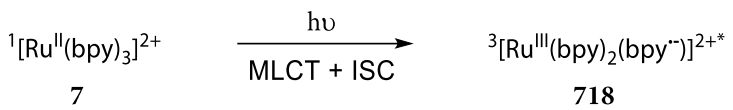

equation 33. Formation of localized lowest energy ^{3}MLCT by visible light irradiation on the example of homoleptic $[Ru(bpy)_3]^{2+}$ (**7**).

Whether the electron is actually localized in a π* orbital on one bipyridine orbital or is distributed in multichelate ring-delocalized orbitals over all bipyridines has been the subject of a long-standing controversy, which was finally decided in favor of a broadly accepted concept of localized MLCT states with the help of a variety of photophysical measurements of ground and excited states, including low-temperature cyclic voltammetry and time-resolved spectroscopy methods.[20, 22, 34, 35, 37-46, 311-313]

For the excitation of heteroleptic complexes, a more complex picture emerges, since different ligands are available for the formal ligand reduction associated with the excitation, whose π* orbital energies and thus reduction potentials differ more or less strongly depending on their substituents. While electron-donating substituents on the ligand lead to an increase in the orbital energies and thus a decrease in the redox potential, electron-withdrawing residues cause the opposite effect.[76, 77] In the case of very similar orbital energies, ^{3}MLCT excitation could still occur into multiple quasi-degenerate π* orbitals despite the heteroleptic nature of the complex, resulting in multiple conceivable localized excited ^{3}MLCT states (**equation 34**). If the π* orbital energies of the different ligands differ more, reduction occurs at the ligand with the π* orbital that is easiest to reduce.[63]

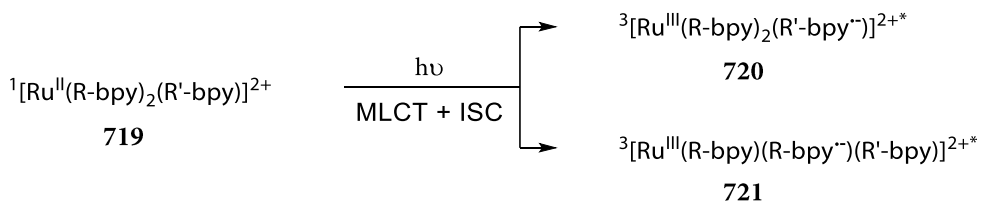

equation 34. Conceivable localized lowest energy ^{3}MLCTs accessible by excitation of heteroleptic complexes with electronically similar ligands.

Since the excitation formally represents an intramolecular charge transfer and the orbitals involved in the redox processes are the same orbitals involved in the MLCT transition, a photophysical and electrochemical investigation of the heteroleptic complexes **532**, **536** and **537** may clarify whether the envisioned concept of electronically disfavoring an achiral catalyst side by localizing the lowest energy π* orbital on the BOX-substituted side has succeeded. The heteroleptic complexes **532**, **536** and **537**, as well as the prototypical $[Ru(bpy)_3](PF_6)_2$ (**7**), were therefore studied by cyclic voltammetry, as well as UV/VIS and emission spectroscopy. The absorption and emission maxima and energies, extinction coefficients, quantum yields and lifetimes and $E_{1/2}$ redox potential of the ground state and the approximated excited state potentials are summarized in **table 6**.

To account for Einstein coefficients, the absorption spectra were divided by the wavenumber and the emission spectra were divided by the third power of the wavenumber before normalizing to the longest wavelength absorption maximum and emission maximum, respectively. Although the comparison of the resulting absorption and emission spectra shows an essentially similar trend in the shift of maxima with respect to the substituents, there is no mirror symmetry, confirming that absorption and emission occur from different states.

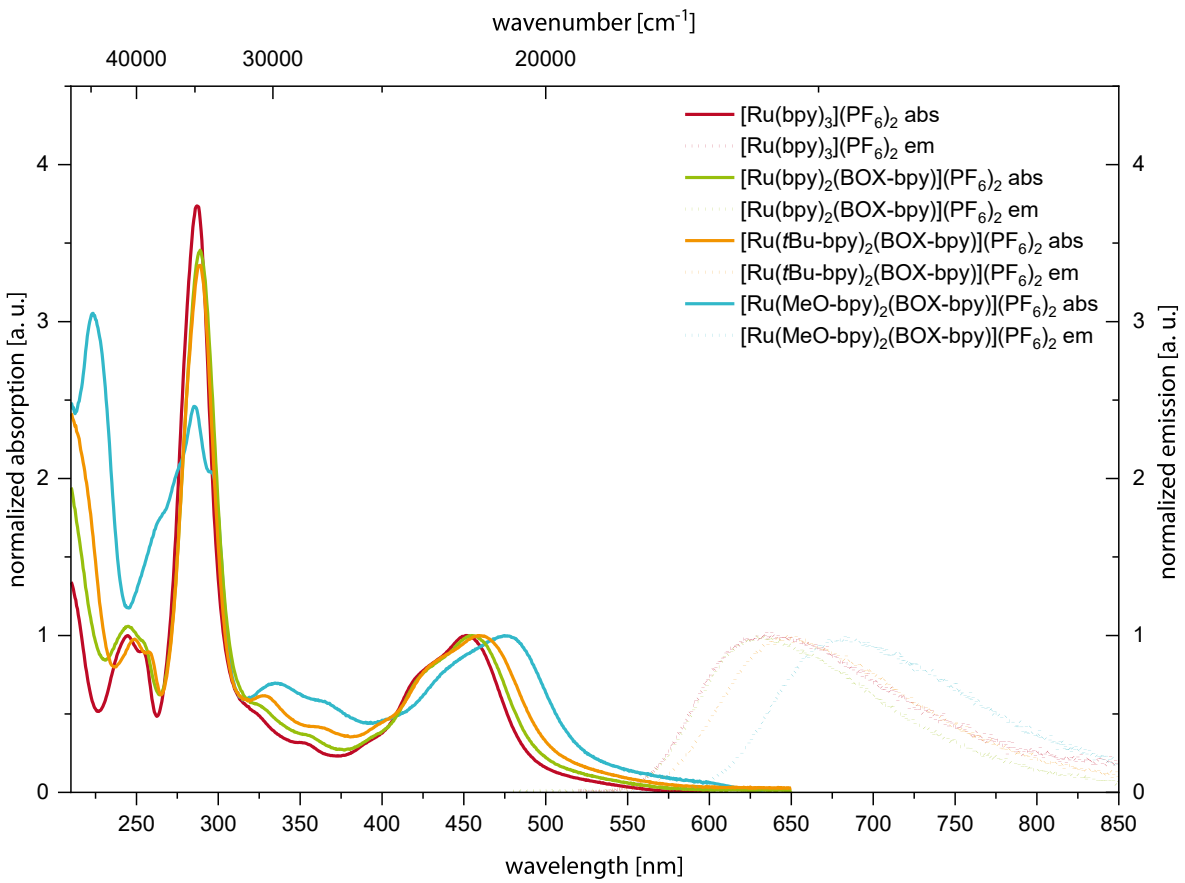

spectrum 10. Corrected and normalized absorption and emission spectra of $[Ru(bpy)_3]^{2+}$ (**7**) and the bifunctional heteroleptic analogues **532**, **536** and **537**.

table 6. Photophysical and electrochemical parameters of $[Ru(bpy)_3]^{2+}$ (**7**) and bifunctional heteroleptic analogues **532**, **536** and **537**.

$[Ru^{II}(R\text{-}bpy)_2(R'\text{-}bpy)]^{2+}$	R	R'	λ_{abs} [nm]	ε [L/(mol·cm)]	$\tilde{\nu}_{abs}$ [cm^{-1}]	E_{abs} [eV]	λ_{em} [nm]	$\tilde{\nu}_{em}$ [cm^{-1}]	E_{em} [eV]	$\tilde{\nu}_{stokes}$ [cm^{-1}]	φ [%]	τ [ns]
$[Ru(bpy)_3](PF_6)_2$	H	H	452	15900	22173	2.74	618	16181	2.01	6000	6.55	759
$[Ru(bpy)_2(BOX\text{-}bpy)](PF_6)_2$	H	BOX	455	12500	22075	2.73	630	16000	1.97	6200	3.28	921
$[Ru(tBu\text{-}bpy)_2(BOX\text{-}bpy)](PF_6)_2$	*t*Bu	BOX	460	16200	21786	2.70	648	15528	1.91	6400	2.82	775
$[Ru(MeO\text{-}bpy)_2(BOX\text{-}bpy)](PF_6)_2$	OMe	BOX	475	9100	21053	2.61	683	14728	1.82	6400		673

R	R'	$E_{1/2}$ [Ru^{III}|Ru^{II}] [V vs. Fc]	$E_{1/2}$ [R-bpy_1|R-$bpy_1^{\cdot-}$] [V vs. Fc]	$E_{1/2}$ [R-bpy_2|R-$bpy_2^{\cdot-}$] [V vs. Fc]	$E_{1/2}$ [R-bpy_3|R-$bpy_3^{\cdot-}$] [V vs. Fc]	$E_{1/2}$ [$Ru(R\text{-}bpy)_2(R'\text{-}bpy)]^{3+}$| $[Ru(R\text{-}bpy)_2(R'\text{-}bpy)]^{2+*}$] [V vs. Fc]	$E_{1/2}$ [$Ru(R\text{-}bpy)_2(R'\text{-}bpy)]^{2+}$| $[Ru(R\text{-}bpy)_2(R'\text{-}bpy)]^{+}$] [V vs. Fc]
H	H	0.890	−1.73	−1.92	−2.16	−1.285	0.455
H	BOX	0.908	−1.71	−1.90	−2.15	−1.218	0.418
*t*Bu	BOX	0.823	−1.70	−1.98	−2.22	−1.252	0.362
OMe	BOX	0.677	−1.72	−1.99	−2.19	−1.351	0.311

R	R'	$E_{1/2}$ [Ru^{III}|Ru^{II}] [V vs. SCE]	$E_{1/2}$ [R-bpy_1|R-$bpy_1^{\cdot-}$] [V vs. SCE]	$E_{1/2}$ [R-bpy_2|R-$bpy_2^{\cdot-}$] [V vs. SCE]	$E_{1/2}$ [R-bpy_3|R-$bpy_3^{\cdot-}$] [V vs. SCE]	$E_{1/2}$ [$Ru(R\text{-}bpy)_2(R'\text{-}bpy)]^{3+}$| $[Ru(R\text{-}bpy)_2(R'\text{-}bpy)]^{2+*}$] [V vs. SCE]	$E_{1/2}$ [$Ru(R\text{-}bpy)_2(R'\text{-}bpy)]^{2+}$| $[Ru(R\text{-}bpy)_2(R'\text{-}bpy)]^{+}$] [V vs. SCE]
H	H	1.27	−1.35	−1.54	−1.78	−0.905	0.835
H	BOX	1.29	−1.33	−1.52	−1.77	−0.838	0.798
*t*Bu	BOX	1.20	−1.32	−1.60	−1.84	−0.872	0.742
OMe	BOX	1.06	−1.34	−1.61	−1.81	−0.971	0.691

The UV/VIS spectra show broad absorption bands in the visible region between 400 - 600 nm, which in the case of $[Ru(bpy)_3]^{2+}$ (**7**) were assigned to the MLCT transition ($[d\pi^6] \rightarrow {}^1[d\pi^5\pi_1{}^{*1}]$).[20-22] Below 300 nm, especially the heteroleptic complexes $[Ru(bpy)_2(BOX\text{-}bpy)]^{2+}$ (**532**) and $[Ru(t\text{Bu-}bpy)_2(BOX\text{-}bpy)]^{2+}$ (**536**) show great similarity to $[Ru(bpy)_3]^{2+}$ (**7**), on the one hand exhibiting a high intensity band for ligand-centred excitation ($\pi \rightarrow \pi^*$) at 287 - 289 nm, furthermore with bands of lower intensity around 250 nm, which in the case of $[Ru(bpy)_3]^{2+}$ (**7**) were assigned to another MLCT transition into energetically higher ligand π^* orbitals ($[d\pi^6] \rightarrow {}^3[d\pi^5\pi_2{}^{*1}]$).[20-22] The direct spin-forbidden triplet excitation results from spin-orbit coupling, merging the orbitals and spin character in the electronic wavefunctions, with the singlet character dictating the absorptivity.[20-23, 76] When the absorption is measured at 77 K in ethanol-methanol glass the direct transition to the lowest ^{3}MLCT-state is also observable in the low energy tail (around 550 nm) of the visible-light MLCT.[20] The MeO-substituted complex **537** exhibits a broader band below 300 nm with indicated shoulders in the region of the ligand-centred excitation, possibly as a result of the overlap of absorptions involving more electronically different BOX-bpy and MeO-bpy orbitals. Alternatively, owing to the raised metal orbitals due to electron donating MeO-bipyridines the band could also arise from the superposition of strongly red-shifted MLCT excitations into higher π_2^* orbitals and ligand-centred excitations ($\pi \rightarrow \pi^*$). An indication of a change in the electronic structure at the metal centre is further indicated by the much more intense band at around 335 nm, which in the case of $[Ru(bpy)_3]^{2+}$ (**7**) was attributed to metal-centred excitations.[20-22] Closer examination of the visible light MLCT transition reveals that the incorporation of BOX-bpy **529** leads to a slight red shift of 4 nm to 455 nm compared to $[Ru(bpy)_3]^{2+}$ (**7**), possibly because the slightly electron-withdrawing BOX fragments lower the BOX-bpy orbital energies (lower LUMO). The incorporation of *t*Bu-residues on the BOX averted side further shifts the absorption maximum to 460 nm, possibly because there is an increased electron density in the *t*Bu-bipyridine orbitals due to the inductive effect of the *t*Bu-residues, which suppresses backbonding and is therefore passed on to the metal-centred Ru orbitals thereby raising their energies. Although the electron-donating nature of the *t*Bu-residues also increases the orbital energies of the *t*Bu-bpy orbitals, the BOX-bpy-centred π^* orbital is still available as an approximately unchanged LUMO, thus requiring a lower energy for MLCT excitation. Such a change in orbital energies was observed in a study of the correlation of *para*-substituent effects with photophysical properties in heteroleptic ruthenium-trisbipyridines.[63] This effect applies even more to the MeO derivative **537**, which shows a significant red shift of the absorption maximum to 475 nm. The emission maxima range from 618 nm for $[Ru(bpy)_3]^{2+}$ (**7**) to 683 nm for MeO-derivative **537** and show the same trend of substituent effects observed for the absorption maxima, with the Stokes shift increasing with electron-donating substituents in the backbone. The lifetimes range from 673 ns to 921 ns which is consistent with the triplet-character of the excited states.

Cyclic voltammetry measurement of each complex was repeated three times at different scan rates of 50-150 mV/s. and the obtained signals were referenced to the signal of the redox couple of ferrocene (Fc^+/Fc) which was used as an internal standard, allowing precise conversion of the obtained potentials against other reference systems (SCE) (**spectrum 11**).[57, 58]

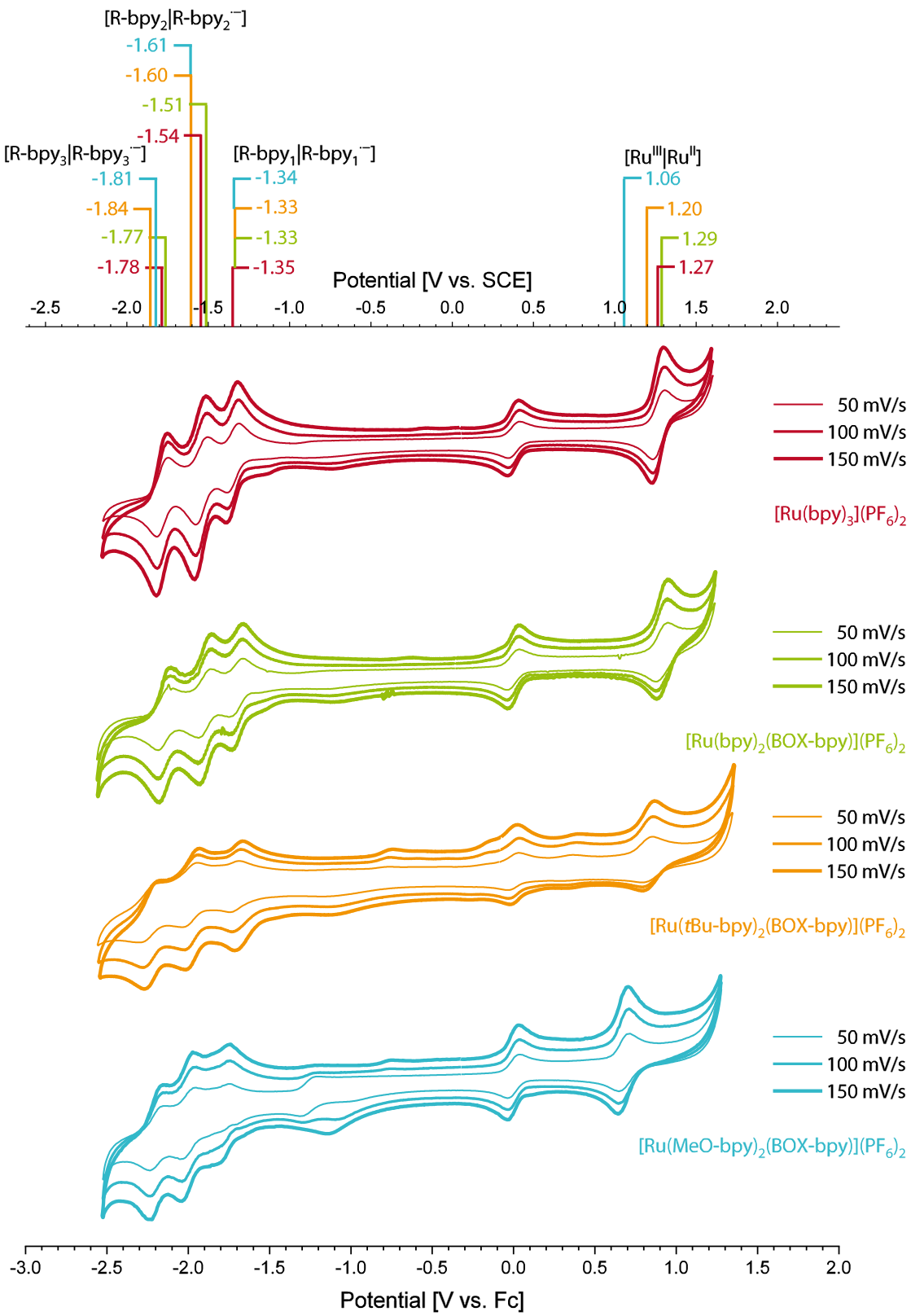

spectrum 11. Stacked cyclic voltammograms of $[Ru(bpy)_3]^{2+}$ (**7**) and heteroleptic complexes **532**, **536** and **537** at different scan rates (50, 100, 150 mV/s) referenced against internal standard redox couple Fc^+/Fc (bottom scale) and against SCE (top scale).

In the cyclic voltammograms of $[Ru(bpy)_3]^{2+}$ (**7**) and the heteroleptic complexes **532**, **536** and **537**, one peak each for the metal-centred redox event ($[Ru^{III}|Ru^{II}]$), and three peaks for the successive reductions of each of the three

bipyridine ligands ([bpy|bpy$^-$]) are visible (**spectrum 11**). In accordance with the literature values of the well-known $[Ru(bpy)_3]^{2+}$ (**7**), the redox potentials of the metal-centred redox events [Ru^{III}|Ru^{II}], and the first bipyridine reduction [bpy_1|bpy_1^-] were determined to be 1.27 V and −1.35 V, respectively, confirming that under the experimental conditions reliable and comparable values were obtained also for the heteroleptic complexes **532**, **536** and **537**.[20, 22]

A comparison of the potentials indicates that the incorporation of a BOX-bpy **529** slightly increases the potential of the ruthenium oxidation compared to $[Ru(bpy)_3]^{2+}$ (**7**), which is in agreement with the spectroscopic observation of a slightly electron-withdrawing effect of the BOX substituents, possibly rendering the BOX-bpy marginally more backbonding. In contrast, the potentials of the *t*Bu- and MeO-derivatives appear significantly lower at 1.20 V and 1.06 V, respectively, presumably due to the electron-donating effect of the corresponding residues and associated increase in electron density at the metal raising the dπ orbitals.

An analysis of the bipyridine reduction potentials determined for the ground state shows that the incorporation of BOX is accompanied by an increase in the first reduction potential of 20 mV compared to $[Ru(bpy)_3]^{2+}$ (**7**) which is consistent with the slightly electron-withdrawing nature found in the previous results. Attachment of *tert*-butyl residues on the backside results in the same potential of the first bipyridine reduction (−1.33 V), and even attachment of the strongly electron-donating MeO substituent only leads to a decrease of only 10 mV (−1.34 V). The extremely small range of redox potentials of the first bipyridine reduction of only 10 mV despite the different substituents in the backbone of the heteroleptic catalysts (R = H, *t*Bu, MeO) indicates that during the first bipyridine reduction, the BOX-substituted ligand, which is common to all three complexes is preferentially reduced. This is also evident when considering the reduction potentials of the second and third ligand reductions, that show much larger span widths of 96 mV and 70 mV, respectively, representing the greater electronic influence of the substituents on the redox potentials of the bipyridines that remain to be reduced in the second and third order and the orbital energies of which vary greatly due to the corresponding substituents. Besides the BOX-bipyridine ligand **529**, which is obviously the easiest to reduce, the largest difference to the potentials of the subsequent reductions is found in the MeO derivative **537**, strongly indicating the successful electronic disfavoring of the achiral catalyst backbone.[63, 76, 78, 314]

To gain further information on the influence of substituents on the orbital energies of metal centre (HOMO) and ligands (LUMO), some of the experimental data were correlated with each other and with Okamoto-Brown parameters. The latter, similar to Hammett parameters, are used to quantify electronic effects of substituents and have been used in extensive studies correlating substituent effects on diimine ligands to redox potentials of ruthenium complexes.[63, 76, 315, 316] For the purpose of comparing the parameters of $[Ru(bpy)_3]^{2+}$ (**7**) and heteroleptic complexes **532**, **536** and **537**, the corresponding values were included in the plots, that are correlating absorption and emission energies with redox potentials, but since $[Ru(bpy)_3]^{2+}$ (**7**) does not contain BOX substituents and the main goal was to investigate the effects of backside substituents, $[Ru(bpy)_3]^{2+}$ (**7**) was not included in the linear fits (**figure 36**).

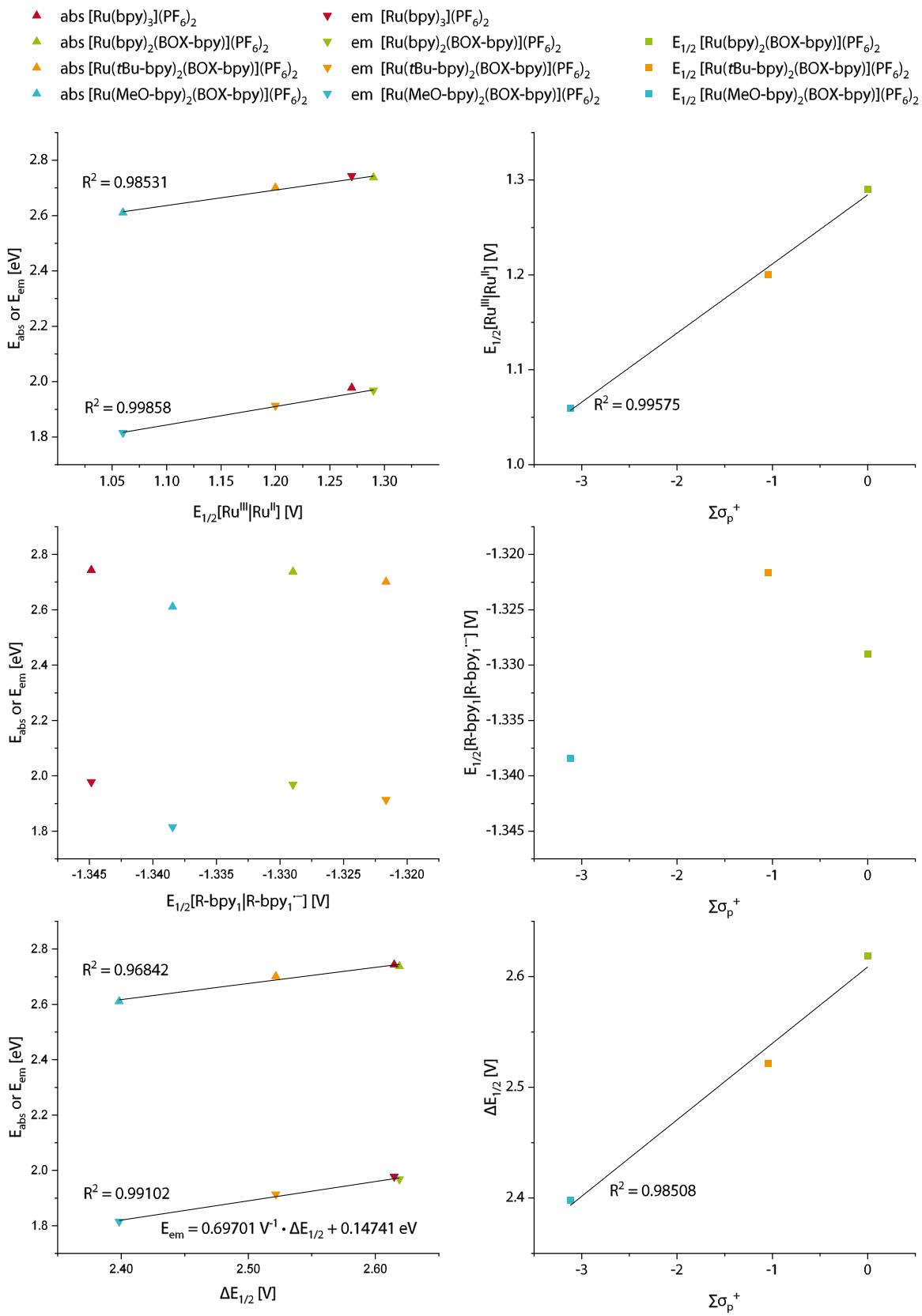

figure 36. Correlations of absorption and emission energies, redox potentials and Okamato-Brown-parameters.[63, 76, 315, 316]

While there is an excellent correlation between both absorption and emission energies with the redox potentials of the metal-centred redox event ($E_{1/2}[Ru^{III}|Ru^{II}]$), no linear correlation of the energies with the potential of the first

bipyridine reduction ($E_{1/2}$[R-bpy$_1$|R-bpy$_1^-$]) can be observed. This observation suggests that the substituent-dependent variation of energy available in the excited MLCT states results mainly from changes in the energy level of the metal-centred dπ-orbitals.[62, 78] The absorption and emission energies were also plotted against $\Delta E_{1/2}$, which is the difference between the potentials of ruthenium oxidation and first ligand reduction ($\Delta E_{1/2} = E_{1/2}[Ru^{III}|Ru^{II}] - E_{1/2}$[R-bpy$_1$|R-bpy$_1^-$]) and related to the HOMO-LUMO-gap.[59, 317] The very good and excellent correlations ($R^2_{abs} = 0.96842$ and $R^2_{em} = 0.99102$) allow several conclusions: First, that a transition to and emission from MLCT excited states occurs,[78] second, that the orbitals involved in electrochemistry are the same as those involved in MLCT absorption and $\pi_1^* \rightarrow d\pi$ emission processes,[59, 317] and furthermore, that the reorganization energies arising from dipole changes during excitation as well as the orbital character of the excited states of all heteroleptic complexes **532**, **536** and **537** are very similar.[76] The y-intercept of the linear fit of 147 mV, could result both from the fact that the measurements were performed at room temperature and because, despite all similarities of involved orbitals, the electron configurations of the electrochemically reduced species $d\pi^6\pi_1^{*1}$ and spectroscopically excited state $d\pi^5\pi_1^{*1}$ still differ.[317] The redox potentials were then correlated with substituent parameters. Although Okamoto and Brown found Hammett parameters to correlate very well with the rate constant of solvolysis of *meta*-substituted phenyldimethylcarbinyl chlorides, worse correlation was observed when *para*-substituted derivatives were used causing them to develop parameters that account for the resonance interactions between *para*-substituents and the electron-deficient reaction centre, showing much better correlations than Hammett parameters in a variety of aromatic substitutions.[315, 316] In addition, Okamoto-Brown parameters also have been shown to correlate very well with electrochemical properties of substituted $[Ru(bpy)_3]^{2+}$ (**7**) derivatives, which has been attributed to dπ/π* overlap and associated substituent influence on resonance stabilization of the positive charge arising during oxidation of the metal centre.[63, 76] In summary, also the correlations of redox potentials to the Okamoto-Brown parameters suggest that the different substituents of the heteroleptic complexes **532**, **536** and **537** mainly raise the orbital energies of the metal centre (dπ), while the lowest energy ligand orbital energy (π* of BOX-bpy **529**) barely changes, as illustrated in the simplified MO-diagram (**figure 37**).

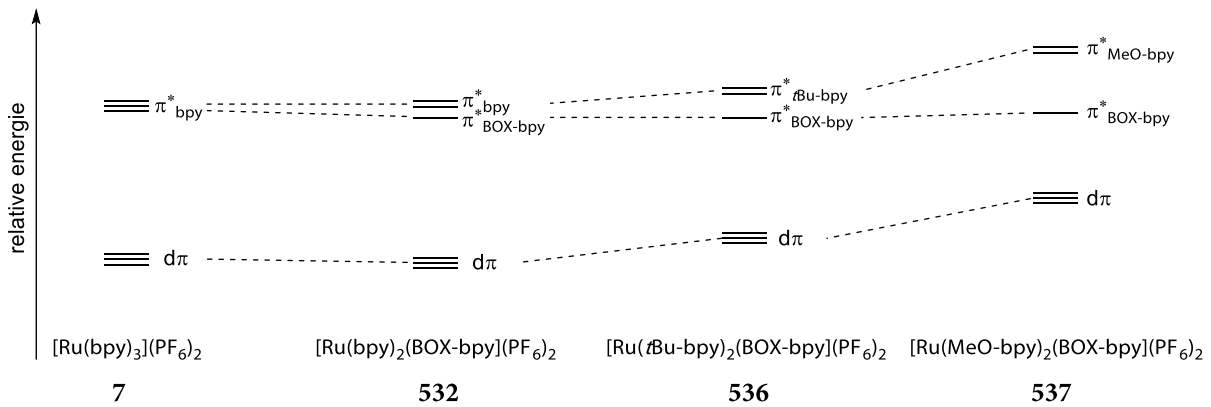

figure 37. Simplified MO-diagram showing assumed relative changes in orbital energies based on experimental absorption and emission energies, redox potentials, Okamoto-Brown parameters and correlations thereof.

To determine which photoredox transformations are suitable for the heteroleptic complexes **532**, **536** and **537** the redox potentials of the excited catalysts were approximated. There are different approaches to determine these potentials: By comparing the electron transfer rate with redox partners of known potential,[64, 65] by phase-modulated cyclic voltammetry,[66] or, most commonly, by calculation from the ground state potentials.[23, 47, 62, 68, 78, 317, 318] The underlying thermodynamic cycle for the calculation of the excited state potentials is shown in **scheme 90** for the example of the literature-known $[Ru(bpy)_3]^{2+}$ (**7**).[20, 22] The underlying model is based on the assumption that the energy present in the excited complex becomes available as an additional driving force for photoredox transformations, and hence the excited state potential is derived from the ground state potentials in addition to the free energy of the ^{3}MLCT (ΔG_{ES}). The free energy ΔG_{ES} is composed of the energy of the lowest vibrational transition ($v = 0 \rightarrow v^* = 0$) E_{00}, in addition to a term accounting for internal relaxation and solvent reorganization (λ).[20, 22]

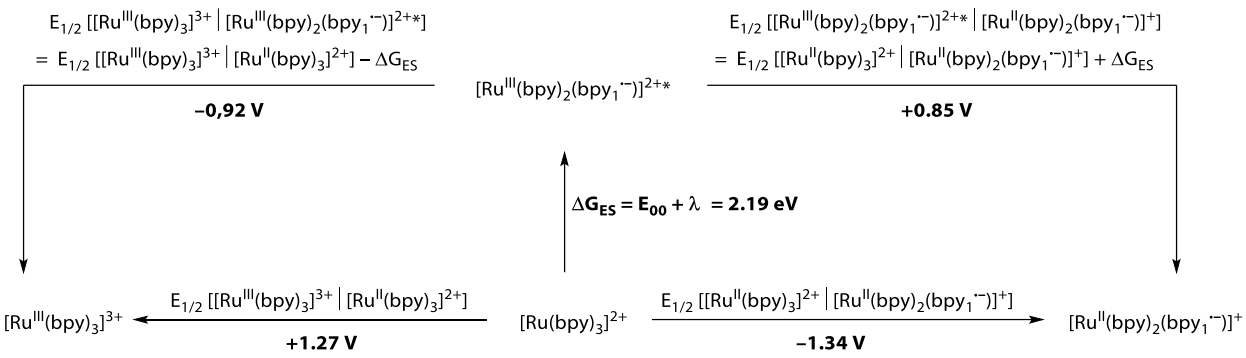

scheme 90. Thermodynamic cycles for the determination of redox potentials of excited states from ground state potentials and the Gibbs free energy of the excited state.[20, 22]

The parameters required to calculate ΔG_{ES} are accessible by Franck-Condon fitting of the emission spectrum.[21, 22, 35, 62, 78, 319, 320] In the single-mode approach this is performed according to

$$I'(\tilde{\nu}) = \sum_{v=0}^{\infty} \left(\frac{E_{00} - v\hbar\omega}{E_{00}}\right)^3 \left(\frac{S^v}{v!}\right) exp\left[-4\ln(2)\left(\frac{\tilde{\nu} - E_{00} + v\hbar\omega}{\Delta\tilde{\nu}_{1/2}}\right)^2\right]$$

with $I'(\tilde{\nu})$ being the ratio of the intensity at $\tilde{\nu}$ to the intensity at the energy gap E_{00} of the $v^* = 0 \rightarrow v = 0$ transition. For an emission spectrum of $[Ru(bpy)_3]^{2+}$ (**7**) at 298 K in acetonitrile the fitting procedure gave the parameter $E_{00} = 16370\ cm^{-1} = 2.03\ eV$, the quantum spacing $\hbar\omega = 1350\ cm^{-1}$, the vibronic band width at half height $\Delta\tilde{\nu}_{1/2} = 1740\ cm^{-1}$ and the Huang-Rhys factor S = 1.03.[22] The vibronic band width at half height $\Delta\tilde{\nu}_{1/2}$ can (after conversion into joules) further be used to calculate the reorganization term λ according to

$$\lambda = \frac{(\Delta\tilde{\nu}_{1/2})^2}{16 k_B T \cdot \ln(2)} = \frac{(3.46 \cdot 10^{-20}\ J)^2}{16\ k_B \cdot 298\ K \cdot \ln(2)} = 0.163\ eV$$

ultimately allowing the determination of the free energy of excited state $[Ru(bpy)_3]^{2+*}$ (**12**) at 298 K in MeCN:[20, 22]

$$\Delta G_{ES} = E_{00} + \lambda = 2.03\ eV + 0.163\ eV = 2.19\ eV$$

According to the thermodynamic cycle given in **scheme 90**, the potentials for oxidative and reductive quenching of the excited state $[Ru(bpy)_3]^{2+*}$ (**12**) are therefore +0.85 V and −0.92 V, respectively (vs. SCE in acetonitrile).[20, 22]

In a widely used approximation, the reorganization term λ is neglected, a reasonable approach if the Stokes shift is small, as this indicates that the ground and excited states are similar in shape, size, and solvation, and hence ultimately in entropy content.[17, 20, 47, 318] E_{00} is approximated in different ways: Most commonly the emission maximum is taken as E_{00} (method a, λ_{max}),[17, 48, 77] although this approach systematically neglects that the transition is vertical and the approximation leads to values that are rather lower limits due to the neglect of internal relaxation to the lowest ground state vibrational level. To improve this approximation, the reorganization term $\lambda_{FC\text{-}fit}$ = 0.163 eV extracted from the Franck-Condon fit of $[Ru(bpy)_3]^{2+}$ (**7**) could be added to the energy of the emission maximum (method a2, $\lambda_{max} + \lambda_{FC\text{-}fit}$). Apart from their energy, the emission bands of the heteroleptic complexes exhibit a very similar shape compared to the band of $[Ru(bpy)_3]^{2+}$ (**7**), indicating that the geometry change associated with the excitation is very similar and thus a very similar underlying reorganization energy is expected. Consequently, approximating the excited state energy by combining the energy of the emission maxima with the reorganization term $\lambda_{FC\text{-}fit}$ of $[Ru(bpy)_3]^{2+}$ (**7**) is also a plausible strategy for the heteroleptic complexes **532**, **536** and **537**.

When neglecting the reorganization term, a shorter wavelength should be used to determine the excited state energy, considering that in low temperature absorption spectroscopy a direct E_{00} transition is resolved in the low energy tail of the MLCT absorption, i.e. at higher energy.[20, 22, 48] Therefore, an alternative approach for the approximating E_{00} could be the determination of the crossing point of the absorption and emission bands (method b, λ_X), which is common in fluorescence spectroscopy, although in case of the ruthenium complexes, the emission originates from a triplet state.[56, 321] Another possibility is to apply a tangent line to the low-energy side of the absorption band at 10% of the maximum intensity and determine the intersection with the abscissa (method c, $\lambda_{0.1\varepsilon}$).[56]

During the determination of emission maxima of the heteroleptic complexes **532**, **536** and **537**, it was found that same values were obtained using either the uncorrected spectra or the spectra corrected to account for the Einstein coefficients. Only in the case of the literature-known $[Ru(bpy)_3]^{2+}$ (**7**), which shows an emission maximum at 618 nm in the uncorrected spectrum in agreement with the literature, the maximum shifted to 635 nm in the corrected spectrum. This is since the recorded emission band of $[Ru(bpy)_3]^{2+}$ (**7**) flattens out slower or scatters more, causing a scattering value that is slightly lower in the uncorrected spectrum but at a slightly higher wavelength to appear higher than the actual maximum of the uncorrected spectrum after division by the third power of the particular wavelength. Further considerations use the literature value of 618 nm for $[Ru(bpy)_3]^{2+}$ (**7**) found in the uncorrected spectrum. The described methods for the approximation of the excited state energy are exemplified by the example of $[Ru(bpy)_3]^{2+}$ (**7**) in **spectrum 12** and the determined wavelength, energies and approximated excited state potentials calculated therefrom as well as the deviation of the energies determined using

the different methods for $[Ru(bpy)_3]^{2+}$ (**7**) from the published ΔG_{ES} calculated by Franck-Condon-fit (2.19 eV) are summarized in **table 7**.

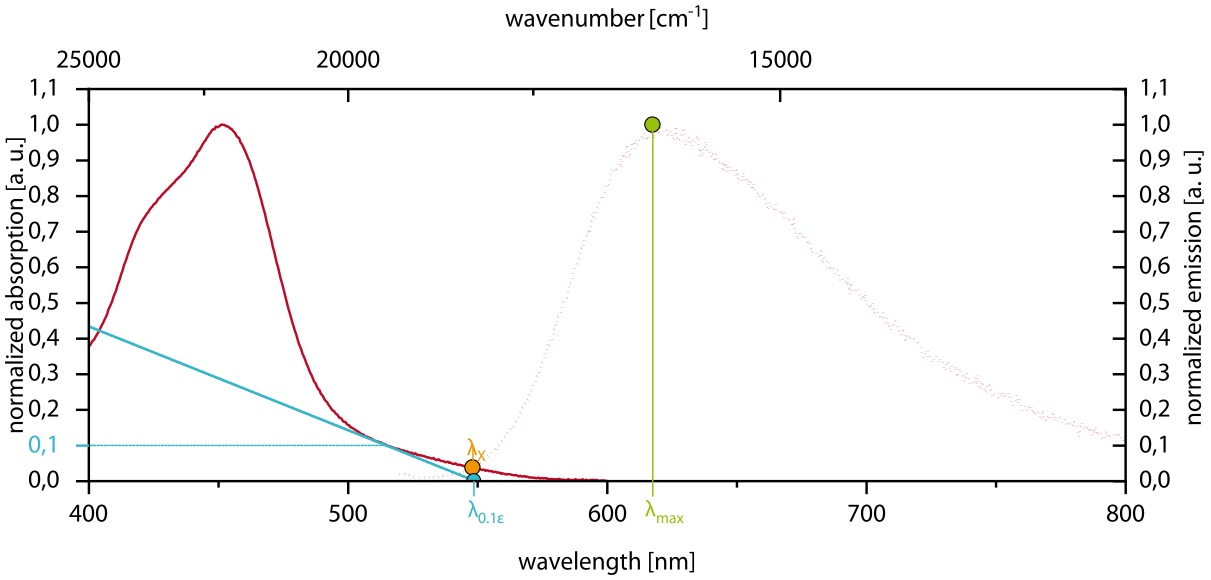

spectrum 12. Common procedures found in the literature for the approximate determination of E_{00}.[17, 48, 56, 77, 321]

table 7. Determination of excited state energies (E) according to three methods (a, b, c), deviation from ΔG_{ES} for the literature known $[Ru(bpy)_3]^{2+}$ (**7**). ground state potentials (E_{red} and E_{ox}) and calculated excited state potentials (E_{red}^* and E_{ox}^*) for $[Ru(bpy)_3]^{2+}$ (**7**), $[Ru(bpy)_2(BOX\text{-}bpy)]^{2+}$ (**532**), $[Ru(tBu\text{-}bpy)_2(BOX\text{-}bpy)]^{2+}$ (**536**) and $[Ru(MeO\text{-}bpy)_2(BOX\text{-}bpy)]^{2+}$ (**537**), as well as averaged potentials

catalyst	method	λ [nm]	E [eV]	$E-\Delta G_{ES}$ [meV]	E_{red} [V]	E_{ox} [V]	E_{red}^* [V]	$\bar{E}_{red}^*$ [V]	E_{ox}^* [V]	$\bar{E}_{ox}^*$ [V]
7	a	618	2.01	−184	−1.35	1.27	−0.736	−0.905	0.666	0.835
	a2	618	2.17	−17.0			−0.900		0.830	
	b	548	2.26	+72.7			−0.993		0.923	
	c	549	2.26	+68.5			−0.989		0.919	
532	a	630	1.97	---	−1.33	1.29	−0.678	−0.838	0.638	0.798
	a2	630	2.13	---			−0,840		0,800	
	b	555	2.23	---			−0.944		0.904	
	c	569	2.18	---			−0.889		0.849	
536	a	648	1.91	---	−1.33	1.20	−0.713	−0.872	0.583	0.742
	a2	648	2.07	---			−0.870		0.740	
	b	566	2.19	---			−0.991		0.861	
	c	587	2.11	---			−0.912		0.782	
537	a	683	1.82	---	−1.34	1.06	−0.755	−0.971	0.475	0.691
	a2	683	1.98	---			−0.920		0.640	
	b	598	2.07	---			−1.020		0.733	
	c	638	1.94	---			−0.883		0.603	

For the literature-known catalyst $[Ru(bpy)_3]^{2+}$ (**7**), a comparison of the frequently used approximations is possible by examining the deviation of the energies obtained with the different approaches from the energy determined by Franck-Condon-fit (ΔG_{ES} = 2.19 eV).[20, 22] Methods b and c, lead to excited state energies that are slightly higher (+72.7 meV and +68.5 meV) than ΔG_{ES}, while method a leads to a significantly lowered energy (−184 meV). The smallest deviation was obtained by the modified method a2 (−17.0 meV). Interestingly, averaging the excited state oxidation and reduction potentials E_{ox}^* and E_{red}^* determined by the different approximations leads to potentials $\overline{E}_{ox}^*$ and $\overline{E}_{red}^*$ with values of 0.835 V and −0.905 V, respectively, exhibiting the smallest deviation from the published potentials (E_{ox}^* = 0.85, E_{red}^* = −0.92). This is plausible, since the averaging of approximation methods that were set too high or too low ultimately leads to results that lay in between and probably differ less from the actual value. The ground state potentials and ranges of excited state potentials, along with the mean values calculated therefrom as well as the deviation from the literature value for $[Ru(bpy)_3]^{2+}$ (**7**) is presented in **figure 38**.

Since the potentials for oxidative quenching of the excited state are calculated from the ground state potentials of the ruthenium centred redox event, which shows a large spanwidth in the ground state due to the substituent influence on the dπ orbital energies, by subtraction of excited state energies determined from also strongly substituent influenced spectroscopic data, a large span of $\overline{E}_{ox}^*$ of 133 mV is obtained. The resulting values embody the trend observed for the ground state of slightly electron-withdrawing (potential raising) BOX fragment and slightly or strongly electron-donating (potential lowering) *tert*-butyl and methoxy residues.

The potentials for reductive quenching range from 691 mV for $[Ru(MeO\text{-}bpy)_2(BOX\text{-}bpy)]^{2+}$ (**537**) to 798 mV for $[Ru(bpy)_2(BOX\text{-}bpy)]^{2+}$ (**532**) and show a slightly smaller span of 107 mV that primarily results from substituent influences on the spectroscopic properties, since the underlying ground-state potentials are roughly the same owing to the energetic similarity of the $\pi^*_{BOX\text{-}bpy}$ orbitals involved.

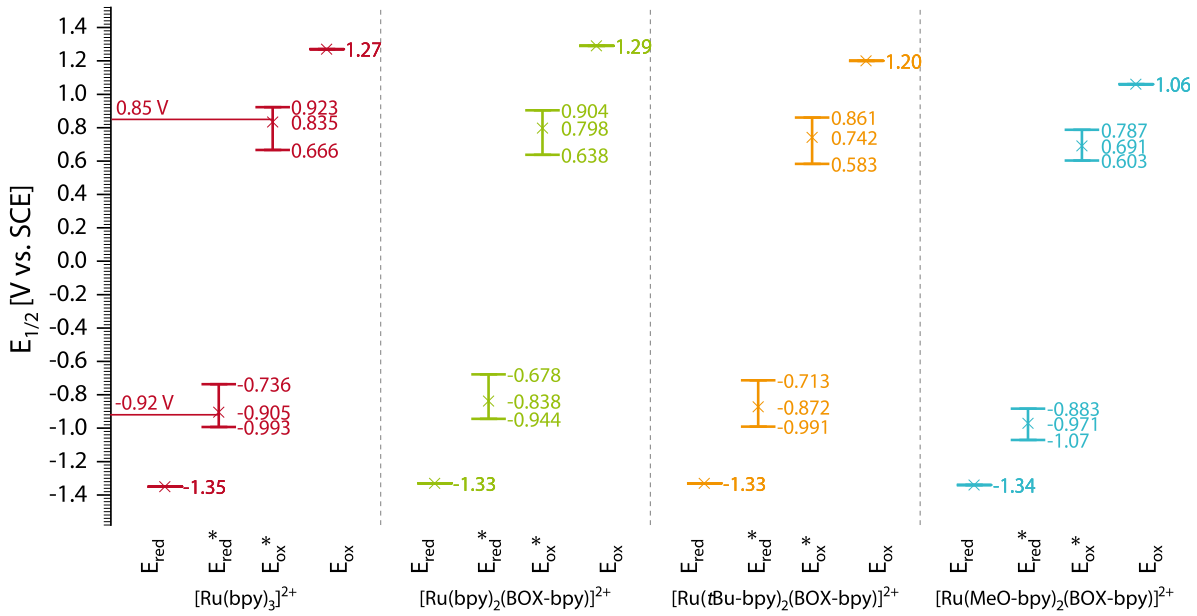

figure 38. Ground state potentials and approximated excited state potentials.

In summary, the photophysical and electrochemical analysis of the novel bifunctional heteroleptic complexes **532**, **536** and **537** confirmed the expected relative trends and substituent influences and moreover even strongly indicated the success of the concept of electronic disfavoring of an achiral catalyst side by rational modification of orbital energies. Although the determination of the excited state redox potentials was only approximated based on different commonly used or modified approaches, the comparison of the obtained values of $[Ru(bpy)_3]^{2+}$ (**7**) with the literature data, as well as the overall reasonable trend of the values, suggests that they are suitable for the estimation of thermodynamically possible reactions to a good approximation. A diagram illustrating all ground state potentials and averaged approximated excited state potentials in the context of oxidative and reductive quenching cycles is shown in **scheme 90**.

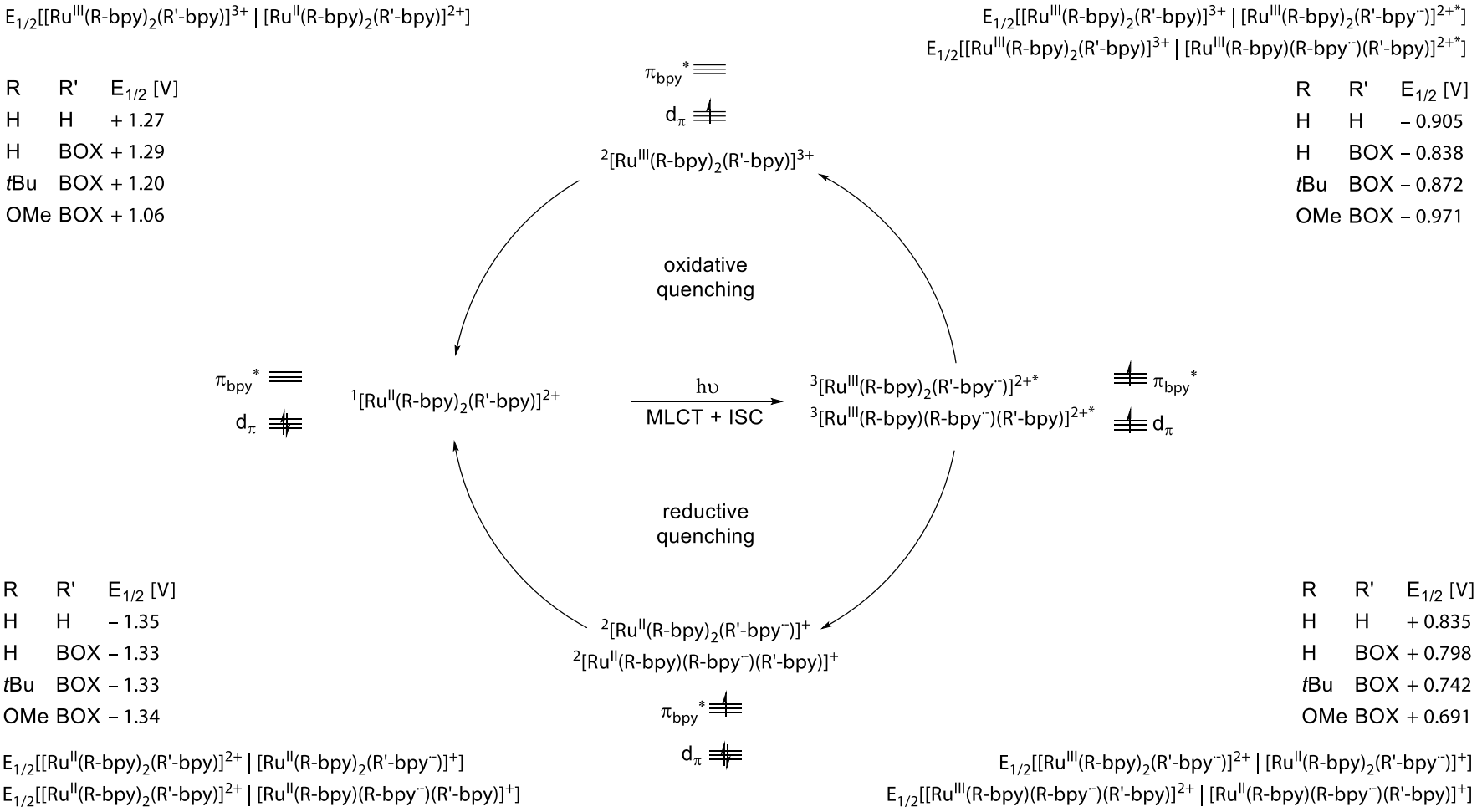

scheme 91. Overview of the ground state potentials and averaged approximated excited state potentials of [Ru(bpy)$_3$]$^{2+}$ (**7**) and the heteroleptic complexes **532**, **536** and **537** in the context of reductive and oxidative quenching cycles.

3.4 Evaluation of the chiral bimetallic photocatalyst in photoredox transformations

For the evaluation of the chiral BOX-substituted ruthenium-tris(bipyridine) analogues **532**, **536** and **537** different literature-known racemic photoredox transformations were examined regarding their enantioselective adaptability (chapters 3.4.1 - 3.4.4), moreover, a literature-known enantioselective photoredox transformation was evaluated (chapter 3.4.5). In order for racemic reactions to be adapted enantioselectively, only those reactions were considered whose substrates exhibit suitable structural features for potentially coordinating to a Lewis acid in the chiral environment of the BOX fragments.

3.4.1 Stephenson's intramolecular radical cyclization

Proceeding out of Stephenson's reductive dehalogenation protocol, the intramolecular radical cyclization represents the direct follow-up development of this reactivity.[12, 16] In this reaction the excited catalyst $[Ru(bpy)_3]^{2+*}$ (**12**) is reductively quenched by triethylamine (**726**). The reduced photocatalyst $[Ru(bpy)_3]^{+}$ (**11**) is a strong reductant itself and thus capable of transferring an electron to the α-bromocarbonyl substrate **722** thereby inducing reductive cleavage of the activated C-Br bond. In contrast to the previously known reductive dehalogenation protocol the resulting α-carbonyl radical intermediate **723** undergoes intramolecular (5-exo-dig) cyclization through addition to the unactivated terminal alkyne before abstracting a hydrogen atom from the amine radical cation **727**. In this way the cyclized product **725** is formed in 85% yield (**scheme 92**).[16]

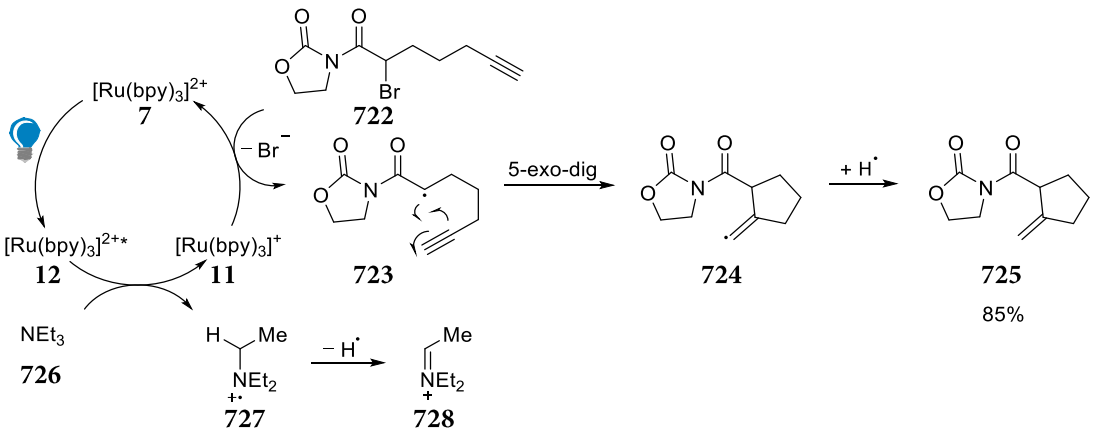

scheme 92. Mechanism of Stephenson's radical cyclization on the example of the oxazolidinone substrate **722**.[16]

Following this reaction mechanism, a large number of 2-bromomalonate substrates and substrates with less activated C-Br bonds were cyclized in good to excellent yields, although the latter require the more reducing iridium complex $[Ir(ppy)_2(dtbbpy)]PF_6$ (**31**) Stephenson *et al.* were also able to expand this reactivity to a cascade radical cyclization, in which the radical formed after the first (5-exo-trig) cyclization **732** undergoes a second (5-exo-dig) cyclization before the hydrogen atom abstraction occurs (**scheme 93**).[16]

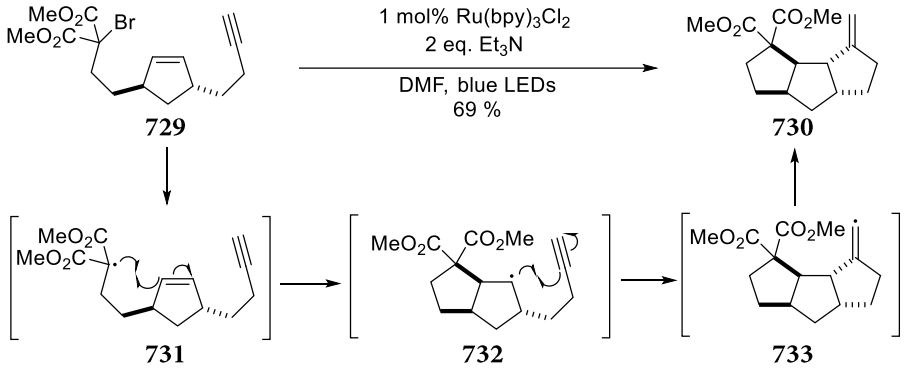

scheme 93. Stephenson's cascade radical cyclization.[16]

The relevant substrates as well as the corresponding products and literature yields for an enantioselective adaptation of Stephenson's radical cyclization using the asymmetric bimetallic BOX-substituted photoredox catalysts are shown in **table 8**.

table 8. Selected substrates for an enantioselective adaption of Stephenson's radical cylization.[16]

entry	substrate	product	yield
1	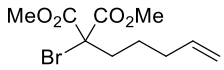 **734**	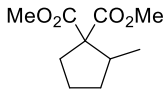 **735**	77%
2	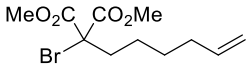 **736**	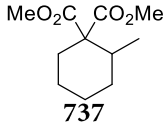 **737**	69%
3	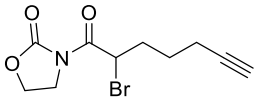 **722**	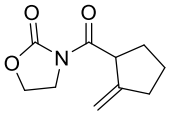 **725**	85%
4	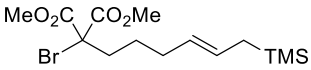 **738**	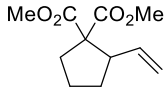 **739**	92%

The alkene substrates **734**, **736** and **738** were prepared starting from dimethylmalonate (**740**) by alkylation with K_2CO_3 and 5-bromopentene (**741**) or 6-bromohexene (**743**) in a THF/DMF mixture at 90 °C in 92% and 78% yield, respectively. The subsequent brominations were achieved by deprotonation with LiHMDS and addition of NBS in excellent yields (98%). The silylated substrate **738** can be synthesized from alkene **734** by metathesis reaction using the Grubbs 2 catalyst and allyl TMS in 54% yield (**scheme 94**).

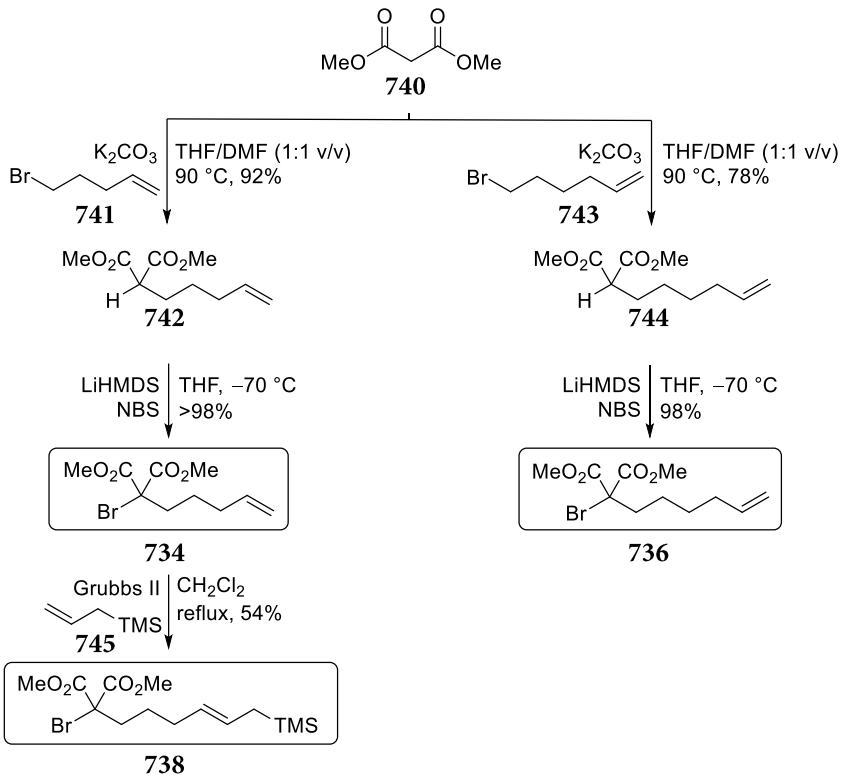

scheme 94. Synthesis of the alkene substrates **734**, **736** and **738** from dimethylmalonate (**740**).

Alkyne substrate **722** was prepared from 2-oxazolidinone (**747**) by conversion into the amide **748** with heptynoic acid (**746**) under Steglich conditions using the coupling reagent DCC and the nucleophilic catalyst DMAP in a moderate yield (61%). The bromination was performed in the same way as for the other substrates using LiHMDS and NBS in a yield of 75% (**scheme 95**). During the bromination reaction, a spontaneous side reaction to a black substance was observed during solvent removal under reduced pressure at 40 °C. All subsequent bromination processes were therefore carried out at room temperature and brominated substrates were always stored in a freezer under inert gas atmosphere and exclusion of light.

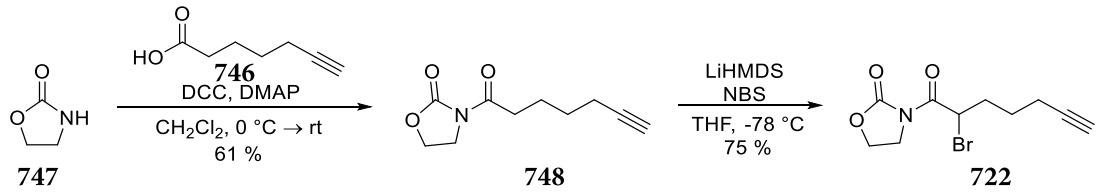

scheme 95. Synthesis of alkyne **722** from 2-oxazolidinon (**747**)

Having prepared selected substrates, the initial approaches focused on racemic reproduction of selected examples of the intramolecular cyclization before an asymmetric adaptation was investigated. The parameters and results of selected experiments are summarized in **table 9**.

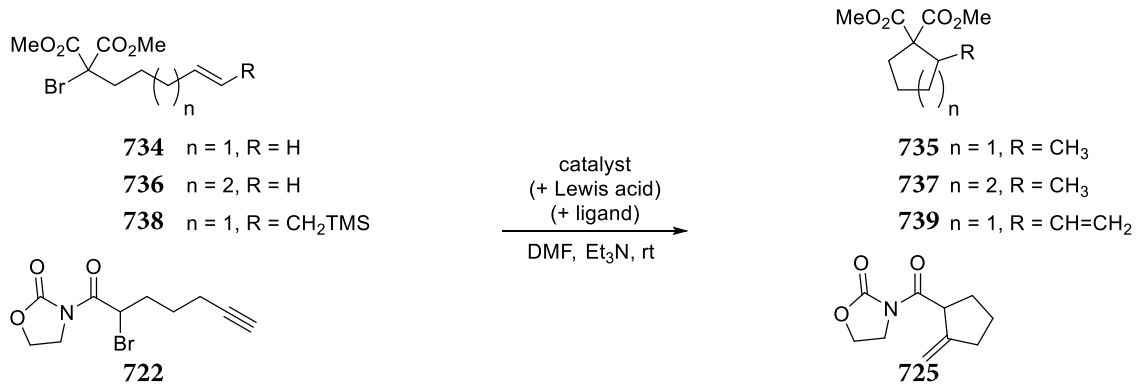

equation 35. Intramolecular radical cyclization according to Stephenson *et al.*

table 9. Parameters and results of selected experiments for Stephenson's intramolecular radical cyclization.

entry	substrate	catalyst	Lewis acid (eq.)	ligand (eq.)	yield [%]	ee [%]
1[a]	**734**	$[Ru(bpy)_3](PF_6)_2$	---	---	---	---
2	**734**	$[Ru(bpy)_3](PF_6)_2$	---	---	<60	---
3	**736**	$[Ru(bpy)_3](PF_6)_2$	---	---	<49	---
4	**734**	$[Ru(bpy)_2(BOX\text{-}bpy)](PF_6)_2$	$Zn(OTf)_2$ (0.01)	---	43	---
5	**722**	$[Ru(bpy)_3](PF_6)_2$	---	---	81	---
6	**738**	$[Ru(bpy)_3](PF_6)_2$	---	---	72	---
7	**722**	$[Ru(bpy)_2(BOX\text{-}bpy)](PF_6)_2$	$Zn(OTf)_2$ (0.02)	---	49	0
8	**722**	$[Ru(t\text{Bu-}bpy)_2(BOX\text{-}bpy)](PF_6)_2$	$Zn(OTf)_2$ (0.02)	---	49	0
9	**722**	$[Ru(MeO\text{-}bpy)_2(BOX\text{-}bpy)](PF_6)_2$	$Zn(OTf)_2$ (0.02)	---	87	0
10	**722**	$[Ru(bpy)_3](PF_6)_2$	$Zn(OTf)_2$ (2.00)	BOX (2.00)	90	0
11	**738**	$[Ru(bpy)_3](PF_6)_2$	$Zn(OTf)_2$ (0.01)	BOX (1.00)	74	0

(a) performed in an uncooled photoreactor.

The published optimized reaction conditions (1 mol% $[Ru(bpy)_3]Cl_2$ (**7**), 2.0 eq. Et_3N, DMF, 435 nm, 4 - 12 h) could not be met exactly, since only the hexahydrate $[Ru(bpy)_3]Cl_2$ x 6 H_2O (**7**) and the hexafluorophosphate $[Ru(bpy)_3](PF_6)_2$ (**7**) were available as achiral photocatalysts. The influence of counterions (hexafluorophosphates instead of chlorides) was neglected.[322] The use of the hexahydrate should not have any negative effects, given that Stephenson's very similar intermolecular atom transfer radical addition (chapter 3.4.2) is performed in a mixture of water/DMF. Nevertheless, for a more accurate reproduction of Stephenson's results all approaches were performed under strict exclusion of water using $[Ru(bpy)_3](PF_6)_2$ (**7**). Another deviation from Stephenson's reaction conditions is the irradiated wavelength, since the available photoreactor is equipped with LEDs of a

different wavelength (460 nm). It was assumed that the irradiation with 460 nm instead of 435 nm should not have a negative effect, as the absorption maximum of the MLCT lies at 452 nm and is thus closer to the irradiated wavelength. Consequently, an even more efficient excitation under milder conditions could be achieved. In an attempt to further bring the wavelength closer to the absorption maximum (and to be closer to the Stephenson group's irradiated wavelength), a simple improvised photoreactor consisting of a 450 nm LED band wrapped inside a beaker was also evaluated.

First, two reaction setups were compared by reproducing the cyclization of α-bromocarbonylalkene **734** using an uncooled simple photoreactor setup made from a beaker and an LED strip (450 nm) and an air-cooled photoreactor made of a heat-dissipating aluminum housing and irradiation at 460 nm (entries 1 & 2). Since the improvised beaker setup lacks sufficient heat dissipation, the reaction mixture heated up significantly, resulting in a very unselective reaction with no detectable product formation. In contrast, a much more selective photoreaction appeared to occur in the cooled aluminum photoreactor, settling on this setup for all further reactions. In this way, photocyclization of alkenes **734** and **736** yielded compounds in yields of < 60% (lit. 77%) and < 49% (lit. 69%), respectively, which showed similarity in ^{1}H-NMR to the reported literature data and thus appeared to confirm overall reactivity. In addition, the spectra contained further small multipletts, which were interpreted as minor impurities at this point (entries 2 & 3). Encouraged by the finding that the general reactivity seemed to work, the photocyclization of alkene **734** was repeated using the asymmetric bimetallic photocatalyst $[Ru(bpy)_2(BOX\text{-}bpy)](PF_6)_2$ (**532**). This catalyst appeared to show the same reactivity as the previously used literature known $[Ru(bpy)_3](PF_6)_2$ (**7**), however attempts to isolate the reaction product **735** in its pure form by repeated column chromatography to separate the additional ^{1}H-NMR signals previously thought to be minor impurities failed, and the spectrum continued to contain sets of signals that did not match Stephenson's experimental details.

The supporting information provided by Stephenson *et al.* do not include all relevant product spectra but instead repeatedly forward to other publications, ultimately guiding to a study by Curran *et al.*, that neither includes the spectrum but instead investigated the regioselectivity and kinetics of a related atom transfer radical cyclization revealing that reverse cyclization (ring openings) are slow but still take place:[16, 323, 324] In the case of esters **749** the reverse cyclization is 4 orders of magnitude slower than iodine addition and thus negligible (**scheme 96**, top). However, for doubly activated malonate derivatives **754** and **756** (which are intermediates in Stephenson's radical cyclization), Curran *et al.* found that although reverse cyclization is slow, it still takes place and the associated equilibrium of 5-exo **754** and 6-endo **756** intermediates requires the irradiation source to be switched off as soon as possible after the starting material has been consumed (**scheme 96**, bottom).[323, 324]

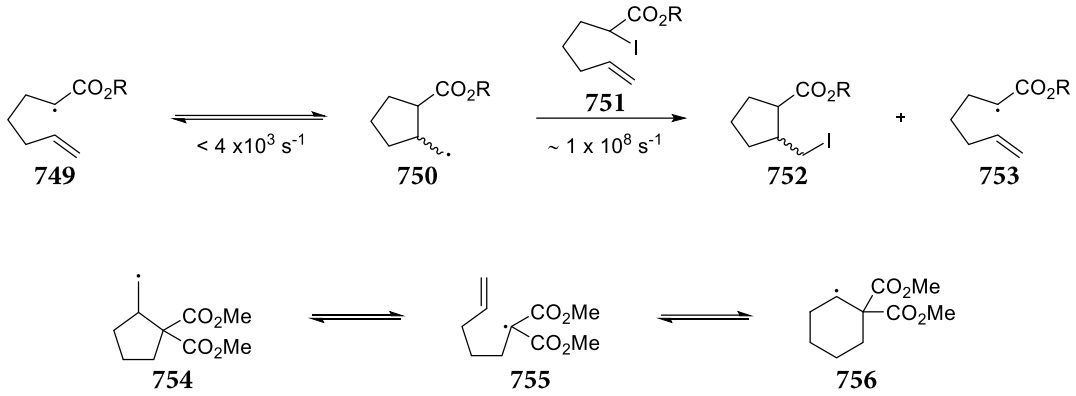

scheme 96. Competitive reversible cyclization and halogen abstraction in atom transfer cyclization of esters (top) and equilibrium of 5-exo **754** and 6-endo **756** intermediates for malonate derivatives (bottom).[323, 324]

Further ^{1}H-NMR analysis of the obtained cyclopentane product **735** indicated a significant change in the signals, including the disappearance of the doublet associated to the methyl group. Due to the described difficulties in reproducing the results, the potential formation of regioisomers, and isomerizations through ring openings, as well as indications of fundamental product instability, the intramolecular radical cyclization was not further investigated using the substrates **734** and **736**.

The racemic reproduction of the cyclizations from substrates **722** and **738** proceeded more smoothly in maximum yields of 81% (entry 5) (lit. 85%) and 72% (entry 6) (lit. 92%), respectively. At this point the stage was set for evaluation of the chiral photocatalysts **532**, **536** and **537**, which was attempted using oxazolidinone alkyne **722** (entries 7 - 9). For this purpose, 1 mol% of each of the three versions of the asymmetric bimetallic catalyst complexes **532**, **536** and **537** was stirred with 2 mol% each of zinc triflate as Lewis acid under exclusion of light for 30 min in order to achieve precoordination, before substrate **722** was added and the reaction was initiated by the addition of Et_3N (**726**). The twofold amount of Lewis acid relative to the catalysts is owing to the fact that each complex contains two asymmetric BOX fragments attached to one of the three bipyridine ligands. Under these conditions, none of the photocatalysts provided any enantiomeric excess.

To verify whether the photocyclization of oxazolidinone substrate **722** is generally suitable for the evaluation of the chiral catalysts **532**, **536** and **537**, an experiment using the separate catalyst system containing the racemic photocatalyst **7** and stoichiometric amounts of BOX **613** and zinc triflate was performed. To ensure that the chiral complex was formed and each substrate molecule was coordinated in its chiral environment, the mixture of BOX **613**, zinc triflate and substrate **722** was allowed to precoordinate for six hours while stirring. Thereafter, the photocatalyst $[Ru(bpy)_3](PF_6)_2$ (**7**) was added, followed by the addition of the reductive quencher Et_3N (**726**). Even under these conditions, no enantiomeric excess could be detected (entry 10). In analogy to this procedure, allylsilane **738** was also reacted with stoichiometric amounts of BOX **613** and zinc triflate, but no enantiomeric excess was detected with this substrate either (entry 11).

The absence of stereoinduction even under the described conditions of complete saturation of each substrate molecule with a chiral catalyst complex can have various reasons. For example, the α-bromocarbonyl substrates

722, **734**, **736** and **738** could be inherently unsuitable for an enantioselective adaption. Moreover, the *i*Pr groups might not be sterically demanding enough to ensure satisfactory stereoinduction for the present substrates **722**, **734**, **736** and **738**. However, since only the *i*Pr residue proved to be practical during the synthesis of the chiral photocatalysts **532**, **536** and **537** no alternative BOX ligands were employed. The choice of Lewis acid is also critical to the success of stereoinduction, as the size and number or type of orbitals determines the spatial linkage of the substrate to the chiral ligand fragment. However, since no signs of enantioselectivity were detected to this point, further optimization was not performed and instead, further approaches focused on an enantioselective adaptation of Stephenson's intermolecular atom transfer radical addition (chapter 3.4.2), which is an extension of the intramolecular cyclization but can be carried out without prior substrate syntheses.

3.4.2 Intermolecular approaches: Stephenson's intermolecular ATRA and related photoreactions

A further development of Stephenson's intramolecular cyclization is the intermolecular atom transfer radical addition (ATRA), which does not require substrate syntheses and may proceed *via* both quenching cycles of the photocatalyst (**scheme 97**).[53, 325] Following the reductive quenching cycle the excited photocatalyst $[Ru(bpy)_3]^{2+*}$ (**12**) is reduced by a reductive quencher such as trialkylamine **764** to $[Ru(bpy)_3]^+$ (**11**), which itself is sufficiently strong reducing to transfer an electron to an activated alkyl halide **759** and initiate the cleavage of the C-Br-bond causing bromide dissociation. The resulting alkyl radical **763** may then add onto an alkene **757** intermolecularly producing a γ-carbonyl radical **765** that can react in two ways: Either abstraction of a bromine atom from bromomalonate **759** occurs (radical propagation), or oxidation by the excited photocatalyst **12** to the carbocation **761** follows, which then binds the previously released bromide anion (nucleophilic trapping).[325] Both pathways lead to an ATRA product **762** containing a bromine-substituted stereocenter at the γ-position. Depending on the halo component used, a stereocenter in the α-position can also be formed in the alkene addition step. Internal alkenes could also lead to stereocenters in the β-position. However, ATRA *via* the reductive quenching cycle is not desirable for intermolecular ATRA for several reasons: The most obvious disadvantage is the use of a sub- or even stoichiometric reductive quencher **764**, but even more problematic is that the resulting intermediately formed radical cations **760** can lead to undesirable side reactions, in particular enamine additions, formation of imines with substrates, or early reaction termination by H-transfer to substrate radicals **765**.[53] One solution is to exploit the oxidative quenching cycle, in which the bromomalonate **759** itself acts as the quencher of the excited state **12** and is reduced to the α-carbonyl radical **763** (**scheme 97**, oxidative quenching). After addition to the alkene component **757**, a γ-alkyl radical **765** is formed, which can react again in two ways. Either through halogen atom abstraction from a substrate molecule **759** (radical propagation) or by closing the photocatalytic cycle through oxidation to the carbocation **761** and addition of the halide released in the course of the first step (nucleophilic trapping). In summary, ATRA *via* oxidative quenching represents a much more atom-economical approach without the negative side effects caused by the quencher **764**.[53]

This mechanism was originally developed with a more reducing iridium photocatalyst, but applying the original reaction conditions (1 mol% photocatalyst, 2.0 eq. atom transfer reagent/bromomalonate, 1.0 eq. alkenes, 2.0 eq. LiBr) also led to the ATRA product **758** in quantitative yield using the less expensive $[Ru(bpy)_3]Cl_2$ (**7**) (**equation 36**).[53]

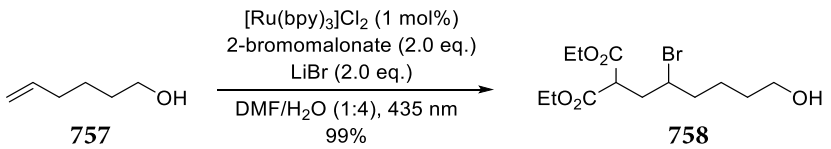

equation 36. ATRA of 2-bromomalonate **759** to 5-hexen-1-ol (**757**).[53]

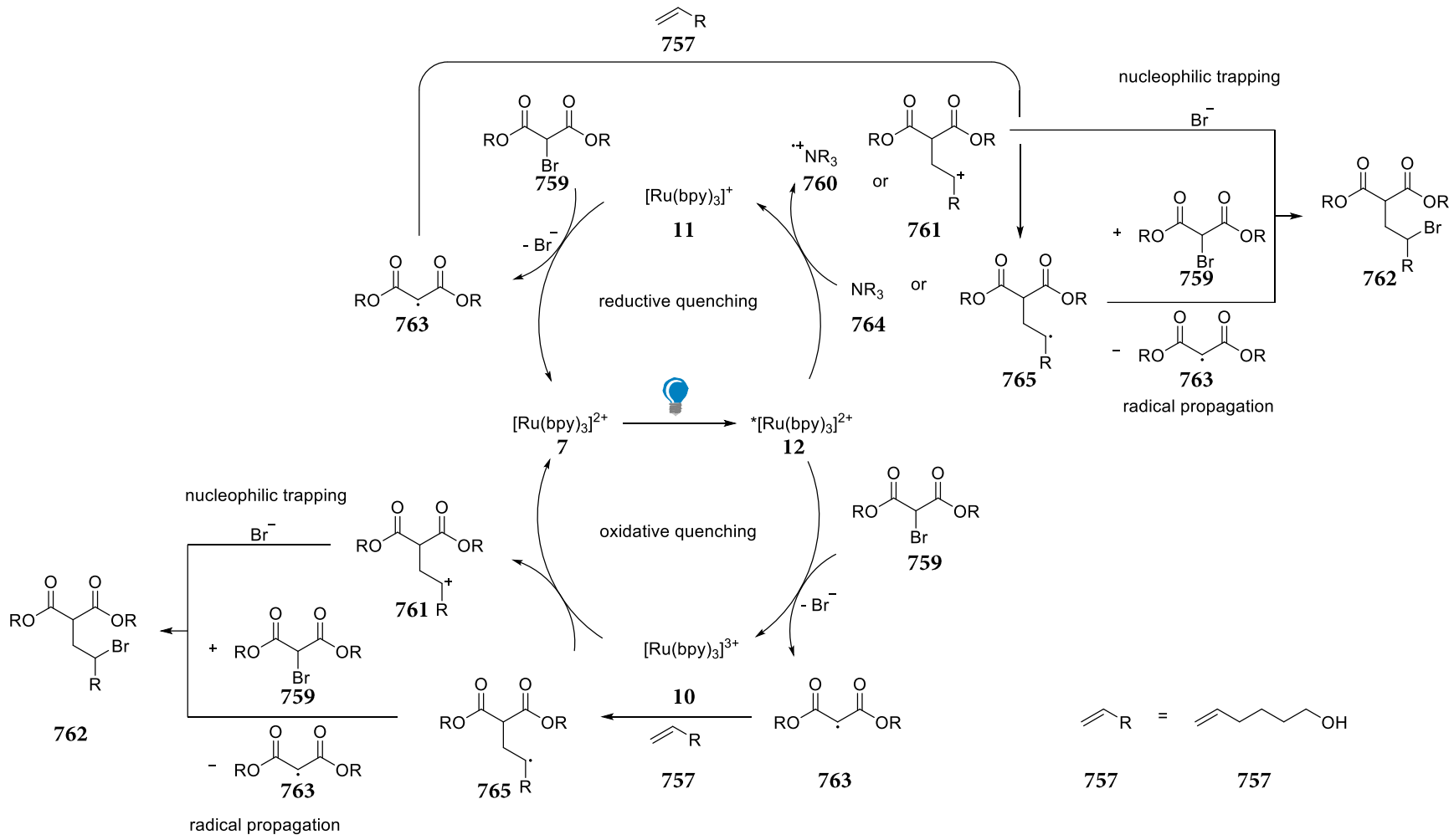

scheme 97. Comparison of the mechanisms of the atom transfer radical addition (ATRA) of 2-bromomalonate **759** and 5-hexene-ol (**757**) *via* a reductive and an oxidative quenching cycle.[53, 325]

A solvent screening revealed that DMSO allows shorter reaction times and highest yields and that the excess of both the atom transfer reagent (bromomalonate **759**) and the lewis acid additive (LiBr) can be reduced from 2.0 eq. to 1.2 eq. and from 2.0 eq. to 0.1 eq. respectively.[53, 325] With these optimized ATRA conditions, a large number of alkenes was successfully functionalized. Instead of α-bromocarbonyl compounds, various other halogenated compounds, e.g. CCl_3Br, CBr_4, CF_2Br_2, CCl_4, were incorporated as well. In summary, Stephenson's intermolecular ATRA, represents a versatile and elegant method for the functionalization of alkenes under mild conditions, which allows the addition of a variety of activated halogenated compounds to non-activated alkenes without the need for a special substrate design.[53, 325] In case of the oxidative quenching cycle no external, stoichiometric electron donor is required rendering it particularly atom-economical.[53]

3.4.2.1 Racemic reproduction of Stephenson's ATRA

In order to adapt Stephenson's ATRA enantioselectively, a racemic reproduction and optimization of the key example from Stephenson's publications on the development of the ATRA had to be accomplished first: The ATRA of 2-bromodiethylmalonate (**766**) to 5-hexene-1-ol (**757**). The parameters and results of selected experiments are summarized in **table 10**.

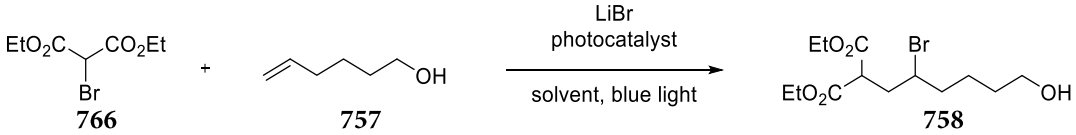

equation 37. Atom transfer radical addition of 2-bromodiethylmalonate (**766**) to 5-hexene-1-ol (**757**).

table 10. Parameters and results of selected experiments of Stephenson's intermolecular atom transfer radical addition.

entry	catalyst	[mol%]	solvent	malonate [eq.]	LiBr [eq.]	time [h]	yield [%]
1	$[Ru(bpy)_3]Cl_2$ 6 H_2O	0.6	DMF/H_2O	1.0	1.0	16	n.r.
2[(b)]	$[Ru(bpy)_3]Cl_2$ 6 H_2O	0.6	DMF/H_2O	1.0	1.0	16	traces
3[(b)]	$[Ru(bpy)_3]Cl_2$ 6 H_2O	0.6	DMF/H_2O	1.2	2.0	16	11
4[(a,b)]	$[Ru(bpy)_3]Cl_2$ 6 H_2O	0.6	DMSO	1.2	2.0	16	3
5[(a,b)]	$[Ru(bpy)_3](PF_6)_2$	1	DMSO	1.2	2.0	40	2
6[(a,b)]	$[Ru(bpy)_3](PF_6)_2$	1	DMSO	2.0	2.0	40	6
7[(a,b)]	$[Ru(bpy)_3](PF_6)_2$	1	DMSO	1.2	0.1	40	18
8[(a,b)]	$[Ru(bpy)_3](PF_6)_2$	3	DMSO	1.2	0.1	40	23
9[(a,b)]	$[Ru(bpy)_3](PF_6)_2$	1	DMF/H_2O	1.2	2.0	40	31
10[(a,b)]	$[Ru(bpy)_3](PF_6)_2$	3	DMF/H_2O	1.2	2.0	40	46

(a) determined by ^{1}H-NMR using an internal standard. (b) mixture degassed by freeze-pump-thaw.

Since different optimal reaction conditions were found in their initial study (2.0 eq. bromomalonate **766**, 2.0 eq. LiBr, DMF/H_2O) and in a later publication on further optimized reactivity (1.2 eq. bromomalonate **766**, 0.1 eq. LiBr, DMSO) the influence of various reaction parameters was investigated.[53, 325] As was the case regarding the reproduction of Stephenson's radical cyclization, the original conditions had to be altered slightly because the

available photoreactor emits at a different wavelength (460 nm instead of 435 nm). This deviation should in spite of the slightly lower energy provided to the reaction mixture not alter the overall reactivity because of the better overlap with the absorption maximum of the MLCT-transition. Furthermore instead of $[Ru(bpy)_3]Cl_2$ (**7**) either the corresponding hexahydrate $[Ru(bpy)_3]Cl_2$ x 6 H_2O (**7**) or the hexafluorophophate $[Ru(bpy)_3](PF_6)_2$ (**7**) was used. Given that the reaction should also proceed quantitatively in a water/DMF mixture, neither use of the hexahydrate nor residual water in solvents or partial hydrolysis of the Lewis acid additive lithium bromide to lithium hydroxide should influence the reaction negatively.

First, the influence of different procedures for degassing the reaction mixture, namely by Ar-sparging or freeze-pump-thaw (fpt), were compared (entries 1 and 2). Although in the original procedure only Ar-sparging was performed, no product formation could be observed in this way. In contrast, some traces of the ATRA-product **758** were detected on TLC in the reaction mixture degassed by fpt. Therefore, in all further approaches, the solids were placed in septum capped vials and the vials were evacuated and filled with argon before the remaining substances were dissolved, thoroughly degassed by fpt and transferred into the vials. Since a very poor yield of only 11% was isolated using Stephenson's original procedure (entry 3), a simultaneous screening followed comparing the individual reaction parameters from Stephenson's original and later general procedures. Both $[Ru(bpy)_3]Cl_2$ x 6 H_2O (**7**) and $[Ru(bpy)_3](PF_6)_2$ (**7**) as well as the solvent systems DMF/H_2O and DMSO were compared. Furthermore the reactant ratios, i.e. catalyst loading and amount of bromomalonate **766** and LiBr were varied. The success of the reactions was investigated using quantitative ^{1}H-NMR spectroscopy by comparing integrals of the β-H-product peak with the integrals of an internal standard (triphenylmethane or *p*-dichlorobenzene) added to the crude product in a defined amount.

The results indicate that, in contrast to Stephenson, the DMF/H_2O solvent mixture from the original studies gave better results than performing the same ATRA in DMSO (entries 3 and 4). The use of $[Ru(bpy)_3](PF_6)_2$ (**7**) instead $[Ru(bpy)_3]Cl_2$ x 6 H_2O (**7**) gave a yield of only 2% despite a much longer reaction time (40 h vs. 16 h) (entries 4 and 5). This slightly poorer yield despite longer reaction time is possibly related to the influence of counterions of photoredox catalysts on their reactivity. Although the ligand structure is generally regarded as the most important regulator for fine-tuning the properties of the photocatalyst, a significant influence of counterions on the energy of excited triplet states and the redox potential of the ground state has recently been observed.[322] The influence can be rationalized by the charge redistribution (MLCT) that takes place during excitation whereby a transfer of an electron from a metal-centred orbital to a ligand-centred orbital occurs. The resulting lower symmetry MLCT state should therefore have a large dipole moment and consequently react sensitively to the coordinating properties of its counterion. Based on this assumption, a more coordinating chloride anion might stabilize the excited triplet state better than a less coordinating hexafluorophosphate anion.[322] However, as the asymmetric bimetallic photoredox catalysts **532**, **536** and **537** the evaluation of which is ultimately to be carried out were prepared as hexafluorophosphates as well, racemic optimization using the hexafluorophosphate is reasonable for better comparability, which is why commercially obtained $[Ru(bpy)_3](PF_6)_2$ (**7**) was used in all

further approaches despite the lower yield. Using a larger excess of bromomalonate **766** (2.0 eq. vs. 1.2 eq.) in analogy to Stephenson's original publication, a higher yield was observed (entries 5 vs. 6). An even larger effect was obtained by using only 0.1 eq. LiBr (instead of 2.0 eq.) similar to Stephenson's more recent publication (entries 5 vs. 7).[53] By increasing the catalyst loading from 1 mol% to 3 mol%, using 0.1 eq. LiBr in DMSO an increase in yield from 18% to 23% (entries 7 and 8) and using 2.0 eq. LiBr in DMF/H_2O an increase from 31% to a maximum of 46% was achieved (entries 9 and 10).

Since none of the approaches produced a result in roughly similar yield to Stephenson's publications, and even the best yield of 46% was not satisfactory, the ATRA of 5-hexene-ol (**757**) and 2-bromomalonate **766** was not pursued further for the evaluation of asymmetric bimetallic photoredox catalysts.[53, 325]

3.4.2.2 ATRA-related approaches

Since the concept of an intermolecular photoreaction and in particular the described ATRA does not require complex substrate syntheses and the reactivity thus represents a promising opportunity to discover a photoreaction suitable for the evaluation of the asymmetric photocatalysts **532**, **536** and **537**, some additional substrate combinations were evaluated. For an enantioselective adaptation, these substrates must contain a 1,3-dicarbonyl group for efficient coordination in the chiral environment of the bisoxazoline fragments. In contrast to the previously discussed ATRA, symmetrical 2-bromomalonates **766** were not used because their corresponding ATRA product would not generate an α-stereocenter. Consequently, only asymmetric esters, or asymmetric 1,3-dicarbonyl compounds such as β-ketoester **767** or 1,3-dicarbonyl compounds containing a bromide substituent that is not positioned between the carbonyl groups **770** could be used as potential substrates. In this way, the ATRA would generate both a stereocenter at the α- and γ-position. Any alkenes could be employed in this reaction allowing examination of the influence of functional groups or sterically demanding substituents on the stereochemical outcome. The alkyl bromide substrates and alkene components accessible by simple bromination or amide formation, as well as the corresponding targeted products, are summarized in **scheme 98**.

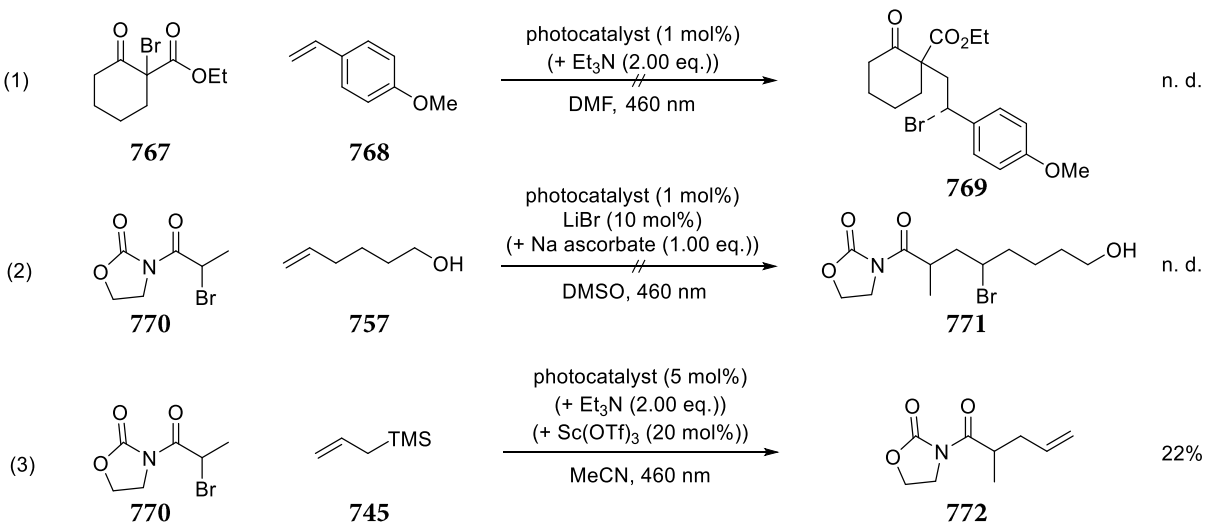

scheme 98. Conditions and results of additional ATRA related photoreactions. Additives in brackets were either added to the ongoing reaction at a later stage or the reaction was carried out with and without the corresponding additive.

First, an ATRA of the β-keto ester **767** with *p*-methoxystyrene (**768**) was investigated (**scheme 98**, equation 1). However, no classical ATRA conditions were used, but conditions of intramolecular radical cyclization (chapter 3.4.1).[16] Aiming at an oxidative quenching cycle, the reaction was set up with and without triethylamine, i.e. with and without a stoichiometric reductive quencher. After 45 minutes, a clear difference was already apparent on a TLC analysis: While a large number of spots was visible in the reaction with reductive quencher triethylamine (**726**), probably resulting from the previously mentioned side reactions with intermediately formed ammoniumyl radical cations **760**, no conversion of the alkyl bromide component **767** was visible in the reaction without triethylamine (**726**). After 20 days, both approaches showed a large number of spots whose mass analysis, however, did not allow an assignment to expected by-products from radical recombination, ATRA, reductive dehalogenation or other side reactions with ammoniumyl radical cations **760**.

In another experiment, the reaction between 5-hexene-ol (**757**) and the oxazolidinone **770** was studied under more typical ATRA conditions (**scheme 98**, equation 2). The latter is of particular interest due to its structural similarity to widely used chiral auxiliaries, as after ATRA has occurred and the oxazolidinone fragment has been cleaved off, asymmetric carboxylic acids would be accessible. Initially, aiming at an atom-economical oxidative quenching cycle, the addition of a stoichiometric quencher was avoided. However, no product formation was apparent in this way, so stoichiometric amounts of sodium ascorbate were added with the aim of product formation *via* the reductive quenching cycle. This quencher had already been used successfully by Stephenson and has the advantage over triethylamine (**726**) that no undesirable side reactions take place.[53] Unfortunately, no ATRA product formation was detected even under these conditions.

The final intermolecular radical addition of an α-halocarbonyl compound to an alkene is not an ATRA but a photoinduced α-allylation based on results of Woo *et al.*[326] They used *fac*-Ir(ppy)$_3$ (**29**) for the photocatalytic reduction of 2-bromoacetophenone (**773**) to form an α-carbonyl radical **774**, which adds to the double bond of allyltrimethylsilane (**745**) similar to the ATRA discussed so far. The TMS radical **778** released in this process can subsequently serve as a reducing agent for the oxidized photocatalyst **776** and thereby complete the photocatalytic cycle while forming trimethylsilyl bromide. In this way, α-allylation also occurs without the addition of a stoichiometric quencher (**scheme 99**).[326] In analogy to the results of Woo *et al.* it was assumed that the oxazolidinone **770** might undergo photoinduced α-allylation with allyltrimethylsilane (**745**). However, a mixture with [Ru(bpy)$_3$](PF$_6$)$_2$ (**7**) in degassed acetonitrile did not result in any conversion within 16 hours. At this point, it was assumed that the redox potential of the excited state [Ru(bpy)$_3$]$^{2+*}$ (**12**) was not sufficient to reduce the oxazolidone substrate **770**, being only activated by one electron withdrawing carbonyl group. Therefore, and given that during the enantioselective run a coordination in a chiral environment takes place, 20 mol% Sc(OTf)$_3$ was added and the reaction was further observed. Unfortunately, no product **772** formation took place in this way either, possibly because no oxidative quenching by the substrate **770** occurred despite activation. It is also conceivable that the ratio of redox potentials from oxidized photocatalyst [Ru(bpy)$_3$]$^{3+}$ (**10**) and trimethylsilyl radi-

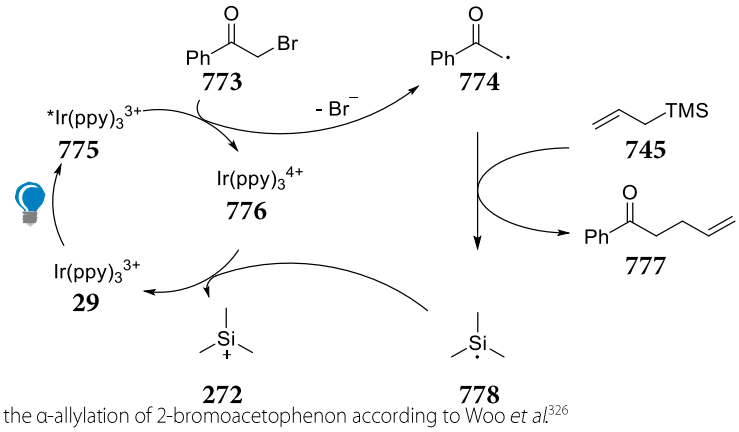

scheme 99. Mechanism of the α-allylation of 2-bromoacetophenon according to Woo *et al.*[326]

cal **778** is not suitable to turn over the photocatalytic cycle. Therefore, 2.0 eq. of the reductive quencher triethylamine (**726**) was added to generate product, albeit *via* a less elegant pathway. After 72 h, the reactant **770** was consumed and a large number of spots became visible, from which, after separating by column chromatography, a species was obtained in poor yield of 22%, showing similarity to the ATRA product **772**.

In summary, several combinations of halo-carbonyls and alkenes under a diverse range of reaction conditions did not result in any efficient intermolecular product formation in satisfactory yields and the search for a suitable photoreaction to evaluate the asymmetric bimetallic photoredox catalysts was continued (chapters 3.4.3 - 3.4.5).

3.4.3 Cascade cyclization of phenylpropynyl-3-oxo-3-phenylpropanoate (**779**)

The reaction evaluated in this section is a cascade cyclization that is mechanistically related to Stephenson's intramolecular cyclization and was first observed by Wu *et al.* and has been optimized racemically in our working group for eosin Y using a variety of substrates.[327, 328] Mechanistically, the excited state $[Ru(bpy)_3]^{2+*}$ (**12**) is reductively quenched by Et_3N (**726**), resulting in the reduced photocatalyst $[Ru(bpy)_3]^{+}$ (**11**) which in turn transfers an electron to the α-brominated β-ketoester **779**, thereby inducing heterolytic cleavage of the C-Br bond. Similar to Stephenson's intramolecular cyclization, the radical **780** undergoes a 5-exo-dig cyclization forming a benzylidenedihydrofurane **781** in which the radical is well stabilized due to the benzylic position. The spatial proximity to the aryl ring allows a 6-endo-trig cyclization to follow forming the product skeleton **782** containing a cyclohexadiene-radical. The latter is finally oxidized and deprotonated, probably by the ammoniumyl radical cation **727** generating a triethylammonium cation **783** and the cyclization product **784**.[327]

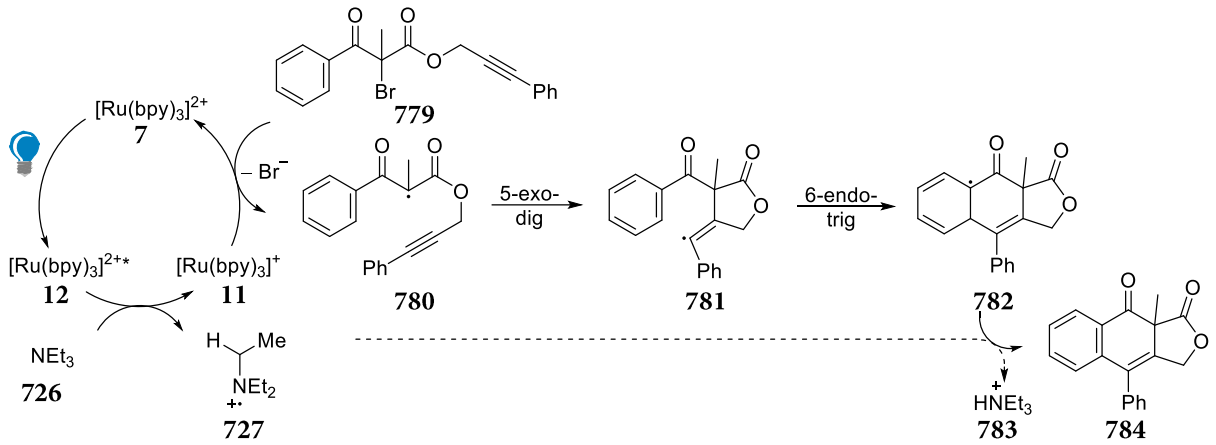

scheme 100. Mechanism of the cascade cyclization of phenylpropynyl-3-oxo-3-phenylpropanoate (**779**).[327]

Starting from β-keto-ethyl ester **785** transesterification with phenylpropynol **786** in the presence of DMAP on a Dean-Stark-trap to continuously remove the azeotrope of toluene and released ethanol gave ester **787** in a maximum yield of 73%. Methylation in the α-position proceeded smoothly in excellent yield and is the key to a configurationally stable product **784** of the photoreaction, since the exchange of the α-proton for this methyl group prevents racemization by keto-enol tautomerism. The subsequent bromination was carried out with NaHMDS and NBS in a maximum yield of 73% (**scheme 101**).

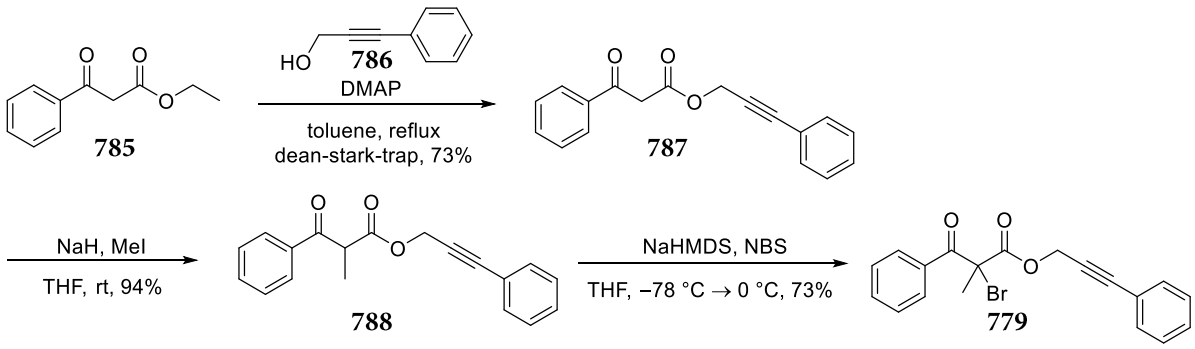

scheme 101. Synthesis of phenylpropynyl-3-oxo-phenylpropanoate (**779**).

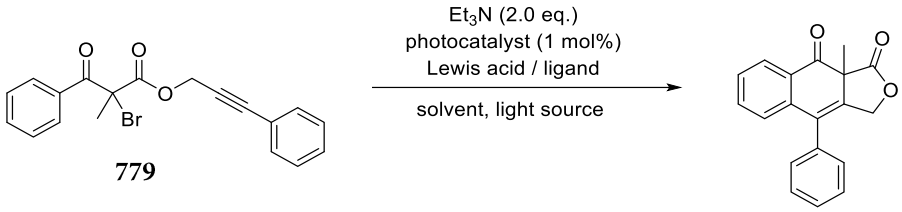

779 **784**

table 11. Parameters and results of selected experiments of the cascade cyclization of phenylpropynyl-3-oxo-phenylpropanoate (**779**).

entry	catalyst	solvent	Lewis acid (eq.)	ligand (eq.)	yield [%]	ee [%]
1	$[Ru(bpy)_3](PF_6)_2$	DMF	---	---	27	---
2	$[Ru(bpy)_3](PF_6)_2$	DMF	$Zn(OTf)_2$ (1.00)	BOX (1.00)	71	0
3	$[Ru(bpy)_3](PF_6)_2$	DMF	$Zn(OTf)_2$ (1.00)	BOX (1.00)	63	0
4[(a)]	$[Ru(bpy)_3](PF_6)_2$	THF	$Zn(OTf)_2$ (1.00)	BOX (1.00)	15	0
5[(a)]	$[Ru(bpy)_3](PF_6)_2$	CH_2Cl_2	$Zn(OTf)_2$ (1.00)	BOX (1.00)	---	0
6[(a)]	$[Ru(bpy)_3](PF_6)_2$	CH_2Cl_2	$Zn(OTf)_2$ (1.00)	BOX (1.00)	40	0
7[(a)]	$[Ru(bpy)_3](PF_6)_2$	$CHCl_3$	$Zn(OTf)_2$ (1.00)	BOX (1.00)	58	0
8[(a)]	$[Ru(bpy)_3](PF_6)_2$	toluene	$Zn(OTf)_2$ (1.00)	BOX (1.00)	81	0
9[(a)]	$[Ru(bpy)_3](PF_6)_2$	$Cl\text{-}C_6H_5$	$Zn(OTf)_2$ (1.00)	BOX (1.00)	65	0
10[(a)]	$[Ru(bpy)_3](PF_6)_2$	dioxane	$Zn(OTf)_2$ (1.00)	BOX (1.00)	27	0
11[(a)]	$[Ru(bpy)_3](PF_6)_2$	$Cl_2\text{-}C_2H_4$	$Zn(OTf)_2$ (1.00)	BOX (1.00)	9	0
12[(a)]	$[Ru(bpy)_3](PF_6)_2$	$Cl_2\text{-}C_6H_4$	$Zn(OTf)_2$ (1.00)	BOX (1.00)	6	0
13	$[Ru(bpy)_3](PF_6)_2$	CH_2Cl_2	$Sc(OTf)_3$ (1.00)	BOX (1.00)	93	0
14	$[Ru(bpy)_3](PF_6)_2$	CH_2Cl_2	$CoCl_2$ (1.00)	BOX (1.00)	47	0
15	$[Ru(bpy)_3](PF_6)_2$	CH_2Cl_2	$Ni(OTf)_2$ (1.00)	BOX (1.00)	57	0
16	$[Ru(bpy)_3](PF_6)_2$	CH_2Cl_2	$CuBr_2$ (1.00)	BOX (1.00)	---	---
17	$[Ru(bpy)_3](PF_6)_2$	CH_2Cl_2	$Cu(OTf)_2$ (1.00)	BOX (1.00)	---	---
18	$[Ru(bpy)_3](PF_6)_2$	CH_2Cl_2	$Zn(OTf)_2$ (1.00)	BOX (1.00)	55	0
19	$[Ru(bpy)_3](PF_6)_2$	CH_2Cl_2	$ZrCl_4$ (1.00)	BOX (1.00)	66	0
20	$[Ru(bpy)_3](PF_6)_2$	CH_2Cl_2	$In(OTf)_3$ (1.00)	BOX (1.00)	42	0
21	$[Ru(bpy)_3](PF_6)_2$	CH_2Cl_2	$La(OTf)_3$ (1.00)	BOX (1.00)	30	0
22	$[Ru(bpy)_3](PF_6)_2$	CH_2Cl_2	$Eu(OTf)_3$ (1.00)	BOX (1.00)	13	0
23	$[Ru(bpy)_3](PF_6)_2$	CH_2Cl_2	$Yb(OTf)_3$ (1.00)	BOX (1.00)	n. r.	0
24	$[Ru(bpy)_3](PF_6)_2$	CH_2Cl_2	$Bi(OTf)_3$ (1.00)	BOX (1.00)	88	0
25	asym. PC. R = H	CH_2Cl_2	$Zn(OTf)_2$ (0.02)	---	67	0
26	asym. PC. R = *t*Bu	CH_2Cl_2	$Zn(OTf)_2$ (0.01)	---	74	0
27	asym. PC. R = OMe	CH_2Cl_2	$Zn(OTf)_2$ (0.014)	---	87	0

asym. PC. = asymmetric photocatalyst of the form $[Ru(R\text{-}bpy)_2(BOX\text{-}bpy)](PF_6)_2$ (a) product isolation by preparative TLC.

The parameters and results of selected experiments for the enantioselective adaption of the cascade cyclization are summarized in **table 11**. The investigation was started with conditions of Stephenson's intramolecular cyclization, confirming, albeit in poor yield, the underlying reactivity (entry 1).[16] Based on this result, the reaction was systematically optimized. First, the reaction was repeated in the presence of stoichiometric amounts of a BOX-Zn and BOX-Sc complex, respectively, increasing the yield to 71% and 63%, respectively, however lacking enantioselectivity (entries 2 and 3). While maintaining a stoichiometric amount of a BOX-Zn complex, a screening of non-coordinating solvents was performed (entries 4 - 12), since the lack of enantioselectivity could result from the blocking of coordination sides on the BOX complex by DMF molecules present in large excess. The focus of the study was mainly on a qualitative comparison in terms of solubility of involved components as well as resulting reaction rates, which were followed by TLC. The product isolation was therefore only performed by preparative TLC, rendering the yields possibly inaccurate (entries 4 - 12). It was assumed that this method would allow faster product isolation and thus determination of the enantiomeric excess, which is the primary goal of the study. Although none of the approaches showed signs of enantioselectivity, it became clear that the best solubility and the fastest conversion occurred in CH_2Cl_2 followed by $CHCl_3$. Due to complete consumption of the reactant after only 1 h in CH_2Cl_2, the reaction was stopped and the dominantly formed spot was isolated by preparative TLC. However, it was not the product but appeared to be a structurally closely related intermediate that was dominant due to the early termination. Repeating the experiment with extended reaction time (10 h) gave the product in a moderate yield of 40% (entries 5 and 6). Rapid consumption was also observed in chlorobenzene within only 2 h, but just as in the other solvents (toluene, dioxane, dichloroethane, dichlorobenzene), the mixture could be described as a suspension rather than a solution. Thus, based on solubility of the reactants and reaction rate, the further approaches were carried out in CH_2Cl_2. Next, a variety of Lewis acids (Mg(II), Sc(III), Co(II), Ni(II), Cu(II), Zn(II), Yb(II)) were evaluated regarding their coordination to BOX **613** and to the substrate **779** by stirring them for 2 h in deuterated chloroform that was previously filtered through neutral aluminiumoxide and analyzing the mixtures by ^{1}H-NMR spectroscopy for changes in chemical shifts and coupling patterns (**spectrum 13**). It was found that the Lewis acids $CoCl_2$ x 6 H_2O, $Ni(SO_4)_2$ x 7 H_2O, and $Cu(SO_4)_2$ neither interacted with BOX **613**, nor with the substrate **779**. With $MgBr_2$, $CuBr_2$, and $Yb(OTf)_3$, there was a significant broadening of the oxazoline ring signals, which in the case of Mg(II) could possibly result from coordination-dissociation equilibria (**scheme 102**) and in the case of Cu(II) and Yb(III) may be due to the paramagnetism of the ions.

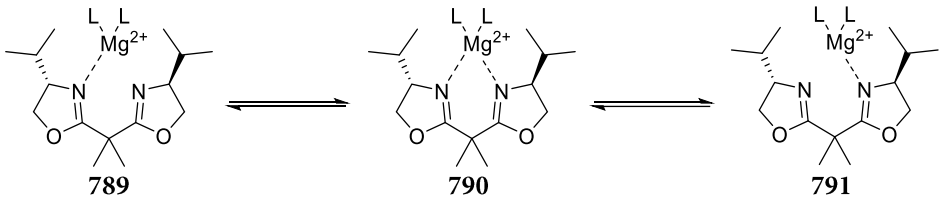

scheme 102. Assumed coordination-dissociation equilibria causing broadend ^{1}H-NMR signals.

The strongest interaction occured with Sc(III) and Zn(II), clearly evident from a shift in oxazoline ring signals and doubled sets of signals for the methyl groups at the ring-bridging C atom and the *i*Pr residues. With the substrate,

none of the Lewis acids examined showed a distinct interaction, possibly due to a coordination-dissociation equilibrium (**spectrum 13**).

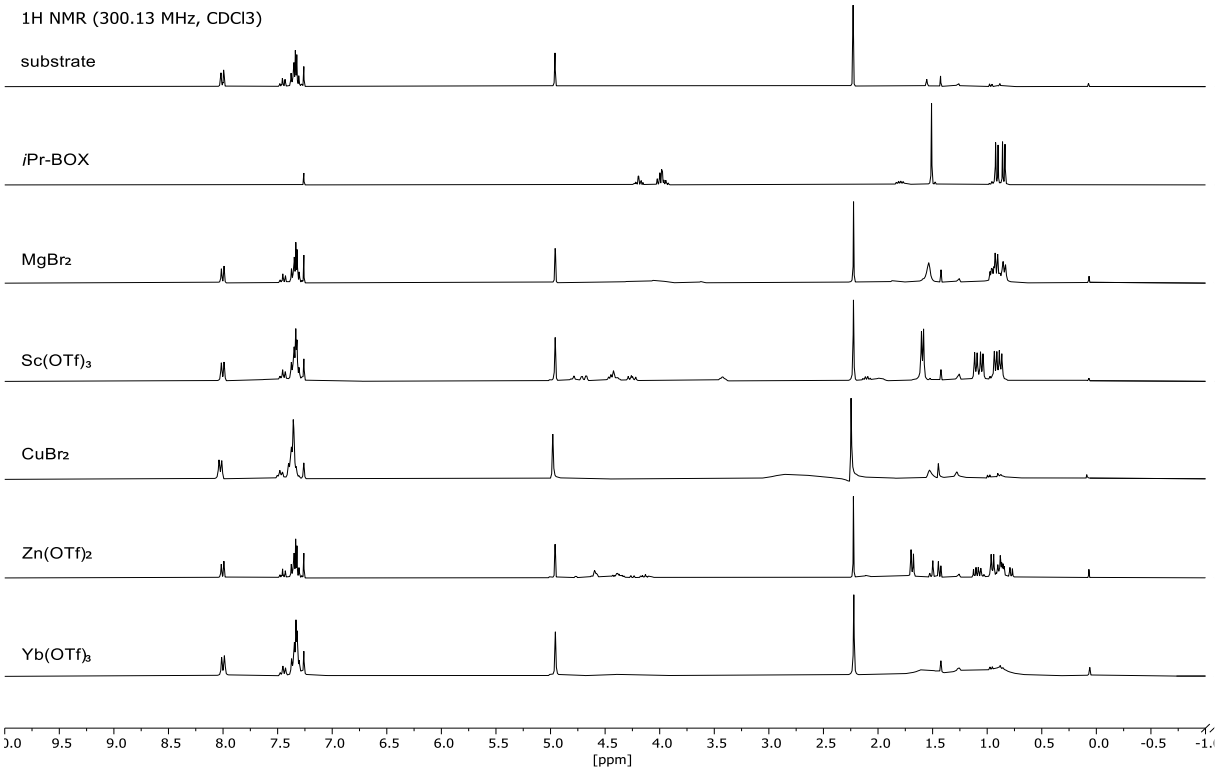

spectrum 13. Stacked ^{1}H-NMR spectra of mixtures of *i*Pr-BOX **613**, substrate **779** and different Lewis acids.

A screening of various Lewis acids in the presence of stoichiometric amounts of the BOX ligand **613** was performed and the reaction products **784** were isolated using flash-chromatography. For this purpose, the Lewis acids were weighed into schlenk tubes, mixed with BOX **613** and the substrate **779** in an Argon counterflow, and the mixtures were stirred for 2 h in the absence of light. Following this precoordination time, the photocatalyst **7** and finally the reductive quencher **726** were added and the mixtures irradiated (entries 13 - 24).With $CuBr_2$ and $Cu(OTf)_2$ only side reactions occurred instead of product formation (entries 16 and 17). In the presence of $Yb(OTf)_3$, even after 18 h, only starting material was present on TLC besides some minor side product spots (entry 23). In the other mixtures, the product **784** was formed in the indicated yields. Product formation was particularly fast with $Ni(OTf)_2$ (entry 15) and $Zn(OTf)_2$ (entry 18), yet all the approaches were irradiated for 18 h. Unfortunately, after purification by flash chromatography, none of the mixtures showed an enantiomeric excess despite theoretically complete saturation of each substrate molecule with a chiral Lewis acid. This may be either an intrinsic problem of the reaction or due to insufficient stereodifferentiation by the *i*Pr-residues of the BOX fragment. Despite the lack of selectivity, the bifunctional complexes **532**, **536** and **537** with $Zn(OTf)_2$ were also subjected to the reaction (entries 25 - 27), since observation of stereoinduction would have been even more remarkable after the sobering results obtained so far using the separate dual catalytic system. However, these experiments also showed no signs enantioselectivity, which finally ruled out this reaction for further evaluation of the asymmetric catalysts **532**, **536** and **537**.

3.4.4 Conjugate addition and [2+2]-enone cycloaddition

After the search for a suitable enantioselective transformation for the evaluation of the bimetallic photoredox catalysts **532**, **536** and **537** by asymmetric adaptation of different literature-known racemic photoreactions failed (chapters 3.4.1 - 3.4.3) sometimes already at the racemic reproduction and *a fortiori* in no approach signs of enantioselectivity were recognizable, further approaches focussed on the evaluation of the catalysts **532**, **536** and **537** in literature-known enantioselective transformations (chapters 3.4.4 - 3.4.5). The first example was a conjugate addition of alkyl radicals from the oxidation of alkyl trifluoroborates **792** to 2-acylimidazoles **794** and *N*-acyl-pyrazoles **795** according to Meggers *et al.* which proceeded in excellent yields and enantioselectivities with a large number of examples (**equation 38**).[205]

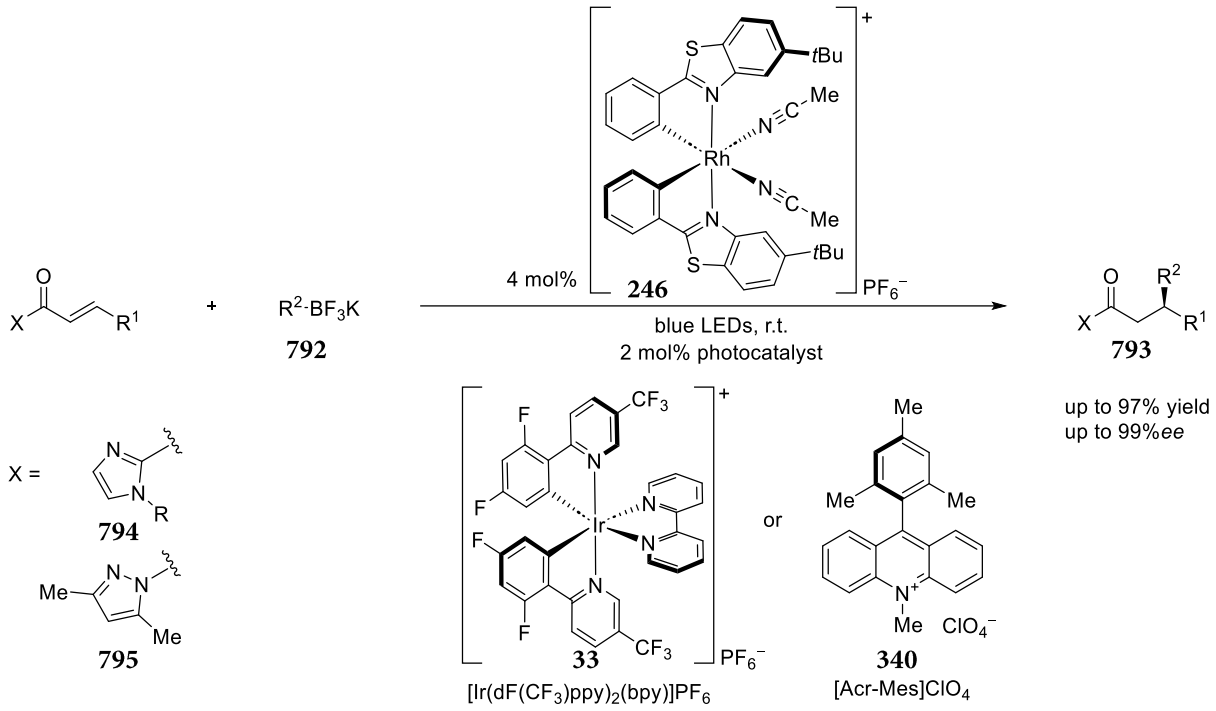

equation 38. Enantioselective conjugate addition of alkyl radicals derived from borotrifluoroborates **792** to 2-acylimidazoles **794** and 2-acylpyrazoles **795** according to Meggers *et al.*[205]

The enantioselectivity of this reaction results from the combination of a photoredox catalytic cycle with another catalytic cycle for asymmetric conversion. The intermediates involved are bound in the chiral environment of the asymmetric rhodium catalyst **246** for the duration of the reaction. Reductive quenching of the excited photocatalyst **798** (**33** or **340**) by the alkyl trifluoroborate **792** is followed by conjugate addition of the released alkyl radical **800** to a substrate molecule coordinated in the chiral environment **802**, forming the new stereocenter. The resulting α-carbonyl radical **801** is reduced to a Rh-bound enolate **796** by the reduced photocatalyst **799**, completing the photocatalytic cycle without the need for stoichiometric amounts of a reducing/oxidizing agent. After hydrolysis of the enolate **796**, the product **793** is released in exchange for a new substrate molecule **794** or **795**.[205]

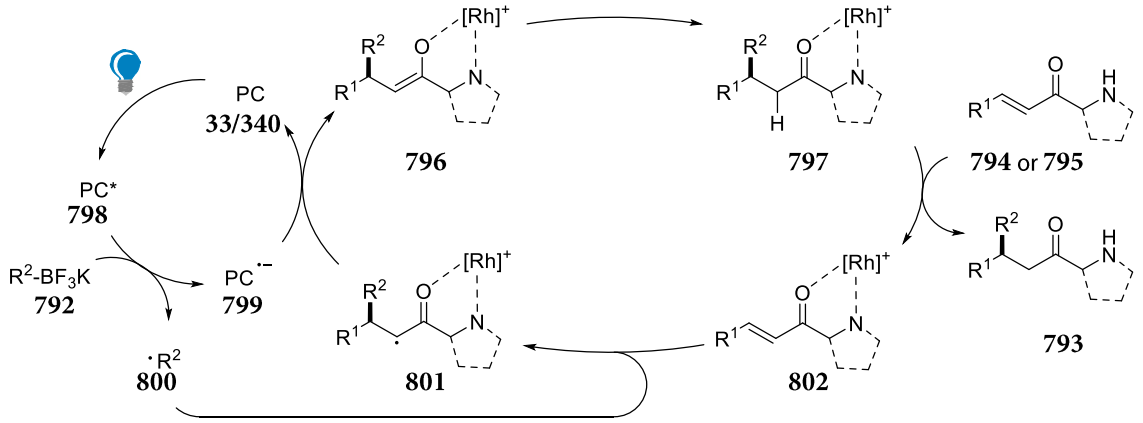

scheme 103. Mechanism of the enantioselective conjugate addition of alkylradicals **800** derived from alkyltrifluoroborates **792** to 2-acylimidazoles **794** or 2-acylpyrazoles **795** according to Meggers *et al.*[205]

Investigations began with the synthesis of 2-acylimidazole substrates **812** and **813**. The α,β-unsaturated 2-acylimidazoles **812** and **813** can be prepared either analogous to Meggers *et al. via* Wittig reaction of α-chloro-2-acylimidazoles **805** or starting from the α,β-unsaturated acids **808** and **809** *via* the corresponding Weinreb amides **810** and **811**.[205, 329] Starting from **804** by reaction with lithiated methylimidazole gave the α-chloro-2-acylimidazole **805** in a yield of 64%, however, the subsequent synthesis of the phosphoranylidene **806** was not successful. Following the other synthetic route starting from cinnamic acid (**808**) or crotonic acid (**809**), the corresponding Weinreb amides **810** and **811** were synthesized in excellent and moderate yields of 93% and 67%, respectively. The subsequent reaction with lithiated methylimidazole or phenylimidazole proceeded smoothly and gave the α,β-unsaturated 2-acylimidazoles **812** and **813** in the indicated yields (**scheme 104**). Benzyl trifluoroborate **792** was synthesized in good yield (69%) by reaction of benzyl Grignard with trimethylborate and KHF_2.

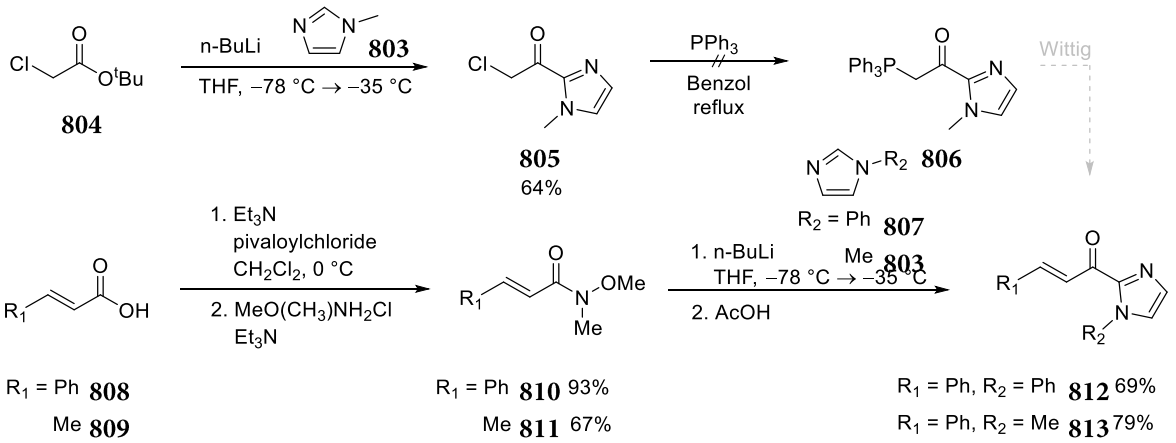

scheme 104. Synthesis of α,β-unsaturated 2-acylimidazoles **812** and **813**.

The first substrate tested is derived from cinnamic acid (**808**) and linked to methylimidazole (R_1 = Ph, R_2 = Me, **813**). After 18 h of irradiation, trace amounts of a substance were obtained with an ^{1}H-NMR spectrum showing high similarity to the starting material **813** along with a multiplett at 4.03 ppm representing 5 H. The

chemical shift indicates that it might be the signal at the stereocenter in the product, however, with an integral of 5 H and a not clearly defined splitting pattern it possibly results from the overlapping of several multipletts, thus it could represent the totality of all five alkyl protons (α-CH_2, β-CH, Ph-CH_2) making it the ^{1}H-NMR spectrum of the desired product. Since a substrate with such a substitution pattern (methyl residue at imidazole and phenyl residue at β-position) was not evaluated in the original literature, no comparison of the obtained spectrum with Meggers *et al.* could be performed.[205] Surprisingly, when the reaction was repeated in dichloromethane the formation of a different product **814** was dominant. ^{1}H-NMR analysis revealed that the product **814** contained a cyclobutane moiety, probably resulting from a (2+2)-enone dimerization (**spectrum 14**).

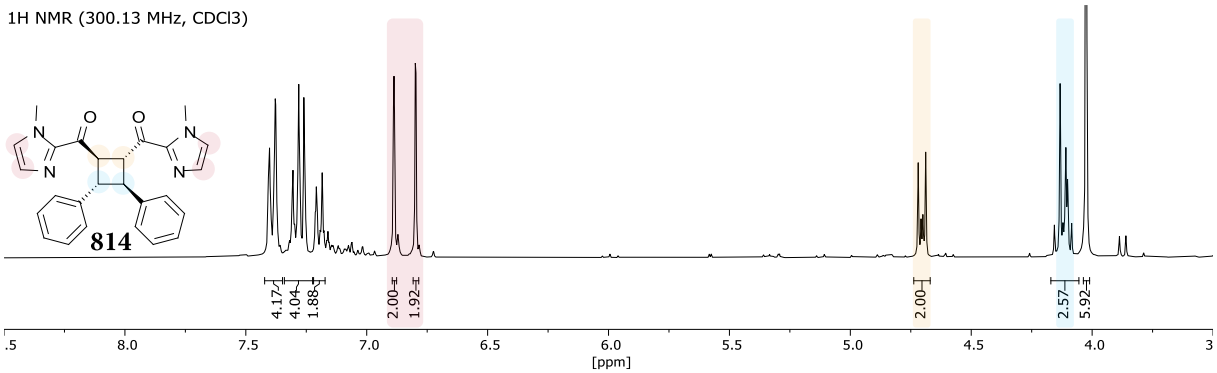

spectrum 14. ^{1}H-NMR spectrum of the dominantly formed cyclobutane side product **814**

Such dimerization products have previously been observed in a different study by Meggers *et al.* on asymmetric alkylation by merging proton coupled electron transfers (PCET), hydrogen atom transfer (1,5-HAT) and chiral Lewis acid catalysis (chapter 1.3.1.2.1, **scheme 29**). In this study, a cyclobutane **815** derived from the (2+2)-homodimerization of related 2-acylimidazoles **812** was isolated in 10% yield (**equation 39**).[208]

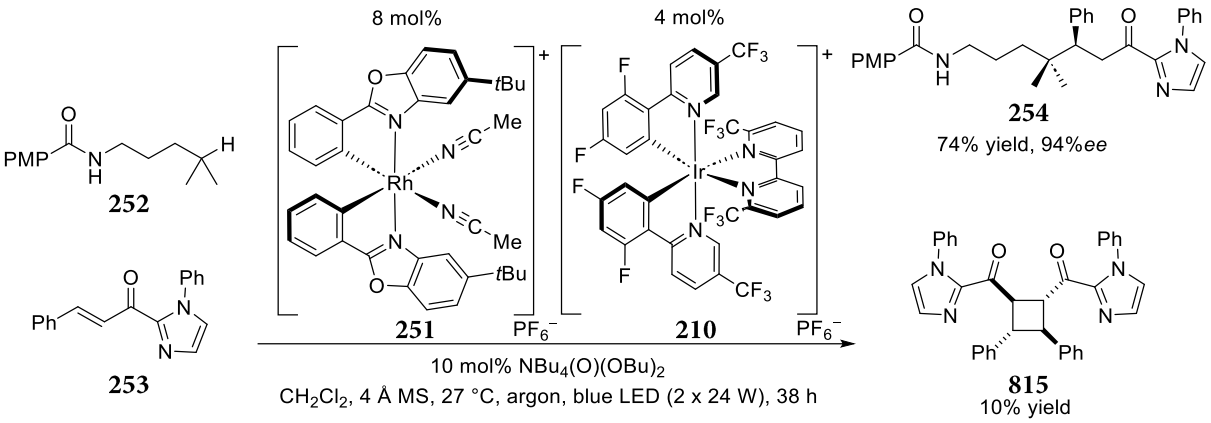

equation 39. Asymmetric alkylation according to Meggers *et al.* and observed cyclobutane side product **815**.[208]

Mechanistically, the formation of cyclobutanes can probably be traced back to a reactivity that has been intensively studied by the Yoon group and is considered to be the first example of photoredox transformations based on the combination of photoredox and Lewis acid catalysis (chapter 1.3.1.2.2, **scheme 31**).[11] Original studies investigated the intramolecular (2+2)-cycloaddition of bisarylenones (**scheme 105**). This reactivity exploits that lithium

coordinated arylenones **273** are readily reduced to lithium enolate radicals **274**, thereby initiating an intramolecular cascade cyclization with another enone moiety, leading to a highly diastereoselective formation of cyclobutane structures.[11]

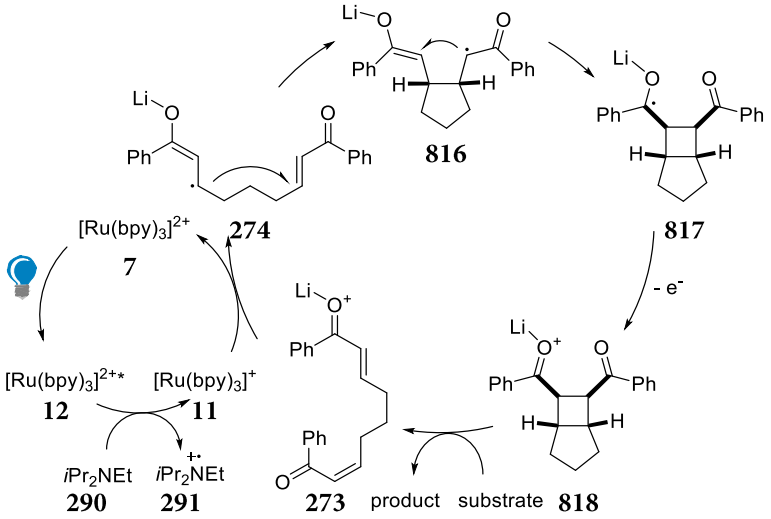

scheme 105. Mechanism of the intramolecular (2+2)-cycloaddition of bisarylenones according to Yoon *et al.*[11]

Given the problematic reproducibility and diverging reactivity of the first two experiments, recourse was made to a substrate containing a phenyl residue on both the double bond and the imidazole ring, which was previously used by Meggers *et al.* in conjugate addition and whose homodimerization product **815** is also literature known.[208, 228] Again, no conjugate addition was detected with this substrate, but instead the corresponding (2+2)-enone-dimerization product **815** formed preferentially. 18% of the starting material **812** was recovered, giving the *all-trans-syn* product **815** in a yield of 31% (based on 82% conversion). In addition, a much more polar substance with identical molecular weight (according to TLC-MS), as well as very similar sets of signals in ^{1}H-NMR but partially different chemical shifts, was isolated in a yield of 16%, which is probably the *all-trans-anti* product **819**.

Comparison of the ^{1}H-NMR spectra of literature-known *syn*-regioisomer **815** (**spectrum 15**, top) with the presumed *anti*-regioisomer **819** (**spectrum 15**, bottom) indicates that the chemical shifts of the signal sets of both the cyclobutane and imidazole rings are significantly low-field shifted in the case of the *anti*-isomer **819**. Furthermore, in the *anti*-isomer **819** the chemical shifts of the protons of the cyclobutane ring differ more significantly. Based on the vicinal position of electron-withdrawing carbonyl groups in the *syn*-regioisomer **815**, it could be hypothesized that the upper half of the ring which is bound to carbonyl groups is much more deshielded than the (lower) β-carbon half of the ring, and thus a greater distinction in the chemical shifts of α- and β-ring atoms should be observed than in the case of the alternately substituted cyclobutane ring of the *anti*-regioisomer **819**. However, for a correct analysis of the electronic situation, the alternating polarization of the carbonyl groups must be taken into account: The theoretical continuation of the alternating partial charges in the

syn-isomer **815** leads to a mismatched pattern of partial charges resulting in less electronic distinguishability of α- and β-cyclobutane

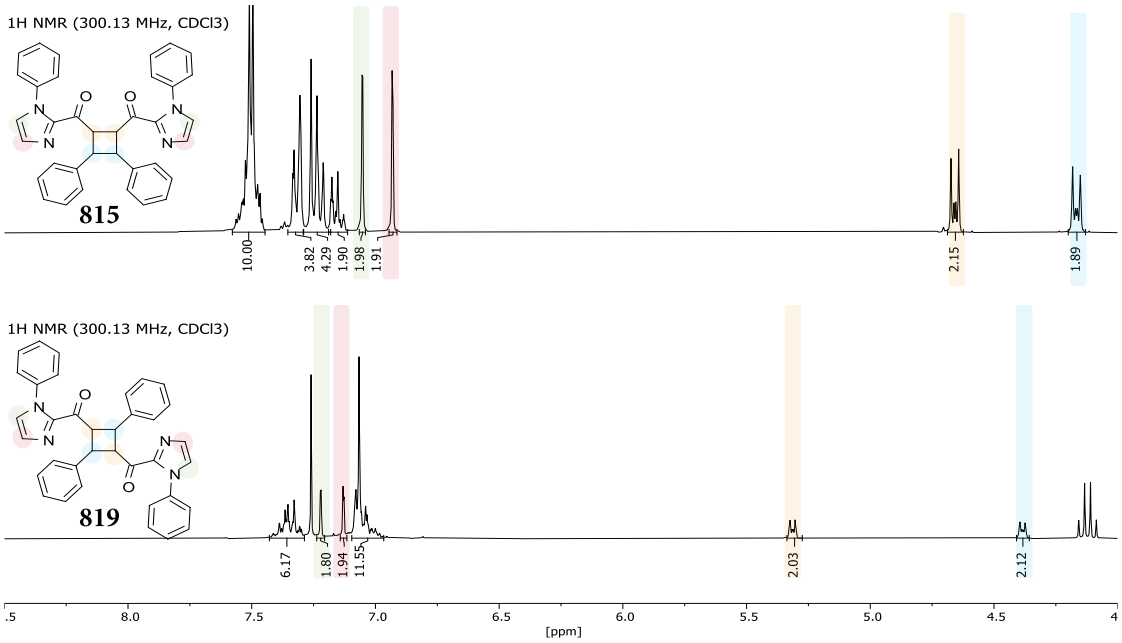

spectrum 15. ^{1}H-NMR spectra of dominantly formed *all-trans-syn*-cyclobutane **815** and its regioisomer **819**.

ring protons (more similar chemical shift), while in the *anti*-isomer **819** the continuation of the polarization reveals a matched pattern resulting in an enhancement of the alternating partially positively and negatively polarized ring protons, respectively, and thus accompanied by a more significant distinction of the chemical shifts. In summary, instead of the targeted conjugate addition of a benzyl radical **800** to be released by oxidation of benzyl trifluoroborate **792**, a (2+2)-enone dimerization proceeded preferentially. The lack of expected reactivity could possibly be due to unsuitable redox potentials, considering that Meggers *et al.* used $Ir[dF(CF_3)ppy]_2(bpy)PF_6$ (**33**) and $[Arc\text{-}Mes]ClO_4$ (**340**) as photocatalysts with reduction potentials $E_{1/2}[cat^*|cat^-]$ of +1.32 V and +2.08 V (vs. SCE), respectively.[330] With a reduction potential $E_{1/2}[[Ru(bpy)_3]^{2+*}|[Ru(bpy)_3]^+]$ = +0.85 V vs. SCE, the excited state of $[Ru(bpy)_3](PF_6)_2$ (**7**) is not sufficiently oxidizing to generate the alkyl radical **800** from the corresponding benzyl trifluoroborate **792** ($E_{1/2}$ = +0.75 V vs. Fc, +1.13 V vs. SCE).[331] In further approaches, therefore, the addition of benzyl trifluoroborate **792** was omitted and the focus was placed on an investigation of the (2+2)-enone dimerization, since in this reaction a cyclobutane with four stereocenters is formed and it is therefore in principle also suitable for the evaluation of the asymmetric bimetallic photoredox catalysts **532**, **536** and **537**. The major challenge of enantioselective adaptation is to ensure that the Lewis acid-catalyzed reaction proceeds significantly faster than the racemic background reaction. The Yoon group met this challenge by exploiting their observation that Li^+ activates the enone **273** for reduction to the enolate and stabilizes the resulting anion **274**. To develop an enantioselective variant, they took advantage of the high kinetic lability of lanthanides and began their screening of asymmetric ligands with $Gd(OTf)_3$. Since neither BINOL (**86**) nor TADDOL (**87**) or PyBOX ligands (**66-69**) gave satisfactory results, more unusual Schiff base dipeptide ligands **281** used by Hoveyda for copper-catalyzed

allylic alkylation were investigated, the optimization of which gave an excellent enantiomeric excess of 92%*ee* after switching to $Eu(OTf)_3$ and lowering the temperature. Moreover, Yoon *et al.* observed that the reaction rate is quite dependent on the L.A. concentration yet it has no effect on the enantiomeric excess, illustrating that no competitive background racemic reaction is taking place in this example (**equation 40**).[211, 244]

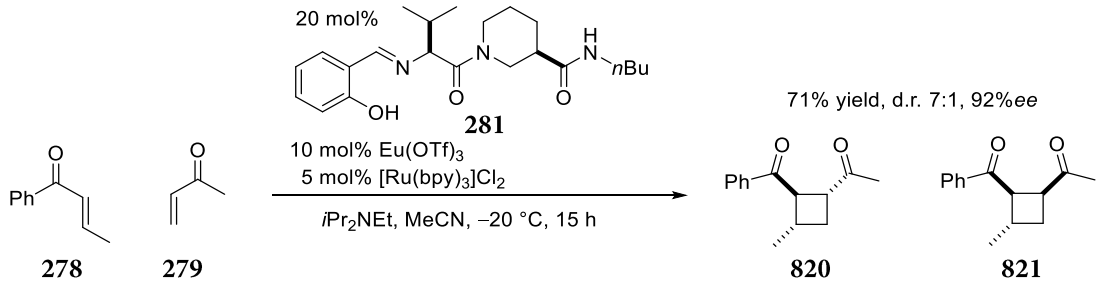

equation 40. Enantioselective crossed (2+2)-dimerization according to Yoon *et al.*[211, 244]

With these valuable insights into the importance of acceleration by L.A. for high enantioselectivities, a ^{1}H-NMR screening was performed to follow the reaction progress in the presence of different Lewis acids (**table 12**). Screening of this type can provide important insights into the nature of the ideal Lewis acid without the use of valuable asymmetric catalyst complexes. Since the asymmetric bimetallic photoredox catalysts contain and thus dictate a BOX structure, no ligand screening was performed. Encouraged by the Yoon groups finding that L.A. activation is required for the one-electron reduction, it was first tested whether this observation also applies to the (2+2)-dimerization of the acylenone **812**.[211, 244] Unfortunately, this investigation revealed that even without the presence of a Lewis acid, the reaction gave a conversion to the product **815** of 51% after 48 h (entry 1). For the Lewis acid screening, the substrate **812** and $[Ru(bpy)_3](PF_6)_2$ (**7**) were dissolved in acetone in a septum vial and the corresponding Lewis acid was weighed into a septum vial in the glovebox and then transferred to the reaction vial as a solution in acetone. After degassing by Ar-sparging, the vials were stirred overnight under exclusion of light and irradiated the next day. After defined periods samples were taken, worked up to remove the photocatalyst and analyzed by ^{1}H-NMR. The values represent the relative ratio of product to substrate signals (**figure 39**).

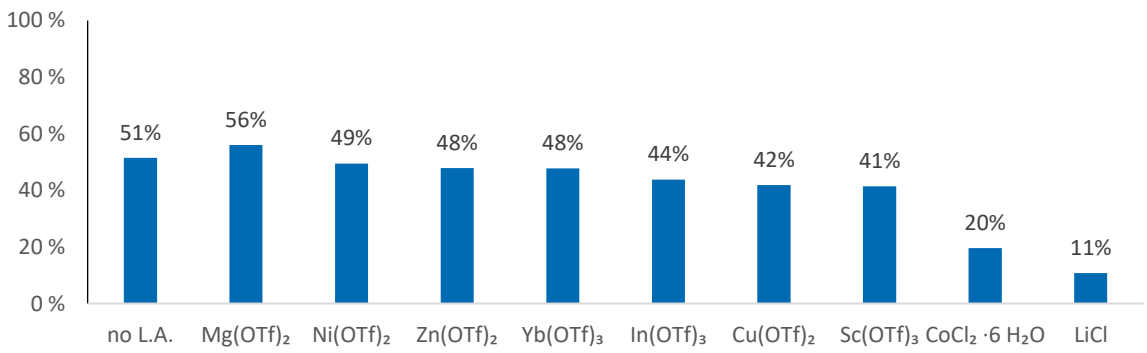

figure 39. Relative ratio of product **815** to substrate **812** signals after 48 h of irradiation.

The corresponding parameters and conversions determined by ^{1}H-NMR are summarized in **table 12**.

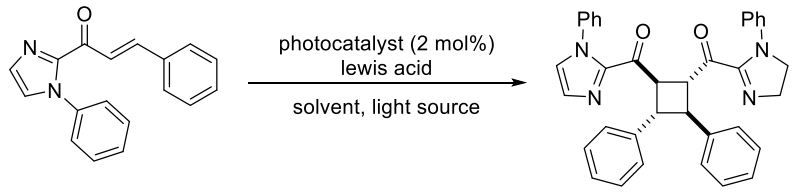

812 **815**

table 12. Parameters and conversions determined by ^{1}H-NMR after the indicated time intervals.

entry	photocatalyst	solvent	Lewis acid	conversion [%]					
				2 h	4 h	6 h	10 h	24 h	48 h
1	$[Ru(bpy)_3](PF_6)_2$	acetone	---	9	14	15	---	38	51
2	$[Ru(bpy)_3](PF_6)_2$	acetone	LiCl	5	7	8	---	10	11
3	$[Ru(bpy)_3](PF_6)_2$	acetone	$Mg(OTf)_2$	16	19	22	29	---	56
4	$[Ru(bpy)_3](PF_6)_2$	acetone	$Sc(OTf)_3$	8	12	10	---	28	41
5	$[Ru(bpy)_3](PF_6)_2$	acetone	$CoCl_2 \cdot 6\ H_2O$	---	4	5	---	13	20
6	$[Ru(bpy)_3](PF_6)_2$	acetone	$Ni(OTf)_2$	10	15	21	28	---	49
7	$[Ru(bpy)_3](PF_6)_2$	acetone	$Cu(OTf)_2$	---	---	10	17	---	42
8	$[Ru(bpy)_3](PF_6)_2$	acetone	$Zn(OTf)_2$	5	8	9	13	33	48
9	$[Ru(bpy)_3](PF_6)_2$	acetone	$In(OTf)_3$	12	15	17	24	---	44
10	$[Ru(bpy)_3](PF_6)_2$	acetone	$Yb(OTf)_3$	trace	6	12	17	34	48
11	$[Ru(bpy)_3](PF_6)_2$	THF	$Zn(OTf)_2$	8	10	12	19	36	---
12	$[Ru(bpy)_3](PF_6)_2$	CH_2Cl_2	$Zn(OTf)_2$	7	10	12	20	36	---
13	$[Ru(bpy)_3](PF_6)_2$	Benzol	$Zn(OTf)_2$	---	3	4	5	7	---
14	$[Ru(bpy)_3](PF_6)_2$	MeCN	$Zn(OTf)_2$	11	19	24	32	47	---
15	$[Ru(bpy)_2(BOX\text{-}bpy)](PF_6)_2$	acetone	$Zn(OTf)_2$	7	7	9	13	29	---

The results of the Lewis acid screening indicate that LiCl and $CoCl_2$ seem to quench the reaction (entry 2 & 5). In case of the cobalt additive, this could be attributed to the absorption at a similar wavelength. However, in case of LiCl, this is surprising given that the Yoon group used LiCl in several publications on similar reactions that are initiated by and based on the one electron reduction of lithium activated substrates to lithium enolate radicals.[11, 203, 210, 244, 245, 332] The greatest L.A. acceleration was observed using $Mg(OTf)_2$ (entry 3), which showed a conversion to product of 56% after 48 h. However, the increase of only about 5% compared to the reaction without Lewis acid is probably within the range of measurement uncertainties, as were the other results for the Lewis acids, which gave slightly lower conversions (entries 6, 8, 10). Overall, it appears the Lewis acids do not have a significant impact on the reaction rate, presumably because the background reaction is too fast without Lewis acid addition. This might also be caused by the large excess of acetone used as a solvent, which might have blocked coordination sides of the Lewis acids that are present only in catalytic amounts, thus making them unavailable for activation of the substrate. Therefore, a solvent screening was carried out using $Zn(OTf)_2$ (entries 11 – 14) (**figure 40**).

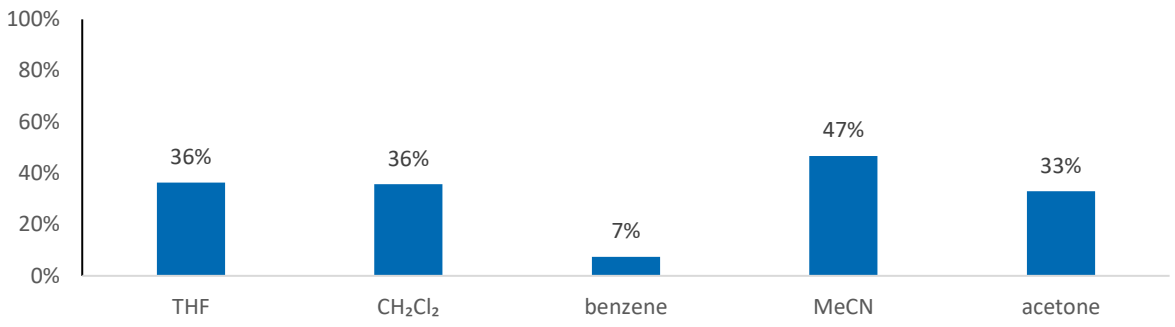

figure 40. Relative ratio of product **815** to substrate **812** signals after 24 h of irradiation in different solvents with $Zn(OTf)_2$.

While in THF and CH_2Cl_2 slightly higher conversions of 36% than in acetone (33%) were observed (entries 11 and 12), hardly any conversion was observed in benzene, which reflects the poor solubility of the reactants in benzene. However, a significant increase in reaction progress to 47% after 24 h (in acetone: 33%) was observed in MeCN (entry 14), rendering it the solvent of choice. At the end, an asymmetric BOX-substituted photocatalyst $[Ru(bpy)_2(BOX\text{-}bpy)](PF_6)_2$ (**532**) was used with $Zn(OTf)_2$ in acetone for a comparison of the photocatalytic activity, which showed a deceleration of 4% to 29% after 24 h only, which probably lies within measurement uncertainties (entry 15).

For further evaluation of the (2+2)-cycloaddition, reactions could be set up in the presence of the best Lewis acids ($Mg(OTf)_2$, $Ni(OTf)_2$, $Zn(OTf)_2$, $Yb(OTf)_3$) in MeCN and analyzed regarding the resulting enantiomeric excesses. In addition, modification of the substrate might contribute to a slower racemic background reaction, however, a background reaction is essential for suitability for comparison of the asymmetric bimetallic catalysts: In contrast to the system of Yoon *et al.* in which no competitive background reaction occurs without Lewis acid activation, a minor racemic background allows differentiation of the efficiency of the various catalysts **532**, **536** and **537**. Instead of 2-acylimidazoles, other arylenones could be evaluated. In addition, the phenyl residue on the Michael system could be exchanged for a methyl group, since the phenyl group in the β-position potentially stabilizes the intermediary formed radical **822** to such an extent that it possibly forms without prior activation of the substrate **812** and subsequent stabilization by a Lewis acid, whereas this would be less likely with a substrate **823** containing a methyl group at the β-position (**scheme 106**).

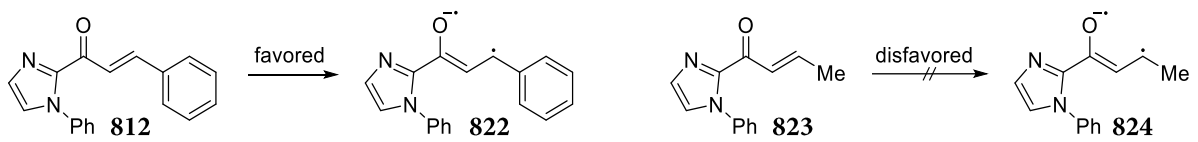

scheme 106. Possible cause for the fast racemic background reaction and potential substrate optimization for slower background reaction.

The transformation with the alternative substrate **823** and screenings under the proposed reaction conditions were not tested, since an alternative reaction - the aerobic oxidation - showed the breakthrough required for the evaluation of the photocatalysts **532**, **536** and **537** in the meantime (chapter 3.4.5).

3.4.5 Aerobic oxidation of β-ketoester **511**

After both the attempt to adapt literature known racemic photoredox reactions enantioselectively and to reproduce a literature known enantioselective reaction using a system of BOX **613** and $[Ru(bpy)_3]^{2+}$ (**7**) were unsuccessful, further approaches focused on the reproduction of an enantioselective photoredox reaction by Xiao *et al.*, which is based on a bifunctional combination of covalently linked thioxanthone photocatalyst substructure with BOX-L.A fragment **510** for asymmetric induction.[243] Assuming the photocatalyst core of the bimetallic asymmetric photocatalysts **532**, **536** and **537** is able to initiate similar reactivity as the thioxanthone fragment of Xiao *et al.*, comparable enantiomeric excesses should be accessible due to the identical asymmetric fragment (**figure 41**).

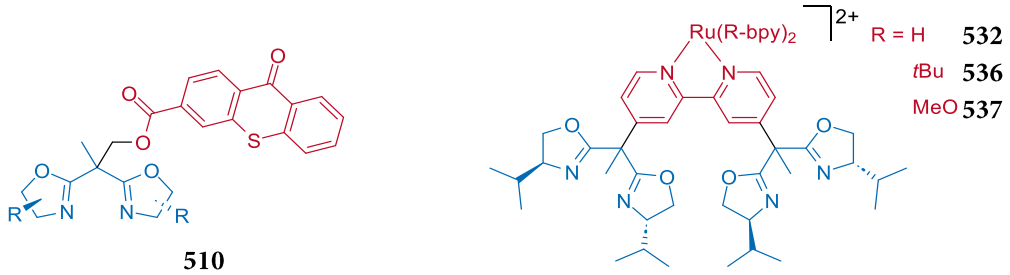

figure 41. Comparison of Xiao *et al.* bifunctional thioxanthone-BOX photocatalyst **510** with heteroleptic complexes **532**, **536** and **537**.[243]

The catalyst structure **510** of the Xiao group is inspired by the first example of a bifunctional chiral hydrogen bonding thioxanthone photocatalyst **322** developed by Bach *et al.* that initiated highly enantioselective intramolecular (2+2)-cycloadditions by energy transfer to 4-(pent-4-enyl)quinolones **323** and heteroatom analogues (**equation 41**).[218]

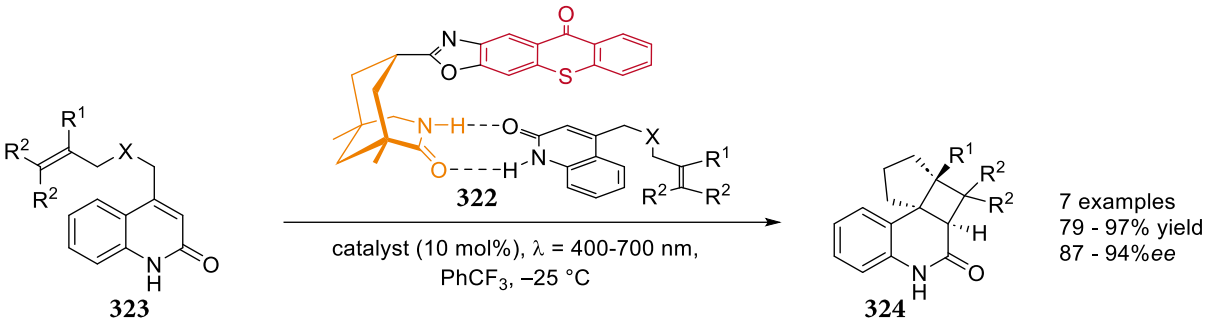

equation 41. Bifunctional thioxanthone photocatalyst **322** for enantioselective (2+2)-cycloadditions according to Bach *et al.*[218]

Instead of the hydrogen bonding moiety, the Xiao group linked their thioxanthone photosensitizer **510** by esterification of the corresponding acid with various hydroxymethyl bisoxazolines containing different residues (indanoyl, *i*Pr, *t*Bu, Ph, Bn, biphenyl) *via* the bridging atom of the bisoxazolines.[243] With this linkage to the photocatalyst and the methyl group at the same position, there is a strong similarity to the linkage in the BOX-substituted ruthenium complexes **532**, **536** and **537**. The linkage was intentionally made at this position as it was shown that substituents at the bridging atom improve stereocontrol.[243, 333] In the case of the ruthenium catalysts **532**, **536** and **537**, the substituents additionally serve to avoid conjugation with the bipyridine and thereby alter

the photophysical properties. In the reaction by Xiao *et al.* the bifunctional catalysts were used for the enantioselective aerobic oxidation of β-ketoesters **511**, more specifically for their α-hydroxylation (**scheme 107**).[243]

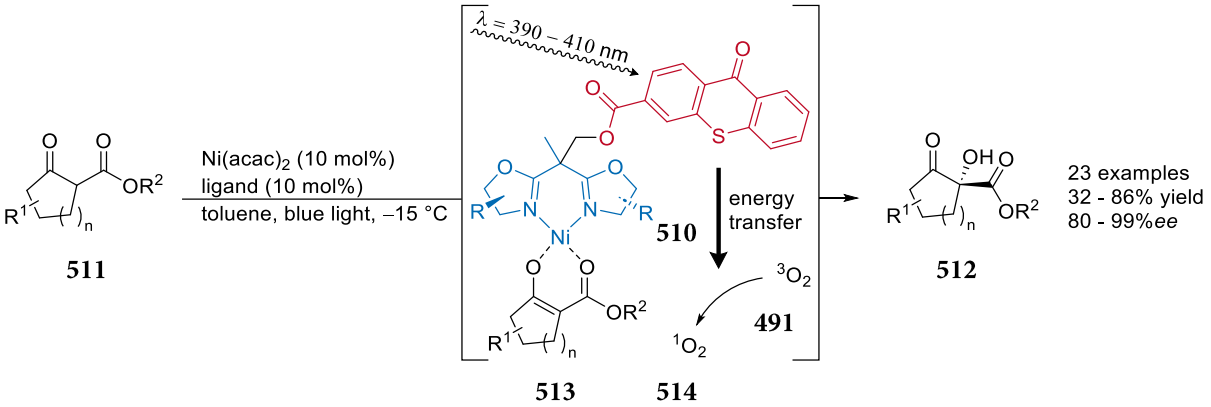

scheme 107. Enantioselective aerobic oxidation of β-ketoester **511** according to Xiao *et al.*[243]

Control experiments for the elucidation of the mechanism have shown that neither energy transfer nor electron transfer to the substrate **511** are dominant in this reaction. Instead, it was observed that the singlet oxygen (**514**) quencher DABCO decreased the yield of the reaction, while the reaction is accelerated in deuterated solvent (wherein the lifetime of singlet oxygen (**514**) is increased).[243] Therefore, it can be assumed that the thioxanthone structure acts as a photosensitizer and generates singlet oxygen (**514**) upon excitation with visible light by energy transfer to atmospheric oxygen (**491**). The Xiao group provides several mechanistic proposals to explain the observed reactivity, either involving energy transfer to triplet oxygen (**491**) with formation of singlet oxygen (**514**) and subsequent conventional two-electron mechanisms, or proceeding along more photoredox-typical one electron pathways.[243] The different proposals differ mainly in the formation of an asymmetric α-hydroperoxide **830**, which is believed to subsequently serve as an oxidant for an asymmetrically-coordinated metal enolate **828**, leading to the formation of the product **512**. Mechanistically, the pathway involving energy transfer begins with the exchange of an acetylacetonate ligand for a substrate molecule that is deprotonated by the acetylacetonate anion, generating the central metallenolate key intermediate **828**, which can react in two ways. The metallenolate **828** can react with singlet oxygen (**514**) previously formed by the thioxanthone photosensitizer in an ene reaction to form a metal-bound peroxide **830**, which is exchanged for a new substrate molecule **511** after proton transfer, generating an α-hydroperoxide while regenerating the central metallenolate intermediate **828** (left cycle). Following the right cycle, the double bond of the enolate **828** is epoxidized by the hydroperoxide **830**, whereby the first equivalent of product **512** is formed. Epoxide **831** is subsequently opened, protonated to the alcohol **512** by the acetylacetone **825** released in the first step, and exchanged for acetylacetonate to liberate another chiral α-hydroxy alcohol product **512**, whereby the initial PS-BOX-Ni(acac)$_2$ complex **827** is regenerated (right cycle) (**scheme 108**). Alternatively, the hydroperoxide **830** might be generated by two consecutive single electron oxidations, first an electron transfer from Ni(II) to the photoexcited thioxanthone and then from the enolate to Ni(III), leading to the formation of a metal-bound α-carbonyl radical **833**. After recombination with triplet oxygen (**491**) and single-electron reduction, the asymmetric α-peroxide **829** is formed, which reacts analogously

to the cycle on the right of the above mechanism to give the product **512** (**scheme 109**). However, the redox potential of the nickel complex is too high (+1.78 V vs. SCE) to be oxidized by the excited thioxanthone, making this pathway rather unlikely.[243]

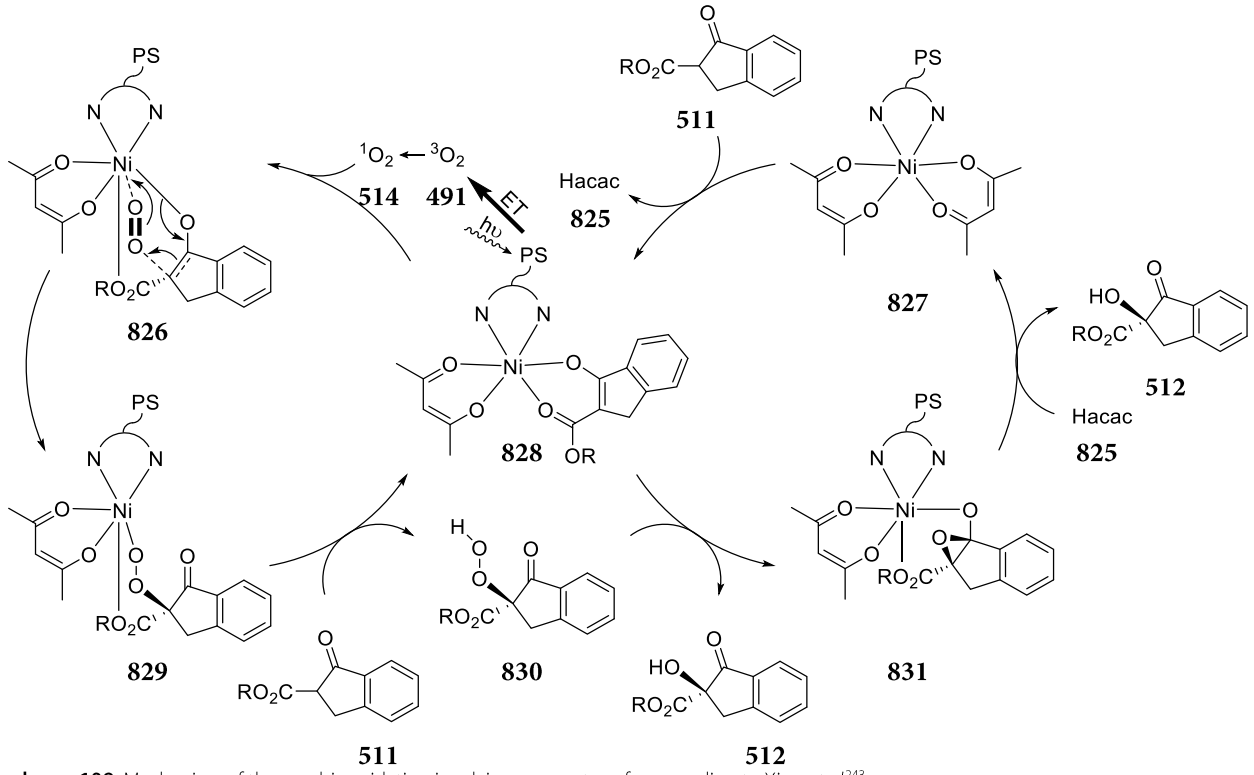

scheme 108. Mechanism of the aerobic oxidation involving energy transfer according to Xiao *et al.*[243]

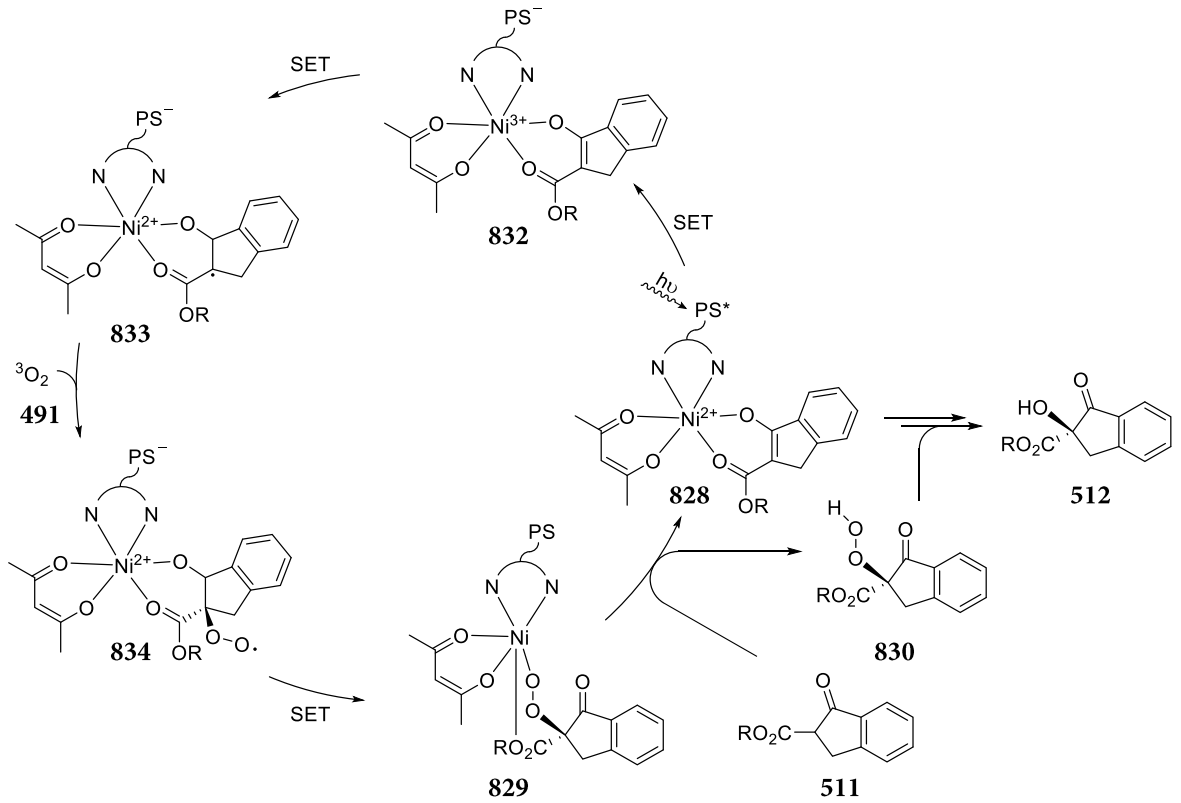

scheme 109. Mechanism of the aerobic oxidation involving SETs according to Xiao *et al.*[243]

Whichever route the formation of the hydroperoxide **830** ultimately takes, this method was used to accomplish enantioselective α-hydroxylations of 21 examples with enantiomeric excesses of up to 95%*ee*.[243]

A Lewis acid screening in CH_2Cl_2 revealed $Ni(acac)_2$ as the most promising Lewis acid (88% yield, 33%*ee*). A solvent switch to toluene increased the enantiomeric excess to 64%*ee*. Screening of the BOX library gave the highest enantiomeric excess of 73%*ee* with biphenyl-BOX. By changing the substrate to adamantyl instead of *i*Pr esters, the yield was increased to 97% and an excellent enantiomeric excess of 95%*ee* was obtained. Not only the ester group and the substituents on the BOX fragment are important for the high enantioselectivity, but also the remaining acetylacetonate substituent contributes to the fixation of the substrate **511** in the chiral environment of the Ni-BOX complex, as shown in **figure 42**. In this way, the *Si* side of the enolate is blocked by the phenyl groups of the rear oxazoline ring and the reaction with singlet oxygen (**514**) or the intermediately formed hydroperoxide **830** occurs from the *Re* side.[243]

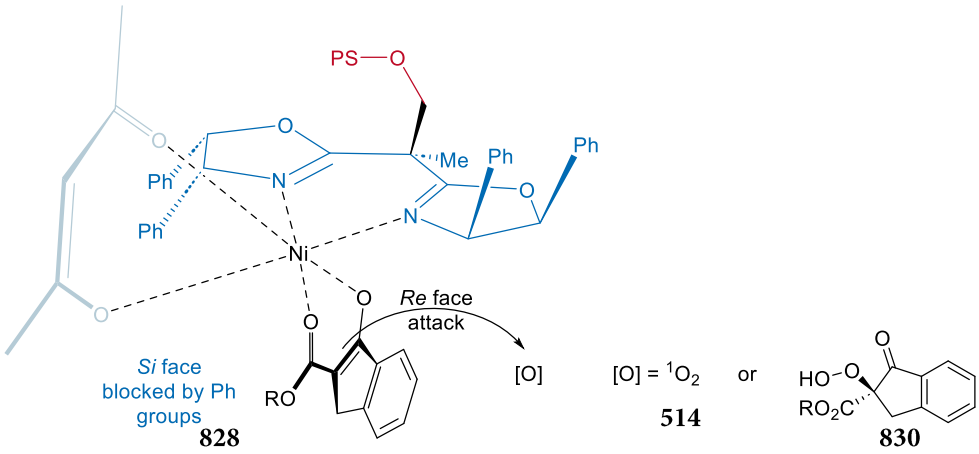

figure 42. Proposed asymmetric induction model according to Xiao *et al.*[243]

Using *i*Pr-BOX, a maximum yield of 73% was observed with an enantiomeric excess of –70%*ee*, which are the values for comparison with the efficiency of the BOX substituted $Ru(bpy)_3$ analogues **532**, **536** and **537**. The reverse configuration of the α-hydroxylated product **512** is due to use of BOX with inverted stereocenters. Although the most common application of $Ru(bpy)_3$-type catalysts today is in photoredox catalysis, its ability to serve as a triplet sensitizer for singlet oxygen (**514**) generation is also well known and the likelihood of similar reactivity with $[Ru(bpy)_3]^{2+}$ (**7**) core is high.[51] Since the asymmetric BOX fragment is suitable for controlling the stereochemical outcome of this reactivity, this reaction is a promising model reaction for the evaluation of the catalysts **532**, **536** and **537**. To verify this, the β-ketoester **511** that was used by Xiao *et al.* under comparable conditions, i.e. using *i*Pr-BOX, was synthesized (**scheme 110**). Starting from dihydroindenone **835**, the formation of the methyl β-keto ester **837** by deprotonation in the α-position and reaction with dimethyl carbonate **836** succeeded in a very good yield of 85%. Subsequent transesterification with isopropanol **838** succeeded under catalysis of dibutyltin oxide in good yield of 72%, paving the way for a screening of reaction parameters, the results of which are summarized in **table 13**.[334]

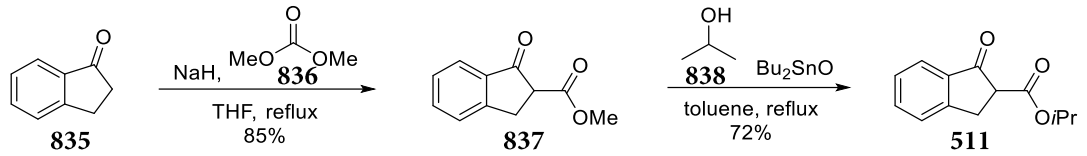

scheme 110. Synthesis of the isopropyl 1-oxo-2,3-dihydro-1*H*-indene-2-carboxylate (**511**) for the aerobic oxidation.

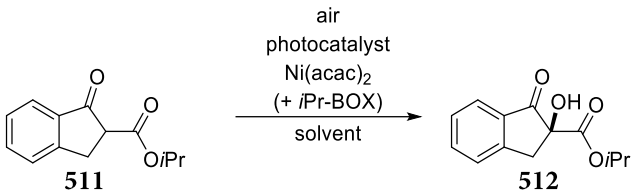

table 13. Parameters and results of the asymmetric aerobic oxidation of isopropyl 1-oxo-2,3-dihydro-1H-indene-2-carboxylate (**511**).

entry	photocatalyst	*i*Pr-BOX, Ni(acac)$_2$ [mol%]	Ni(acac)$_2$ [mol%]	solvent	t [h]	yield [%]	*ee* [%]
1	[Ru(bpy)$_3$](PF$_6$)$_2$	10	---	toluene	24	71	60
2	[Ru(bpy)$_3$](PF$_6$)$_2$	5.0	---	toluene	24	70	63
3	[Ru(bpy)$_3$](PF$_6$)$_2$	2.5	---	toluene	48	42	57
4	[Ru(bpy)$_3$](PF$_6$)$_2$	1.2	---	toluene	48	84	50
5	[Ru(bpy)$_3$](PF$_6$)$_2$	1.0	---	toluene	48	62	53
6	[Ru(bpy)$_3$](PF$_6$)$_2$	0.80	---	toluene	48	82	52
7	[Ru(bpy)$_3$](PF$_6$)$_2$	0.60	---	toluene	48	82	48
8	[Ru(bpy)$_2$(BOX-bpy)](PF$_6$)$_2$	---	0.81	toluene	48	89	17
9	[Ru(*t*Bu-bpy)$_2$(BOX-bpy)](PF$_6$)$_2$	---	0.77	toluene	48	30	21
10	[Ru(MeO-bpy)$_2$(BOX-bpy)](PF$_6$)$_2$	---	0.69	toluene	48	55	35
11	[Ru(bpy)$_3$](PF$_6$)$_2$	2.5	---	Cl-C$_6$H$_5$	48	92	32
12	[Ru(bpy)$_3$](PF$_6$)$_2$	2.5	---	CHCl$_3$	48	38	49
13	[Ru(bpy)$_3$](PF$_6$)$_2$	2.5	---	THF	48	6	10
14	[Ru(bpy)$_3$](PF$_6$)$_2$	2.5	---	acetone	48	67	32
15	[Ru(bpy)$_3$](PF$_6$)$_2$	2.5	---	MeCN	48	98	24
16	[Ru(MeO-bpy)$_2$(BOX-bpy)](PF$_6$)$_2$	---	2.5	acetone	48	65	25
17	[Ru(MeO-bpy)$_2$(BOX-bpy)](PF$_6$)$_2$	---	2.5	MeCN	48	43	11

The reaction was initially carried out in analogy to Xiao *et al.* using 10 mol% of the separated catalyst system consisting of [Ru(bpy)$_3$](PF$_6$)$_2$ (**7**), *i*Pr-BOX **613** and Ni(acac)$_2$. Encouraged by a clean conversion to α-hydroxy-β-ketoester **512** and an isolated yield of 71% with an enantiomeric excess of 60%*ee* (entry 1), an optimization process began in which the influence of *i*Pr-BOX **613** and Ni(acac)$_2$ loading on the resulting enantiomeric excess was mainly evaluated (entries 2 - 7), since the ultimate focus was the comparison of the

different asymmetric catalysts and not the maximization of the enantiomeric excess, and the amount of catalyst used for this purpose should be kept as low as possible (less than 10 mol%). In addition, this results in a calibration curve, which allows for better comparison of results for which the intended catalyst amount could not be weighed accurately enough. The calibration curve and a graphical representation of the other results are shown in **figure 43**.

figure 43. Graphical representation of the dependency of the enantiomeric excess on asymmetric catalyst loading, along with other screening results of both the separate catalyst system (blue) and the bimetallic asymmetric photoredox catalysts **532** (green), **536** (yellow) and **537** (red) in different solvents.

The dependence of the enantiomeric excess on catalyst loading is indicated clearly by the blue calibration curve of mixtures of different loadings of catalyst in toluene, although presumably an outlier using 1.2 mol% asymmetric Lewis acid complex yielded only 50%*ee* (entry 4) lowering the coefficient of determination of the implied regression. The somewhat lower enantiomeric excess at a catalyst loading of 10 mol% of 60%*ee* (entry 1) compared to the result of 63%*ee* for 5.0 mol% (entry 2) is probably due to measurement uncertainties, indicating that a maximum enantiomeric excess of about 60%*ee* is accessible using the available photoreactor, whose temperature cannot be regulated but which is equipped only with an air flow to avoid heat-up caused by the LEDs to a temperature above about 32 °C. Xiao *et al.* carried out the reaction at −10 °C and achieved an enantiomeric excess of 70%*ee*, with a yield of 73%, using their bifunctional photocatalyst containing *i*Pr-BOX.[243] Considering the high temperature difference of more than 40 °C, the enantiomeric excess lower by only 10%*ee* is a promising result.

The calibration curve also illustrates that further decreasing the catalyst loading to 1.0 mol% resulted in a significant decrease in enantiomeric excess by about 7%*ee* to 53%*ee*, a value large enough for comparison of the bifunctional complexes, while saving catalyst amount (entry 5). Therefore, to evaluate $[Ru(bpy)_2(BOX\text{-}bpy)](PF_6)_2$ (**532**), $[Ru(tBu\text{-}bpy)_2(BOX\text{-}bpy)](PF_6)_2$ (**536**) and $[Ru(MeO\text{-}bpy)_2(BOX\text{-}bpy)](PF_6)_2$ (**537**) the amount of catalyst complex and Lewis acid ($Ni(acac)_2$) calculated for a 1.0 mol% reaction was weighed into a septum-vial and the mixture was stirred in toluene for 30 min under nitrogen and light exclusion, to ensure coordination of the Lewis acid to the BOX fragments. The β-ketoester **511** was added, the septum caps of the vials were removed and the irradiation in the photoreactor was started. After addition of the substrate **511**, the corresponding syringes were weighed again, and the balance showed negative masses in all three experiments, although the balance had previously been tared to a syringe the dead volume of which had been filled with substrate **511**. Accordingly, since a slightly higher amount of substrate **511** was added in all approaches, there was no loading of exactly 1.0 mol% in any of the approaches. The actual loadings of $[Ru(bpy)_2(BOX\text{-}bpy)](PF_6)_2$ (**532**), $[Ru(tBu\text{-}bpy)_2(BOX\text{-}bpy)](PF_6)_2$ (**536**) and $[Ru(MeO\text{-}bpy)_2(BOX\text{-}bpy)](PF_6)_2$ (**537**), were instead 0.81 mol%, 0.77 mol% and 0.69 mol%, respectively (entries 8 - 10). The resulting enantiomeric excesses of 17%*ee*, 21%*ee* and 35%*ee* are not directly comparable to the enantiomeric excess of 53%*ee* from the use of 1.0 mol% of the separate system due to the dependence of the enantiomeric excess on the catalyst loading, which is clearly evident on the separate system. However, when compared to the calibration curve, an enantiomeric excess of about 50%*ee* (instead of 35%*ee*) should have been obtained with the bifunctional methoxy catalyst loaded at 0.69 mol% for a stereoinduction similar in efficiency to that of the separate system. The inferior performance of the asymmetric catalyst complexes **532**, **536** and **537** could possibly reflect differences in solubility of the catalysts in the previously used solvent toluene. Neither $[Ru(bpy)_3](PF_6)_2$ (**7**) from the separate catalyst system nor the asymmetric bimetallic catalyst complexes **532**, **536** and **537** showed good solubility in toluene and all the approaches rather resembled turbid suspensions than clear solutions. Based on the size difference of the separated catalyst system and asymmetric catalysts **532**, **536** and **537** alone, poorer solubility of the latter can be assumed. This could be a reason for the much lower enantiomeric

excesses obtained. The actual catalyst loading in solution therefore remains uncertain for the reactions carried out in toluene. Therefore, a solvent screening ($CHCl_3$, Cl-benzene, acetone, MeCN, THF) was performed using the separate system with 2.5 mol% of each photocatalyst **7** and chiral Lewis acid (entries 11 - 15). In chlorobenzene, $CHCl_3$ and THF, the reaction mixture was rather turbid (similar to the approaches in toluene), due to incomplete dissolution of the photocatalyst **7** and accompanied by a distorted ratio of photocatalyst **7** and chiral Lewis acid in solution. In acetone and MeCN, the reaction mixture was a clear, intense red solution. In THF, the conversion was incomplete after 48 h and many byproduct spots were indicated; the enantiomeric excess of only 10%*ee* was also far below the values obtained in other solvents. The highest enantiomeric excess (49%*ee*) was obtained in $CHCl_3$, which, however, was lower than the comparative value in toluene (57%*ee*). It is noteworthy that the apparently better solubility in acetone and MeCN leads to poorer enantiomeric excesses. Presumably, the photocatalyst **7** is only partially dissolved in the other approaches and the relative ratio of BOX complex to photocatalyst **7** is higher, causing more BOX-L.A. substrate complexes to be converted by the traces of dissolved photocatalyst **7**. By completely dissolving the photocatalyst **7**, the ratio approaches 1:1 and relatively more racemic background reactions can occur. The stereoinduction of separated and combined systems can only be compared when both systems are completely dissolved, on the one hand because less catalyst is present due to the assumed lower solubility of the bimetallic system, resulting in a lower *ee* due to the quantity dependence of the enantiomeric excess, and on the other hand since the ratio of BOX-LA substrate complex and photocatalyst **7** in the separated system otherwise differs from the fixed ratio (2:1) in the combined system **532**, **536** and **537**.

The comparison of the separate system **7** with the bifunctional catalysts **532**, **536** and **537** must therefore be performed in acetone or MeCN. Using the catalyst $[Ru(MeO\text{-}bpy)_2(BOX\text{-}bpy)](PF_6)_2$ (**537**) which performed best in toluene for photoreactions in acetone and MeCN gave 25%*ee* and 11%*ee*, respectively (entries 16 & 17). These values are 11% and 13% lower, respectively, than the enantiomeric excesses obtained with the separate catalyst system. This deviation, and thus the difference in the efficiency of stereoinduction between the bifunctional and the separated system, is much smaller in case of complete solution, i.e. in MeCN or acetone, than the deviation of the enantiomeric excesses obtained in toluene, confirming the above assumptions on the influence of solubility on enantioselectivity. A possible explanation for the lower selectivity despite complete solubility could be the distance dependency of both single electron transfer and energy transfer. Mechanistically, unlike in the other photoreactions, the reaction does not involve electron transfer to a substrate molecule **511** coordinated in the chiral BOX environment, but instead involves the generation of singlet oxygen (**514**). Studies on the generation of singlet oxygen (**514**) with $[Ru(bpy)_3]^{2+}$ (**7**) and analogues have shown that this occurs either by energy transfer to triplet oxygen (**491**) or by reduction to the superoxide radical anion and subsequent oxidation of the same.[51] Both processes are strongly distance-dependent. Given this distance dependency, a review of the heteroleptic catalyst structures **532**, **536** and **537** suggests that the lower enantiomeric excesses may be the result of steric shielding of one side of the catalyst in terms of enlargement of the distance towards dissolved $^3O_2$ due to the attached BOX-fragments: Presumably, the distance is increased to such an extent that no competitive concentrations of singlet

oxygen (**514**) is formed compared to the achiral catalyst backbone, and thus the substrates bound in a chiral environment have no reaction partner, resulting in a smaller reaction rate constant of the enantioselective transformation. In contrast, the distance between the photoredox active core and the triplet oxygen (**491**) is much smaller on the backside, which presumably leads to an enrichment of $^1O_2$, so that substrate molecules **511** on this side of the catalyst can react through the ene-reaction to the α-hydroperoxide and ultimately to the racemic product, despite the lack of activation through *i*Pr-BOX-Ni coordination. Indeed, a control experiment in the absence of $Ni(acac)_2$ proved that the reaction yields the racemic product in very good yields.

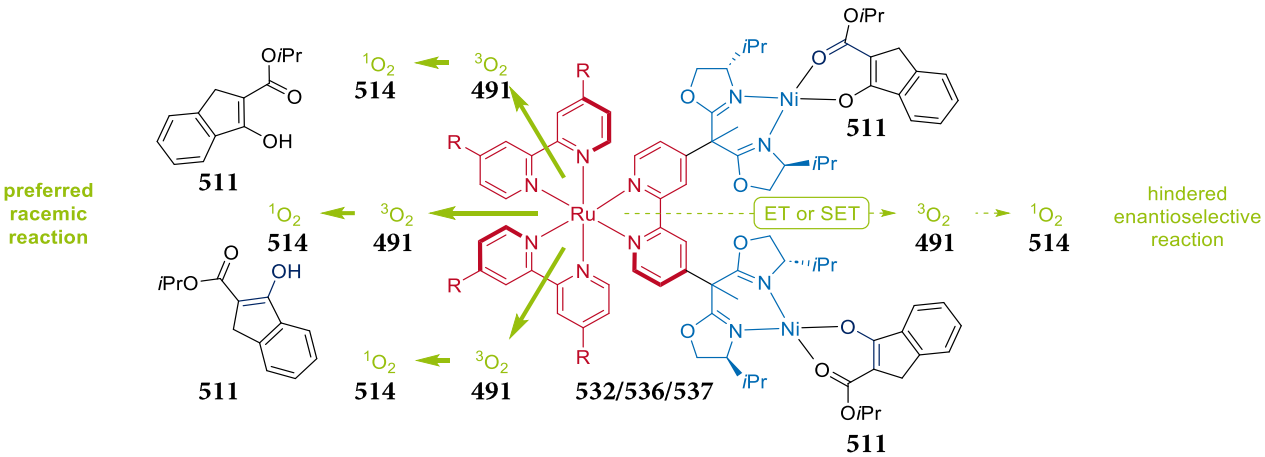

figure 44. Illustration of distances and associated probability for efficient singlet oxygen (**514**) formation by energy transfer or single electron transfer in the bifunctional heteroleptic catalysts **532**, **536** and **537**.

This contrasts the separated catalyst system, for which enantiomeric excesses of > 48%*ee* were obtained when the calibration curve was established, and even >50%*ee* with >0.80 mol% *i*Pr-BOX-Ni complex. Thus, in almost all reactions, the rate constant of the enantioselective transformation k_{en} was larger than the rate constant of the racemic transformation k_{rac}. In the separated system, the distance dependency is not a hindering factor for the enantioselective reaction because the *i*Pr-BOX-Ni substrate complexes are free to move just like uncoordinated substrates, and the probability of diffusing towards a side with elevated singlet oxygen concentration is comparable to free substrate (**figure 45**). The fact that k_{en} is greater than k_{rac} in these cases is eventually owing to the Lewis acid activation, which at 10 mol% accounts for only an acceleration to 1.5 times the racemic reaction constant (10 mol%: 60%*ee*, $k_{en} = 1.5\ k_{rac}$).

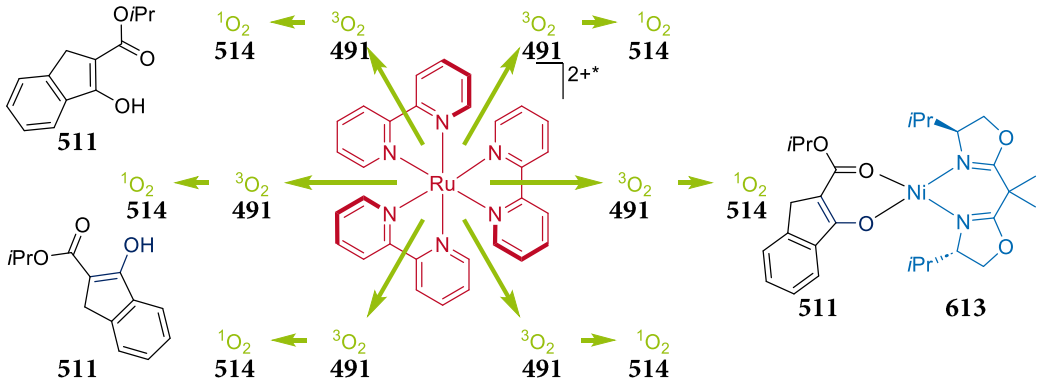

figure 45. Illustration of distances and associated probability for efficient singlet oxygen (**514**) formation by energy transfer or single electron transfer in the separate catalyst system.

The structure of the Xiao group's bifunctional catalyst is very similar to the BOX-substituted $[Ru(bpy)_3]^{2+}$-analogues **532**, **536** and **537**, yet there is a crucial difference that may be responsible for the fact that the Xiao group achieved fewer racemic background reactions resulting from the distance dependence of energy transfer and SET. The thioxanthone was esterified with hydroxymethyl-bisoxazolines, resulting in a longer but more flexible linker. Depending on the conformation of the linker, the distance between the photosensitizer and the asymmetrically coordinated reaction centre may vary. Conformational analysis considering stereoelectronic orbital interactions further suggests that the interaction of the antibonding orbital of the ester-methylene bond ($\sigma^*_{C\text{-}O}$) with the $\sigma_{C\text{-}C}$ bond between bridging atom and methyl group is energetically more favorable due to more similar orbital energies than an alignment of $\sigma^*_{C\text{-}O}$ parallel to the C-C bonds between bridging atom and the electron-deficient formimide-carbon atoms of the oxazoline rings (**figure 46**, left). In contrast, the linkage of the photoredox-active Ru complex to BOX occurs *via* a short and comparatively rigid C-C single bond which can rotate freely, but without forming a conformer in which the distance between the photoredox-active core and the asymmetric reaction centre is substantially reduced (**figure 46**, right).

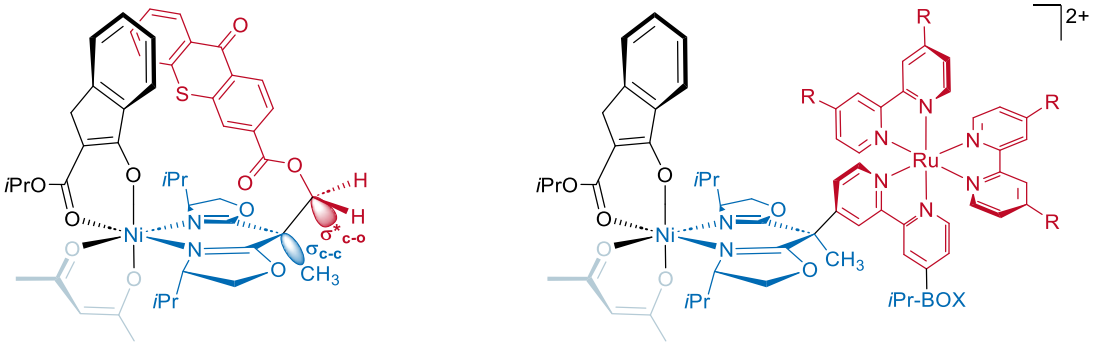

figure 46. Conformational analysis of the distance between photoredox active fragments and Ni-coordinated substrate in thioxanthone-BOX catalyst **510** and BOX substituted ruthenium complexes **532**, **536** and **537**.

Designing the linker between BOX and bipyridine as short as possible derives from the original goal to prepare a homoleptic bifunctional catalyst of the form $[Ru(BOX\text{-}bpy)_3](PF_6)_2$ (**542**). Due to the complete saturation of all spatial directions of the photoredox-active $[Ru(bpy)_3]^{2+}$ core with asymmetric BOX ligands and the distance dependence of energy transfer and single electron transfer, presumably only substrates in close proximity to the

asymmetric BOX sphere would have been converted and no competitive racemic excitation could have taken place on an achiral catalyst backbone. To ensure the most efficient excitation, or to make sure that the distance was not too great for excitation of substrates outside the asymmetric BOX sphere, the linkage of bipyridine and BOX was kept as short as possible. After the synthesis of the homoleptic complex **542** was unsuccessful and instead focus was placed on the synthesis of heteroleptic complexes of the form $[Ru(R\text{-}bpy)_2(BOX\text{-}bpy)](PF_6)_2$ (**532**, **536** and **537**) with different substituents in the backbone to shield this achiral side, the BOX-bpy ligand structure was not adapted to meet the challenges of the heteroleptic catalyst structure and instead the linkage *via* a C-C bond between the 4-positions of the bipyridine and the bridging atom of the BOX fragment was maintained. Perhaps a more efficient enantioselective transformation would be accessible by modifying the BOX-bpy linkage toward a more flexible linker.

Although the heteroleptic bimetallic catalyst complexes **532**, **536** and **537** did not achieve similar enantiomeric excesses as the separate system, the experimental results obtained allow a comparison of the influence of substituents in the achiral backbone. In addition to an unsubstituted complex (R = H, complex **532**) serving as a reference model, a sterically shielded complex (R = *t*Bu, **536**) and an electronically modified complex (R = MeO, **537**) were prepared and evaluated, yielding the enantiomeric excesses and rate constants calculated therefrom, which are summarized in **table 14** for direct comparison.

table 14. Ratio of enantiomers, enantiomeric excesses and rate constants calculated therefrom for the aerobic oxidation in toluene.

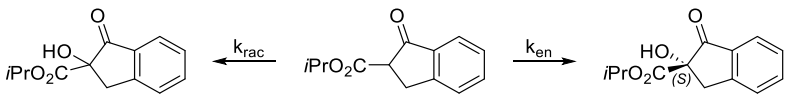

512 + ent-512 **511** **512**

catalyst	*R* : *S*	%*ee*	k_{rac} : k_{en}	k_{en}	Factor k_{en}(H)
$[Ru(bpy)_2(BOX\text{-}bpy)](PF_6)_2$	41.5 : 58.5	17	83 : 17	0.20 k_{rac}	x1.00
$[Ru(t\text{Bu-}bpy)_2(BOX\text{-}bpy)](PF_6)_2$	39.5 : 60.5	21	79 : 21	0.27 k_{rac}	x1.35
$[Ru(MeO\text{-}bpy)_2(BOX\text{-}bpy)](PF_6)_2$	32.5 : 67.5	35	65 : 35	0.54 k_{rac}	x2.70

Comparison of the enantiomeric excess of reference catalyst (R = H) of 17%*ee* with the sterically shielded catalyst **536** (R = *t*Bu) shows that the incorporation of the alkyl substituents leads to an increase in enantiomeric excess of only 4%, thus in the range of measurement uncertainties. Taking into account the helical arrangement of three bidentate bipyridine ligands around the octahedrally coordinated ruthenium centre and the remaining gaps, the *t*Bu residues employed might be too small for efficient sterical shielding of the achiral side (**figure 47**). Moreover, for efficient shielding, the steric demand of the residues on the side to be shielded should be larger than the *i*Pr-BOX fragments in order to preferentially allow the photoreaction to proceed on the chiral side.

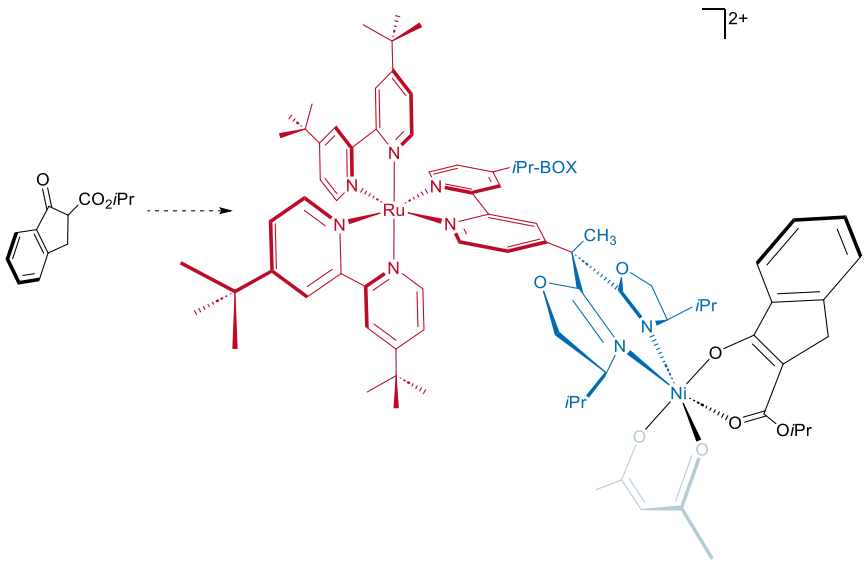

figure 47. Three-dimensional visualization of sterically unshielded gaps in the helical arrangement of the three bipyridine ligands around the octahedrally coordinated ruthenium centre.

The slightly elevated enantiomeric excess could be due to the electron-donating effect of the alkyl substituents and associated removal of the degeneracy of ligand-centred π^* orbitals, as it has been shown by photophysical and electrochemical measurements that the metal-centred dπ orbitals and the $\pi_{tBu\text{-}bpy}^*$ orbitals are energetically elevated, rendering the $\pi_{BOX\text{-}bpy}^*$ orbital the LUMO, which preferentially accepts the electron in the course of MLCT excitation (chapter 3.3).

A comparison of the reference catalyst **532** (R = H) with the electronically modified complex **537** (R = MeO) reflects the observed changes in orbital energies even more and extends the photophysically and electrochemically observed trends to the application in enantioselective catalysis. In fact, the enantiomeric excess of the MeO-catalyst **537** (35%*ee*) is more than twice as high as the enantiomeric excess of the reference catalyst **532** (17%*ee*). After conversion to ratios of the reaction constant k_{en} to k_{rac}, this difference corresponds roughly to an increase in the asymmetric reaction rate by a factor of 2.7. This increase may in fact be a result of electronic disfavoring of the MeO-substituted achiral bipyridine ligands, through energetic raising of the associated MeO-bipyridine centred π^* orbitals, while the energy of the π^* orbital of BOX-bpy remains almost unchanged, thereby causing MLCT excitation to preferentially proceed into orbitals on the BOX-substituted side and transformation to take place on the asymmetric catalyst side.

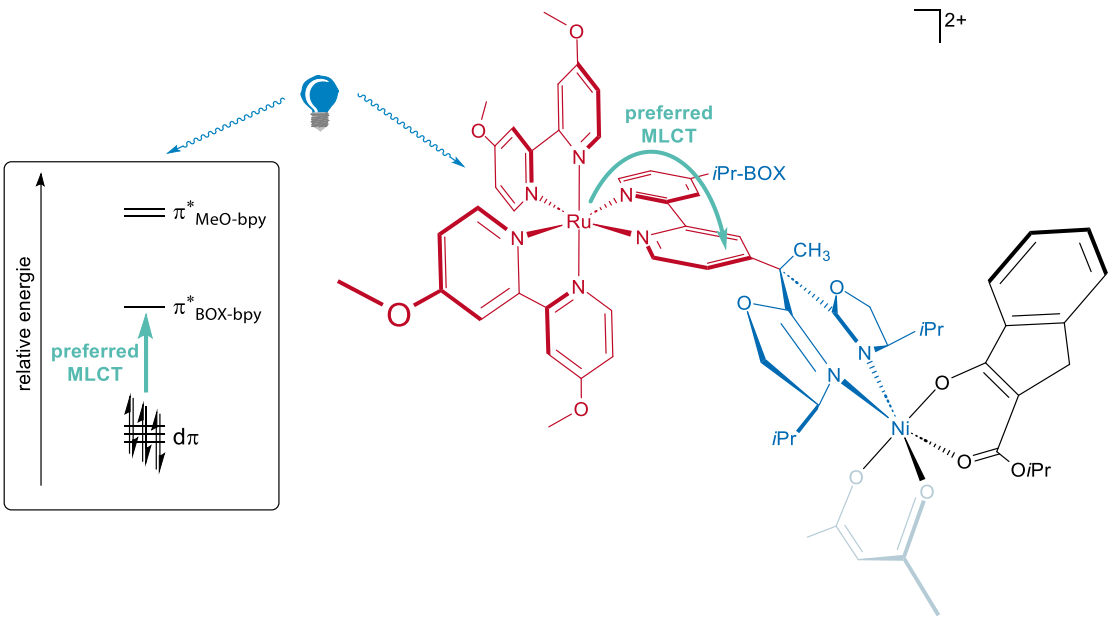

figure 48. Three-dimensional schematic visualization of the assumed concept of electronic disfavoring through modification of orbital energies.

Although the electronically modified heteroleptic complex **537** provided lower enantiomeric excesses than were accessible with the separate catalyst system, the concept of adjusting orbital energies and directing of the MLCT excitation on the desired asymmetric catalyst side was proven both theoretically by photophysical and electrochemical measurements as well as practically in enantioselective catalysis and it represents a fundamentally new and promising strategy in the toolbox of rational catalyst development.

4 Summary and outlook

The goal of this thesis was to synthesize and evaluate asymmetric bimetallic photoredox catalysts for combining photoredox reactivity with asymmetric Lewis acid catalysis in one chiral catalyst structure derived from the structure of the prototypical $[Ru(bpy)_3]^{2+}$ (**7**). For this purpose, three different synthetic strategies for linking a bipyridine ligand with an asymmetric bisoxazoline fragment were investigated (**scheme 111**).

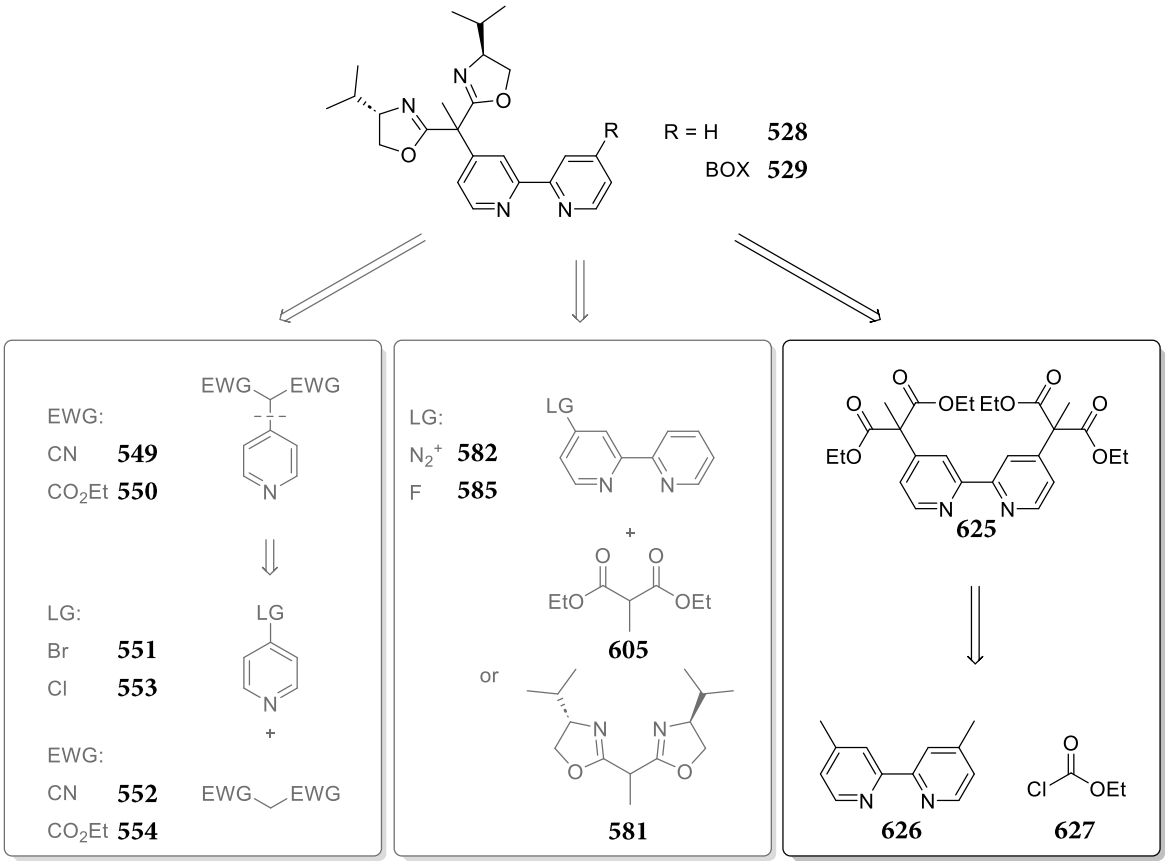

scheme 111. Overview of the evaluated synthetic strategies for linking a bipyridine ligand with an asymmetric bisoxazoline fragment. Left: *Via* substitution on 4-halopyridines (**551** and **553**) and coupling to another pyridine. Middle: *Via* nucleophilic aromatic substitution on diazo- or fluorobipyridine. (**582** and **585**) Right: *Via* side-chain functionalization of 4,4'-dimethylbipyridine **626**.

The linkage of a 2-malonyl fragment with a bipyridine turned out to be the major hurdle of all ligand syntheses, at which various approaches of aromatic substitutions failed (**scheme 111**, left & middle) and which was ultimately overcome by exploiting the heterobenzylic acidity of 4,4'-dimethylbipyridine **626** and side-chain functionalization thereof through benzylic acylation involving consecutive benzylic deprotonation and reaction with ethyl chloroformate (**627**) (**scheme 112**). Methylation at the benzylic α-position for the separation of the bipyridine and BOX fragment by preventing imine-enamine tautomerism occurred in very good yield (85%) and the subsequent formation of a tetra-γ-hydroxyamide **636** with L-valinol (**603**) also succeeded in an excellent yield (95%) despite the challenge of four reaction centres to be converted and repeatedly observed side reactions of decarboxylation, paving the way for the second key step of the synthetic route - the ring closure leading to the bisoxazoline **529**. Once again, a major challenge of this step arose from the requirement of four amide strands to undergo formal cyclodehydration, which was not selectively achieved following the rather conventional routes of converting the

terminal hydroxy groups into suitable leaving groups and intramolecular substitution. The Burgess dehydration reagent **619** enabled the most selective conversion to the BOX-bpy ligand **529** in good yield (75%). Starting from 4,4'-dimethylbipyridine **626**, the BOX-bpy ligand **529** was successfully synthesized in only four linear steps in an overall yield of 18% with the benzylic acylation being the bottle neck, due to difficulties in controlling the degree of substitution. Besides the low number of steps, another remarkable feature of the developed pathway is the simplicity of purification of all reaction products by precipitation, eliminating the need for time-consuming and uneconomical purification by column chromatography and rendering the ligand synthesis straightforward and easily scalable (**scheme 112**).

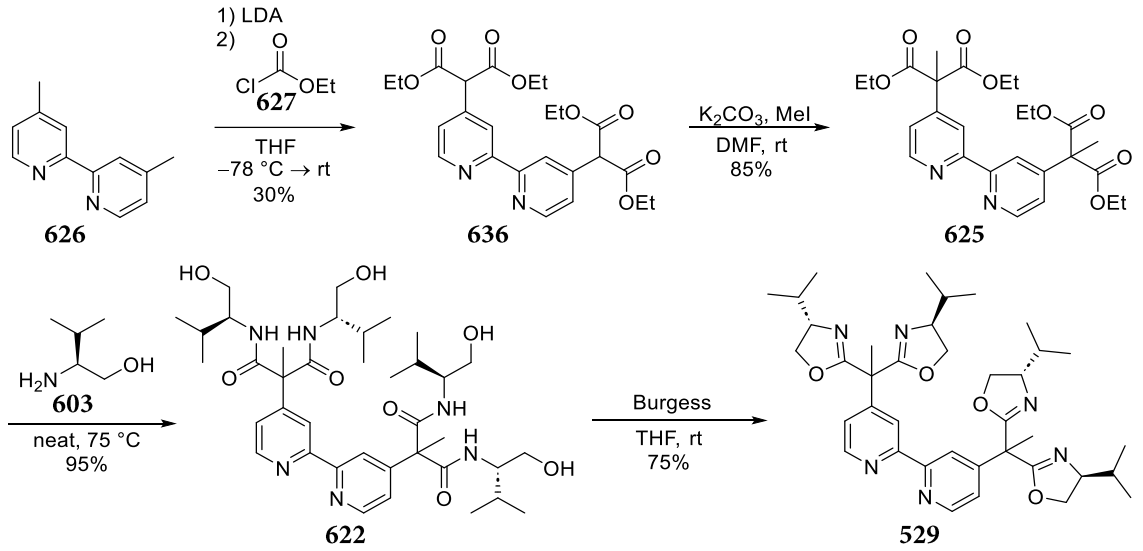

scheme 112. Synthetic route for the synthesis of BOX-bpy **529** from dimethylbipyridine **626** by side-chain functionalization.

Attempts to exploit the potential of the route for diversification and to vary the residue of the bisoxazoline fragments by employing L-phenylalaninol (**604**) instead of L-valinol (**603**) led in several approaches in different solvents and neat in the molten amino alcohol **604** only to side products from decarboxylation.

After successful ligand synthesis, initial complexation approaches focused on the synthesis of a homoleptic complex of the form $[Ru(BOX\text{-}bpy)_3]^{2+}$ (**542**). Thereby, both conventional synthetic strategies, using $RuCl_3$ x H_2O (**676**) under reducing conditions, as well as approaches starting from the ruthenium(II) precursor complex *cis,fac*-$RuCl_2$(dmso-*S*)$_3$(dmso-*O*) (**679**), were evaluated, however only the addition of two BOX-bpy ligands **529** leading to the formation of precursor complexes of the form $Ru(BOX\text{-}bpy)_2(X)(Y)$ with mixed ligands X and Y of varying composition of Cl, H_2O or dmso were identified by mass spectrometry. Furthermore, in all mass spectrometric analyses, multiple sets of peaks with ruthenium-typical splitting patterns were observed at much higher masses than that of the desired homoleptic complex **542**, which was attributed to the triple bidentate ligand structure and therefore conceivable formation of BOX-bridged multinuclear clusters. To overcome this problem, an ^{1}H-NMR study was performed, revealing the tendency of Zn(II) to preferentially saturate the BOX fragments prior to coordination to bipyridines, which became the basis for a complexation experiment in the presence of Zn(II) for blocking the BOX fragments, which, however, neither led to the selective formation of

$[Ru((OTf)_2Zn\text{-}BOX\text{-}bpy)_3]^{2+}$ (**691**) nor $[Ru(BOX\text{-}bpy)_3]^{2+}$ (**542**). Another evaluated synthetic strategy for the homoleptic complex **542** was the approach of constructing the BOX fragments by side-chain functionalization starting from precursor complexes containing intermediates **626** and **625** from the BOX-bpy **529** synthesis as ligands. Considering that one difficulty of the BOX-bpy **529** synthesis was to ensure conversion at four reaction centres, and that in several experiments the formation of side products due to decarboxylation was observed, it is not surprising that both owing to the increased number of 12 reaction centres in a complex bearing three ligands as well as the increased risk of decarboxylation reactions due to Ru coordination, the homoleptic complex **542** was not accessible in this way either. The synthesis of the homoleptic complex $[Ru(BOX\text{-}bpy)_3]^{2+}$ (**542**) was therefore not pursued further and instead a new concept of heteroleptic complexes of the form $[Ru(R\text{-}bpy)_2(BOX\text{-}bpy)]^{2+}$ was developed, the complexes synthesized and evaluated both by photophysical and electrochemical measurements as well as in enantioselective photoredox transformations.

In contrast to the homoleptic catalyst $[Ru(BOX\text{-}bpy)_3]^{2+}$ (**542**), whose photoredox-active core is completely surrounded by asymmetric BOX fragments, causing substrates to react preferentially in the chiral environment given the distance dependency of both electron and energy transfer, the heteroleptic complexes **532**, **536** and **537** poses an increased risk of racemic background reactions on the achiral sides of the catalysts. Besides the simplest heteroleptic complex $[Ru(bpy)_2(BOX\text{-}bpy)]^{2+}$ (**532**), which allows investigations on the change of photophysical properties resulting from the incorporation of BOX and provides insights on the competition of racemic background reactions, two further heteroleptic complexes, $[Ru(t\text{Bu-}bpy)_2(BOX\text{-}bpy)]^{2+}$ (**536**) and $[Ru(MeO\text{-}bpy)_2(BOX\text{-}bpy)]^{2+}$ (**537**), were synthesized, which on the one hand embody the common concept of steric and on the other hand the fundamentally new concept of electronic disfavoring of the achiral catalyst side. The synthesis of the heteroleptic complexes **532**, **536** and **537** succeeded in moderate yields (46% - 60%) starting from the corresponding precursor complexes (**717**, **701**, **702**) of the form $Ru(R\text{-}bpy)_2Cl_2$ by abstraction of the chlorido ligands with a silver salt thereby forming a solvate complex which readily allowed the incorporation of BOX-bpy **529** under mild conditions (**equation 42**).

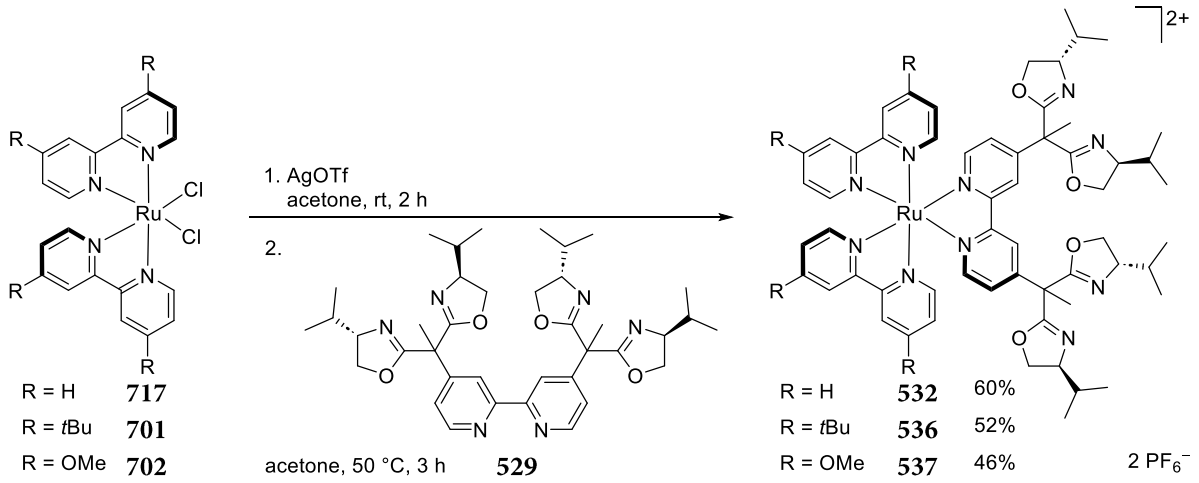

equation 42. Synthesis of heteroleptic complexes **532**, **536** and **537** from $Ru(R\text{-}bpy)_2Cl_2$ (**717**, **701**, **702**) by chloride abstraction with silver triflate.

The heteroleptic complexes complexes **532**, **536** and **537** were subjected to photophysical and electrochemical measurements to explore the influence of BOX incorporation, determine the redox potentials of their excited states and, in particular, to investigate the envisioned concept of electronic disfavoring of an achiral catalyst side. The idea of electronic disfavoring is based on the broadly accepted concept of localized MLCT states and aims at exploiting the systematic raising of the orbital energies of the achiral ligands, causing visible light irradiation and ISC to preferably form a long-lived ^{3}MLCT state in which the excited electron is localized on the ligand that is easiest to reduce, e.g. on the BOX-substituted catalyst side. Absorption and emission spectra of the heteroleptic complexes **532**, **536** and **537** exhibited similar transitions as found for the literature-known $[Ru(bpy)_3]^{2+}$ (**7**). The different band shapes, the lack of mirror symmetry and the lifetimes confirmed that absorption and emission originate from different states. Moreover, the energetic position of MLCT absorption and emission indicated that the electron-donating nature of substituents in the achiral catalyst backbone is accompanied by a red shift, presumably due to an increased electron density in the ligands with associated elevated ligand orbitals, resulting in weaker backbonding properties and consequently increased electron density at the metal. This is accompanied by increased metal-centred dπ-orbital energies (HOMO), while the $\pi^*_{BOX\text{-}bpy}$-orbital, which is common to all complexes, remains available as an almost energetically unchanged LUMO. Consistent with these spectroscopic observations, cyclic voltammetry revealed a wide range of redox potentials for the metal-centred redox event (230 mV) and a very narrow range of redox potentials for the ligand-centred first reduction event (10 mV). Therefore, while variation of the substituents in the achiral catalyst backbone strongly influenced the energetic levels of the metal-centred HOMO, the energy of the ligand-centred LUMO remained unaffected, strongly suggesting that the latter is indeed localized on the BOX-bpy ligand **529** common to all three complexes. This observation was supported by correlations of absorption and emission energies with redox potentials and summed Okamoto-Brown substituent parameters, again strongly indicating the successful electronic disfavoring of the achiral catalyst side by rational modification of orbital energies, as summarized in the simplified MO diagram (**figure 49**).

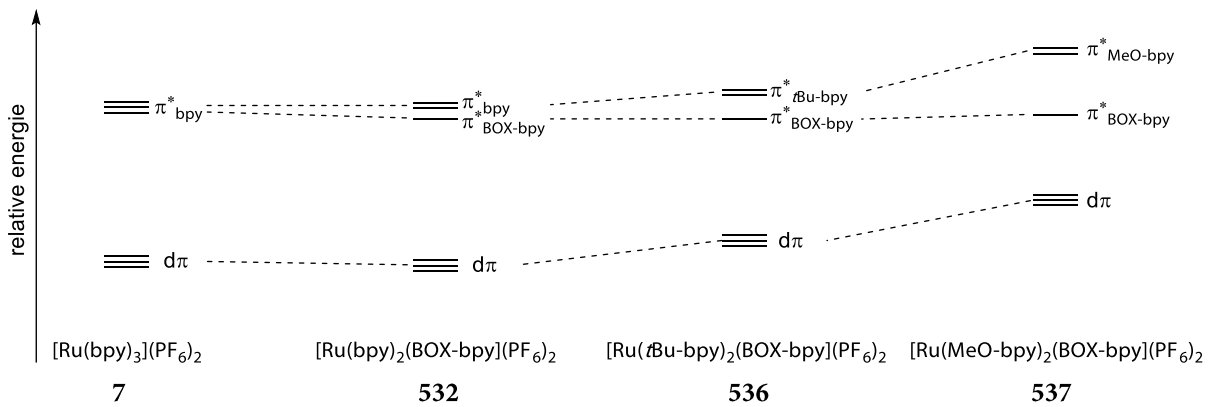

figure 49. Simplified MO-diagram showing assumed relative changes in orbital energies based on experimental absorption and emission energies, redox potentials, Okamoto-Brown parameters and correlations thereof.

For the determination of the excited state redox potentials, three common approximation methods were compared and the most common method of approximating the emission maximum as the free energy of the excited state ΔG_{ES}, which systematically neglects the vertical nature of the transitions as well as internal relaxation to the lowest

ground state vibrational level, resulting in values that are rather lower limits, was modified by the addition of the reorganisation energy determined from a Franck-Condon fit of $[Ru(bpy)_3]^{2+}$ (**7**). Based on the similar shape of the emission bands of the heteroleptic complexes **532**, **536** and **537** and $[Ru(bpy)_3]^{2+}$ (**7**), it can be assumed that the geometry changes during the excitation and therefore the reorganisation energy are likewise similar. A comparison of the excited state redox potentials determined for $[Ru(bpy)_3]^{2+}$ (**7**) according the three common approximations and using the modified approach showed that the latter leads to the smallest deviation from the published excited state redox potentials. Consideration of different approximation methods as statistical sampling around the actual value suggested averaging, which in fact for $[Ru(bpy)_3]^{2+}$ (**7**) yielded the potentials of $\overline{E}_{ox}^*$ and $\overline{E}_{red}^*$ with values of 0.835 V and –0.905 V, exhibiting an even smaller deviation from published potentials ($E_{ox}^* = 0.85$ V, $E_{red}^* = -0.92$ V). Although the redox potentials of the excited states were not determined precisely by low-temperature spectroscopy and Franck-Condon fits, phase-modulated cyclic voltammetry or with the aid of computational methods, their small deviation from literature values and the overall plausible trend indicate that the determined values are suitable for the prediction of thermodynamically possible reactions in a good approximation (**scheme 113**).

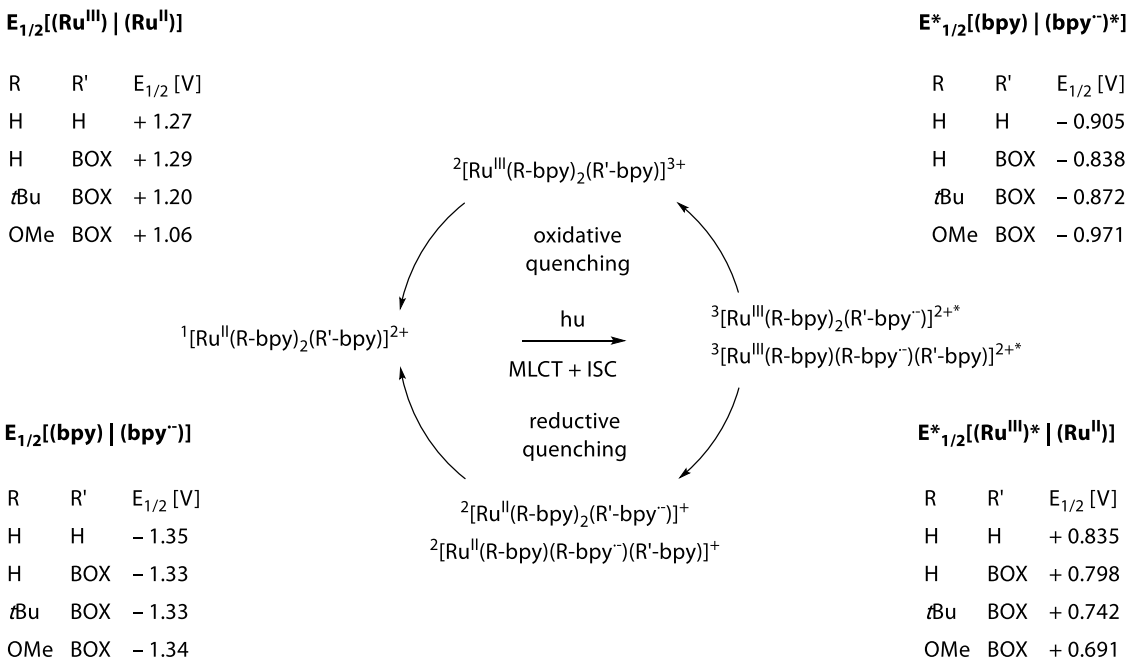

scheme 113. Overview of the ground state potentials and averaged approximated excited state potentials of $[Ru(bpy)_3]^{2+}$ (**7**) and the heteroleptic complexes **532**, **536** and **537** in the context of reductive and oxidative quenching cycles.

To gain insight into the actual applicability of the concept of electronic disfavoring of an achiral catalyst side in the field of enantioselective photoredox catalysis, several literature-known photoredox transformations were investigated (**scheme 114**). Aiming at an asymmetric adaptation of literature-known racemic photoredox reactions, Stephenson's intramolecular radical cyclization, Stephenson's intermolecular atom transfer radical addition (ATRA) and an intramolecular cascade cyclization of phenylpropynyl-3-oxo-phenylpropanoate (**779**) that has been optimized in our working group for eosin Y were investigated.[16, 53, 327]

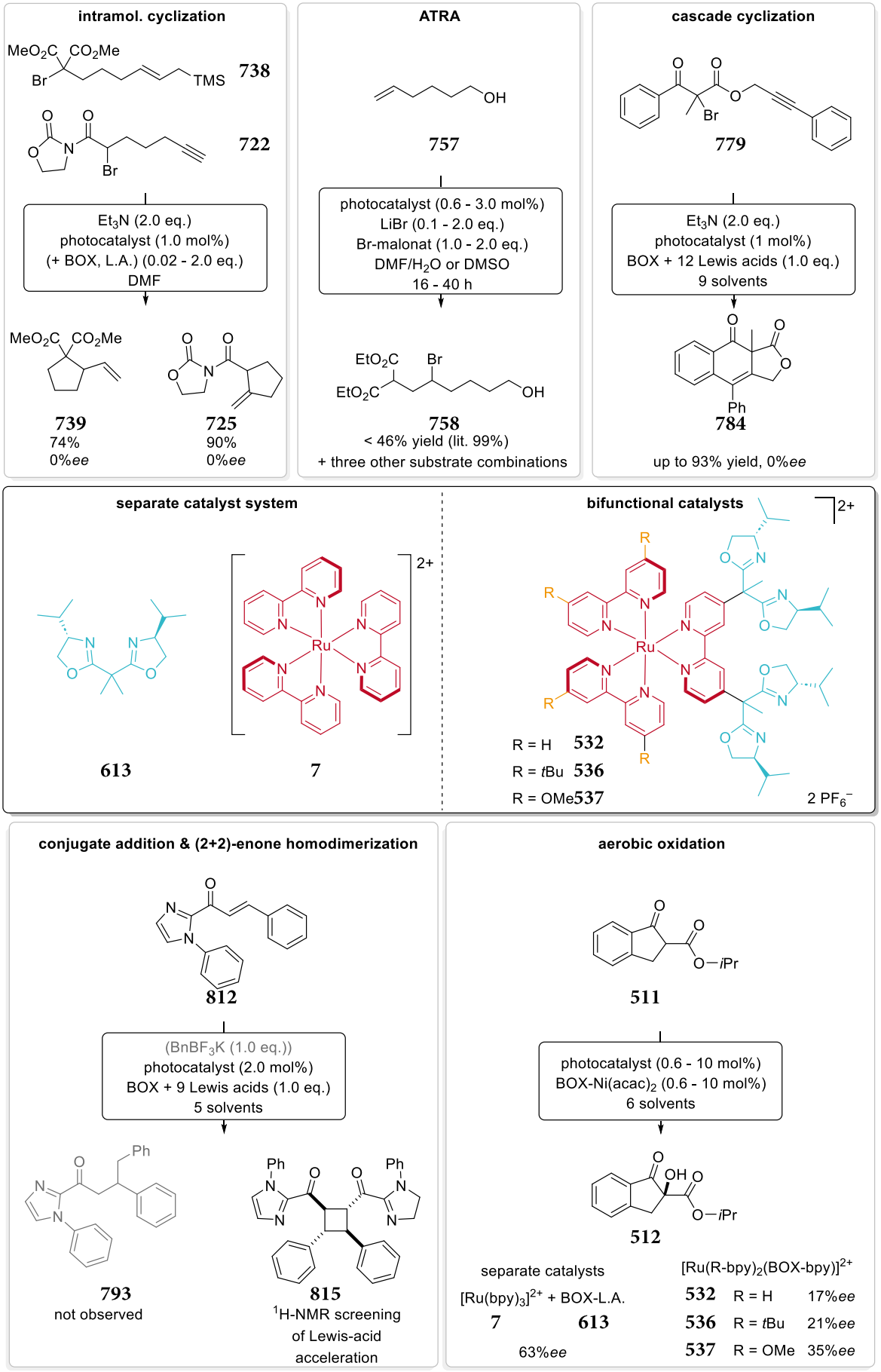

scheme 114. Overview of investigated literature-known racemic (top) and enantioselective (bottom) photoredox transformations.[16, 53, 243, 327]

When investigating Stephenson's intramolecular radical cyclization, some substrates failed to allow racemic reproduction of published results due to observed product instabilities and isomerizations. The cyclization of malonate **738** and oxazolidinone **722** did not provide evidence of enantioselectivity neither with catalytic amounts of the heteroleptic catalysts **532**, **536** and **537**, nor with a separate catalyst system of $[Ru(bpy)_3]^{2+}$ (**7**) and stoichiometric amounts of BOX-$Zn(OTf)_2$. The investigation of Stephenson's ATRA was performed without the presence of an asymmetric Lewis acid and analyzed the influence of different experimental procedures, solvent, catalyst, reactant ratio of substrate and Lewis acid additive, as well as catalyst loading by quantitative ^{1}H-NMR spectroscopy, detecting only a maximum yield of 46% (lit. 99%) for Stephenson's main example of the ATRA.[53] Therefore, the combination of other halocarbonyls and alkenes was evaluated that did not lead to ATRA products or only in unsatisfactory yields. Far more successful was the racemic reproduction of the cascade cyclization, which was systematically screened for enantioselective adaptation with stoichiometric addition of BOX using 12 different Lewis acids and 10 different solvents. However, neither the separate catalyst system nor the heteroleptic complexes **532**, **536** and **537** provided the cyclization product **784** in an enantioenriched form.

After the enantioselective adaptation of several racemic photoreactions failed, further approaches focused on the evaluation of heteroleptic complexes **532**, **536** and **537** in literature-known enantioselective reactions such as the conjugate addition of alkyl radicals from the oxidation of alkyl trifluoroborates to 2-acylimidazoles **812** according to Meggers *et al.* which presumably did not proceed due to unsuitable redox potentials and instead led to (2+2)-enone homodimerization. An ^{1}H-NMR screening for the investigation of the acceleration of the reaction in the presence of 9 different Lewis acids and in five solvents showed no significant differences in the reaction rate, possibly because the substrate **812** employed contains a β-Ph group and therefore readily forms benzylic-radical intermediates even without prior Lewis acid activation. To further optimize the (2+2)-enone dimerization, the substrate structure could be modified by exchange of the β-Ph residue for a Me group, as the formation of the intermediary radical should only occur after L.A. activation, thereby eliminating the racemic background reaction.

Finally, the aerobic oxidation by Xiao *et al.* based on a structurally related bifunctional catalyst combining a thioxanthone photosensitizer with different BOX fragments was evaluated. A calibration curve was established indicating the influence of catalyst loading (between 0.6 mol% and 10 mol%) on the enantiomeric excess using the separate system of $[Ru(bpy)_3]^{2+}$ (**7**) and BOX-$Ni(acac)_2$. It was found that a maximum enantiomeric excess of about 60%*ee* can be obtained with the available photoreactor, which is only about 10%*ee* lower than published results, despite a significantly higher temperature (about 32 °C instead of −10 °C). A comparison of the enantiomeric excesses obtained using the heteroleptic complexes **532**, **536** and **537** revealed a superior performance of the electronically modified complex $[Ru(MeO\text{-}bpy)_2(BOX\text{-}bpy)]^{2+}$ **537** (35%*ee*) compared to the sterically shielded $[Ru(t\text{Bu-}bpy)_2(BOX\text{-}bpy)]^{2+}$ **536** (21%*ee*) or unsubstituted $[Ru(bpy)_2(BOX\text{-}bpy)]^{2+}$ **532** (17%*ee*). The inferior performance of all heteroleptic catalysts **532**, **536** and **537** compared to the separate system (max 63%*ee*) was attributed to solubility-induced variation in the ratios of photosensitizer to chiral BOX fragment, which is fixed in the heteroleptic complexes **532**, **536** and **537** due to the covalent linkage, but shifted towards an increased ratio of

chiral L.A. to photosensitizer in the separated system due to different solubilities of BOX-Ni(acac)$_2$ and $[Ru(bpy)_3]^{2+}$ (**7**). This assumption was supported by a smaller differences in stereochemical outcome when ensuring complete dissolution of both the bifunctional catalysts **532**, **536** and **537** and the separated system. The remaining difference was attributed to an increased distance between BOX-coordinated substrate and photoredox active catalyst core accompanied by lower concentration of $^1O_2$ on the chiral side compared to the achiral back side, whereas in the separated catalyst system the BOX-coordinated substrates can diffuse to sides close to the photosensitizer with increased $^1O_2$ concentration with a preference for the asymmetric reaction due to L.A. activation. A structural comparison of the heteroleptic catalysts **532**, **536** and **537** with the bifunctional catalysts of the Xiao group, taking into account stereoelectronic orbital interactions, also suggests the described consideration of increased distance by the BOX fragments themselves and provides an explanation for the inferior performance compared to the thioxanthone-BOX system, in which a flexible linker allows formation of a conformer with a shorter distance between photosensitizer and chiral BOX-fragment.

The incorporation of *t*Bu groups in the sterically shielded complex **536** only led to an increase of the enantiomeric excess of 4%*ee*, possibly because *t*Bu-groups are smaller than BOX fragments and furthermore because they are too small to block gaps in the helical tris(bipyridine) structure. The slight increase could be the result of the weak electron-donating nature of the *t*Bu groups, considering the superior performance of the electronically modified MeO-substituted complex **537**, which yielded more than twice the enantiomeric excess of the unsubstituted catalyst **532**. This represents a practical proof of the concept of electronic disfavoring of an achiral catalyst side, laying the foundation for the promising concept of directed excitation in the toolbox of rational catalyst development.

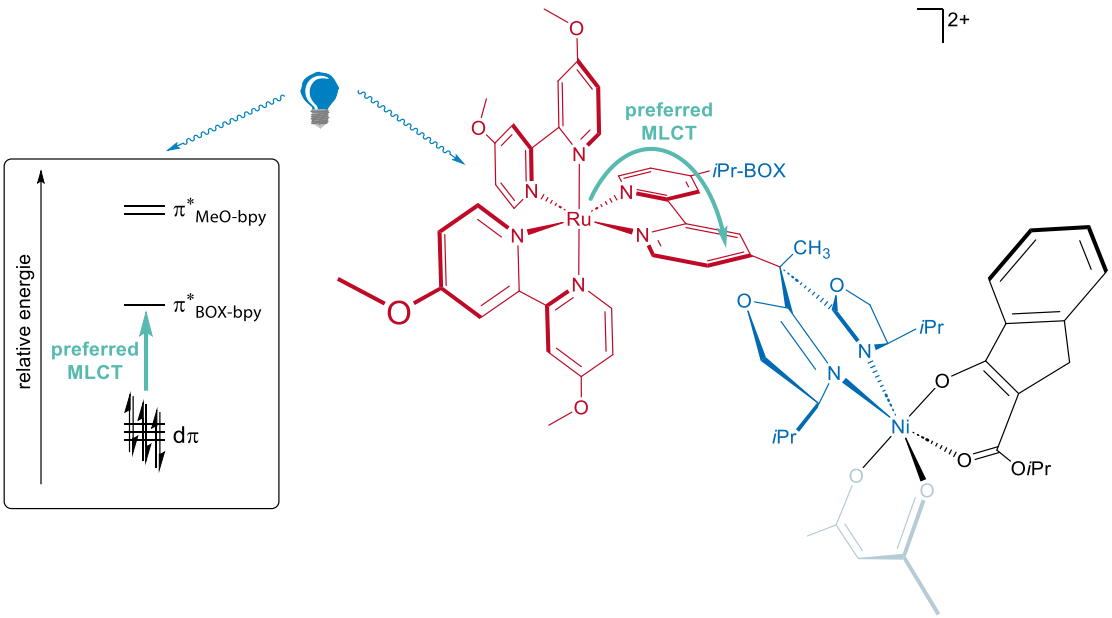

figure 50. Three-dimensional schematic visualization of the assumed concept of electronic disfavoring of an achiral catalyst side and directed excitation through modification of orbital energies.

The concept might further be confirmed by more extended photophysical investigations, i.e. low-temperature emission spectroscopy and Franck-Condon-fit, as well as computational methods for calculating the orbital energies. Based on the discussed findings, the catalyst structure could be modified in various ways. In addition to varying the residues on the bisoxazoline rings by employing other chiral amino alcohols in the ligand synthesis, a different concept of linking the BOX fragment and bipyridine, aiming at a more flexible linker to potentially reduce the distance between the chiral reaction centre and the photoredox-active fragment, could be investigated. Furthermore, instead of ruthenium-based bipyridine ligands, bifunctional iridium complexes with BOX-substituted phenylpyridine ligands could also be synthesized, possibly paving the way for a multitude of alternative transformations due to the change in redox potentials associated with the change of the metal centre. In addition, the concept of electronic disfavoring could be further explored in three ways: Instead of methoxy substituents in the achiral backbone, sterically demanding alkyloxy substituents could be incorporated. Furthermore, stronger electron-donating substituents, e.g. dimethylamine, or even multiple electron-donating substituents per pyridine ring ligand could be connected to the achiral backbone. Complementary to the electron disfavoring of the catalyst backside by raising the corresponding ligand orbitals, electron-withdrawing substituents on the BOX-substituted ligand might lead to the lowering of the corresponding orbital energies and consequently also to the preferred MLCT excitation into orbitals on the BOX-substituted ligand.

5 Experimental procedures

5.1 General information

All reactions were performed under a nitrogen atmosphere using established Schlenk techniques. The glassware was dried at 120 °C for two hours and cooled in high vacuum using a high vacuum rotary vane oil pump (vacuubrand RZ 6). Chemicals and solvents were purchased from Alfa Aesar, Fluka, TCI, VWR, Merck or Sigma Aldrich and used without further purification, unless otherwise stated. Dry solvents (tetrahydrofuran (THF), toluene, dichloromethane, diethylether) were taken from a MBraun Solvent Purification System (MB-SPS800). *N*,*N*-Dimethylformamide (DMF) was distilled from CaH_2 and stored over molecular sieve (4 Å). Other chemicals or solvents were purified according to common laboratory methods.

For thin-layer chromatography (TLC) analysis, Macherey-Nagel precoated plates (ALUGRAM® Xtra G/UV254) with fluorescence indicator were used. The detection occurred by UV radiation (254 nm) and by staining with cerium molybdophosphoric acid solution (16.0 mL concentrated H_2SO_4, 200 mL distilled water, 5.00 g molybdophosphoric acid, 2.00 g $Ce(SO_4)_2$ x 4 H_2O). For preparative silica-gel chromatography or flash chromatography Macherey-Nagel silica-gel (60 Mesh, 0.04 - 0.063 mm) was used. Medium pressure chromatography (MPLC) was performed using a Büchi Sepacore® X50 system.

For quantitative TLC analysis, the TLC-MS system Advion expression CMS was used. High resolution electrospray ionization mass spectra (HRMS ESI) were measured on a Bruker Daltonics UHR-QTOF maXis 4G.

Enantiomeric excesses were measured using a VWR-Hitachi LaChrom ELITE® HPLC system with Daicel CHIRALPAK® columns (length: 25 cm, diameter: 0.46 cm).

^{1}H-NMR, ^{13}C-NMR and ^{19}F-NMR spectra were recorded on a Bruker Avance III 300 or 600 spectrometer. The NMR samples were dissolved in deuterated chloroform ($CDCl_3$), methanol (CD_3OD), acetonitrile (CD_3CN), acetone ($(CD_3)_2CO$) or DMSO ($(CD_3)_2SO$). The recorded spectra were calibrated on the corresponding solvent signal ($CDCl_3$: ^{1}H-NMR – δ = 7.26 ppm; ^{13}C-NMR – δ = 77.0 ppm; CD_3OD: ^{1}H-NMR – δ = 4.87 ppm; ^{13}C-NMR – δ = 49.0 ppm; CD_3CN: ^{1}H-NMR – δ = 1.94 ppm; ^{13}C-NMR – δ = 118.26 ppm; $(CD_3)_2CO$: 1H-NMR - δ = 2.05 ppm; ^{13}C-NMR – δ = 29.8 ppm; $(CD_3)_2SO$: 1H-NMR - δ = 2.50 ppm; ^{13}C-NMR – δ = 39.5 ppm). Chemical shifts are expressed in parts per million (ppm). Splitting patterns are indicated as follows: br, broad; s, singlet; d, doublet; t, triplet; q, quartet; m, multiplet.

Infrared (IR) spectra were recorded on a Jasco FT/IR 6200 as a thin film on a NaCl single crystal at 499 – 4000 cm^{-1}.

All spectroscopic measurements in solution were performed using solvents in spectroscopic grade. UV/VIS absorption spectra were recorded on the Perkin Elmer UV/VIS/NIR Lambda 19 dual beam spectrometer between 210 nm and 650 nm at room temperature. The substances were measured as solutions in acetonitrile and their molar absorption coefficients were determined using a five-point linear regression. Emission spectra, quantum yields and lifetimes of excited states were acquired on the Edinburgh instruments Spectrofluorometer FS5. Excitation was performed either at the lowest energy absorption maximum or using an EPL-450 laser at 450 nm.

Detection occurred between 470 nm and 900 nm. To account for Einstein's coefficients, absorption and emission spectra were divided by the wavenumber or the third power of the wavenumber, respectively. Quantum yields were measured using an integration sphere SC30. Absolute quantum yields were determined in reference to acetonitrile.

Cyclic voltammetry was measured in a flame-dried and argon-flushed one compartment cell containing a glassy carbon working electrode, AgCl/Ag reference electrode and a Pt-disc counter electrode on a Autolab Potentiostat/Galvanostat (PGSTAT204, Software: Autolab Nova 2.1). All measurements were performed in degassed acetonitrile in the presence of NBu_4PF_6 (100 mM) as supporting electrolyte and the internal standard ferrocene. After measurement of a blanc spectrum of the electrolyte, the analyte as well as a solution of the internal standard ferrocene were added ensuring that the corresponding concentrations during measurement are 1.00 mM and 0.250 mM, respectively. The ohmic-drop was measured by positive feedback and the open circuit potential was measured before each scan and used as the starting potential. The internal standard ferrocene was sublimed twice and electrolyte NBu_4PF_6 was recrystallized three times from absolute ethanol and dried for 48 h at 115 °C in vacuum prior to use. The electrolyte solution was thoroughly degassed by freeze-pump-thaw, all other solutions were prepared inertly with the degassed electrolyte solution. To ensure inert measuring conditions, the cell was degassed by N_2-sparging for five minutes after the addition of analyte or internal standard before each measurement. The measurements were recorded at scan-rates of 50 - 150 mV/s and referenced to the signal of the redox couple of the internal standard.

5.2 Synthesis of bipyridine derivatives

5.2.1 2,2′-Bipyridine-*N*-oxide (**588**)

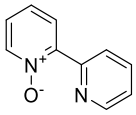

588

2,2'-Bipyridine-*N*-oxide (**588**) was prepared according to a modified published procedure:[335] To a solution of 2,2'-bipyridine (**587**) (5.00 g, 32.0 mmol, 1.00 eq.) in trifluoroacetic acid (24 mL) was added H_2O_2-solution (30%, 3.71 mL, 36.3 mmol, 1.21 eq.). After stirring for 1 h at room temperature, $CHCl_3$ (60 mL) was added and the mixture was washed with NaOH-solution (5 M, 2 x 20 mL). The aqueous phase was extracted with $CHCl_3$ (3 x 60 mL). The combined organic extracts were dried over Na_2SO_4 and concentrated in vacuo to give pure 2,2'-bipyridine-*N*-oxide (**588**) (5.40 g, 31.4 mmol, 98%).

^{1}**H NMR** (300 MHz, $CDCl_3$) δ 8.89 (dt, *J* = 8.1, 1.1 Hz, 1H), 8.72 (ddd, *J* = 4.8, 1.9, 1.0 Hz, 1H), 8.31 (ddd, *J* = 6.4, 1.4, 0.6 Hz, 1H), 8.17 (ddd, *J* = 8.0, 2.3, 0.6 Hz, 1H), 7.82 (ddd, *J* = 8.1, 7.5, 1.9 Hz, 1H), 7.39 – 7.31 (m, 2H), 7.30 – 7.22 (m, 1H).

5.2.2 4-Nitro-2,2′-bipyridine-*N*-oxide (**589**)

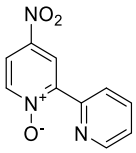

589

4-Nitro-2,2'-bipyridine-*N*-oxide (**589**) was prepared according to a modified published procedure:[335] To a cooled (0 °C) suspension of KNO_3 (28.4 g, 28.1 mmol, 1.07 eq.) in concentrated H_2SO_4 (75 mL) was added 2,2'-bipyridine-*N*-oxide (**588**) (4.50 g, 26.2 mmol, 1.00 eq.). The ice bath was removed and the mixture was heated to 120 °C for 72 h. After cooling to room temperature, ice (50 g) was added. Under constant pH control using a pH meter was slowly added NaOH-solution (25%) until the pH value was adjusted to pH = 9-10. The white precipitate was filtered off and dissolved in CH_2Cl_2. Undissolved solids were filtered off and washed with CH_2Cl_2. Removal of the solvent gave 4-nitro-2,2'-bipyridine-*N*-oxide (**589**) (3.93 g, 18.1 mmol, 69%).

^{1}**H NMR** (300 MHz, $CDCl_3$) δ 9.17 (d, *J* = 3.3 Hz, 1H), 8.89 (ddd, *J* = 8.1, 1.1 Hz, 1H), 8.79 (ddd, *J* = 4.7, 1.9, 1.0 Hz, 1H), 8.36 (d, *J* = 7.2 Hz, 1H), 8.06 (dd, *J* = 7.2, 3.3 Hz, 1H), 7.88 (ddd, *J* = 8.1, 7.6, 1.8 Hz, 1H), 7.43 (ddd, *J* = 7.6, 4.7, 1.1 Hz, 1H).

5.2.3 4-Amino-2,2′-bipyridine (**590**)

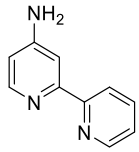

590

4-Amino-2,2'-bipyridine (**590**) was prepared according to a modified published procedure:[336] Sodium borohydride (3.41 g, 90.1 mmol, 4.98 eq.) was added portionwise to a mixture of 4-nitro-2,2'-bipyridine-*N*-oxide (**589**) (3.93 g, 18.1 mmol, 1.00 eq.) and palladium on charcoal (10%, 645 mg, 68.6 mmol, 3.79 eq.) in MeOH (65 mL). After 15 h, the catalyst was filtered off and the solvent was removed under reduced pressure. H_2O (60 mL) was added and the aqueous phase was extracted with Et_2O (6 x 70 mL). The combined organic extracts were concentrated in vacuo to give 4-amino-2,2'-bipyridine (**590**) (2.99 g, 17.5 mmol, 97%) as a beige solid.

^{1}H NMR (600 MHz, $CDCl_3$) δ 8.63 (ddd, *J* = 4.8, 1.8, 0.9 Hz, 1H), 8.35 (dt, *J* = 7.9, 1.1 Hz, 1H), 8.30 (d, *J* = 5.5 Hz, 1H), 7.78 (td, *J* = 7.7, 1.8 Hz, 1H), 7.66 (d, *J* = 2.4 Hz, 1H), 7.29 – 7.26 (m, 1H), 6.54 (dd, J = 5.5, 2.4 Hz, 1H), 4.28 (s, 2H).

5.2.4 2,2′-Bipyridine-4-diazonium tetrafluoroborate (**582**)

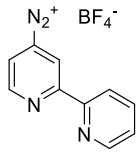

582

2,2'-Bipyridine-4-diazonium tetrafluoroborate (**582**) was prepared according to a modified published procedure:[337] To a suspension of 4-amino-2,2'-bipyridine (**590**) (1.00 g, 5.85 mmol, 1.00 eq.) in HBF_4-solution (50%, 17.1 mL, 120 mmol, 20.0 eq.) was added a solution of $NaNO_2$ (1.10 g, 15.9 mmol, 2.73 eq.) in water (10 mL). The green solution was cooled in liquid nitrogen and allowed to warm to 0 °C over 15 minutes. The precipitate was filtered off. The mother liquor was subjected to the precipitation sequence again. The combined precipitates were dried in the desiccator over P_2O_5 giving 2,2'-bipyridine-4-diazonium tetrafluoroborate (**582**) (1.33 g, 4.91 mmol, 84%) as a beige solid, that was used without further purification and analysis.

5.2.5 4-Fluoro-2,2′-bipyridine (**585**)

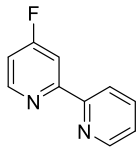

585

4-Fluoro-2,2'-bipyridine (**585**) was prepared according to a modified published procedure:[337] 2,2'-Bipyridine-4-diazonium tetrafluoroborate (**582**) (302 mg, 1.12 mmol, 1.00 eq.) was heated with a heat gun until gas evolution and a color change from beige to brown occurred. NaOH-solution (20%, 5 mL), H_2O (10 mL) and EtOAc (15 mL) were added and the aqueous phase was extracted with EtOAc (3 x 15 mL). The combined organic extracts were dried over Na_2SO_4 and concentrated in vacuo to give 4-fluoro-2,2'-bipyridine (**585**) (125 mg, 0.718 mmol, 64%).

^{1}H NMR (600 MHz, $CDCl_3$) δ 8.68 (ddd, *J* = 4.8, 1.8, 0.9 Hz, 1H), 8.63 (dd, *J* = 8.5, 5.5 Hz, 1H), 8.41 (dt, *J* = 7.9, 1.1 Hz, 1H), 8.17 (dd, *J* = 10.4, 2.5 Hz, 1H), 7.83 (td, *J* = 7.7, 1.8 Hz, 1H), 7.34 (ddd, *J* = 7.5, 4.8, 1.2 Hz, 1H), 7.04 (ddd, *J* = 8.1, 5.5, 2.5 Hz, 1H).

^{19}F NMR (565 MHz, $CDCl_3$) δ −101.97.

5.2.6 4,4′-Dihydroxy-2,2′-bipyridine (**704**)

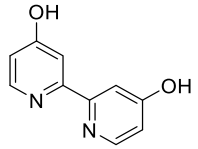

704

4,4'-Dihydroxybipyridine (**704**) was prepared according to a modified published procedure:[309] To a solution of 4,4'-dimethoxybipyridine (**699**) (1.00 g, 4.60 mmol, 1.00 eq.) in acetic acid (60 mL) was added HBr (33% in HOAc, 16.0 mL, 92.7 mmol, 20.1 eq.) and the mixture refluxed for 72 h. The solvent was removed in vacuo and water (70 mL) was added to the residue. Undissolved solids were filtered off and the aqueous solution was neutralized with ammonia solution (25%) to precipitate a white solid, which was filtered off and dried in vacuo to give 4,4'-dihydroxybipyridine (**704**) (580 mg, 3.08 mmol, 67%).

^{1}H NMR (300 MHz, CD_3OD) δ 8.15 (s, 2H), 7.21 (s, 2H), 6.71 (s, 2H)

5.2.7 4,4′-Diisopropyloxy-2,2′-bipyridine (**700**)

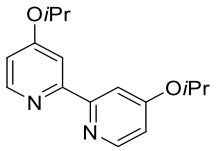

700

To a solution of 4,4'-dihydroxybipyridine (**704**) (100 mg, 0.532 mmol, 1.00 eq.) in DMF (2.5 mL) were added K_2CO_3 (436 mg, 3.15 mmol, 5.93 eq.), KI (8.8 mg, 53 µmol, 0.10 eq.) and isopropylbromide (0.148 mL, 1.58 mmol, 2.98 eq.) and the mixture was heated to 75 °C for 48 h. The solvent was removed in vacuo and to the residue was added CH_2Cl_2 (10 mL) and water (10 mL). The aqueous phase was extracted with CH_2Cl_2 (4 x 10 mL) and the combined organic extracts were dried (Na_2SO_4) and concentrated in vacuo to give 4,4'-diisopropyloxybipyridine (**700**) (144 mg, 0.529 mmol, 99%) as an off-white solid. Following this procedure in a bigger scale using 500 mg 4,4'-dihydroxybipyridine (**700**) gave 84% yield.

^{1}H NMR (300 MHz, Chloroform-*d*) δ 8.42 (d, *J* = 5.7 Hz, 2H), 7.91 (d, *J* = 2.5 Hz, 2H), 6.77 (dd, *J* = 5.7, 2.6 Hz, 2H), 4.79 (hept, *J* = 6.1 Hz, 2H), 1.37 (d, *J* = 6.1 Hz, 12H).

^{13}C NMR (75 MHz, $CDCl_3$) δ 165.22, 158.05, 150.33, 112.12, 107.61, 77.16, 70.11, 21.99.

IR (film on NaCl) ϋ [cm^{-1}] = 3330, 2959, 2873, 2478, 1662, 1637, 1595, 1544, 1463, 1409, 1375, 1213, 1283, 1223, 1175, 1120, 1078, 1028, 1002, 974, 909, 749, 677.

HRMS (ESI) m/z calculated for $C_{16}H_{21}N_2O_2$ [M + H] - 273.1598, found 273.1600.

5.2.8 Tetraethyl 2,2′-([2,2′-bipyridine]-4,4′-diyl)dimalonate (**636**)

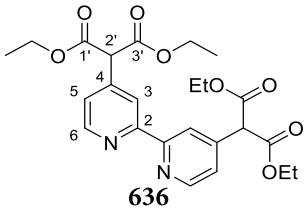

636

To a solution of 4,4'-dimethylbipyridine (**626**) (7.50 g, 40.7 mmol, 1.00 eq.) in THF (250 mL) in a three-necked flask equipped with a mechanical stirrer was added a freshly prepared LDA solution (1.0 M, 40.7 mL, 40.7 mmol, 1.00 eq.) dropwise at −78 °C. After 15 minutes, ethyl chloroformate (**627**) (3.87 mL, 40.7 mmol, 1.00 eq.) was added and the resulting mixture was stirred until the color changed from deep red to yellow. The described addition sequence was repeated five more times. NH_4Cl-solution (200 mL) was added and the aqueous phase was extracted with EtOAc (3 x 100 mL). The combined organic extracts were washed with brine (2 x 100 mL), dried over Na_2SO_4 and concentrated under reduced pressure. Purification using a filter column (diameter: 10 cm, length: 8 cm, gradient: *n*-Hexane/EtOAc = 80:20 → 70:30) and precipitation from $CHCl_3$/*n*-hexane gave tetraethyl 2,2'-([2,2'-bipyridine]-4,4'-diyl)dimalonate (**636**) (5.74 g, 12.2 mmol, 30%) as colorless crystals.

^{1}H NMR (300 MHz, $CDCl_3$) δ 8.68 (d, *J* = 5.1 Hz, 2H, *H*-6), 8.41 (d, *J* = 1.7 Hz, 2H, *H*-3), 7.46 (dd, *J* = 5.1, 1.8 Hz, 2H, *H*-5), 4.72 (s, 2H, *H*-2'), 4.24 (2 x q, *J* = 7.0, 8H, OCH_2Me), 1.27 (t, *J* = 7.1 Hz, 12H, OCH_2CH_3).

^{13}C NMR (75 MHz, $CDCl_3$) δ 167.07 (*C*-1'), 156.09 (*C*-2), 149.49 (*C*-6), 142.69 (*C*-4), 124.37 (*C*-5), 122.41 (*C*-3), 62.39 (OCH_2Me), 57.69 (*C*-2'), 14.11(OCH_2CH_3).

IR (film on NaCl) $\tilde{\upsilon}$ [cm^{-1}] = 3061, 2983, 2939, 2907, 1748, 1735, 1594, 1557, 1460, 1388, 1368, 1305, 1276, 1223, 1175, 1149, 1111, 1095, 1077, 1032, 993, 863, 771, 610.

HRMS (ESI) m/z calculated for $C_{24}H_{29}N_2O_8$ [M + H$^+$] - 473.1918, found 473.1912.

5.2.9 Tetraethyl 2,2′-([2,2′-bipyridine]-4,4′-diyl)bis(2-methylmalonate) (**625**)

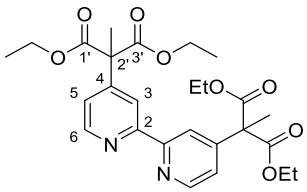

625

A mixture of tetraethyl 2,2'-([2,2'-bipyridine]-4,4'-diyl)dimalonate (**636**) (4.50 g, 9.53 mmol, 1.00 eq.) and K_2CO_3 (3.29 g, 23.8 mmol, 2.50 eq.) in DMF (60 mL) was cooled to 0 °C and methyl iodide (1.31 mL, 20.9 mmol, 2.20 eq.) was added. The mixture was allowed to warm up to room temperature overnight. After 24 h NH_4Cl solution was added and the aqueous phase was extracted with CH_2Cl_2 (3 x 150 mL). The combined organic extracts were washed with water (3 x 250 mL) and brine (250 mL) and dried over Na_2SO_4. Precipitation from $CHCl_3$/*n*-hexane yielded tetraethyl 2,2'-([2,2'-bipyridine]-4,4'-diyl)bis(2-methylmalonate) (**625**) (4.05 g, 8.10 mmol, 85%) as colorless crystals.

^{1}H NMR (300 MHz, $CDCl_3$) δ 8.63 (d, *J* = 5.1 Hz, 2H, *H*-6), 8.46 (dt, *J* = 1.9, 0.8 Hz, 2H, *H*-3), 7.32 (ddd, *J* = 5.3, 2.0, 0.7 Hz, 2H, *H*-5), 4.25 (q, *J* = 7.0 Hz, 8H, OCH_2Me), 1.93 (s, 6H, *H*-2'), 1.26 (t, *J* = 7.1 Hz, 12H, OCH_2CH_3).

^{13}C NMR (75 MHz, $CDCl_3$) δ 170.51 (*C*-1'), 156.11 (*C*-2), 149.03 (*C*-6), 148.31 (*C*-4), 123.18 (*C*-5), 119.91 (*C*-3), 62.22 (OCH_2Me), 58.87 (*C*-2'), 21.99 (CH_3), 14.07 (OCH_2CH_3).

IR (film on NaCl) ϋ [cm^{-1}] = 3063, 2983, 2940, 2906, 2874, 1735, 1591, 1550, 1462, 1380, 1365, 1297, 1262, 1173, 1109, 1072, 1018, 995, 930, 861, 761, 706, 668, 622.

HRMS (ESI) m/z calculated for $C_{26}H_{33}N_2O_8$ [M + H] - 501.2231, found 501.2241.

5.2.10 2,2'-([2,2'-Bipyridine]-4,4'-diyl)bis(*N* ^{1},*N* ^{3}-bis((*S*)-1-hydroxy-3-methylbutan-2-yl)-2-methylmalonamide) (**622**)

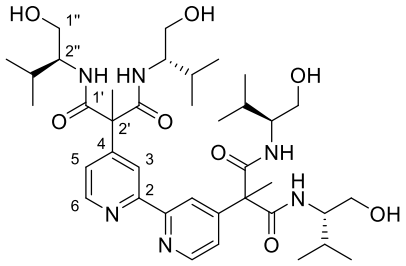

622

A mixture of tetraethyl 2,2'-([2,2'-bipyridine]-4,4'-diyl)bis(2-methylmalonate) (**625**) (500 mg, 1.00 mmol, 1.00 eq.), NaH (10.0 mg, 0.250 mmol, 0.250 eq.) and L-valinol (**603**) (0.500 mL, 4.49 mmol, 4.49 eq.), that was thoroughly dried by azeotropic distillation with $CHCl_3$ on an inverse Dean-Stark-trap and freshly distilled, was heated to 80 °C for five days. Excess L-valinol (**603**) was regained by bulb-to-bulb distillation in high vacuum at a temperature not exceeding 80 °C. The residue was purified by a short column chromatography (CH_2Cl_2/MeOH/NH_3 (25%) = 3.72 : 0.25 : 0.03) and recrystallization from *n*-hexane/CH_2Cl_2 to give 2,2'-([2,2'-Bipyridine]-4,4'-diyl)bis(*N* ^{1},*N* ^{3}-bis((*S*)-1-hydroxy-3-methylbutan-2-yl)-2-methylmalonamide) (**622**) (414 mg, 5.68 mmol, 95%) as colorless crystals. In an entirely analogous fashion, a bigger scale (4.05 g, 8.10 mmol) provided the tetraamide **622** in 73% yield.

^{1}H NMR (300 MHz, MeOD) δ 8.64 (d, *J* = 5.2 Hz, 2H, *H*-6), 8.45 (d, *J* = 1.9 Hz, 2H, *H*-3), 7.48 (dd, *J* = 5.3, 1.9 Hz, 2H, *H*-5), 3.93 – 3.28 (m, 12H, *H*-1''& *H*-2''), 1.93 (s, 6H, CH_3), 1.85 (ddd, *J* = 13.7, 11.7, 6.9 Hz, 4H, *i*Pr-C*H*), 0.95 (dd, *J* = 6.8, 4.7 Hz, 12H, *i*Pr-CH_3), 0.87 (t, *J* = 7.3 Hz, 12H, *i*Pr-CH_3).

^{13}C NMR (75 MHz, MeOD) δ 173.71 (*C*-1'), 173.17 (*C*-1'), 157.04 (*C*-2), 153.76 (*C*-4), 150.41 (*C*-6), 124.28 (*C*-3), 121.52 (*C*-5), 63.04 (*C*-1''/*C*-2''), 62.98 (*C*-1''/*C*-2''), 60.84 (*C*-2'), 58.80 (*C*-1''/*C*-2''), 30.15 (*i*Pr-CH), 23.55 (CH_3), 20.20 (*i*Pr-CH_3), 20.15 (*i*Pr-CH_3), 19.21 (*i*Pr-CH_3), 19.14 (*i*Pr-CH_3).

IR (film on NaCl) ϋ [cm^{-1}] = 3330, 2959, 2873, 2478, 1662, 1637, 1595, 1544, 1463, 1409, 1375, 1313, 1283, 1223, 1175, 1120, 1078, 1028, 1002, 974, 909, 749, 677.

HRMS (ESI) m/z calculated for $C_{38}H_{61}N_6O_8$ [M + H] - 729.4545, found 729.4547.

5.2.11 4,4′-Bis(1,1-bis((*S*)-4-isopropyl-4,5-dihydrooxazol-2-yl)ethyl)-2,2′-bipyridine (**529**)

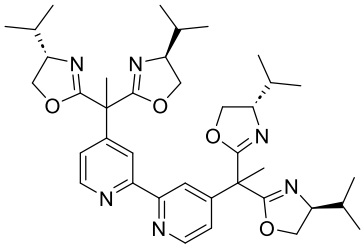

529

To a solution of the tetra-γ-hydroxyamide **622** (300 mg, 0.412 mmol, 1.00 eq.) in THF (5 mL) was added Burgess reagent (**619**) (589 mg, 2.47 mmol, 6.00 eq.), which was previously weighed inside the glovebox into a septum capped vial, as a solution in THF (3 mL) and rinsed with THF (2 x 3 mL). After 24 h the white precipitate was filtered off and rinsed with THF, before concentration in vacuo. The residue was purified in two ways: Using reverse phase HPLC (C18, gradient over 60 min.: H_2O/MeOH = 30:70 → 5:95) followed by removal of the methanol at the rotary evaporator and removal of the water by lyophilization gave 4,4'-bis(1,1-bis((*S*)-4-isopropyl-4,5-dihydrooxazol-2-yl)ethyl)-2,2'-bipyridine (**529**) (189 mg, 0.288 mmol, 70%) as a colorless oil. Alternatively, the residue can be purified by the addition of an excess amount of *n*-hexane to a concentrated solution of the crude product in dichloromethane, leading to the precipitation of all by-products, i.e. not fully cyclized intermediates, and after filtration and removal of the solvent provides the product **529** in 75% yield.

^{1}H NMR (300 MHz, $CDCl_3$) δ 8.58 (dd, *J* = 5.2, 0.7 Hz, 2H), 8.43 (d, *J* = 1.9 Hz, 2H), 7.34 (dd, *J* = 5.2, 2.0 Hz, 2H), 4.35 – 3.90 (m, 12H), 1.97 (s, 6H), 1.94 – 1.73 (m, 4H), 0.95 (d, *J* = 6.9, 1.2 Hz, 12H), 0.89 (dd, *J* = 6.8, 1.4 Hz, 12H).

^{1}H NMR (300 MHz, MeOD) δ 8.61 (dd, *J* = 5.3, 0.7 Hz, 2H), 8.46 (dd, *J* = 2.0, 0.8 Hz, 2H), 7.47 (dd, *J* = 5.3, 2.0 Hz, 2H), 4.36 (ddd, *J* = 9.9, 8.5, 7.4 Hz, 4H), 4.16 (ddd, *J* = 8.4, 7.4, 5.8 Hz, 4H), 4.10 – 3.99 (m, 4H), 1.96 (s, 6H), 1.91 – 1.76 (m, 4H), 0.97 – 0.85 (m, 24H).

^{13}C NMR (75 MHz, $CDCl_3$) δ 166.41, 166.36, 156.22, 150.08, 148.89, 122.62, 119.76, 70.42, 70.40, 47.54, 32.44, 32.33, 24.18, 18.74, 18.68, 17.91, 17.77.

^{13}C NMR (75 MHz, MeOD) δ 168.69, 168.53, 156.93, 151.77, 150.27, 124.17, 121.27, 72.72, 72.70, 71.62, 33.37, 33.30, 30.75, 24.21, 18.88, 18.78, 18.00, 17.98.

IR (film on NaCl) $\tilde{\upsilon}$ [cm^{-1}] = 2959, 2903, 2873, 1660, 1590, 1550, 1463, 1377, 1348, 1300, 1274, 1235, 1177, 1119, 1084, 1033, 973, 932, 895, 842, 752, 665, 628.

HRMS (ESI) m/z calculated for $C_{38}H_{52}N_6O_4$ [M + H] - 657.4123, found 657.4134.

ESI: Calculated for M+H: 657, found: 657.

5.3 Synthesis of bisoxazoline derivatives

5.3.1 L-Phenylalaninol (**604**)

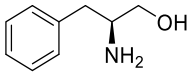

604

Into a three-necked flask equipped with a mechanical stirrer and a metal cooler was added THF (400 mL) and the solution was cooled in an ice bath. $LiAlH_4$ (20 g, 527 mmol, 2.20 eq.) was added portionwise over 25 minutes, before L-phenylalanine (**601**) (39.6 g, 240 mmol, 1.00 eq.) was slowly added and the mixture was allowed to warm up to room temperature. After refluxing for 24 h the mixture was cooled to 0 °C and quenched by the addition of crushed ice (100 g). The solid was filtered off and extracted by repeated refluxing in THF/H_2O (4:1 v/v) (3 x 150 mL). THF was removed under reduced pressure and the residual oil was mixed with $CHCl_3$ (150 mL). The mixture was subjected to an azeotropic distillation on an inverse Dean-Stark-trap until no more separation of water was visible. The solvent was removed under reduced pressure and the crude product was purified recrystallization from EtOAc give L-phenylalaninol (**604**) (33.0 g, 218 mmol, 91%) as colorless crystals. Analytical data was consisted with the literature.[338]

^{1}**H NMR** (300 MHz, MeOD) δ 7.35 – 7.19 (m, 5H), 3.54 (dd, *J* = 10.7, 4.5 Hz, 1H), 3.39 (dd, *J* = 10.7, 6.8 Hz, 1H), 3.10 – 3.00 (m, 1H), 2.80 (dd, *J* = 13.4, 6.1 Hz, 1H), 2.58 (dd, *J* = 13.4, 7.7 Hz, 1H).

5.3.2 L-Valinol (**603**)

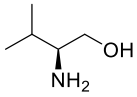

603

Into a three-necked flask equipped with a mechanical stirrer and a metal cooler was added THF (250 mL) and the solution was cooled in an ice bath. $LiAlH_4$ (16.1 g, 425 mmol, 2.20 eq.) was added portionwise over 15 minutes, before L-valine (**600**) (22.7 g, 193 mmol, 1.00 eq.) was slowly added and the mixture was allowed to warm up to room temperature. After refluxing for 22 h the mixture was cooled to 0 °C and quenched by the addition of crushed ice (60 g). The solid was filtered off and extracted by repeated refluxing in THF/H_2O (4:1 v/v) (3 x 150 mL). THF was removed under reduced pressure and the residual oil was mixed with $CHCl_3$ (150 mL). The mixture was subjected to an azeotropic distillation on an inverse Dean-Stark-trap until no more separation of water was visible. The solvent was removed under reduced pressure and the crude product was purified by bulb-to-bulb-distillation to give L-valinol (**603**) (18.2 g, 177 mmol, 92%) as a colorless oil, which crystallized below 30 °C. Analytical data was consisted with the literature.[339]

^{1}**H NMR** (300 MHz, $CDCl_3$) δ 3.61 (ddd, *J* = 10.5, 3.9, 1.2 Hz, 1H), 3.27 (dd, *J* = 10.5, 8.7 Hz, 1H), 2.54 (ddd, *J* = 8.5, 6.3, 3.9 Hz, 1H), 2.04 (s, 3H), 1.55 (dq, *J* = 13.5, 6.7 Hz, 1H), 0.90 (ddd, *J* = 6.8, 3.7, 1.1 Hz, 6H).

5.3.3 L-*O*-TBDMS-Valinol (**661**)

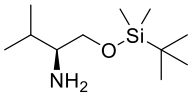

661

To a solution of L-valinol (**603**) (500 mg, 4.85 mmol, 1.00 eq.) in CH_2Cl_2 (15 mL), were added imidazole (396 mg, 5.82 mmol, 1.20 eq.) and TBDMSCl (877 mg, 5.82 mmol, 1.20 eq.) and the mixture was stirred for 9 days at room temperature. After addition of saturated NH_4Cl-solution (15 mL), the aqueous phase was extracted with CH_2Cl_2 (4 x 20 mL). The combined organic extracts were washed with brine (30 mL), dried ($MgSO_4$) and concentrated in vacuo to give L-*O*-TBDMS-Valinol (**661**) (1.04 g, 4.80 mmol, 99%) as a white solid. Analytical data was consistent with the literature.[340]

^{1}H NMR (300 MHz, $CDCl_3$) δ 3.73 (dd, *J* = 10.2, 4.4 Hz, 1H), 3.55 (dd, *J* = 10.2, 6.8 Hz, 1H), 2.74 (ddd, *J* = 6.5, 6.5, 4.3 Hz, 1H), 1.84 (dq, *J* = 13.5, 6.7 Hz, 1H), 0.99 (d, *J* = 6.8 Hz, 3H), 0.96 (d, *J* = 6.8 Hz, 3H), 0.89 (s, 9H), 0.07 (s, 6H).

IR (film on NaCl) $\tilde{\upsilon}$ [cm^{-1}] = 2954, 2930, 2882, 2859, 1596, 1519, 1469, 1256, 1220, 1147, 1116, 1095, 1057, 838, 671.

5.3.4 Diethyl-2-methylmalonate (605)

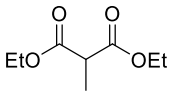

605

Diethyl-2-methylmalonate (**605**) was prepared according to a modified published procedure:[341] To a suspension of K_2CO_3 (12.9 g, 93.6 mmol, 1.50 eq.) in DMF (150 mL) were subsequently added diethylmalonate (**554**) (9.52 mL, 62.4 mmol, 1.00 eq.) and 4.27 mL MeI (4.27 mL, 68.6 mmol, 1.10 eq.) and the mixture was stirred at room temperature for 20 h. H_2O (150 mL) was added and the aqueous phase was extracted with EtOAc (5 x 50 mL). The combined organic layers were washed with H_2O (100 mL) and brine (100 mL), dried over Na_2SO_4 and concentrated in vacuo. The residue was purified by flash-chromatography (gradient over 90 min.: *n*-Hexane/EtOAc = 97:3 → 95:5, flow: 30 mL/min., length: 15 cm, diameter: 4 cm) to give diethyl-2-methylmalonate (**605**) (8.44 g, 48.4 mmol, 78%) as a colorless oil.

^{1}H NMR (300 MHz, $CDCl_3$) δ 4.18 (qd, *J* = 7.1, 1.3 Hz, 4H), 3.41 (q, *J* = 7.3 Hz, 1H), 1.40 (d, *J* = 7.2 Hz, 3H), 1.26 (t, *J* = 7.1 Hz, 6H).

5.3.5 2,2-Dimethylmalonyl dichloride (**606**)

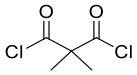

606

2,2-Dimethylmalonyl dichloride (**606**) was prepared according to a modified published procedure:[342] To a cooled (0 °C) solution of 2,2-dimethylmalonic acid (5.00 g, 37.9 mmol, 1.00 eq.) and DMF (0.38 mL, 4.92 mmol, 0.13 eq.) in CH_2Cl_2 (60 mL) oxalyl chloride (9.75 mL, 114 mmol, 3.01 eq.) was slowly added *via* a dropping funnel. After

three hours the reaction mixture was purified by distillation (bath temperature 200 °C) to give 2,2-dimethylmalonyl dichloride (**606**) (5.29 g, 31.5 mmol, 83%) as a colorless oil.

^{1}H NMR (300 MHz, $CDCl_3$) δ 3.64 (s, 6H).

5.3.6 *N*^{1},*N*^{3}-Bis((*S*)-1-hydroxy-3-methylbutan-2-yl)malonamide (**608**)

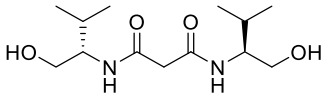

608

N^1,*N*^{3}-Bis((*S*)-1-hydroxy-3-methylbutan-2-yl)malonamide (**608**) was prepared according to a modified published procedure:[343] To a suspension of dimethylmalonate (**740**) (2.75 mL, 23.9 mmol, 1.00. eq.) and L-valinol (**603**) (5.00 g, 48.5 mmol, 2.03 eq.) was added a tip of a spatula of NaH (60%, 2.0 mg, 50 µmol, 0.2 mol%.). The mixture was heated to 150 °C for 14 h. After cooling to room temperature MeOH was removed under reduced pressure to give a slightly yellow solid that was dissolved in CH_2Cl_2 (20 mL) and precipitated by the addition of Et_2O (70 mL). Filtration of the white precipitate and drying under reduced pressure gave *N*^{1},*N*^{3}-bis((*S*)-1-hydroxy-3-methylbutan-2-yl)malonamide (**608**) (5.98 g, 21.8 mmol, 91%) as a white powder.

^{1}H NMR (300 MHz, $CDCl_3$) δ 7.51 – 7.41 (d, *J* = 8.84 Hz, 2H), 3.85 – 3.75 (m, 2H), 3.71 (dd, *J* = 11.4, 3.4 Hz, 2H), 3.51 (dd, *J* = 11.4, 7.9 Hz, 2H), 3.30 (s, 2H), 1.80 (h, *J* = 6.8 Hz, 2H), 0.94 (d, *J* = 5.6 Hz, 6H), 0.92 (d, *J* = 6.0 Hz, 6H).

5.3.7 *N*^{1},*N*^{3}-Bis((*S*)-1-hydroxy-3-methylbutan-2-yl)-2-methylmalonamide (**609**)

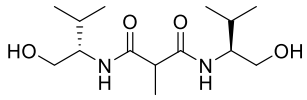

609

N^1,*N*^{3}-Bis((*S*)-1-hydroxy-3-methylbutan-2-yl)-2-methylmalonamide (**609**) was prepared according to a modified published procedure:[343] Diethyl-2-methylmalonate (**605**) (2.94 mL, 17.2 mmol, 1.00 eq.) and L-valinol (**603**) (4.80 mL, 43.0 mmol, 2.50 eq.) were stirred at 120 °C for 21 h. After cooling to room temperature, the mixture was subjected to silica gel column chromatography (gradient from *n*-hexane/EtOAc = 50:50 for removal of the malonate to EtOAc/MeOH =50:50 for flushing the malonamide). The reaction gave *N*^{1},*N*^{3}-Bis((*S*)-1-hydroxy-3-methylbutan-2-yl)-2-methylmalonamide (**609**) (4.56 g, 15.9 mmol, 92%) as an off-white solid.

^{1}H NMR (300 MHz, $CDCl_3$) δ 7.24 (d, *J* = 9.6 Hz, 1H), 7.14 (d, *J* = 9.3 Hz, 1H), 3.98 (s, 2H), 3.87 – 3.62 (m, 4H), 3.54 (dd, *J* = 11.4, 7.6 Hz, 1H), 3.43 (dd, *J* = 11.4, 8.1 Hz, 1H), 3.32 (q, *J* = 7.2 Hz, 1H), 1.89 – 1.71 (m, 2H), 1.49 (d, *J* = 7.2 Hz, 3H), 0.99 – 0.86 (m, 12H).

5.3.8 N^1,N^3-Bis((*S*)-1-hydroxy-3-methylbutan-2-yl)-2,2-dimethylmalonamide (**610**)

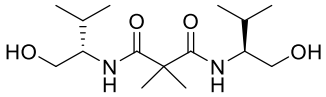

610

Bismalonamide **610** was prepared according to a modified published procedure:[344] To a cooled (0 °C) solution of aminoalcohol **603** (2.50 g, 24.2 mmol, 2.04 eq.) in CH_2Cl_2 (25 mL) was added Et_3N (7.93 mL, 59.55 mmol, 5.00 eq.) and then dropwisely a solution of dimethylmalonyldichloride (**606**) (2.00 g, 11.9 mmol, 1.00 eq) in CH_2Cl_2 (10 mL). After 48 h, the mixture was transferred into a separatory funnel and sequentially washed with HCl (1 M, 20 mL), $NaHCO_3$ (20 mL) and brine (20 mL). After reextraction with CH_2Cl_2 (2 x 20 mL) the combined organic extracts were dried (Na_2SO_4) and concentrated in vacuo to give the corresponding bismalonamide **610** (1.63 g, 5.39 mmol, 45%) as white solid, which was used without further purification.

^{1}**H NMR** (300 MHz, $CDCl_3$) δ 6.44 (d, *J* = 8.9 Hz, 2H), 3.85 – 3.43 (m, 8H), 1.80 (h, *J* = 6.8 Hz, 2H), 1.48 (s, 6H), 0.94 (d, *J* = 6.8 Hz, 6H), 0.90 (d, *J* = 6.8 Hz, 6H).

5.3.9 N^1,N^3-Bis((*S*)-1-hydroxy-3-phenylpropan-2-yl)-2,2-dimethylmalonamide (**611**)

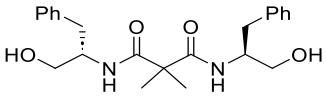

611

Bismalonamide **611** was prepared according to a modified published procedure:[344] To a cooled (0 °C) solution of aminoalcohol **604** (3.60 g, 23.8 mmol, 2.00 eq.) in CH_2Cl_2 (25 mL) was added Et_3N (7.93 mL, 59.55 mmol, 5.00 eq.) and then dropwisely a solution of dimethylmalonyldichloride (**606**) (2.00 g, 11.9 mmol, 1.00 eq) in CH_2Cl_2 (10 mL). After 48 h, the mixture was transferred into a separatory funnel and sequentially washed with HCl (1 M, 20 mL), $NaHCO_3$ (20 mL) and brine (20 mL). After reextraction with CH_2Cl_2 (2 x 20 mL) the combined organic extracts were dried (Na_2SO_4) and concentrated in vacuo to give the corresponding bismalonamide **611** (3.63 g, 9.12 mmol, 77%) as a slightly yellow solid, which was used without further purification.

^{1}**H NMR** (300 MHz, $CDCl_3$) δ 7.32 - 7.14 (m, 10H), 6.40 (d, *J* = 7.1 Hz, 2H), 4.28 – 4.15 (m, 2H), 3.72 (d, *J* = 11.0 Hz, 2H), 3.51 – 3.40 (m, 2H), 3.32 (s, 2H), 2.84 (dd, *J* = 13.8, 6.7 Hz, 2H), 2.73 (dd, *J* = 13.9, 8.0 Hz, 2H), 1.22 (s, 6H).

5.3.10 Bis((*S*)-4-isopropyl-4,5-dihydrooxazol-2-yl)methane (**612**)

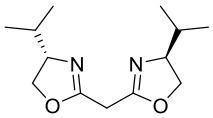

612

BOX-ligand **612** was prepared according to a modified published procedure:[256] To a solution of N^1,N^3-Bis((*S*)-1-hydroxy-3-methylbutan-2-yl)malonamide (**608**) (2.00 g, 8.46 mmol, 1.00 eq.) in CH_2Cl_2 (25 mL) were added Et_3N (5.81 mL, 41.9 mmol, 5.00 eq.) and methanesulfonyl chloride (1.62 mL, 20.9 mmol, 2.50 eq.) and the mixture was stirred for 18 h. NH_4Cl-solution (20 mL) was added and the aqueous phase was extracted with Et_2O (4 x 20 mL).

The combined organic extracts were concentrated under reduced pressure. NaOH-solution (0.5 M, 25 mL in MeOH/H_2O = 50:50) was added and the mixture was heated to reflux for 4 h. After cooling to room temperature, the aqueous phase was extracted with CH_2Cl_2 (3 x 20 mL) and the combined organic extracts were dried over Na_2SO_4. Removal of the solvent under reduced pressure and flash-chromatography (EtOAc, length: 15 cm, diameter: 4 cm) gave bis((*S*)-4-isopropyl-4,5-dihydrooxazol-2-yl)methane (**612**) (432 mg, 1.81 mmol, 21%) as a slightly yellow oil.

^{1}H NMR (300 MHz, $CDCl_3$) δ 4.28 – 4.19 (m, 2H), 4.00 – 3.85 (m, 4H), 3.31 (s, 1H), 1.71 (dp, *J* = 12.4, 6.3, 5.8 Hz, 2H), 0.91 (d, *J* = 6.8 Hz, 6H), 0.84 (d, *J* = 6.8 Hz, 6H).

5.3.11 (4*S*,4′*S*)-2,2′-(Ethane-1,1-diyl)bis(4-isopropyl-4,5-dihydrooxazole) (**581**)

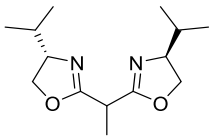

581

BOX-ligand **581** was prepared according to a modified published procedure:[256] To a solution of N^1,N^3-bis((*S*)-1-hydroxy-3-methylbutan-2-yl)-2-methylmalonamide (**609**) (320 mg, 1.27 mmol, 1.00 eq.) in CH_2Cl_2 (12 mL) were added Et_3N (0.78 mL, 5.63 mmol, 4.43 eq.) and methanesulfonyl chloride (0.25 mL, 3.23 mmol, 2.54 eq.) and the mixture was stirred for 24 h. NH_4Cl-solution (20 mL) was added and the aqueous phase was extracted with Et_2O (4 x 20 mL). The combined organic extracts were concentrated under reduced pressure. NaOH-solution (0.5 M, 5 mL in MeOH/H_2O = 50:50) was added and the mixture was heated to reflux for 6 h. After cooling to room temperature, the aqueous phase was extracted with CH_2Cl_2 (3 x 20 mL) and the combined organic extracts were dried over Na_2SO_4. Removal of the solvent under reduced pressure and Flash-chromatography (EtOAc, length: 15 cm, diameter: 4 cm) gave (4*S*,4'*S*)-2,2'-(ethane-1,1-diyl)bis(4-isopropyl-4,5-dihydrooxazole) (**581**) (92.0 mg, 0.364 mmol, 29%) as a lilac oil.

^{1}H NMR (300 MHz, $CDCl_3$) δ 4.23 (ddd, *J* = 7.8, 1.0 Hz, 2H), 4.02 – 3.88 (m, 4H), 3.53 (q, *J* = 7.2 Hz, 1H), 1.77 (dddd, *J* = 12.9, 7.5, 6.4, 4.9 Hz, 2H), 1.48 (d, *J* = 7.2 Hz, 3H), 0.93 (dd, *J* = 6.8, 1.7 Hz, 6H), 0.86 (d, *J* = 6.8 Hz, 6H).

5.3.12 (4*S*,4′*S*)-2,2′-(Propane-2,2-diyl)bis(4-benzyl-4,5-dihydrooxazole) (**614**)

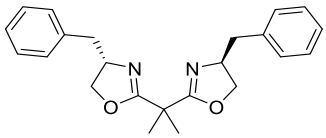

614

To a solution of N^1,N^3-bis((*S*)-1-hydroxy-3-phenylpropan-2-yl)-2,2-dimethylmalonamide (**611**) in THF (20.0 mL) was transferred a solution of Burgess reagent (1.60 g, 6.71 mmol, 3.00 eq.), which was previously weighed inside the glovebox into a septum capped vial, as a solution in THF (3 mL) and rinsed with THF (2 x 3 mL). The mixture was stirred for 18 h, before it was filtered, the solids rinsed with THF and the solvent was removed in vacuo. Purification by column chromatography (*n*-hexane:EtOAc = 60:40 → EtOAc:MeOH = 90:10) gave

(4*S*,4'*S*)-2,2'-propane-2,2-diyl)bis(4-benzyl-4,5-dihydrooxazole) (**614**) (529 mg, 1.46 mmol, 65%). Analytical data was consistent with the literature.[345]

^{1}**H NMR** (300 MHz, $CDCl_3$) δ 7.33 – 7.26 (m, 4H), 7.21 (td, *J* = 6.9, 1.5 Hz, 6H), 4.41 (dddd, *J* = 9.3, 8.6, 6.9, 4.7 Hz, 2H), 4.17 (dd, *J* = 9.3, 8.4 Hz, 2H), 4.01 (dd, *J* = 8.5, 6.8 Hz, 2H), 3.10 (dd, *J* = 13.7, 4.7 Hz, 2H), 2.65 (dd, *J* = 13.7, 8.5 Hz, 2H), 1.46 (s, 6H).

5.4 Synthesis of ruthenium complexes

5.4.1 *cis,fac*-$RuCl_2$(dmso-*S*)$_3$(dmso-*O*) (**677**)

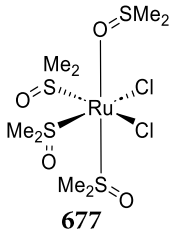

677

Method A: According to a modified published procedure:[291] In a H_2 atmosphere a solution of $RuCl_3$ x H_2O (**676**) (200 mg) in DMSO (5.00 mL) was heated to 80 °C for 48 h. After cooling to room temperature, acetone (200 mL) was added and the solution was cooled in the refrigerator for three days. Filtering off the yellow crystals and drying in a high vacuum gave tetrakis(dimethylsulfoxide)dichlororuthenium(II) (**677**) (198 mg, 0.765 mmol), which corresponds to a yield of 53%, assuming that the ruthenium trichloride trihydrate (**676**) was employed.

Anal. Calcd for $C_8H_{24}Cl_2O_4RuS_4$: C 19.83, H 4.99, S 26.47%. Found: C 19.96, H 4.99, S 26.47%.

Method B: According to a modified published procedure:[292] $RuCl_3$ x H_2O (**676**) (2.00 g, 7.64 mmol assuming x = 3) was refluxed for 3 h in degassed ethanol (50 mL). Undissolved particles were filtered off and the solvent was evaporated in vacuo. The dark green oily residue was dissolved in DMSO (8.00 mL) and stirred at 150 °C for 2.5 h. After cooling to room temperature acetone (60 mL) was added and the mixture allowed to stand at room temperature for 24 h before the precipitate was filtered off, washed with acetone (5 x 5.00 mL) and recrystallized from DMSO/acetone (1:6 v/v) to give *cis,fac*-$RuCl_2$(dmso-S)$_3$(dmso-O) (**677**) (2.36 g, 4.88 mmol, 64%) as a bright yellow crystalline solid.

^{1}H NMR (300 MHz, $CDCl_3$) δ 3.50 (s, 6H, dmso-*S*), 3.44 (s, 6H, dmso-*S*), 3.33 (s, 6H, dmso-*S*), 2.73 (s, 6H, dmso-*O*); additional signals resulting from partial hydrolysis to *cis,fac*-$RuCl_2$(dmso)$_3$(H_2O) and free dmso at δ 3.53, 3.48, 3.42, 2.62.

5.4.2 *μ*-Chloro-(η^4-cycloocta-1,5-diene)ruthenium(II)-polymer (**683**)

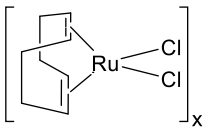

683

$RuCl_3$ x H_2O (**676**) (1.00 g, 3.83 mmol, 1.00 eq.) and 1,5-cyclooctadiene (**681**) (9.25 mL, 75 mmol, 19.6 eq.) were added in a strong counterflow into a flask containing thoroughly degassed EtOH (100 mL). Argon was bubbled through the stirred mixture for 15 minutes before it was heated to reflux for 48 h. After cooling to room temperature the brown precipitate was filtered off and washed with EtOH (3 x 5 mL) and Et_2O (3 x 5 mL) and dried in high vacuum to give [$RuCl_2$(η^4-cod)]$_x$ (**683**) (977 mg, 3.49 mmol, 91%) as a brown powder. In accordance with the literature and owing to the undefined polymer composition, the substance was not further analyzed and used in subsequent steps without further purification.[293, 346, 347]

5.4.3 *cis*-Ru(*t*Bu-bpy)$_2$Cl$_2$ (**701**)

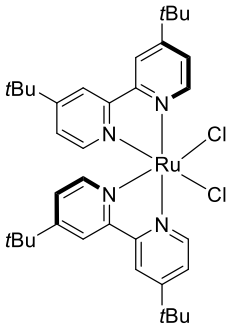

701

cis-Ru(*t*Bu-bpy)$_2$Cl$_2$ (**701**) was prepared according to a modified published procedure:[310] A suspension of [RuCl$_2$(η^4-cod)]$_x$ (**683**) (100 mg, 357 µmol, 1.00 eq.) and 4,4'-*tert*-butyl-2,2'-bipyridine (**698**) (191 mg, 714 µmol, 2.00 eq.) in degassed 1,2-dichlorobenzene (1.8 mL) was heated to 140 °C for 3 h. After cooling to room temperature, the product **701** was precipitated by the addition of *n*-hexane and the supernatant solution was removed after sedimentation of the microcrystalline solid using a syringe. Repeated slurrying with *n*-hexane (total 200 mL), sedimentation and removal of the supernatant liquid inside the flask separated the 1,2-dichlorobenzene. Removal of residual *n*-hexane in vacuo gave *cis*-Ru(*t*Bu-bpy)$_2$Cl$_2$ (**701**) as a lilac solid (249 mg, 352 µmol, 98%).

^{1}H NMR (300 MHz, $CDCl_3$) δ 10.17 (d, *J* = 6.0 Hz, 2H), 8.06 (d, *J* = 2.1 Hz, 2H), 7.91 (d, *J* = 2.1 Hz, 2H), 7.59 – 7.47 (m, 4H), 6.91 (dd, *J* = 6.2, 2.1 Hz, 2H), 1.46 (s, 18H), 1.26 (s, 18H).

^{13}C NMR (75 MHz, CD_3CN) δ 159.56, 153.53, 132.76, 131.57, 129.39, 123.69, 122.80, 120.36, 120.14, 35.96, 35.48, 30.75, 30.65, 30.44.

IR (film on NaCl) ṽ [cm^{-1}] = 3455, 2962, 2870, 1612, 1535, 1478, 1412, 1365, 1314, 1254, 1220, 1125, 1017, 882, 846, 660.

5.4.4 *cis*-Ru(MeO-bpy)$_2$Cl$_2$ (**702**)

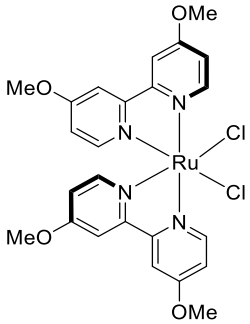

702

cis-Ru(MeO-bpy)$_2$Cl$_2$ (**702**) was prepared according to a modified published procedure:[310] A suspension of [RuCl$_2$(η^4-cod)]$_x$ (**683**) (131 mg, 469 µmol, 1.00 eq.) and 4,4'-dimethoxy-2,2'-bipyridine (**699**) (203 mg, 938 µmol, 2.00 eq.) in degassed 1,2-dichlorobenzene (3 mL) was thoroughly sparged with nitrogen (25 min.) before the mixture was heated to 180 °C for 3 h. After cooling to room temperature, the product **702** was precipitated by the addition of *n*-hexane and the supernatant solution was removed after sedimentation of the microcrystalline solid using a syringe. Repeated slurrying with *n*-hexane (total 200 mL), sedimentation and removal of the supernatant

liquid inside the flask separated the 1,2-dichlorobenzene. Removal of residual *n*-hexane in vacuo gave *cis*-Ru(MeO-bpy)$_2$Cl$_2$ (**702**) as a brown solid (232 mg, 385 µmol, 82%).

^{1}H NMR (300 MHz, (CD$_3$)$_2$SO) δ 9.72 (d, *J* = 6.5 Hz, 1H), 8.27 (d, *J* = 2.7 Hz, 1H), 8.12 (d, *J* = 2.8 Hz, 1H), 7.43 (dd, *J* = 6.6, 2.7 Hz, 1H), 7.29 (d, *J* = 6.5 Hz, 1H), 6.79 (dd, *J* = 6.6, 2.7 Hz, 1H), 4.07 (s, 3H), 3.86 (s, 3H).

^{13}C NMR (75 MHz, (CD$_3$)$_2$SO) δ 166.19, 156.82, 150.50, 110.73, 106.03, 55.41.

IR (film on NaCl) ῡ [cm^{-1}] = 3049, 3014, 2971, 2941, 2839, 1608, 1587, 1560, 1478, 1459, 1435, 1424, 1389, 1294, 1256, 1232, 1222, 1191, 1175, 1029, 999, 986, 897, 845, 829, 819, 772, 742.

HRMS (ESI) m/z calculated for $C_{24}H_{27}ClN_4O_5Ru$ (Ru(MeO-bpy)$_2$(MeO)Cl) [M + H] - 600.0713, found 600.0713.

5.4.5 [Ru(dmb)$_3$](PF$_6$)$_2$ (**692**)

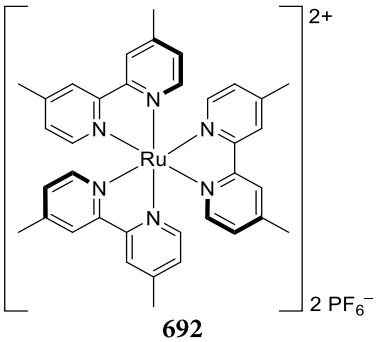

692

Under exclusion of light, a solution of *cis*-RuCl$_2$(dmso)$_4$ (**677**) (50.0 mg, 0.103 mmol, 1.00 eq.) and 4,4'-dimethylbipyridine **626** (57.0 mg, 0.310 mmol, 3.00 eq.) in a degassed mixture of ethylene glycol (8.00 mL) and water (1.00 mL) was heated to 120 °C for 2 h. After cooling to room temperature a saturated solution of KPF$_6$ (5.00 mL) was added to precipitate an orange solid, which was filtered and sequentially washed with water (2 x 20 mL), toluene (2 x 20 mL) and *n*-hexane (5 x 5 mL). The solid was rinsed into a flask with MeCN and the solvent was removed to give [Ru(dmb)$_3$](PF$_6$)$_2$ (**692**) (96.4 mg, 0.102 mmol, 99%) as an orange solid, that was used without further purification as analytical data was consistent with the literature.[348]

^{1}H NMR (300 MHz, CD$_3$CN) δ 8.33 (d, *J* = 1.8 Hz, 2H), 7.53 (d, *J* = 5.8 Hz, 2H), 7.21 (ddd, *J* = 5.8, 1.9, 0.9 Hz, 2H), 2.52 (s, 6H).

5.4.6 [Ru(DiMeMal-bpy)$_3$](PF$_6$)$_2$ (**693**)

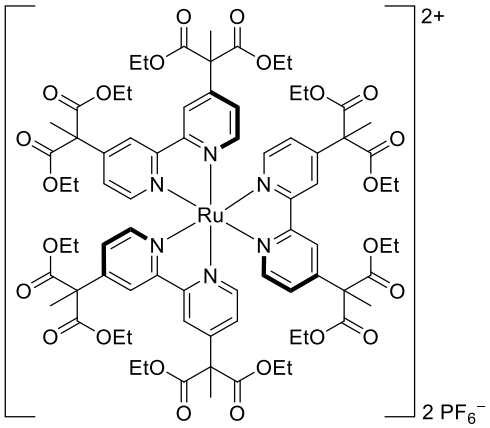

693

Under exclusion of light, a solution of *cis*-RuCl$_2$(dmso)$_4$ **677** (15.0 mg, 31.0 µmol, 1.00 eq.) and tetraethyl 2,2'-([2,2'-bipyridine]-4,4'-diyl)bis(2-methylmalonate) (**626**) (72.1 mg, 0.144 mmol, 4.66 eq.) in a degassed mixture of ethylenglycol (4.5 mL) and water (0.5 mL) was heated to 80 °C for 18 h. After cooling to room temperature a saturated solution of KPF$_6$ (5.00 mL) was added to precipitate an orange solid, which was filtered and purified by column chromatography (CH$_2$Cl$_2$:MeOH:NH$_4$OH (25%) = 91:8:1 → 72:25:3) to give Ru(DiMeMal-bpy)$_3$X$_2$ (**693**) (38.1 mg, 20.1 µmol, 65%, assuming X = PF$_6$).

^{1}H NMR (300 MHz, CD$_3$CN) δ 8.43 (t, *J* = 1.8 Hz, 2H), 7.68 (d, *J* = 6.0 Hz, 2H), 7.36 (dt, *J* = 6.0, 1.6 Hz, 2H), 4.24 (qd, *J* = 7.1, 1.8 Hz, 8H), 1.90 (s, 6H), 1.22 (td, *J* = 7.1, 1.3 Hz, 12H).

^{13}C NMR (75 MHz, CD$_3$CN) δ 170.36, 157.51, 152.41, 150.59, 127.65, 124.66, 63.60, 59.80, 22.37, 14.22, 1.32.

IR (film on NaCl) ῡ [cm^{-1}] = 2984, 2941, 1733, 1616, 1546, 1467, 1416, 1382, 1366, 1265, 1111, 1017, 928, 839, 758.

HRMS (ESI) m/z calculated for C$_{78}$H$_{96}$N$_6$O$_{24}$Ru [M^{2+}]– 801.2754, found 801.2766.

5.4.7 [Ru(bpy)$_3$]Cl$_2$ x 6 H$_2$O (7)

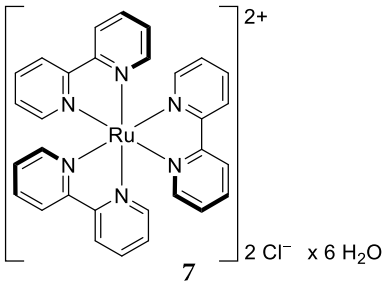

7

Ruthenium(III) chloride hydrate (**676**) was heated to 120 °C in a vacuum drying oven for 3 h. A suspension of the resulting ruthenium(III) chloride (400 mg, 1.93 mmol, 1.00 eq.), bipyridine (900 mg, 5.76 mmol, 2.98 eq.) and hypophosphorous acid (31% + NaOH, 2.00 mL) in H$_2$O (40 mL) was refluxed for 1 h. While still hot, the undissolved solids were filtered off and KCl (12.9 g, 173 mmol, 89.7 eq.) was added to the solution to precipitate [Ru(bpy)$_3$]Cl$_2$. After heating to reflux the solution was cooled to room temperature overnight. The precipitate was filtered off and the mother liquor was concentrated in vacuo and left for further precipitation overnight. After filtering off again, the reaction gave Ruthenium-tris(2,2'-bipyridyl) dichloride hexahydrate (**7**) (835 mg, 1.12 mmol, 58%) as red, plate-like crystals. Analytical data was consistent with the literature.[348]

^{1}H NMR (300 MHz, CD_3CN) δ 8.48 (dt, *J* = 8.2, 1.2 Hz, 6H), 8.04 (td, *J* = 7.9, 1.5 Hz, 6H), 7.71 (ddd, *J* = 5.7, 1.5, 0.8 Hz, 6H), 7.38 (ddd, *J* = 7.6, 5.6, 1.3 Hz, 6H).

^{13}C NMR (75 MHz, CD_3CN) δ 157.98, 152.69, 138.79, 128.57, 125.26.

IR (film on NaCl) ῡ [cm^{-1}] = 2357, 1220, 772.

MS (ESI) m/z calculated for $C_{30}H_{24}N_6Ru$ [M^{2+}]– 285.1, found 285.3.

5.4.8 [Ru(bpy)$_2$(BOX-bpy)](PF$_6$)$_2$ (**532**)

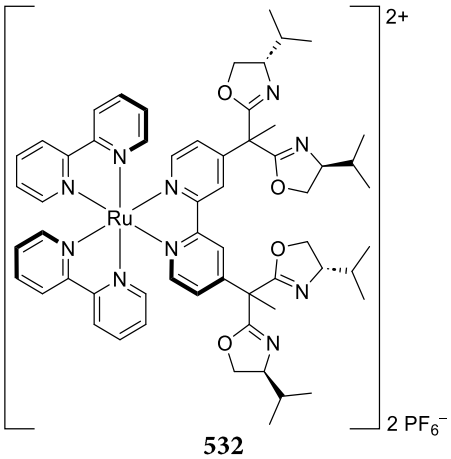

532

To a solution of Ru(bpy)$_2$Cl$_2$ (**717**) (80.1 mg, 165 µmol, 1.00 eq.) in degassed acetone (5.00 mL) was added a solution of AgOTf (85.0 mg, 331 µmol, 2.00 eq.), that was stored inside a nitrogen glovebox and weighed into a septum capped vial, in degassed acetone (3 x 5 mL) and the mixture was allowed to stir for 2 h. The silver chloride was removed by transferring the reaction mixture through a syringe filter into a second purged and nitrogen filled flask, containing a solution of BOX-bpy **529** in acetone (109 mg, 165 µmol, 1.00 eq.). After rinsing residues from the first flask into the second flask using acetone (2 x 2 mL), the mixture was heated to 50 °C for 4 h. Removal of the solvent and purification of the residue by column chromatography (CH_2Cl_2:MeOH:NH_4OH (25%) = 91:8:1) followed by dissolving the complex in CH_2Cl_2 and washing with a saturated KPF_6-solution gave the complex [Ru(bpy)$_2$(BOX-bpy)](PF$_6$)$_2$ (**532**) (103.5 mg, 76.1 µmol, 46%) as a red solid.

^{1}H NMR (300 MHz, CD_3CN) δ 8.56 – 8.45 (m, 6H), 8.07 (dddd, *J* = 8.2, 7.7, 5.5, 1.5 Hz, 4H), 7.74 – 7.65 (m, 6H), 7.45 – 7.36 (m, 6H), 4.34 – 4.22 (m, 4H), 4.08 – 3.98 (m, 3H), 3.91 (tdd, *J* = 9.7, 7.8, 6.0 Hz, 3H), 1.90 (s, 5H), 1.71 (dtt, *J* = 13.5, 6.8, 3.4 Hz, 3H), 0.95 – 0.77 (m, 24H).

^{13}C NMR (75 MHz, CD_3CN) δ 165.99, 157.85, 152.64, 138.80, 128.55, 127.33, 125.26, 124.25, 72.83, 71.77, 48.29, 33.40, 18.78, 18.47.

IR (film on NaCl) ῡ [cm^{-1}] = 2961, 2931, 2910, 2874, 1717, 1656, 1616, 1604, 1466, 1446, 1418, 1362, 1273, 1257, 1241, 1222, 1175, 1091, 1031, 970, 934, 875, 770, 732, 702, 666, 637.

HRMS (ESI) m/z calculated for $C_{58}H_{68}N_{10}O_4Ru$ ([Ru(bpy)$_2$(BOX-bpy)]$^{2+}$) [M^{2+}]– 535.2229, found 535.2234.
$C_{58}H_{70}N_{10}O_5Ru$ (1x hydrolyzed oxazoline) [(H_2O)-M^{2+}]– 544.2282, found 544.2285.
$C_{58}H_{72}N_{10}O_6Ru$ (2x hydrolyzed oxazoline) [(H_2O)$_2$-M^{2+}]– 553.2335, found 553.2338.

5.4.9 [Ru(*t*Bu-bpy)$_2$(BOX-bpy)](PF$_6$)$_2$ (**536**)

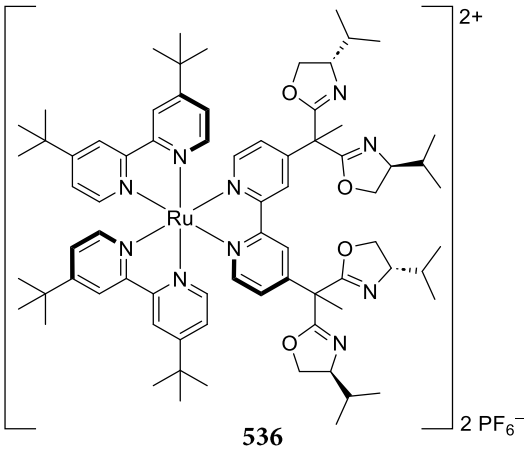

536

To a solution of Ru(*t*Bu-bpy)$_2$Cl$_2$ (**701**) (118 mg, 165 µmol, 1.00 eq.) in degassed acetone (5.00 mL) was added a solution of AgOTf (85.0 mg, 331 µmol, 2.00 eq.), that was stored inside a nitrogen glovebox and weighed into a septum capped vial, in degassed acetone (3 x 5 mL) and the mixture was allowed to stir for 2 h. The silver chloride was removed by transferring the reaction mixture through a syringe filter into a second purged and nitrogen filled flask, containing a solution of BOX-bpy **529** in acetone (109 mg, 165 µmol, 1.00 eq.). After rinsing residues from the first flask into the second flask using acetone (2 x 2 mL), the mixture was heated to 50 °C for 4 h. Removal of the solvent and purification of the residue by column chromatography (CH_2Cl_2:MeOH:NH_4OH (25%) = 91:8:1) followed by dissolving the complex in CH_2Cl_2 and washing with a saturated KPF_6-solution gave the complex [Ru(*t*Bu-bpy)$_2$(BOX-bpy)](PF$_6$)$_2$ (**536**) (136 mg, 85.8 µmol, 52%) as a red solid.

^{1}H NMR (300 MHz, CD_3CN) δ 8.48 (dd, *J* = 5.0, 3.0 Hz, 6H), 7.66 (dd, *J* = 6.0, 1.3 Hz, 2H), 7.56 (td, *J* = 4.3, 2.2 Hz, 4H), 7.41 (ddt, *J* = 6.0, 4.1, 2.2 Hz, 6H), 4.40 – 4.22 (m, 4H), 4.13 – 3.84 (m, 8H), 1.91 (s, 6H), 1.77 – 1.65 (m, 4H), 1.41 (s, 36H), 0.99 – 0.76 (m, 24H).

^{13}C NMR (75 MHz, CD_3CN) δ 163.34, 157.89, 151.73, 125.56, 122.40, 36.30, 30.47.

IR (film on NaCl) ϋ [cm^{-1}] = 2962, 2909, 2873, 1656, 1614, 1542, 1481, 1467, 1415, 1367, 1251, 1203, 1175, 1092, 1030, 970, 934, 899, 749, 703, 666, 638, 607.

HRMS (ESI) m/z calculated for $C_{74}H_{100}N_{10}O_4Ru$ ([Ru(*t*Bu-bpy)$_2$(BOX-bpy)]$^{2+}$) [M^{2+}]– 647.3481, found 647.3492.

$C_{74}H_{102}N_{10}O_5Ru$ (1x hydrolyzed oxazoline) [(H_2O)-M^{2+}]– 656.3534, found 656.3542.

$C_{74}H_{104}N_{10}O_6Ru$ (2x hydrolyzed oxazoline) [(H_2O)$_2$-M^{2+}]– 665.3587, found 665.3583.

5.4.10 [Ru(MeO-bpy)$_2$(BOX-bpy)](PF$_6$)$_2$ (**537**)

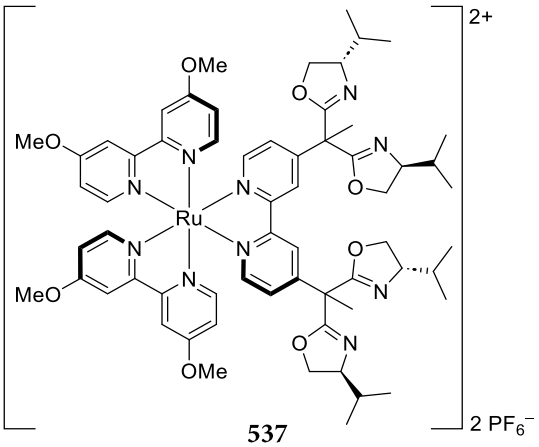

537

To a solution of Ru(MeO-bpy)$_2$Cl$_2$ (**702**) (99.9 mg, 165 µmol, 1.00 eq.) in degassed acetone (5.00 mL) was added a solution of AgOTf (85.3 mg, 332 µmol, 2.00 eq.), that was stored inside a nitrogen glovebox and weighed into a septum capped vial, in degassed acetone (3 x 5 mL) and the mixture was allowed to stir for 2 h. The silver chloride was removed by transferring the reaction mixture through a syringe filter into a second purged and nitrogen filled flask, containing a solution of BOX-bpy **529** in acetone (109 mg, 165 µmol, 1.00 eq.). After rinsing residues from the first flask into the second flask using acetone (2 x 2 mL), the mixture was heated to 50 °C for 4 h. Removal of the solvent and purification of the residue by column chromatography (CH_2Cl_2:MeOH:NH_4OH (25%) = 91:8:1) followed by dissolving the complex in CH_2Cl_2 and washing with a saturated KPF_6-solution gave the complex [Ru(MeO-bpy)$_2$(BOX-bpy)](PF$_6$)$_2$ (**537**) (113 mg, 76.2 µmol, 46%) as a red solid.

^{1}H NMR (300 MHz, CD_3CN) δ 8.43 (d, *J* = 2.3 Hz, 2H), 8.01 (s, 4H), 7.73 (d, *J* = 6.0 Hz, 2H), 7.51 (d, *J* = 6.4 Hz, 2H), 7.49 – 7.31 (m, 4H), 7.02 – 6.87 (m, 4H), 4.35 – 4.20 (m, 2H), 4.11 – 3.85 (m, 22H), 1.94 – 1.85 (m, 6H), 1.00 – 0.76 (m, 24H).

^{13}C NMR (75 MHz, CD_3CN) δ 166.80, 151.75, 143.94, 117.00, 110.70, 87.67, 79.69, 71.56, 56.37, 22.97, 17.52.

IR (film on NaCl) $\tilde{\upsilon}$ [cm^{-1}] = 2961, 2875, 1663, 1615, 1557, 1492, 1471, 1441, 1417, 1389, 1361, 1338, 1311, 1279, 1264, 1250, 1225, 1175, 1100, 1042, 1035, 1018, 968, 934, 841, 751, 666.

HRMS (ESI) m/z calculated for $C_{62}H_{76}N_{10}O_8Ru$ ([Ru(MeO-bpy)$_2$(BOX-bpy)]$^{2+}$) [M^{2+}]– 595.2440, found 595.2450.

$C_{62}H_{78}N_{10}O_9Ru$ (1x hydrolyzed oxazoline) [(H_2O)-M^{2+}]– 604.2493, found 604.2509.

$C_{62}H_{80}N_{10}O_{10}Ru$ (2x hydrolyzed oxazoline) [(H_2O)$_2$-M^{2+}]– 613.2546, found 613.2560.

5.5 Synthesis of substrates

5.5.1 Substrates for intramolecular radical cyclization

5.5.1.1 Dimethyl 2-(pent-4-en-1-yl)malonate (**742**)

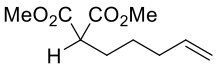

742

Dimethyl 2-(pent-4-en-1-yl)malonate (**742**) was prepared according to a modified published procedure:[349] To a solution of dimethylmalonate (**740**) (1.00 g, 7.57 mmol, 1.00 eq) in THF/DMF (1:1 v/v, 15 mL) was added K_2CO_3 (1.36 g, 9.84 mmol, 1.30 eq.) and the mixture was stirred for 15 minutes at room temperature before 5-bromopent-1-ene (**741**) (1.18 g, 7.95 mmol, 1.05 eq.) was added and stirring was continued at 90 °C for 18 h. After cooling water (50 mL) was added and the aqueous phase was extracted with CH_2Cl_2 (3 x 30 mL). The combined organic extracts were washed with water (5 x 50 mL), dried (Na_2SO_4) and concentrated in vacuo. Purification by column chromatography (gradient: *n*-Hexane/EtOAc = 90:10 → 85:15) gave dimethyl 2-(pent-4-en-1-yl)malonate (**742**) (1.40 g, 6.98 mmol, 92%) as a colorless oil. Analytical data was consistent with the literature.[350]

^{1}H NMR (300 MHz, $CDCl_3$) δ 5.77 (ddt, *J* = 16.9, 10.2, 6.6 Hz, 1H), 5.07 – 4.92 (m, 2H), 3.73 (s, 6H), 3.36 (t, *J* = 7.5 Hz, 1H), 2.13 – 2.01 (m, 2H), 1.97 – 1.85 (m, 2H), 1.48 – 1.34 (m, 2H).

5.5.1.2 Dimethyl 2-(hex-5-en-1-yl)malonate (**744**)

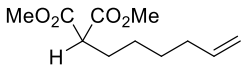

744

Dimethyl 2-(hex-5-en-1-yl)malonate (**744**) was prepared according to a modified published procedure:[349] To a suspension of K_2CO_3 (2.51 g, 18.2 mmol, 1.20 eq.) in THF/DMF (1:1 v/v, 30 mL) was added dimethylmalonate (**740**) (2.00 g, 15.1 mmol, 1.00 eq) and the mixture was stirred for 15 minutes at room temperature before 5-bromohex-1-ene (2.59 g, 15.9 mmol, 1.05 eq.) was added and stirring was continued at 90 °C for 24 h. After cooling water (150 mL) was added and the aqueous phase was extracted with CH_2Cl_2 (3 x 50 mL). The combined organic extracts were dried (Na_2SO_4) and concentrated in vacuo. Purification by column chromatography (gradient: *n*-Hexane/EtOAc = 90:10 → 85:15) gave dimethyl 2-(hex-5-en-1-yl)malonate (**744**) (2.52 g, 11.7 mmol, 78%) as a colorless oil. Analytical data was consistent with the literature.[351]

^{1}H NMR (300 MHz, $CDCl_3$) δ 5.78 (ddt, *J* = 16.9, 10.2, 6.7 Hz, 1H), 5.06 - 4.88 (m, 1H), 4.96 (dq, *J* = 2.2, 1.0 Hz, 1H), 3.73 (s, 6H), 3.35 (t, *J* = 7.6 Hz, 1H), 2.10 - 2.00 (m, 2H), 1.95 - 1.85 (m, 2H), 1.48 - 1.24 (m, 4H).

5.5.1.3 Dimethyl 2-bromo-2-(pent-4-en-1-yl)malonate (**734**)

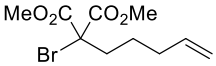

734

Dimethyl 2-bromo-2-(pent-4-en-1-yl)malonate (**734**) was prepared according to a modified published procedure:[16] A solution of dimethyl 2-(pent-4-en-1-yl)malonate (**742**) (1.02 g, 5.11 mmol, 1.00 eq.) in THF

(50 mL) was cooled to –78 °C and mixed with LiHMDS (0.97 M solution in THF, 5.79 mL, 5.62 mmol, 1.10 eq.) and NBS (1.18 g, 6.64 mmol, 1.30 eq.). After stirring at –78 °C for 18 h, the reaction was quenched by transferring the mixture into a separating funnel containing H_2O (50 mL) and Et_2O (50 mL). The aqueous phase was extracted with Et_2O (3 x 50 mL) and the combined organic extracts were dried (Na_2SO_4). Removal of the solvent under reduced pressure and purification of the residue by column chromatography (*n*-hexane/EtOAc = 90:10) gave dimethyl 2-bromo-2-(pent-4-en-1-yl)malonate (**734**) (1.38 g, 4.98 mmol, 97%) as a colorless oil.

^{1}H NMR (300 MHz, $CDCl_3$) δ 5.75 (ddt, *J* = 16.9, 10.2, 6.6 Hz, 1H), 5.09 – 4.89 (m, 2H), 3.80 (s, 6H), 2.33 – 2.19 (m, 2H), 2.09 (qt, *J* = 7.2, 1.4 Hz, 2H), 1.49 (ddt, *J* = 10.9, 9.0, 6.1 Hz, 2H).

5.5.1.4 Dimethyl 2-bromo-2-(hex-5-en-1-yl)malonate (**737**)

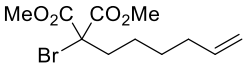

737

Dimethyl 2-bromo-2-(hex-5-en-1-yl)malonate (**737**) was prepared according to a modified published procedure:[16] A solution of dimethyl 2-(hex-5-en-1-yl)malonate (**744**) (1.00 g, 4.67 mmol, 1.00 eq.) in THF (50 mL) was cooled to –78 °C and mixed with LiHMDS (0.97 M solution in THF, 5.80 mL, 5.63 mmol, 1.21 eq.) and NBS (1.08 g, 6.07 mmol, 1.30 eq.). After stirring at –78 °C for 18 h, the reaction was quenched by transferring the mixture into a separating funnel containing H_2O (50 mL) and Et_2O (50 mL). The aqueous phase was extracted with Et_2O (3 x 50 mL) and the combined organic extracts were dried (Na_2SO_4). Removal of the solvent under reduced pressure and purification of the residue by flash chromatography (gradient over 90 min.: *n*-Hexane/EtOAc = 98:2 → 95:5, flow: 30 mL/min., length: 15 cm, diameter: 4 cm) gave dimethyl 2-bromo-2-(hex-5-en-1-yl)malonate (**737**) (1.34 g, 4.58 mmol, 98%) as a colorless oil.

^{1}H NMR (300 MHz, $CDCl_3$) δ 5.78 (ddt, *J* = 16.9, 10.2, 6.7 Hz, 1H), 5.07 – 4.90 (m, 1H), 4.97 (dq, *J* = 2.4, 1.4 Hz, 1H), 3.82 (s, 6H), 2.35 – 2.21 (m, 2H), 2.13 – 2.00 (m, 2H), 1.53 – 1.36 (m, 4H).

5.5.1.5 Dimethyl (*E*)-2-bromo-2-(6-(trimethylsilyl)hex-4-en-1-yl)malonate (**738**)

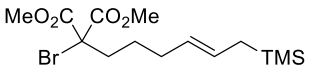

738

Dimethyl-(*E*)-2-bromo-2-(6-(trimethylsilyl)hex-4-en-1-yl)malonate (**738**) was prepared according to a modified published procedure:[16] Inside a nitrogen glovebox Grubbs II-catalyst (43.0 mg, 0.051 mmol, 5 mol%) was weighed into a flame dried two necked flask that was attached to a flame dried reflux condenser using established schlenk techniques. Inhibitor free CH_2Cl_2 (5 mL) was filtered through a neutral aluminium oxide column was thoroughly degassed by freeze-pump-thaw and transferred into the catalyst containing reaction flask. Dimethyl-2-bromo-2-(pent-4-en-1-yl)malonate (**734**) (280 mg, 1.01 mmol, 1.00 eq.) and allyltrimethylsilane (**745**) (346 mg, 3.03 mmol, 3.00 eq.) were added and the mixture was heated to reflux until full conversion was indicated by TLC. After cooling to room temperature ethyl vinyl ether (8.50 mg, 101 µmol, 10 mol%) was added and the mixture stirred for 30 minutes. The solvent was removed in vacuo and the residue

purified by flash chromatography (gradient over 90 min.: *n*-Hexane/EtOAc = 99:1 → 95:5, flow: 30 mL/min., length: 15 cm, diameter: 4 cm) to give dimethyl-(*E*)-2-bromo-2-(6-(trimethylsilyl)hex-4-en-1-yl)malonate (**738**) (212 mg, 582 mmol, 58%).

^{1}**H NMR** (300 MHz, $CDCl_3$) δ 5.50 – 5.34 (m, 1H), 5.29 – 5.13 (m, 1H), 3.81 (d, *J* = 0.7 Hz, 6H), 2.36 – 2.21 (m, 2H), 2.10 – 1.96 (m, 2H), 1.54 – 1.35 (m, 4H), –0.01 (d, *J* = 3.5 Hz, 9H).

5.5.1.6 3-(Hept-6-ynoyl)oxazolidin-2-one (**748**)

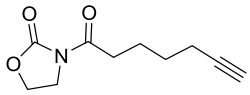

748

3-(Hept-6-ynoyl)oxazolidin-2-one (**748**) was prepared according to a modified published procedure:[352] To a cooled (0 °C) solution of oxazolidin-2-one (**747**) (628 mg, 7.21 mmol, 1.00 eq.) in CH_2Cl_2 (25 mL) were added heptynoic acid (**746**) (1.00 g, 7.93 mmol, 1.10 eq.), DMAP (96.9 mg, 0.793 mmol, 10 mol%) and DCC (1.64 g, 7.93 mmol, 1.10 eq.). The mixture was allowed to warm up to room temperature and stirring was continued for 4 days. The solid was filtered off and rinsed with CH_2Cl_2. The filtrate was washed with $NaHCO_3$-solution (100 mL) and the aqueous phase was extracted with CH_2Cl_2 (2 x 30 mL). The combined organic extracts were dried (Na_2SO_4) and concentrated in vacuo. Purification by column chromatography (*n*-hexane/EtOAc = 70:30) gave 3-(hept-6-ynoyl)oxazolidin-2-one (**748**) (859 mg, 4.40 mmol, 61%) as a colorless oil that crystallized upon standing.

^{1}**H NMR** (600 MHz, $CDCl_3$) δ 4.39 (td, *J* = 8.1, 2.2 Hz, 2H), 4.00 (td, *J* = 8.1, 2.2 Hz, 2H), 2.96 – 2.88 (m, 2H), 2.21 (td, *J* = 7.0, 2.8 Hz, 2H), 1.93 (d, *J* = 2.7 Hz, 1H), 1.76 (pd, *J* = 7.6, 2.2 Hz, 2H), 1.58 (pd, *J* = 7.3, 2.2 Hz, 2H).

5.5.1.7 3-(2-Bromohept-6-ynoyl)oxazolidin-2-one (**722**)

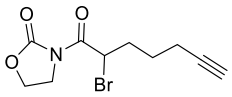

722

3-(2-Bromohept-6-ynoyl)oxazolidin-2-one (**722**) was prepared according to a modified published procedure:[16] A solution of 3-(hept-6-ynoyl)oxazolidin-2-one (**722**) (100 mg, 0.513 mmol, 1.00 eq.) in THF (15 mL) was cooled to –78 °C and mixed with LiHMDS (0.97 M solution in THF, 0.581 mL, 0.564 mmol, 1.10 eq.) and NBS (119 mg, 0.667 mmol, 1.30 eq.). After stirring at –78 °C for 48 h, the reaction was quenched by transferring the mixture into a separating funnel containing H_2O (30 mL) and Et_2O (30 mL). The aqueous phase was extracted with Et_2O (3 x 25 mL) and the combined organic extracts were dried (Na_2SO_4). Removal of the solvent under reduced pressure and purification of the residue by column chromatography (*n*-hexane/EtOAc = 70:30) gave 3-(2-bromohept-6-ynoyl)oxazolidin-2-one (**722**) (105 mg, 0.384 mmol, 75%) as a yellow oil.

^{1}**H NMR** (300 MHz, $CDCl_3$) δ 5.59 (dd, *J* = 8.0, 6.4 Hz, 1H), 4.50 – 4.34 (m, 3H), 4.14 – 3.94 (m, 2H), 2.28 – 2.06 (m, 4H), 1.94 (dt, *J* = 8.8, 2.7 Hz, 1H), 1.81 – 1.65 (m, 1H), 1.65 – 1.50 (m, 1H).

5.5.2 Substrates for intermolecular atom transfer radical addition

5.5.2.1 2-(2-Bromopropanoyl)cyclopentan-1-one (**770**)

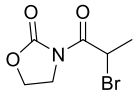

770

2-(2-Bromopropanoyl)cyclopentane-1-one (**770**) was prepared according to a modified published procedure:[353] To a cooled (–78 °C) solution of 2-oxazolidinone (**747**) (4.79 g, 55.0 mmol, 1.00 eq.) in THF (100 mL) was slowly added *n*-BuLi (2.48 M in *n*-hexane, 26.6 mL, 66.0 mmol, 1.20 eq.) and stirring was continued for 30 minutes before 2-bromopropanoyl bromide (5.83 mL, 55 mmol, 1.00 eq.) were added. The mixture was allowed to warm up to room temperature overnight. Water (100 mL) was added and THF was removed under reduced pressure. The aqueous phase was extracted with EtOAc (3 x 50 mL). The combined organic extracts were washed with brine (100 mL), dried (Na_2SO_4) and concentrated in vacuo. Purification by flash chromatography (gradient over 90 min.: *n*-Hexane/EtOAc = 85:15 → 70:30, flow: 30 mL/min., length: 15 cm, diameter: 4 cm) gave 2-(2-bromopropanoyl)cyclopentane-1-one (**770**) (5.64 g, 25.5 mmol, 46%).

^{1}**H NMR** (300 MHz, $CDCl_3$) δ 5.75 – 5.65 (m, 1H), 4.47 (ddt, *J* = 8.9, 7.6, 0.9 Hz, 2H), 4.11 – 4.03 (m, 2H), 1.84 (ddd, *J* = 6.8, 1.8, 1.1 Hz, 3H).

5.5.2.2 Ethyl 1-bromo-2-oxocyclohexane-1-carboxylate (**767**)

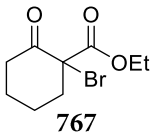

767

Ethyl 1-bromo-2-oxocyclohexane-1-carboxylate (**767**) was prepared according to a modified published procedure:[354] To a solution of ethyl 2-oxocyclohexane-1-carboxylate (100 mg, 0.588 mmol, 1.00 eq.) in CH_2Cl_2 (10.0 mL) were added NBS (105 mg, 0.589 mmol, 1.00 eq.) and *p*-toluenesulfonic acid monohydrate (112 mg, 0.589 mmol, 1.00 eq.) and the mixture was stirred for 18 h. Water (20 mL) was added and the aqueous phase was extracted with CH_2Cl_2 (20 mL) and EtOAc (2 x 20 mL). The combined organic extracts were washed with brine (50 mL), dried (Na_2SO_4) and concentrated in mild vacuum to give ethyl 1-bromo-2-oxocyclohexane-1-carboxylate (**767**) as a colorless oil in quantitative yield (144 mg, 581 mmol, 99%).

^{1}**H NMR** (300 MHz, $CDCl_3$) δ 4.24 (qd, *J* = 7.2, 1.8 Hz, 2H), 2.94 – 2.74 (m, 2H), 2.70 (d, *J* = 1.5 Hz, 1H), 2.40 (ddd, *J* = 16.4, 9.2, 5.4 Hz, 1H), 2.25 – 2.10 (m, 1H), 1.95 – 1.60 (m, 4H), 1.25 (td, *J* = 7.1, 1.8 Hz, 3H).

5.5.3 Substrates for cascade cyclization

5.5.3.1 3-Phenylprop-2-yn-1-yl-3-oxo-3-phenylpropanoate (**787**)

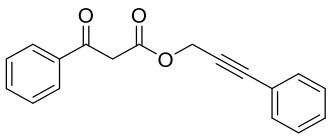

787

3-Phenylprop-2-yn-1-yl-3-oxo-3-phenylpropanoate (**787**) was prepared according to a modified published procedure:[355] A solution of ethyl-3-oxo-3-phenylpropanoate (**785**) (8.00 g, 41.6 mmol, purity 90%, 8.89 mL, 1.00 eq.), 3-phenylprop-2-yn-1-ol (**786**) (16.5 g, 124.8 mmol, 3.00 eq.) and DMAP (5.08 g, 41.6 mmol, 1.00 eq.) in toluene (400 mL) was refluxed using a Dean-Stark trap. Over the course of the reaction solvent was continuously removed and replaced with a total of 500 mL fresh toluene until TLC indicated full conversion. After cooling to room temperature water (500 mL) was added and the aqueous phase was extracted with EtOAc (5 x 100 mL). The combined organic extracts were washed with brine (2 x 50 mL), dried (Na_2SO_4) and concentrated in vacuo. Purification by column chromatography (*n*-hexane/EtOAc = 95:5, length: 27 cm, diameter: 8 cm) gave 3-phenylprop-2-yn-1-yl-3-oxo-3-phenylpropanoate (**787**) (7.62 g, 27.4 mmol, 66%). Following the described procedure in a smaller scale provided a maximum yield of 73%.

^{1}**H NMR** (300 MHz, $CDCl_3$) δ 12.35 (s, 0.30H, enol), 7.99 – 7.92 (m, 2.03H), 7.82 – 7.77 (m, 0.58H, enol), 7.64 – 7.56 (m, 0.98H, enol), 7.53 – 7.39 (m, 5.30H), 7.32 (dddd, J = 5.2, 4.1, 2.5, 1.2 Hz, 3.60H), 5.76 (s, 0.29H, enol), 5.06 (s, 0.60H, enol), 5.00 (s, 2H), 4.09 (s, 2H).

HRMS (ESI) m/z calculated for $C_{18}H_{18}NO_3$ [M + NH_4^+] - 296.1281, found 296.1282.

5.5.3.2 3-Phenylprop-2-yn-1-yl 2-methyl-3-oxo-3-phenylpropanoate (**788**)

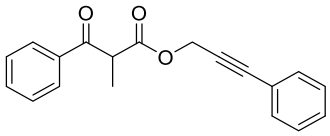

788

To a cooled (0 °C) solution of 3-phenylprop-2-yn-1-yl-3-oxo-3-phenylpropanoate (**787**) (5.00 g, 18.0 mmol, 1.00 eq.) in THF (80 mL) was added NaH (719 mg, 60% in mineral oil, 18.0 mmol, 1.00 eq.) and stirring was continued for 30 minutes before MeI (1.12 mL, 2.55 g, 18.0 mmol, 1.00 eq.) was added. After 22 h the reaction was quenched by the addition of H_2O (100 mL). The aqueous phase was extracted with EtOAc (3 x 100 mL), dried (Na_2SO_4) and concentrated in vacuo. Purification by flash chromatography (gradient over 90 min.: *n*-Hexane/EtOAc = 95:5 → 85:15, flow: 30 mL/min., length: 15 cm, diameter: 4 cm) gave 3-phenylprop-2-yn-1-yl-2-methyl-3-oxo-3-phenylpropanoate (**788**) (4.96 g, 17.0 mmol, 94%).

^{1}**H NMR** (300 MHz, $CDCl_3$) δ 8.04 – 7.95 (m, 2H), 7.61 – 7.53 (m, 1H), 7.50 – 7.43 (m, 2H), 7.42 – 7.36 (m, 2H), 7.31 (td, *J* = 5.3, 2.6 Hz, 3H), 4.98 (d, *J* = 15.6 Hz, 1H), 4.88 (d, *J* = 15.6 Hz, 1H), 4.46 (q, *J* = 7.1 Hz, 1H), 1.54 (d, *J* = 7.1 Hz, 3H).

^{13}C NMR (75 MHz, $CDCl_3$) δ 195.59, 170.41, 135.76, 133.72, 132.03, 128.99, 128.94, 128.82, 128.66, 128.41, 122.17, 86.92, 82.51, 53.81, 48.35, 29.86, 13.99.

IR (film on NaCl) ϋ [cm^{-1}] = 2923, 2852, 2362, 2333, 1541, 1507, 1457, 1220, 772, 688.

HRMS (ESI) m/z calculated for $C_{19}H_{16}NaO_3$ [M + Na^+] - 315.0992, found 315.0989.

5.5.3.3 3-Phenylprop-2-yn-1-yl 2-bromo-2-methyl-3-oxo-3-phenylpropanoate (**779**)

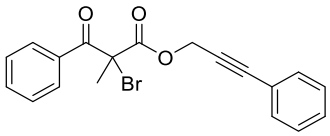

779

To a cooled (–78 °C) solution of 3-phenylprop-2-yn-1-yl-2-methyl-3-oxo-3-phenylpropanoate (**788**) (4.96 g, 17.0 mmol, 1.00 eq.) in THF (150 mL) was added NaHMDS (1 M in THF, 18.7 mL, 18.7 mmol, 1.10 eq.). After 20 min. *N*-bromosuccinimide (3.93 g, 22.1 mmol, 1.30 eq.) was added and stirring at –78 °C was continued for 40 min. before the mixture was allowed to warm up to 0 °C. After 18 h the reaction was quenched by the addition of H_2O (100 mL) and the mixture was extracted with EtOAc (5 x 50 mL). The combined organic extracts were dried (Na_2SO_4) and concentrated in vacuo. Purification by column chromatography (*n*-hexane/EtOAc = 95:5 → 85:15) gave 3-phenylprop-2-yn-1-yl-2-bromo-2-methyl-3-oxo-3-phenylpropanoate (**779**) (4.59 g, 12.4 mmol, 73%) as a colorless oil that crystallized upon standing.

^{1}H NMR (300 MHz, $CDCl_3$) δ 7.98 – 7.92 (m, 2H), 7.43 – 7.35 (m, 1H), 7.35 – 7.16 (m, 6H), 4.90 (s, 2H), 2.17 (s, 3H).

^{13}C NMR (75 MHz, $CDCl_3$) δ 188.85, 168.67, 133.48, 133.07, 132.03, 129.78, 129.10, 128.55, 128.36, 121.77, 87.55, 81.35, 77.16, 60.40, 55.29, 27.38.

IR (film on NaCl) ϋ [cm^{-1}] = 3060, 2936, 1759, 1732, 1690, 1597, 1582, 1490, 1445, 1376, 1367, 1255, 1212, 1187, 1125, 1103, 1061, 1030, 1003, 986, 959, 940, 812, 800, 771, 758, 737, 689, 666, 639.

HRMS (ESI) m/z calculated for $C_{19}H_{16}BrO_3$ [M + H^+]– 371.0277, found 371.0278.

5.5.4 Substrates for [2+2]-enone cycloaddition

5.5.4.1 Potassium benzyltrifluoroborate (**792**)

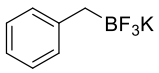

792

Potassium benzyltrifluoroborate (**792**) was prepared according to a modified published procedure:[205] Magnesium chips (668 mg, 27.5 mmol, 1.10 eq.) were covered with Et_2O (50.0 mL) and benzyl bromide (2.97 mL, 4.28 g, 25.0 mmol) was added to the mixture. A heat gun was used to warm up the flask until the mixture kept itself boiling for 30 minutes. Then the flask was placed in an oil bath and refluxed for 1 h. The Grignard solution was added dropwise to a cooled (–78 °C) solution of trimethylborate (4.20 mL, 37.5 mmol, 1.50 eq.) in Et_2O (25.0 mL) and stirring at that temperature was continued for 30 min before the mixture was allowed to warm up to room temperature and stirred for 1 h. After cooling to 0 °C KHF_2 (11.7 g, 150 mmol, 6.00 eq.) was added in one portion and H_2O (20.0 mL) was added dropwise over 20 min. before the mixture was stirred for 1 h at room temperature. Et_2O and H_2O were evaporated consecutively on the rotary evaporator at 40 °C by attaching a high vacuum pump and cooling the collecting flask. After drying the white solid at 40 °C in high vacuum for 1 h it was extracted in hot acetone (4 x 100 mL), filtered and concentrated. The crude solid was purified by dissolving in hot acetone and precipitating with Et_2O to give potassium benzyltrifluoroborate (**792**) (3.42 g, 17.3 mmol, 69%) as a white solid.

^{1}**H NMR** (600 MHz, $(CD_3)_2CO$) δ 7.38 – 7.00 (m, 4H), 6.86 (ttd, J = 8.6, 6.0, 2.3 Hz, 1H), 1.62 (m, 2H).

^{19}**F NMR** (565 MHz, $(CD_3)_2CO$) δ –140.65 (dd, J = 117.5, 54.2 Hz).

^{11}**B NMR** (193 MHz, $(CD_3)_2CO$) δ 4.42 (q, J = 62.2 Hz).

5.5.4.2 2-Chloro-1-(1-methyl-1*H*-imidazol-2-yl)ethan-1-one (**805**)

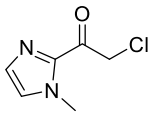

805

2-Chloro-1-(1-methyl-1*H*-imidazol-2-yl)ethan-1-one (**805**) was prepared according to a modified published procedure:[229, 356] To a cooled (–78 °C) solution of *N*-methylimidazole (**803**) (1.31 g, 1.27 mL, 15.9 mmol, 1.00 eq.) in THF (45.0 mL) was added *n*-BuLi (2.60 M in *n*-hexane, 6.36 mL, 15.9 mmol, 1.00 eq.) dropwise. The mixture was allowed to warm up to room temperature over 30 min, cooled down to –78 °C and stirred for 20 min. before *tert*-butylchloroacetate (**804**) (2.85 mL, 19.9 mmol, 1.25 eq.) was added and stirring was continued for 3 h. H_2O (3.00 mL) and brine (50.0 mL) were added and the aqueous phase was extracted with EtOAc (5 x 30 mL). The combined organic extracts were dried (Na_2SO_4) and concentrated in vacuo. The residue was purified by flash-chromatography (gradient over 90 min.: *n*-Hexane/EtOAc = 85:5 → 75:25, flow: 30 mL/min., length: 15 cm, diameter: 4 cm) to give 2-chloro-1-(1-methyl-1*H*-imidazol-2-yl)ethan-1-one (**805**) (1.59 g, 10.1 mmol, 64%) as a white solid.

^{1}**H NMR** (300 MHz, $CDCl_3$) δ 7.17 (d, J = 0.9 Hz, 1H), 7.11 (d, J = 0.9 Hz, 1H), 4.94 (s, 2H), 4.03 (s, 3H).

5.5.4.3 (*E*)-*N*-Methoxy-*N*-methylcinnamamide (**810**)

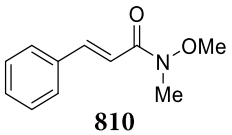

810

(*E*)-*N*-Methoxy-*N*-methylcinnamamide (**810**) was prepared according to a modified published procedure:[329] To a cooled (0 °C) solution of cinnamic acid (**808**) (1.48 g, 10.0 mmol, 1.00 eq.) in CH_2Cl_2 (25 mL) was added Et_3N (1.52 mL, 11.0 mmol, 1.10 eq.) and the mixture was stirred for 15 min. before pivaloyl chloride (1.23 mL, 10.0 mmol, 1.00 eq.) was added and stirring was continued for 1 h. *N*,*O*-Dimethylhydroxylamine hydrochloride (975 mg, 10.0 mmol, 1.00 eq.) was added followed by a dropwise addition of Et_3N (2.77 mL, 2.02 g, 20.0 mmol, 2.00 eq.). After two hours, hydrochloric acid (1 M, 5.00 mL) and water (30 mL) were added, and the aqueous phase was extracted with CH_2Cl_2 (3 x 30 mL). The combined organic extracts were dried (Na_2SO_4) and concentrated in vacuo. The residue was purified by flash chromatography (gradient over 90 min.: *n*-Hexane/EtOAc = 85:5 → 75:25, flow: 30 mL/min., length: 15 cm, diameter: 4 cm) to give (*E*)-*N*-methoxy-*N*-methylcinnamamide (**810**) (1.77 g, 9.25 mmol, 93%). Analytical data was consistent with the literature.[357]

^{1}**H NMR** (300 MHz, $CDCl_3$) δ 7.74 (d, *J* = 15.8 Hz, 1H), 7.60 – 7.55 (m, 2H), 7.43 – 7.34 (m, 3H), 7.04 (d, *J* = 15.8 Hz, 1H), 3.77 (s, 3H), 3.31 (s, 3H).

5.5.4.4 (*E*)-*N*-Methoxy-*N*-methylbut-2-enamide (**811**)

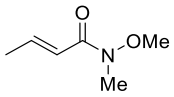

811

(*E*)-*N*-Methoxy-*N*-methylbut-2-enamide (**811**) was prepared according to a modified published procedure:[356] To a cooled (0 °C) solution of crotonic acid (**809**) (1.72 g, 20.0 mmol, 1.00 eq.) in CH_2Cl_2 (25 mL) was added Et_3N (3.04 mL, 22.0 mmol, 1.10 eq.) and the mixture was stirred for 15 min. before pivaloyl chloride (2.46 mL, 20.0 mmol, 1.00 eq.) was added and stirring was continued for 1 h. *N*,*O*-Dimethylhydroxylamine hydrochloride (1.95 mg, 20.0 mmol, 1.00 eq.) was added followed by a dropwise addition of Et_3N (5.54 mL, 40.0 mmol, 2.00 eq.). After two hours hydrochlorid acid (1 M, 10.0 mL) and water (60 mL) were added and the aqueous phase was extracted with CH_2Cl_2 (4 x 30 mL). The combined organic extracts were dried (Na_2SO_4) and concentrated in vacuo. The residue was purified by flash chromatography (gradient over 90 min.: *n*-Hexane/EtOAc = 85:15 → 75:25, flow: 30 mL/min., length: 15 cm, diameter: 4 cm) to give (*E*)-*N*-methoxy-*N*-methylbut-2-enamide (**811**) (1.74 g, 13.5 mmol, 67%).

^{1}**H NMR** (300 MHz, $CDCl_3$) δ 6.97 (m, 1H), 6.40 (dq, *J* = 15.4, 1.8 Hz, 1H), 3.74 – 3.65 (m, 3H), 3.22 (q, *J* = 1.3 Hz, 3H), 1.94 – 1.84 (m, 3H).

5.5.4.5 (*E*)-1-(1-Methyl-1*H*-imidazol-2-yl)-3-phenylprop-2-en-1-one (**813**)

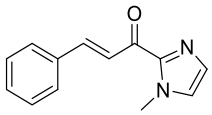

813

(*E*)-1-(1-Methyl-1-*H*-imidazol-2-yl)-3-phenylprop-2-en-1-one (**813**) was prepared according to a modified published procedure:[358] To a cooled (−78 °C) solution of *N*-methylimidazole (**803**) (379 mg, 4.62 mmol, 1.00 eq.) in THF (25.0 mL) was added *n*-butyllithium (2.60 M, 1.77 mL, 4.62 mmol, 1.00 eq.) dropwise. After 30 min the mixture was allowed to warm up to −40 °C and stirring was continued for one hour before the solution was cooled back to −78 °C. *N*-Methoxy-*N*-methylcinnamamide (**810**) (883 mg, 4.62 mmol, 1.00 eq.) was added and the solution was first stirred at −78 °C for 2 h, then at −40 °C for 2 h, and finally warmed to room temperature overnight. To obtain complete conversion, the mixture was again cooled to −40°C and treated with additional stock solution of lithiated methylimidazole (total amount: 0.4 eq.). The reaction was quenched by the addition of diluted acetic acid solution (0.5 M, 20.0 mL). The organic layer was washed with $NaHCO_3$, H_2O and brine. The aqueous phase was extracted with CH_2Cl_2 (4 x 30 mL) and the combined organic extracts were dried (Na_2SO_4), concentrated in vacuo and purified by flash chromatography (gradient over 90 min.: *n*-Hexane/EtOAc = 75:25 → 60:40, flow: 30 mL/min., length: 15 cm, diameter: 4 cm) to give (*E*)-1-(1-methyl-1-*H*-imidazol-2-yl)-3-phenylprop-2-en-1-one (**813**) (879 mg, 4.14 mmol, 79%) as an off white solid. Analytical data was consistent with the literature.[356]

^{1}**H NMR** (300 MHz, $CDCl_3$) δ 8.08 (d, *J* = 16.0 Hz, 1H), 7.83 (d, *J* = 16.0 Hz, 1H), 7.75 – 7.66 (m, 2H), 7.44 – 7.36 (m, 3H), 7.22 (d, *J* = 0.9 Hz, 1H), 7.08 (d, *J* = 0.9 Hz, 1H), 4.10 (s, 3H).

5.5.4.6 (*E*)-3-Phenyl-1-(1-phenyl-1*H*-imidazol-2-yl)prop-2-en-1-one (**812**)

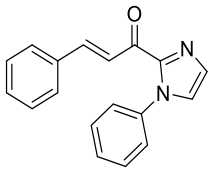

812

(*E*)-2-Phenyl-1-(1-phenyl-1-*H*-imidazol-2-yl)prop-2-en-1-one (**812**) was prepared according to a modified published procedure:[358] To a cooled (−78 °C) solution of *N*-phenylimidazole (**807**) (666 mg, 4.62 mmol, 1.00 eq.) in THF (25.0 mL) was added *n*-butyllithium (2.50 M, 1.84 mL, 4.60 mmol, 1.00 eq.) dropwise. After 30 min the mixture was allowed to warm up to −40 °C and stirring was continued for one hour before the solution was cooled back to −78 °C. *N*-Methoxy-*N*-methylcinnamamide (**810**) (883 mg, 4.62 mmol, 1.00 eq.) was added and the solution was first stirred at −78 °C for 1.5 h, then at −40 °C for 1 h and finally warmed to room temperature overnight. The reaction was quenched by the addition of diluted acetic acid solution (0.5 M, 20.0 mL). The organic layer was washed with $NaHCO_3$, H_2O and brine. The aqueous phase was extracted with CH_2Cl_2 (4 x 30 mL) and the combined organic extracts were dried (Na_2SO_4), concentrated in vacuo and purified by flash chromatography (gradient over 90 min.: *n*-Hexane/EtOAc = 75:25 → 60:40, flow: 30 mL/min., length: 15 cm, diameter: 4 cm) and

precipitation (*n*-hexane/CH_2Cl_2) to give (*E*)-2-phenyl-1-(1-phenyl-1-*H*-imidazol-2-yl)prop-2-en-1-one (**812**) (875 mg, 3.19 mmol, 69%).

^{1}**H NMR** (300 MHz, $CDCl_3$) δ 8.07 (d, *J* = 16.0 Hz, 1H), 7.75 (d, *J* = 16.0 Hz, 1H), 7.71 – 7.62 (m, 2H), 7.53 – 7.45 (m, 3H), 7.39 (dp, *J* = 4.7, 1.8 Hz, 3H), 7.37 – 7.30 (m, 3H), 7.24 (d, *J* = 1.0 Hz, 1H).

5.5.5 Substrates for aerobic oxidation

5.5.5.1 Methyl-1-indanone-2-carboxylate (**837**)

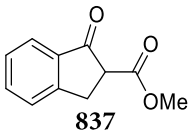

837

Methyl-1-indanone-2-carboxylate (**837**) was prepared according to a modified published procedure:[359] To a suspension of NaH (60% in mineral oil, 2.86 g, 71.5 mmol, 2.50 eq.) in THF (40.0 mL) was added dimethyl carbonate (**836**) (14.4 mL, 172 mmol, 6.01 eq.) and the mixture was heated to 60 °C. A solution of 1-indanone (**835**) (3.78 g, 28.6 mmol, 1.00 eq.) in THF (40.0 mL) was added dropwise over 1 h before the mixture was heated to reflux for 22 h until full conversion was indicated by ^{1}H-NMR-spectroscopy. After cooling to room temperature HCl (2 M, 30 mL) and H_2O (50 mL) were added and the aqueous phase was extracted with CH_2Cl_2 (4 x 30 mL). The combined organic extracts were washed with brine (2 x 40 mL), dried (Na_2SO_4), concentrated in vacuo and purified by flash-chromatography (gradient over 90 min.: *n*-Hexane/EtOAc = 90:10 → 80:20, flow: 15 mL/min., length: 15 cm, diameter: 4 cm) to give methyl-1-indanone-2-carboxylate (**837**) (4.64 g, 24.4 mmol, 85%) as a mixture of keto and enol tautomers (ratio 4:1 by ^{1}H-NMR).

^{1}H NMR (300 MHz, $CDCl_3$) δ 10.37 (br-s, 0.24H, enol), 7.82 – 7.75 (m, 0.97H, keto), 7.63 (m, 1.21H, keto/enol), 7.51 (d, *J* = 7.8 Hz, 1.04H, keto), 7.50 – 7.34 (m, 1.43H, keto/enol), 3.86 (s, 0.67H, enol), 3.80 (s, 2.77H, keto), 3.74 (dd, *J* = 8.3, 4.1 Hz, 1.02H, keto), 3.58 (dd, *J* = 17.3, 4.1 Hz, 1.09H, keto), 3.52 (s, 0.41H, enol), 3.38 (dd, *J* = 17.3, 8.3 Hz, 1.00H, keto).

5.5.5.2 Isopropyl 1-*oxo*-2,3-dihydro-1*H*-indene-2-carboxylate (**511**)

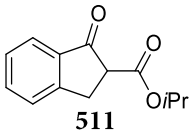

511

Isopropyl-1-*oxo*-2,3-dihydro-1-*H*-indene-2-carboxylate (**511**) was prepared according to a modified published procedure:[360] To a solution of methyl-1-indanone-2-carboxylate (**837**) (2.00 g, 10.5 mmol, 1.00 eq.) in toluene (30.0 mL) were added 2-propanol (**838**) (10.0 mL, 131 mmol, 12.5 eq.) and dibutyl tin oxide (524 mg, 2.10 mmol, 20 mol%) and the mixture was refluxed for 96 h. Removal of the solvent and purification by flash-chromatography (gradient over 90 min.: *n*-Hexane/EtOAc = 95:5 → 90:10, flow: 15 mL/min., length: 15 cm, diameter: 4 cm) gave isopropyl-1-*oxo*-2,3-dihydro-1-*H*-indene-2-carboxylate (**511**) (1.65 g, 7.56 mmol, 72%) as a mixture of keto and enol tautomers (ratio 6.6:1 by ^{1}H NMR).

^{1}H NMR (300 MHz, $CDCl_3$) δ 10.37 (br-s, 0.24H, enol), 7.82 – 7.75 (m, 0.97H, keto), 7.63 (m, 1.21H, keto/enol), 7.51 (d, *J* = 7.8 Hz, 1.04H, keto), 7.50 – 7.34 (m, 1.43H, keto/enol), 3.86 (s, 0.67H, enol), 3.80 (s, 2.77H, keto), 3.74 (dd, *J* = 8.3, 4.1 Hz, 1.02H, keto), 3.58 (dd, *J* = 17.3, 4.1 Hz, 1.09H, keto), 3.52 (s, 0.41H, enol), 3.38 (dd, *J* = 17.3, 8.3 Hz, 1.00H, keto).

5.6 Photoredox transformations

5.6.1 Enantioselective approaches for intramolecular radical cyclization

Procedure A: Intramolecular radical cyclization using separate catalysts

In a heated Schlenk tube, a solution of the photocatalyst, chiral ligand and zinc triflate were mixed in thoroughly degassed DMF and stirred under exclusion of light for 1 h before the reaction was started by the addition of freshly distilled and degassed triethylamine and irradiation. After 18 h the mixture was transferred into a separatory funnel containing Et_2O (25 mL) and H_2O (25 mL). The aqueous layer was extracted with Et_2O (3 x 50 mL) and the combined organic extracts were dried (Na_2SO_4) and concentrated in vacuo. The residue was purified by flash-chromatography to give the corresponding cyclization product.

Procedure B: Intramolecular radical cyclization using bimetallic asymmetric photoredox catalysts

In a heated Schlenk tube, a solution of the photocatalyst and zinc triflate were mixed in thoroughly degassed DMF and stirred under exclusion of light for 1 h before the reaction was started by the addition of freshly distilled and degassed triethylamine and irradiation. After 18 h the mixture was transferred into a separatory funnel containing Et_2O (25 mL) and H_2O (25 mL). The aqueous layer was extracted with Et_2O (3 x 50 mL) and the combined organic extracts were dried (Na_2SO_4) and concentrated in vacuo. The residue was purified by flash-chromatography to give the corresponding cyclization product.

5.6.1.1 Dimethyl 2-vinylcyclopentane-1,1-dicarboxylate (**739**)

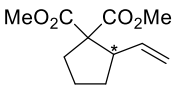

739

According to general procedure A, using dimethyl-(*E*)-2-bromo-2-(6-(trimethylsilyl)hex-4-en-1-yl)-malonate (**738**) (50.0 mg, 137 µmol, 1.00 eq.), $[Ru(bpy)_3](PF_6)_2$ (**7**) (1.00 mg, 1.16 µmol, 0.849 mol%), 2,2-bis((4*S*)-(-)-4-isopropyloxazolin)propan (**613**) (38.4 mg, 144 µmol, 1.05 eq.), zinc triflate (52.4 mg, 144 µmol, 1.05 eq.) and Et_3N (0.380 mL, 27.8 mg, 275 µmol, 2.00 eq.) in DMF (6.00 mL) gave dimethyl-2-vinylcyclopentane-1,1-dicarboxylate (**739**) (21.5 mg, 101 µmol, 74%) after purification by flash chromatography (gradient over 90 min.: *n*-Hexane/EtOAc = 97:3 → 80:20, flow: 15 mL/min., length: 15 cm, diameter: 1.5 cm). Analytical data was consistent with the literature.[16]

^{1}**H NMR** (300 MHz, $CDCl_3$) δ 5.78 (ddd, *J* = 17.1, 10.2, 7.9 Hz, 1H), 5.14 – 4.97 (m, 2H), 3.72 (s, 3H), 3.65 (s, 3H), 3.23 (tdd, *J* = 8.3, 6.5, 1.2 Hz, 1H), 2.51 – 2.40 (m, 1H), 2.16 – 2.01 (m, 1H), 2.00 – 1.79 (m, 2H), 1.76 – 1.56 (m, 2H).

5.6.1.2 3-(2-Methylenecyclopentanecarbonyl)oxazolidine-2-one (**725**)

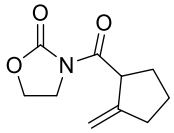

725

According to general procedure A, using 3-(2-bromohept-6-ynoyl)oxazolidin-2-one (**722**) (30.0 mg, 110 µmol, 1.00 eq.), $[Ru(bpy)_3](PF_6)_2$ (**7**) (0.80 mg, 0.93 µmol, 0.845 mol%), 2,2-bis((4*S*)-(–)-4-isopropyloxazolin)propan (**613**) (58.5 mg, 220 µmol, 2.00 eq.), zinc triflate (79.9 mg, 220 µmol, 2.00 eq.) and Et_3N (0.380 mL, 27.8 mg, 275 µmol, 2.00 eq.) in DMF (6.00 mL) gave 3-(2-methylenecyclopentanecarbonyl)oxazolidine-2-one (**725**) (19.4 mg, 99.4 µmol, 90%) after purification by flash chromatography (gradient over 90 min.: *n*-Hexane/EtOAc = 97:3 → 80:20, flow: 15 mL/min., length: 15 cm, diameter: 1.5 cm).

According to general procedure B, using 3-(2-bromohept-6-ynoyl)oxazolidine-2-one (**722**) (30.0 mg, 110 µmol, 1.00 eq.), $[Ru(bpy)_2(BOX\text{-}bpy)](PF_6)_2$ (**532**) (1.50 mg, 1.10 µmol, 1.00 mol%) or $[Ru(t\text{Bu-}bpy)_2(BOX\text{-}bpy)](PF_6)_2$ (**536**) (1.70 mg, 1.07 µmol, 1.06 mol%) or $[Ru(MeO\text{-}bpy)_2(BOX\text{-}bpy)](PF_6)_2$ (**537**) (1.60 mg, 1.08 µmol, 0.983 mol%) and Et_3N (0.03 mL, 220 µmol, 2.00 eq.) in DMF (6.00 mL) gave 3-(2-methylenecyclopentanecarbonyl)oxazolidine-2-one (**725**) (10.6 – 18.7 mg, 54.4 - 95.9 µmol, 49 - 87%) after purification by flash chromatography (gradient over 90 min.: *n*-Hexane/EtOAc = 97:3 → 80:20, flow: 15 mL/min., length: 15 cm, diameter: 1.5 cm). Analytical data was consistent with the literature.[16]

^{1}**H NMR** (300 MHz, $CDCl_3$) δ 5.03 (dd, *J* = 2.2, 2.2 Hz, 1H), 4.90 (dd, *J* = 2.2, 2.2 Hz, 1H), 4.72 (td, *J* = 7.5, 2.1 Hz, 1H), 4.42 (t, *J* = 8.2 Hz, 2H), 4.12 – 3.98 (m, 2H), 2.52 – 2.32 (m, 2H), 2.04 (tt, *J* = 7.7, 5.8 Hz, 2H), 1.97 – 1.81 (m, 1H), 1.69 (dq, *J* = 12.2, 7.8 Hz, 1H).

5.6.2 Intermolecular approaches: ATRA and α-allylation

Procedure C: ATRA

Into a previously heated and argon-filled septum-capped vial were placed the photocatalyst (1-3 mol%) and LiBr (2.0 eq. or 0.1 eq.) and the vial was flushed with argon again. A solution of 2-bromomalonate (**766**) (2.0 eq. or 1.2 eq.) and 5-hexen-ol (**757**) (1.0 eq.) in DMF/H_2O (1/4 v/v, 1.00 mL) was thoroughly degassed by freeze-pump-thaw and transferred into the reaction vial. The mixture was irradiated for 40 h before it was transferred into a separatory funnel containing Et_2O (25 mL) and H_2O (25 mL). The aqueous layer was extracted with Et_2O (3 x 50 mL) and the combined organic extracts were dried (Na_2SO_4) and concentrated in vacuo. The residue was either purified by column chromatography or mixed with a defined amount of internal standard (triphenylmethane or *p*-dichlorobenzene) to determine the yield by quantitative ^{1}H-NMR spectroscopy.

5.6.2.1 Diethyl 2-(2-bromo-6-hydroxyhexyl)malonate (**758**)

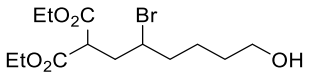

758

According to general procedure C, using 2-bromomalonate (**766**) (239 mg, 1.00 mmol, 1.20 eq.), 5-hexene-ol (**757**) (83.0 mg, 828 µmol, 1.00 eq.), $[Ru(bpy)_3](PF_6)_2$ (**7**) (21.6 mg, 25.1 µmol, 3.0 mol%), LiBr (144 mg, 1,66 mmol, 2.00 eq.). After workup, the crude product was mixed with the internal standard *p*-dichlorobenzene (30.6 mg, 208 µmol, 0.25 eq.) to determine a yield of 46% by comparing the integral of the internal standard with the integrals of the product β-H signals. Analytical data was consistent with the literature.[53, 325]

^{1}H NMR (300 MHz, $CDCl_3$) δ 4.27 – 4.06 (m, 4H, OC*H*$_2$CH$_3$), 4.00 – 3.88 (m, 1H, Br-C*H*), 3.71 (dd, *J* = 10.2, 4.3 Hz, 1H, α-CH), 3.63 – 3.53 (m, 2H, RC*H*$_2$OH), 2.40 (ddd, *J* = 14.8, 10.2, 3.1 Hz, 1H, β-C*H*$_2$), 2.19 (ddd, *J* = 14.8, 10.6, 4.3 Hz, 1H, β-C*H*$_2$'), 1.82 (dd, *J* = 14.4, 7.7 Hz, 4H, -C*H*$_2$- (C4' & C6')), 1.63 – 1.37 (m, 2H, -C*H*$_2$- (C5')), 1.20 (td, *J* = 7.5, 3.3 Hz, 6H, OCH$_2$C*H*$_3$).

5.6.2.2 3-(2-Methylpent-4-enoyl)oxazolidin-2-one (**772**)

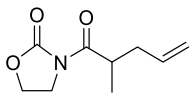

772

To a solution of $[Ru(bpy)_3](PF_6)_2$ (**7**) (1.94 mg, 2.26 µmol, 1 mol%) in thoroughly degassed MeCN (5.00 mL) were added 3-(2-bromopropanoyl)oxazolidin-2-one (**770**) (50.0 mg, 226 µmol, 1.00 eq.) and allyltrimethylsilane (**745**) (0.110 mL, 79.1 mg, 692 µmol, 3.06 eq.) and the mixture was irradiated. After 20 h $Sc(OTf)_3$ (22,4 mg, 45.3 µmol, 20 mol%), Et_3N (45.8 mg, 452 µmol, 2.00 eq.) and additional $[Ru(bpy)_3](PF_6)_2$ (7.76 mg, 9.04 µmol, 4 mol%) were added and irradiation was continued. After 72 h the mixture was transferred into a separatory funnel containing Et_2O (25 mL) and H_2O (25 mL). The aqueous layer was extracted with Et_2O (3 x 50 mL) and the combined organic extracts were dried (Na_2SO_4) and concentrated in vacuo. The residue was purified by column chromatography (*n*-hexane/EtOAc = 70:30) to give 3-(2-methylpent-4-enoyl)oxazolidine-2-one (**772**) (9.00 mg, 49.2 µmol, 22%)

the ^{1}H-NMR spectrum of which was consistent with the literature. Analytical data was consistent with the literature.[358, 361]

^{1}H NMR (300 MHz, $CDCl_3$) δ 5.71 (ddt, *J* = 17.1, 10.1, 7.0 Hz, 1H, R-C*H*=CH_2), 5.05 – 4.91 (m, 2H, CH=CH_2), 4.42 – 4.28 (m, 2H, ring-CH_2), 4.02 – 3.89 (m, 2H, ring-CH_2), 3.77 (h, *J* = 6.8 Hz, 1H, α-C*H*), 2.40 (dtt, *J* = 13.8, 6.8, 1.3 Hz, 1H, β-CH_2), 2.17 – 2.06 (m, 1H, β-CH_2'), 1.11 (d, *J* = 6.8 Hz, 3H, α-CHCH_3).

5.6.3 Cascade cyclization of phenylpropynyl-3-oxo-3-phenylpropanoate (**779**)

Procedure D: Cascade cyclization using separate catalysts

A mixture of Lewis-acid, BOX-ligand and substrate was dissolved and stirred for 2 h under exclusion of light before the photocatalyst and finally Et_3N were added and the mixture was irradiated for 18 h. The mixture was transferred into a separatory funnel containing H_2O (25 mL), saturated $NaHCO_3$-solution (25 mL) and Et_2O (25 mL). The aqueous layer was extracted with Et_2O (3 x 50 mL) and the combined organic extracts were dried (Na_2SO_4) and concentrated in vacuo and the crude product was purified by flash chromatography.

Procedure E: Cascade cyclization using bimetallic asymmetric photoredox catalysts

A solution of Lewis-acid and photocatalyst in CH_2Cl_2 (6.00 mL) was stirred for 1 h under exclusion of light before the substrate was added and stirring in the dark was continued for 1 Et_3N was added and the mixture was irradiated for 18 h. The mixture was transferred into a separatory funnel containing H_2O (25 mL), saturated $NaHCO_3$-solution (25 mL) and Et_2O (25 mL). The aqueous layer was extracted with Et_2O (3 x 50 mL) and the combined organic extracts were dried (Na_2SO_4) and concentrated in vacuo and the crude product was purified by flash chromatography.

5.6.3.1 9a-Methyl-4-phenylnaphtho[2,3-c]furan-1,9(3*H*,9a*H*)-dione (**784**)

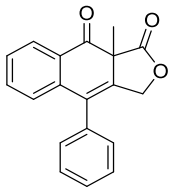

784

According to general procedure D, using $Zn(OTf)_2$ (29.4 mg, 80.9 µmol, 1.00 eq.), 2,2-bis((4*S*)-(−)-4-isopropyloxazolin)propane (**613**) (21.6 mg, 81.1 µmol, 1.00 eq.) and phenylpropynyl-3-oxo-3-phenylpropanoate (**779**) (30.0 mg, 81.1 µmol, 1.00 eq.) in CH_2Cl_2 with $[Ru(bpy)_3](PF_6)_2$ (**7**) (0.060 mg, 0.698 µmol, 0.863 mol%) and Et_3N (0.023 mL, 165 µmol, 2.03 eq.) gave 9a-methyl-4-phenylnaphtho[2,3-c]furan-1,9(3H,9aH)-dione (**784**) (13.0 mg, 44.8 µmol, 55%) after purification by flash chromatography (gradient over 90 min.: *n*-Hexane/EtOAc = 85:15 → 80:20, flow: 15 mL/min., length: 15 cm, diameter: 1.5 cm).

According to general procedure E, using $Zn(OTf)_2$ (0.40 mg, 1.10 µmol, 1.36 mol%), $[Ru(MeO\text{-}bpy)_2(BOX\text{-}bpy)](PF_6)_2$ (**537**) (1.65 mg, 1.11 µmol, 1.37 mol%), phenylpropynyl-3-oxo-3-phenylpropanoate (**779**) (30.0 mg, 81.1 µmol, 1.00 eq.) and Et_3N (0.023 mL, 165 µmol, 2.03 eq.) gave 9a-methyl-4-phenylnaphtho[2,3-c]furan-1,9(3*H*,9a*H*)-dione (**783**) (20.5 mg, 70.7 µmol, 87%) after purification by flash chromatography (gradient over 90 min.: *n*-Hexane/EtOAc = 85:15 → 80:20, flow: 15 mL/min., length: 15 cm, diameter: 1.5 cm).

Chiral HPLC: Chiralpak IB, flow 0.9 mL/min., *n*-hexane/isopropanol 95:5

^{1}H NMR (300 MHz, $CDCl_3$) δ 8.11 (dd, *J* = 7.7, 1.5 Hz, 1H), 7.64 – 7.39 (m, 5H), 7.27 (d, *J* = 3.9 Hz, 1H), 7.18 (d, *J* = 5.5 Hz, 1H), 7.10 (dd, *J* = 7.8, 1.3 Hz, 1H), 5.07 (d, *J* = 13.7 Hz, 1H), 4.53 (d, *J* = 13.6 Hz, 1H), 1.77 (s, 3H).

^{13}C NMR (75 MHz, $CDCl_3$) δ 193.69, 171.36, 137.83, 136.57, 134.99, 134.77, 132.46, 129.92, 129.22, 129.09, 128.74, 128.49, 128.30, 127.26, 67.71, 51.03, 24.48.

IR (film on NaCl) ῡ [cm^{-1}] = 2925, 2361, 1697, 1592, 1541, 1507, 1445, 1350, 1284, 1109, 1081, 1005, 704, 686, 673.

HRMS (ESI) m/z calculated for $C_{19}H_{15}O_3$ [M + H]– 291.1016, found 291.1022.

5.6.4 [2+2]-Enone cycloaddition

General procedure F: ^{1}H-NMR-Screening of the conversion of the (2+2)-enone dimerization

A solution of substrate and catalyst in 2.00 mL solvent was mixed with a solution of a Lewis acid in 1.00 mL solvent and the mixture was degassed by Ar-sparging for 15 min. After defined time intervals, 0.100 mL samples were taken, subjected to a work-up procedure involving washing with water, extraction with Et_2O, drying (Na_2SO_4) and removal of the solvent. The crude product was analyzed by ^{1}H-NMR spectroscopy, whereby the reaction progress was determined from the ratio of the signals of starting material at 8.00 ppm and 7.68 ppm with the cyclobutane product signals at 4.58 ppm and 4.09 ppm, as shown in the following example.

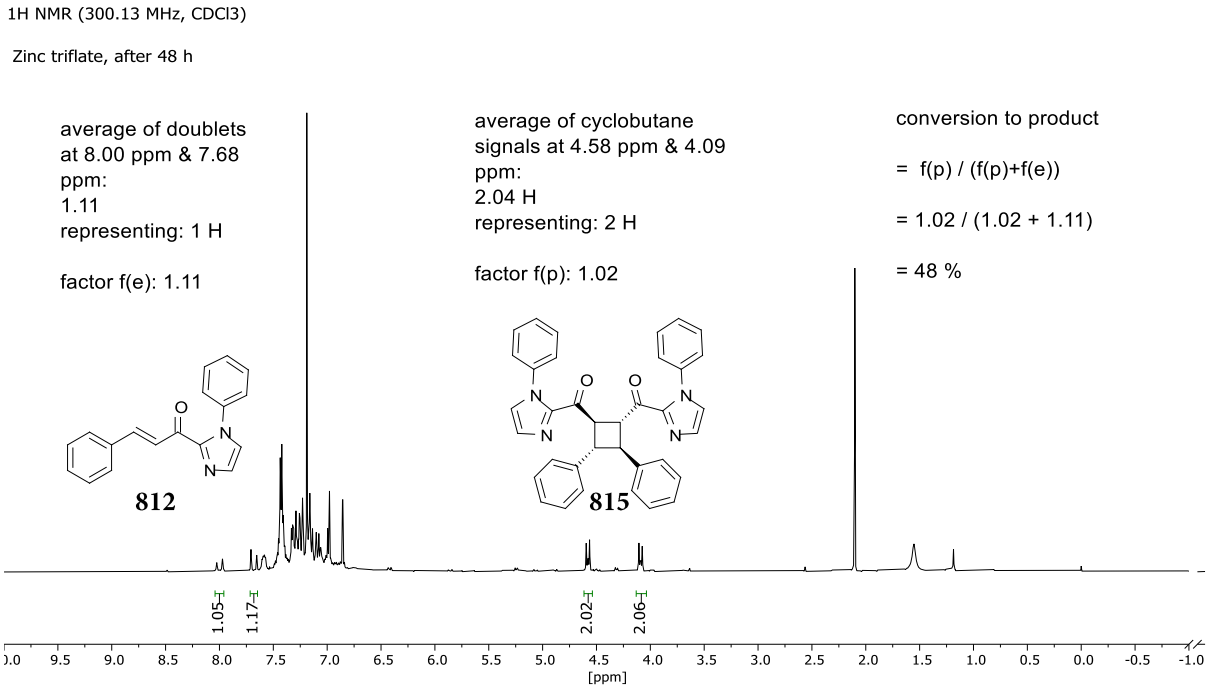

General procedure G: (2+2)-Enone dimerization

A solution of substrate and catalyst in 2.00 mL solvent was mixed with a solution of a Lewis acid in 1.00 mL solvent and the mixture was degassed by Ar-sparging for 15 min. After 48 h the mixture was transferred into a separating funnel containing H_2O (15.0 mL) and Et_2O (15.0 mL). The aqueous phase was extracted with Et_2O (3 x 30 mL). The combined organic extracts were dried (Na_2SO_4) and concentrated in *vacuo*. The residue was purified by flash chromatography (gradient over 90 min.: *n*-Hexane/EtOAc = 85:15 → 80:20, flow: 15 mL/min., length: 15 cm, diameter: 1.5 cm) to give the dimerization product.

5.6.4.1 (3,4-Diphenylcyclobutane-1,2-diyl)bis((1-methyl-1*H*-imidazol-2-yl)methanone) (**814**)

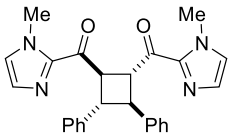

814

According to general procedure G in the presence of potassium benzyltrifluoroborate (**792**) (59.4 mg, 0.300 mmol, 1.50 eq.) using (*E*)-1-(1-methyl-1*H*-imidazol-2-yl)-3-phenylprop-2-en-1-one (42.4 mg, 0.200 mmol, 1.00 eq.),

$[Ru(bpy)_3](PF_6)_2$ (**7**) (3.40 mg, 4.00 µmol, 2.00 mol%), $Zn(OTf)_2$ (2.90 mg, 8.00 µmol, 4.00 mol%) in CH_2Cl_2 gave (3,4-diphenylcyclobutane-1,2-diyl)bis((1-methyl-1*H*-imidazol-2-yl)methanone) (**814**) (10.1 mg in a mixture with 1.87 mg EtOAc as determined by NMR, 23.9 mmol, 12%)

^{1}H NMR (300 MHz, $CDCl_3$) δ 7.42 – 7.35 (m, 4H), 7.34 – 7.22 (m, 4H), 7.22 – 7.17 (m, 2H), 6.89 (d, *J* = 0.9 Hz, 2H), 6.80 (d, *J* = 0.9 Hz, 2H), 4.74 – 4.67 (m, 2H), 4.12 (d, *J* = 9.3 Hz, 2H), 4.02 (s, 6H).

IR (film on NaCl) ϋ [cm^{-1}] = 3107, 3060, 3027, 2955, 1667, 1628, 1602, 1508, 1496, 1473, 1456, 1417, 1405, 1364, 1289, 1233, 1220, 1155, 1078, 1031, 1004, 990, 917, 896, 851, 772, 720, 699, 667.

HRMS (ESI) m/z calculated for $C_{26}H_{25}N_4O_2$ [M – H$^+$] - 425.1972, found 425.1983.

5.6.4.2 (3,4-Diphenylcyclobutane-1,2-diyl)bis((1-phenyl-1*H*-imidazol-2-yl)methanone) (**815**) and (2,4-Diphenylcyclobutane-1,3-diyl)bis((1-phenyl-1*H*-imidazol-2-yl)methanone) (**819**)

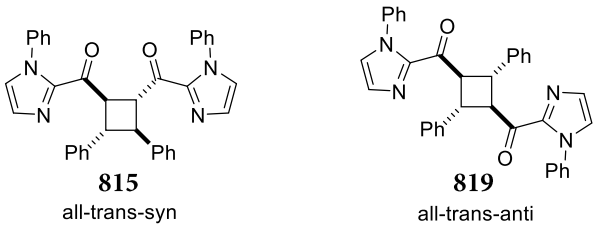

According to general procedure G in the presence of potassium benzyltrifluoroborate (**792**) (35.6 mg, 0.180 mmol, 1.50 eq.) using (*E*)-3-phenyl-1-(1-phenyl-1*H*-imidazol-2-yl)prop-2-en-1-one (**812**) (32.9 mg, 0.120 mmol, 1.00 eq.), $[Ru(bpy)_3](PF_6)_2$ (**7**) (2.10 mg, 2.40 µmol, 2.00 mol%), $Zn(OTf)_2$ (1.70 mg, 4.80 µmol, 4.00 mol%) in acetone gave the *all-trans-syn*-(3,4-diphenylcyclobutane-1,2-diyl)bis((1-phenyl-1*H*-imidazol-2-yl)methanone) (**815**) (11.2 mg product, 30.6 µmol, 25%) as well as the *all-trans-anti*-regioisomer **819** (10.5 mg, 19.2 µmol, 16%). Analytical data was consistent with the literature.[208, 228]

Syn-product:

^{1}H NMR (300 MHz, $CDCl_3$) δ 7.58 – 7.45 (m, 10H), 7.35 – 7.29 (m, 4H), 7.29 – 7.18 (m, 4H), 7.19 – 7.11 (m, 2H), 7.05 (d, *J* = 1.0 Hz, 2H), 6.93 (d, *J* = 1.0 Hz, 2H), 4.69 – 4.62 (m, 2H), 4.20 – 4.13 (m, 2H).

Anti-product:

^{1}H NMR (300 MHz, $CDCl_3$) δ 7.43 – 7.29 (m, 7H), 7.22 (d, *J* = 1.0 Hz, 2H), 7.13 (d, *J* = 1.0 Hz, 2H), 7.10 – 6.97 (m, 13H), 5.34 – 5.27 (m, 2H), 4.41 – 4.36 (m, 2H).

IR (film on NaCl) ϋ [cm^{-1}] = 2360, 2341, 2337, 1686, 1597, 1504, 1494, 1447, 1407, 1310, 1219, 1075, 934, 909, 835, 772, 695, 673.

HRMS (ESI) m/z calculated for $C_{36}H_{29}N_4O_2$ [M – H$^+$]– 549.2285, found 549.2285.

5.6.5 Aerobic oxidation

Procedure H: Aerobic oxidation using separate catalysts

BOX-ligand and $Ni(acac)_2$ were mixed in toluene (0.01 M) and stirred for 30 min. under nitrogen and exclusion of light, before transferal into open vials containing a solution of photocatalyst **7** and substrate **511** (total volume: 2.00 mL) and the mixture was irradiated for 24 – 48 h. Removal of the solvent in vacuo and purification by flash-chromatography (*n*-hexane/EtOAc = 95:5, flow 15 mL/min., length: 15 cm, diameter: 1.5 cm) gave isopropyl (*S*)-2-hydroxy-1-oxo-2,3-dihydro-1*H*-indene-2-carboxylate (**512**).

Procedure I: Aerobic oxidation using bimetallic asymmetric photoredox catalysts

Photocatalyst and $Ni(acac)_2$ were weighed into a septum-capped vial, dissolved in toluene and stirred under exclusion of light for 1 h, before the substrate **511** was added either *via* syringe or as a solution in toluene (100 mM). and the solution (total volume: 2.00 mL) was irradiated for 48 h. Removal of the solvent in vacuo and purification by flash-chromatography (*n*-hexane/EtOAc = 95:5, flow 15 mL/min., length: 15 cm, diameter: 1.5 cm) gave isopropyl (*S*)-2-hydroxy-1-oxo-2,3-dihydro-1*H*-indene-2-carboxylate (**512**).

5.6.5.1 Isopropyl (*S*)-2-hydroxy-1-oxo-2,3-dihydro-1*H*-indene-2-carboxylate (**512**)

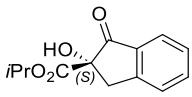

512

According to procedure H using isopropyl 1-oxo-2,3-dihydro-1*H*-indene-2-carboxylate (**511**) (21.8 mg, 100 µmol, 1.00 eq.), $[Ru(bpy)_3](PF_6)_2$ (**7**) (4.30 mg, 5.00 µmol, 5.00 mol%), *i*Pr-BOX **613** (1.33 mg, 4.99 µmol, 4.99 mol%), $Ni(acac)_2$ (1.28 mg, 4.98 µmol, 4.98 mol%) in toluene (2.00 mL) and irradiation for 24 h gave isopropyl (*S*)-2-hydroxy-1-oxo-2,3-dihydro-1*H*-indene-2-carboxylate (**512**) (16.4 mg, 70.1 µmol, 70%) in 63%*ee*.

According to procedure I by dissolving $[Ru(MeO\text{-}bpy)_2(BOX\text{-}bpy)](PF_6)_2$ (**537**)(1.50 mg, 101 µmol, 0.69 mol%) and $Ni(acac)_2$ (0.250 mg, 100 µmol, 0.68 mol%) in toluene (2.00 mL) and addition of isopropyl 1-oxo-2,3-dihydro-1*H*-indene-2-carboxylate (**511**) (32.0 mg, 147 µmol, 1.00 eq.) *via* syringe gave isopropyl (*S*)-2-hydroxy-1-oxo-2,3-dihydro-1*H*-indene-2-carboxylate (**512**) (19.0 mg, 81.2 µmol, 55%) in 35%*ee*. Analytical data was consistent with the literature.[362]

Chiral HPLC: Chiralpak IB, flow 0.6 mL/min., *n*-hexane/isopropanol 97:3

^{1}H NMR (300 MHz, $CDCl_3$) δ 7.79 (d, *J* = 7.7 Hz, 1H), 7.66 (td, *J* = 7.5, 1.3 Hz, 1H), 7.49 (dt, *J* = 7.7, 1.0 Hz, 1H), 7.46 – 7.39 (m, 1H), 5.07 (p, *J* = 6.3 Hz, 1H), 3.99 (s, 1H), 3.69 (d, *J* = 17.2 Hz, 1H), 3.23 (d, *J* = 17.2 Hz, 1H), 1.19 (d, *J* = 6.2 Hz, 3H), 1.13 (d, *J* = 6.3 Hz, 3H).

6 IR and NMR spectra

6.1 Spectra of bipyridine derivatives

6.1.1 2,2′-Bipyridine-*N*-oxide (**588**)

1H NMR (300.13 MHz, CDCl3)

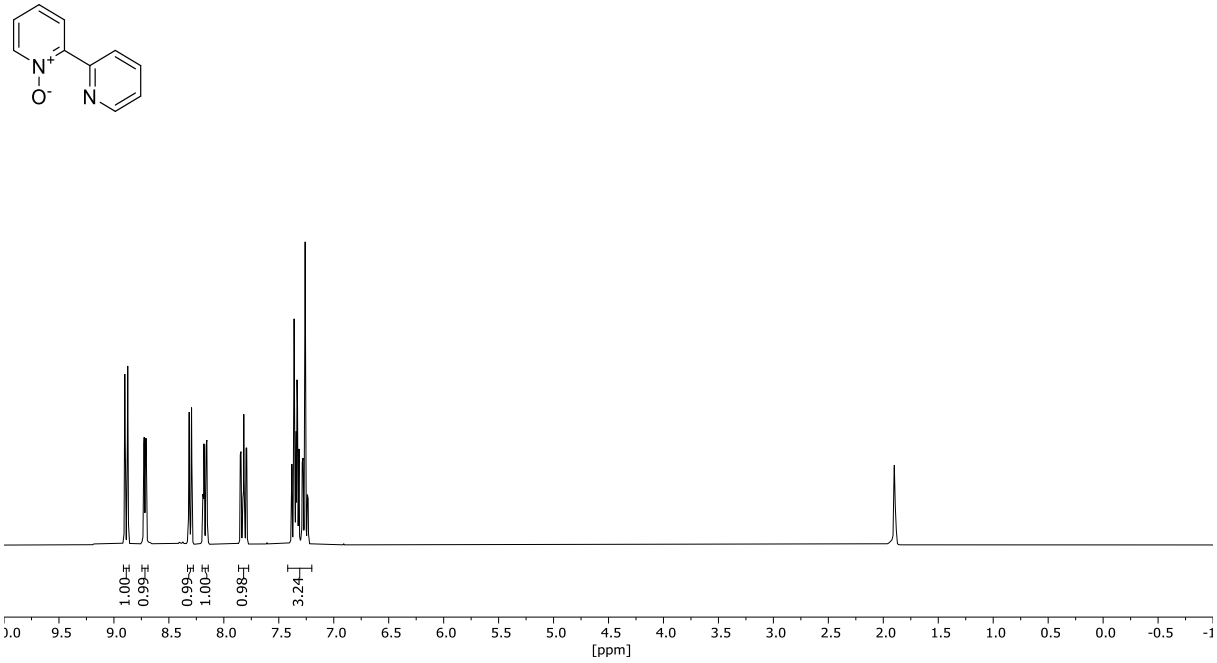

6.1.2 4-Nitro-2,2′-bipyridine-*N*-oxide (**589**)

1H NMR (300.13 MHz, CDCl3)

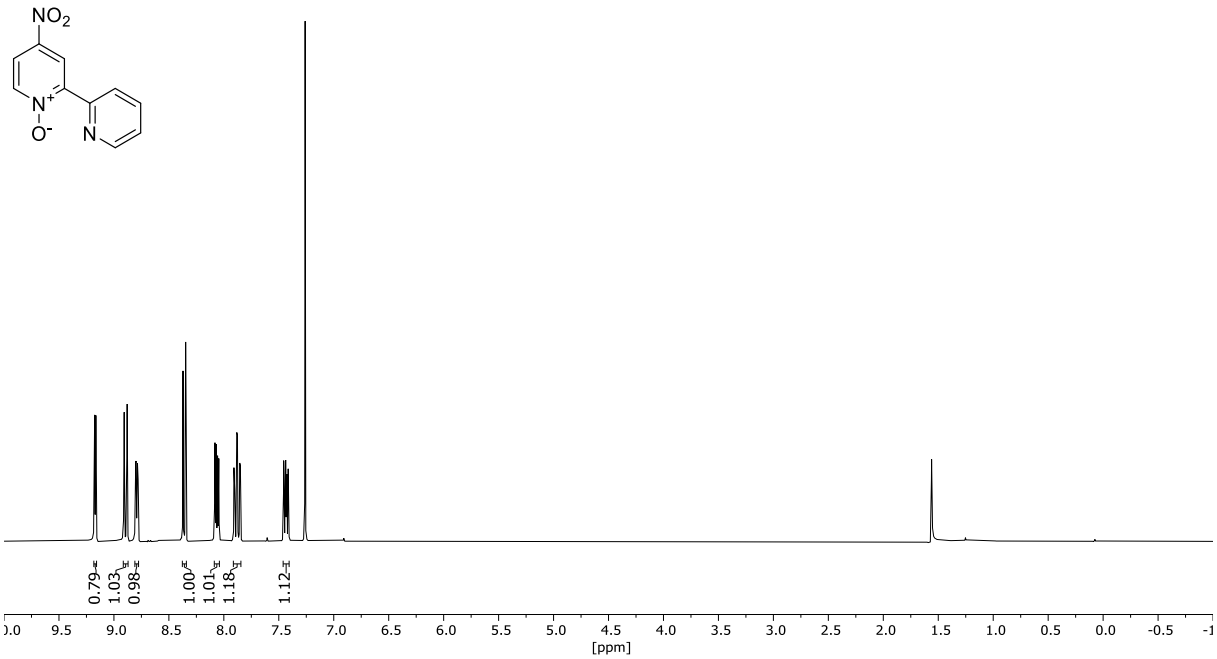

6.1.3 4-Amino-2,2′-bipyridine (**590**)

1H NMR (600.13 MHz, CDCl3)

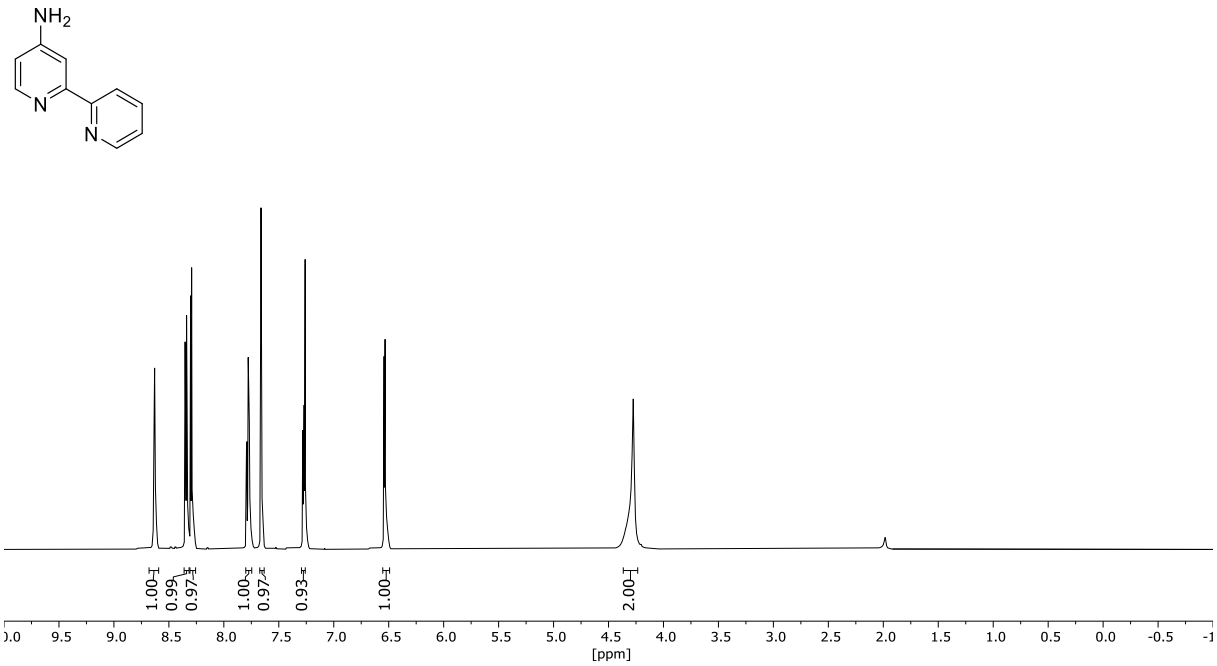

6.1.4 4-Fluoro-2,2′-bipyridine (**585**)

1H NMR (600.13 MHz, CDCl3)

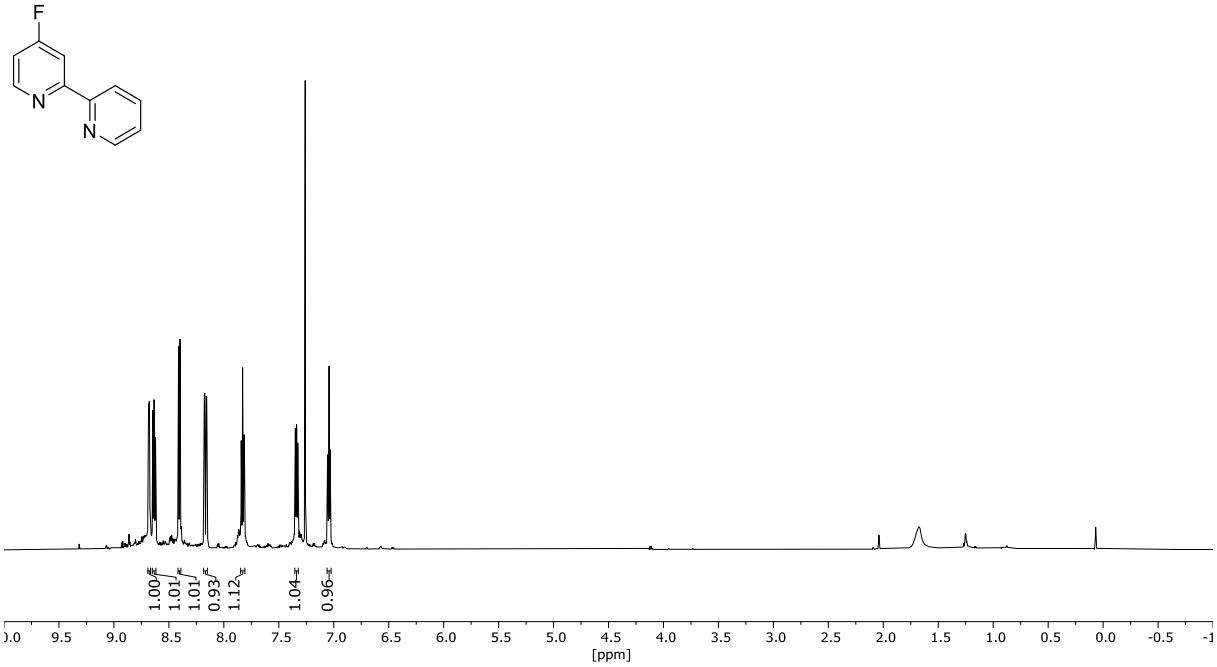

19F NMR (564.63 MHz, CDCl3)

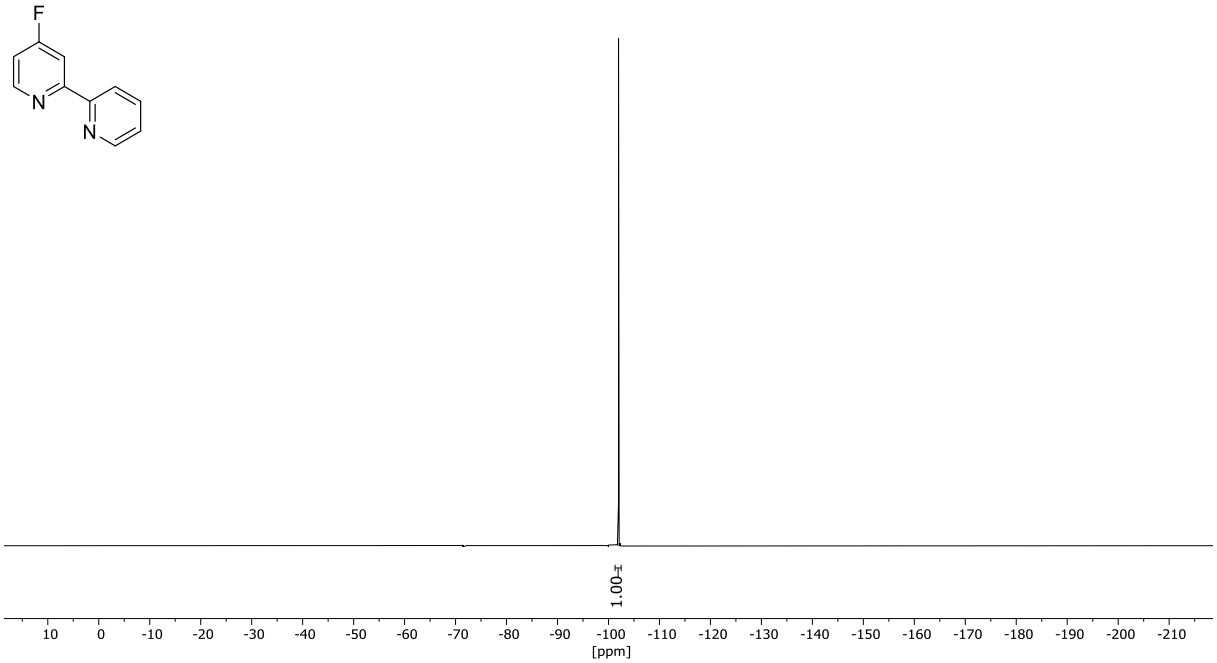

6.1.5 4,4′-Dihydroxy-2,2′-bipyridine (**704**)

1H NMR (300.13 MHz, MeOD)

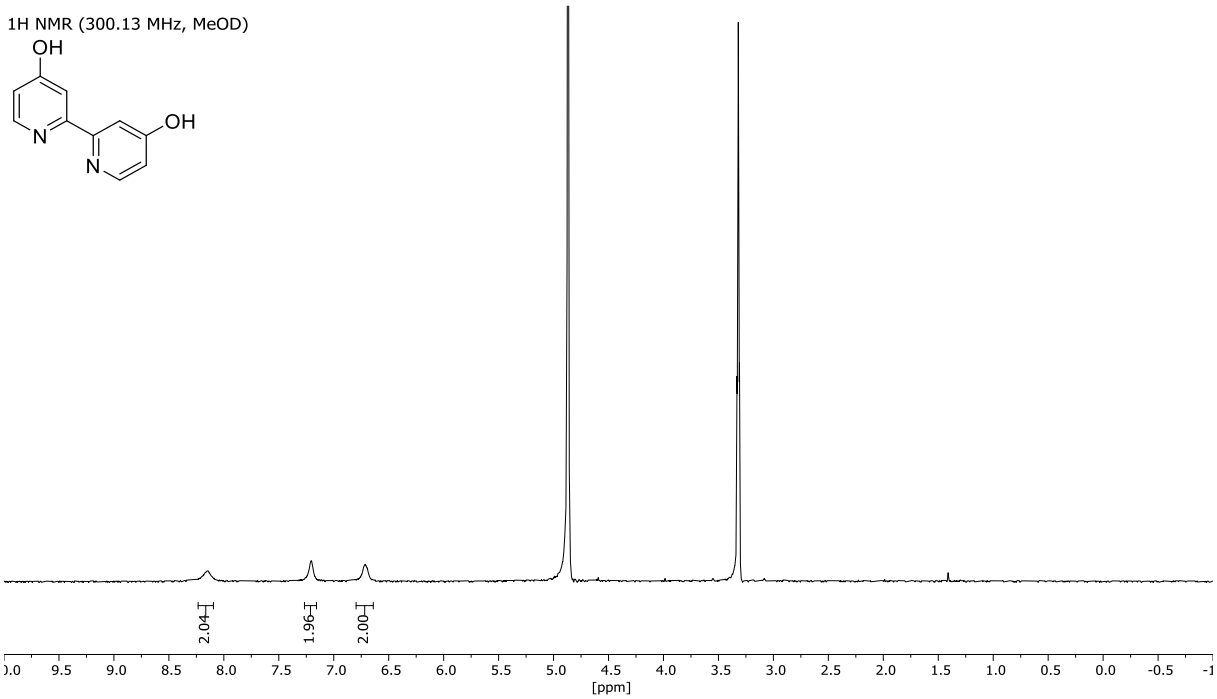

6.1.6 4,4′-Diisopropyloxy-2,2′-bipyridine (**700**)

1H NMR (300.13 MHz, CDCl3)

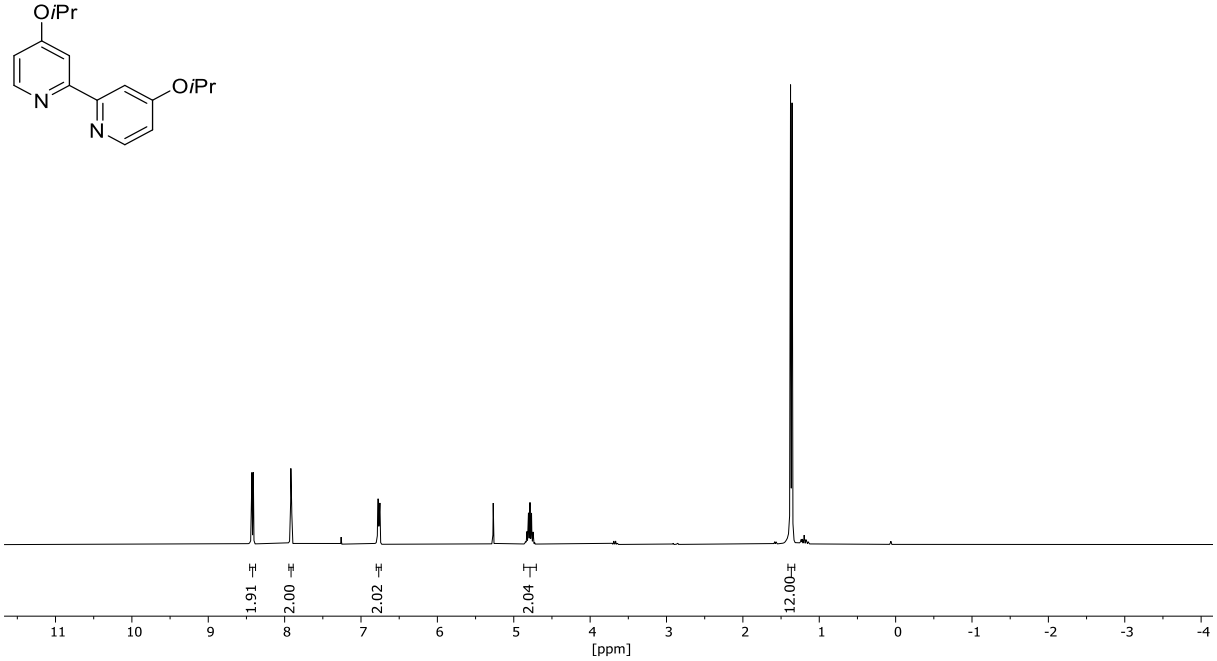

13C NMR (75.48 MHz, CDCl3)

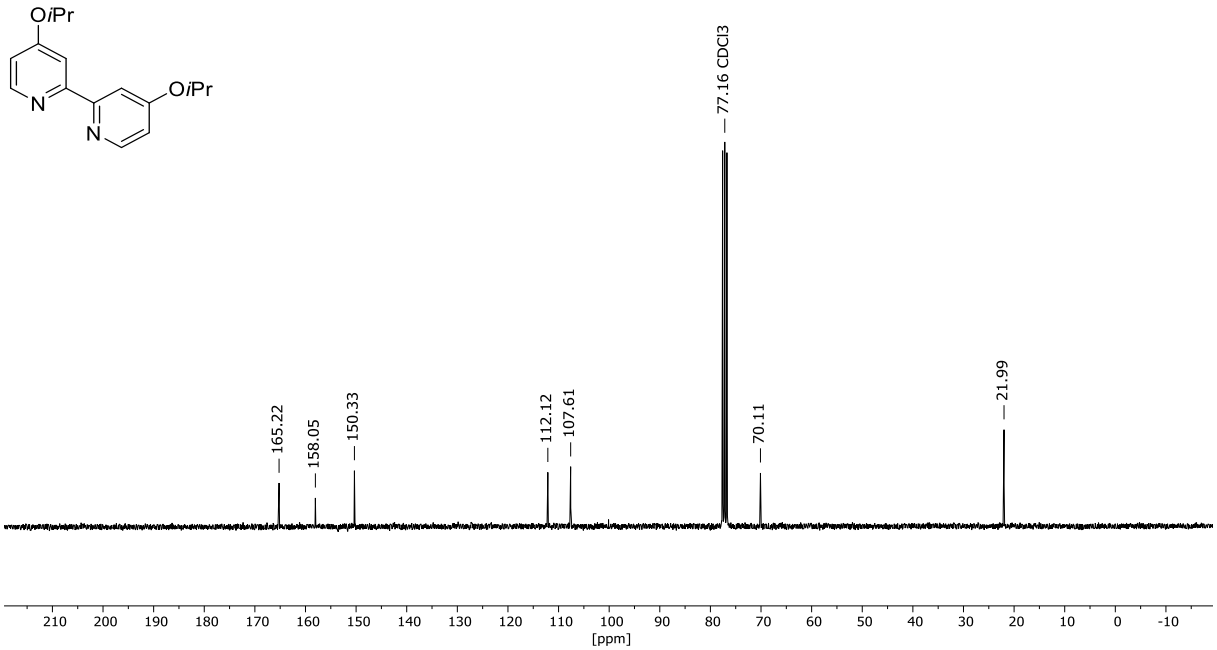

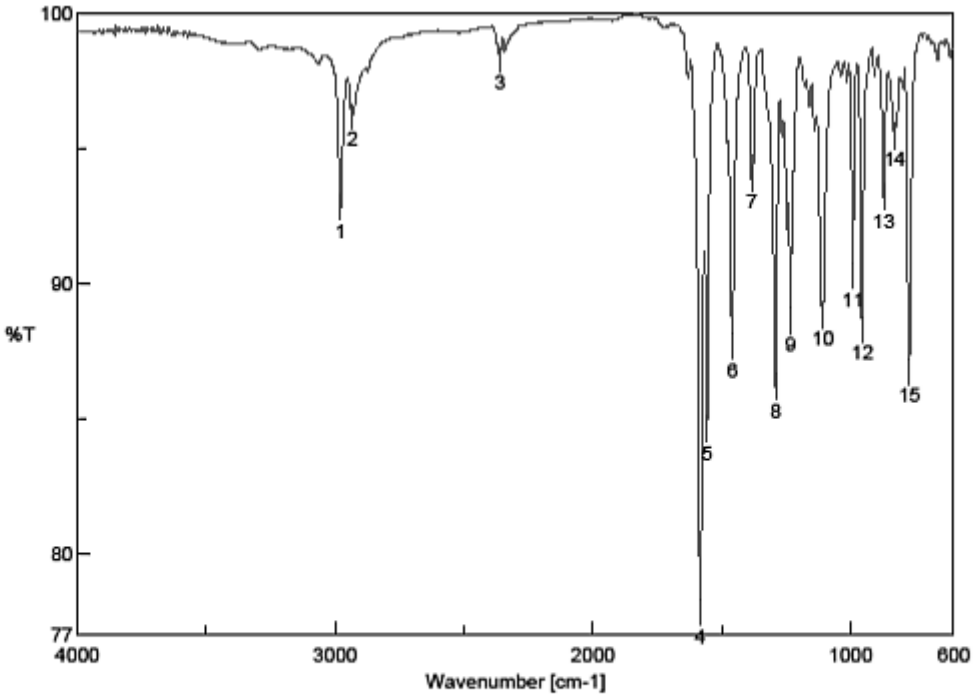

[Result of Peak Picking]

No.	Position	Intensity	No.	Position	Intensity	No.	Position	Intensity
1	2978.52	92.8069	2	2933.2	96.217	3	2360.44	98.2925
4	1583.27	77.7911	5	1556.27	84.5734	6	1458.89	87.6305
7	1384.64	93.8693	8	1290.14	86.1527	9	1232.29	88.5944
10	1107.9	88.8175	11	991.232	90.2679	12	955.555	88.2793
13	871.667	93.1885	14	829.241	95.4775	15	772.351	86.7009

6.1.7 Tetraethyl 2,2′-([2,2′-bipyridine]-4,4′-diyl)dimalonate (**636**)

1H NMR (300.13 MHz, CDCl3)

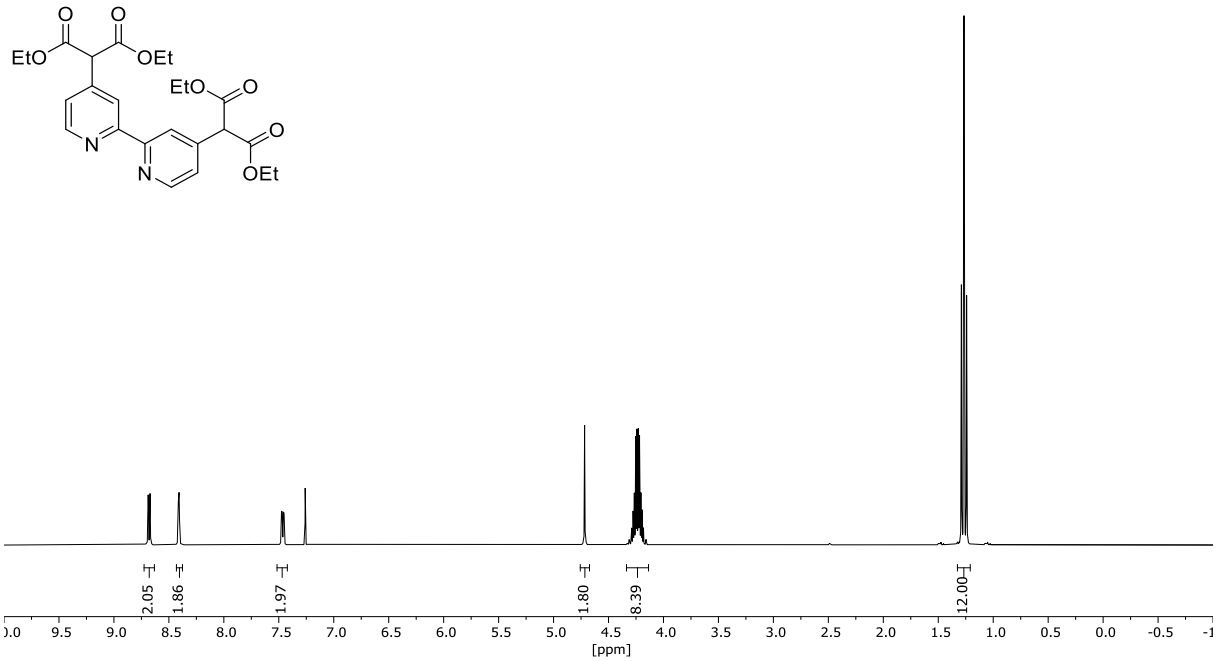

13C NMR (75.48 MHz, CDCl3)

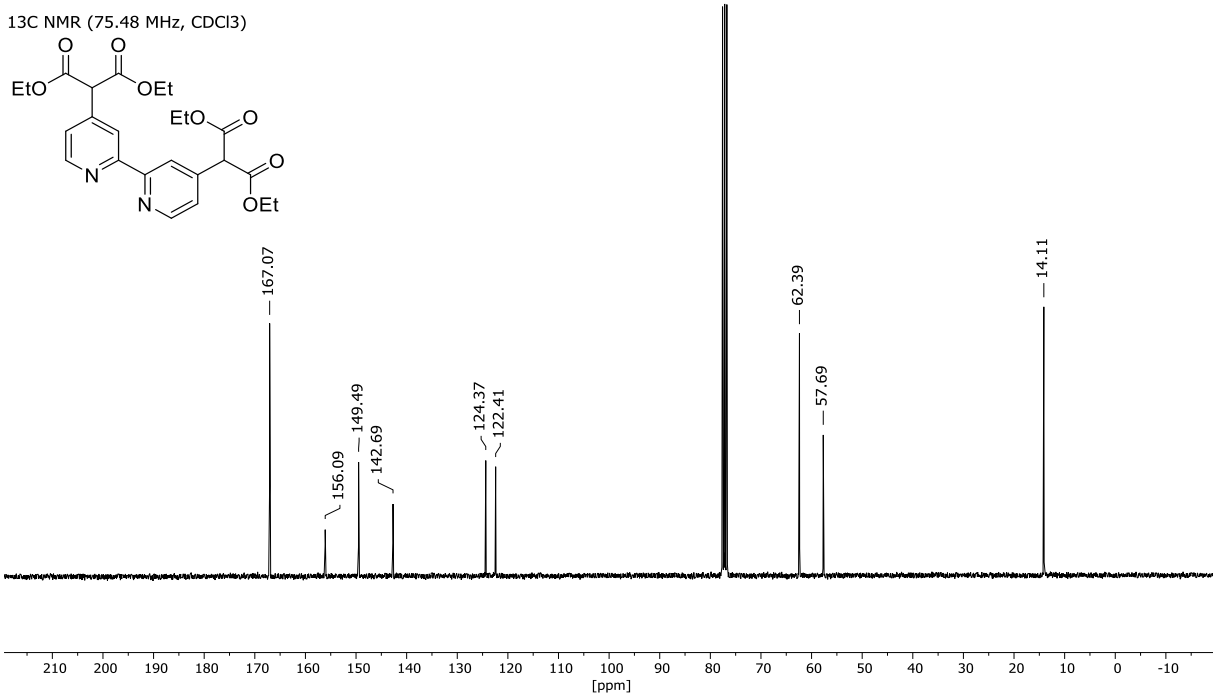

DEPT135 NMR (75.48 MHz, CDCl3)

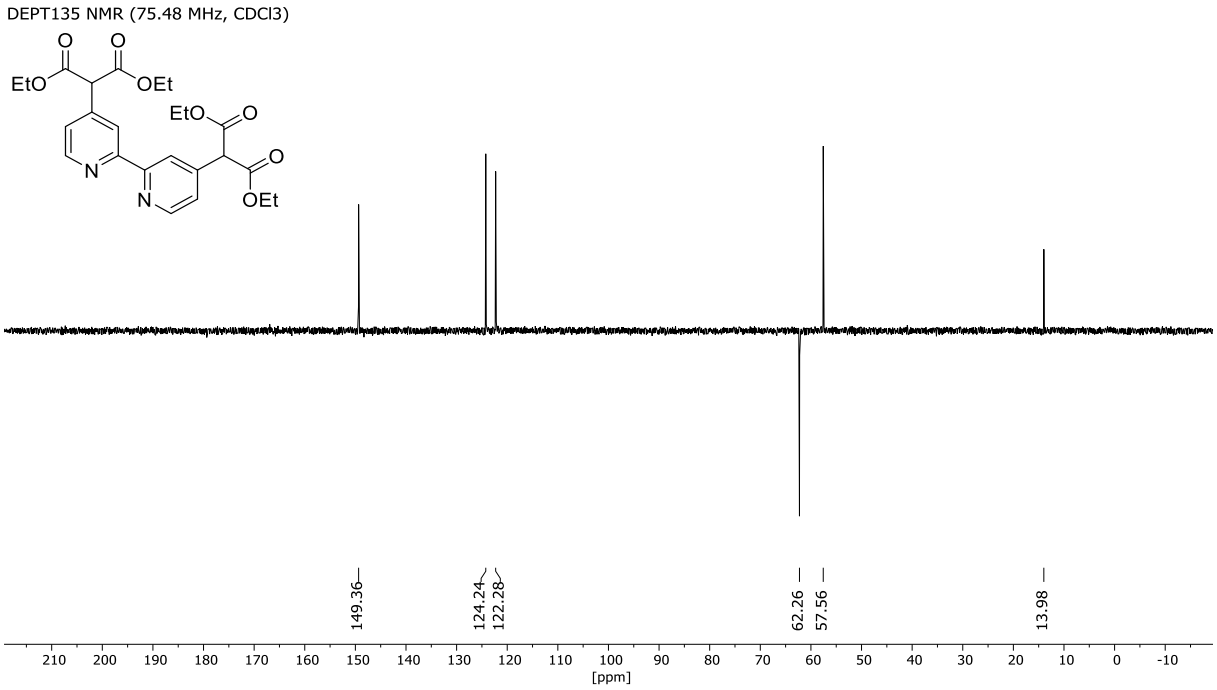

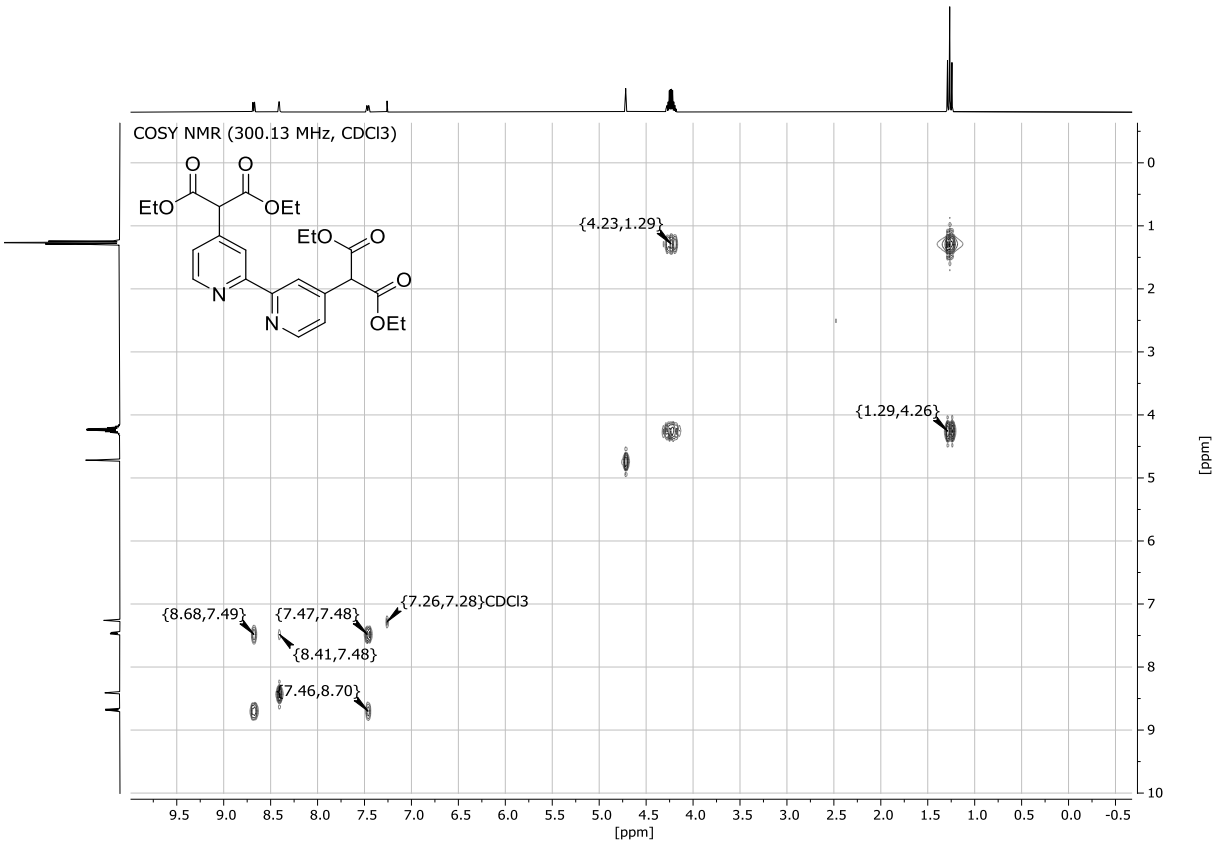
COSY NMR (300.13 MHz, CDCl3)
EtO
OEt
EtO
O
O
OEt
N
N
{4.23,1.29}
{1.29,4.26}
{8.68,7.49}
{7.47,7.48}
{7.26,7.28}CDCl3
{8.41,7.48}
{7.46,8.70}
[ppm]
[ppm]

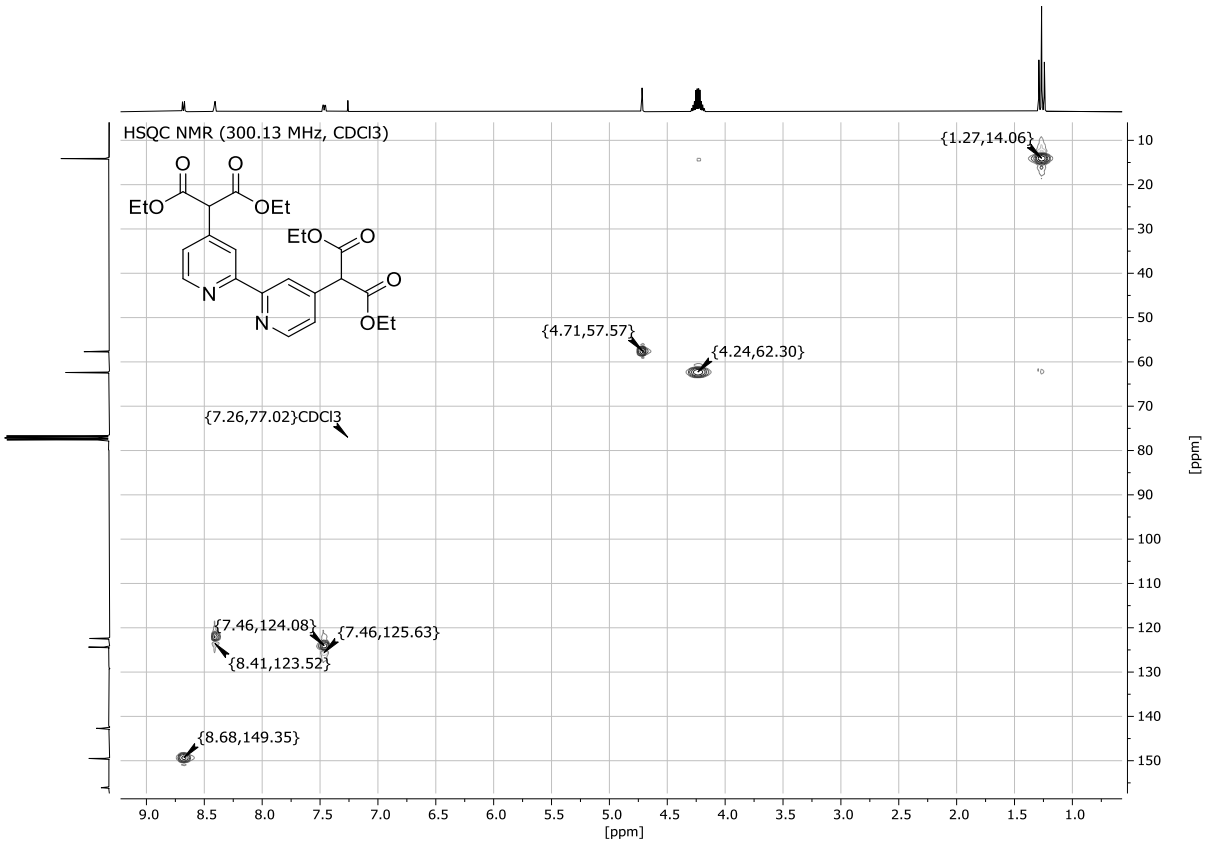
HSQC NMR (300.13 MHz, CDCl3)
EtO
OEt
EtO
O
O
OEt
N
N
{1.27,14.06}
{4.71,57.57}
{4.24,62.30}
{7.26,77.02}CDCl3
{7.46,124.08}
{7.46,125.63}
{8.41,123.52}
{8.68,149.35}
[ppm]
[ppm]

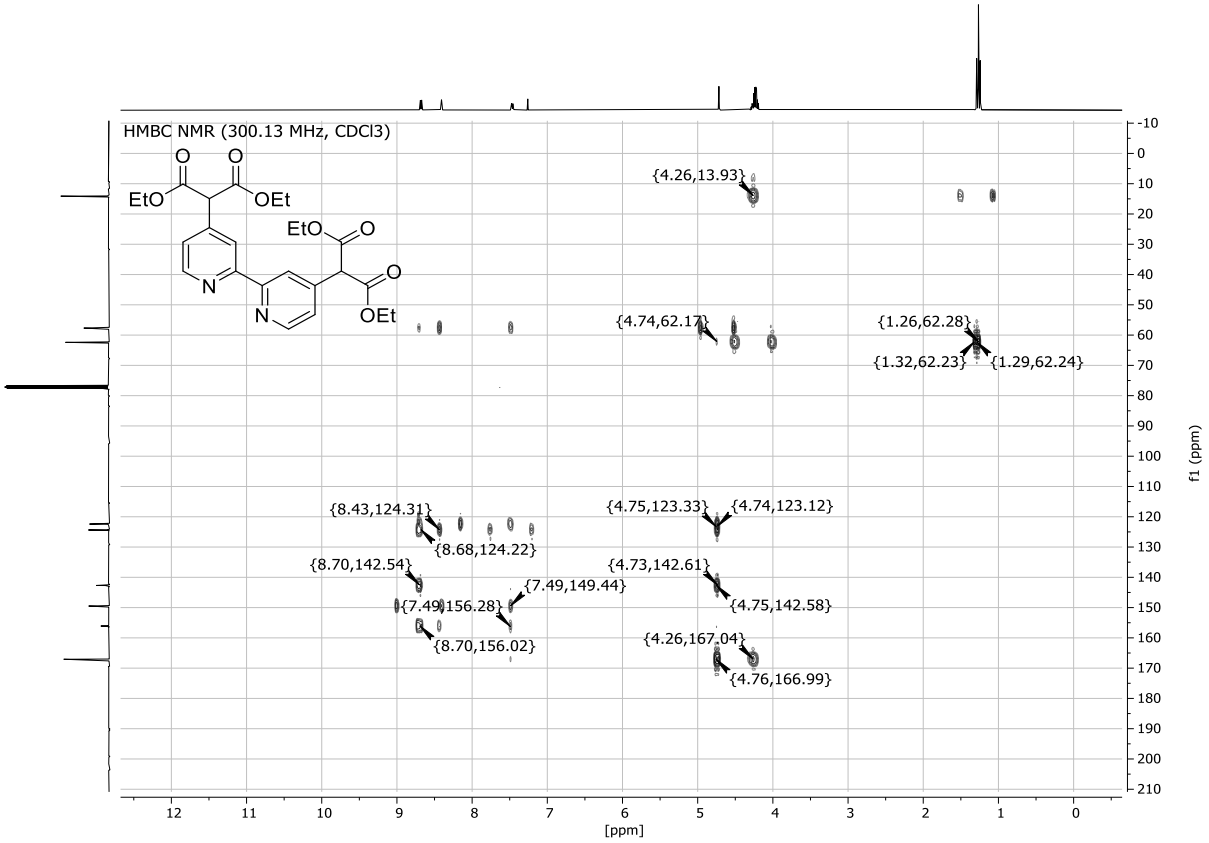

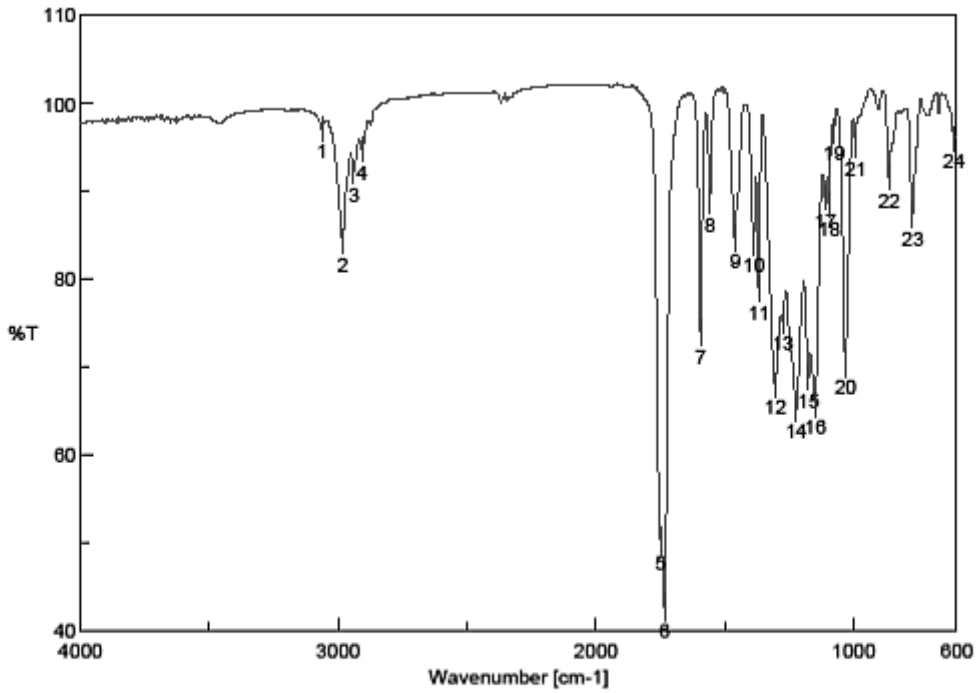

[Result of Peak Picking]

No.	Position	Intensity	No.	Position	Intensity	No.	Position	Intensity
1	3061.44	97.043	2	2983.34	84.2361	3	2938.98	92.2209
4	2907.16	94.7371	5	1748.16	50.3495	6	1734.66	42.5298
7	1593.88	73.7886	8	1557.24	88.8282	9	1459.85	84.556
10	1387.53	84.1692	11	1368.25	78.7865	12	1304.61	67.9097
13	1275.68	75.2021	14	1222.65	65.2476	15	1175.4	68.7427
16	1149.37	65.6982	17	1110.8	89.2247	18	1095.37	88.3183
19	1077.05	96.7965	20	1031.73	70.2828	21	993.16	95.1588
22	862.989	91.516	23	771.387	87.1951	24	610.36	95.9275

6.1.8 Tetraethyl 2,2′-([2,2′-bipyridine]-4,4′-diyl)bis(2-methylmalonate) (**625**)

1H NMR (300.13 MHz, CDCl3)

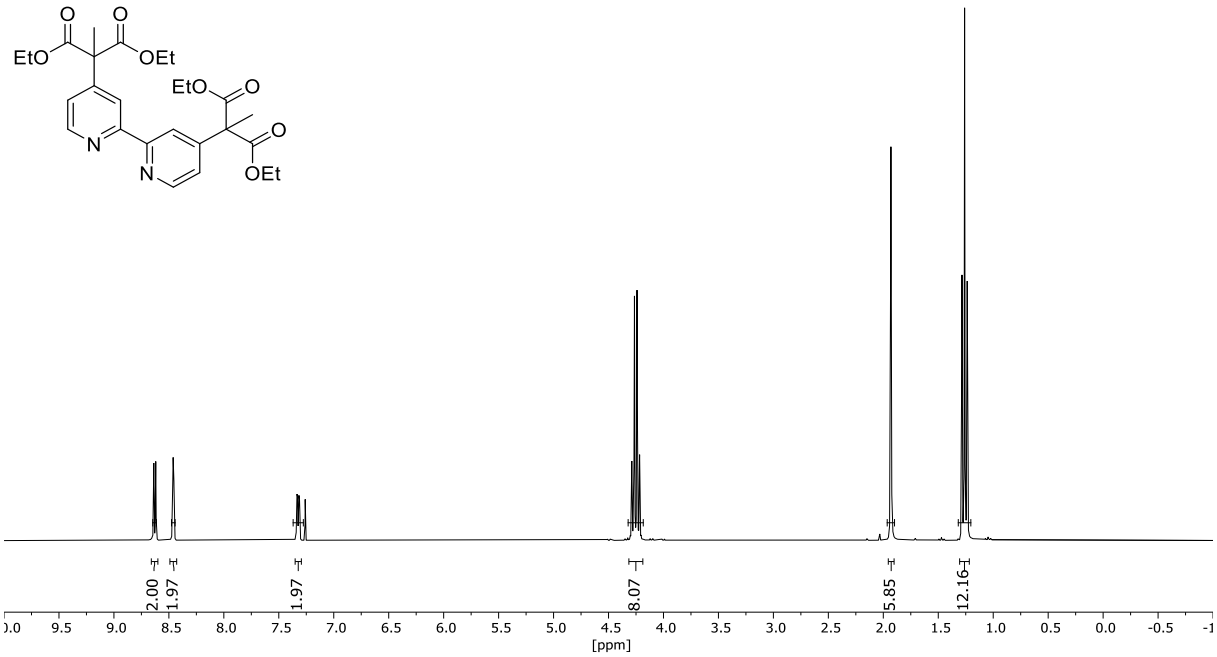

13C NMR (75.48 MHz, CDCl3)

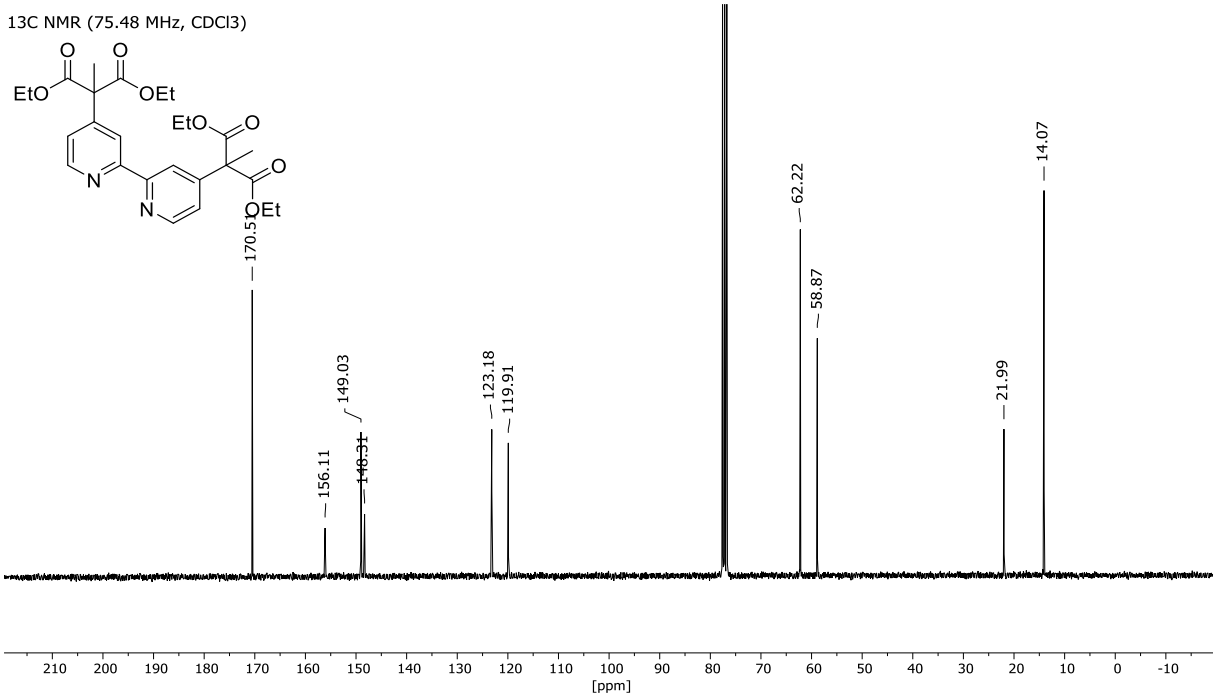

DEPT135 NMR (75.48 MHz, CDCl3)

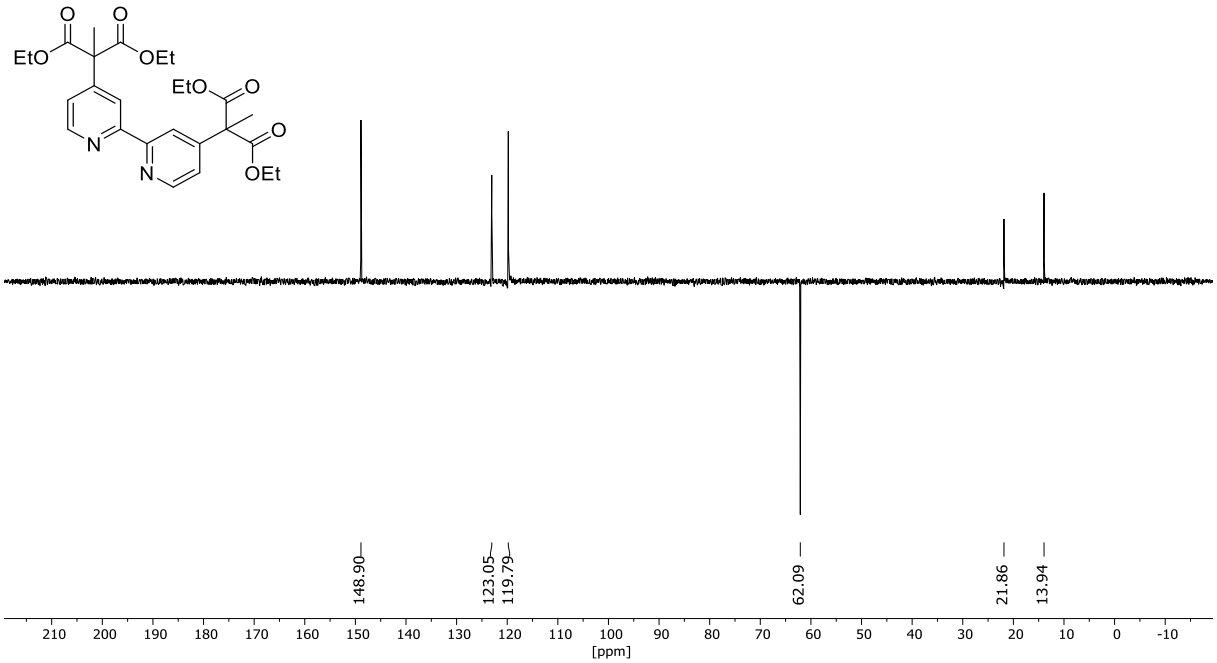

COSY NMR (300.13 MHz, CDCl3)

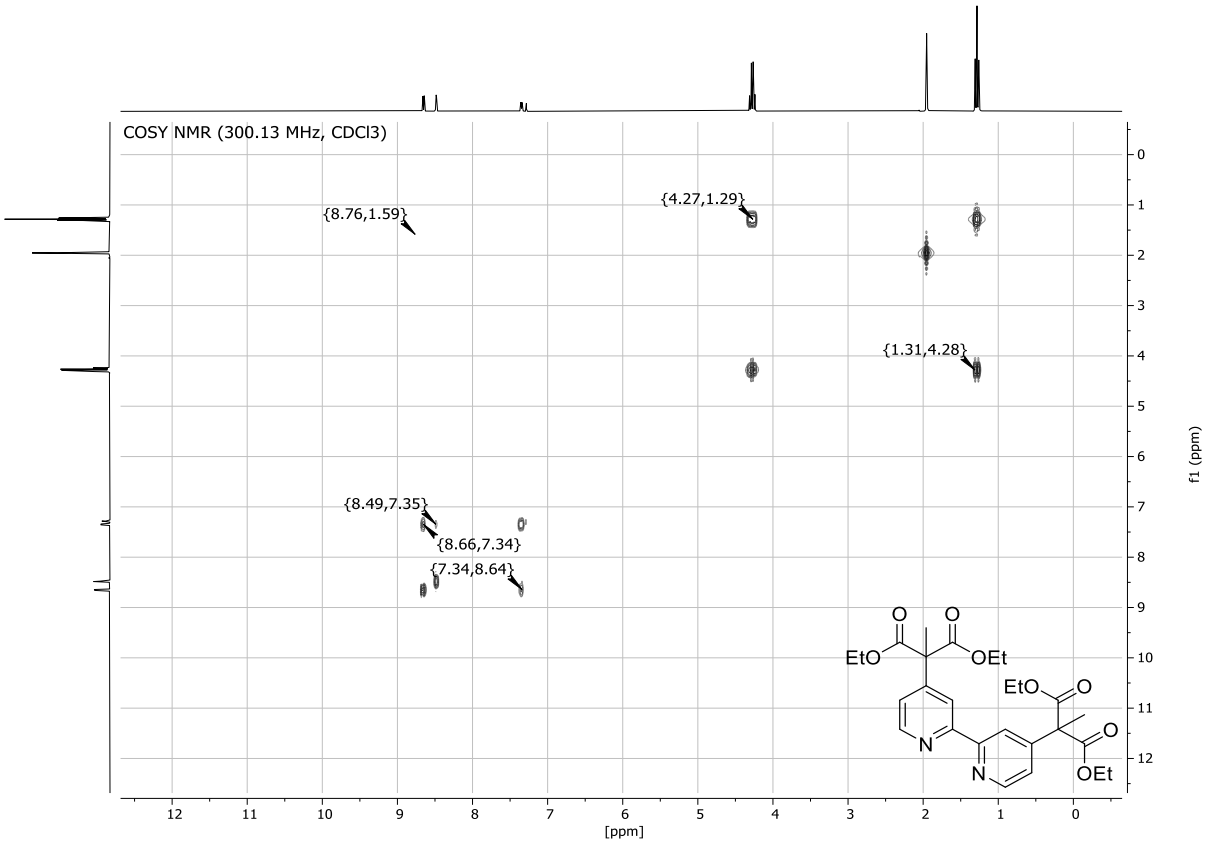

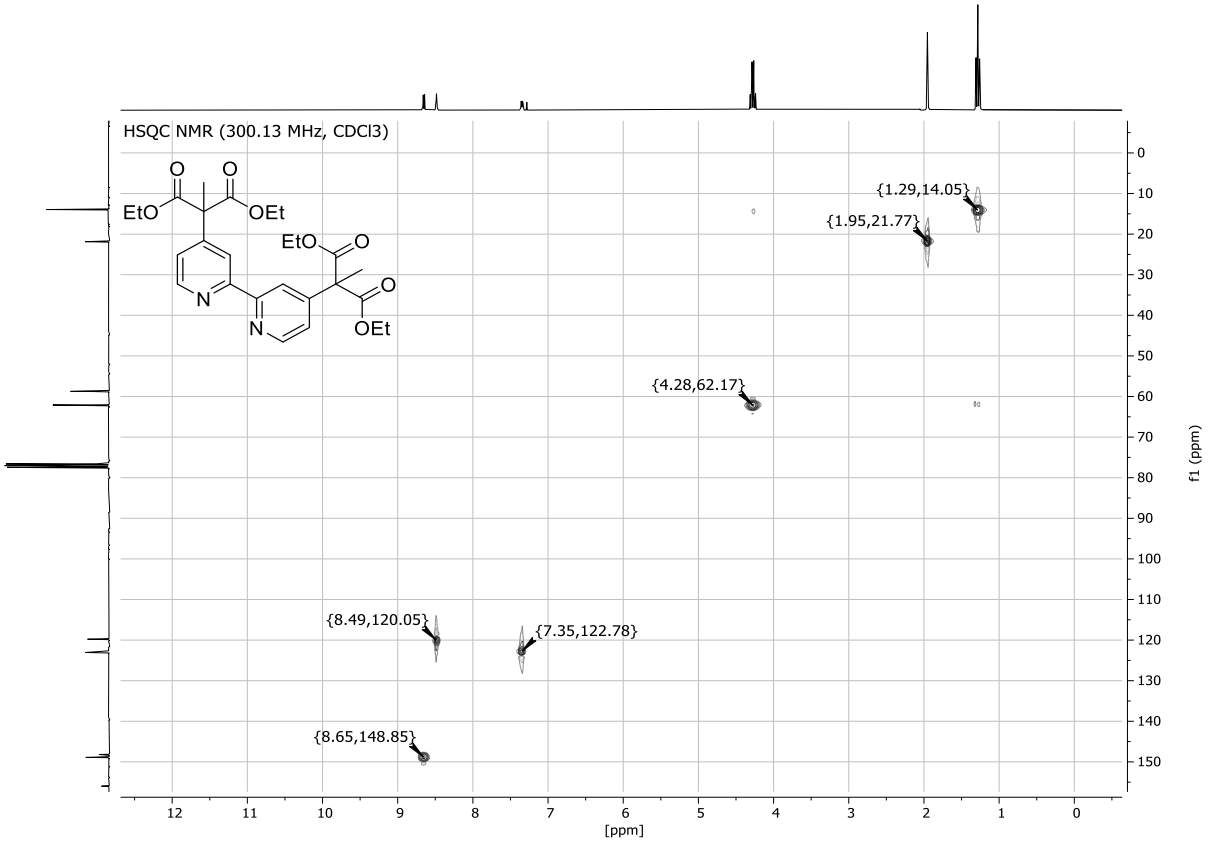
HSQC NMR (300.13 MHz, CDCl3)
{1.29,14.05}
{1.95,21.77}
{4.28,62.17}
{8.49,120.05}
{7.35,122.78}
{8.65,148.85}
f1 (ppm)
[ppm]

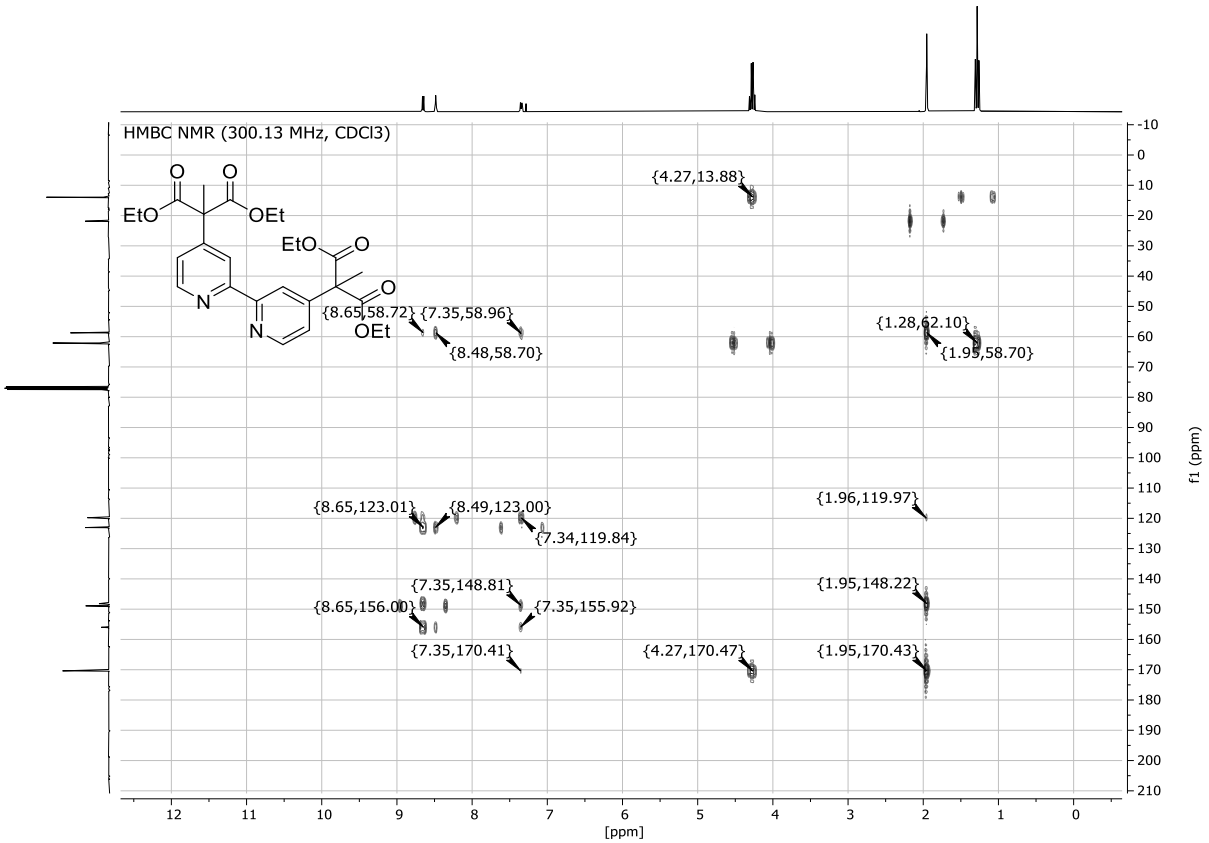
HMBC NMR (300.13 MHz, CDCl3)
{4.27,13.88}
{8.65,58.72}
{7.35,58.96}
{8.48,58.70}
{1.28,62.10}
{1.95,58.70}
{8.65,123.01}
{8.49,123.00}
{7.34,119.84}
{1.96,119.97}
{7.35,148.81}
{8.65,156.00}
{7.35,155.92}
{1.95,148.22}
{7.35,170.41}
{4.27,170.47}
{1.95,170.43}
f1 (ppm)
[ppm]

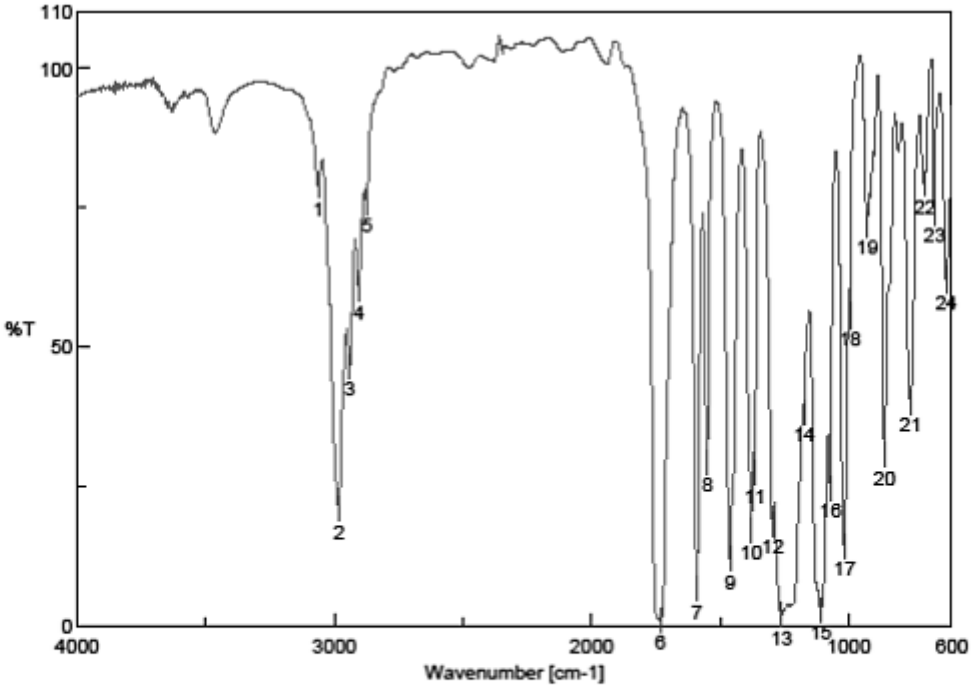

[Result of Peak Picking]

No.	Position	Intensity	No.	Position	Intensity	No.	Position	Intensity
1	3063.37	78.8767	2	2983.34	20.9476	3	2939.95	46.3935
4	2906.2	60.2205	5	2874.38	75.7452	6	1734.66	1.01572
7	1590.99	6.51783	8	1550.49	29.2331	9	1461.78	11.9203
10	1379.82	17.0327	11	1365.35	27.2542	12	1296.89	18.1107
13	1262.18	1.98307	14	1173.47	38.1627	15	1108.87	2.80012
16	1072.23	24.6224	17	1018.23	14.1991	18	995.089	55.5063
19	929.521	71.9263	20	861.06	30.5949	21	760.78	39.9016
22	705.819	79.1758	23	668.214	73.998	24	621.931	61.878

6.1.9 2,2′-([2,2′-Bipyridine]-4,4′-diyl)bis(N^1,N^3-bis((*S*)-1-hydroxy-3-methylbutan-2-yl)-2-methylmalonamide) (**622**)

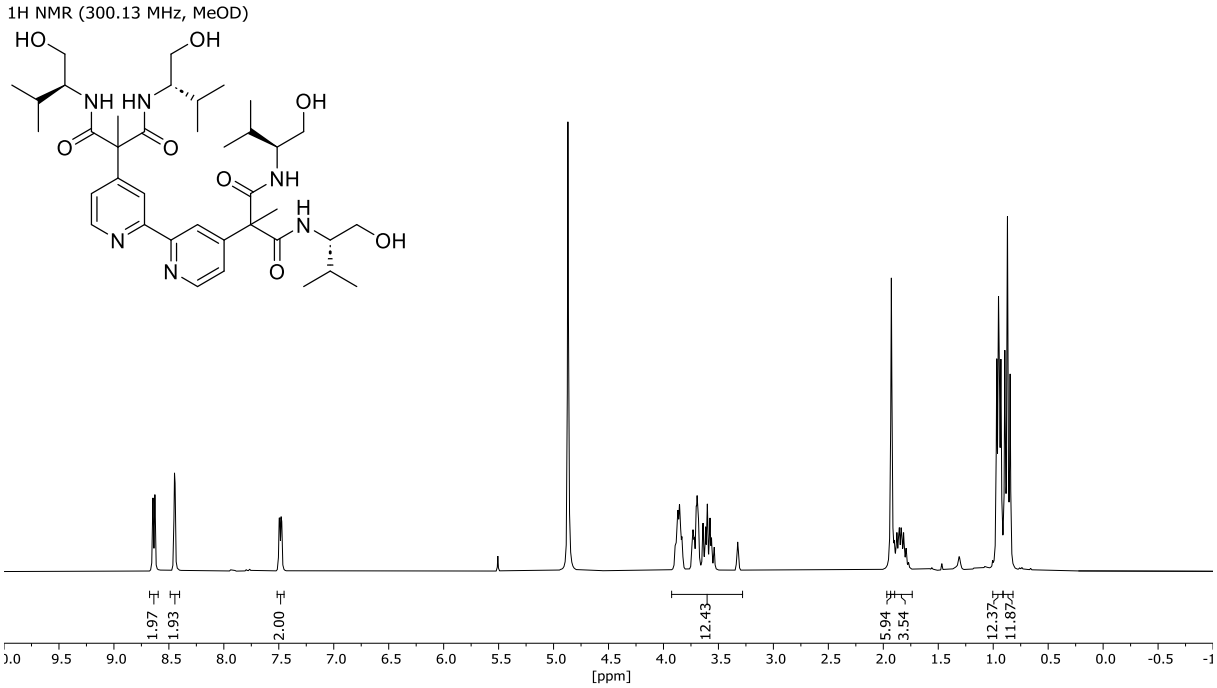

13C NMR (75.48 MHz, MeOD)

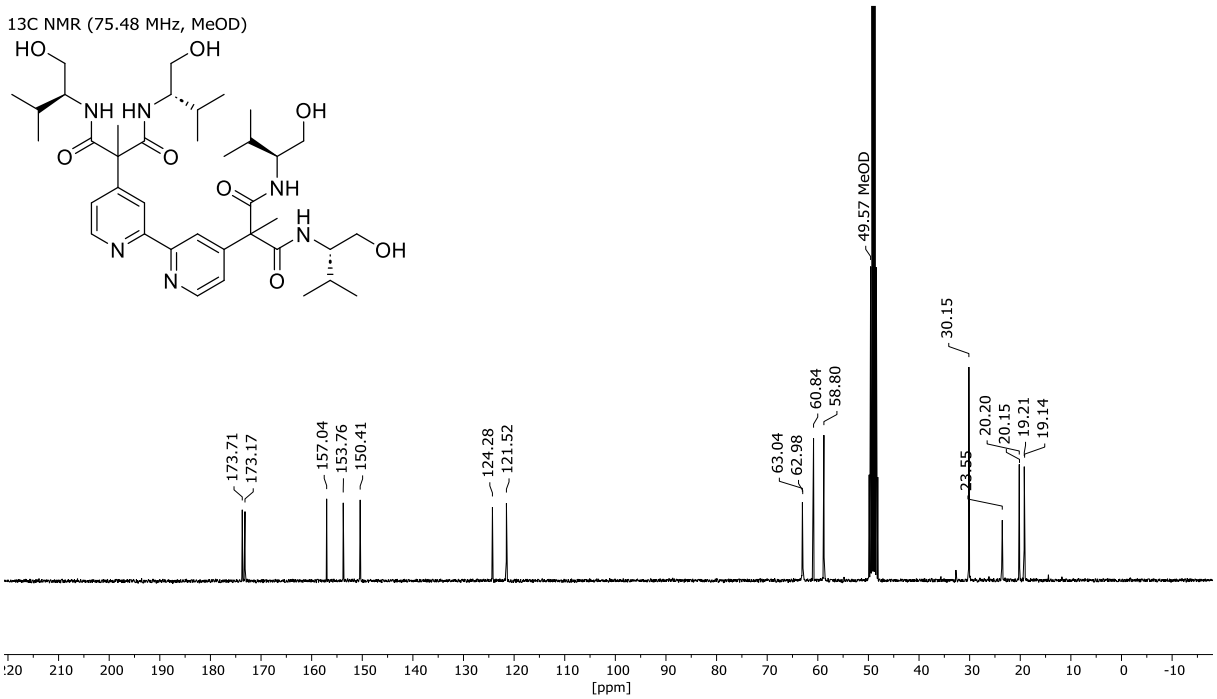

DEPT135 NMR (75.48 MHz, MeOD)

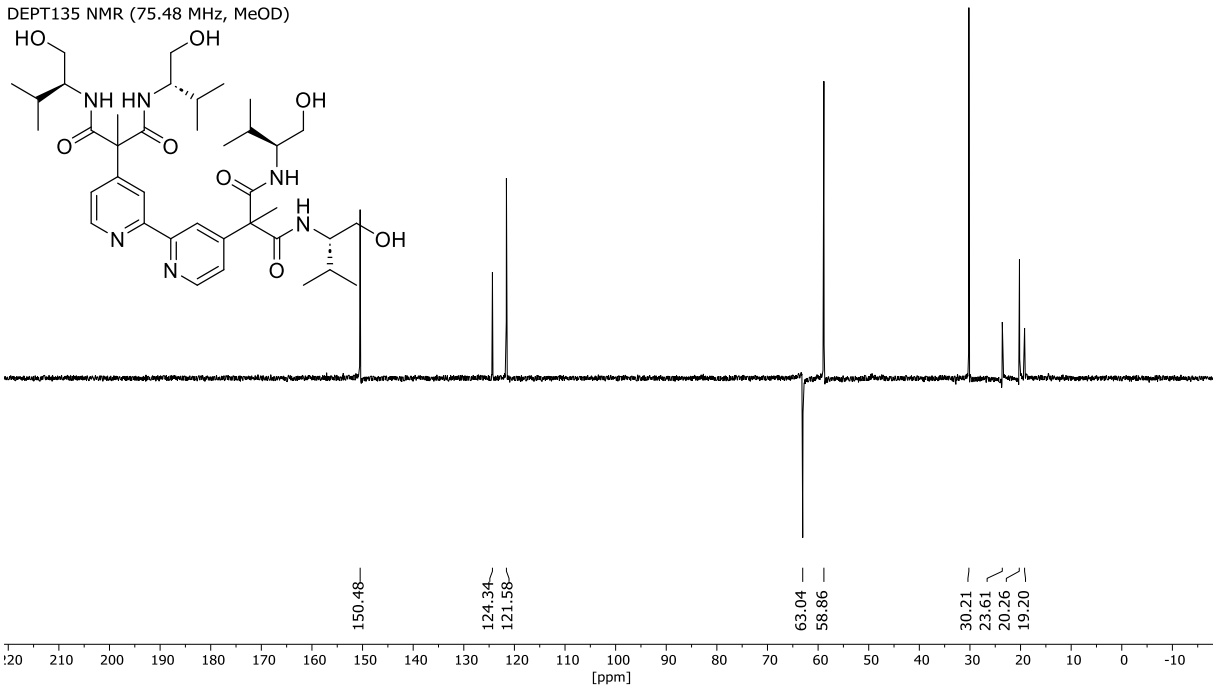

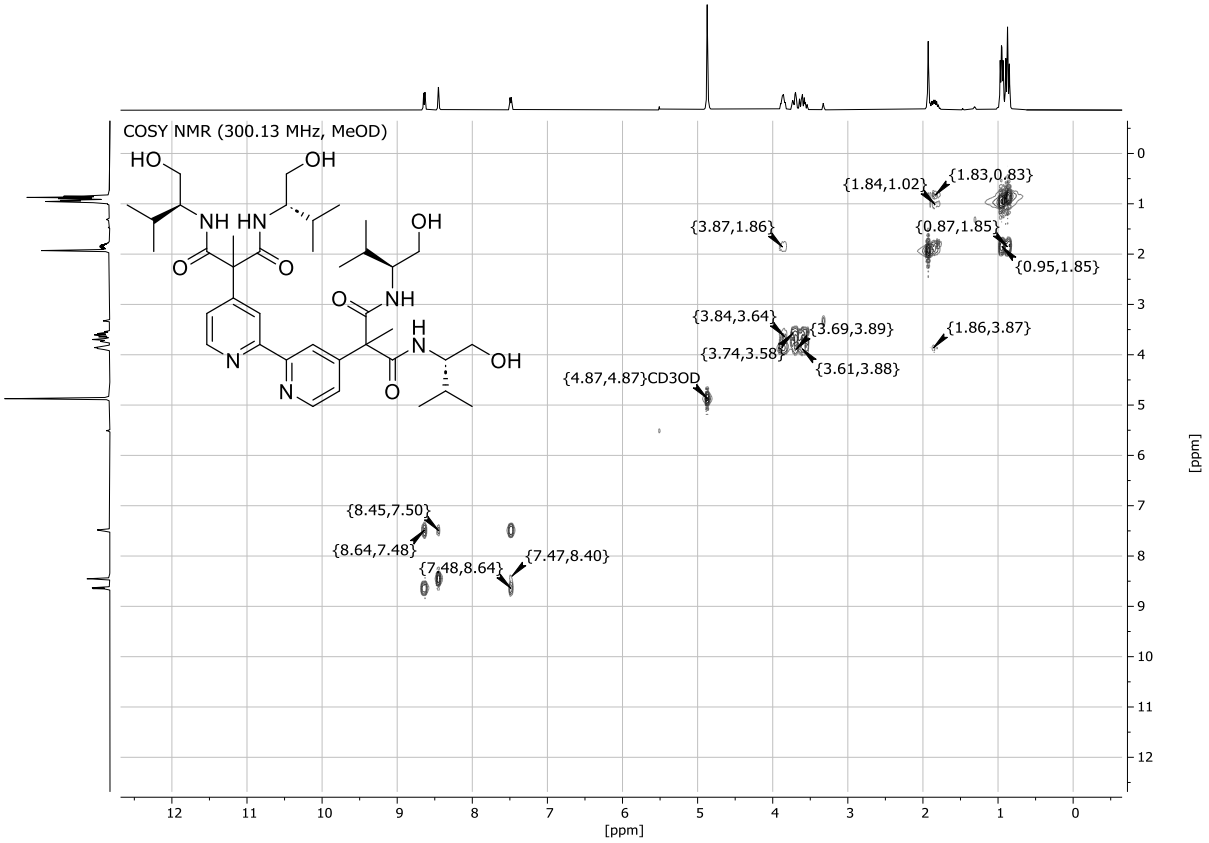
COSY NMR (300.13 MHz, MeOD)
{1.84,1.02}
{1.83,0.83}
{3.87,1.86}
{0.87,1.85}
{0.95,1.85}
{3.84,3.64}
{3.69,3.89}
{1.86,3.87}
{3.74,3.58}
{3.61,3.88}
{4.87,4.87}CD3OD
{8.45,7.50}
{8.64,7.48}
{7.48,8.64}
{7.47,8.40}
[ppm]

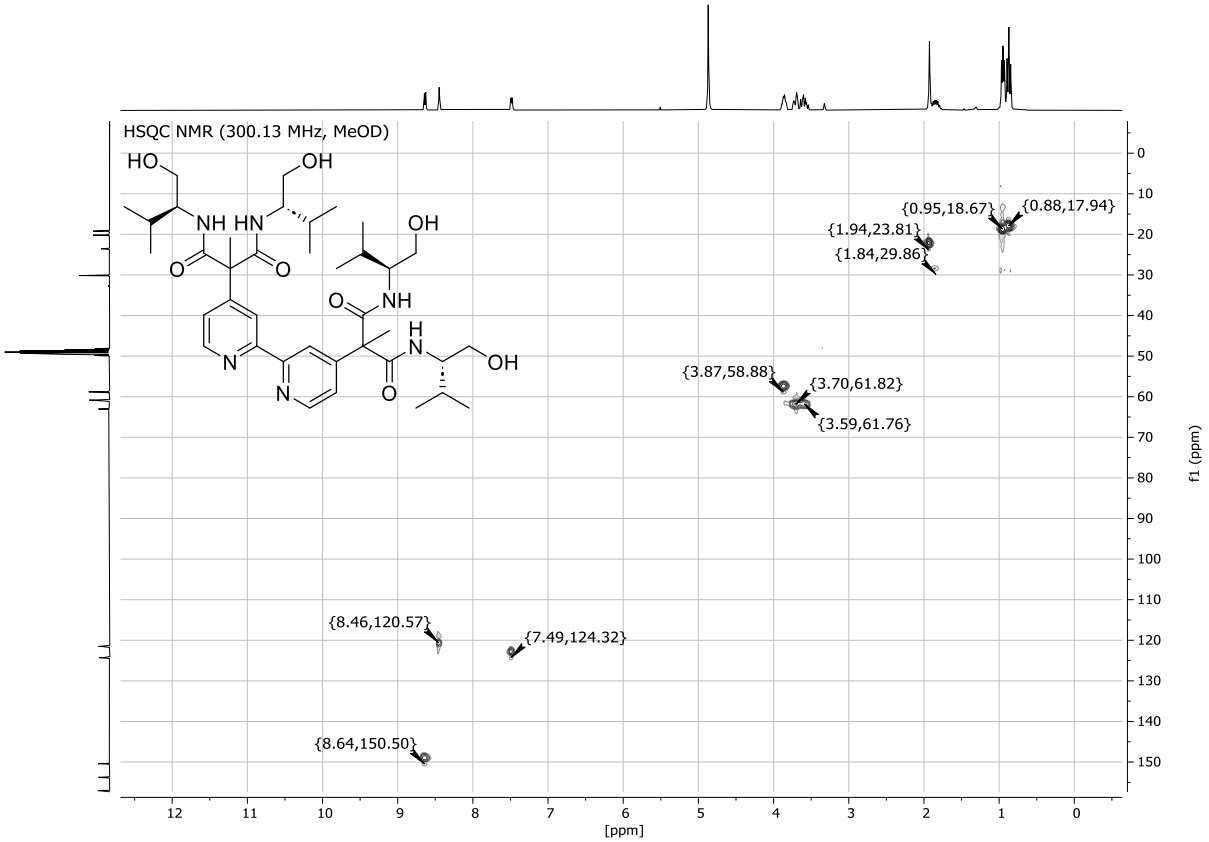
HSQC NMR (300.13 MHz, MeOD)
{0.95,18.67}
{0.88,17.94}
{1.94,23.81}
{1.84,29.86}
{3.87,58.88}
{3.70,61.82}
{3.59,61.76}
{8.46,120.57}
{7.49,124.32}
{8.64,150.50}
[ppm]
f1 (ppm)

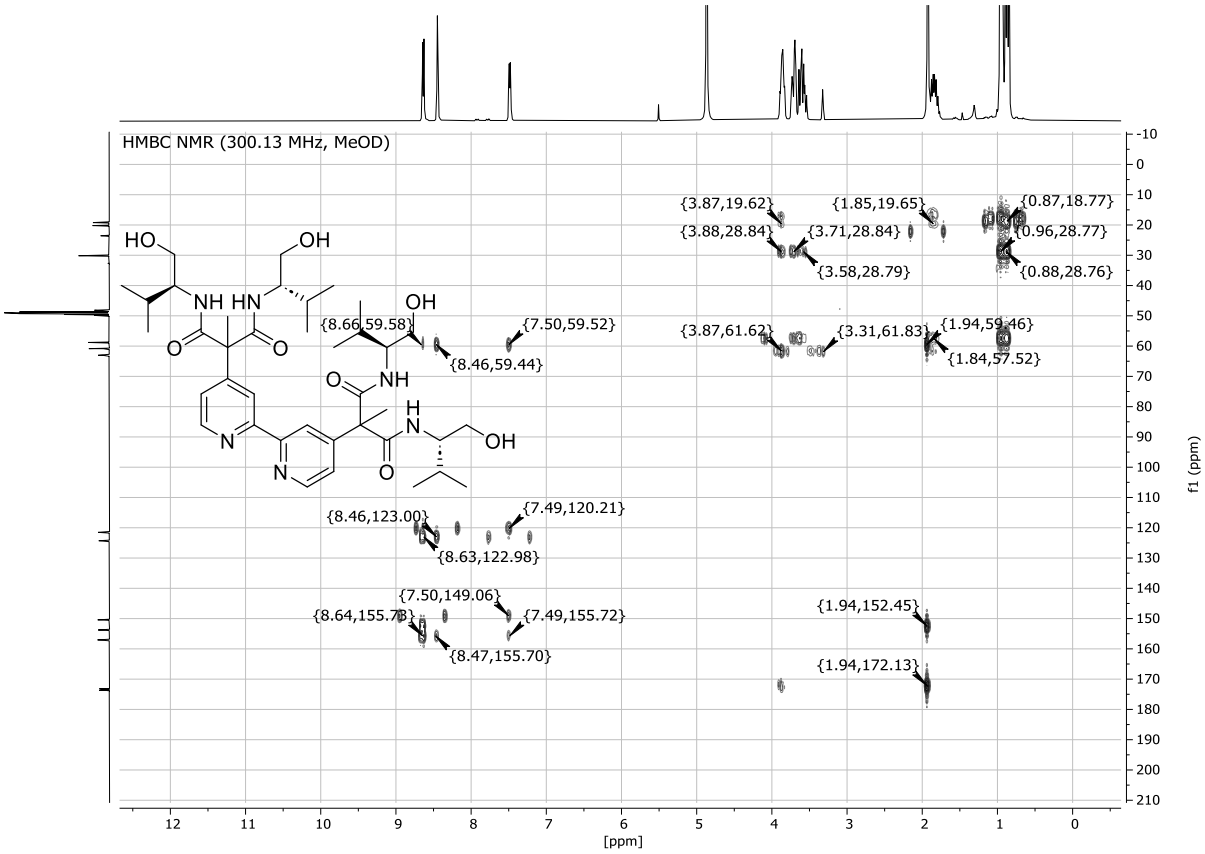

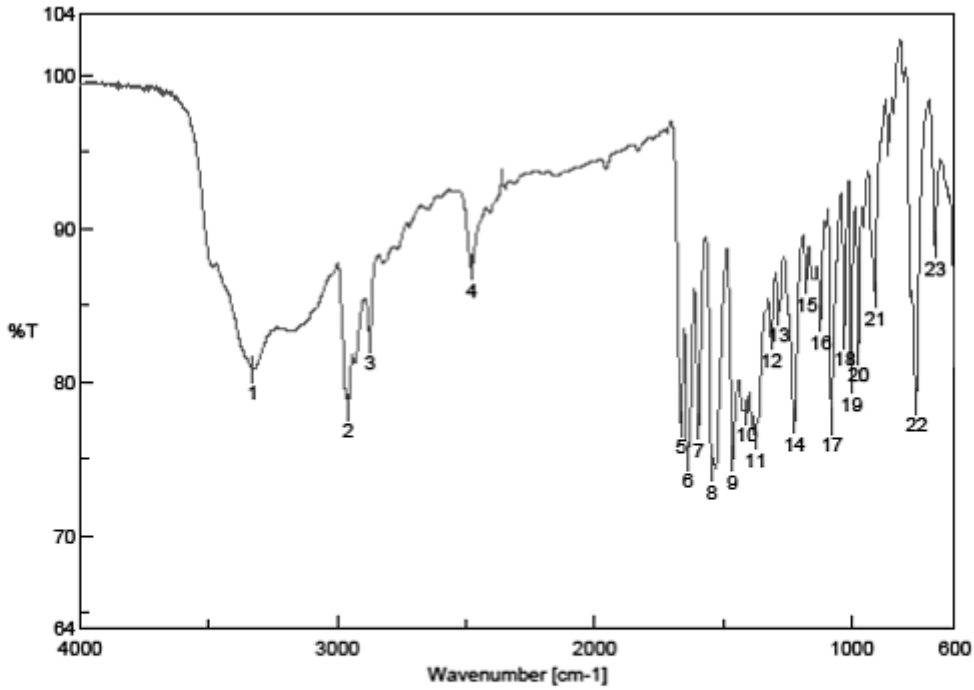

[Result of Peak Picking]

No.	Position	Intensity	No.	Position	Intensity	No.	Position	Intensity
1	3329.5	80.7784	2	2959.23	78.3113	3	2873.42	82.7253
4	2478.08	87.4494	5	1662.34	77.2302	6	1637.27	75.0014
7	1594.84	77.0859	8	1543.74	74.3237	9	1462.74	74.9871
10	1408.75	78.0302	11	1375	76.4267	12	1313.29	82.883
13	1283.39	84.5655	14	1222.65	77.4289	15	1175.4	86.5394
16	1120.44	84.056	17	1078.01	77.3885	18	1027.87	82.973
19	1001.84	80.0294	20	973.876	81.8993	21	909.272	85.6482
22	749.209	78.7166	23	676.892	88.9133			

6.1.10 4,4′-Bis(1,1-bis((*S*)-4-isopropyl-4,5-dihydrooxazol-2-yl)ethyl)-2,2′-bipyridine (**529**)

1H NMR (300.13 MHz, CDCl3)

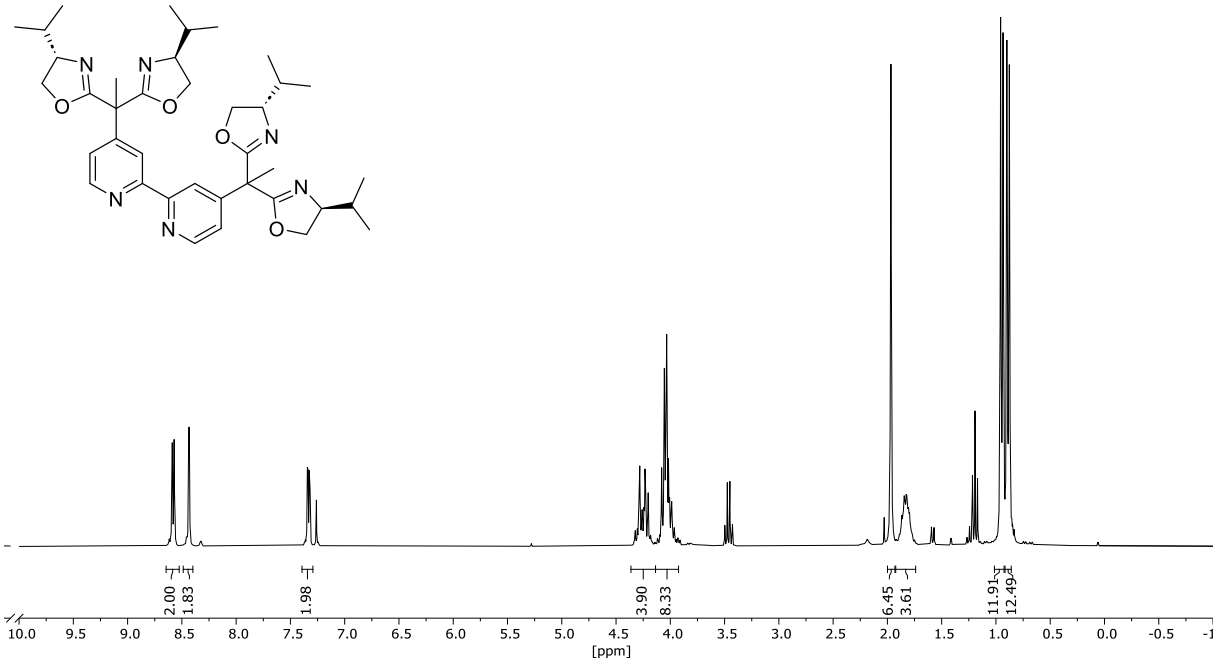

1H NMR (300.13 MHz, MeOD)

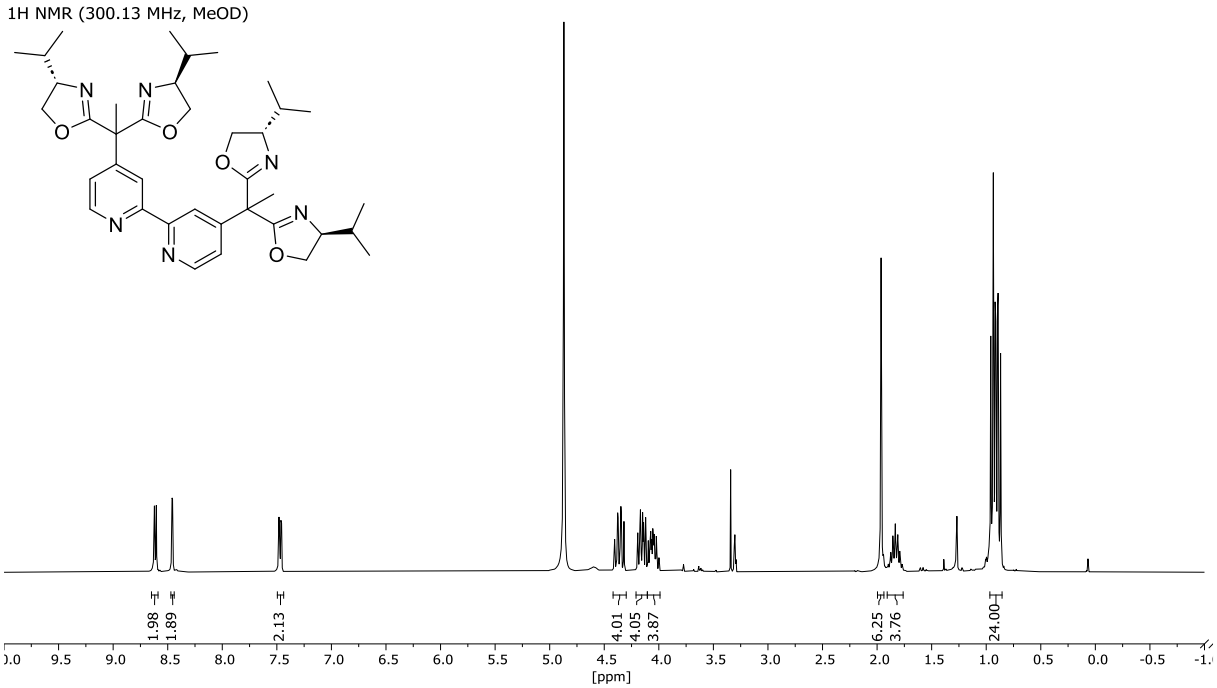

13C NMR (75.48 MHz, CDCl3)

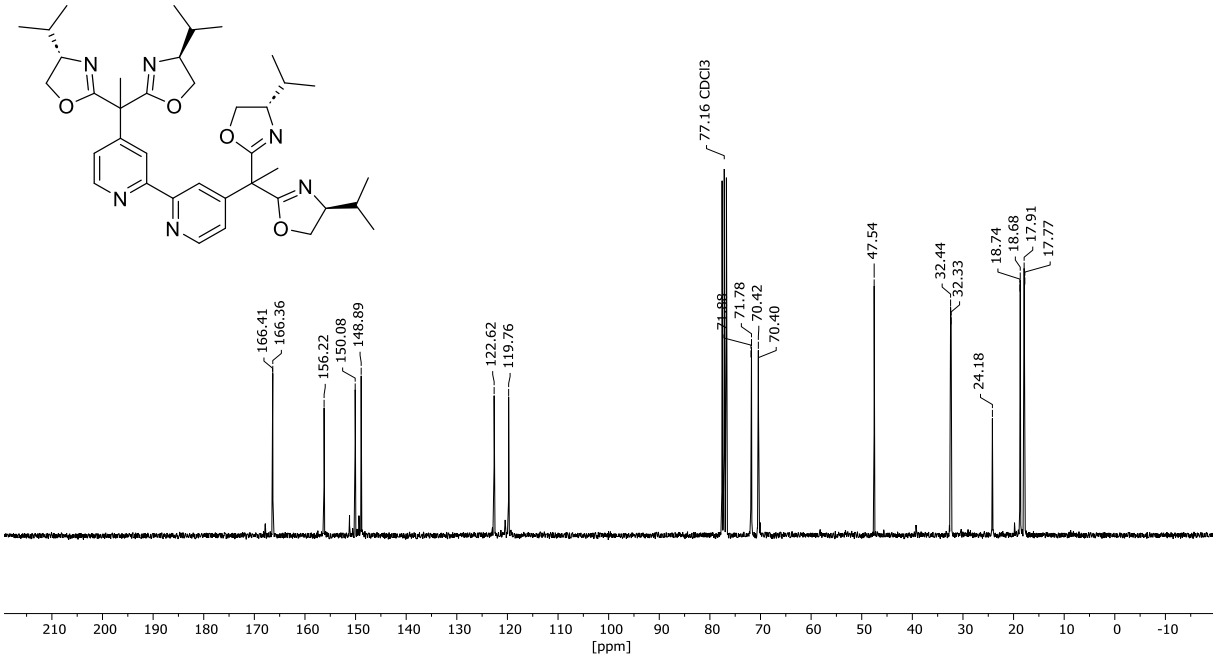

13C NMR (75.48 MHz, MeOD)

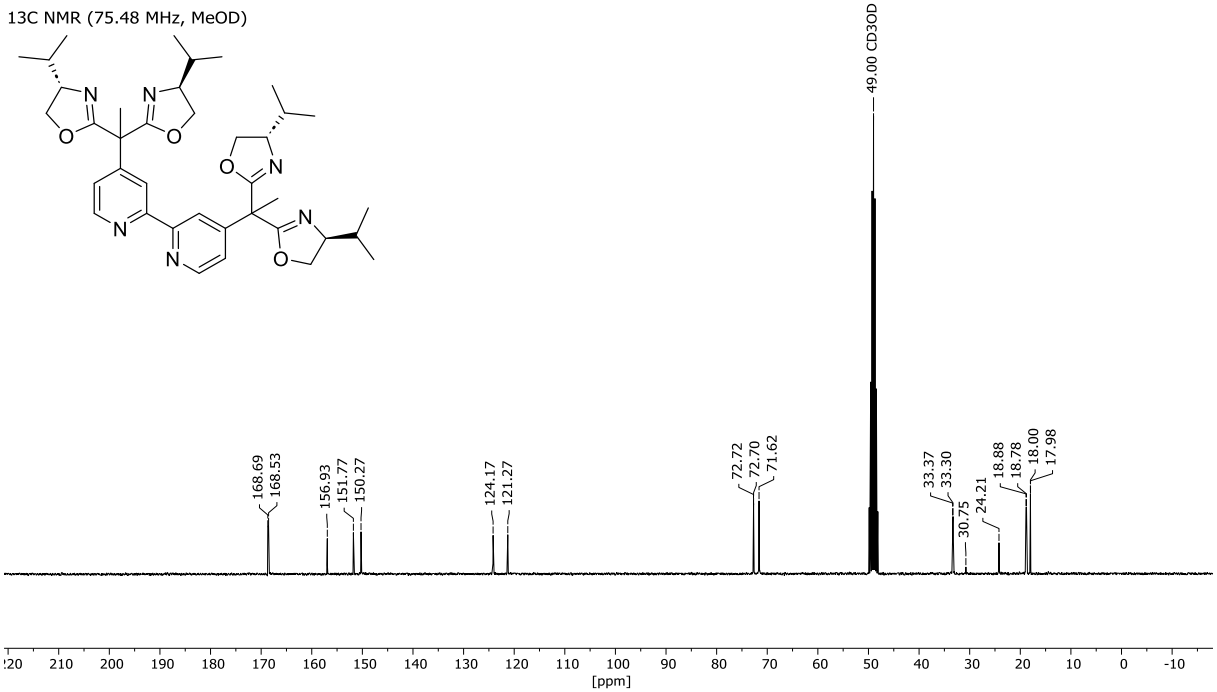

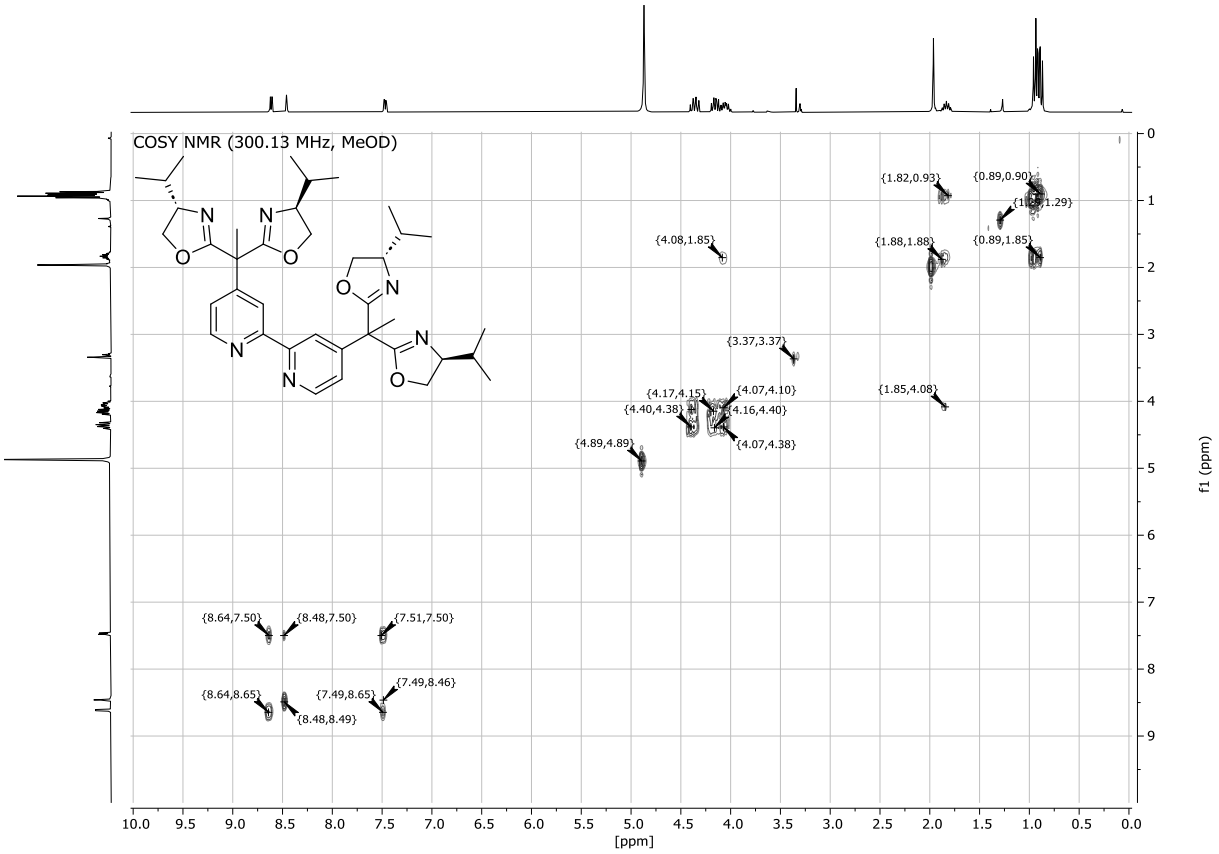
COSY NMR (300.13 MHz, MeOD)
{1.82,0.93}
{0.89,0.90}
{1.29}
{4.08,1.85}
{1.88,1.88}
{0.89,1.85}
{3.37,3.37}
{4.17,4.15}
{4.07,4.10}
{4.40,4.38}
{4.16,4.40}
{4.07,4.38}
{1.85,4.08}
{4.89,4.89}
{8.64,7.50}
{8.48,7.50}
{7.51,7.50}
{8.64,8.65}
{7.49,8.65}
{7.49,8.46}
{8.48,8.49}
[ppm]
f1 (ppm)

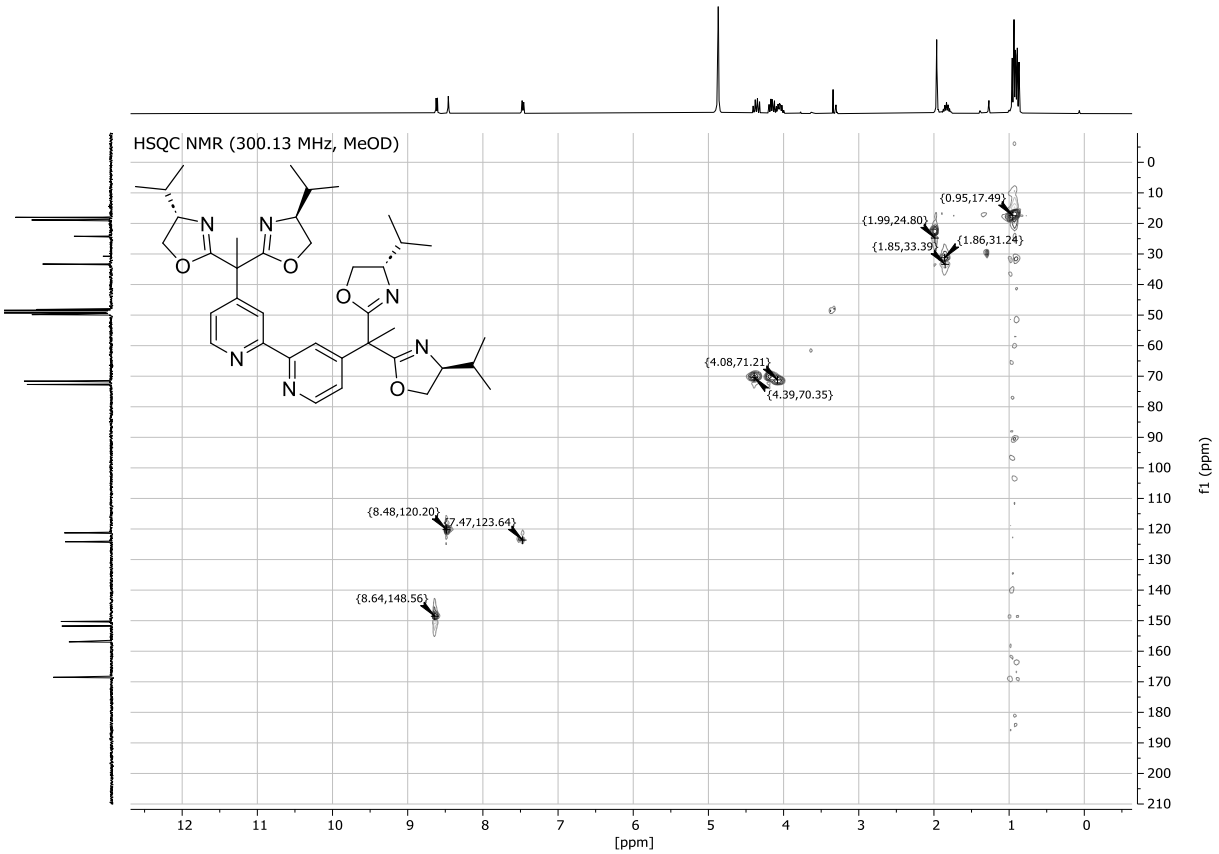
HSQC NMR (300.13 MHz, MeOD)
{0.95,17.49}
{1.99,24.80}
{1.85,33.39}
{1.86,31.24}
{4.08,71.21}
{4.39,70.35}
{8.48,120.20}
{7.47,123.64}
{8.64,148.56}
[ppm]
f1 (ppm)

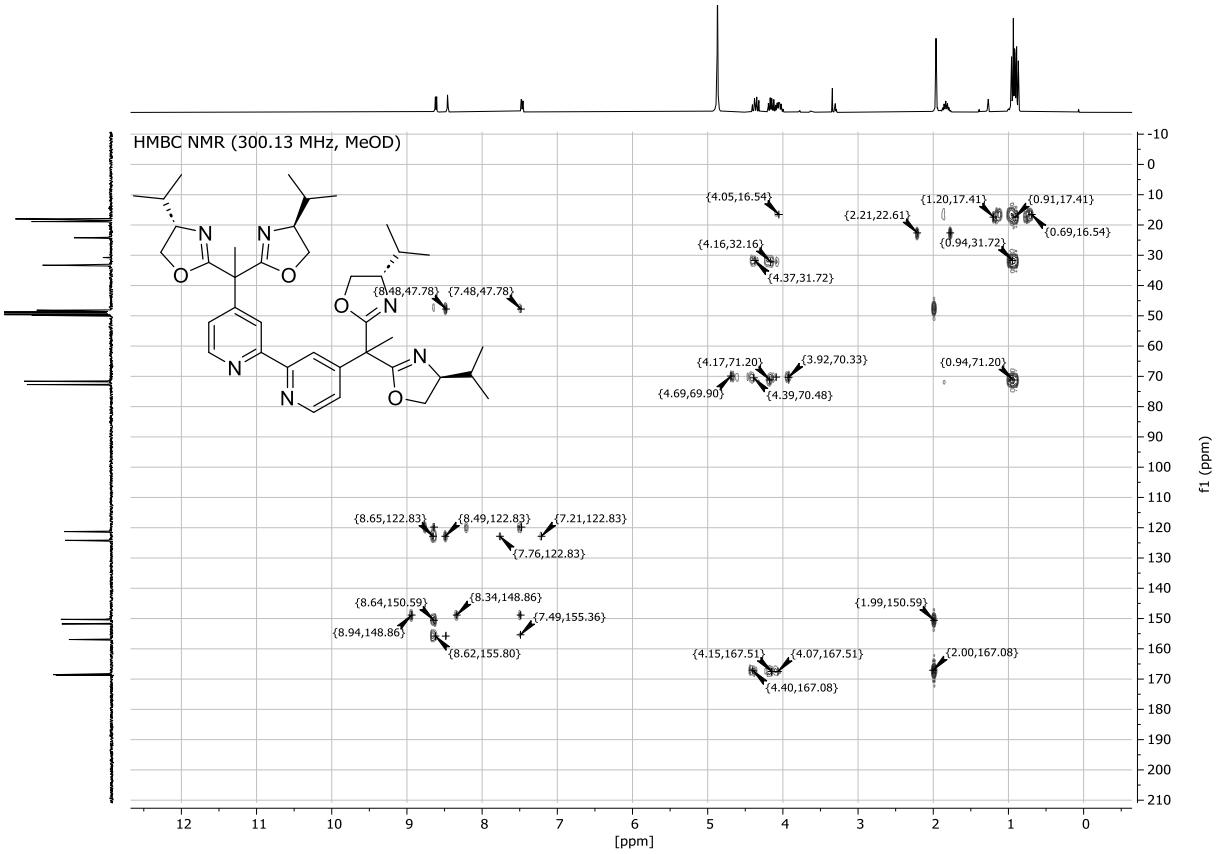

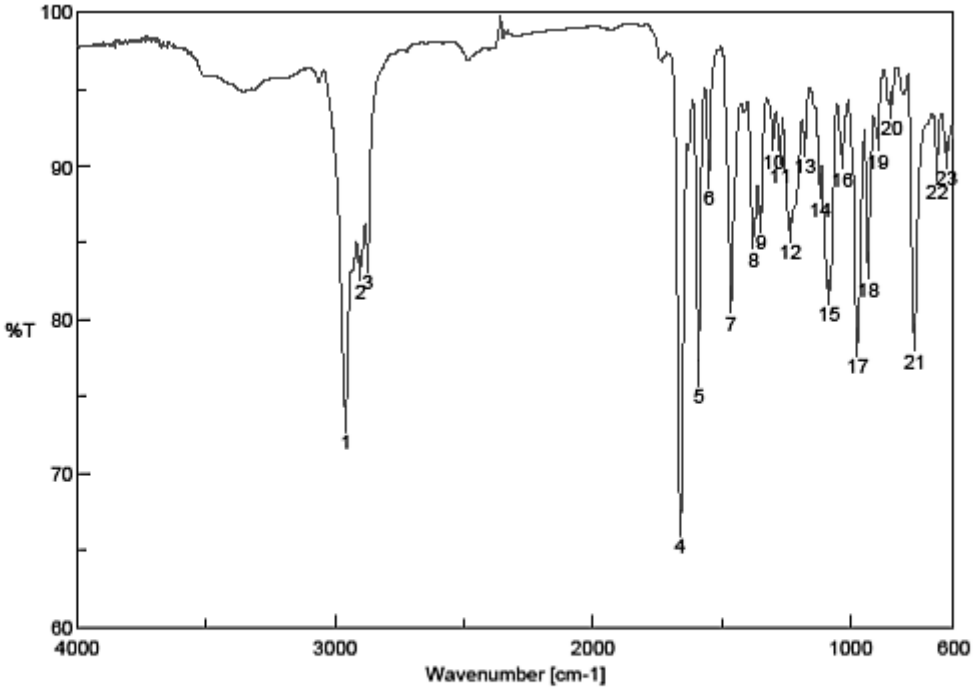

[Result of Peak Picking]

No.	Position	Intensity	No.	Position	Intensity	No.	Position	Intensity
1	2959.23	73.5184	2	2903.31	83.355	3	2873.42	83.9371
4	1660.41	66.7149	5	1590.02	76.481	6	1549.52	89.3913
7	1462.74	81.2725	8	1376.93	85.4019	9	1348	86.5298
10	1299.79	91.7763	11	1273.75	90.8497	12	1235.18	85.8513
13	1177.33	91.4695	14	1118.51	88.6778	15	1083.8	81.8221
16	1032.69	90.6339	17	972.912	78.4825	18	932.414	83.4362
19	894.809	91.7862	20	841.776	93.9597	21	752.102	78.7684
22	665.321	89.8562	23	627.716	90.6967			

6.2 Spectra from the synthesis of bisoxazoline derivatives

6.2.1 L-Phenylalaninol (**604**)

1H NMR (300.13 MHz, MeOD)

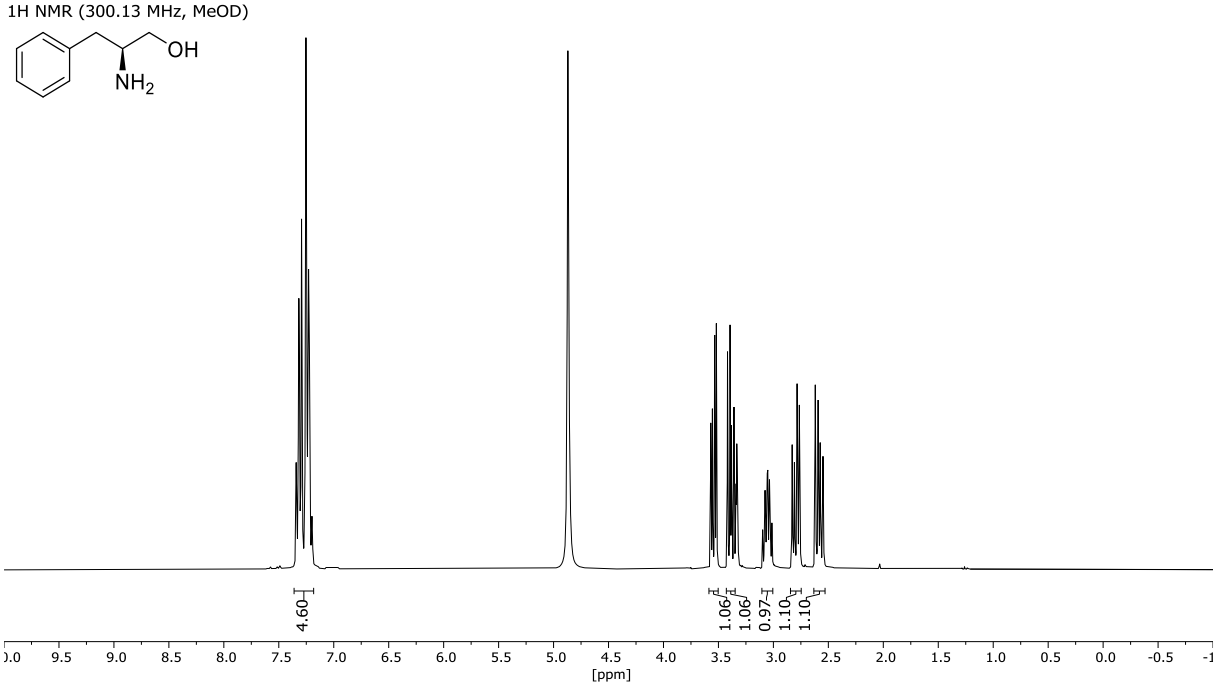

6.2.2 L-Valinol (**603**)

1H NMR (300.13 MHz, CDCl3)

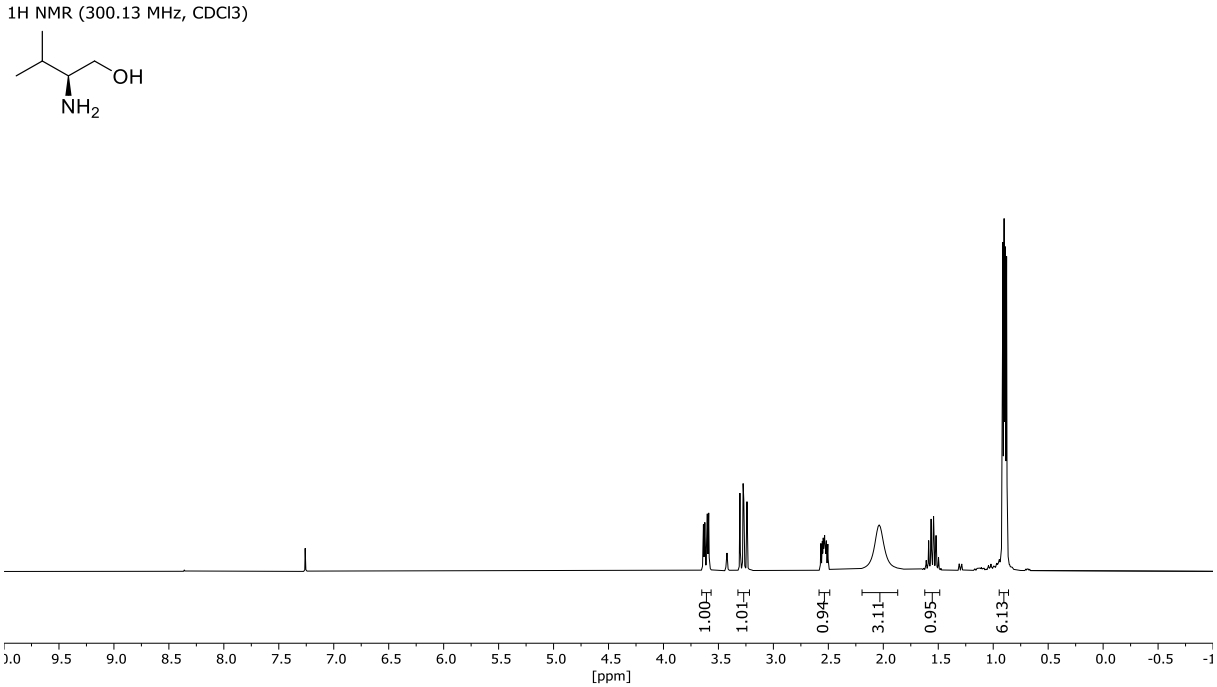

6.2.3 L-*O*-TBDMS-Valinol (**661**)

1H NMR (300.13 MHz, CDCl3)

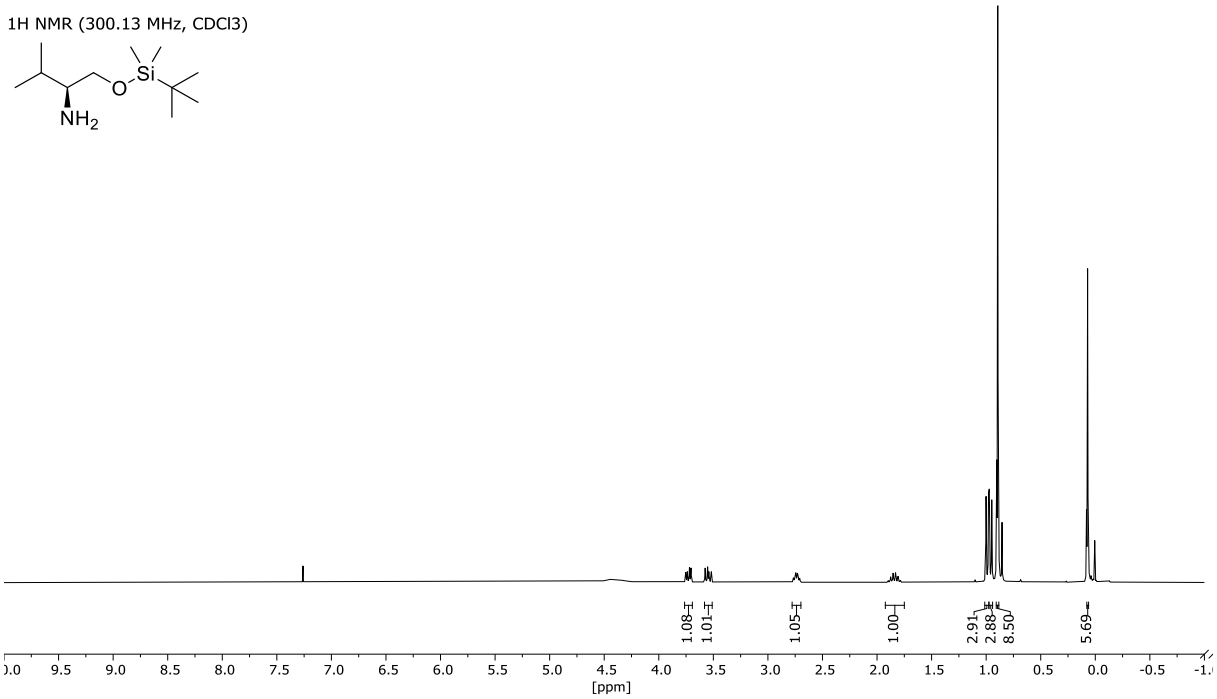

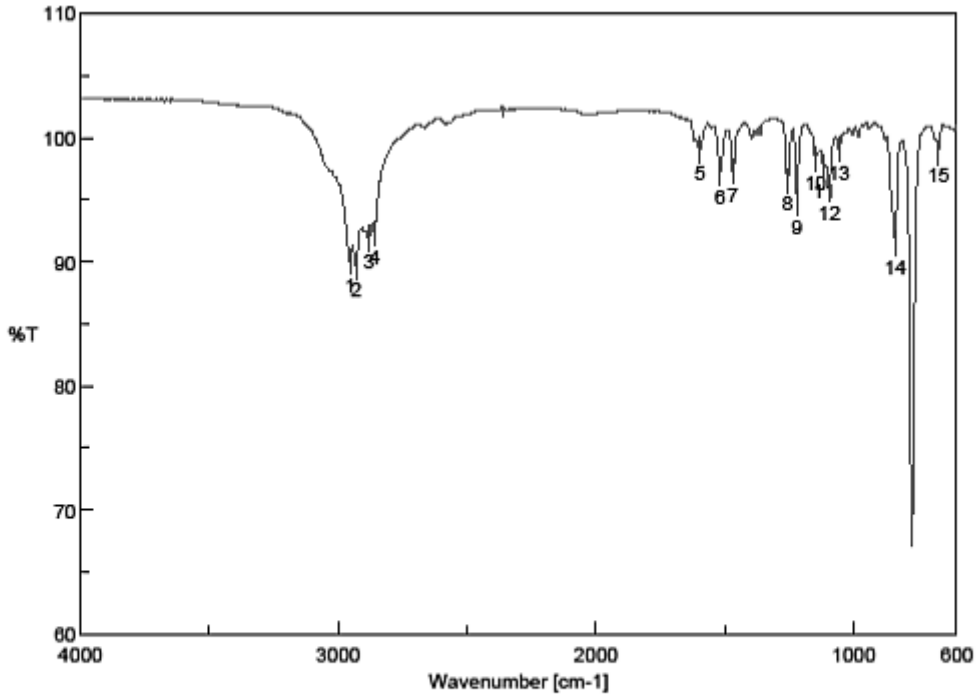

[Result of Peak Picking]

No.	Position	Intensity	No.	Position	Intensity	No.	Position	Intensity
1	2954.41	89.9812	2	2930.31	89.5547	3	2882.09	91.8511
4	2858.95	92.2185	5	1595.81	99.0235	6	1518.67	97.0981
7	1469.49	97.2803	8	1256.4	96.5387	9	1219.76	94.6647
10	1147.44	98.2354	11	1115.62	97.586	12	1095.37	95.86
13	1056.8	99.0986	14	837.919	91.4328	15	671.106	98.8058

6.2.4 Diethyl-2-methylmalonate (**605**)

1H NMR (300.13 MHz, CDCl3)

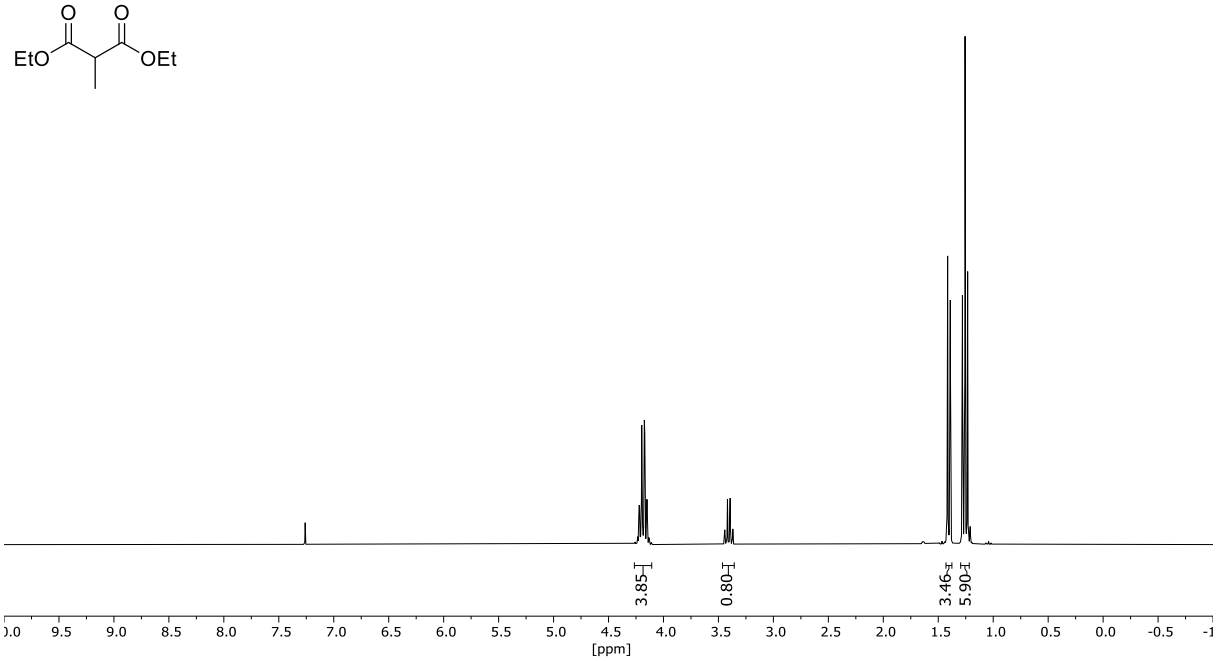

6.2.5 2,2-Dimethylmalonyldichloride (**606**)

1H NMR (300.13 MHz, CDCl3)

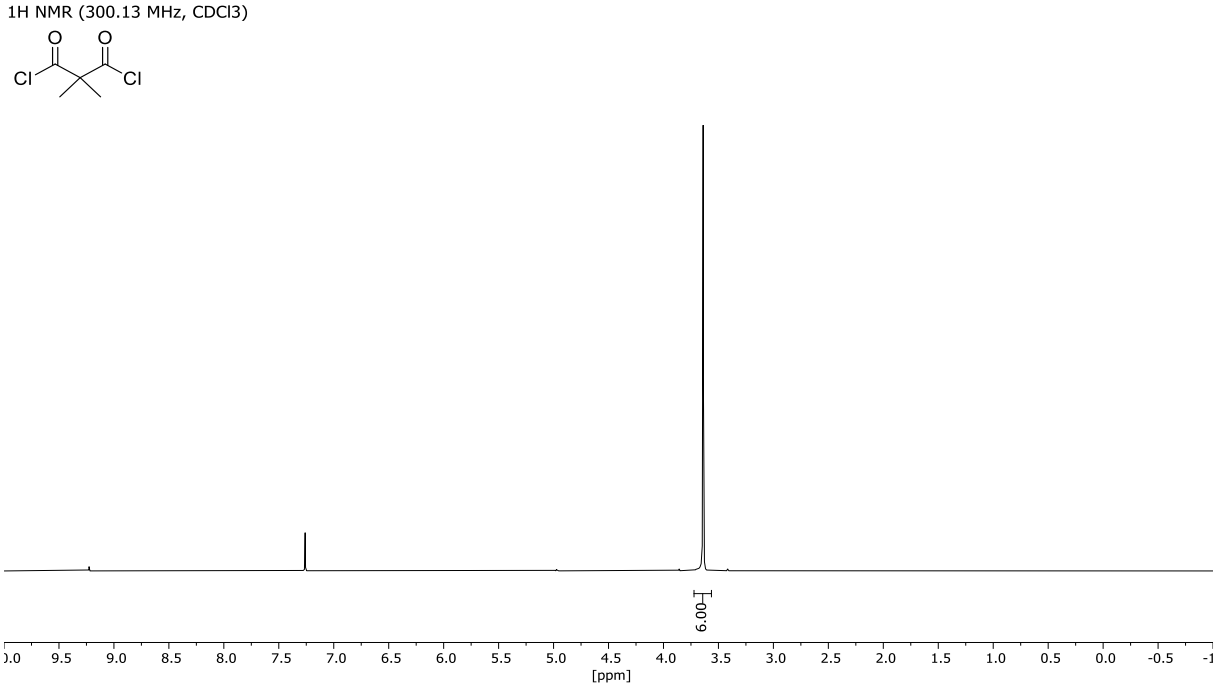

6.2.6 N^1,N^3-Bis((*S*)-1-hydroxy-3-methylbutan-2-yl)malonamide (**608**)

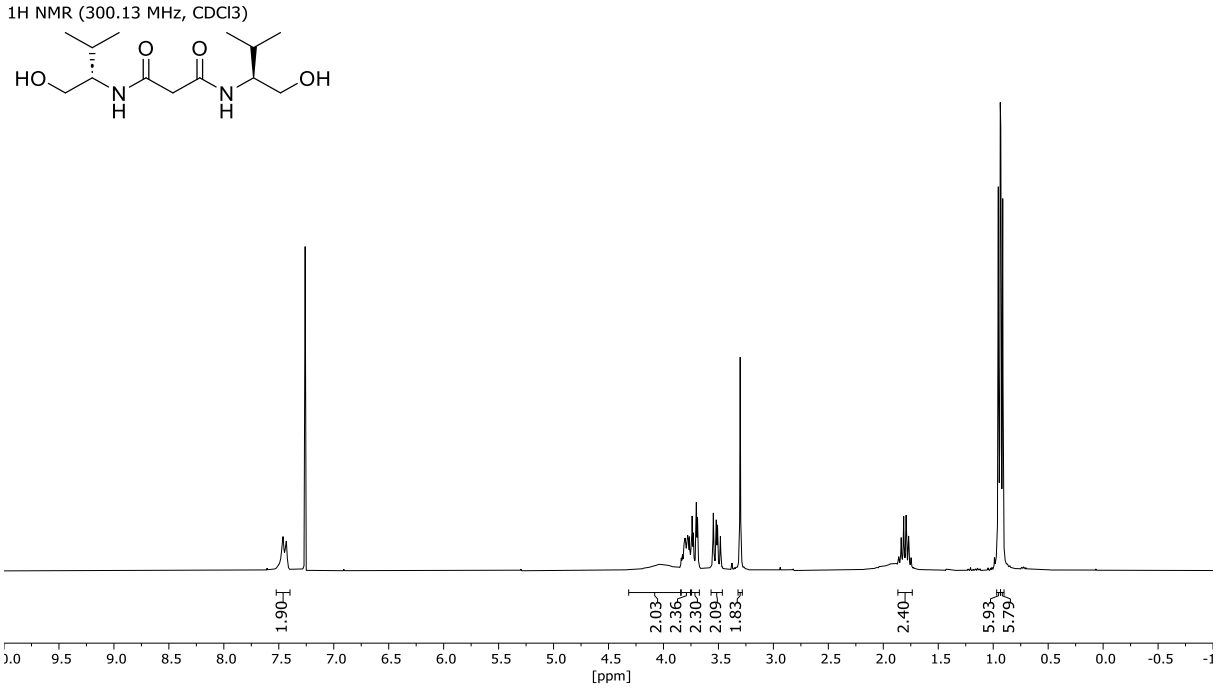

6.2.7 N^1,N^3-Bis((*S*)-1-hydroxy-3-methylbutan-2-yl)-2-methylmalonamide (**609**)

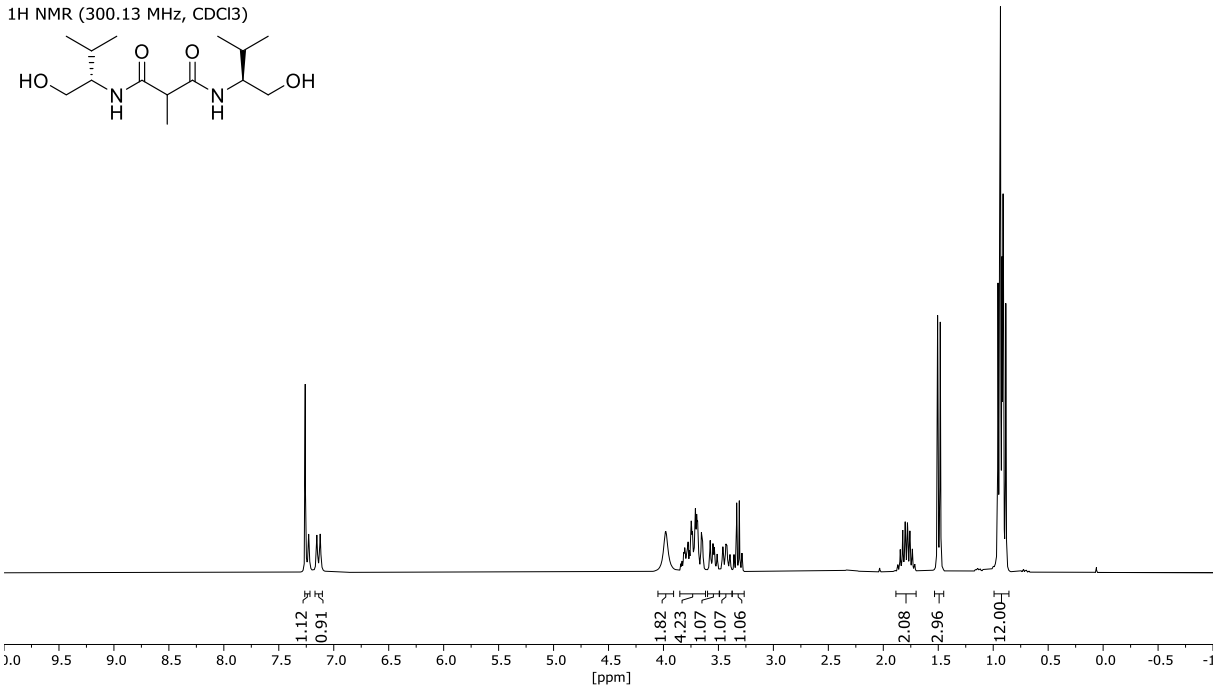

6.2.8 N^1,N^3-Bis((*S*)-1-hydroxy-3-methylbutan-2-yl)-2,2-dimethylmalonamide (**610**)

1H NMR (300.13 MHz, CDCl3)

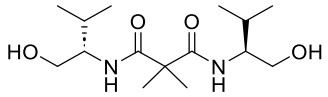

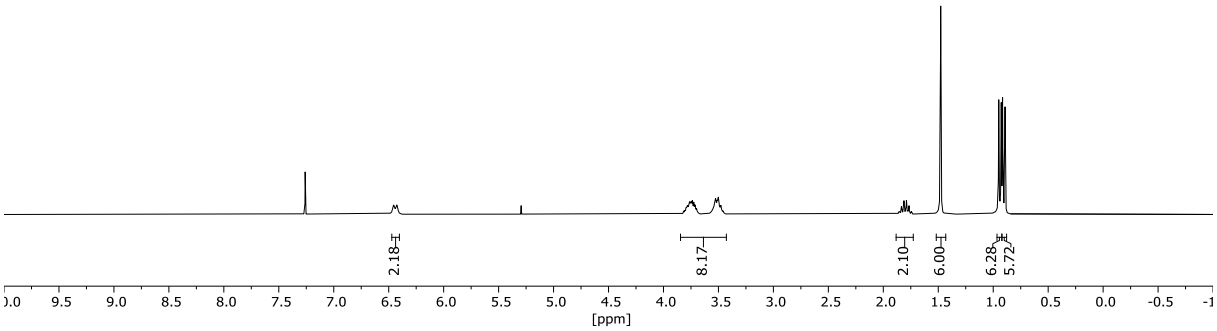

6.2.9 N^1,N^3-Bis((*S*)-1-hydroxy-3-phenylpropan-2-yl)-2,2-dimethylmalonamide (**611**)

1H NMR (300.13 MHz, CDCl3)

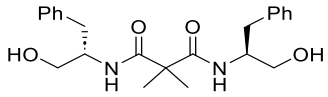

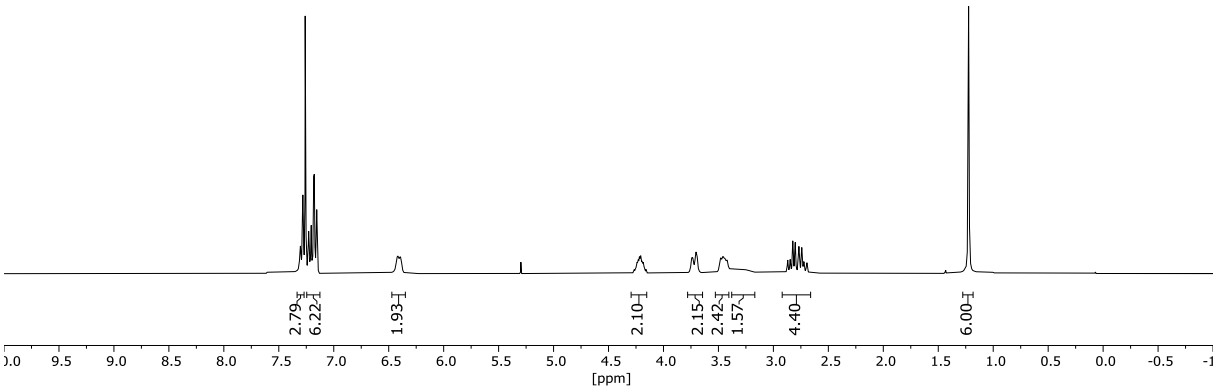

6.2.10 Bis((*S*)-4-isopropyl-4,5-dihydrooxazol-2-yl)methane (**612**)

1H NMR (300.13 MHz, CDCl3)

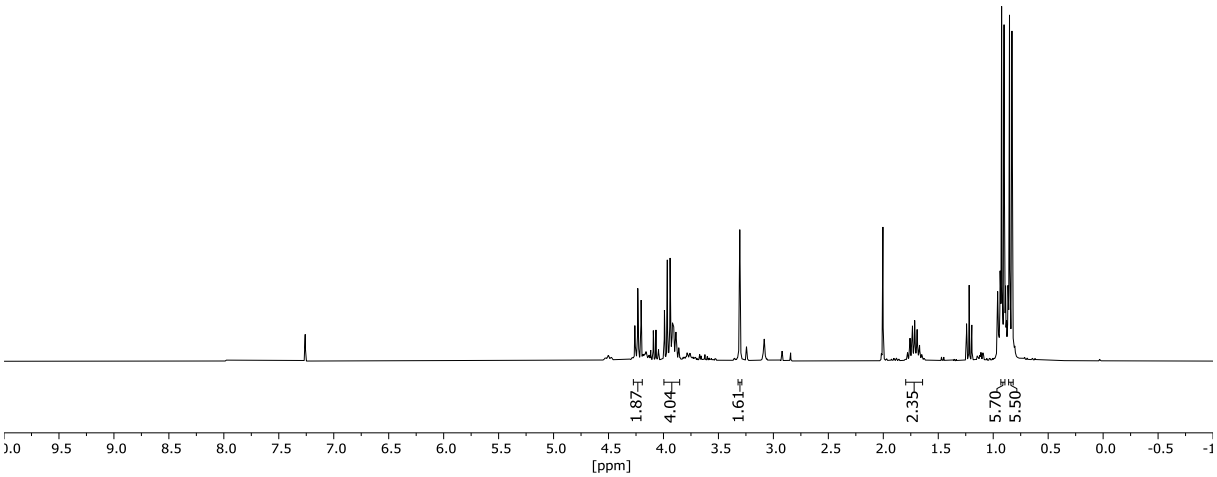

6.2.11 (4*S*,4′*S*)-2,2′-(Ethane-1,1-diyl)bis(4-isopropyl-4,5-dihydrooxazole) (**581**)

1H NMR (300.13 MHz, CDCl3)

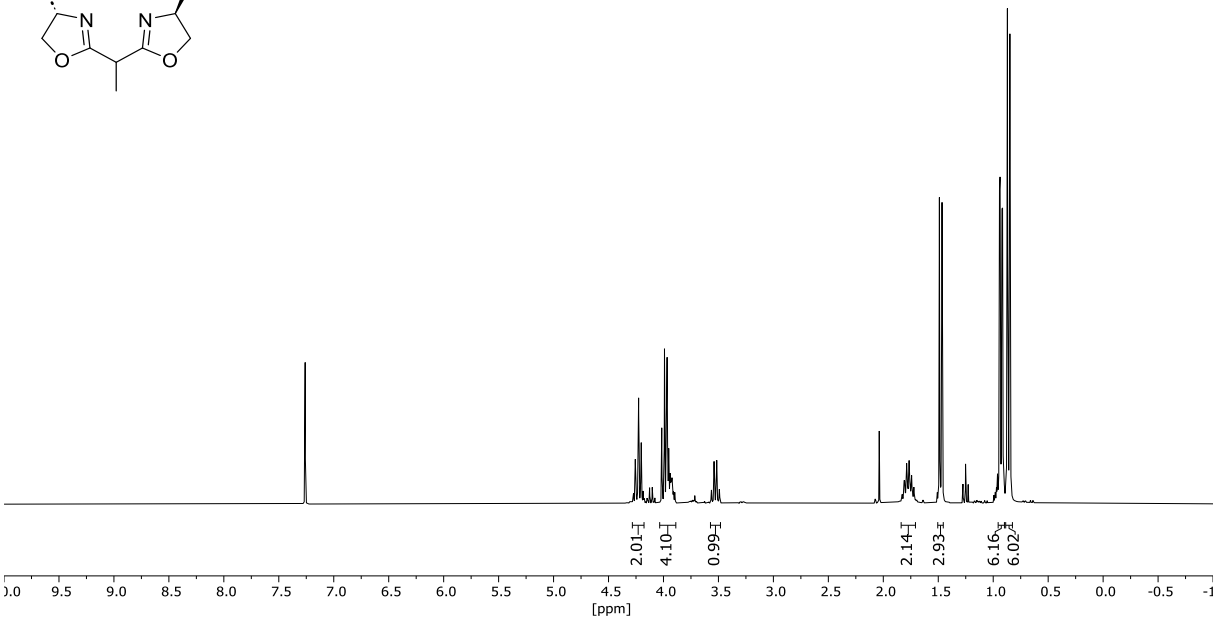

6.2.12 (4*S*,4′*S*)-2,2′-(Ethane-1,1-diyl)bis(4-benzyl-4,5-dihydrooxazole) (**614**)

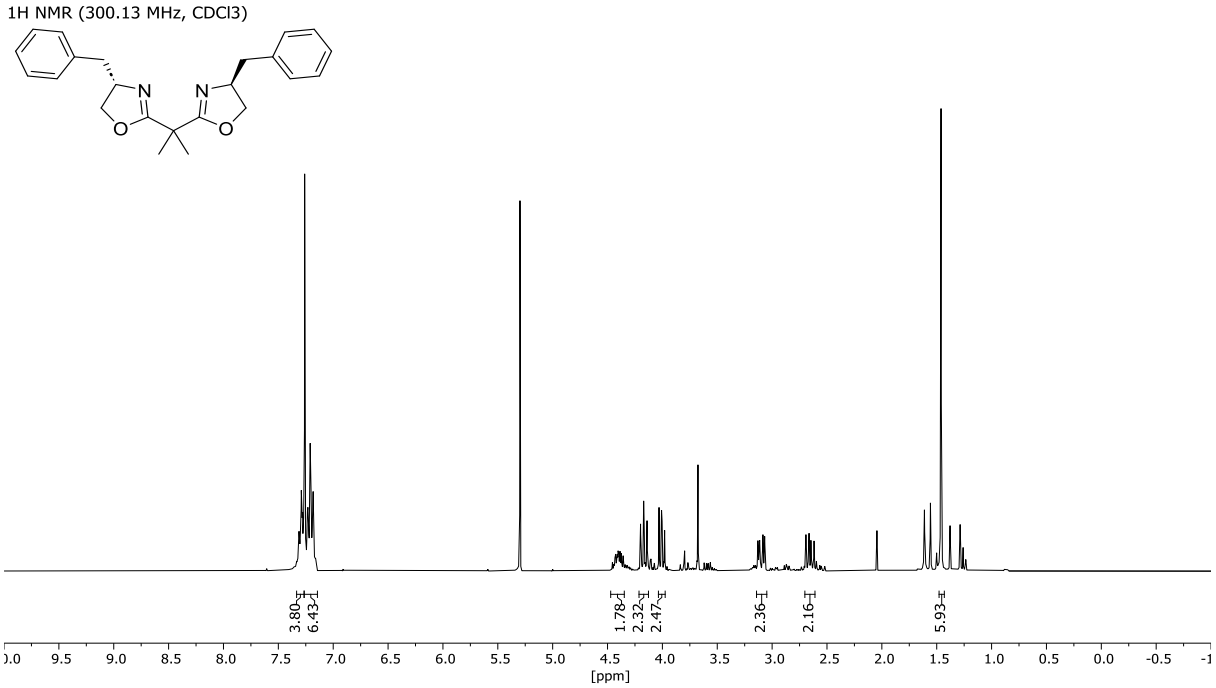

6.3 Spectra of ruthenium complexes

6.3.1 *cis,fac*-$RuCl_2$(dmso-*S*)$_3$(dmso-*O*) (**677**)

1H NMR (300.13 MHz, CDCl3)

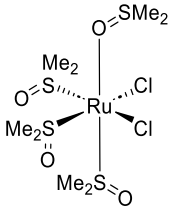

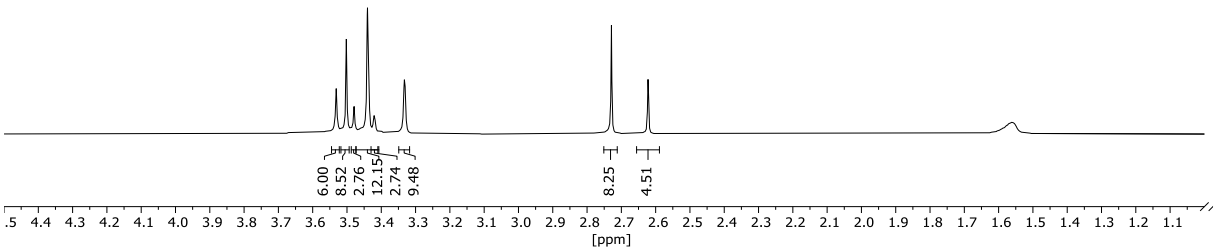

6.3.2 *cis*-Ru(*t*Bu-bpy)$_2$Cl$_2$ (**701**)

1H NMR (300.13 MHz, CDCl3)

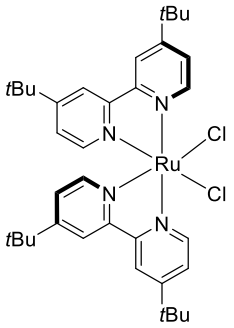

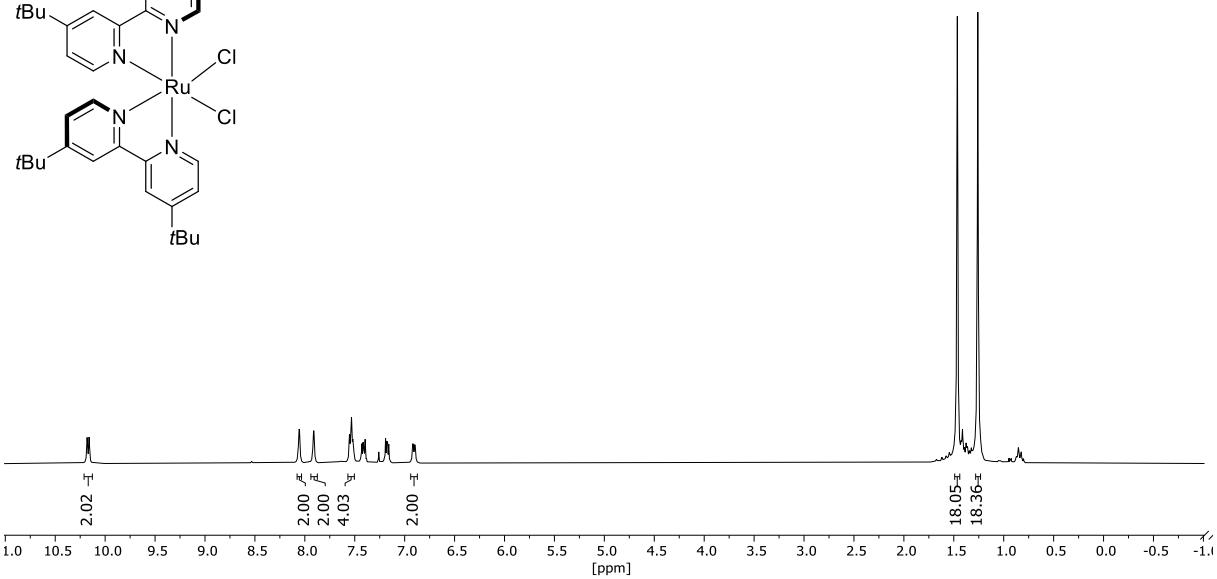

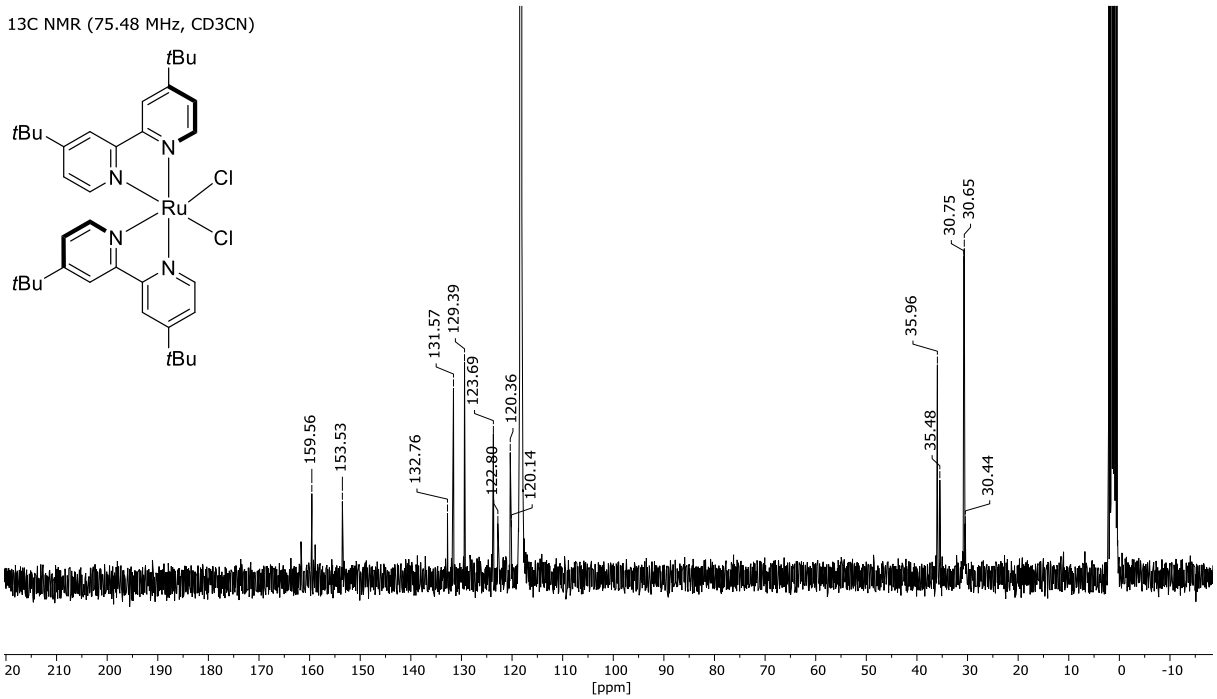

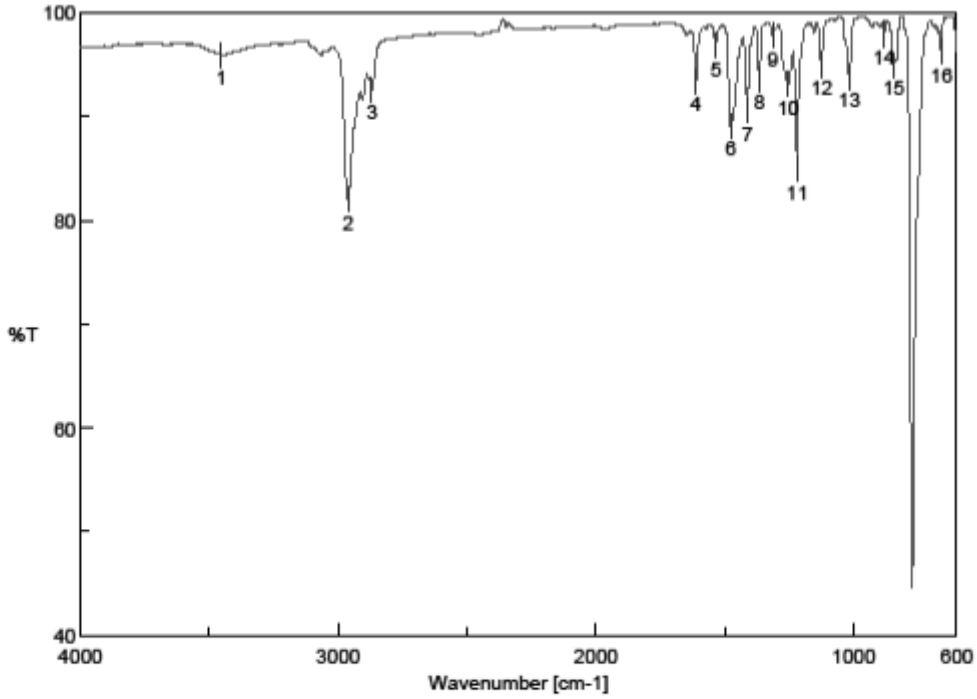

[Result of Peak Picking]

No.	Position	Intensity	No.	Position	Intensity	No.	Position	Intensity
1	3454.85	95.9824	2	2962.13	82.0013	3	2869.56	92.6225
4	1612.2	93.3769	5	1535.06	96.8232	6	1478.17	89.1461
7	1411.64	90.6351	8	1365.35	93.5981	9	1314.25	97.7929
10	1253.5	93.1076	11	1219.76	84.932	12	1125.26	95.0171
13	1017.27	93.8148	14	882.274	97.9574	15	845.633	94.9875
16	659.536	96.2431						

6.3.3 *cis*-Ru(MeO-bpy)$_2$Cl$_2$ (**702**)

1H NMR (300.13 MHz, DMSO)

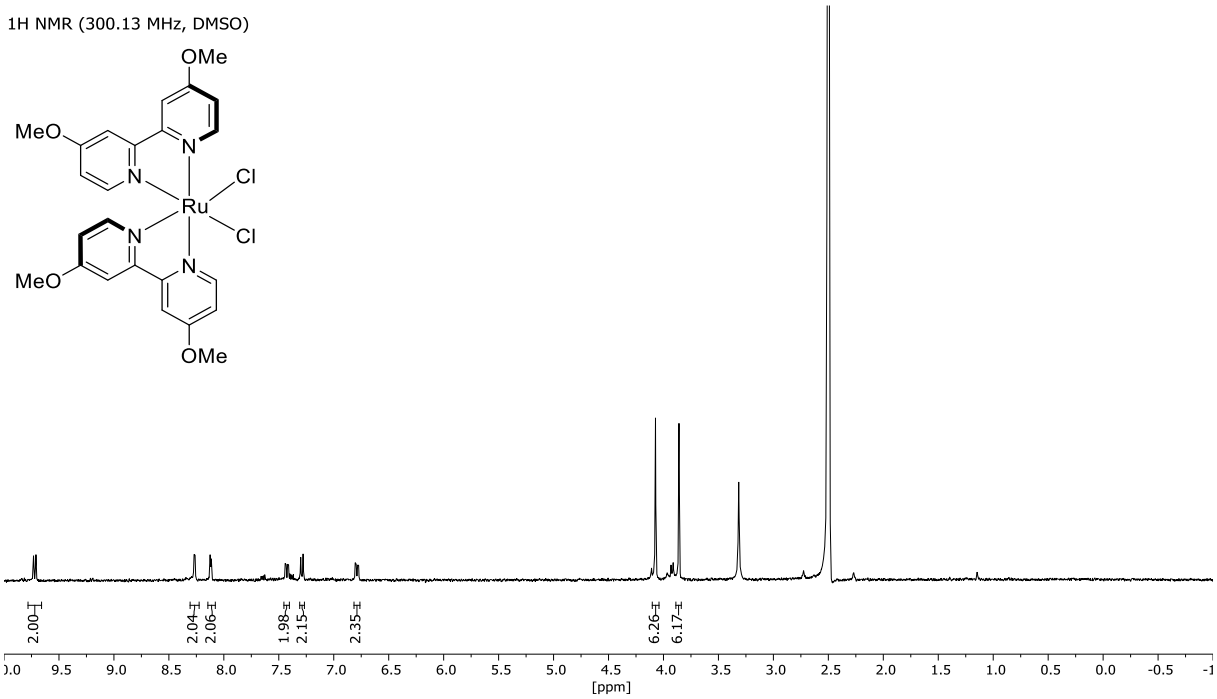

13C NMR (75.48 MHz, DMSO)

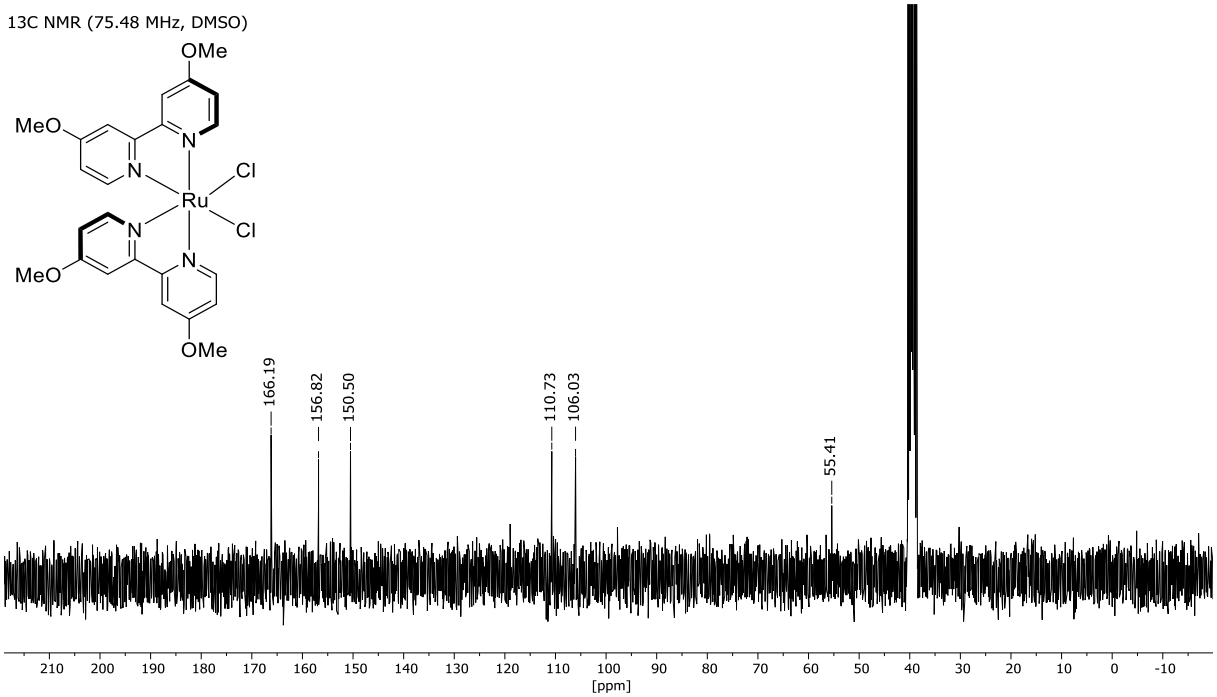

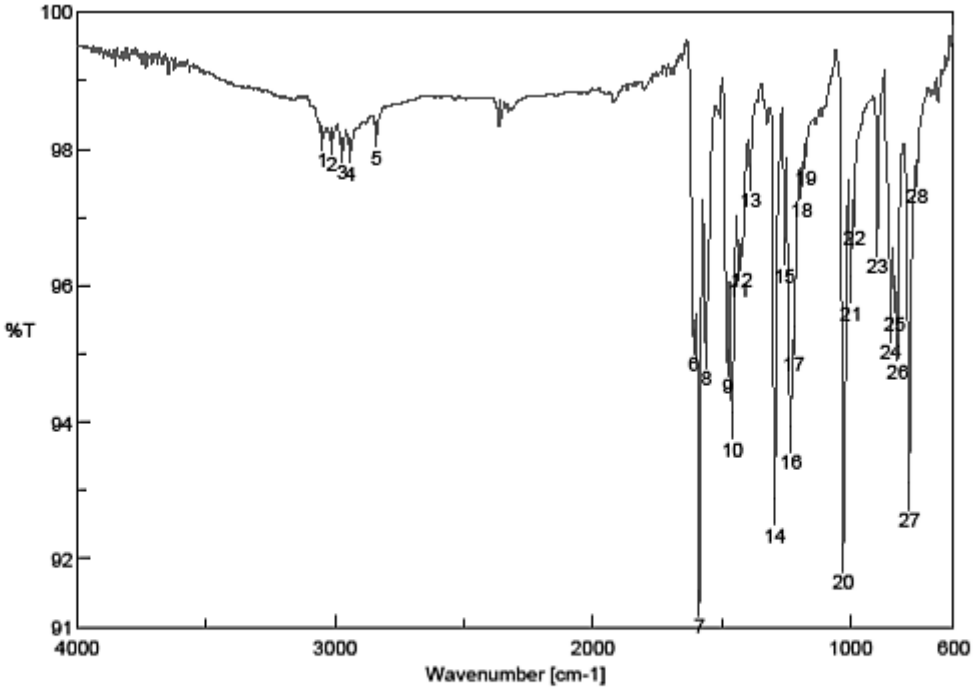

[Result of Peak Picking]

No.	Position	Intensity	No.	Position	Intensity	No.	Position	Intensity
1	3048.91	98.1685	2	3014.19	98.1113	3	2970.8	97.9903
4	2940.91	97.9774	5	2838.7	98.213	6	1608.34	95.1773
7	1587.13	91.3406	8	1560.13	94.9684	9	1478.17	94.8668
10	1458.89	93.9387	11	1434.78	96.2624	12	1424.17	96.4151
13	1389.46	97.5805	14	1294	92.6794	15	1256.4	96.482
16	1232.29	93.7454	17	1221.68	95.1868	18	1190.83	97.444
19	1175.4	97.9001	20	1028.84	91.9941	21	998.946	95.9311
22	986.411	97.0422	23	896.737	96.6128	24	844.669	95.3616

6.3.4 $[Ru(dmb)_3](PF_6)_2$ (**692**)

1H NMR (300.13 MHz, CD3CN)

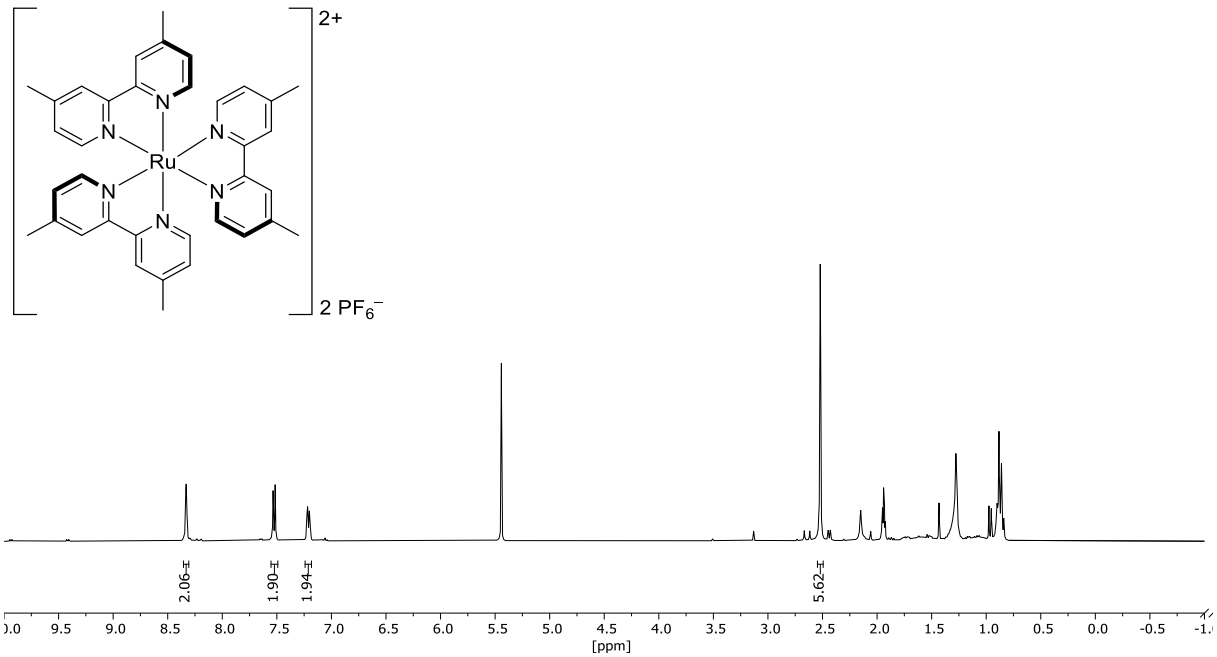

6.3.5 [Ru(DiMeMal-bpy)$_3$](PF$_6$)$_2$ (**693**)

1H NMR (300.13 MHz, CD3CN)

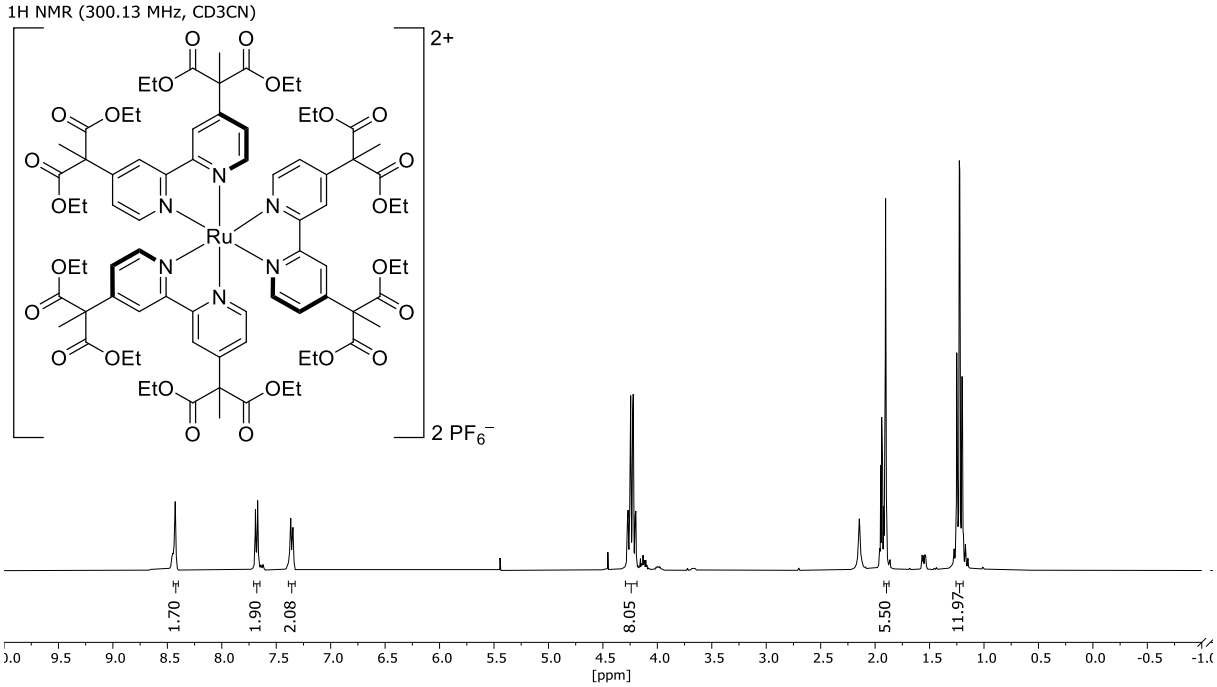

13C NMR (75.48 MHz, CD3CN)

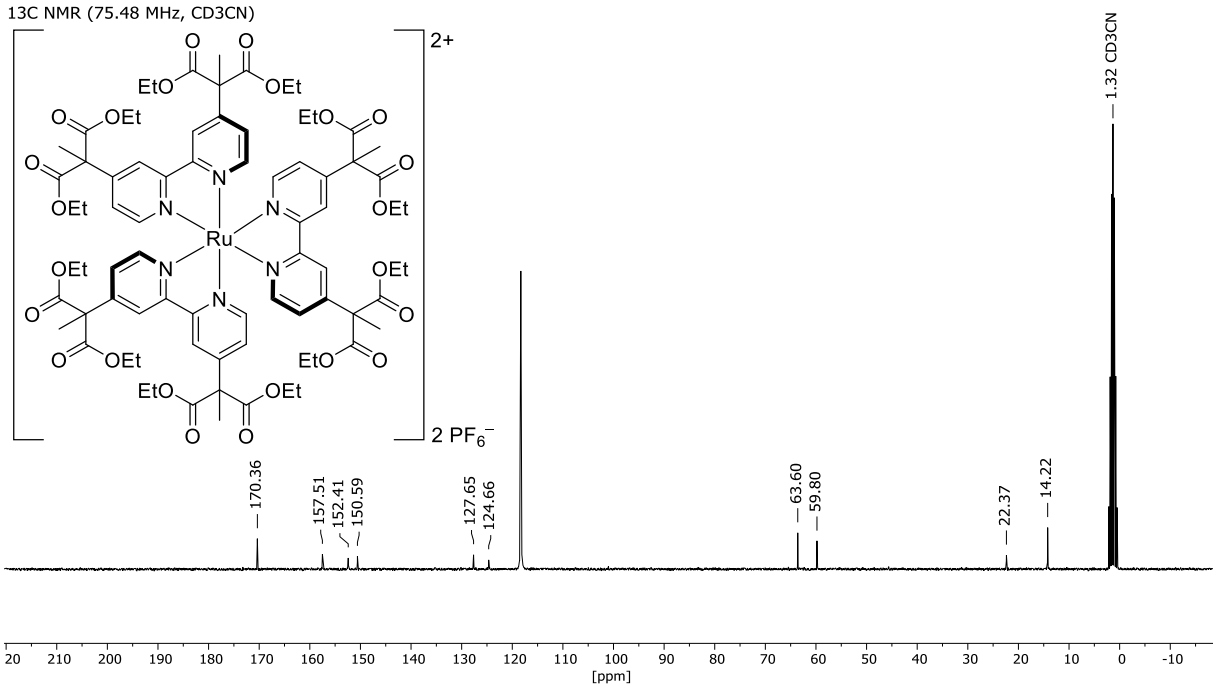

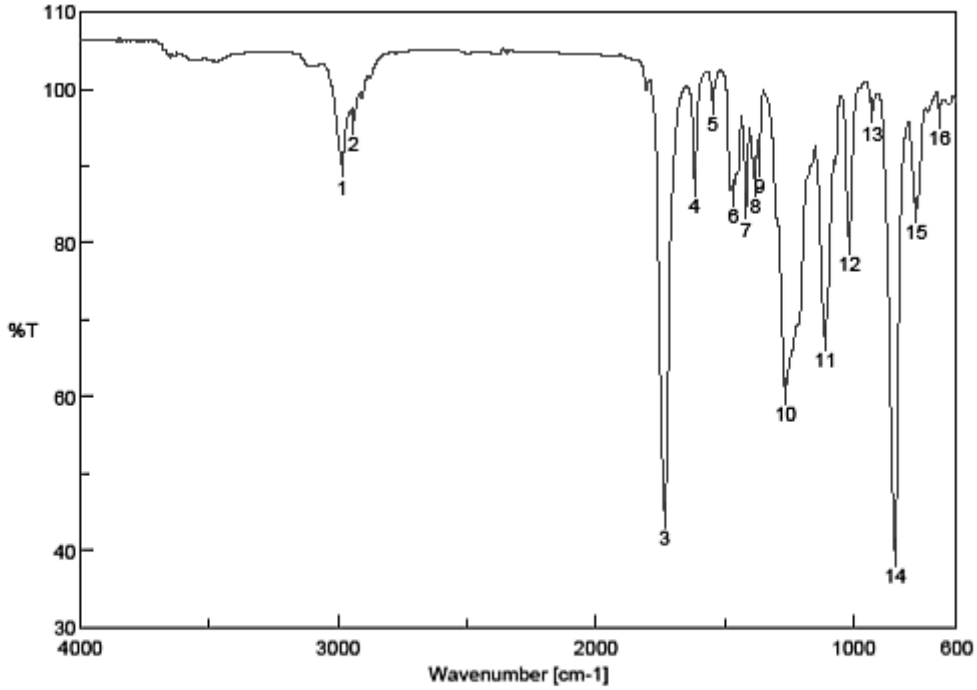

[Result of Peak Picking]

No.	Position	Intensity	No.	Position	Intensity	No.	Position	Intensity
1	2984.3	90.2155	2	2940.91	95.8398	3	1732.73	44.4801
4	1616.06	87.6444	5	1545.67	98.4637	6	1466.6	86.4579
7	1416.46	84.6964	8	1381.75	87.6516	9	1366.32	90.3507
10	1265.07	60.68	11	1110.8	67.6415	12	1017.27	80.1924
13	927.593	97.2011	14	838.883	39.643	15	757.888	84.3362
16	667.25	96.5597						

6.3.6 $[Ru(bpy)_3](PF_6)_2$ (7)

1H NMR (300.13 MHz, CD3CN)

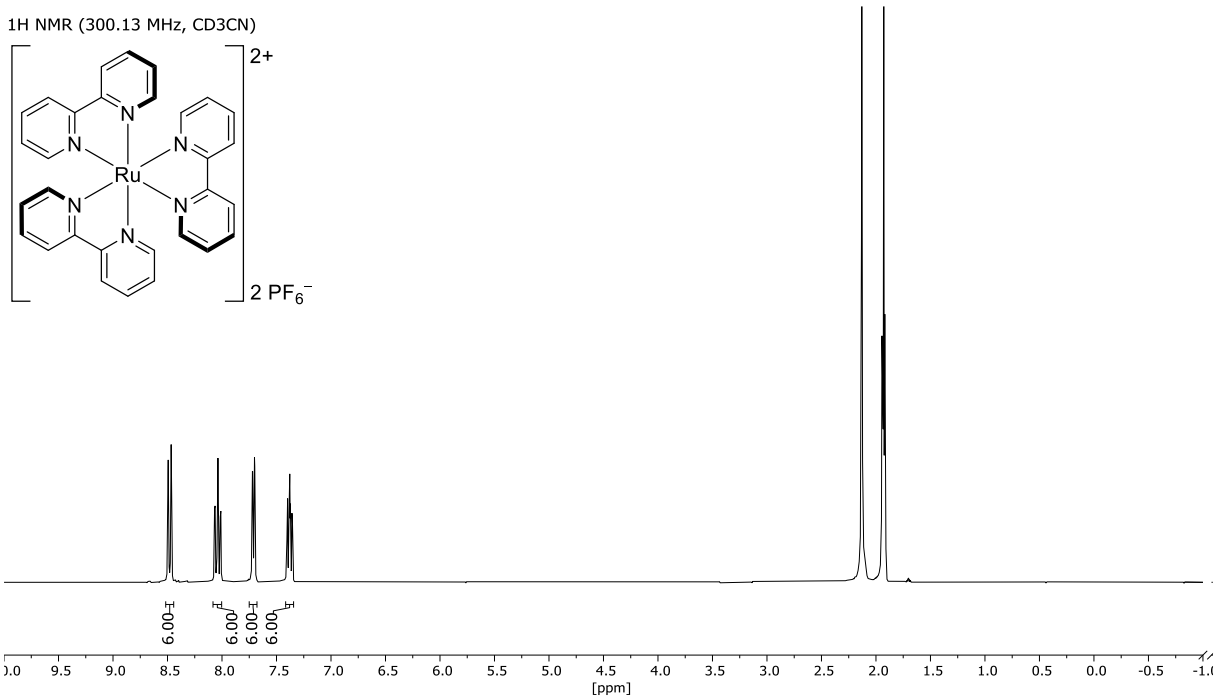

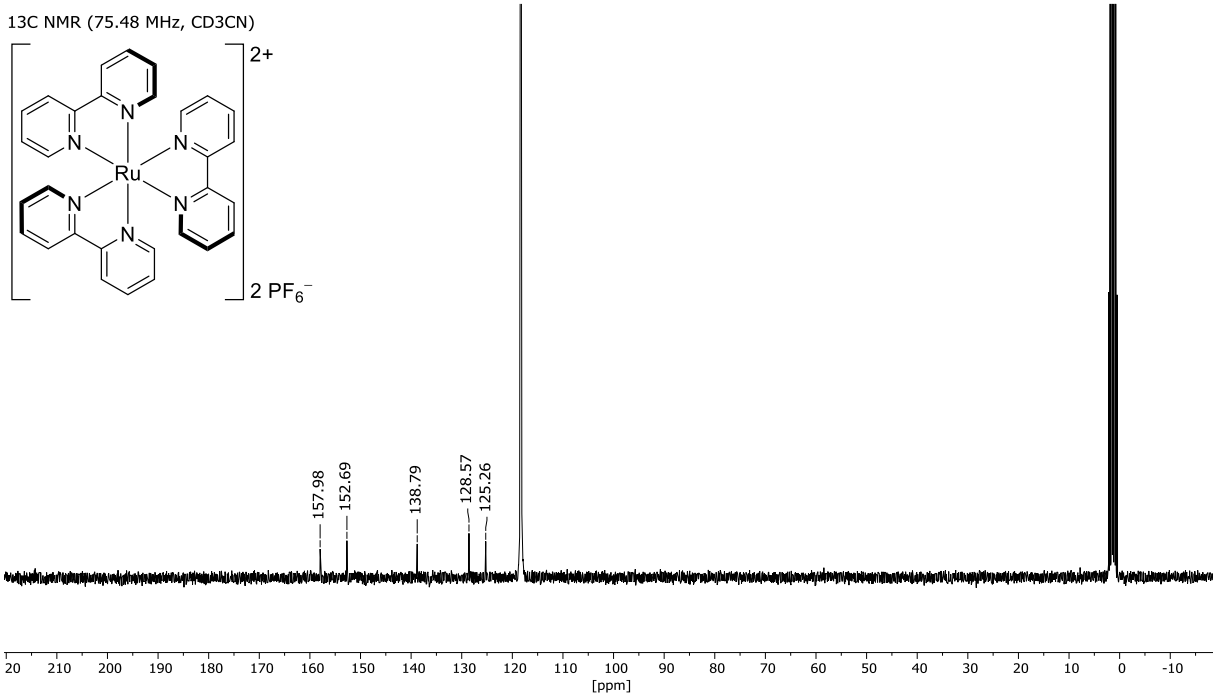

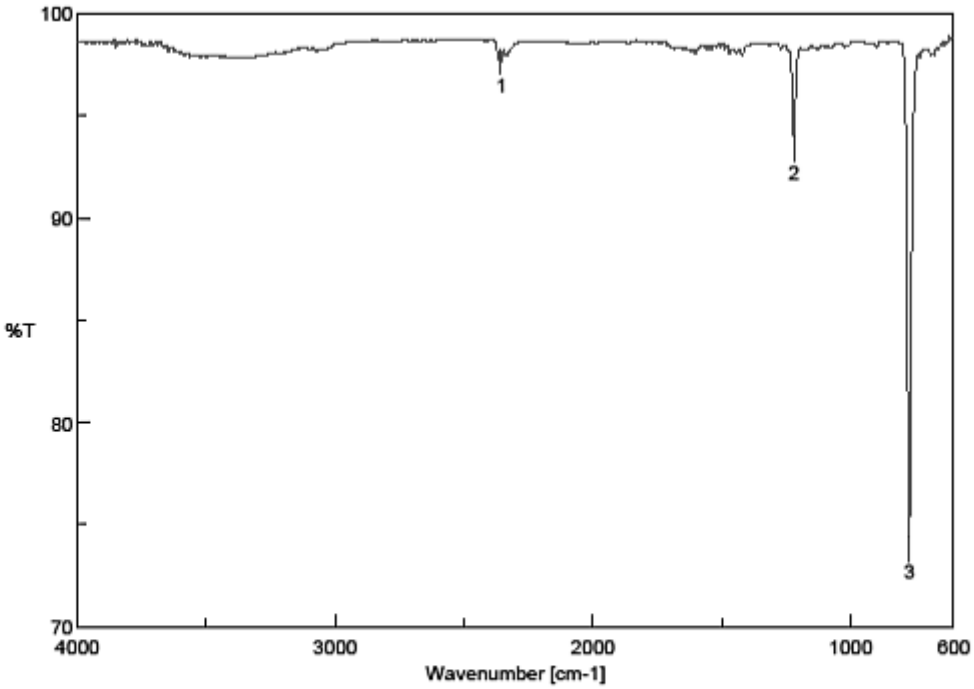

[Result of Peak Picking]

No.	Position	Intensity	No.	Position	Intensity	No.	Position	Intensity
1	2356.59	97.6286	2	1219.76	93.3608	3	772.351	73.7645

6.3.7 $[Ru(bpy)_2(BOX\text{-}bpy)](PF_6)_2$ (**532**)

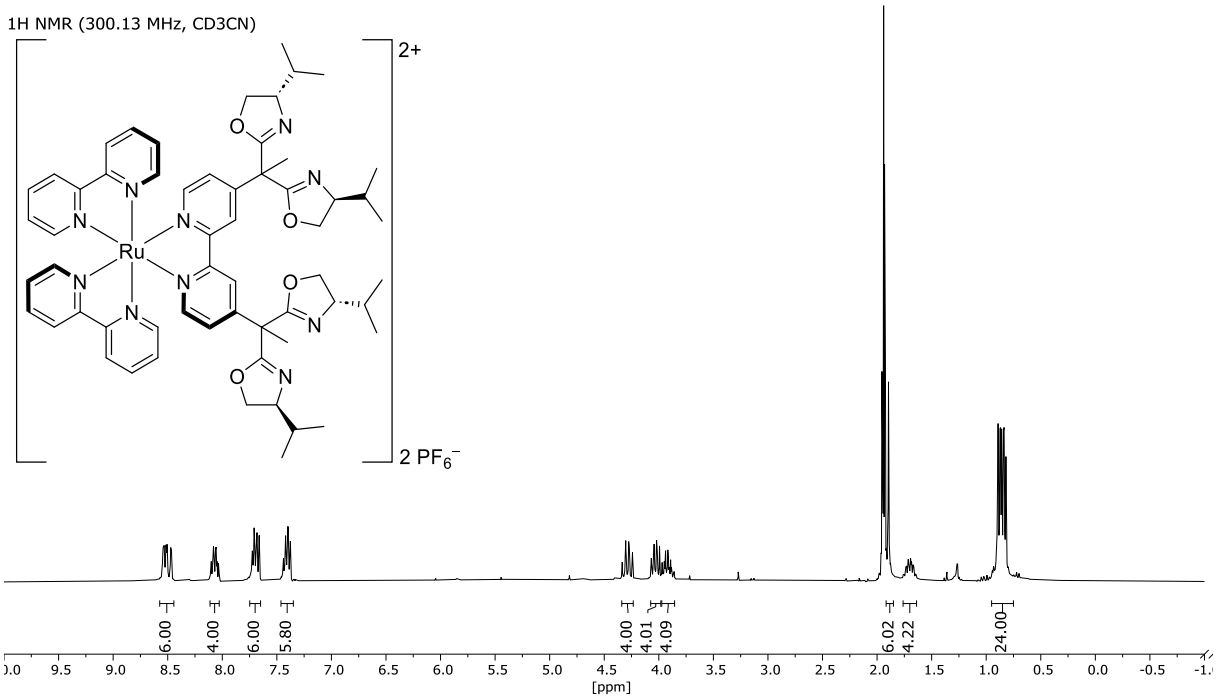

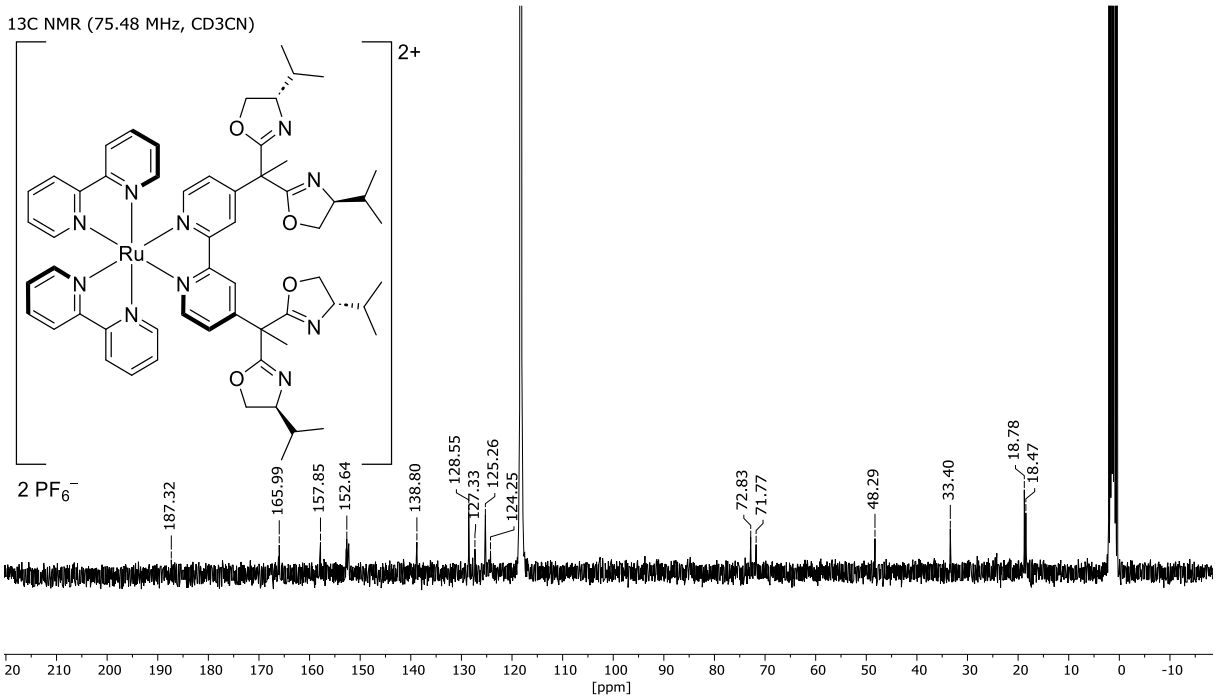

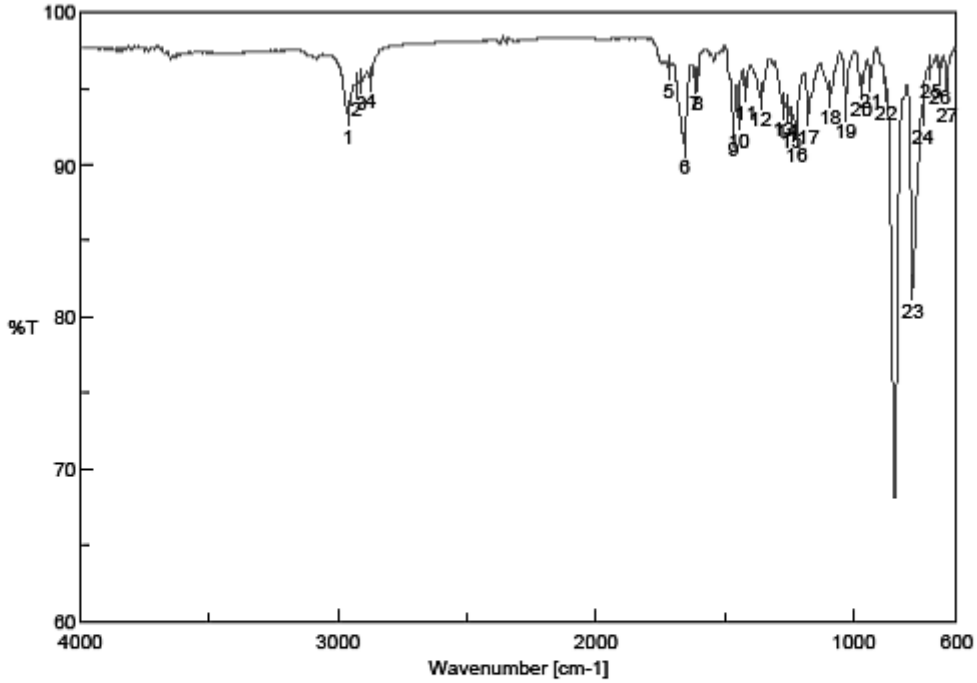

[Result of Peak Picking]

No.	Position	Intensity	No.	Position	Intensity	No.	Position	Intensity
1	2961.16	93.3209	2	2931.27	95.1825	3	2910.06	95.4596
4	2874.38	95.6217	5	1717.3	96.3382	6	1655.59	91.3598
7	1616.06	95.5152	8	1604.48	95.5457	9	1465.63	92.5095
10	1446.35	93.0931	11	1418.39	94.9126	12	1361.5	94.4521
13	1272.79	93.812	14	1257.36	93.6791	15	1240.97	92.9932
16	1221.68	92.1201	17	1175.4	93.3404	18	1090.55	94.6005
19	1030.77	93.6999	20	970.019	95.0891	21	934.342	95.6288
22	874.56	94.9092	23	770.423	81.8777	24	731.853	93.3441
25	701.962	96.3349	26	666.285	95.9463	27	637.358	94.7696

6.3.8 [Ru(*t*Bu-bpy)$_2$(BOX-bpy)](PF$_6$)$_2$ (**536**)

1H NMR (300.13 MHz, CD3CN)

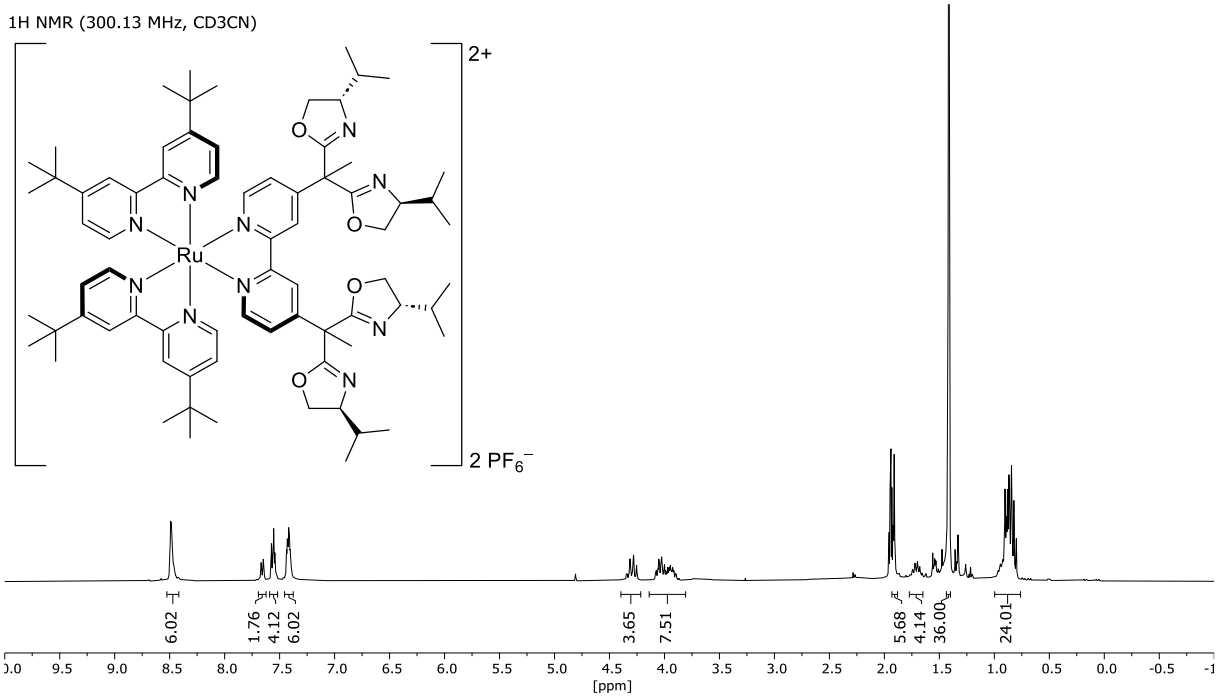

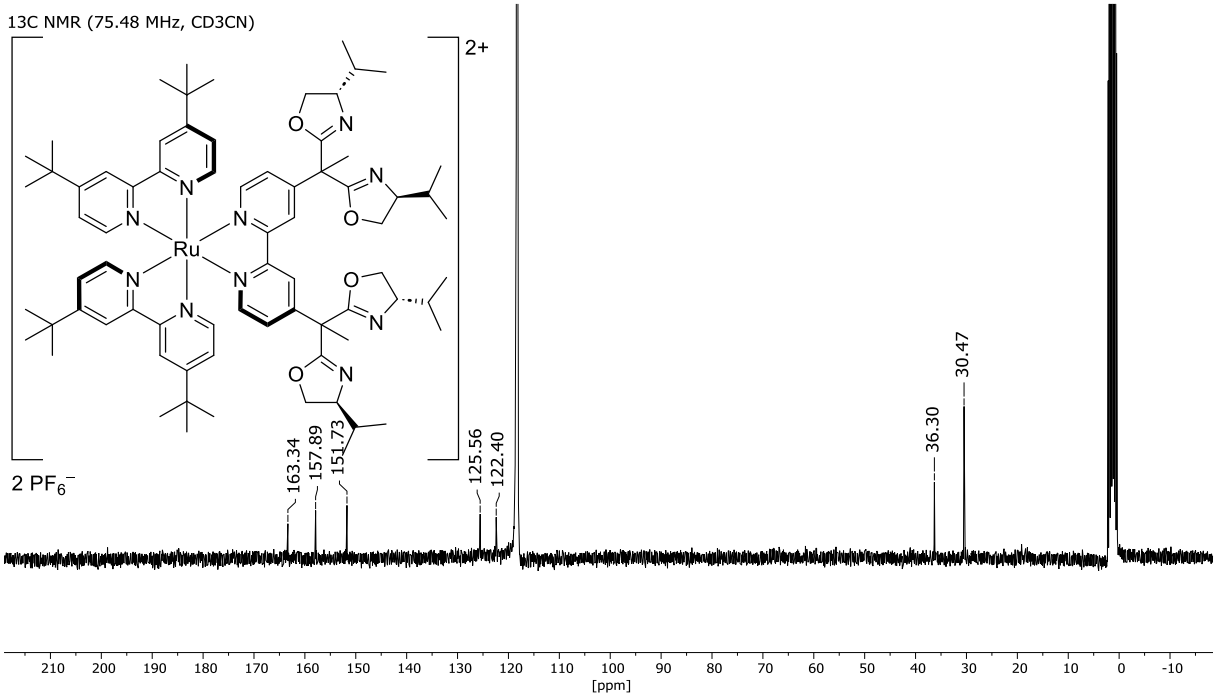

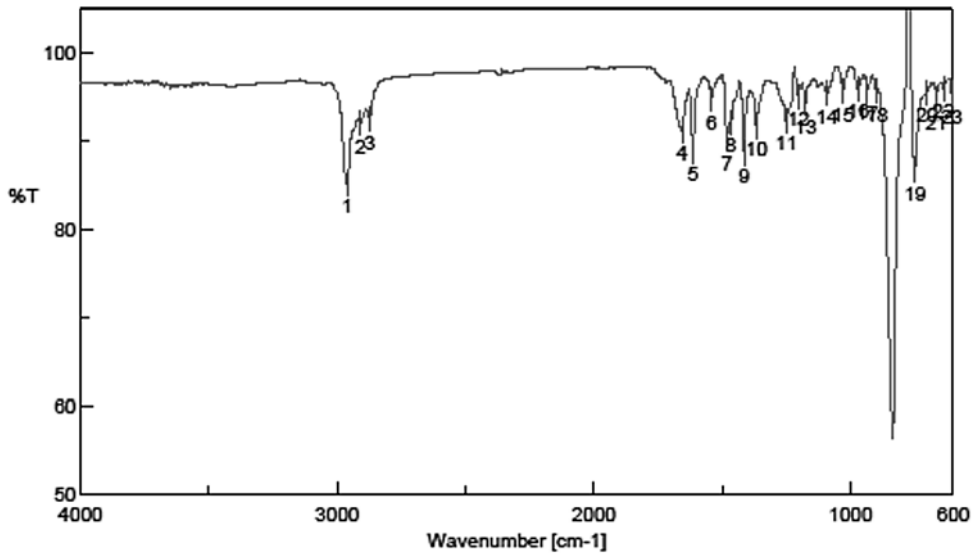

[Result of Peak Picking]

No.	Position	Intensity	No.	Position	Intensity	No.	Position	Intensity
1	2962.13	85.2684	2	2909.09	91.9108	3	2873.42	92.4484
4	1655.59	91.1135	5	1614.13	88.9229	6	1541.81	94.6632
7	1481.06	90.1778	8	1466.6	92.0357	9	1414.53	88.6856
10	1367.28	91.6703	11	1250.61	92.3159	12	1203.36	94.9722
13	1175.4	94.2742	14	1091.51	95.4312	15	1029.8	95.6344
16	970.019	95.874	17	934.342	95.7588	18	898.666	95.5755
19	749.209	86.7617	20	702.926	95.511	21	666.285	94.6276
22	638.323	95.8854	23	606.503	95.3745			

6.3.9 [Ru(MeO-bpy)$_2$(BOX-bpy)](PF$_6$)$_2$ (**537**)

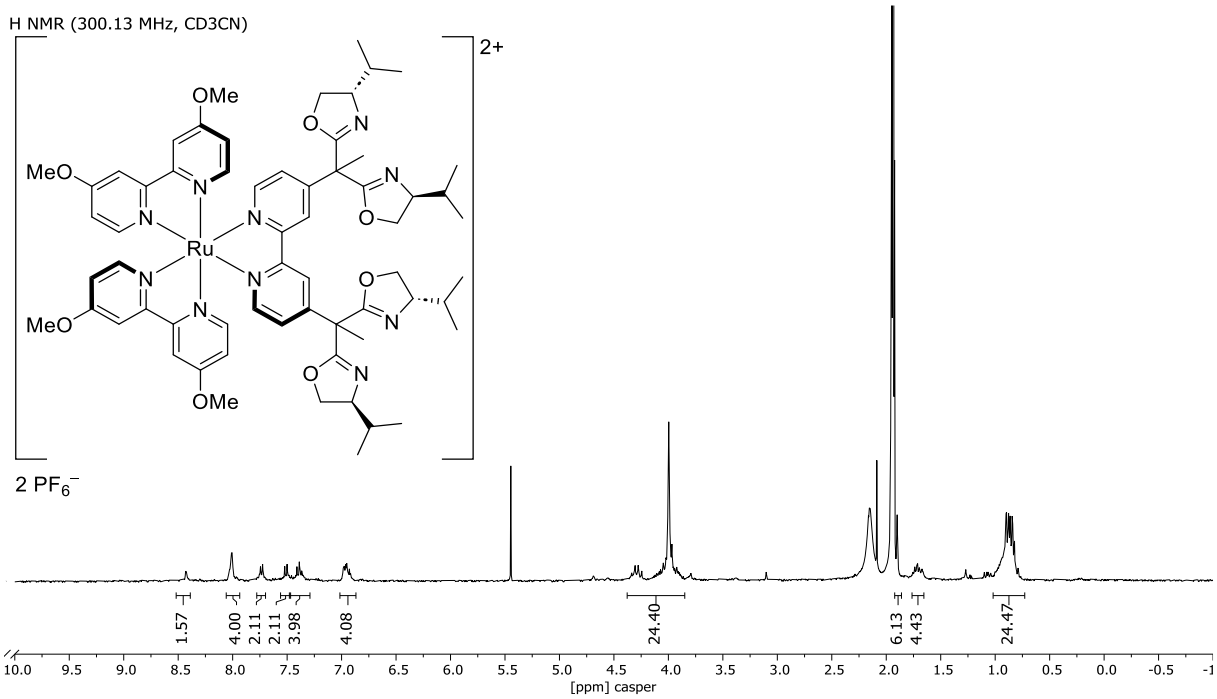

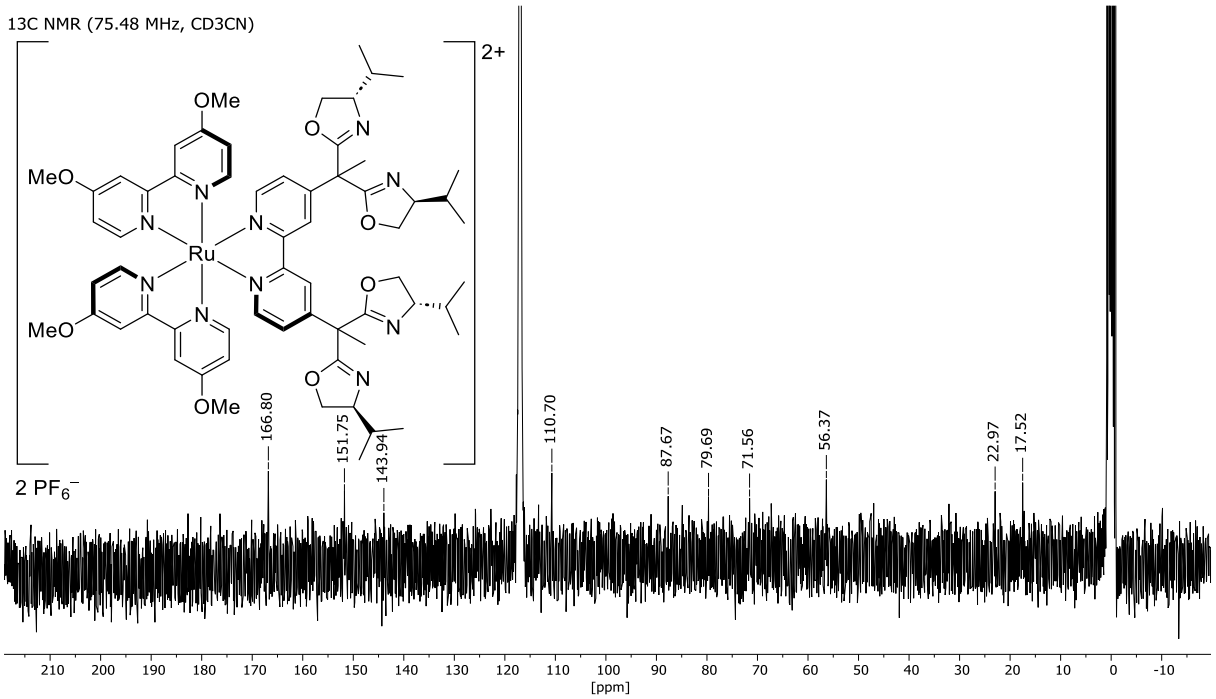

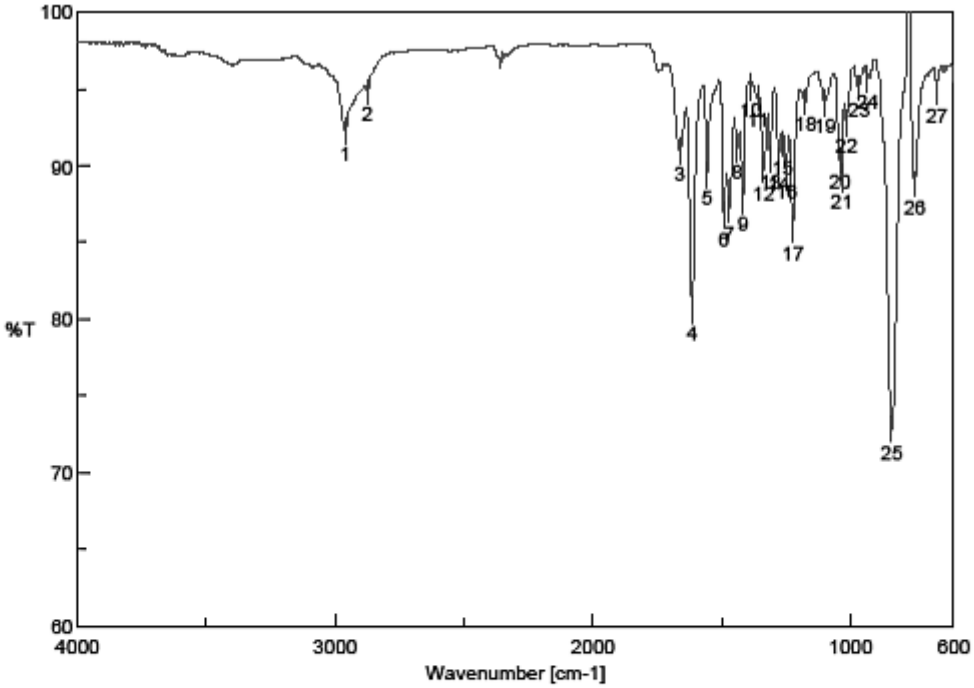

[Result of Peak Picking]

No.	Position	Intensity	No.	Position	Intensity	No.	Position	Intensity
1	2961.16	92.2623	2	2875.34	94.8211	3	1663.3	90.9546
4	1615.09	80.5578	5	1557.24	89.3403	6	1491.67	86.7273
7	1471.42	87.13	8	1440.56	91.0785	9	1417.42	87.685
10	1388.5	95.122	11	1360.53	94.4491	12	1338.36	89.7203
13	1311.36	90.3807	14	1278.57	90.2978	15	1264.11	91.4112
16	1249.65	89.7632	17	1224.58	85.8132	18	1175.4	94.1677
19	1100.19	94.073	20	1042.34	90.3802	21	1034.62	89.1399
22	1018.23	92.7966	23	968.09	95.0614	24	934.342	95.6468
25	840.812	72.8092	26	751.138	88.7978	27	666.285	94.7921

6.4 Substrate spectra

6.4.1 Substrates for intramolecular radical cyclization

6.4.1.1 Dimethyl 2-(pent-4-en-1-yl)malonate (**742**)

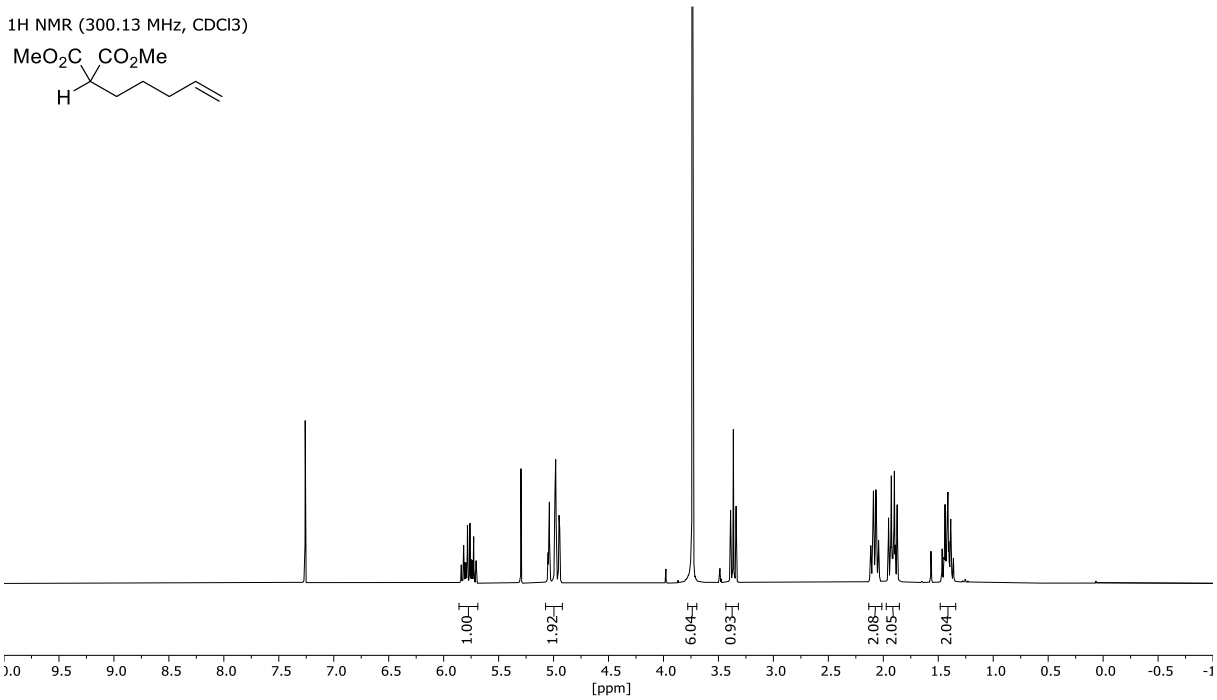

6.4.1.2 Dimethyl 2-(hex-5-en-1-yl)malonate (**744**)

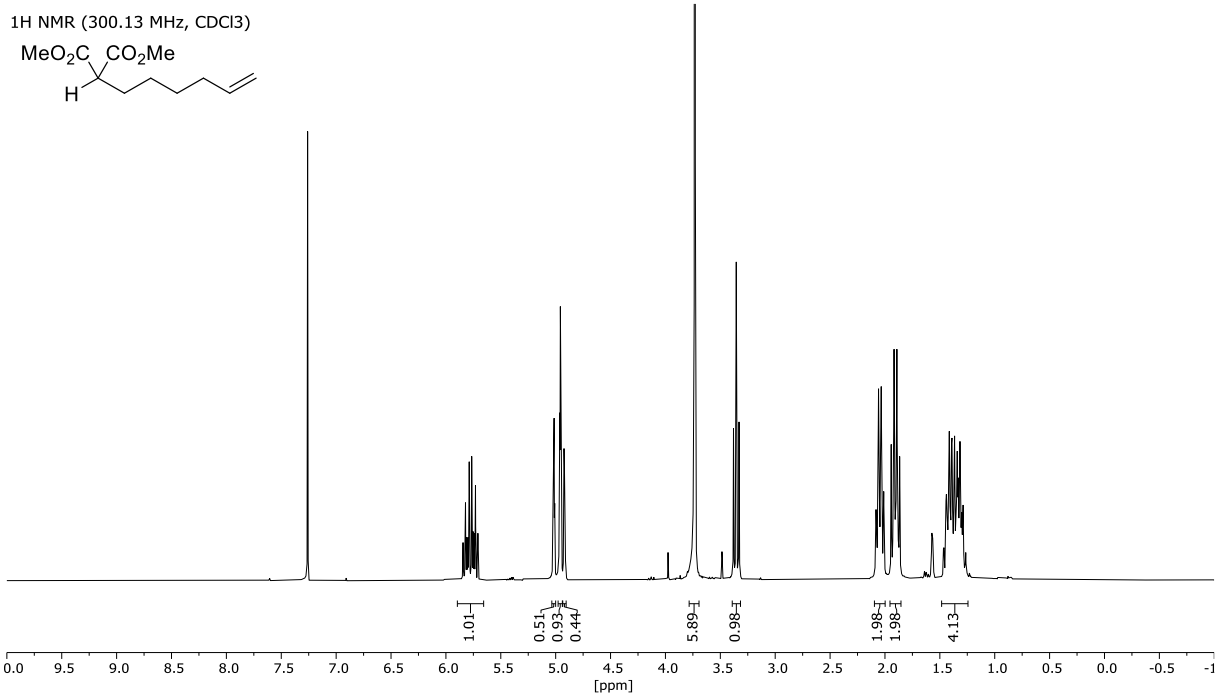

6.4.1.3 Dimethyl 2-bromo-2-(pent-4-en-1-yl)malonate (**734**)

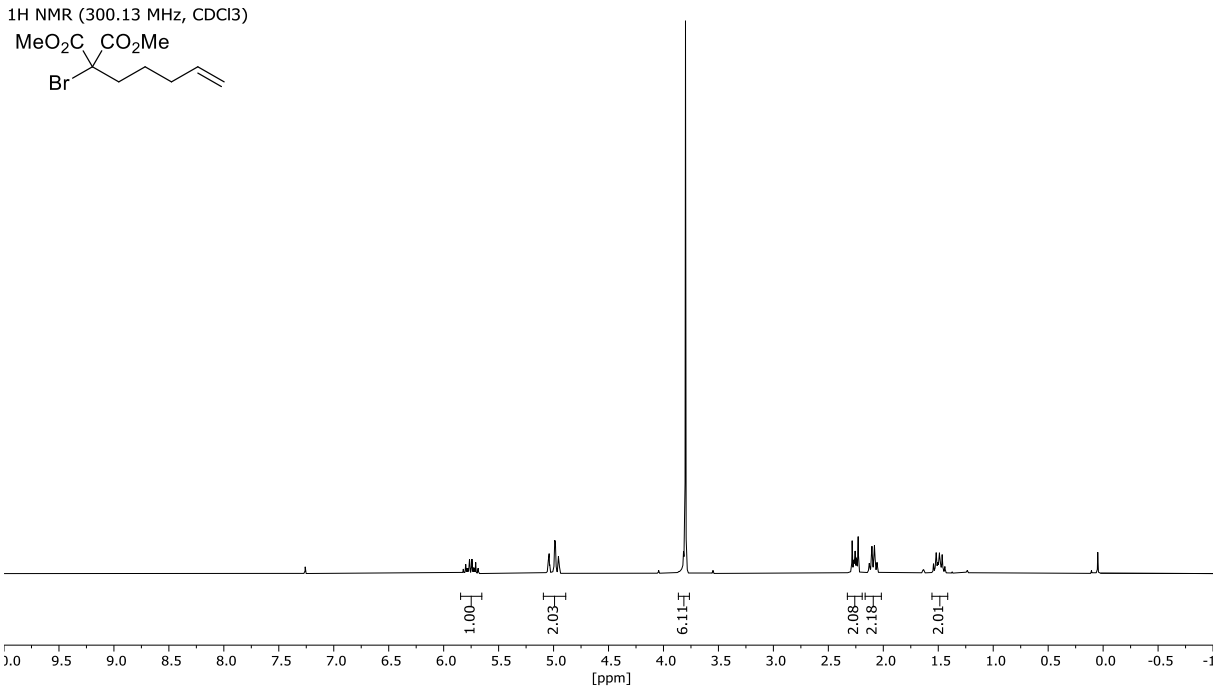

6.4.1.4 Dimethyl 2-bromo-2-(hex-5-en-1-yl)malonate (**737**)

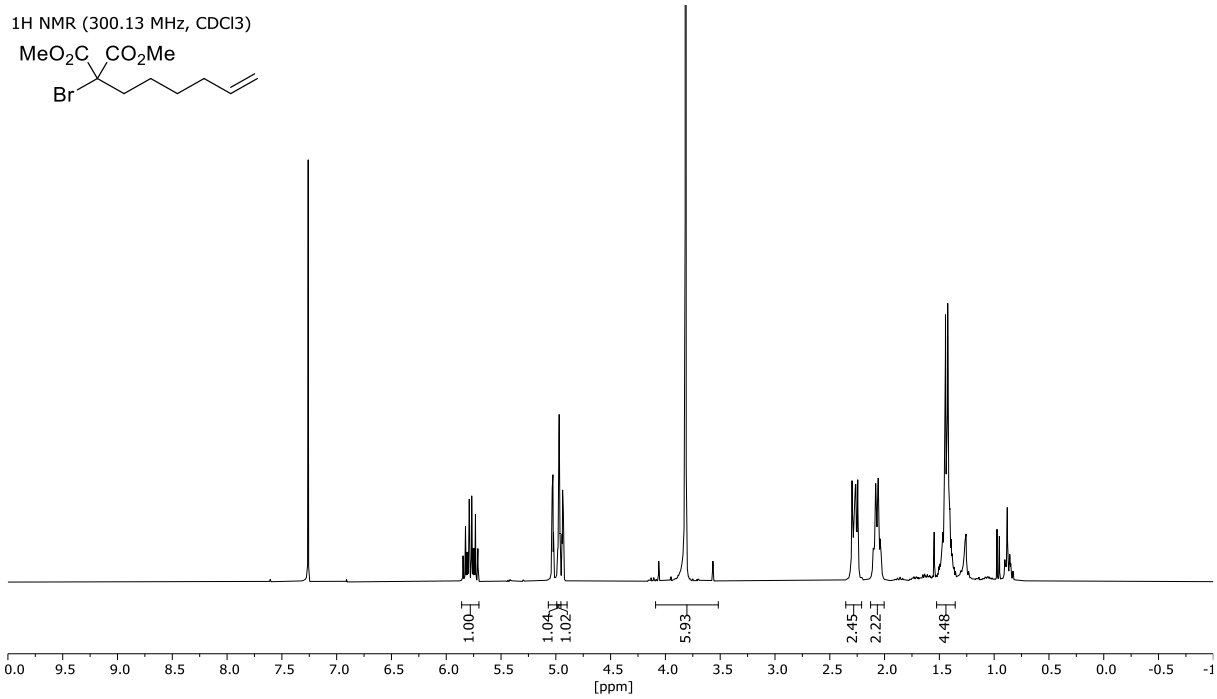

6.4.1.5 Dimethyl (*E*)-2-bromo-2-(6-(trimethylsilyl)hex-4-en-1-yl)malonate (**738**)

1H NMR (300.13 MHz, CDCl3)

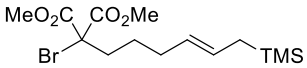

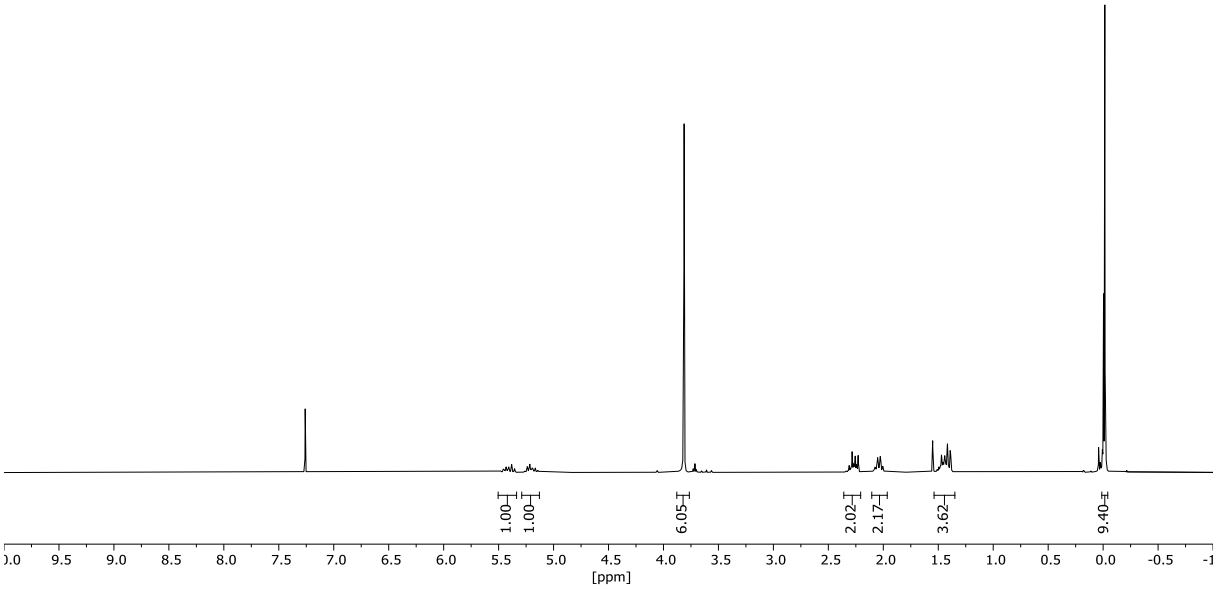

6.4.1.6 3-(Hept-6-ynoyl)oxazolidin-2-one (**748**)

1H NMR (600.13 MHz), CDCl3

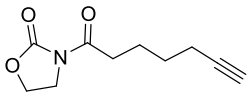

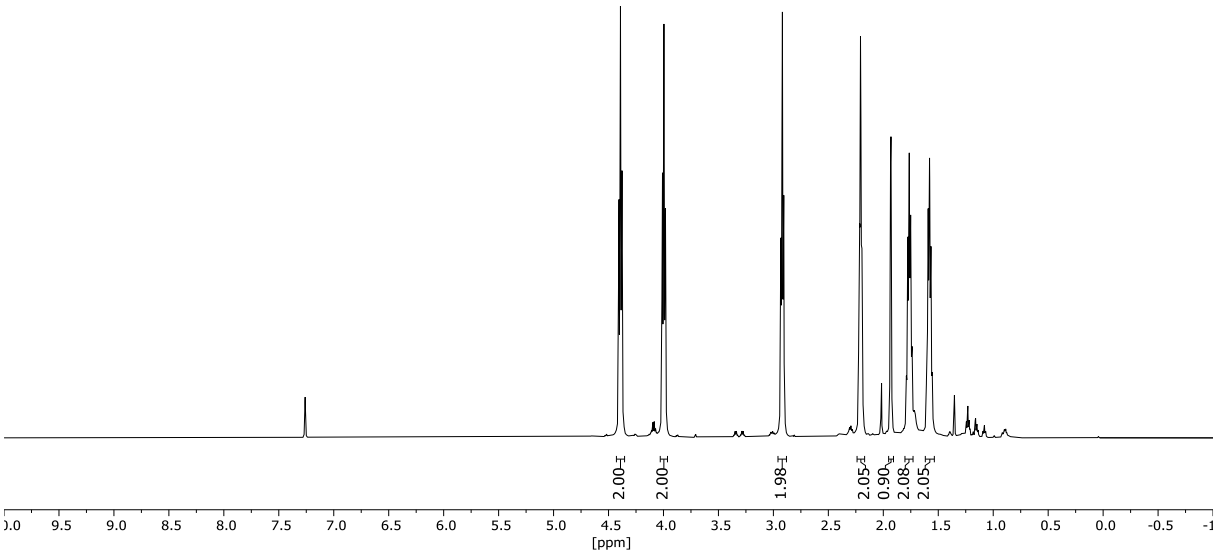

6.4.1.7 3-(2-Bromohept-6-ynoyl)oxazolidin-2-one (**722**)

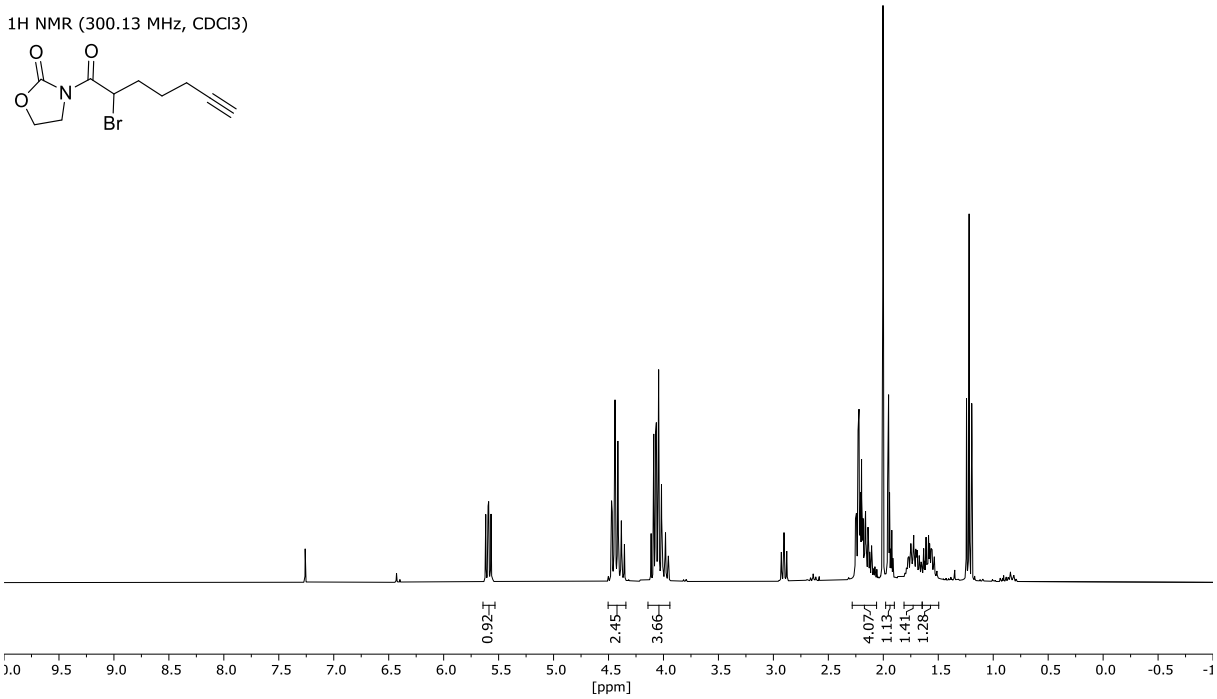

6.4.2 Substrates for intermolecular atom transfer radical addition

6.4.2.1 2-(2-Bromopropanoyl)cyclopentan-1-one (**770**)

1H NMR (300.13 MHz, CDCl3)

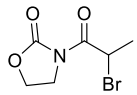

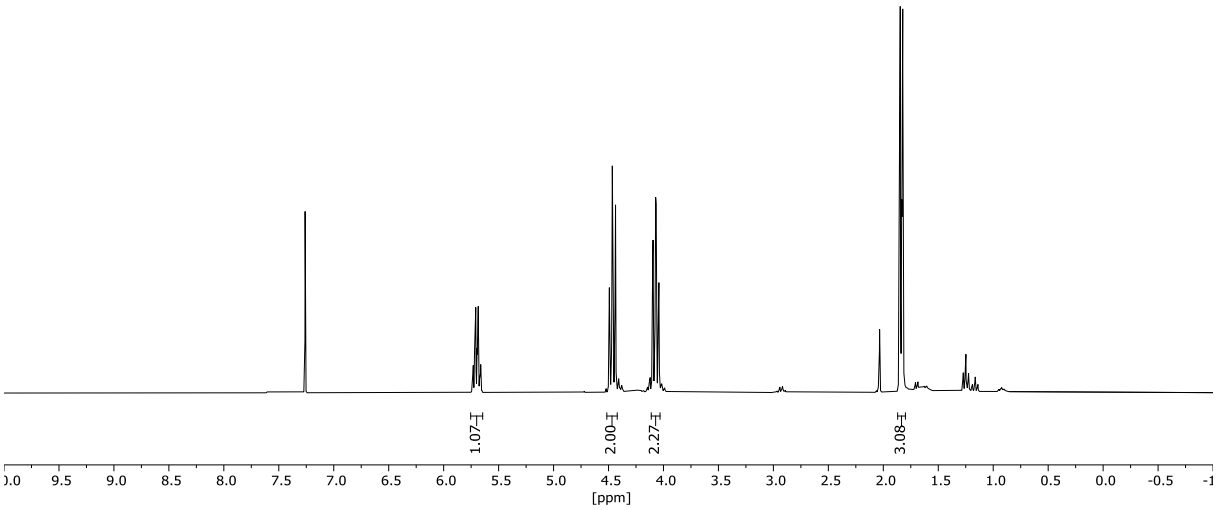

6.4.2.2 Ethyl 1-bromo-2-oxocyclohexane-1-carboxylate (**767**)

1H NMR (300.13 MHz, CDCl3)

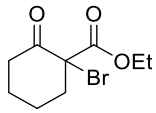

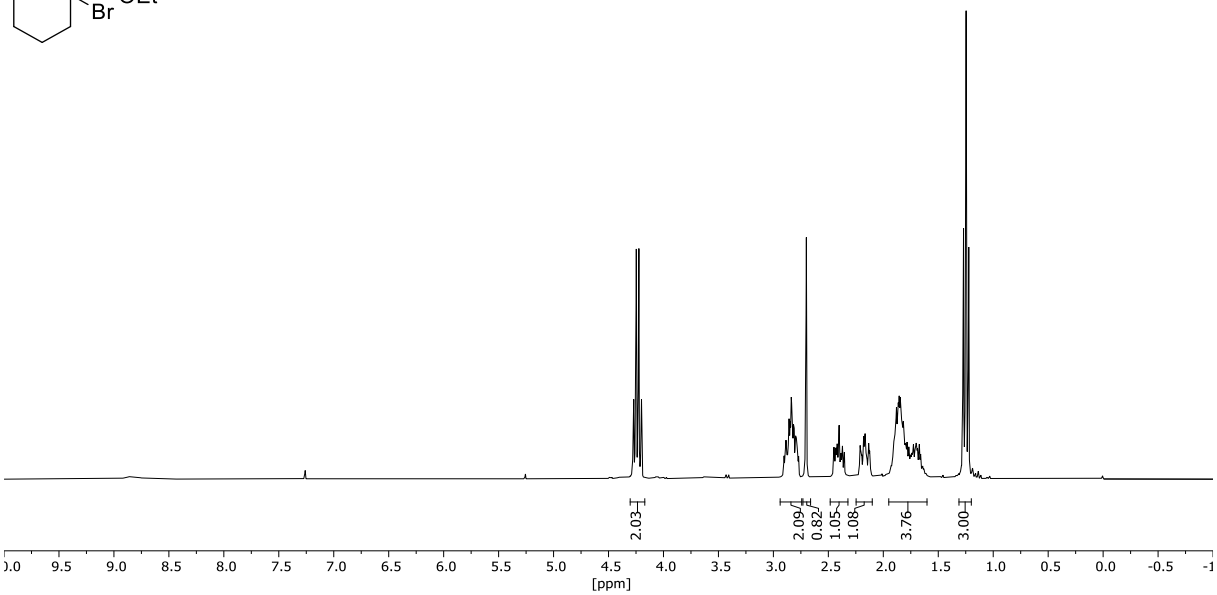

6.4.3 Substrates for cascade cyclization

6.4.3.1 3-Phenylprop-2-yn-1-yl-3-oxo-3-phenylpropanoate (**787**)

1H NMR (300.13 MHz, CDCl3)

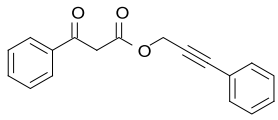

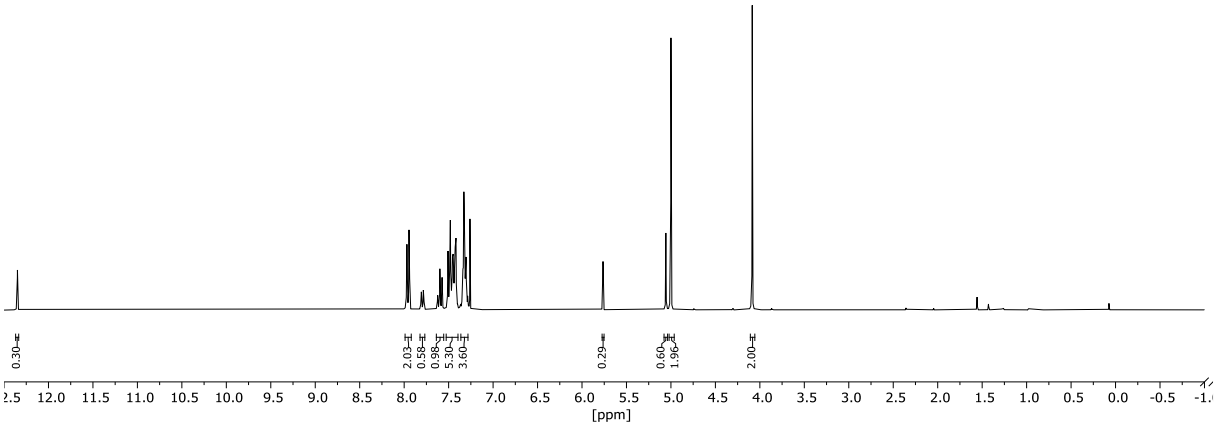

6.4.3.2 3-Phenylprop-2-yn-1-yl 2-methyl-3-oxo-3-phenylpropanoate (**788**)

1H NMR (300.13 MHz, CDCl3)

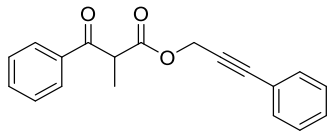

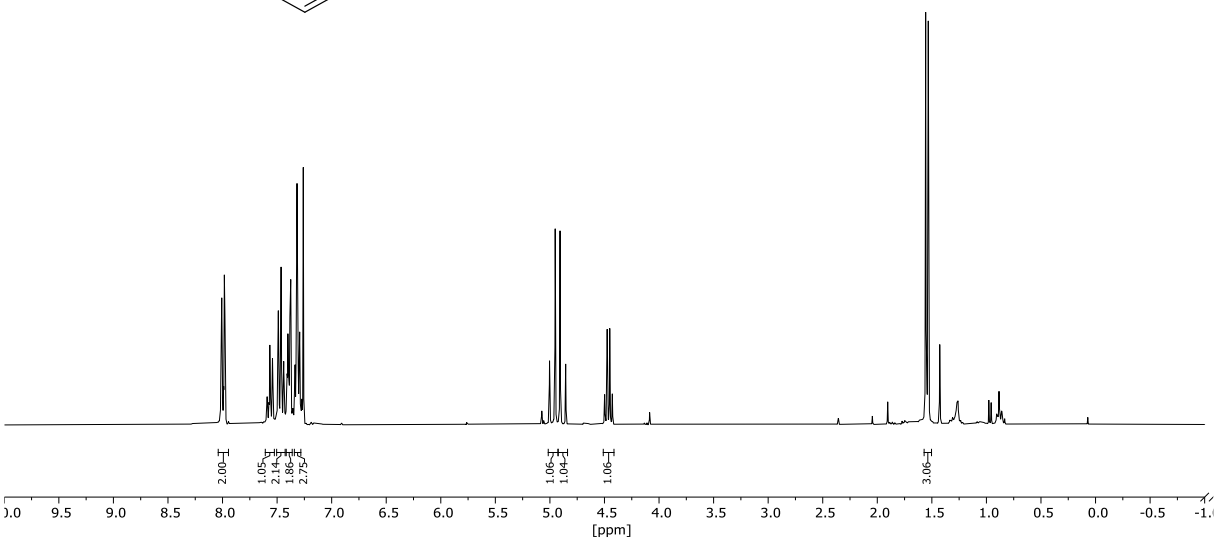

13C NMR (75.48 MHz, CDCl3)

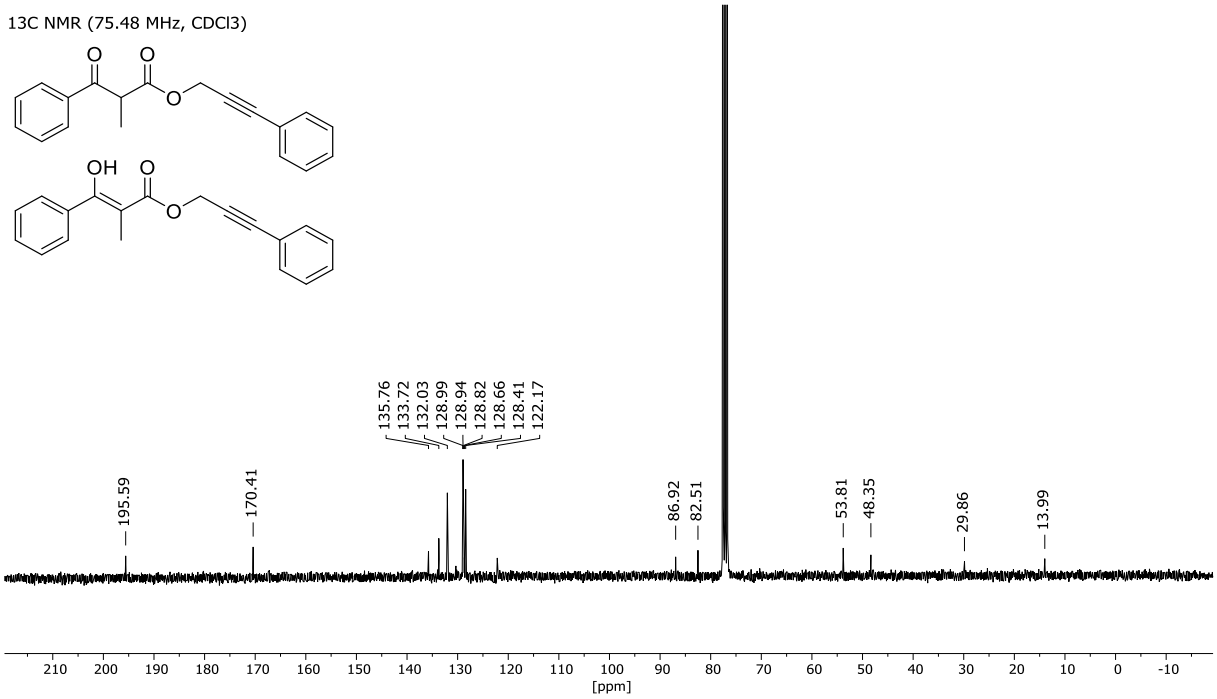

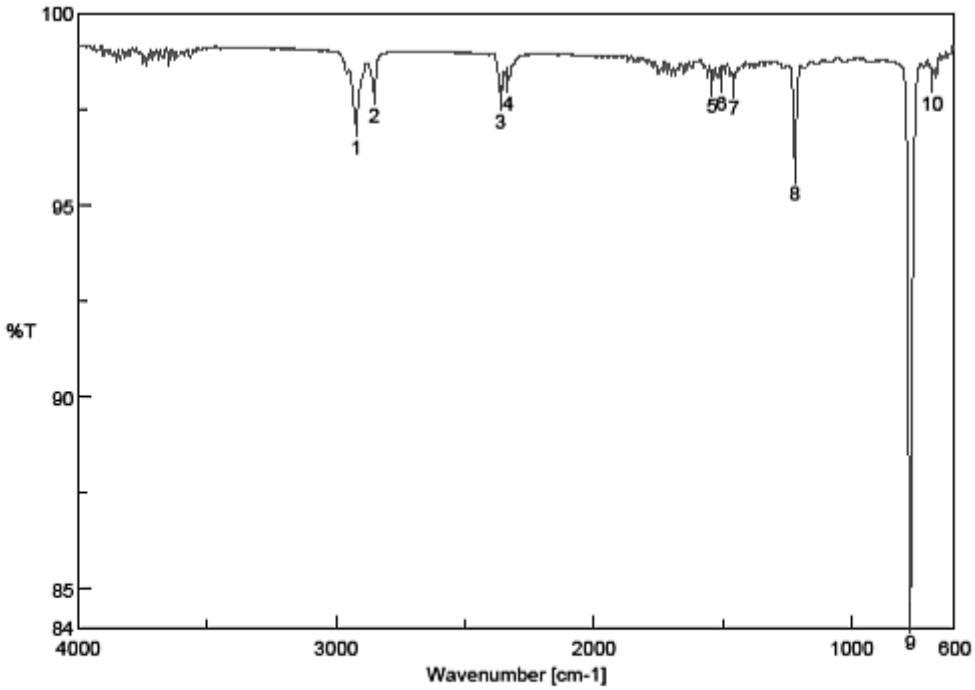

[Result of Peak Picking]

No.	Position	Intensity	No.	Position	Intensity	No.	Position	Intensity
1	2922.59	97.1233	2	2852.2	97.9718	3	2362.37	97.8103
4	2333.45	98.277	5	1540.85	98.1912	6	1507.1	98.2619
7	1456.98	98.1445	8	1219.76	95.8952	9	772.351	84.2139
10	688.463	98.2728						

6.4.3.3 3-Phenylprop-2-yn-1-yl 2-bromo-2-methyl-3-oxo-3-phenylpropanoate (**779**)

1H NMR (300.13 MHz, CDCl3)

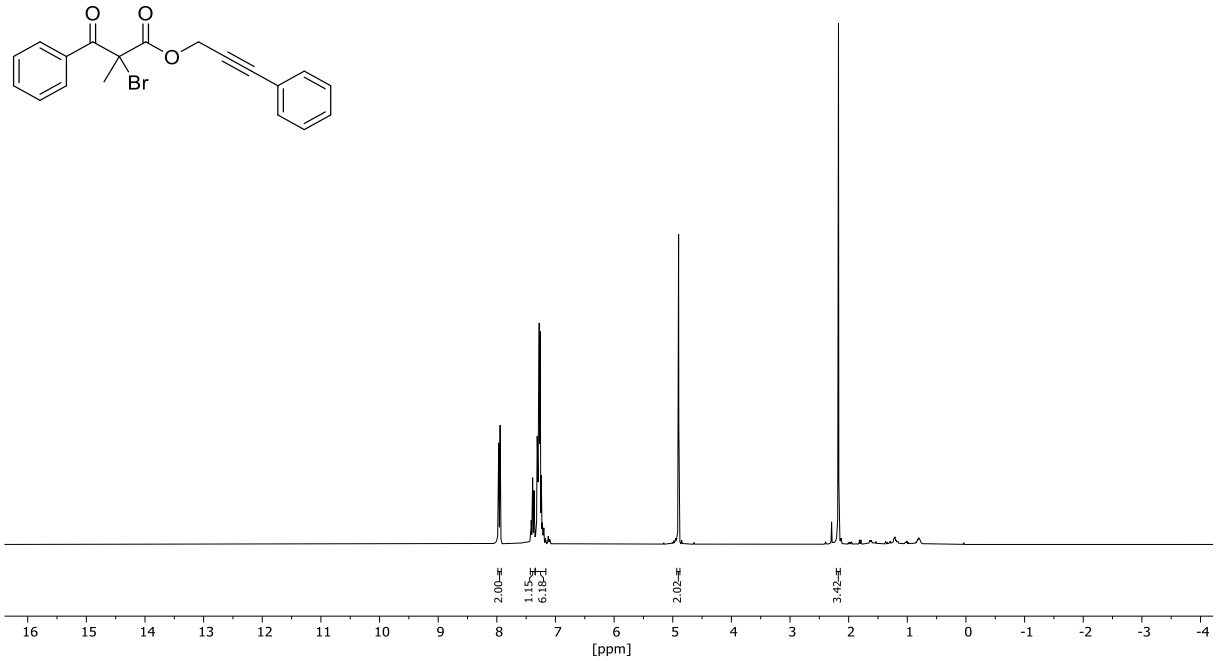

13C NMR (75.48 MHz, CDCl3)

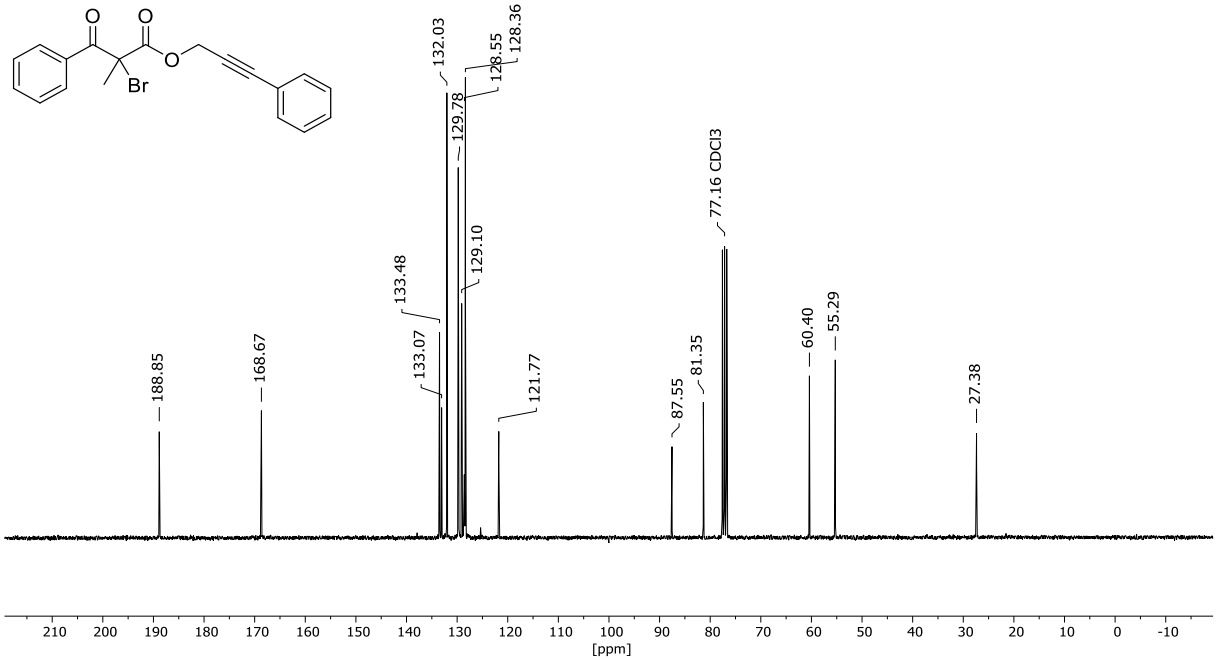

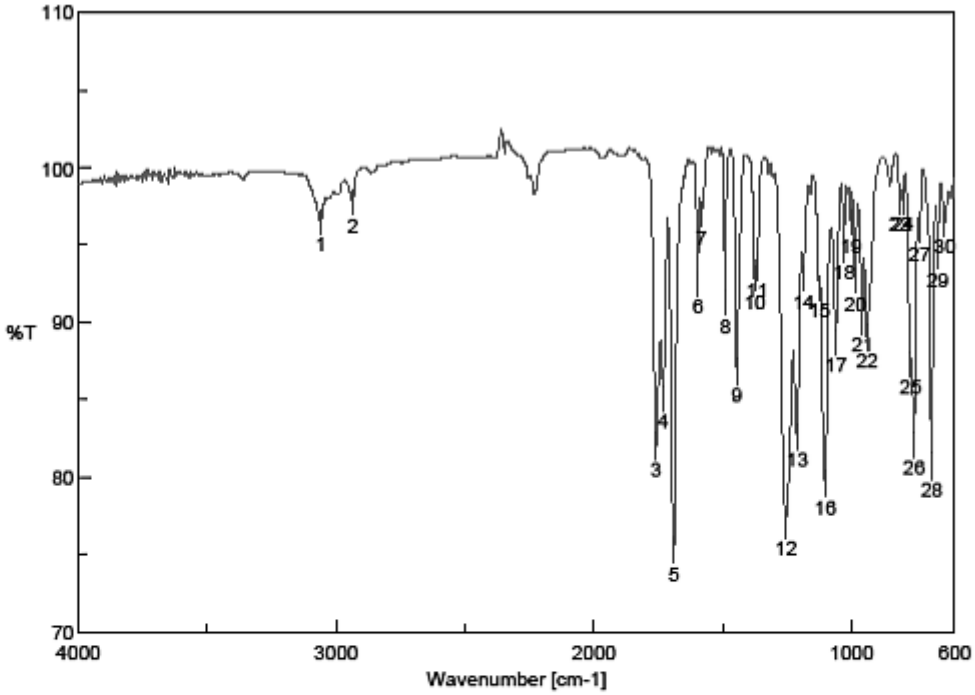

[Result of Peak Picking]

No.	Position	Intensity	No.	Position	Intensity	No.	Position	Intensity
1	3059.51	96.487	2	2936.09	97.7715	3	1758.76	81.9668
4	1731.76	85.047	5	1690.3	75.2258	6	1596.77	92.4952
7	1582.31	96.947	8	1489.74	91.2792	9	1445.39	86.7708
10	1375.96	92.8339	11	1367.28	93.5436	12	1255.43	76.9041
13	1212.04	82.5942	14	1186.97	92.84	15	1125.26	92.2299
16	1103.08	79.527	17	1060.66	88.675	18	1029.8	94.6513
19	1002.8	96.4543	20	986.411	92.6839	21	959.412	90.0101
22	940.128	88.9989	23	811.885	97.8296	24	800.314	97.849
25	771.387	87.2553	26	757.888	82.0434	27	736.674	95.9024
28	689.427	80.6545	29	666.285	94.2509	30	639.287	96.3821

6.4.4 Substrates for [2+2]-enone cycloaddition

6.4.4.1 Potassium benzyltrifluoroborate (**792**)

1H NMR (600.13 MHz, Acetone)

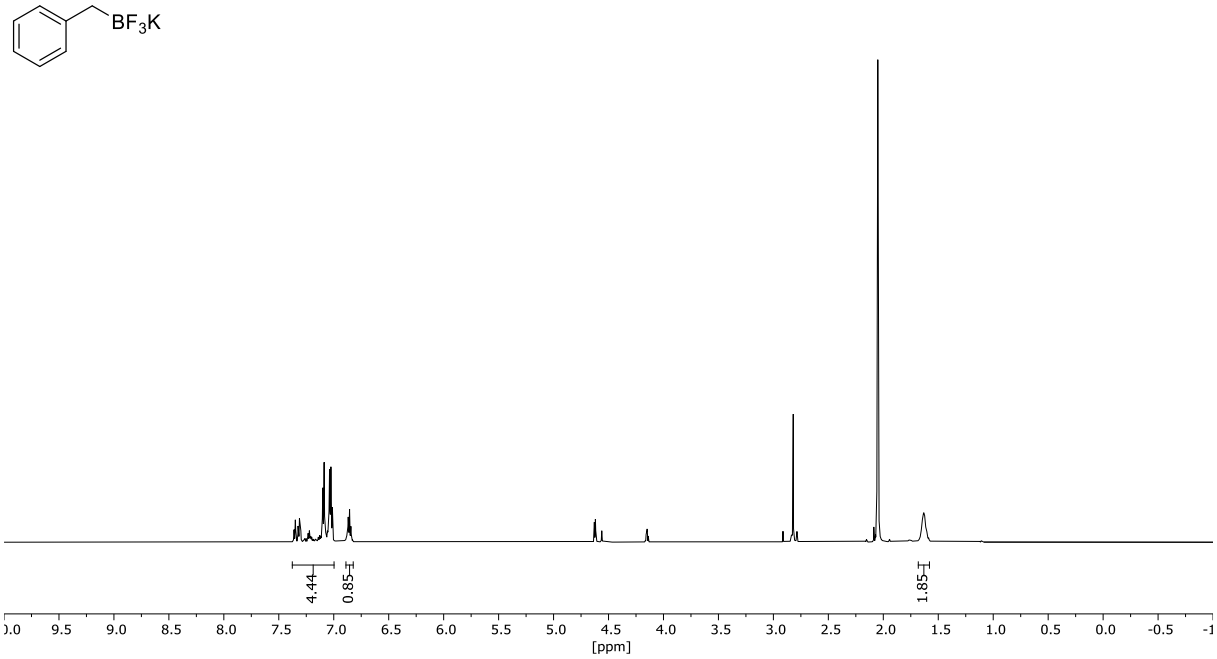

19F NMR (564.63 MHz, Acetone)

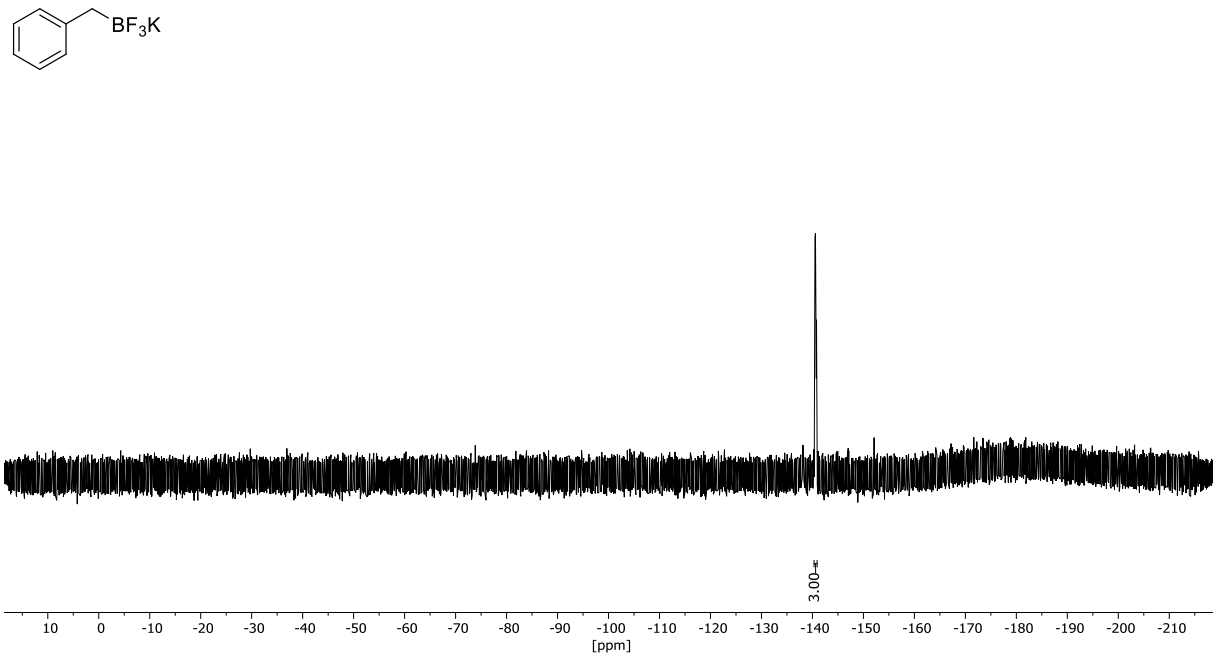

11B NMR (192.55 MHz, Acetone)

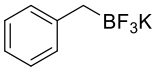

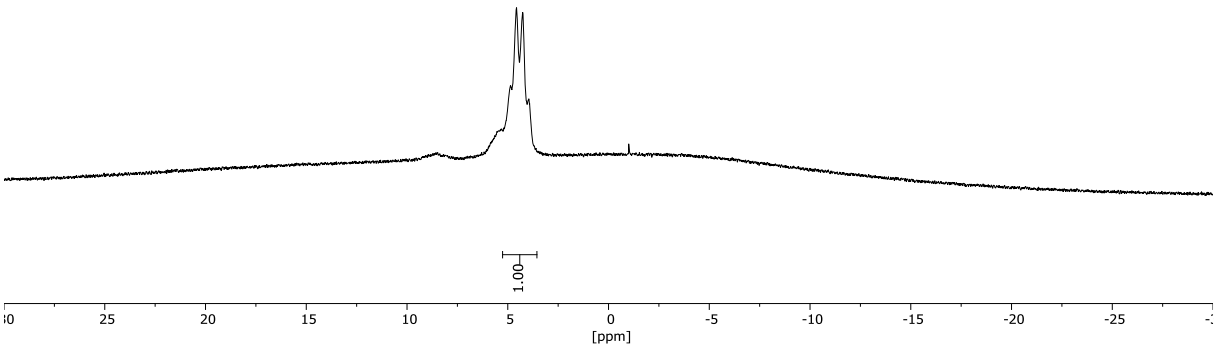

6.4.4.2 2-Chloro-1-(1-methyl-1*H*-imidazol-2-yl)ethan-1-one (**805**)

1H NMR (300.13 MHz, CDCl3)

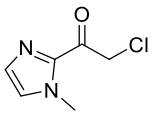

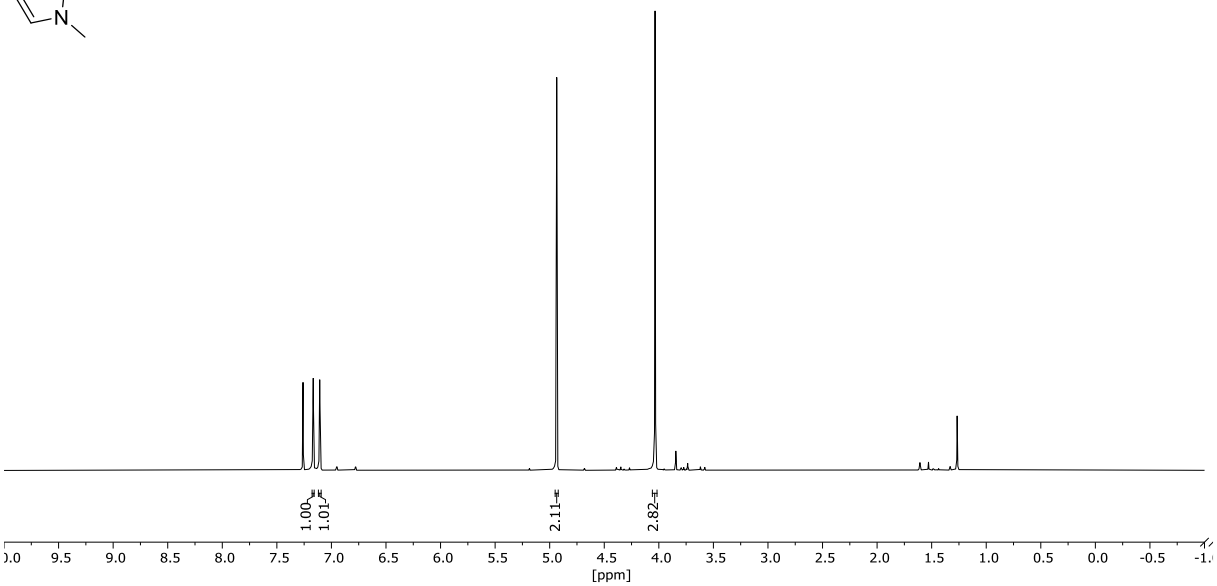

6.4.4.3 (*E*)-*N*-Methoxy-*N*-methylcinnamamide (**810**)

H NMR (300.13 MHz, CDCl3)

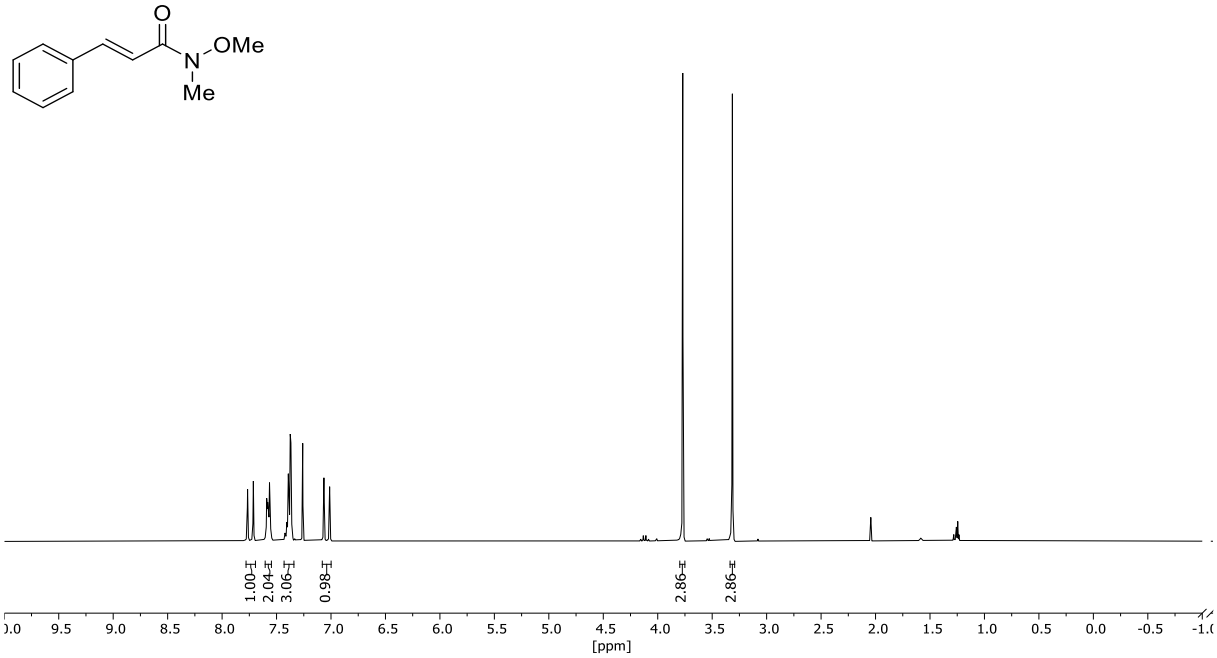

6.4.4.4 (*E*)-*N*-Methoxy-*N*-methylbut-2-enamide (**811**)

H NMR (300.13 MHz, CDCl3)

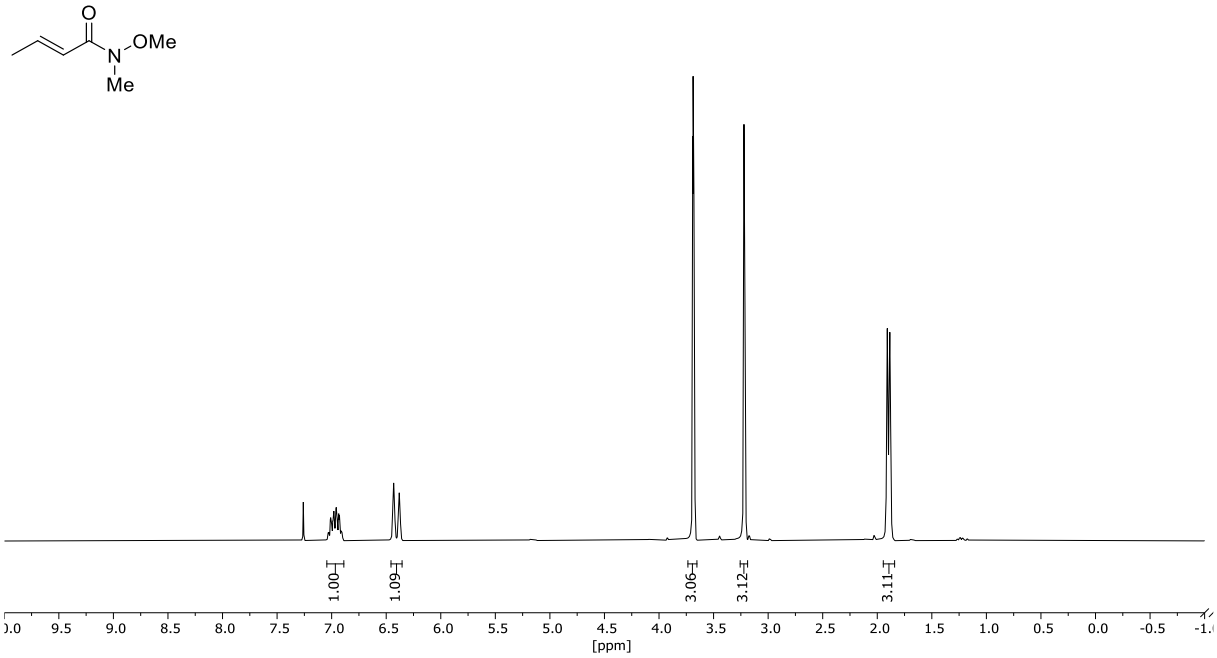

6.4.4.5 (*E*)-1-(1-Methyl-1*H*-imidazol-2-yl)-3-phenylprop-2-en-1-one (**813**)

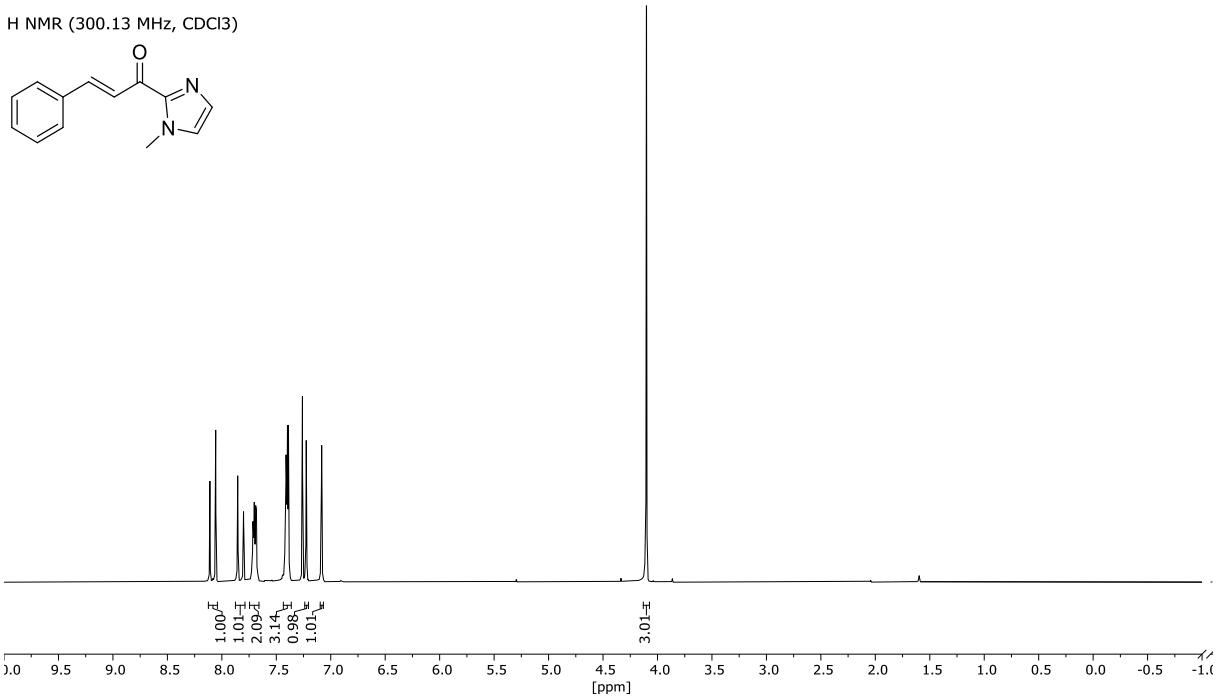

6.4.4.6 (*E*)-3-Phenyl-1-(1-phenyl-1*H*-imidazol-2-yl)prop-2-en-1-one (**812**)

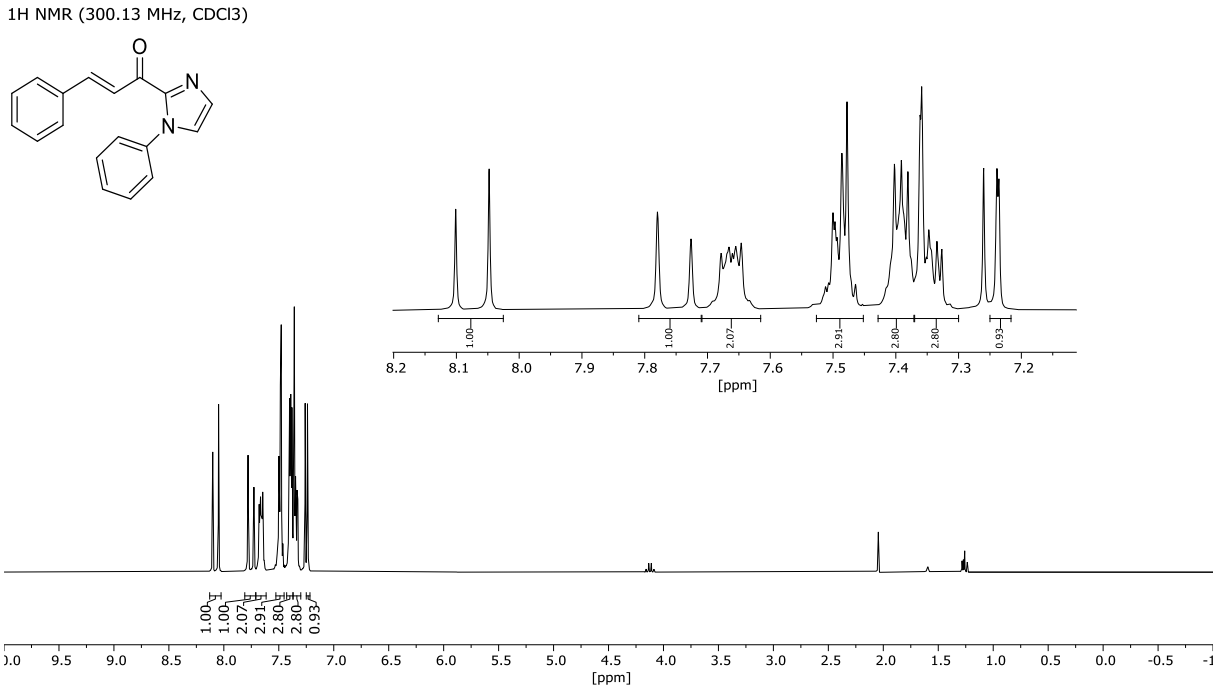

6.4.5 Substrates for aerobic oxidation

6.4.5.1 Methyl-1-indanone-2-carboxylate (**837**)

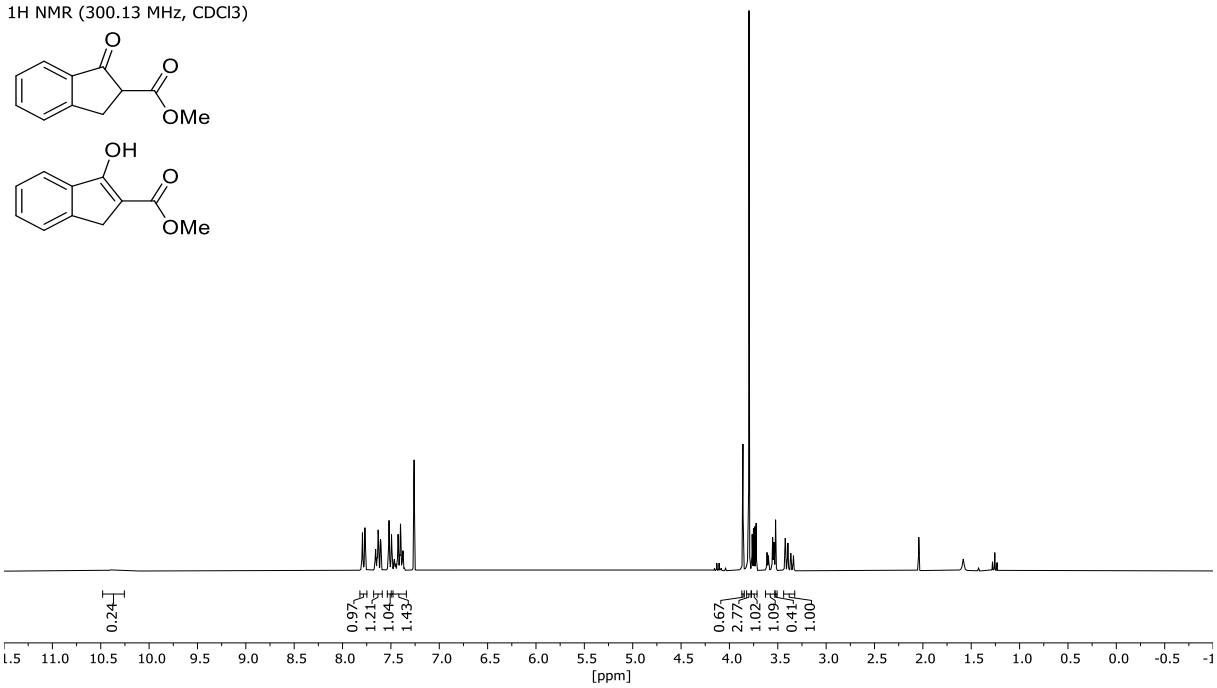

6.4.5.2 Isopropyl 1-*oxo*-2,3-dihydro-1*H*-indene-2-carboxylate (**511**)

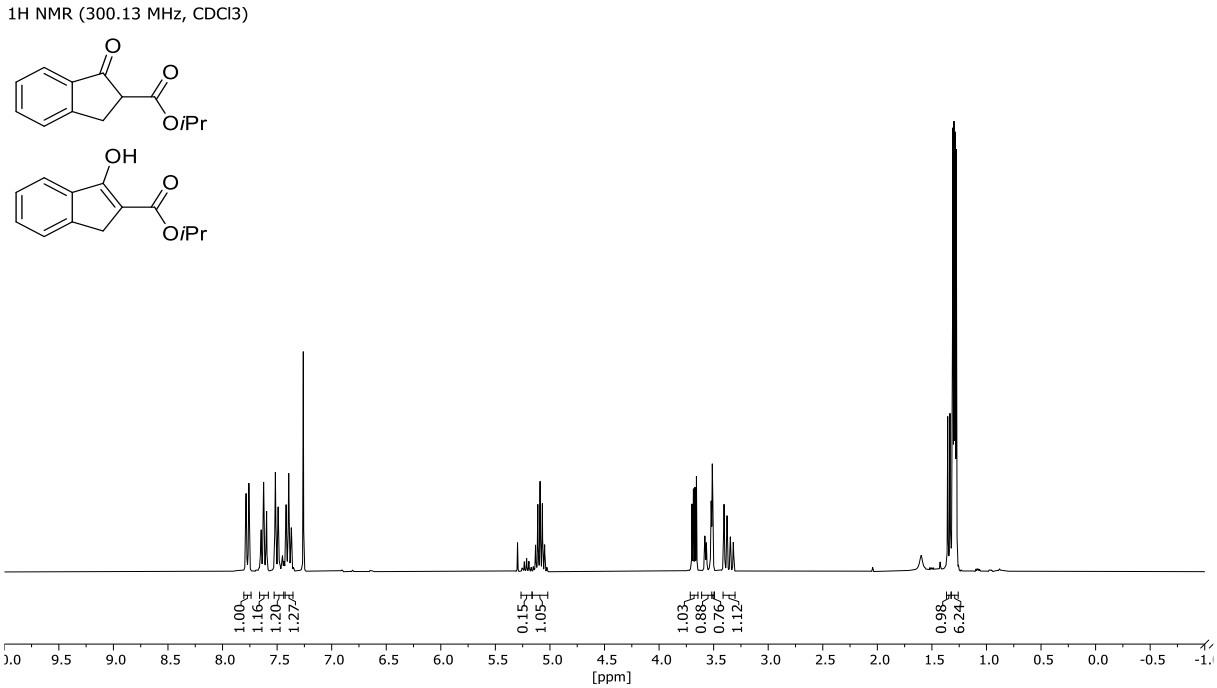

6.5 Spectra of photoredox transformations

6.5.1 Intramolecular radical cyclization

6.5.1.1 Dimethyl 2-vinylcyclopentane-1,1-dicarboxylate (**739**)

1H NMR (300.13 MHz, CDCl3)

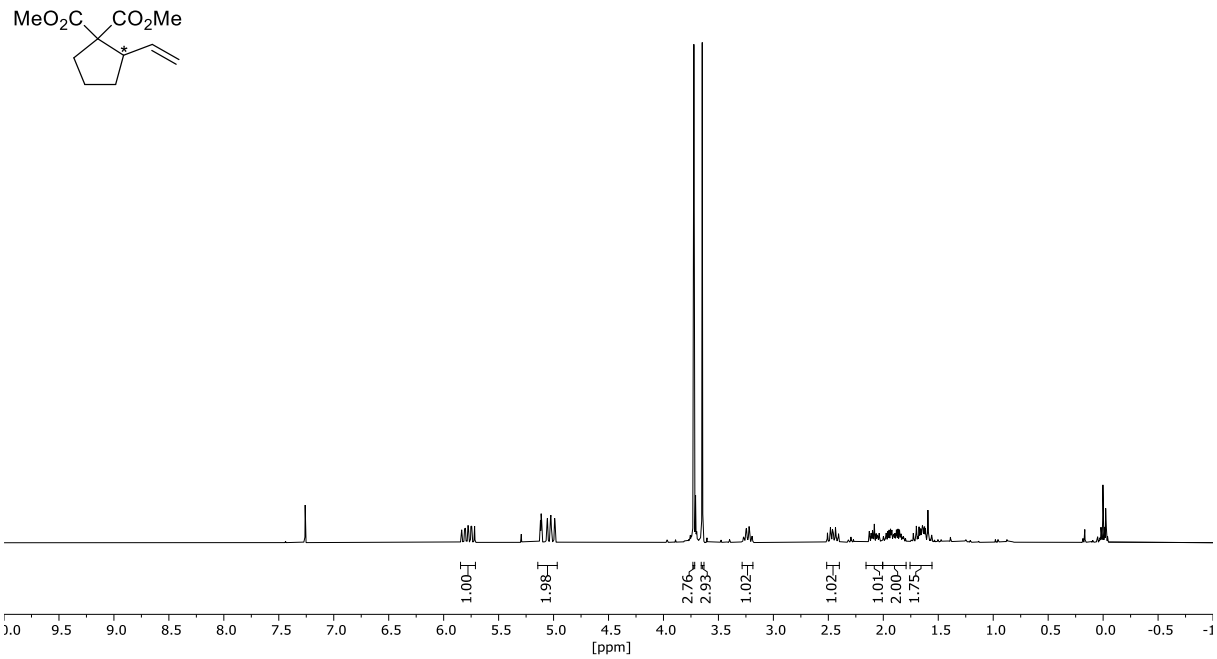

6.5.1.2 3-(2-Methylenecyclopentanecarbonyl)oxazolidine-2-one (**725**)

1H NMR (300.13 MHz, CDCl3)

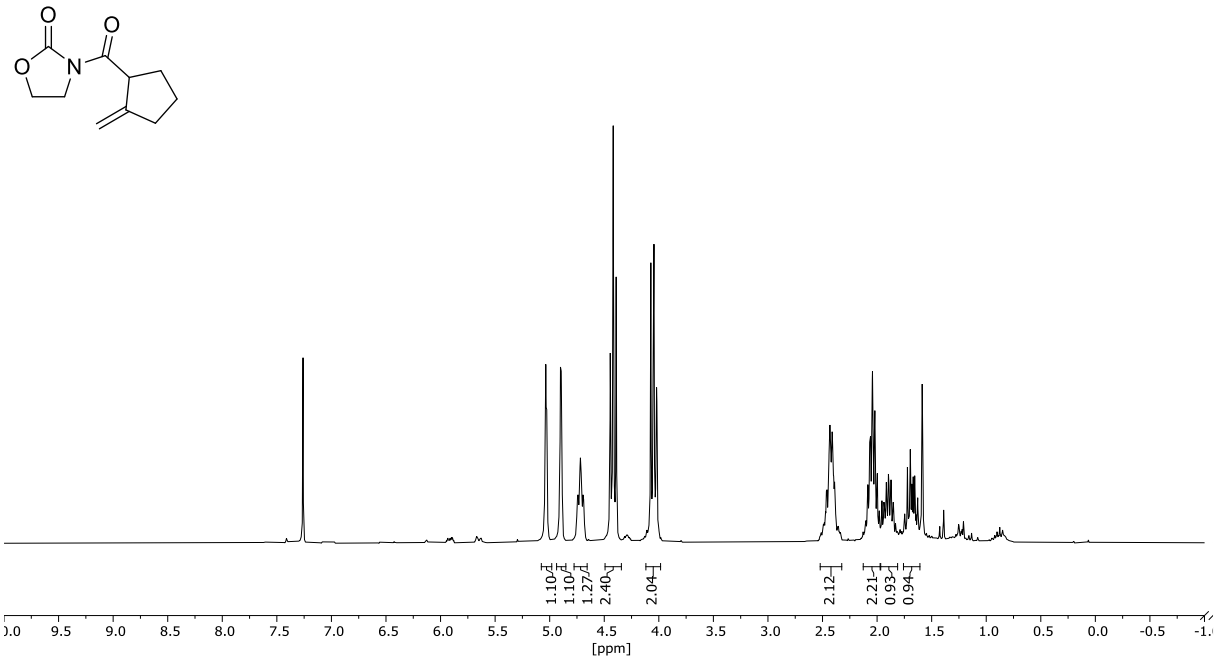

6.5.2 Intermolecular approaches: ATRA and α-allylation

6.5.2.1 Diethyl 2-(2-bromo-6-hydroxyhexyl)malonate (**758**)

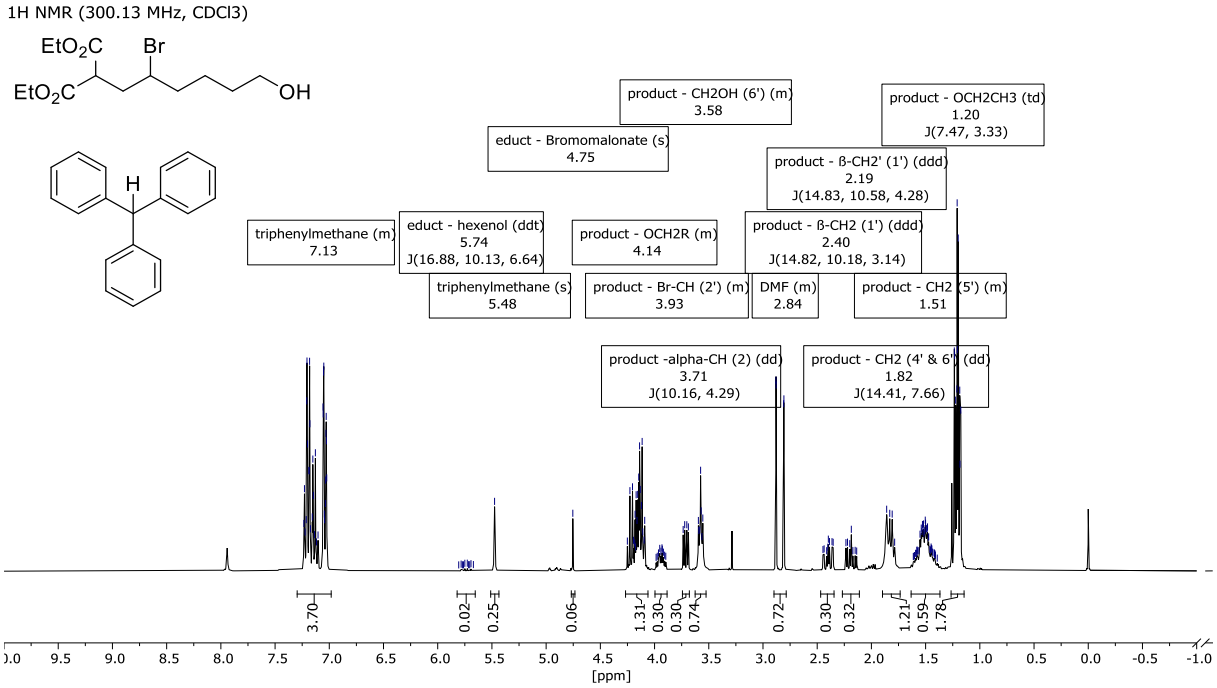

Setting the Ph_3CH-signal (s, 5.48 ppm) of 0.25 eq. triphenylmethane to 0.25 makes product β-CH_2 integral correspond to a yield of 31%.

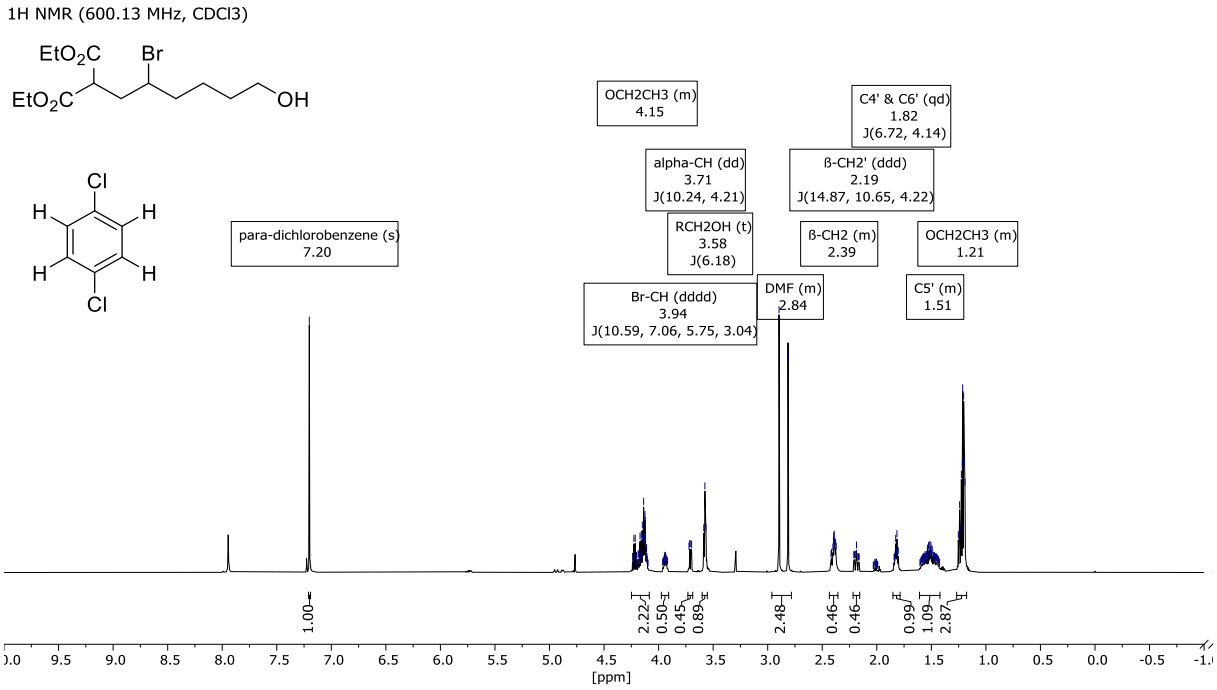

Setting the p-$Cl_2C_6H_4$ signal (s, 7.20 ppm) of 0.25 eq. *para*-dichlorobenzene to 0.25 makes product β-CH_2 integral correspond to a yield of 46%.

6.5.2.2 3-(2-Methylpent-4-enoyl)oxazolidin-2-one (**772**)

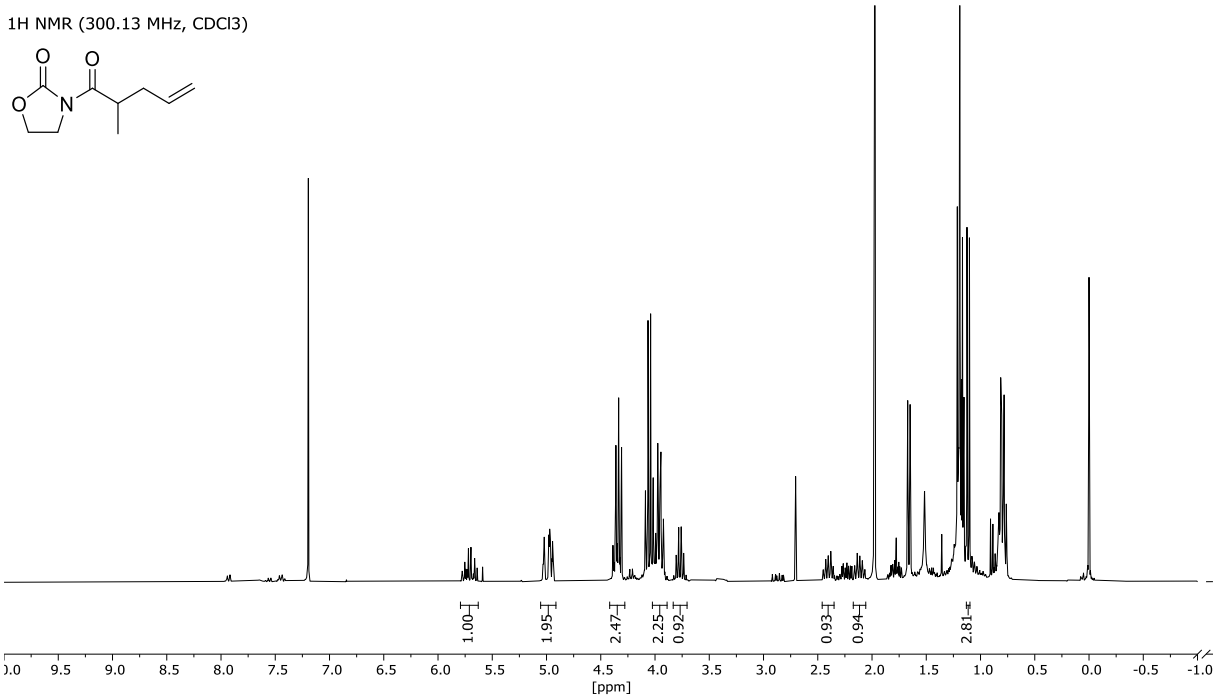

6.5.3 Cascade cyclization of phenylpropynyl-3-oxo-3-phenylpropanoate (**779**)

6.5.3.1 9a-Methyl-4-phenylnaphtho[2,3-c]furan-1,9(3*H*,9a*H*)-dione (**784**)

1H NMR (300.13 MHz, CDCl3)

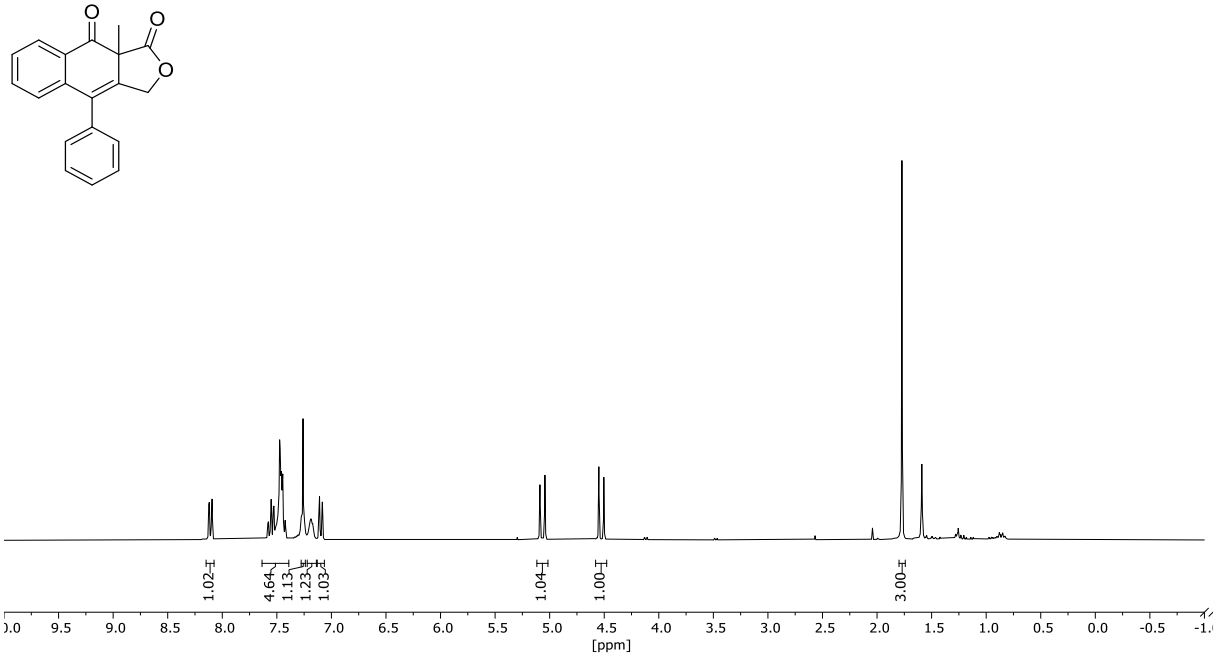

13C NMR (75.48 MHz, CDCl3)

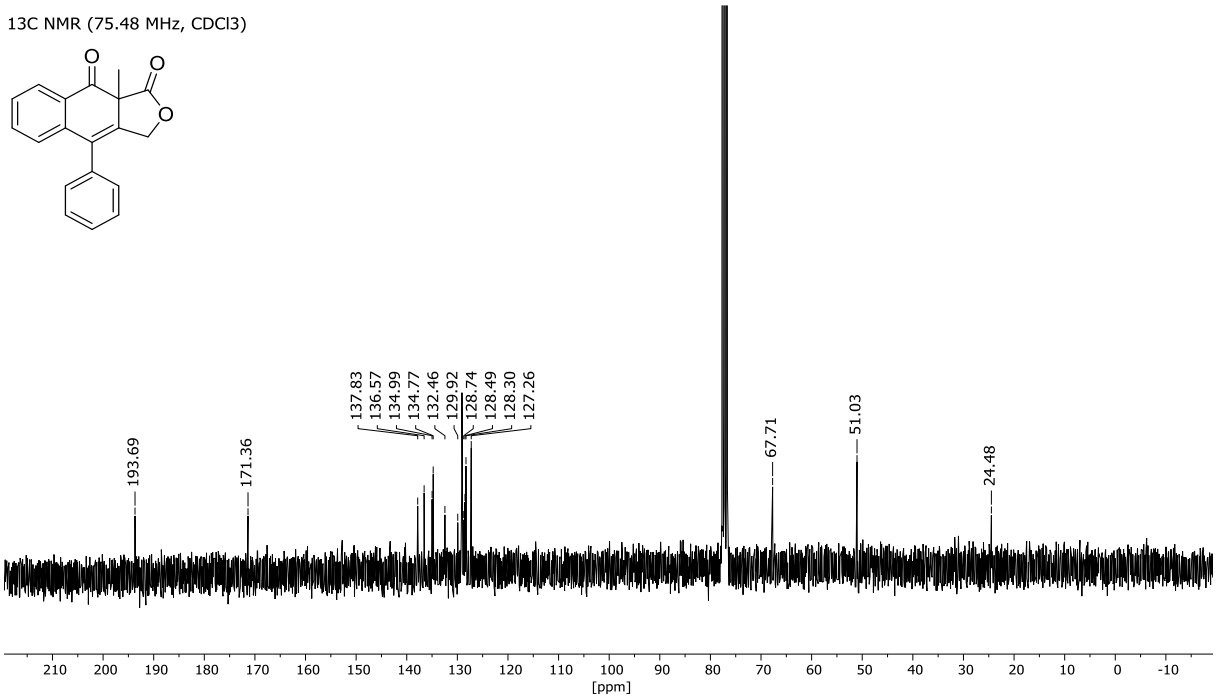

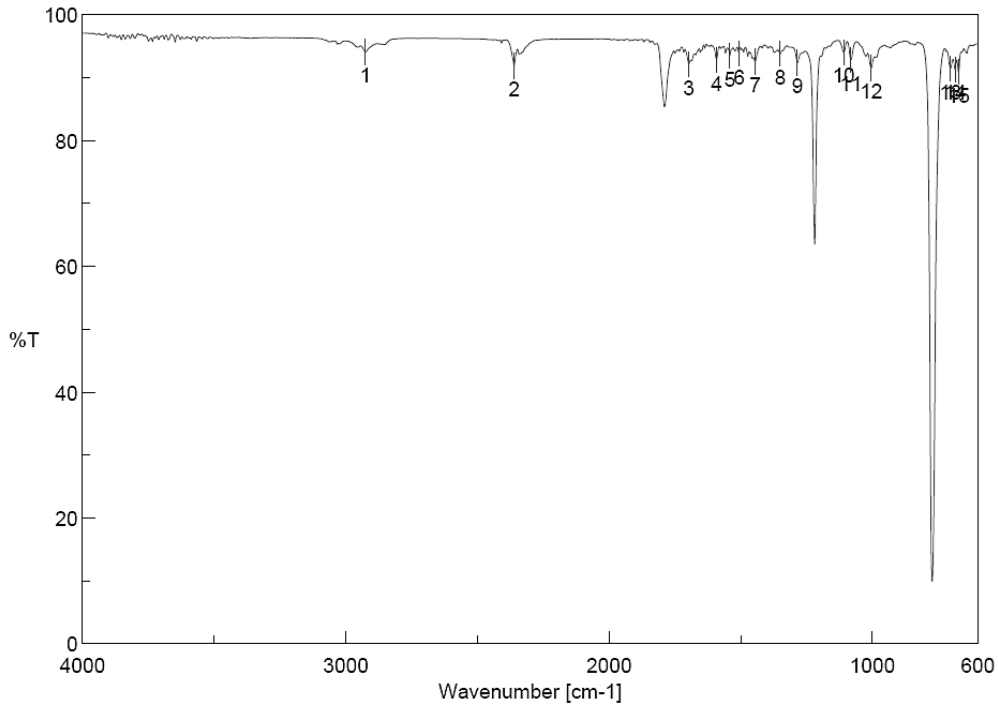

[Result of Peak Picking]

No.	Position	Intensity	No.	Position	Intensity	No.	Position	Intensity
1	2925.48	94.0205	2	2361.41	91.824	3	1697.05	92.0753
4	1591.95	92.7889	5	1540.85	93.4487	6	1507.1	93.808
7	1445.39	92.4628	8	1349.93	93.737	9	1284.36	92.3494
10	1108.87	93.9832	11	1080.91	92.7436	12	1004.73	91.4715
13	703.89	91.4267	14	685.57	91.2671	15	673.035	90.8573

6.5.4 [2+2]-Enone cyclization

6.5.4.1 (3,4-Diphenylcyclobutane-1,2-diyl)bis((1-methyl-1*H*-imidazol-2-yl)methanone) (**814**)

1H NMR (300.13 MHz, CDCl3)

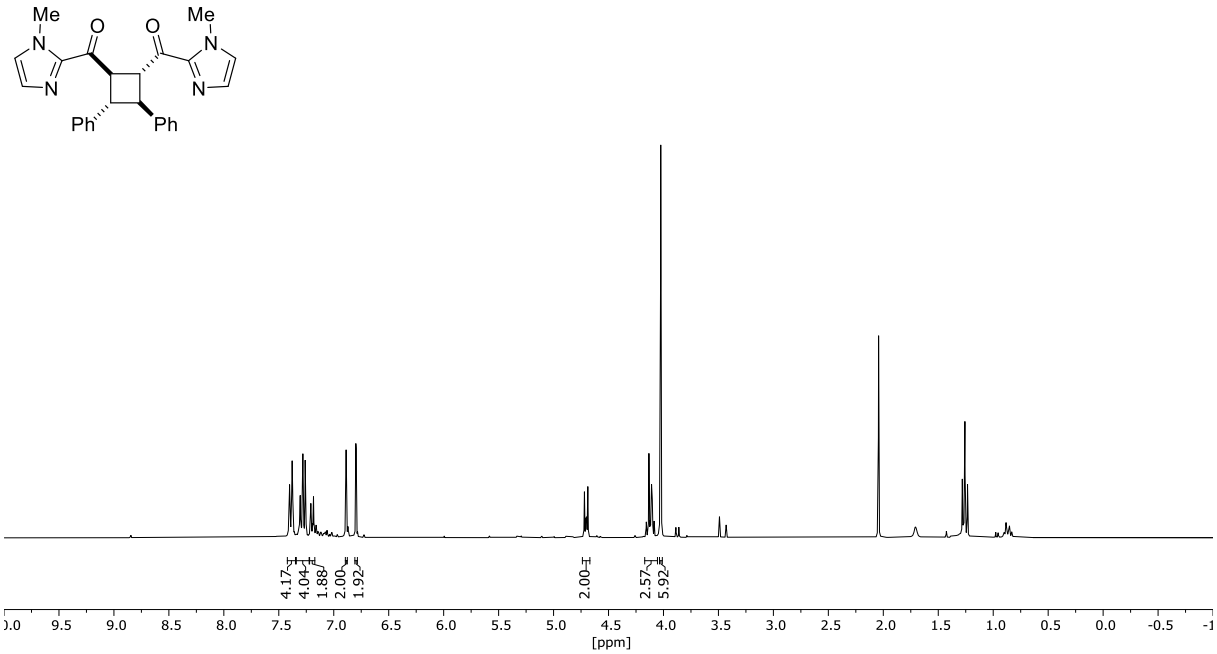

13C NMR (75.48 MHz, CDCl3)

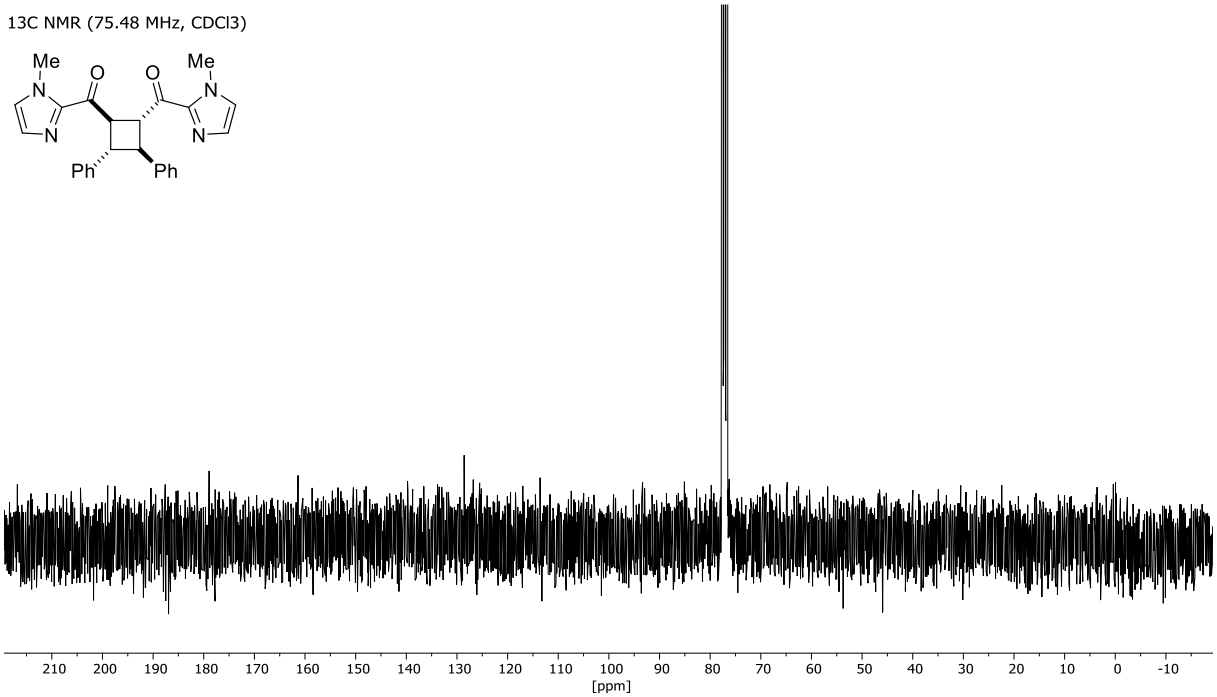

6.5.4.2 (3,4-Diphenylcyclobutane-1,2-diyl)bis((1-phenyl-1*H*-imidazol-2-yl)methanone) (**815**)

1H NMR (300.13 MHz, CDCl3)

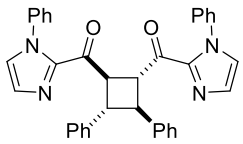

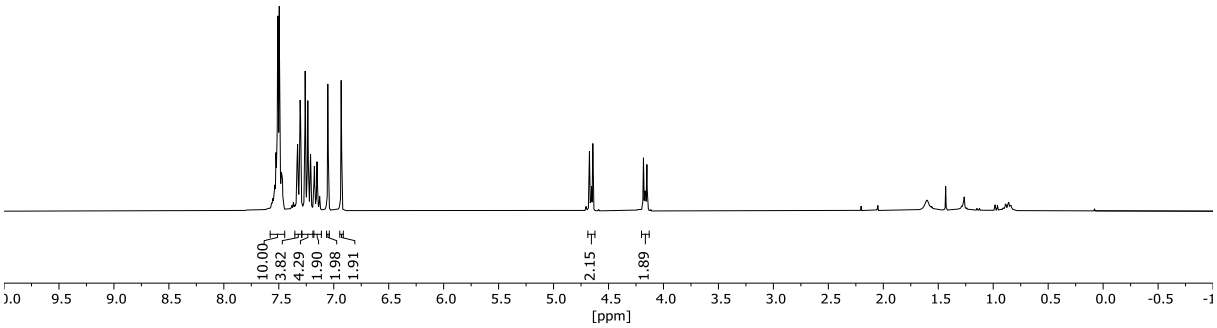

6.5.4.3 (2,4-Diphenylcyclobutane-1,3-diyl)bis((1-phenyl-1*H*-imidazol-2-yl)methanone) (**819**)

1H NMR (300.13 MHz, CDCl3)

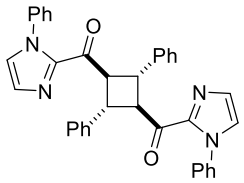

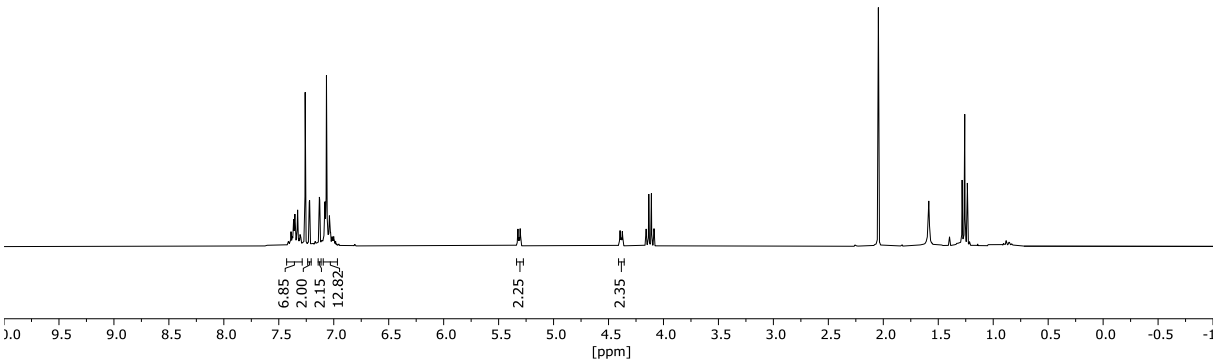

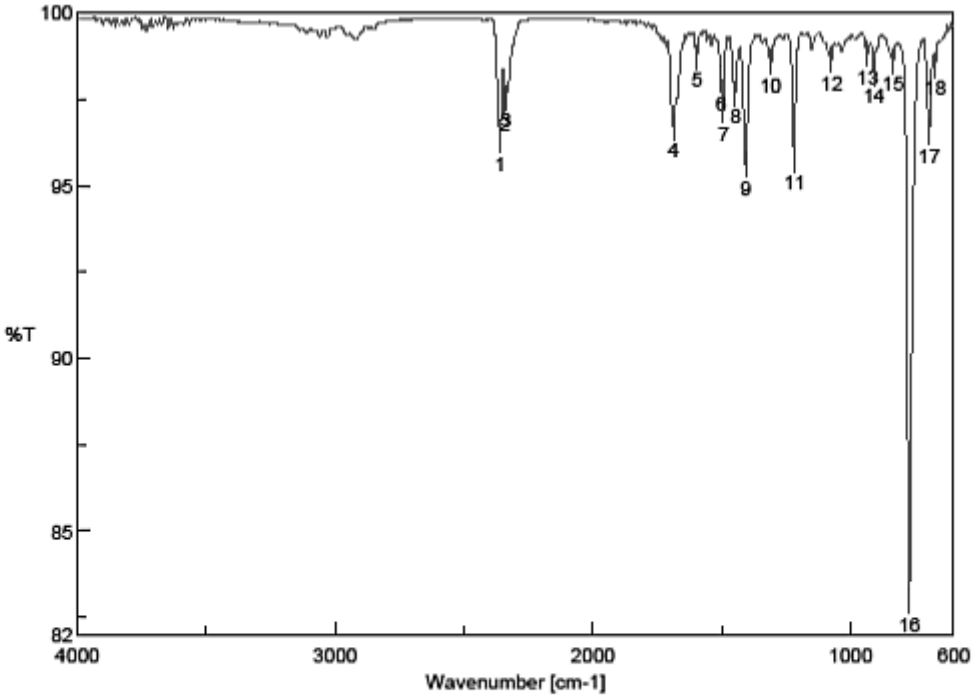

[Result of Peak Picking]

No.	Position	Intensity	No.	Position	Intensity	No.	Position	Intensity
1	2360.44	96.2952	2	2341.16	97.4816	3	2337.3	97.5507
4	1686.44	96.6845	5	1596.77	98.7141	6	1504.2	98.063
7	1493.6	97.1825	8	1447.31	97.6776	9	1406.82	95.5892
10	1310.39	98.5857	11	1218.79	95.7366	12	1075.12	98.6523
13	934.342	98.8266	14	909.272	98.2653	15	835.026	98.6078
16	772.351	82.9497	17	695.212	96.5411	18	673.035	98.4843

6.5.5 Aerobic oxidation

6.5.5.1 Isopropyl (*S*)-2-hydroxy-1-oxo-2,3-dihydro-1*H*-indene-2-carboxylate (**512**)

1H NMR (300.13 MHz, CDCl3)

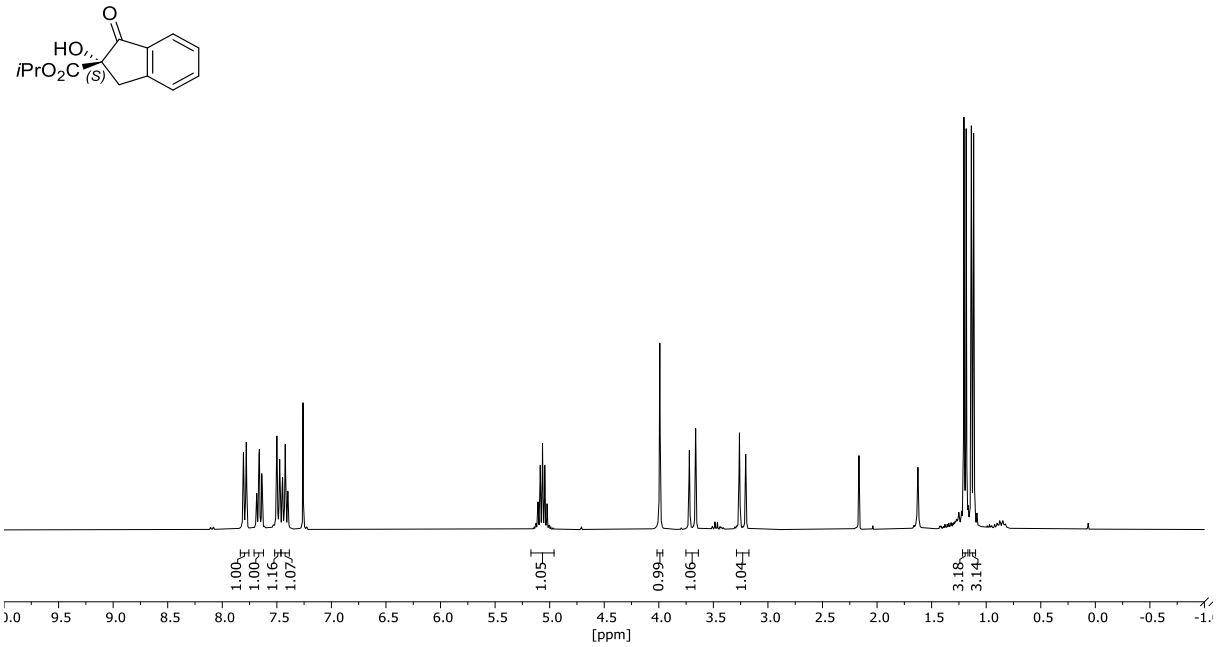

7 HPLC-traces

7.1 Aerobic oxidation

Racemic reference

Chiralpak IB, *n*-hexane/isopropanol 97:3, flow 0.6 mL/min.

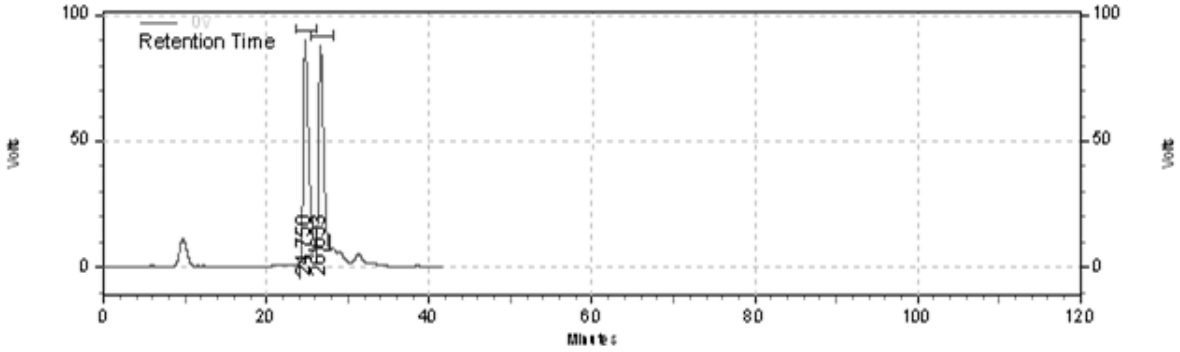

UV Results

Retention Time	Area	Area %	Height	Height %
24,750	15223437	54,26	345964	51,85
26,633	12835245	45,74	321226	48,15

HPLC trace for table 13, entry 1 (10 mol% $[Ru(bpy)_3](PF_6)_2$, 10 mol% iPr-BOX, 10 mol% $Ni(acac)_2$)

Chiralpak IB, *n*-hexane/isopropanol 97:3, flow 0.6 mL/min.

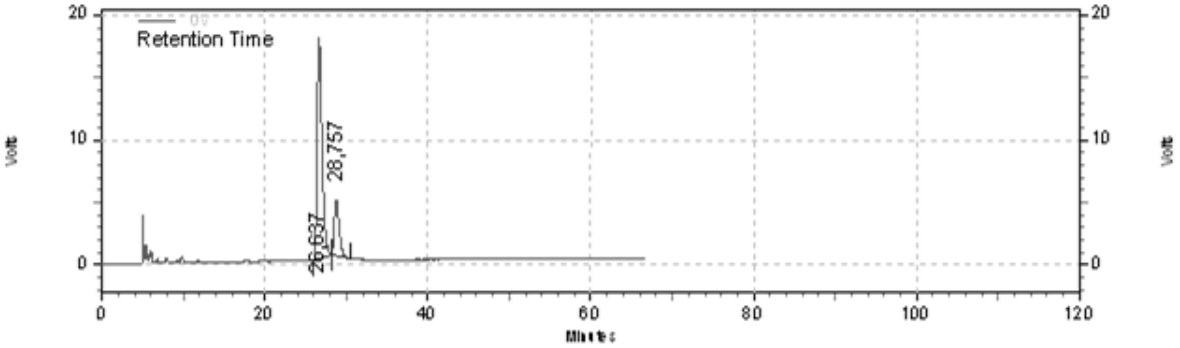

UV Results

Retention Time	Area	Area %	Height	Height %
26,637	2977035	79,48	70785	80,01
28,757	768679	20,52	17680	19,99

HPLC trace for table 13, entry 2 (5 mol% $[Ru(bpy)_3](PF_6)_2$, 5 mol% iPr-BOX, 5 mol% $Ni(acac)_2$)

Chiralpak IB, *n*-hexane/isopropanol 97:3, flow 0.6 mL/min.

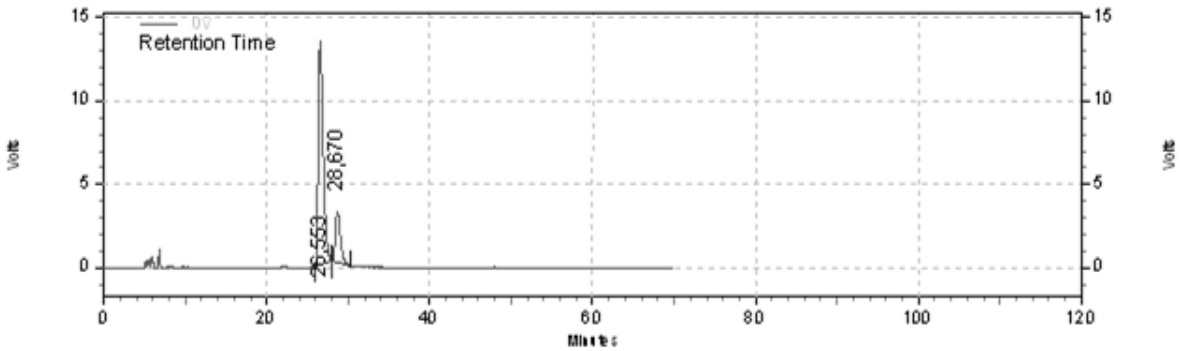

UV Results

Retention Time	Area	Area %	Height	Height %
26,553	2252437	80,75	53577	81,26
28,670	536821	19,25	12352	18,74

HPLC trace for table 13, entry 5 (1 mol% $[Ru(bpy)_3](PF_6)_2$, 1 mol% iPr-BOX, 1 mol% $Ni(acac)_2$)

Chiralpak IB, *n*-hexane/isopropanol 97:3, flow 0.6 mL/min.

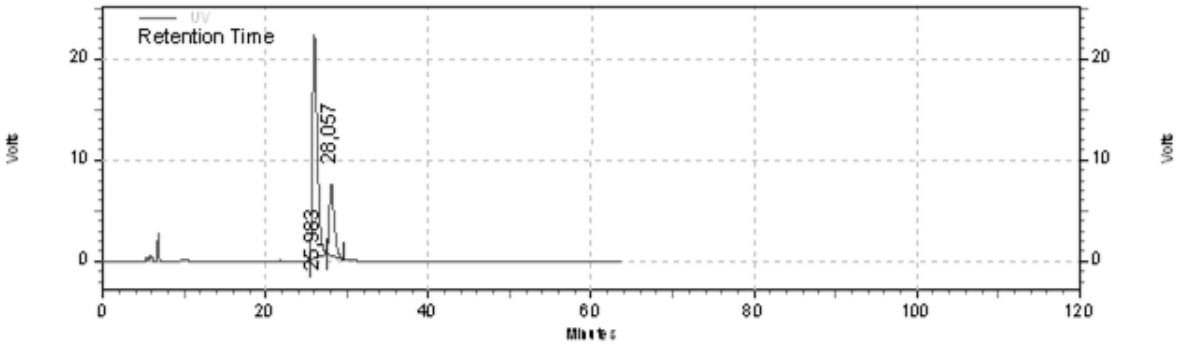

UV Results

Retention Time	Area	Area %	Height	Height %
25,983	3599351	75,47	88355	75,87
28,057	1170198	24,53	28098	24,13

HPLC trace for table 13, entry 8 (0.81 mol% [Ru(bpy)$_2$(BOX-bpy)](PF$_6$)$_2$, 0.81 mol% Ni(acac)$_2$)

Chiralpak IB, *n*-hexane/isopropanol 97:3, flow 0.6 mL/min.

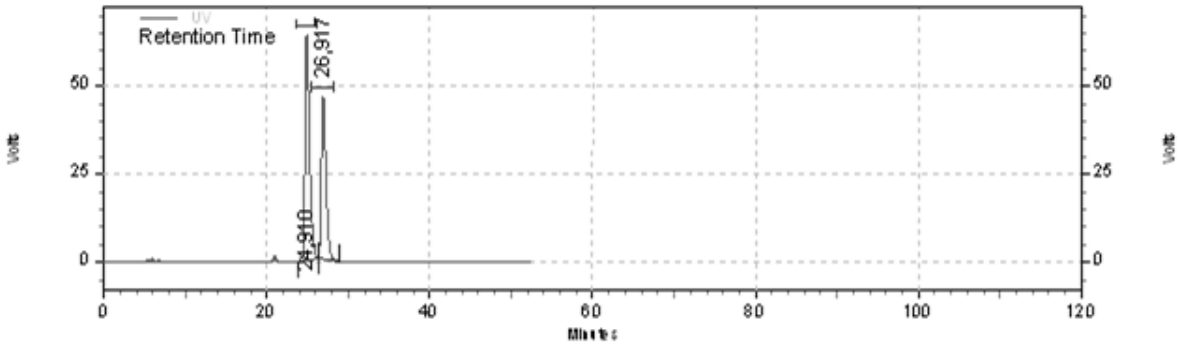

UV Results

Retention Time	Area	Area %	Height	Height %
24,910	9838911	57,76	255943	58,30
26,917	7194842	42,24	183060	41,70

HPLC trace for table 13, entry 9 (0.77 mol% [Ru(*t*Bu-bpy)$_2$(BOX-bpy)](PF$_6$)$_2$, 0.74 mol% Ni(acac)$_2$)

Chiralpak IB, *n*-hexane/isopropanol 97:3, flow 0.6 mL/min.

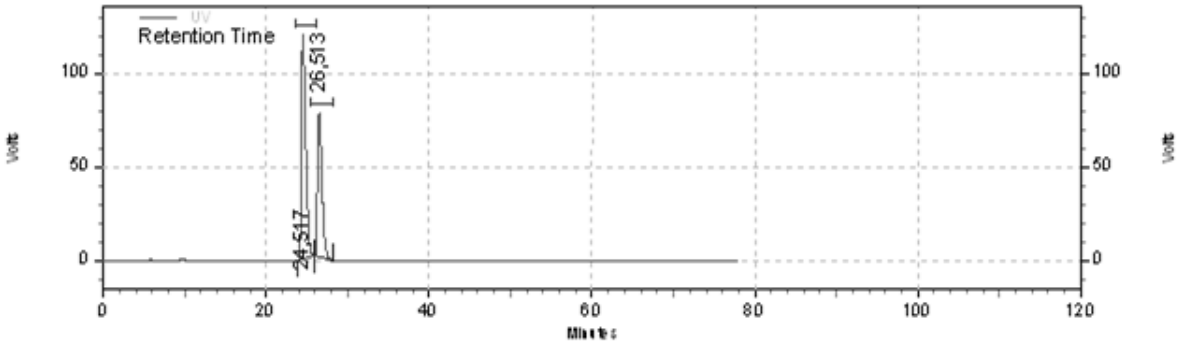

UV Results

Retention Time	Area	Area %	Height	Height %
24,517	17584366	59,98	478909	60,98
26,513	11734608	40,02	306425	39,02

HPLC trace for table 13, entry 10 (0.69 mol% [Ru(MeO-bpy)$_2$(BOX-bpy)](PF$_6$)$_2$, 0.68 mol% Ni(acac)$_2$)

Chiralpak IB, *n*-hexane/isopropanol 97:3, flow 0.6 mL/min.

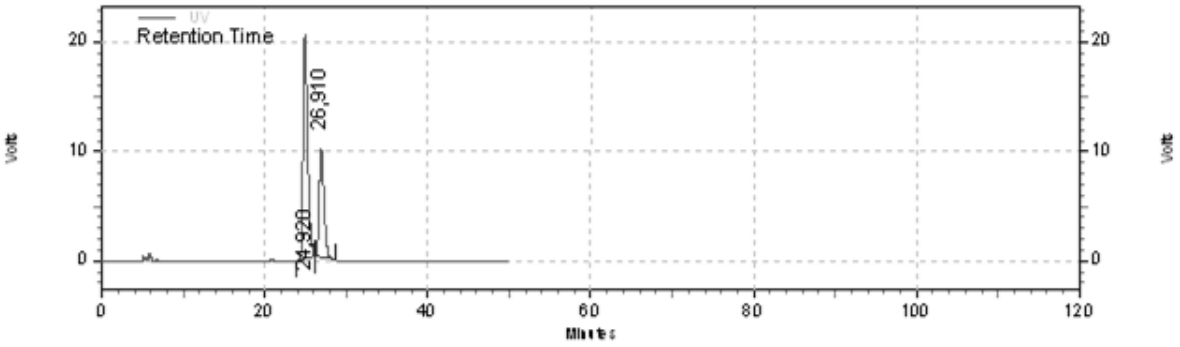

UV Results

Retention Time	Area	Area %	Height	Height %
24,920	3232966	66,61	82345	67,60
26,910	1620877	33,39	39470	32,40

8 Photophysical and electrochemical measurements

8.1 UV/VIS

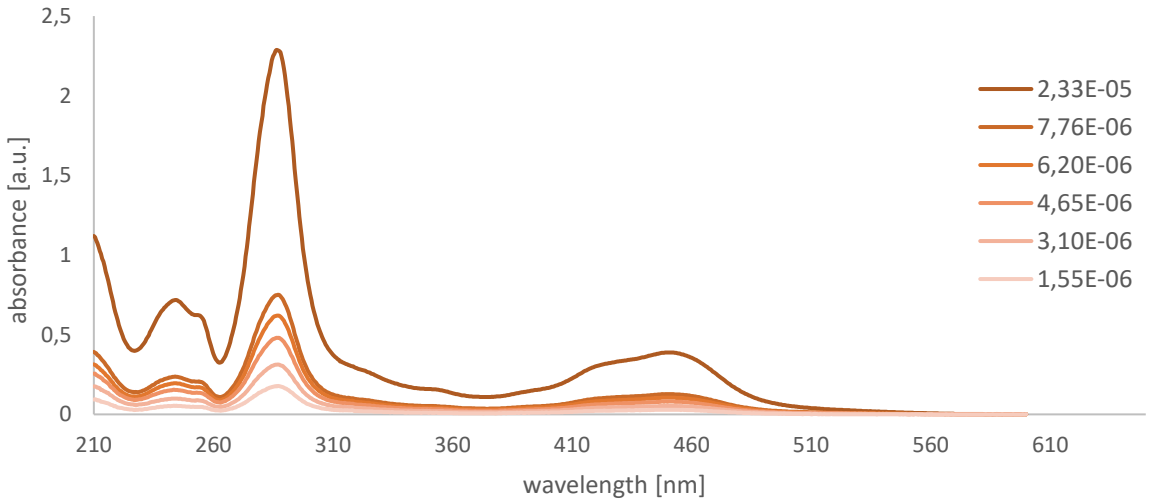

spectrum 16. UV/VIS spectra of $[Ru(bpy)_3](PF_6)_2$ (**7**) in acetonitrile at different concentrations.

table 15. Determination of the molar absorptivity of $[Ru(bpy)_3](PF_6)_2$ (**7**) by linear regression.

concentration	absorbance	
[mol/L]	287 nm	452 nm
$7.76 \cdot 10^{-6}$	0.7508	0.1269
$6.20 \cdot 10^{-6}$	0.6201	0.1056
$4.65 \cdot 10^{-6}$	0.4800	0.0810
$3.10 \cdot 10^{-6}$	0.3129	0.0533
$1.55 \cdot 10^{-6}$	0.1784	0.0294
slope	93605	15943
r^2	0.9984	0.9983
ε [L/(mol·cm^{-1}]	93600	15900

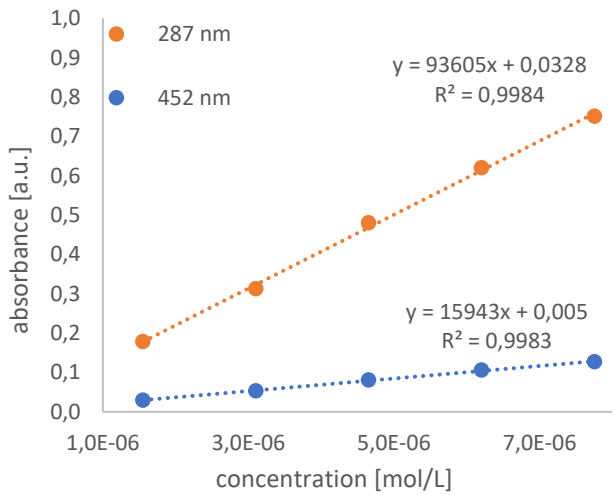

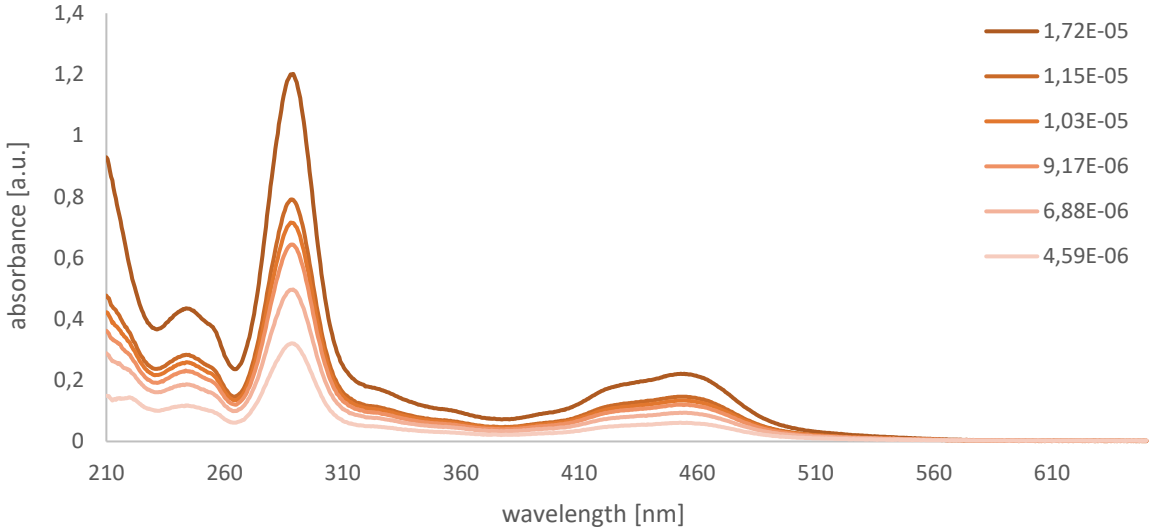

spectrum 17. UV/VIS spectra of $[Ru(bpy)_2(BOX\text{-}bpy)](PF_6)_2$ (**532**) in acetonitrile at different concentrations.

table 16. Determination of the molar absorptivity of $[Ru(bpy)_2(BOX\text{-}bpy)](PF_6)_2$ (**532**) by linear regression.

concentration	absorbance	
[mol/L]	289 nm	455 nm
$1.72 \cdot 10^{-5}$	1.2020	0.2214
$1.15 \cdot 10^{-5}$	0.7913	0.1467
$1.03 \cdot 10^{-5}$	0.7158	0.1340
$9.17 \cdot 10^{-6}$	0.6438	0.1202
$6.88 \cdot 10^{-6}$	0.4969	0.0942
$4.59 \cdot 10^{-6}$	0.3209	0.0612
slope	69125	12537
r^2	0.9992	0.9990
ε [L/(mol·cm^{-1}]	69100	12500

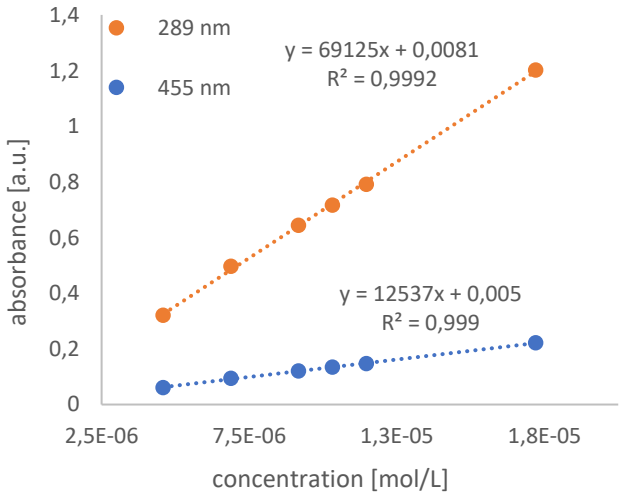

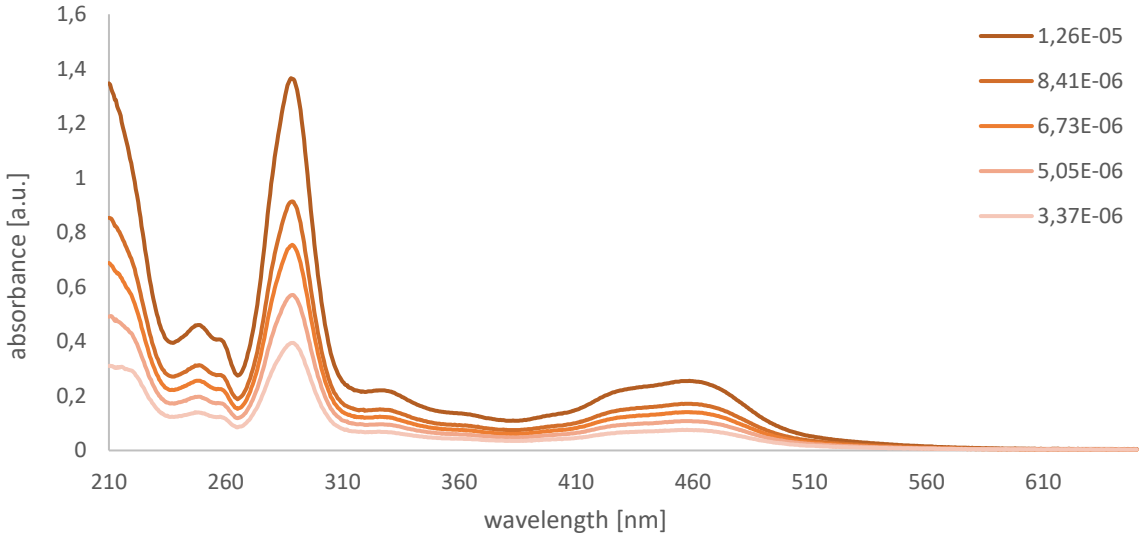

spectrum 18. UV/VIS spectra of [Ru(*t*Bu-bpy)$_2$(BOX-bpy)](PF$_6$)$_2$ (**536**) in acetonitrile at different concentrations.

table 17. Determination of the molar absorptivity of [Ru(*t*Bu-bpy)$_2$(BOX-bpy)](PF$_6$)$_2$ (**536**) by linear regression.

concentration [mol/L]	absorbance 289 nm	absorbance 460 nm
$1.26 \cdot 10^{-5}$	1.3656	0.2554
$8.41 \cdot 10^{-6}$	0.9137	0.1716
$6.73 \cdot 10^{-6}$	0.7544	0.1410
$5.05 \cdot 10^{-6}$	0.5700	0.1081
$3.37 \cdot 10^{-6}$	0.2767	0.0756
slope	104653	19386
r^2	0.9997	0.9998
ε [L/(mol·cm^{-1}]	104600	19400

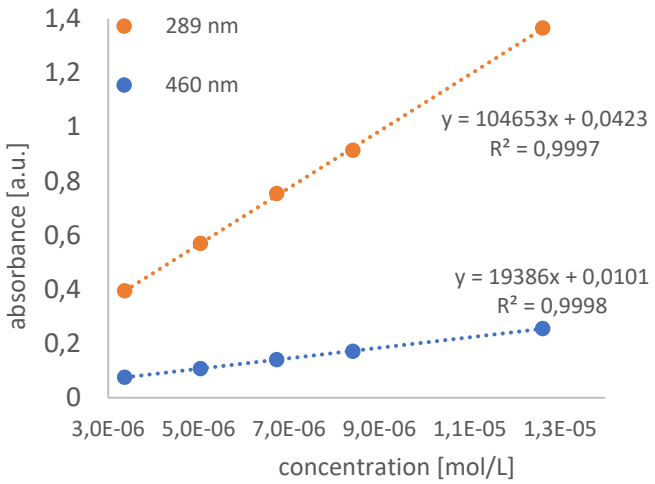

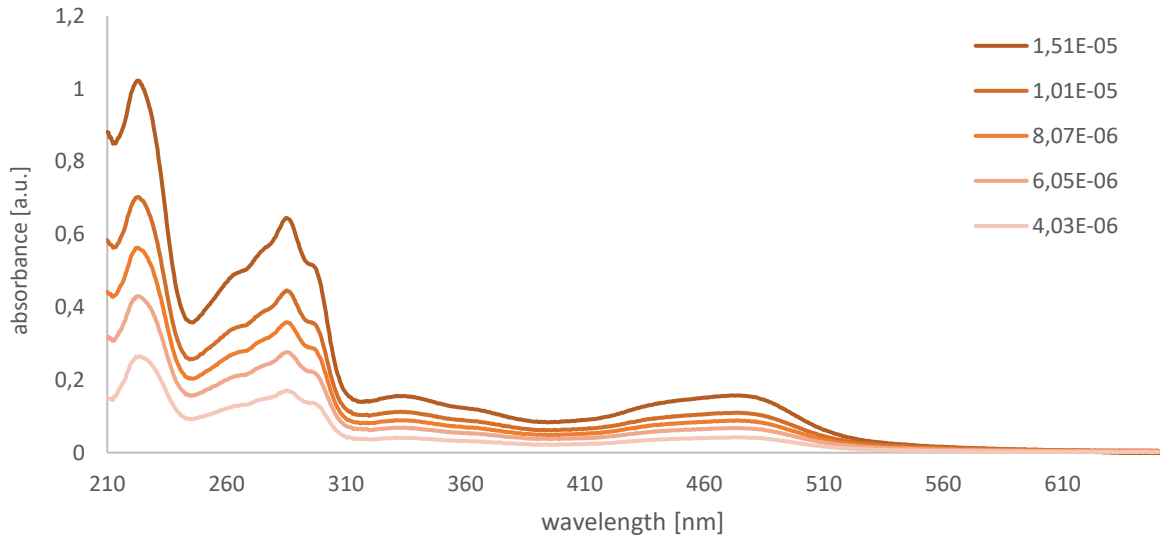

spectrum 19. UV/VIS spectra of [Ru(MeO-bpy)$_2$(BOX-bpy)](PF$_6$)$_2$ (**537**) in acetonitrile at different concentrations.

table 18. Determination of the molar absorptivity of [Ru(MeO-bpy)$_2$(BOX-bpy)](PF$_6$)$_2$ (**537**) by linear regression.

concentration	absorbance	
[mol/L]	285 nm	475 nm
$1.51 \cdot 10^{-5}$	0.6451	0.1573
$1.01 \cdot 10^{-6}$	0.4460	0.1097
$8.07 \cdot 10^{-6}$	0.3586	0.0886
$6.05 \cdot 10^{-6}$	0.2761	0.0678
$4.03 \cdot 10^{-6}$	0.1711	0.0423
slope	42243	10255
r^2	0.9975	0.9968
ε [L/(mol·cm^{-1}]	42200	10300

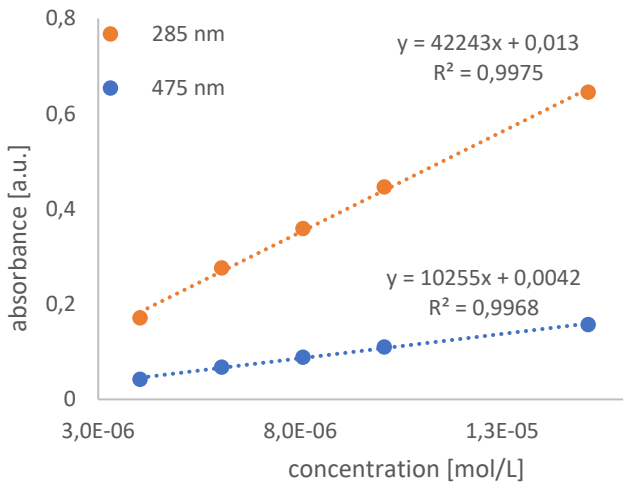

8.2 Cyclic voltammetry

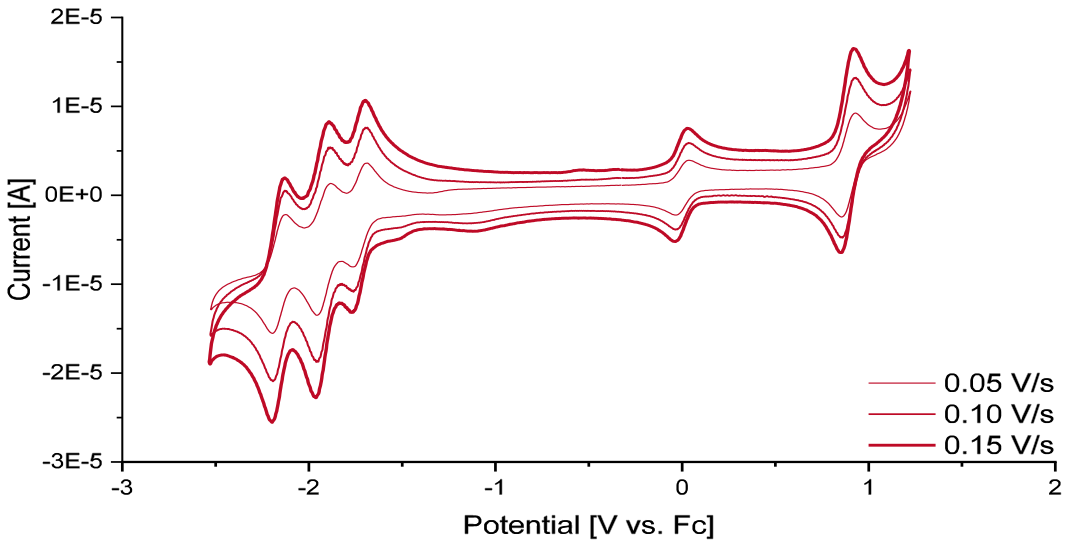

figure 51. Cyclic voltammograms of 1 mM $[Ru(bpy)_3](PF_6)_2$ (**7**) at scan rates 0.050 V/s to 0.150 V/s in degassed acetonitrile with 0.100 M $TBAPF_6$ as supporting electrolyte.

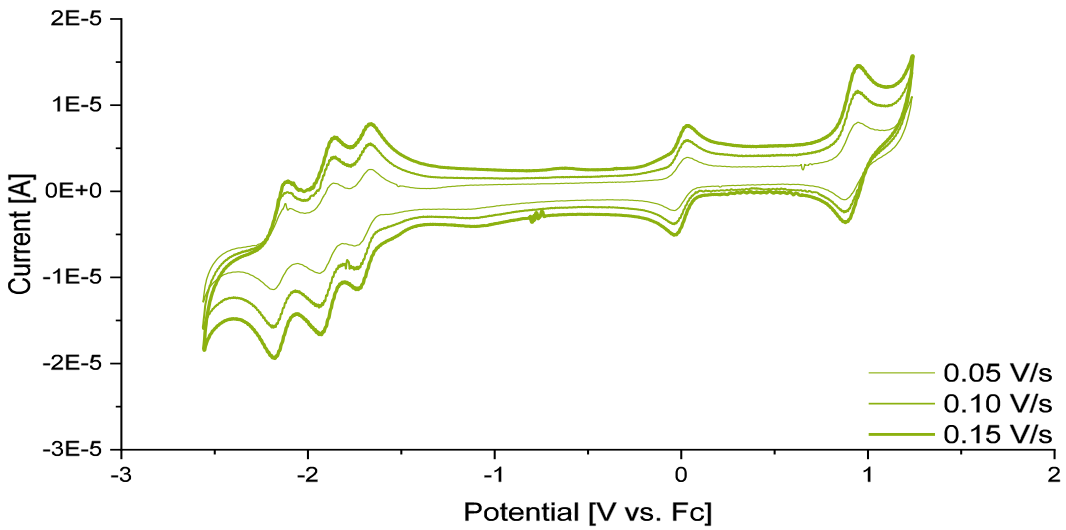

figure 52. Cyclic voltammograms of 1 mM $[Ru(bpy)_2(BOX\text{-}bpy)](PF_6)_2$ (**532**) at scan rates 0.050 V/s to 0.150 V/s in degassed acetonitrile with 0.100 M $TBAPF_6$ as supporting electrolyte.

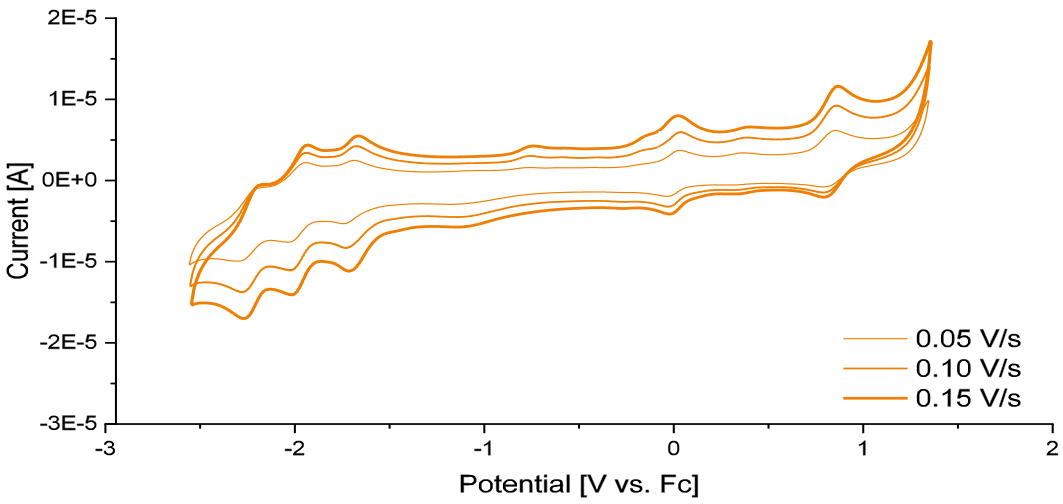

figure 53. Cyclic voltammograms of 1 mM [Ru(*t*Bu-bpy)$_2$(BOX-bpy)](PF$_6$)$_2$ (**536**) at scan rates 0.050 V/s to 0.150 V/s in degassed acetonitrile with 0.100 M TBAPF$_6$ as supporting electrolyte.

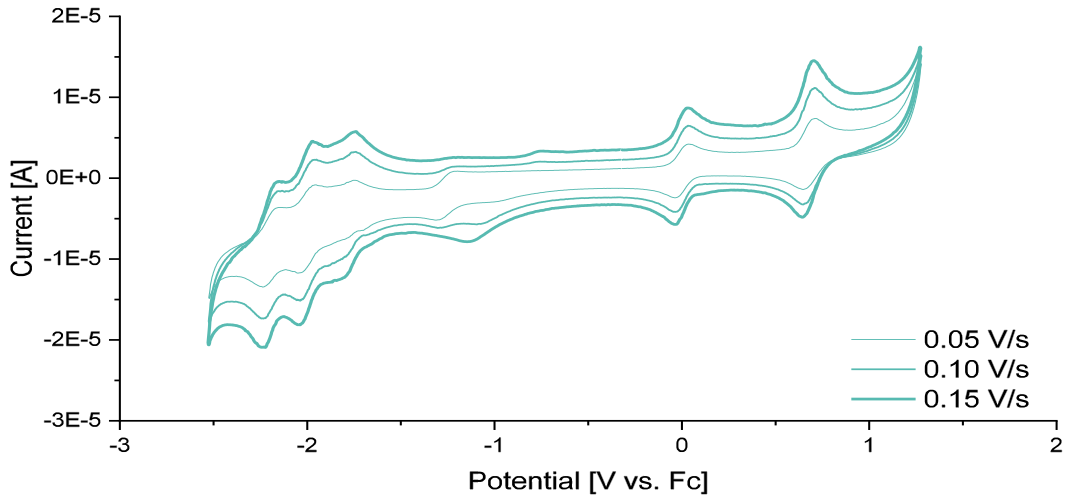

figure 54. Cyclic voltammograms of 1 mM [Ru(MeO-bpy)$_2$(BOX-bpy)](PF$_6$)$_2$ (**537**) at scan rates 0.050 V/s to 0.150 V/s in degassed acetonitrile with 0.100 M TBAPF$_6$ as supporting electrolyte.

9 Literature

1. Hopkinson, M. N.; Sahoo, B.; Li, J.-L.; Glorius, F., Dual Catalysis Sees the Light: Combining Photoredox with Organo-, Acid, and Transition-Metal Catalysis. *Chemistry – A European Journal* **2014,** *20* (14), 3874-3886.
2. Shaw, M. H.; Twilton, J.; MacMillan, D. W. C., Photoredox Catalysis in Organic Chemistry. *The Journal of Organic Chemistry* **2016,** *81* (16), 6898-6926.
3. Prier, C. K.; Rankic, D. A.; MacMillan, D. W. C., Visible Light Photoredox Catalysis with Transition Metal Complexes: Applications in Organic Synthesis. *Chemical Reviews* **2013,** *113* (7), 5322-5363.
4. Romero, N. A.; Nicewicz, D. A., Organic Photoredox Catalysis. *Chemical Reviews* **2016,** *116* (17), 10075-10166.
5. Corrigan, N.; Shanmugam, S.; Xu, J.; Boyer, C., Photocatalysis in organic and polymer synthesis. *Chemical Society Reviews* **2016,** *45* (22), 6165-6212.
6. Cauwenbergh, R.; Das, S., Photocatalysis: A Green Tool for Redox Reactions. *Synlett* **2021,** (YIW), 129-149.
7. Creutz, C.; Sutin, N., Reaction of tris(bipyridine)ruthenium(III) with hydroxide and its application in a solar energy storage system. *Proceedings of the National Academy of Sciences* **1975,** *72* (8), 2858.
8. Kalyanasundaram, K.; Kiwi, J.; Grätzel, M., Hydrogen Evolution from Water by Visible Light, a Homogeneous Three Component Test System for Redox Catalysis. *Helvetica Chimica Acta* **1978,** *61* (7), 2720-2730.
9. Kiwi, J.; Graetzel, M., Projection, size factors, and reaction dynamics of colloidal redox catalysts mediating light induced hydrogen evolution from water. *Journal of the American Chemical Society* **1979,** *101* (24), 7214-7217.
10. Nicewicz, D. A.; MacMillan, D. W. C., Merging Photoredox Catalysis with Organocatalysis: The Direct Asymmetric Alkylation of Aldehydes. *Science* **2008,** *322* (5898), 77.
11. Ischay, M. A.; Anzovino, M. E.; Du, J.; Yoon, T. P., Efficient Visible Light Photocatalysis of [2+2] Enone Cycloadditions. *Journal of the American Chemical Society* **2008,** *130* (39), 12886-12887.
12. Narayanam, J. M. R.; Tucker, J. W.; Stephenson, C. R. J., Electron-Transfer Photoredox Catalysis: Development of a Tin-Free Reductive Dehalogenation Reaction. *Journal of the American Chemical Society* **2009,** *131* (25), 8756-8757.
13. Fukuzumi, S.; Jung, J.; Lee, Y.-M.; Nam, W., Effects of Lewis Acids on Photoredox Catalysis. *Asian Journal of Organic Chemistry* **2017,** *6* (4), 397-409.
14. Twilton, J.; Le, C.; Zhang, P.; Shaw, M. H.; Evans, R. W.; MacMillan, D. W. C., The merger of transition metal and photocatalysis. *Nature Reviews Chemistry* **2017,** *1* (7), 0052.
15. Silvi, M.; Melchiorre, P., Enhancing the potential of enantioselective organocatalysis with light. *Nature* **2018,** *554* (7690), 41-49.
16. Tucker, J. W.; Nguyen, J. D.; Narayanam, J. M. R.; Krabbe, S. W.; Stephenson, C. R. J., Tin-free radical cyclization reactions initiated by visible light photoredox catalysis. *Chemical Communications* **2010,** *46* (27), 4985-4987.
17. Arias-Rotondo, D. M.; McCusker, J. K., The photophysics of photoredox catalysis: a roadmap for catalyst design. *Chemical Society Reviews* **2016,** *45* (21), 5803-5820.
18. Arias-Rotondo, D. M.; McCusker, J. K., An Overview of the Physical and Photophysical Properties of $[Ru(bpy)_3]^{2+}$. In *Visible Light Photocatalysis in Organic Chemistry*, 2018; pp 1-24.
19. Balzani, V.; Ceroni, P.; Credi, A.; Venturi, M., Ruthenium tris(bipyridine) complexes: Interchange between photons and electrons in molecular-scale devices and machines. *Coordination Chemistry Reviews* **2021,** *433*, 213758.
20. Juris, A.; Balzani, V.; Barigelletti, F.; Campagna, S.; Belser, P.; von Zelewsky, A., Ru(II) polypyridine complexes: photophysics, photochemistry, eletrochemistry, and chemiluminescence. *Coordination Chemistry Reviews* **1988,** *84*, 85-277.
21. Campagna, S.; Puntoriero, F.; Nastasi, F.; Bergamini, G.; Balzani, V., Photochemistry and Photophysics of Coordination Compounds: Ruthenium. In *Photochemistry and Photophysics of Coordination Compounds I*, Balzani, V.; Campagna, S., Eds. Springer Berlin Heidelberg: Berlin, Heidelberg, 2007; pp 117-214.
22. David, W. T.; Akitaka, I.; Thomas, J. M., $[Ru(bpy)_3]^{2+*}$ and other remarkable metal-to-ligand charge transfer (MLCT) excited states. *Pure and Applied Chemistry* **2013,** *85* (7), 1257-1305.

23. Kalyanasundaram, K., Photophysics, photochemistry and solar energy conversion with tris(bipyridyl)ruthenium(II) and its analogues. *Coordination Chemistry Reviews* **1982,** *46*, 159-244.
24. Riedel, J., 3 Komplex-/ Koordinationschemie. 2012.
25. Klassen, D. M.; Crosby, G. A., Spectroscopic Studies of Ruthenium(II) Complexes. Assignment of the Luminescence. *The Journal of Chemical Physics* **1968,** *48* (4), 1853-1858.
26. Kober, E. M.; Meyer, T. J., Concerning the absorption spectra of the ions $M(bpy)_3^{2+}$ (M = Fe, Ru, Os; bpy = 2,2'-bipyridine). *Inorganic Chemistry* **1982,** *21* (11), 3967-3977.
27. Lytle, F. E.; Hercules, D. M., Luminescence of tris(2,2'-bipyridine)ruthenium(II) dichloride. *Journal of the American Chemical Society* **1969,** *91* (2), 253-257.
28. Scattergood, P. A.; Elliott, P. I. P., An unexpected journey from highly tunable phosphorescence to novel photochemistry of 1,2,3-triazole-based complexes. *Dalton Transactions* **2017,** *46* (47), 16343-16356.
29. Soupart, A.; Alary, F.; Heully, J.-L.; Elliott, P. I. P.; Dixon, I. M., Recent progress in ligand photorelease reaction mechanisms: Theoretical insights focusing on Ru(II) ^{3}MC states. *Coordination Chemistry Reviews* **2020,** *408*, 213184.
30. Weber, B., Lumineszenz bei Komplexen. In *Koordinationschemie: Grundlagen und aktuelle Trends*, Weber, B., Ed. Springer Berlin Heidelberg: Berlin, Heidelberg, 2021; pp 215-232.
31. Knoll, J. D.; Albani, B. A.; Turro, C., New Ru(II) Complexes for Dual Photoreactivity: Ligand Exchange and $^1O_2$ Generation. *Accounts of Chemical Research* **2015,** *48* (8), 2280-2287.
32. Sutin, N.; Creutz, C., Properties and Reactivities of the Luminescent Excited States of Polypyridine Complexes of Ruthenium(II) and Osmium(II). In *Inorganic and Organometallic Photochemistry*, 1978; Vol. 168, pp 1-27.
33. Kandoth, N.; Pérez Hernández, J.; Palomares, E.; Lloret-Fillol, J., Mechanisms of photoredox catalysts: the role of optical spectroscopy. *Sustainable Energy & Fuels* **2021,** *5* (3), 638-665.
34. De Armond, M. K.; Myrick, M. L., The life and times of $[Ru(bpy)_3]^{2+}$: localized orbitals and other strange occurrences. *Accounts of Chemical Research* **1989,** *22* (10), 364-370.
35. Wang, X.-y.; Del Guerzo, A.; Schmehl, R. H., Photophysical behavior of transition metal complexes having interacting ligand localized and metal-to-ligand charge transfer states. *Journal of Photochemistry and Photobiology C: Photochemistry Reviews* **2004,** *5* (1), 55-77.
36. Ardo, S.; Meyer, G. J., Photodriven heterogeneous charge transfer with transition-metal compounds anchored to TiO_2 semiconductor surfaces. *Chemical Society Reviews* **2009,** *38* (1), 115-164.
37. Dallinger, R. F.; Woodruff, W. H., Time-resolved resonance Raman study of the lowest ($d\pi^*$, ^{3}CT) excited state of Tris(2,2'-bipyridine)ruthenium(II). *Journal of the American Chemical Society* **1979,** *101* (15), 4391-4393.
38. Bradley, P. G.; Kress, N.; Hornberger, B. A.; Dallinger, R. F.; Woodruff, W. H., Vibrational spectroscopy of the electronically excited state. 5. Time-resolved resonance Raman study of tris(bipyridine)ruthenium(II) and related complexes. Definitive evidence for the "localized" MLCT state. *Journal of the American Chemical Society* **1981,** *103* (25), 7441-7446.
39. Motten, A. G.; Hanck, K.; DeArmound, M. K., ESR of the reduction products of $[Fe(bpy)_3]^{2+}$ and $[Ru(bpy)_3]^{2+}$. *Chemical Physics Letters* **1981,** *79* (3), 541-546.
40. Heath, G. A.; Yellowlees, L. J.; Braterman, P. S., Ligand-ligand inter-valence charge-transfer absorption in reduced ruthenium(II) bipyridine complexes. *Chemical Physics Letters* **1982,** *92* (6), 646-648.
41. Morris, D. E.; Hanck, K. W.; DeArmond, M. K., Electrochemical and ESR studies of $[Fe(terpy)_2]^{2+}$ and $[Ru(terpy)_2]^{2+}$ and their reduction products. *Journal of Electroanalytical Chemistry and Interfacial Electrochemistry* **1983,** *149* (1), 115-130.
42. Morris, D. E.; Hanck, K. W.; DeArmond, M. K., ESR studies of the redox orbitals in diimine complexes of iron(II) and ruthenium(II). *Journal of the American Chemical Society* **1983,** *105* (10), 3032-3038.
43. Angel, S. M.; DeArmond, M. K.; Donohoe, R. J.; Hanck, K. W.; Wertz, D. W., Resonance Raman spectra of the first three reduction products of tris(bipyridyl)ruthenium(II). *Journal of the American Chemical Society* **1984,** *106* (12), 3688-3689.
44. DeArmond, M. K.; Hanck, K. W.; Wertz, D. W., Spatially ioslated redox orbitals - an update. *Coordination Chemistry Reviews* **1985,** *64*, 65-81.
45. Omberg, K. M.; Schoonover, J. R.; Treadway, J. A.; Leasure, R. M.; Dyer, R. B.; Meyer, T. J., Mid-Infrared Spectrum of [Ru(bpy)3]2+*. *Journal of the American Chemical Society* **1997,** *119* (30), 7013-7018.

46. Yeh, A. T.; Shank, C. V.; McCusker, J. K., Ultrafast Electron Localization Dynamics Following Photo-Induced Charge Transfer. *Science* **2000,** *289* (5481), 935-938.
47. Balzani, V.; Bolletta, F.; Scandola, F.; Ballardini, R., Excited state electron-transfer reactions of transition metal complexes. *Pure and Applied Chemistry* **1979,** *51* (2), 299-311.
48. Tucker, J. W.; Stephenson, C. R. J., Shining Light on Photoredox Catalysis: Theory and Synthetic Applications. *The Journal of Organic Chemistry* **2012,** *77* (4), 1617-1622.
49. Dexter, D. L., A Theory of Sensitized Luminescence in Solids. *The Journal of Chemical Physics* **1953,** *21* (5), 836-850.
50. Förster, T., Transfer Mechanisms of Electronic Excitation Energy. *Radiation Research Supplement* **1960,** *2*, 326-339.
51. Zhang, X.; Rodgers, M. A. J., Energy and Electron Transfer Reactions of the MLCT State of Ruthenium Tris(bipyridyl) with Molecular Oxygen: A Laser Flash Photolysis Study. *The Journal of Physical Chemistry* **1995,** *99* (34), 12797-12803.
52. Abdel-Shafi, A. A.; Beer, P. D.; Mortimer, R. J.; Wilkinson, F., Photosensitized Generation of Singlet Oxygen from (Substituted Bipyridine)ruthenium(II) Complexes. *Helvetica Chimica Acta* **2001,** *84* (9), 2784-2795.
53. Wallentin, C.-J.; Nguyen, J. D.; Finkbeiner, P.; Stephenson, C. R. J., Visible Light-Mediated Atom Transfer Radical Addition via Oxidative and Reductive Quenching of Photocatalysts. *Journal of the American Chemical Society* **2012,** *134* (21), 8875-8884.
54. Roth, H. G.; Romero, N. A.; Nicewicz, D. A., Experimental and Calculated Electrochemical Potentials of Common Organic Molecules for Applications to Single-Electron Redox Chemistry. *Synlett* **2016,** *27* (05), 714-723.
55. Wu, Y.; Kim, D.; Teets, T. S., Photophysical Properties and Redox Potentials of Photosensitizers for Organic Photoredox Transformations. *Synlett* **2021,** *33* (12), 1154-1179.
56. Melchiorre, P.; Crisenza, G. E. M.; Buzzetti, L., Mechanistic Studies in Photocatalysis. *Angew. Chem. Int. Ed.* **2019,** (58), 3730 –3747.
57. Pavlishchuk, V. V.; Addison, A. W., Conversion constants for redox potentials measured versus different reference electrodes in acetonitrile solutions at 25°C. *Inorganica Chimica Acta* **2000,** *298* (1), 97-102.
58. Elgrishi, N.; Rountree, K. J.; McCarthy, B. D.; Rountree, E. S.; Eisenhart, T. T.; Dempsey, J. L., A Practical Beginner's Guide to Cyclic Voltammetry. *Journal of Chemical Education* **2018,** *95* (2), 197-206.
59. Juris, A.; Belser, P.; Barigelletti, F.; Von Zelewsky, A.; Balzani, V., Excited-state properties of ruthenium(II) tris chelate complexes containing the ligands 2,2'-bipyridine (bpy) and dipyrido[3,2-c:2',3'-e]pyridazine (taphen). *Inorganic Chemistry* **1986,** *25* (3), 256-259.
60. Akasheh, T. S.; Jibril, I.; Shraim, A. M., Ligand-metal interactions and excited state properties in ruthenium(II)-diimine complexes. *Inorganica Chimica Acta* **1990,** *175* (2), 171-180.
61. Kawanishi, Y.; Kitamura, N.; Tazuke, S., Dependence of spectroscopic, electrochemical, and excited-state properties of tris chelate ruthenium(II) complexes on ligand structure. *Inorganic Chemistry* **1989,** *28* (15), 2968-2975.
62. Ashford, D. L.; Brennaman, M. K.; Brown, R. J.; Keinan, S.; Concepcion, J. J.; Papanikolas, J. M.; Templeton, J. L.; Meyer, T. J., Varying the Electronic Structure of Surface-Bound Ruthenium(II) Polypyridyl Complexes. *Inorganic Chemistry* **2015,** *54* (2), 460-469.
63. Shalan, H.; Colbert, A.; Nguyen, T. T.; Kato, M.; Cheruzel, L., Correlating the para-Substituent Effects on Ru(II)-Polypyridine Photophysical Properties and on the Corresponding Hybrid P450 BM3 Enzymes Photocatalytic Activity. *Inorganic Chemistry* **2017,** *56* (11), 6558-6564.
64. Ballardini, R.; Varani, G.; Indelli, M. T.; Scandola, F.; Balzani, V., Free energy correlation of rate constants for electron transfer quenching of excited transition metal complexes. *Journal of the American Chemical Society* **1978,** *100* (23), 7219-7223.
65. Bock, C. R.; Connor, J. A.; Gutierrez, A. R.; Meyer, T. J.; Whitten, D. G.; Sullivan, B. P.; Nagle, J. K., Estimation of excited-state redox potentials by electron-transfer quenching. Application of electron-transfer theory to excited-state redox processes. *Journal of the American Chemical Society* **1979,** *101* (17), 4815-4824.
66. Jones, W. E.; Fox, M. A., Determination of Excited-State Redox Potentials by Phase-Modulated Voltammetry. *The Journal of Physical Chemistry* **1994,** *98* (19), 5095-5099.
67. Stevenson, K. L., Oxidation-reduction potentials and Hess' Law. *Journal of Chemical Education* **1976,** *53* (7), 453.

68. Rillema, D. P.; Allen, G.; Meyer, T. J.; Conrad, D., Redox properties of ruthenium(II) tris chelate complexes containing the ligands 2,2'-bipyrazine, 2,2'-bipyridine, and 2,2'-bipyrimidine. *Inorganic Chemistry* **1983,** *22* (11), 1617-1622.
69. Sutin, N.; Creutz, C., Electron-transfer reactions of excited states. *Journal of Chemical Education* **1983,** *60* (10), 809.
70. Ito, A.; Meyer, T. J., The Golden Rule. Application for fun and profit in electron transfer, energy transfer, and excited-state decay. *Physical Chemistry Chemical Physics* **2012,** *14* (40), 13731-13745.
71. Meyer, T. J., Photochemistry of metal coordination complexes: metal to ligand charge transfer excited states. **1986,** *58* (9), 1193-1206.
72. Flamigni, L.; Barbieri, A.; Sabatini, C.; Ventura, B.; Barigelletti, F., Photochemistry and Photophysics of Coordination Compounds: Iridium. In *Photochemistry and Photophysics of Coordination Compounds II*, Balzani, V.; Campagna, S., Eds. Springer Berlin Heidelberg: Berlin, Heidelberg, 2007; pp 143-203.
73. Wagenknecht, P. S.; Ford, P. C., Metal centered ligand field excited states: Their roles in the design and performance of transition metal based photochemical molecular devices. *Coordination Chemistry Reviews* **2011,** *255* (5), 591-616.
74. Englman, R.; Jortner, J., The energy gap law for radiationless transitions in large molecules. *Molecular Physics* **1970,** *18* (2), 145-164.
75. Koike, T.; Akita, M., Visible-light radical reaction designed by Ru- and Ir-based photoredox catalysis. *Inorganic Chemistry Frontiers* **2014,** *1* (8), 562-576.
76. Al-Rawashdeh, N. A. F.; Chatterjee, S.; Krause, J. A.; Connick, W. B., Ruthenium Bis-diimine Complexes with a Chelating Thioether Ligand: Delineating 1,10-Phenanthrolinyl and 2,2′-Bipyridyl Ligand Substituent Effects. *Inorganic Chemistry* **2014,** *53* (1), 294-307.
77. Rozenel, S. S.; Azpilcueta, C. R.; Flores-Leonar, M. M.; Rebolledo-Chávez, J. P. F.; Ortiz-Frade, L.; Amador-Bedolla, C.; Martin, E., Ruthenium tris bipyridine derivatives and their photocatalytic activity in [4+2] cycloadditions. An experimental and DFT study. *Catalysis Today* **2018,** *310*, 2-10.
78. Ashford, D. L.; Glasson, C. R. K.; Norris, M. R.; Concepcion, J. J.; Keinan, S.; Brennaman, M. K.; Templeton, J. L.; Meyer, T. J., Controlling Ground and Excited State Properties through Ligand Changes in Ruthenium Polypyridyl Complexes. *Inorganic Chemistry* **2014,** *53* (11), 5637-5646.
79. Taylor, J. O.; Pižl, M.; Kloz, M.; Rebarz, M.; McCusker, C. E.; McCusker, J. K.; Záliš, S.; Hartl, F.; Vlček, A., Optical and Infrared Spectroelectrochemical Studies of CN-Substituted Bipyridyl Complexes of Ruthenium(II). *Inorganic Chemistry* **2021,** *60* (6), 3514-3523.
80. Wagnière, G. H., Pathways to Homochirality. In *On Chirality and the Universal Asymmetry*, 2007; pp 167-195.
81. Hancu, G.; Modroiu, A., Chiral Switch: Between Therapeutical Benefit and Marketing Strategy. *Pharmaceuticals* **2022,** *15* (2).
82. He, Y., Chiral analysis in drug discovery and development. *Innov Pharm Technol* **2010,** *35*, 18-23.
83. Nguyen, L. A.; He, H.; Pham-Huy, C., Chiral drugs: an overview. *Int J Biomed Sci* **2006,** *2* (2), 85-100.
84. Winkler, C. K.; Schrittwieser, J. H.; Kroutil, W., Power of Biocatalysis for Organic Synthesis. *ACS Central Science* **2021,** *7* (1), 55-71.
85. Agranat, I.; Caner, H.; Caldwell, J., Putting chirality to work: the strategy of chiral switches. *Nature Reviews Drug Discovery* **2002,** *1* (10), 753-768.
86. Caner, H.; Groner, E.; Levy, L.; Agranat, I., Trends in the development of chiral drugs. *Drug Discov Today* **2004,** *9* (3), 105-10.
87. Peepliwala, A.; Bagade, S.; Bonde, C., A Review: Stereochemical consideration and eudismic ratio in chiral drug development. *Journal of Biomedical Sciences and Research* **2010,** *2*.
88. Fischer, E., Einfluss der Konfiguration auf die Wirkung der Enzyme. *Berichte der deutschen chemischen Gesellschaft* **1894,** *27* (3), 2985-2993.
89. Ariëns, E. J., Stereochemistry, a basis for sophisticated nonsense in pharmacokinetics and clinical pharmacology. *European Journal of Clinical Pharmacology* **1984,** *26* (6), 663-668.
90. Lenz, W.; Knapp, K., Die Thalidomid-Embryopathie*. *Dtsch Med Wochenschr* **1962,** *87* (24), 1232-1242.
91. Purser, S.; Moore, P. R.; Swallow, S.; Gouverneur, V., Fluorine in medicinal chemistry. *Chem. Soc. Rev.* **2008,** *37* (2), 320-330.

92. Collins, T. F., History and evolution of reproductive and developmental toxicology guidelines. *Curr Pharm Des* **2006,** *12* (12), 1449-65.
93. Food, U. S.; Administration, D., *FDA's Policy Statement for the Development of New Stereoisomeric Drugs*. Food and Drug Administration: 1992.
94. Agency, E. M., Investigation of chiral active substances. 1994.
95. Murakami, H., From Racemates to Single Enantiomers – Chiral Synthetic Drugs over the last 20 Years. In *Novel Optical Resolution Technologies*, Sakai, K.; Hirayama, N.; Tamura, R., Eds. Springer Berlin Heidelberg: Berlin, Heidelberg, 2007; pp 273-299.
96. Mansfield, P.; Henry, D.; Tonkin, A., Single-enantiomer drugs: elegant science, disappointing effects. *Clin Pharmacokinet* **2004,** *43* (5), 287-90.
97. Eichelbaum, M.; Gross, A. S., Stereochemical aspects of drug action and disposition. In *Advances in drug research*, Elsevier: 1996; Vol. 28, pp 1-64.
98. Kaiser, D. G.; Vangiessen, G. J.; Reischer, R. J.; Wechter, W. J., Isomeric inversion of ibuprofen (*R*)-enantiomer in humans. *J Pharm Sci* **1976,** *65* (2), 269-73.
99. Gladiali, S., Guidelines and methodologies in asymmetric synthesis and catalysis. *Comptes Rendus Chimie* **2007,** *10* (3), 220-231.
100. Flack, H. D., Louis Pasteur's discovery of molecular chirality and spontaneous resolution in 1848, together with a complete review of his crystallographic and chemical work. *Acta Crystallogr A* **2009,** *65* (Pt 5), 371-89.
101. Okamoto, Y.; Yashima, E., Polysaccharide Derivatives for Chromatographic Separation of Enantiomers. *Angewandte Chemie International Edition* **1998,** *37* (8), 1020-1043.
102. Kagan, H. B.; Fiaud, J. C., Kinetic Resolution. In *Topics in Stereochemistry*, 1988; pp 249-330.
103. Ward, R. S., Dynamic kinetic resolution. *Tetrahedron: Asymmetry* **1995,** *6* (7), 1475-1490.
104. Maier, N. M.; Franco, P.; Lindner, W., Separation of enantiomers: needs, challenges, perspectives. *Journal of Chromatography A* **2001,** *906* (1), 3-33.
105. Lichtenthaler, F. W., Emil Fischer's Proof of the Configuration of Sugars: A Centennial Tribute. *Angewandte Chemie International Edition in English* **1992,** *31* (12), 1541-1556.
106. Kagan, H. B.; Gopalaiah, K., Early history of asymmetric synthesis: who are the scientists who set up the basic principles and the first experiments? *New Journal of Chemistry* **2011,** *35* (10), 1933-1937.
107. Diaz-Muñoz, G.; Miranda, I. L.; Sartori, S. K.; de Rezende, D. C.; Alves Nogueira Diaz, M., Use of chiral auxiliaries in the asymmetric synthesis of biologically active compounds: A review. *Chirality* **2019,** *31* (10), 776-812.
108. Nozaki, H.; Moriuti, S.; Takaya, H.; Noyori, R., Asymmetric induction in carbenoid reaction by means of a dissymmetric copper chelate. *Tetrahedron Letters* **1966,** *7* (43), 5239-5244.
109. Knowles, W. S., Asymmetric Hydrogenations (Nobel Lecture). *Angewandte Chemie International Edition* **2002,** *41* (12), 1998-2007.
110. Noyori, R., Asymmetric Catalysis: Science and Opportunities (Nobel Lecture). *Angewandte Chemie International Edition* **2002,** *41* (12), 2008-2022.
111. Sharpless, K. B., Searching for New Reactivity (Nobel Lecture). *Angewandte Chemie International Edition* **2002,** *41* (12), 2024-2032.
112. Noyori, R., Centenary Lecture. Chemical multiplication of chirality: science and applications. *Chemical Society Reviews* **1989,** *18* (0), 187-208.
113. Arnold, F. H., Innovation by Evolution: Bringing New Chemistry to Life (Nobel Lecture). *Angewandte Chemie International Edition* **2019,** *58* (41), 14420-14426.
114. Hargittai, I., The 2021 chemistry Nobel laureates and asymmetric organocatalysis. *Structural Chemistry* **2022,** *33* (1), 303-305.
115. Walsh, P. J., Principles of Catalysis. In *Organotransition Metal Chemistry: From Bonding to Catalysis*, Hartwig, J. F., Ed. 2009.
116. Knowles, W. S.; Sabacky, M. J., Catalytic asymmetric hydrogenation employing a soluble, optically active, rhodium complex. *Chemical Communications (London)* **1968,** (22), 1445-1446.
117. Knowles, W. S.; Sabacky, M. J.; Vineyard, B. D., Catalytic asymmetric hydrogenation. *Journal of the Chemical Society, Chemical Communications* **1972,** (1), 10-11.

118. Knowles, W. S.; Sabacky, M. J.; Vineyard, B. D. Verfahren zur Herstellung von 3-(3,4-Dihydroxyphenyl)-L-alanin. 1972.
119. Kagan, H. B.; Dang, T.-P., Asymmetric catalytic reduction with transition metal complexes. I. Catalytic system of rhodium (I) with (−)-2, 3-0-isopropylidene-2, 3-dihydroxy-1, 4-bis (diphenylphosphino) butane, a new chiral diphosphine. *Journal of the American Chemical Society* **1972,** *94* (18), 6429-6433.
120. Dang, T. P.; Kagan, H. B., The asymmetric synthesis of hydratropic acid and amino-acids by homogeneous catalytic hydrogenation. *Journal of the Chemical Society D: Chemical Communications* **1971,** (10), 481-481.
121. Knowles, W. S.; Sabacky, M. J.; Vineyard, B. D. Asymmetrische Katalyse. DE2456937A1, 1975.
122. Miyashita, A.; Yasuda, A.; Takaya, H.; Toriumi, K.; Ito, T.; Souchi, T.; Noyori, R., Synthesis of 2,2'-bis(diphenylphosphino)-1,1'-binaphthyl (BINAP), an atropisomeric chiral bis(triaryl)phosphine, and its use in the rhodium(I)-catalyzed asymmetric hydrogenation of α-(acylamino)acrylic acids. *Journal of the American Chemical Society* **1980,** *102* (27), 7932-7934.
123. Dylong, D.; Hausoul, P. J. C.; Palkovits, R.; Eisenacher, M., Synthesis of (−)-menthol: Industrial synthesis routes and recent development. *Flavour and Fragrance Journal* **2022,** *37* (4), 195-209.
124. Kumobayashi, H.; Akutagawa, S. Rhodium-phosphine complex 1984.
125. Katsuki, T.; Sharpless, K. B., The first practical method for asymmetric epoxidation. *J. Am. Chem. Soc.* **1980,** *102* (18), 5974-5976.
126. Jacobsen, E. N.; Marko, I.; Mungall, W. S.; Schroeder, G.; Sharpless, K. B., Asymmetric dihydroxylation via ligand-accelerated catalysis. *Journal of the American Chemical Society* **1988,** *110* (6), 1968-1970.
127. Trost, B. M., Asymmetric catalysis: An enabling science. *Proceedings of the National Academy of Sciences* **2004,** *101* (15), 5348-5355.
128. Zhang, W.; Loebach, J. L.; Wilson, S. R.; Jacobsen, E. N., Enantioselective epoxidation of unfunctionalized olefins catalyzed by salen manganese complexes. *Journal of the American Chemical Society* **1990,** *112* (7), 2801-2803.
129. Irie, R.; Noda, K.; Ito, Y.; Matsumoto, N.; Katsuki, T., Catalytic asymmetric epoxidation of unfunctionalized olefins. *Tetrahedron Letters* **1990,** *31* (50), 7345-7348.
130. Fritschi, H.; Leutenegger, U.; Pfaltz, A., Chiral Copper-Semicorrin Complexes as Enantioselective Catalysts for the Cyclopropanation of Olefins by Diazo Compounds. *Angewandte Chemie International Edition in English* **1986,** *25* (11), 1005-1006.
131. Fritschi, H.; Leutenegger, U.; Pfaltz, A., Semicorrin metal complexes as enantioselective catalysts. Part 2. Enantioselective cyclopropane formation from olefins with diazo compounds catalyzed by chiral (semicorrinato)copper complexes. *Helvetica Chimica Acta* **1988,** *71* (6), 1553-1565.
132. Lowenthal, R. E.; Abiko, A.; Masamune, S., Asymmetric catalytic cyclopropanation of olefins: bis-oxazoline copper complexes. *Tetrahedron Letters* **1990,** *31* (42), 6005-6008.
133. Evans, D. A.; Woerpel, K. A.; Hinman, M. M.; Faul, M. M., Bis(oxazolines) as chiral ligands in metal-catalyzed asymmetric reactions. Catalytic, asymmetric cyclopropanation of olefins. *Journal of the American Chemical Society* **1991,** *113* (2), 726-728.
134. Nishiyama, H.; Kondo, M.; Nakamura, T.; Itoh, K., Highly enantioselective hydrosilylation of ketones with chiral and C2-symmetrical bis(oxazolinyl)pyridine-rhodium catalysts. *Organometallics* **1991,** *10* (2), 500-508.
135. Evans, D. A.; Murry, J. A.; Kozlowski, M. C., C2-Symmetric Copper(II) Complexes as Chiral Lewis Acids. Catalytic Enantioselective Aldol Additions of Silylketene Acetals to (Benzyloxy)acetaldehyde. *Journal of the American Chemical Society* **1996,** *118* (24), 5814-5815.
136. Evans, D. A.; Barnes, D. M.; Johnson, J. S.; Lectka, T.; von Matt, P.; Miller, S. J.; Murry, J. A.; Norcross, R. D.; Shaughnessy, E. A.; Campos, K. R., Bis(oxazoline) and Bis(oxazolinyl)pyridine Copper Complexes as Enantioselective Diels−Alder Catalysts: Reaction Scope and Synthetic Applications. *Journal of the American Chemical Society* **1999,** *121* (33), 7582-7594.
137. Mikami, K.; Lautens, M., *New frontiers in asymmetric catalysis.* John Wiley & Sons: 2007.
138. Takahashi, H.; Achiwa, K., Efficient Asymmetric Hydrogenations of (Z)-2-Acetamidoacrylic Acid Derivatives with the Cationic Rhodium Complex of (2*S*,4*S*)-MOD-BPPM. *Chemistry Letters* **1989,** *18* (2), 305-308.
139. Inoguchi, K.; Sakuraba, S.; Achiwa, K., Design Concepts for Developing Highly Efficient Chiral Bisphosphine Ligands in Rhodium-Catalyzed Asymmetric Hydrogenations. *Synlett* **1992,** *1992* (03), 169-178.

140. Morimoto, T.; Chiba, M.; Achiwa, K., Synthesis of Efficient Chiral Bisphosphine Ligands, Modified DIOPs, (4*R*, 5*R*)-4-(Diaryl- or dialkylphosphino)methyl-5-(diarylphosphino)methyl-2, 2-dimethyl-1, 3-dioxolanes, and Their Use in Rhodium(I)-Catalyzed Asymmetric Hydrogenations. *chemical pharmaceutical bulletin* **1993,** *41* (6), 1149-1156.
141. Pfaltz, A.; Drury, W. J., Design of chiral ligands for asymmetric catalysis: from C2-symmetric *P,P*- and *N,N*-ligands to sterically and electronically nonsymmetrical *P,N*-ligands. *Proceedings of the National Academy of Sciences of the United States of America* **2004,** *101* (16), 5723-5726.
142. Dawson, G. J.; Frost, C. G.; Williams, J. M. J.; Coote, S. J., Asymmetric palladium catalysed allylic substitution using phosphorus containing oxazoline ligands. *Tetrahedron Letters* **1993,** *34* (19), 3149-3150.
143. Sprinz, J.; Helmchen, G., Phosphinoaryl- and phosphinoalkyloxazolines as new chiral ligands for enantioselective catalysis: Very high enantioselectivity in palladium catalyzed allylic substitutions. *Tetrahedron Letters* **1993,** *34* (11), 1769-1772.
144. von Matt, P.; Pfaltz, A., Chiral Phosphinoaryldihydrooxazoles as Ligands in Asymmetric Catalysis: Pd-Catalyzed Allylic Substitution. *Angewandte Chemie International Edition in English* **1993,** *32* (4), 566-568.
145. Yoon, T. P.; Jacobsen, E. N., Privileged Chiral Catalysts. *Science* **2003,** *299* (5613), 1691-1693.
146. Ahrendt, K. A.; Borths, C. J.; MacMillan, D. W. C., New Strategies for Organic Catalysis: The First Highly Enantioselective Organocatalytic Diels–Alder Reaction. *Journal of the American Chemical Society* **2000,** *122* (17), 4243-4244.
147. List, B.; Lerner, R. A.; Barbas, C. F., Proline-Catalyzed Direct Asymmetric Aldol Reactions. *Journal of the American Chemical Society* **2000,** *122* (10), 2395-2396.
148. Bulger, P. G., 9.10 Industrial Applications of Organocatalysis. In *Comprehensive Chirality*, Carreira, E. M.; Yamamoto, H., Eds. Elsevier: Amsterdam, 2012; pp 228-252.
149. Barbas III, C. F., Organocatalysis Lost: Modern Chemistry, Ancient Chemistry, and an Unseen Biosynthetic Apparatus. *Angewandte Chemie International Edition* **2008,** *47* (1), 42-47.
150. Hajos, Z. G.; Parrish, D. R., Asymmetric synthesis of bicyclic intermediates of natural product chemistry. *The Journal of Organic Chemistry* **1974,** *39* (12), 1615-1621.
151. Eder, U.; Sauer, G.; Wiechert, R., New Type of Asymmetric Cyclization to Optically Active Steroid CD Partial Structures. *Angewandte Chemie International Edition in English* **1971,** *10* (7), 496-497.
152. Hayashi, Y., Asymmetric enamine and iminium ion catalysis. In *Catalytic Asymmetric Synthesis*, 2022; pp 1-28.
153. Akiyama, T., Asymmetric acid organocatalysis. In *Catalytic Asymmetric Synthesis*, 2022; pp 29-80.
154. Kondoh, A.; Terada, M., Asymmetric Base Organocatalysis. In *Catalytic Asymmetric Synthesis*, 2022; pp 81-115.
155. MacMillan, D. W. C., The advent and development of organocatalysis. *Nature* **2008,** *455* (7211), 304-308.
156. Heckmann, C. M.; Paradisi, F., Looking Back: A Short History of the Discovery of Enzymes and How They Became Powerful Chemical Tools. *ChemCatChem* **2020,** *12* (24), 6082-6102.
157. Maicas, S., The Role of Yeasts in Fermentation Processes. *Microorganisms* **2020,** *8* (8), 1142.
158. Rehm, H.-J., Glycerin. In *Industrielle Mikrobiologie*, Rehm, H.-J., Ed. Springer Berlin Heidelberg: Berlin, Heidelberg, 1967; pp 287-294.
159. Wang, Z.; Zhuge, J.; Fang, H.; Prior, B. A., Glycerol production by microbial fermentation: A review. *Biotechnology Advances* **2001,** *19* (3), 201-223.
160. Neuberg, C.; Hirsch, J., Über ein Kohlenstoffketten knüpfendes Ferment (Carboligase). *Biochemische Zeitung* **1921,** *115*, 282 - 310.
161. Hilderbrandt, G.; Mann, W. Manufacture of Laevo-1-phenyl-2-methylaminopropanol-1. 1934.
162. Hughes, G.; Lewis, J. C., Introduction: Biocatalysis in Industry. *Chemical Reviews* **2018,** *118* (1), 1-3.
163. Reichstein, T.; Grüssner, A.; Oppenauer, R., Die Synthese der D-Ascorbinsäure (D-Form des C-Vitamins). *Helvetica Chimica Acta* **1933,** *16* (1), 561-565.
164. Reichstein, T.; Grüssner, A., Eine ergiebige Synthese der L-Ascorbinsäure (C-Vitamin). *Helvetica Chimica Acta* **1934,** *17* (1), 311-328.
165. Sanger, F., The Chemistry of Insulin. *Nobel Lectures, Chemistry 1942-1962* **1958**, 544.
166. Kendrew, J. C., Myoglobin and the structure of proteins. *Nobel Lecture* **1962**.
167. Perutz, M. F., X-ray Analysis of Haemoglobin. *Nobel Lecture* **1962**.

168. Reetz, M. T., Laboratory Evolution of Stereoselective Enzymes: A Prolific Source of Catalysts for Asymmetric Reactions. *Angewandte Chemie International Edition* **2011,** *50* (1), 138-174.
169. Bornscheuer, U. T.; Huisman, G. W.; Kazlauskas, R. J.; Lutz, S.; Moore, J. C.; Robins, K., Engineering the third wave of biocatalysis. *Nature* **2012,** *485* (7397), 185-194.
170. Devine, P. N.; Howard, R. M.; Kumar, R.; Thompson, M. P.; Truppo, M. D.; Turner, N. J., Extending the application of biocatalysis to meet the challenges of drug development. *Nature Reviews Chemistry* **2018,** *2* (12), 409-421.
171. Chen, K.; Arnold, F. H., Engineering new catalytic activities in enzymes. *Nature Catalysis* **2020,** *3* (3), 203-213.
172. Sheldon, R. A.; Brady, D.; Bode, M. L., The Hitchhiker's guide to biocatalysis: recent advances in the use of enzymes in organic synthesis. *Chemical Science* **2020,** *11* (10), 2587-2605.
173. Bell, E. L.; Finnigan, W.; France, S. P.; Green, A. P.; Hayes, M. A.; Hepworth, L. J.; Lovelock, S. L.; Niikura, H.; Osuna, S.; Romero, E.; Ryan, K. S.; Turner, N. J.; Flitsch, S. L., Biocatalysis. *Nature Reviews Methods Primers* **2021,** *1* (1), 46.
174. Sciences, T. R. S. A. o., A (r)evolution in chemistry. KVA: 2018.
175. Anastas, P. T.; Warner, J. C., *Green chemistry: theory and practice* Oxford University Press: New York, 1998.
176. Emmanuel, M. A.; Greenberg, N. R.; Oblinsky, D. G.; Hyster, T. K., Accessing non-natural reactivity by irradiating nicotinamide-dependent enzymes with light. *Nature* **2016,** *540* (7633), 414-417.
177. Biegasiewicz, K. F.; Cooper, S. J.; Emmanuel, M. A.; Miller, D. C.; Hyster, T. K., Catalytic promiscuity enabled by photoredox catalysis in nicotinamide-dependent oxidoreductases. *Nature Chemistry* **2018,** *10* (7), 770-775.
178. Biegasiewicz, K. F.; Cooper, S. J.; Gao, X.; Oblinsky, D. G.; Kim, J. H.; Garfinkle, S. E.; Joyce, L. A.; Sandoval, B. A.; Scholes, G. D.; Hyster, T. K., Photoexcitation of flavoenzymes enables a stereoselective radical cyclization. *Science* **2019,** *364* (6446), 1166-1169.
179. Black, M. J.; Biegasiewicz, K. F.; Meichan, A. J.; Oblinsky, D. G.; Kudisch, B.; Scholes, G. D.; Hyster, T. K., Asymmetric redox-neutral radical cyclization catalysed by flavin-dependent 'ene'-reductases. *Nature Chemistry* **2020,** *12* (1), 71-75.
180. Huang, X.; Wang, B.; Wang, Y.; Jiang, G.; Feng, J.; Zhao, H., Photoenzymatic enantioselective intermolecular radical hydroalkylation. *Nature* **2020,** *584* (7819), 69-74.
181. Nakano, Y.; Black, M. J.; Meichan, A. J.; Sandoval, B. A.; Chung, M. M.; Biegasiewicz, K. F.; Zhu, T.; Hyster, T. K., Photoenzymatic Hydrogenation of Heteroaromatic Olefins Using 'Ene'-Reductases with Photoredox Catalysts. *Angewandte Chemie International Edition* **2020,** *59* (26), 10484-10488.
182. Schwochert, T. D.; Cruz, C. L.; Watters, J. W.; Reynolds, E. W.; Nicewicz, D. A.; Brustad, E. M., Design and Evaluation of Artificial Hybrid Photoredox Biocatalysts. *ChemBioChem* **2020,** *21* (21), 3146-3150.
183. Millet, A.; Cesana, P. T.; Sedillo, K.; Bird, M. J.; Schlau-Cohen, G. S.; Doyle, A. G.; MacMillan, D. W. C.; Scholes, G. D., Bioinspired Supercharging of Photoredox Catalysis for Applications in Energy and Chemical Manufacturing. *Accounts of Chemical Research* **2022,** *55* (10), 1423-1434.
184. Guo, X.; Okamoto, Y.; Schreier, M. R.; Ward, T. R.; Wenger, O. S., Enantioselective synthesis of amines by combining photoredox and enzymatic catalysis in a cyclic reaction network. *Chemical Science* **2018,** *9* (22), 5052-5056.
185. He, Y.-H.; Xiang, Y.; Yang, D.-C.; Guan, Z., Combining enzyme and photoredox catalysis for aminoalkylation of indoles via a relay catalysis strategy in one pot. *Green Chemistry* **2016,** *18* (19), 5325-5330.
186. Pitre, S. P.; Overman, L. E., Strategic Use of Visible-Light Photoredox Catalysis in Natural Product Synthesis. *Chemical Reviews* **2022,** *122* (2), 1717-1751.
187. Lyu, J.; Claraz, A.; Masson, G., Asymmetric Visible-light Photoredox Catalysis. In *Catalytic Asymmetric Synthesis*, 2022; pp 277-327.
188. Prentice, C.; Morrisson, J.; Smith, A. D.; Zysman-Colman, E., Recent developments in enantioselective photocatalysis. *Beilstein Journal of Organic Chemistry* **2020,** *16*, 2363-2441.
189. Nagib, D. A.; Scott, M. E.; MacMillan, D. W. C., Enantioselective α-Trifluoromethylation of Aldehydes via Photoredox Organocatalysis. *Journal of the American Chemical Society* **2009,** *131* (31), 10875-10877.
190. Gualandi, A.; Marchini, M.; Mengozzi, L.; Natali, M.; Lucarini, M.; Ceroni, P.; Cozzi, P. G., Organocatalytic Enantioselective Alkylation of Aldehydes with $[Fe(bpy)_3]Br_2$ Catalyst and Visible Light. *ACS Catalysis* **2015,** *5* (10), 5927-5931.

191. Gualandi, A.; Marchini, M.; Mengozzi, L.; Kidanu, H. T.; Franc, A.; Ceroni, P.; Cozzi, P. G., Aluminum(III) Salen Complexes as Active Photoredox Catalysts. *European Journal of Organic Chemistry* **2020,** *2020* (10), 1486-1490.
192. Neumann, M.; Füldner, S.; König, B.; Zeitler, K., Metal-Free, Cooperative Asymmetric Organophotoredox Catalysis with Visible Light. *Angewandte Chemie International Edition* **2011,** *50* (4), 951-954.
193. Fidaly, K.; Ceballos, C.; Falguières, A.; Veitia, M. S.-I.; Guy, A.; Ferroud, C., Visible light photoredox organocatalysis: a fully transition metal-free direct asymmetric α-alkylation of aldehydes. *Green Chemistry* **2012,** *14* (5), 1293-1297.
194. Zhu, Y.; Zhang, L.; Luo, S., Asymmetric α-Photoalkylation of β-Ketocarbonyls by Primary Amine Catalysis: Facile Access to Acyclic All-Carbon Quaternary Stereocenters. *Journal of the American Chemical Society* **2014,** *136* (42), 14642-14645.
195. Shih, H.-W.; Vander Wal, M. N.; Grange, R. L.; MacMillan, D. W. C., Enantioselective α-Benzylation of Aldehydes via Photoredox Organocatalysis. *Journal of the American Chemical Society* **2010,** *132* (39), 13600-13603.
196. Nacsa, E. D.; MacMillan, D. W. C., Spin-Center Shift-Enabled Direct Enantioselective α-Benzylation of Aldehydes with Alcohols. *Journal of the American Chemical Society* **2018,** *140* (9), 3322-3330.
197. Capacci, A. G.; Malinowski, J. T.; McAlpine, N. J.; Kuhne, J.; MacMillan, D. W. C., Direct, enantioselective α-alkylation of aldehydes using simple olefins. *Nature Chemistry* **2017,** *9* (11), 1073-1077.
198. Murphy, J. J.; Bastida, D.; Paria, S.; Fagnoni, M.; Melchiorre, P., Asymmetric catalytic formation of quaternary carbons by iminium ion trapping of radicals. *Nature* **2016,** *532* (7598), 218-222.
199. Zhao, J.-J.; Zhang, H.-H.; Shen, X.; Yu, S., Enantioselective Radical Hydroacylation of Enals with α-Ketoacids Enabled by Photoredox/Amine Cocatalysis. *Organic Letters* **2019,** *21* (4), 913-916.
200. Lin, L.; Bai, X.; Ye, X.; Zhao, X.; Tan, C.-H.; Jiang, Z., Organocatalytic Enantioselective Protonation for Photoreduction of Activated Ketones and Ketimines Induced by Visible Light. *Angewandte Chemie International Edition* **2017,** *56* (44), 13842-13846.
201. Roos, C. B.; Demaerel, J.; Graff, D. E.; Knowles, R. R., Enantioselective Hydroamination of Alkenes with Sulfonamides Enabled by Proton-Coupled Electron Transfer. *Journal of the American Chemical Society* **2020,** *142* (13), 5974-5979.
202. Li, J.; Kong, M.; Qiao, B.; Lee, R.; Zhao, X.; Jiang, Z., Formal enantioconvergent substitution of alkyl halides via catalytic asymmetric photoredox radical coupling. *Nature Communications* **2018,** *9* (1), 2445.
203. Ruiz Espelt, L.; McPherson, I. S.; Wiensch, E. M.; Yoon, T. P., Enantioselective Conjugate Additions of α-Amino Radicals via Cooperative Photoredox and Lewis Acid Catalysis. *Journal of the American Chemical Society* **2015,** *137* (7), 2452-2455.
204. Pagire, S. K.; Kumagai, N.; Shibasaki, M., Introduction of a 7-aza-6-MeO-indoline auxiliary in Lewis-acid/photoredox cooperative catalysis: highly enantioselective aminomethylation of α,β-unsaturated amides. *Chemical Science* **2020,** *11* (20), 5168-5174.
205. Huo, H.; Harms, K.; Meggers, E., Catalytic, Enantioselective Addition of Alkyl Radicals to Alkenes via Visible-Light-Activated Photoredox Catalysis with a Chiral Rhodium Complex. *Journal of the American Chemical Society* **2016,** *138* (22), 6936-6939.
206. Zhang, K.; Lu, L.-Q.; Jia, Y.; Wang, Y.; Lu, F.-D.; Pan, F.; Xiao, W.-J., Exploration of a Chiral Cobalt Catalyst for Visible-Light-Induced Enantioselective Radical Conjugate Addition. *Angewandte Chemie International Edition* **2019,** *58* (38), 13375-13379.
207. de Assis, F. F.; Huang, X.; Akiyama, M.; Pilli, R. A.; Meggers, E., Visible-Light-Activated Catalytic Enantioselective β-Alkylation of α,β-Unsaturated 2-Acyl Imidazoles Using Hantzsch Esters as Radical Reservoirs. *The Journal of Organic Chemistry* **2018,** *83* (18), 10922-10932.
208. Yuan, W.; Zhou, Z.; Gong, L.; Meggers, E., Asymmetric alkylation of remote C(sp^3)–H bonds by combining proton-coupled electron transfer with chiral Lewis acid catalysis. *Chemical Communications* **2017,** *53* (64), 8964-8967.
209. Ma, J.; Harms, K.; Meggers, E., Enantioselective rhodium/ruthenium photoredox catalysis en route to chiral 1,2-aminoalcohols. *Chemical Communications* **2016,** *52* (66), 10183-10186.
210. Du, J.; Yoon, T. P., Crossed Intermolecular [2+2] Cycloadditions of Acyclic Enones via Visible Light Photocatalysis. *Journal of the American Chemical Society* **2009,** *131* (41), 14604-14605.

211. Du, J.; Skubi Kazimer, L.; Schultz Danielle, M.; Yoon Tehshik, P., A Dual-Catalysis Approach to Enantioselective [2 + 2] Photocycloadditions Using Visible Light. *Science* **2014,** *344* (6182), 392-396.
212. Lu, Z.; Shen, M.; Yoon, T. P., [3+2] Cycloadditions of Aryl Cyclopropyl Ketones by Visible Light Photocatalysis. *Journal of the American Chemical Society* **2011,** *133* (5), 1162-1164.
213. Amador, A. G.; Sherbrook, E. M.; Yoon, T. P., Enantioselective Photocatalytic [3 + 2] Cycloadditions of Aryl Cyclopropyl Ketones. *Journal of the American Chemical Society* **2016,** *138* (14), 4722-4725.
214. Huang, X.; Webster, R. D.; Harms, K.; Meggers, E., Asymmetric Catalysis with Organic Azides and Diazo Compounds Initiated by Photoinduced Electron Transfer. *Journal of the American Chemical Society* **2016,** *138* (38), 12636-12642.
215. Schmermund, L.; Jurkaš, V.; Özgen, F. F.; Barone, G. D.; Büchsenschütz, H. C.; Winkler, C. K.; Schmidt, S.; Kourist, R.; Kroutil, W., Photo-Biocatalysis: Biotransformations in the Presence of Light. *ACS Catalysis* **2019,** *9* (5), 4115-4144.
216. Sandoval, B. A.; Hyster, T. K., Emerging strategies for expanding the toolbox of enzymes in biocatalysis. *Current Opinion in Chemical Biology* **2020,** *55*, 45-51.
217. Bauer, A.; Westkämper, F.; Grimme, S.; Bach, T., Catalytic enantioselective reactions driven by photoinduced electron transfer. *Nature* **2005,** *436* (7054), 1139-1140.
218. Alonso, R.; Bach, T., A Chiral Thioxanthone as an Organocatalyst for Enantioselective [2+2] Photocycloaddition Reactions Induced by Visible Light. *Angewandte Chemie International Edition* **2014,** *53* (17), 4368-4371.
219. Tröster, A.; Alonso, R.; Bauer, A.; Bach, T., Enantioselective Intermolecular [2 + 2] Photocycloaddition Reactions of 2(1*H*)-Quinolones Induced by Visible Light Irradiation. *Journal of the American Chemical Society* **2016,** *138* (25), 7808-7811.
220. Mayr, F.; Mohr, L.-M.; Rodriguez, E.; Bach, T., Synthesis of Chiral Thiourea-Thioxanthone Hybrids. *Synthesis* **2017,** *49* (23), 5238-5250.
221. Pecho, F.; Zou, Y.-Q.; Gramüller, J.; Mori, T.; Huber, S. M.; Bauer, A.; Gschwind, R. M.; Bach, T., A Thioxanthone Sensitizer with a Chiral Phosphoric Acid Binding Site: Properties and Applications in Visible Light-Mediated Cycloadditions. *Chemistry – A European Journal* **2020,** *26* (23), 5190-5194.
222. Rigotti, T.; Casado-Sánchez, A.; Cabrera, S.; Pérez-Ruiz, R.; Liras, M.; de la Peña O'Shea, V. A.; Alemán, J., A Bifunctional Photoaminocatalyst for the Alkylation of Aldehydes: Design, Analysis, and Mechanistic Studies. *ACS Catalysis* **2018,** *8* (7), 5928-5940.
223. Yang, Z.; Li, H.; Li, S.; Zhang, M.-T.; Luo, S., A chiral ion-pair photoredox organocatalyst: enantioselective anti-Markovnikov hydroetherification of alkenols. *Organic Chemistry Frontiers* **2017,** *4* (6), 1037-1041.
224. Morse, P. D.; Nguyen, T. M.; Cruz, C. L.; Nicewicz, D. A., Enantioselective counter-anions in photoredox catalysis: The asymmetric cation radical Diels-Alder reaction. *Tetrahedron* **2018,** *74* (26), 3266-3272.
225. Uraguchi, D.; Kimura, Y.; Ueoka, F.; Ooi, T., Urea as a Redox-Active Directing Group under Asymmetric Photocatalysis of Iridium-Chiral Borate Ion Pairs. *Journal of the American Chemical Society* **2020,** *142* (46), 19462-19467.
226. Wang, C.; Chen, L.-A.; Huo, H.; Shen, X.; Harms, K.; Gong, L.; Meggers, E., Asymmetric Lewis acid catalysis directed by octahedral rhodium centrochirality. *Chemical Science* **2015,** *6* (2), 1094-1100.
227. Huo, H.; Fu, C.; Harms, K.; Meggers, E., Asymmetric Catalysis with Substitutionally Labile yet Stereochemically Stable Chiral-at-Metal Iridium(III) Complex. *Journal of the American Chemical Society* **2014,** *136* (8), 2990-2993.
228. Zhou, Z.; Li, Y.; Han, B.; Gong, L.; Meggers, E., Enantioselective catalytic β-amination through proton-coupled electron transfer followed by stereocontrolled radical–radical coupling. *Chemical Science* **2017,** *8* (8), 5757-5763.
229. Huo, H.; Shen, X.; Wang, C.; Zhang, L.; Röse, P.; Chen, L.-A.; Harms, K.; Marsch, M.; Hilt, G.; Meggers, E., Asymmetric photoredox transition-metal catalysis activated by visible light. *Nature* **2014,** *515* (7525), 100-103.
230. Wang, C.; Qin, J.; Shen, X.; Riedel, R.; Harms, K.; Meggers, E., Asymmetric Radical–Radical Cross-Coupling through Visible-Light-Activated Iridium Catalysis. *Angewandte Chemie International Edition* **2016,** *55* (2), 685-688.

231. Huang, X.; Quinn, T. R.; Harms, K.; Webster, R. D.; Zhang, L.; Wiest, O.; Meggers, E., Direct Visible-Light-Excited Asymmetric Lewis Acid Catalysis of Intermolecular [2+2] Photocycloadditions. *Journal of the American Chemical Society* **2017,** *139* (27), 9120-9123.
232. Huo, H.; Wang, C.; Harms, K.; Meggers, E., Enantioselective, Catalytic Trichloromethylation through Visible-Light-Activated Photoredox Catalysis with a Chiral Iridium Complex. *Journal of the American Chemical Society* **2015,** *137* (30), 9551-9554.
233. Huo, H.; Huang, X.; Shen, X.; Harms, K.; Meggers, E., Visible-Light-Activated Enantioselective Perfluoroalkylation with a Chiral Iridium Photoredox Catalyst. *Synlett* **2016,** *27* (05), 749-753.
234. Ma, J.; Rosales, A. R.; Huang, X.; Harms, K.; Riedel, R.; Wiest, O.; Meggers, E., Visible-Light-Activated Asymmetric β-C–H Functionalization of Acceptor-Substituted Ketones with 1,2-Dicarbonyl Compounds. *Journal of the American Chemical Society* **2017,** *139* (48), 17245-17248.
235. Huang, X.; Lin, J.; Shen, T.; Harms, K.; Marchini, M.; Ceroni, P.; Meggers, E., Asymmetric [3+2] Photocycloadditions of Cyclopropanes with Alkenes or Alkynes through Visible-Light Excitation of Catalyst-Bound Substrates. *Angewandte Chemie International Edition* **2018,** *57* (19), 5454-5458.
236. Kainz, Q. M.; Matier, C. D.; Bartoszewicz, A.; Zultanski, S. L.; Peters, J. C.; Fu, G. C., Asymmetric copper-catalyzed C-N cross-couplings induced by visible light. *Science* **2016,** *351* (6274), 681-684.
237. Guo, Q.; Wang, M.; Peng, Q.; Huo, Y.; Liu, Q.; Wang, R.; Xu, Z., Dual-Functional Chiral Cu-Catalyst-Induced Photoredox Asymmetric Cyanofluoroalkylation of Alkenes. *ACS Catalysis* **2019,** *9* (5), 4470-4476.
238. Zhang, Y.; Sun, Y.; Chen, B.; Xu, M.; Li, C.; Zhang, D.; Zhang, G., Copper-Catalyzed Photoinduced Enantioselective Dual Carbofunctionalization of Alkenes. *Organic Letters* **2020,** *22* (4), 1490-1494.
239. Li, Y.; Zhou, K.; Wen, Z.; Cao, S.; Shen, X.; Lei, M.; Gong, L., Copper(II)-Catalyzed Asymmetric Photoredox Reactions: Enantioselective Alkylation of Imines Driven by Visible Light. *Journal of the American Chemical Society* **2018,** *140* (46), 15850-15858.
240. Han, B.; Li, Y.; Yu, Y.; Gong, L., Photocatalytic enantioselective α-aminoalkylation of acyclic imine derivatives by a chiral copper catalyst. *Nature Communications* **2019,** *10* (1), 3804.
241. Zhou, K.; Yu, Y.; Lin, Y.-M.; Li, Y.; Gong, L., Copper-catalyzed aerobic asymmetric cross-dehydrogenative coupling of C(sp3)–H bonds driven by visible light. *Green Chemistry* **2020,** *22* (14), 4597-4603.
242. Shen, X.; Li, Y.; Wen, Z.; Cao, S.; Hou, X.; Gong, L., A chiral nickel DBFOX complex as a bifunctional catalyst for visible-light-promoted asymmetric photoredox reactions. *Chemical Science* **2018,** *9* (20), 4562-4568.
243. Ding, W.; Lu, L.-Q.; Zhou, Q.-Q.; Wei, Y.; Chen, J.-R.; Xiao, W.-J., Bifunctional Photocatalysts for Enantioselective Aerobic Oxidation of β-Ketoesters. *Journal of the American Chemical Society* **2017,** *139* (1), 63-66.
244. Yoon, T. P., Photochemical Stereocontrol Using Tandem Photoredox–Chiral Lewis Acid Catalysis. *Accounts of Chemical Research* **2016,** *49* (10), 2307-2315.
245. Daub, M. E.; Jung, H.; Lee, B. J.; Won, J.; Baik, M.-H.; Yoon, T. P., Enantioselective [2+2] Cycloadditions of Cinnamate Esters: Generalizing Lewis Acid Catalysis of Triplet Energy Transfer. *Journal of the American Chemical Society* **2019,** *141* (24), 9543-9547.
246. Liao, L.-Y.; Kong, X.-R.; Duan, X.-F., Reductive Couplings of 2-Halopyridines without External Ligand: Phosphine-Free Nickel-Catalyzed Synthesis of Symmetrical and Unsymmetrical 2,2′-Bipyridines. *The Journal of Organic Chemistry* **2014,** *79* (2), 777-782.
247. Sasse, W. H. F.; Snieckus, V. A.; Boeckelheide, V., 2,2'-Bipyridine. *Organic Syntheses* **1966,** *46* (5), 5 - 8.
248. Eicher, T.; Hauptmann, S.; Speicher, A., *The chemistry of heterocycles: structures, reactions, synthesis, and applications.* John Wiley & Sons: 2013.
249. Witte, H.; Seeliger, W., Cyclische Imidsäureester aus Nitrilen und Aminoalkoholen. *Justus Liebigs Annalen der Chemie* **1974,** *1974* (6), 996-1009.
250. Bolm, C.; Weickhardt, K.; Zehnder, M.; Ranff, T., Synthesis of Optically Active Bis(2-oxazolines): Crystal Structure of a 1,2-Bis(2-oxazolinyl)benzene $ZnCl_2$ Complex. *Chemische Berichte* **1991,** *124* (5), 1173-1180.
251. Allen, J. V.; Williams, J. M. J., Enantiomerically pure oxazolines tethered to alcohols. Preparation and use in asymmetric catalysis. *Tetrahedron: Asymmetry* **1994,** *5* (2), 277-282.
252. Ghosh, A. K.; Mathivanan, P.; Cappiello, J., C (2)-Symmetric chiral bis(oxazoline)-metal complexes in catalytic asymmetric synthesis. *Tetrahedron Asymmetry* **1998,** *9* (1), 1-45.

253. Corey, E. J.; Imai, N.; Zhang, H. Y., Designed catalyst for enantioselective Diels-Alder addition from a C2-symmetric chiral bis(oxazoline)-iron(III) complex. *Journal of the American Chemical Society* **1991,** *113* (2), 728-729.
254. Müller, D.; Umbricht, G.; Weber, B.; Pfaltz, A., C2-Symmetric 4,4′,5,5′-Tetrahydrobi(oxazoles) and 4,4′,5,5′-Tetrahydro-2,2′-methylenebis[oxazoles] as Chiral Ligands for Enantioselective Catalysis Preliminary Communication. *Helvetica Chimica Acta* **1991,** *74* (1), 232-240.
255. Vorbrüggen, H.; Krolikiewicz, K., A simple synthesis of Δ^2-oxazines, Δ^2-oxazines, Δ^2-thiazolines and 2-substituted benzoxazoles. *Tetrahedron* **1993,** *49* (41), 9353-9372.
256. Denmark, S. E.; Nakajima, N.; Nicaise, O. J. C.; Faucher, A.-M.; Edwards, J. P., Preparation of Chiral Bisoxazolines: Observations on the Effect of Substituents. *The Journal of Organic Chemistry* **1995,** *60* (15), 4884-4892.
257. Chow, H.-F.; Mak, C. C., Dendritic Bis(oxazoline)copper(II) Catalysts. 2.1 Synthesis, Reactivity, and Substrate Selectivity. *The Journal of Organic Chemistry* **1997,** *62* (15), 5116-5127.
258. Evans, D. A.; Peterson, G. S.; Johnson, J. S.; Barnes, D. M.; Campos, K. R.; Woerpel, K. A., An Improved Procedure for the Preparation of 2,2-Bis[2-[4(*S*)- tert-butyl-1,3-oxazolinyl]]propane [(*S*,*S*)-tert-Butylbis(oxazoline)] and Derived Copper(II) Complexes. *The Journal of Organic Chemistry* **1998,** *63* (13), 4541-4544.
259. Corey, E. J.; Ishihara, K., Highly enantioselective catalytic Diels-Alder addition promoted by a chiral bis(oxazoline)-magnesium complex. *Tetrahedron Letters* **1992,** *33* (45), 6807-6810.
260. Wipf, P.; Miller, C. P., An investigation of the mitsunobu reaction in the preparation of peptide oxazolines, thiazolines, and aziridines. *Tetrahedron Letters* **1992,** *33* (42), 6267-6270.
261. Wipf, P.; Miller, C. P., A short, stereospecific synthesis of dihydrooxazoles from serine and threonine derivatives. *Tetrahedron Letters* **1992,** *33* (7), 907-910.
262. Gupta, A. D.; Bhuniya, D.; Singh, V. K., Synthesis of homochiral bis (oxazolinyl) pyridine type ligands for asymmetric cyclopropanation reactions. *Tetrahedron* **1994,** *50* (48), 13725-13730.
263. Pirrung, M. C.; Tumey, L. N., Oxazoline Synthesis from Hydroxyamides by Resin Capture and Ring-Forming Release. *Journal of Combinatorial Chemistry* **2000,** *2* (6), 675-680.
264. Davies, I. W.; Gerena, L.; Lu, N.; Larsen, R. D.; Reider, P. J., Concise Synthesis of Conformationally Constrained Pybox Ligands. *The Journal of Organic Chemistry* **1996,** *61* (26), 9629-9630.
265. Desimoni, G.; Faita, G.; Mella, M., A stereodivergent synthesis of chiral 4,5-disubstituted bis(oxazolines). *Tetrahedron* **1996,** *52* (43), 13649-13654.
266. Zeng, Y.; Zheng, H.-l.; Yang, Z.; Liu, C.-K.; Fang, Z.; Guo, K., Copper(I) Iodide-Catalyzed (Het)arylation of Diethyl Malonate with (Het)aryl Bromides by Using 1,3-Benzoxazole as a Ligand. *Synlett* **2018,** *29* (01), 79-84.
267. Brückner, R., *Reaktionsmechanismen: organische Reaktionen, Stereochemie, moderne Synthesemethoden.* Springer-Verlag: 2014.
268. Ismail, M. M., Synthesis and cyclization reactions of 2-(6-methylquinolin-4-yl)malononitriles and ethyl 2-cyano-2-(6-methylquinolin-4-yl)acetates. *Journal of the Serbian Chemical Society* **2006,** *71* (7), 721 - 732.
269. Matthews, W. S.; Bares, J. E.; Bartmess, J. E.; Bordwell, F. G.; Cornforth, F. J.; Drucker, G. E.; Margolin, Z.; McCallum, R. J.; McCollum, G. J.; Vanier, N. R., Equilibrium acidities of carbon acids. VI. Establishment of an absolute scale of acidities in dimethyl sulfoxide solution. *Journal of the American Chemical Society* **1975,** *97* (24), 7006-7014.
270. Arnett, E. M.; Maroldo, S. G.; Schilling, S. L.; Harrelson, J. A., Ion pairing and reactivity of enolate anions. 5. Thermodynamics of ionization of .beta.-di- and tricarbonyl compounds in dimethyl sulfoxide solution and ion pairing of their alkali salts. *Journal of the American Chemical Society* **1984,** *106* (22), 6759-6767.
271. Meyers, A. I.; Knaus, G.; Kamata, K.; Ford, M. E., Asymmetric synthesis of *R* and *S* α-alkylalkanoic acids from metalation and alkylation of chiral 2-oxazolines. *Journal of the American Chemical Society* **1976,** *98* (2), 567-576.
272. Hall, J.; Lehn, J.-M.; DeCian, A.; Fischer, J., Synthesis and Structure of the Copper(II) Complex of a Chiral Bis(dihydrooxazole) Ligand. *Helvetica Chimica Acta* **1991,** *74* (1), 1-6.
273. Meyers, A. I.; Schmidt, W.; McKennon, M. J., Asymmetric Addition to Chiral Aromatic and Unsaturated Oxazolines Using a Novel Chiral Auxiliary. *Synthesis* **1993,** *1993* (02), 250-262.

274. Atkins, G. M.; Burgess, E. M., The reactions of an *N*-sulfonylamine inner salt. *Journal of the American Chemical Society* **1968,** *90* (17), 4744-4745.
275. Cornejo, A.; Fraile, J. M.; García, J. I.; Gil, M. J.; Martínez-Merino, V.; Mayoral, J. A.; Pires, E.; Villalba, I., An Efficient and General One-Pot Method for the Synthesis of Chiral Bis(oxazoline) and Pyridine Bis(oxazoline) Ligands. *Synlett* **2005,** *2005* (15), 2321-2324.
276. Yaroslavsky, S., Reaction of aryldiazonium salts with dimethylformamide. *Tetrahedron Letters* **1965,** *6* (20), 1503-1507.
277. Lehn, J.-M., Molecular Ribbons from Molecular Recognition directed Self-assembly of Self -complementary Molecular Components. *J. Chem. Soc. Perkin Trans* **1992,** *2*, 461-467.
278. Renaud, P., Regioselective Radical Additions to 7-Oxabicyclo(2.2.l]hept-5-en-2-one. *Helvetica Chimica Acta* **1993,** *76*, 2490-2499.
279. Miller, C. P., Mild and Efficient Dehydration of Oximes to Nitriles Mediated by the Burgess Reagent. *Synlett* **2000,** *8*, 1169-1171.
280. Walli, A.; Dechert, S.; Meyer, F., Tautomerism in Bis(oxazoline)s. *European Journal of Organic Chemistry* **2013,** *2013* (31), 7044-7049.
281. Hackbart, W.; Hartmann, M., Notiz über eine neue Darstellungsmethode für α,α-disubstituierte Malonsäurediamide. *Journal für Praktische Chemie* **1961,** *14* (1-2), 1-3.
282. Sasai, H., Design and synthesis of chiral hybrid spiro (isoxazole–isoxazoline) ligands. *Tetrahedron: Asymmetry* **2007,** *18*, 919–923.
283. Nemoto, H.; Kubota, Y.; Yamamoto, Y., Development of a new acyl anion equivalent for the preparation of masked activated esters, and their use to prepare a dipeptide. *The Journal of Organic Chemistry* **1990,** *55* (15), 4515-4516.
284. Binev, Y. I., The conversion of phenylpropanedinitrile (phenylmalononitrile) into the carbanion, followed by IR spectra, ab initio and DFT force field calculations. *Spectrochimica Acta Part A* **2003,** *59*, 3041-3052.
285. Burstall, F. H., 34. Optical activity dependent on co-ordinated bivalent ruthenium. *Journal of the Chemical Society (Resumed)* **1936,** (0), 173-175.
286. Miller, R. R.; Brandt, W. W.; Puke Sr, M.; Puke, O., Metal-Amine Coördination Compounds. V. The Ruthenium-2, 2'-Bipyridine System1, 2, 3. *Journal of the American Chemical Society* **1955,** *77* (12), 3178-3180.
287. Palmer, R. A.; Piper, T. S., 2,2'-Bipyridine Complexes. I. Polarized Crystal Spectra of Tris (2,2'-bipyridine)copper(II), -nickel(II), -cobalt(II), -iron(II), and -ruthenium(II). *Inorganic Chemistry* **1966,** *5* (5), 864-878.
288. Braddock, J. N.; Meyer, T. J., Kinetics of the oxidation of $Fe(H_2O)_6^{2+}$ by polypyridine complexes of ruthenium(III). Negative enthalpies of activation. *Journal of the American Chemical Society* **1973,** *95* (10), 3158-3162.
289. Broomhead, J. A.; Young, C. G.; Hood, P., Tris(2,2'-Bipyridine)Ruthenium(II) Dichloride Hexahydrate. In *Inorganic Syntheses*, 1990; pp 338-340.
290. James, B. R.; Ochiai, E.; Rampel, G. L., Ruthenium (II) halide dimethylsulphoxide complexes from hydrogenation reactions. *Inorganic and Nuclear Chemistry Letters* **1971,** *7* (8), 781-784.
291. Evans, I. P.; Spencer, A.; Wilkinson, G., Dichlorotetrakis(dimethyl sulphoxide)ruthenium(II) and its use as a source material for some new ruthenium(II) complexes. *Journal of the Chemical Society, Dalton Transactions* **1973,** (2), 204-209.
292. Alessio, E.; Mestroni, G.; Nardin, G.; Attia, W. M.; Calligaris, M.; Sava, G.; Zorzet, S., *Cis*- and *trans*-dihalotetrakis(dimethyl sulfoxide)ruthenium(II) complexes ($RuX_2(DMSO)_4$; X = Cl, Br): synthesis, structure, and antitumor activity. *Inorganic Chemistry* **1988,** *27* (23), 4099-4106.
293. Saito, R.; Chung, K.-g.; Nishimura, H.; Sakai, T., Ruthenium film-forming material and ruthenium film-forming method. Google Patents: 2012.
294. Ioannis Bratsos; Enzo Alessio; Mark E. Ringenberg, T. B. R., Ruthenium Complexes. In *Inorganic Syntheses*, Rauchfuss, T. B., Ed. 2010; pp 148-163.
295. Jaswal, J. S.; Rettig, S. J.; James, B. R., Ruthenium(III) complexes containing dimethylsulfoxide or dimethylsulfide ligands, and a new route to *trans*-dichlorotetrakis(dimethylsulfoxide)ruthenium(II). *Canadian Journal of Chemistry* **1990,** *68* (10), 1808-1817.

296. Fu, S.; Liu, Y.; Ding, Y.; Du, X.; Song, F.; Xiang, R.; Ma, B., A mononuclear cobalt complex with an organic ligand acting as a precatalyst for efficient visible light-driven water oxidation. *Chemical Communications* **2014,** *50* (17), 2167-2169.
297. Jia, W.-G.; Cheng, M.-X.; Gao, L.-L.; Tan, S. M.; Wang, C.; Liu, X.; Lee, R., A ruthenium bisoxazoline complex as a photoredox catalyst for nitro compound reduction under visible light. *Dalton Transactions* **2019,** *48* (27), 9949-9953.
298. Faller, J. W.; Lavoie, A., Highly enantioselective Diels–Alder catalysis with a chiral ruthenium bisoxazoline complex. *Journal of Organometallic Chemistry* **2001,** *630* (1), 17-22.
299. Desimoni, G.; Faita, G.; Jørgensen, K. A., C2-Symmetric Chiral Bis(Oxazoline) Ligands in Asymmetric Catalysis. *Chemical Reviews* **2006,** *106* (9), 3561-3651.
300. Stanley, L. M.; Sibi, M. P., Chiral Bisoxazoline Ligands. In *Privileged Chiral Ligands and Catalysts*, 2011; pp 171-219.
301. Hossain, A.; Bhattacharyya, A.; Reiser, O., Copper's rapid ascent in visible-light photoredox catalysis. *Science* **2019,** *364* (6439), eaav9713.
302. Sandoval-Pauker, C.; Molina-Aguirre, G.; Pinter, B., Status report on copper (I) complexes in photoredox catalysis; photophysical and electrochemical properties and future prospects. *Polyhedron* **2021,** *199*, 115105.
303. Vila, C., Merging Visible-Light-Photoredox and Nickel Catalysis. *ChemCatChem* **2015,** *7* (12), 1790-1793.
304. Badir, S. O.; Molander, G. A., Developments in Photoredox/Nickel Dual-Catalyzed 1,2-Difunctionalizations. *Chem* **2020,** *6* (6), 1327-1339.
305. Zuo, Z.; Ahneman, D. T.; Chu, L.; Terrett, J. A.; Doyle, A. G.; MacMillan, D. W. C., Merging photoredox with nickel catalysis: Coupling of α-carboxyl sp^3-carbons with aryl halides. *Science* **2014,** *345* (6195), 437-440.
306. Cavalcanti, L. N.; Molander, G. A., Photoredox Catalysis in Nickel-Catalyzed Cross-Coupling. *Topics in Current Chemistry* **2016,** *374* (4), 39.
307. Vidal, A.; Calligaro, R.; Gasser, G.; Alberto, R.; Balducci, G.; Alessio, E., cis-Locked Ru(II)-DMSO Precursors for the Microwave-Assisted Synthesis of Bis-Heteroleptic Polypyridyl Compounds. *Inorganic Chemistry* **2021,** *60* (10), 7180-7195.
308. Viala, C.; Coudret, C., An expeditious route to *cis*-$Ru(bpy)_2Cl_2$ (bpy=2,2′-bipyridine) using carbohydrates as reducers. *Inorganica Chimica Acta* **2006,** *359* (3), 984-989.
309. Wu, Z.; Mu, J.; Wang, Q.; Chen, X.; Jensen, L.; Yi, C.; Li, M.-J., Hydroxyl and amino functionalized cyclometalated Ir(III) complexes: Synthesis, characterization and cytotoxicity studies. *Journal of Organometallic Chemistry* **2015,** *791*, 175-182.
310. Mack, J. B. C.; Walker, K. L.; Robinson, S. G.; Zare, R. N.; Sigman, M. S.; Waymouth, R. M.; Du Bois, J., Mechanistic Study of Ruthenium-Catalyzed C–H Hydroxylation Reveals an Unexpected Pathway for Catalyst Arrest. *Journal of the American Chemical Society* **2019,** *141* (2), 972-980.
311. Heath, G. A.; Yellowlees, L. J.; Braterman, P. S., Spectro-electrochemical studies on tris-bipyridyl ruthenium complexes; ultra-violet, visible, and near-infrared spectra of the series $[Ru(bipyridyl)_3]^{2+/1+/0/1-}$. *Journal of the Chemical Society, Chemical Communications* **1981,** (6), 287-289.
312. Caspar, J. V.; Westmoreland, T. D.; Allen, G. H.; Bradley, P. G.; Meyer, T. J.; Woodruff, W. H., Molecular and electronic structure in the metal-to-ligand charge-transfer excited states of d6 transition-metal complexes in solution. *Journal of the American Chemical Society* **1984,** *106* (12), 3492-3500.
313. Ohsawa, Y.; DeArmond, M. K.; Hanck, K. W.; Moreland, C. G., A proton NMR study of reduced paramagnetic tris(2,2'-bipyridine) complexes of iron(II), ruthenium(II) and osmium(II). *Journal of the American Chemical Society* **1985,** *107* (19), 5383-5386.
314. Dodsworth, E. S.; Lever, A. B. P., Correlations between electrochemical potentials and optical charge transfer energies in ruthenium bipyridine derivatives. *Chemical Physics Letters* **1986,** *124* (2), 152-158.
315. Brown, H. C.; Okamoto, Y., Substituent Constants for Aromatic Substitution1-3. *Journal of the American Chemical Society* **1957,** *79* (8), 1913-1917.
316. Brown, H. C.; Okamoto, Y., Electrophilic Substituent Constants. *Journal of the American Chemical Society* **1958,** *80* (18), 4979-4987.
317. Barbante, G. J.; Hogan, C. F.; Wilson, D. J. D.; Lewcenko, N. A.; Pfeffer, F. M.; Barnett, N. W.; Francis, P. S., Simultaneous control of spectroscopic and electrochemical properties in functionalised electrochemiluminescent tris(2,2′-bipyridine)ruthenium(II) complexes. *Analyst* **2011,** *136* (7), 1329-1338.

318. Balzani, V.; Bolletta, F.; Gandolfi, M. T.; Maestri, M. In *Bimolecular electron transfer reactions of the excited states of transition metal complexes*, Organic Chemistry and Theory, Berlin, Heidelberg, 1978//; Springer Berlin Heidelberg: Berlin, Heidelberg, 1978; pp 1-64.
319. Claude, J. P.; Meyer, T. J., Temperature Dependence of Nonradiative Decay. *The Journal of Physical Chemistry* **1995,** *99* (1), 51-54.
320. Ito, A.; Kobayashi, N.; Teki, Y., Low-Energy and Long-Lived Emission from Polypyridyl Ruthenium(II) Complexes Having A Stable-Radical Substituent. *Inorganic Chemistry* **2017,** *56* (7), 3794-3808.
321. Lakowicz, J. R., *Principles of fluorescence spectroscopy*. Springer: 2006.
322. Farney, E. P.; Chapman, S. J.; Swords, W. B.; Torelli, M. D.; Hamers, R. J.; Yoon, T. P., Discovery and Elucidation of Counteranion Dependence in Photoredox Catalysis. *Journal of the American Chemical Society* **2019,** *141* (15), 6385-6391.
323. Curran, D. P.; Bosch, E.; Kaplan, J.; Newcomb, M., Rate constants for halogen atom transfer from representative α-halo carbonyl compounds to primary alkyl radicals. *The Journal of Organic Chemistry* **1989,** *54* (8), 1826-1831.
324. Curran, D. P.; Chang, C. T., Atom transfer cyclization reactions of α-iodo esters, ketones, and malonates: examples of selective 5-exo, 6-endo, 6-exo, and 7-endo ring closures. *The Journal of Organic Chemistry* **1989,** *54* (13), 3140-3157.
325. Nguyen, J. D.; Tucker, J. W.; Konieczynska, M. D.; Stephenson, C. R. J., Intermolecular Atom Transfer Radical Addition to Olefins Mediated by Oxidative Quenching of Photoredox Catalysts. *Journal of the American Chemical Society* **2011,** *133* (12), 4160-4163.
326. Gontala, A.; Jang, G. S.; Woo, S. K., Visible-Light Photoredox-Catalyzed α-Allylation of α-Bromocarbonyl Compounds Using Allyltrimethylsilane. *Bulletin of the Korean Chemical Society* **2021,** *42* (3), 506-509.
327. Festersen, L. Eosin Y-katalysierte Kaskadencyclisierung von Alkinyl-α-brom-acetophenonen.
328. Yang, X.-L.; Guo, J.-D.; Xiao, H.; Feng, K.; Chen, B.; Tung, C.-H.; Wu, L.-Z., Photoredox Catalysis of Aromatic β-Ketoesters for in Situ Production of Transient and Persistent Radicals for Organic Transformation. *Angewandte Chemie International Edition* **2020,** *59* (13), 5365-5370.
329. Raghuram, T.; Vijaysaradhi, S.; Singh, I.; Singh, J., Convenient Conversion of Acid to Weinreb's Amide. *Synthetic Communications* **1999,** *29* (18), 3215-3219.
330. Bryden, M. A.; Zysman-Colman, E., Organic thermally activated delayed fluorescence (TADF) compounds used in photocatalysis. *Chemical Society Reviews* **2021,** *50* (13), 7587-7680.
331. Luo, J.; Hu, B.; Wu, W.; Hu, M.; Liu, T. L., Nickel-Catalyzed Electrochemical $C(sp^3)–C(sp^2)$ Cross-Coupling Reactions of Benzyl Trifluoroborate and Organic Halides. *Angewandte Chemie International Edition* **2021,** *60* (11), 6107-6116.
332. Tyson, E. L.; Farney, E. P.; Yoon, T. P., Photocatalytic [2 + 2] Cycloadditions of Enones with Cleavable Redox Auxiliaries. *Organic Letters* **2012,** *14* (4), 1110-1113.
333. Liao, S.; Sun, X.-L.; Tang, Y., Side Arm Strategy for Catalyst Design: Modifying Bisoxazolines for Remote Control of Enantioselection and Related. *Accounts of Chemical Research* **2014,** *47* (8), 2260-2272.
334. Meneghetti, M. R.; Meneghetti, S. M. P., Sn(IV)-based organometallics as catalysts for the production of fatty acid alkyl esters. *Catalysis Science & Technology* **2015,** *5* (2), 765-771.
335. Zalas, M.; Gierczyk, B.; Klein, M.; Siuzdak, K.; Pędziński, T.; Łuczak, T., Synthesis of a novel dinuclear ruthenium polypyridine dye for dye-sensitized solar cells application. *Polyhedron* **2014,** *67*, 381-387.
336. Kodama, K.; Kobayashi, A.; Hirose, T., Synthesis and spectral properties of ruthenium(II) complexes based on 2,2′-bipyridines modified by a perylene chromophore. *Tetrahedron Letters* **2013,** *54* (40), 5514-5517.
337. Nguyen, T. Q.; Qu, F.; Huang, X.; Janzen, A. F., Preparation and NMR spectra of $PF_4(N\text{-}N)^+$ and $SiF_4(N\text{-}N)$, where N-N = 2,2′-bipyridine, 4-fluoro-2,2′-bipyridine, and 1,10-phenanthroline. *Canadian Journal of Chemistry* **1992,** *70* (7), 2089-2093.
338. Reddy, R. B.; Dudhe, P.; Chauhan, P.; Sengupta, S.; Chelvam, V., Synthesis of tubuphenylalanine and epi-tubuphenylalanine via regioselective aziridine ring opening with carbon nucleophiles followed by hydroboration-oxidation of 1,1-substituted amino alkenes. *Tetrahedron* **2018,** *74* (48), 6946-6953.
339. Dickman, D. A.; Meyers, A. I.; Smith, G. A.; Gawley, R. E.; Smith, K. M.; Heathcock, C. H.; Johnson, A. T.; Yager, K. M.; White, J. D., Reduction of alpha-amino acids: L-Valinol. *Organic Syntheses* **1985,** *63*, 136.

340. Theodoropoulou, M. A.; Koutoulogenis, G. S.; Zhang, L.; Akrani, I.; Mikros, E.; Hilgenfeld, R.; Kokotos, G. Identification of a Dual Inhibitor of Secreted Phospholipase A_2 (GIIA $sPLA_2$) and SARS-CoV-2 Main Protease *Pharmaceuticals* [Online], 2022.
341. Ton, T. M. U.; Tejo, C.; Tiong, D. L. Y.; Chan, P. W. H., Copper(II) Triflate Catalyzed Amination and Aziridination of 2-Alkyl Substituted 1,3-Dicarbonyl Compounds. *Journal of the American Chemical Society* **2012,** *134* (17), 7344-7350.
342. Breising, V. M.; Gieshoff, T.; Kehl, A.; Kilian, V.; Schollmeyer, D.; Waldvogel, S. R., Electrochemical Formation of 3,5-Diimido-1,2-dithiolanes by Dehydrogenative Coupling. *Organic Letters* **2018,** *20* (21), 6785-6788.
343. Marinova, M.; Bonnefont, A.; Achard, T.; Maisse-François, A.; Bellemin-Laponnaz, S., Chiral stimuli-responsive metallo-supramolecular assembly induced by Cu^{II}/Cu^{I} redox change. *Chemical Communications* **2020,** *56* (61), 8703-8706.
344. Evans, D. A.; Woerpel, K. A.; Nosse, B.; Schall, A.; Shinde, Y.; Jezek, E.; Haque, M. M.; Wipf, P., Synthesis of (–)-(*S*,*S*)- Bis(4-isopropyloxazoline); (4S, 4S')-2,2'-(Propane-2,2-diyl)bis(4-isopropyl-4,5-dihydrooxazole). *Organic Syntheses* **2006,** *83*, 97 - 102.
345. Guan, Y.; Attard, J. W.; Mattson, A. E., Copper Bis(oxazoline)-Catalyzed Enantioselective Alkynylation of Benzopyrylium Ions. *Chemistry – A European Journal* **2020,** *26* (8), 1742-1747.
346. Qu, F.; Park, S.; Martinez, K.; Gray, J. L.; Thowfeik, F. S.; Lundeen, J. A.; Kuhn, A. E.; Charboneau, D. J.; Gerlach, D. L.; Lockart, M. M.; Law, J. A.; Jernigan, K. L.; Chambers, N.; Zeller, M.; Piro, N. A.; Kassel, W. S.; Schmehl, R. H.; Paul, J. J.; Merino, E. J.; Kim, Y.; Papish, E. T., Ruthenium Complexes are pH-Activated Metallo Prodrugs (pHAMPs) with Light-Triggered Selective Toxicity Toward Cancer Cells. *Inorganic Chemistry* **2017,** *56* (13), 7519-7532.
347. Poulsen, B. C.; Estalayo-Adrián, S.; Blasco, S.; Bright, S. A.; Kelly, J. M.; Williams, D. C.; Gunnlaugsson, T., Luminescent ruthenium polypyridyl complexes with extended 'dppz' like ligands as DNA targeting binders and cellular agents. *Dalton Transactions* **2016,** *45* (45), 18208-18220.
348. Rutherford, T. J.; Keene, F. R., Stereochemical Control of Donor and Acceptor Groups in a Monomeric Chromophore–Quencher Complex of Ruthenium(II). *Inorganic Chemistry* **1997,** *36* (13), 2872-2878.
349. Ylijoki, K. E. O.; Kirk, A. D.; Böcklein, S.; Witherell, R. D.; Stryker, J. M., Cobalt-Mediated η5-Pentadienyl/Alkyne [5 + 2] Cycloaddition Reactions: Substitution Effects, Bicyclic Synthesis, and Photochemical η4-Cycloheptadiene Demetalation. *Organometallics* **2015,** *34* (13), 3335-3357.
350. Kammerer, C.; Prestat, G.; Gaillard, T.; Madec, D.; Poli, G., Allylic Alkylation and Ring-Closing Metathesis in Sequence: A Successful Cohabitation of Pd and Ru. *Organic Letters* **2008,** *10* (3), 405-408.
351. Sugimoto, K.; Kobayashi, A.; Kohyama, A.; Sakai, H.; Matsuya, Y., Divinylcarbinol Desymmetrization Strategy: A Concise and Reliable Approach to Chiral Hydroxylated Fatty Acid Derivatives. *The Journal of Organic Chemistry* **2021,** *86* (5), 3970-3980.
352. Falck, J. R.; Gao, S.; Prasad, R. N.; Koduru, S. R., Electrophilic α-thiocyanation of chiral and achiral N-acyl imides. A convenient route to 5-substituted and 5,5-disubstituted 2,4-thiazolidinediones. *Bioorganic & Medicinal Chemistry Letters* **2008,** *18* (6), 1768-1771.
353. Sibi, M. P.; Miyabe, H., Crotylations of α-Carbonyl Radicals with Crotylstannane. *Organic Letters* **2002,** *4* (20), 3435-3438.
354. Fang, L.-Z.; Shen, J.-M.; Lv, Q.-H.; Yan, F.-L., Facile and Efficient Method for α-Monobromination of Dicarbonyl Compounds with *N*-Bromosuccinimide. *Asian Journal of Chemistry* **2011,** *23* (8), 3425-3427.
355. Yang, H.-M.; Liu, M.-L.; Tu, J.-W.; Miura-Stempel, E.; Campbell, M. G.; Chuang, G. J., Bimetallic Photoredox Catalysis: Visible Light-Promoted Aerobic Hydroxylation of Arylboronic Acids with a Dirhodium(II) Catalyst. *The Journal of Organic Chemistry* **2020,** *85* (4), 2040-2047.
356. Evans, D. A.; Fandrick, K. R.; Song, H.-J., Enantioselective Friedel–Crafts Alkylations of α,β-Unsaturated 2-Acyl Imidazoles Catalyzed by Bis(oxazolinyl)pyridine–Scandium(III) Triflate Complexes. *Journal of the American Chemical Society* **2005,** *127* (25), 8942-8943.
357. Salaverri, N.; Carli, B.; Díaz-Tendero, S.; Marzo, L.; Alemán, J., Enantioselective Addition of Remote Alkyl Radicals to Double Bonds by Photocatalytic Proton-Coupled Electron Transfer (PCET) Deconstruction of Unstrained Cycloalkanols. *Organic Letters* **2022,** *24* (17), 3123-3127.

358. Trost, B. M.; Lam, T. M., Development of Diamidophosphite Ligands and Their Application to the Palladium-Catalyzed Vinyl-Substituted Trimethylenemethane Asymmetric [3 + 2] Cycloaddition. *Journal of the American Chemical Society* **2012,** *134* (28), 11319-11321.
359. Poeira, D. L.; Negrão, A. C. R.; Faustino, H.; Coelho, J. A. S.; Gomes, C. S. B.; Gois, P. M. P.; Marques, M. M. B., Hypervalent Iodine(III) Reagents with Transferable Primary Amines: Structure and Reactivity on the Electrophilic α-Amination of Stabilized Enolates. *Organic Letters* **2022,** *24* (2), 776-781.
360. Ding, T.; Jiang, L.; Yang, J.; Xu, Y.; Wang, G.; Yi, W., Highly Carbon-Selective Monofluoromethylation of β-Ketoesters with Fluoromethyl Iodide. *Organic Letters* **2019,** *21* (15), 6025-6028.
361. Trost, B. M.; Michaelis, D. J.; Charpentier, J.; Xu, J., Palladium-Catalyzed Allylic Alkylation of Carboxylic Acid Derivatives: *N*-Acyloxazolinones as Ester Enolate Equivalents. *Angewandte Chemie International Edition* **2012,** *51* (1), 204-208.
362. Meng, Q.; Zhao, J.; Yang, F.; Liu, G.; Tang, X.; Wu, Y.; Yin, H.; Feng, S. Method for preparing α-hydroxy-β-dicarbonyl compound by visible light excited disulfide catalysis. 2018.